

**APPLICATION OF AQUIFER TESTS AND  
SEDIMENTOLOGICAL CONCEPTS TO CHARACTERIZE THE  
HYDROLOGICAL PROPERTIES OF  
A FLUVIAL DEPOSIT**

by

**Steven C. Young**

A thesis

presented to the University of Waterloo

in fulfillment of the thesis requirement for the degree of

Doctor of Philosophy

in

Earth Sciences

Waterloo, Ontario, Canada, 1997

© Steven C. Young, 1997



**National Library  
of Canada**

**Acquisitions and  
Bibliographic Services**

395 Wellington Street  
Ottawa ON K1A 0N4  
Canada

**Bibliothèque nationale  
du Canada**

**Acquisitions et  
services bibliographiques**

395, rue Wellington  
Ottawa ON K1A 0N4  
Canada

*Your file Votre référence*

*Our file Notre référence*

**The author has granted a non-exclusive licence allowing the National Library of Canada to reproduce, loan, distribute or sell copies of his/her thesis by any means and in any form or format, making this thesis available to interested persons.**

**The author retains ownership of the copyright in his/her thesis. Neither the thesis nor substantial extracts from it may be printed or otherwise reproduced with the author's permission.**

**L'auteur a accordé une licence non exclusive permettant à la Bibliothèque nationale du Canada de reproduire, prêter, distribuer ou vendre des copies de sa thèse de quelque manière et sous quelque forme que ce soit pour mettre des exemplaires de cette thèse à la disposition des personnes intéressées.**

**L'auteur conserve la propriété du droit d'auteur qui protège sa thèse. Ni la thèse ni des extraits substantiels de celle-ci ne doivent être imprimés ou autrement reproduits sans son autorisation.**

0-612-21400-1

## **BORROWER'S PAGE**

The University of Waterloo requires the signatures of all persons using or photocopying this thesis. Please sign below, and give address and date.

## **ABSTRACT**

The dissertation focuses on the interpretation and evaluation of pump and tracer tests from a heterogeneous unconfined aquifer in Columbus, Mississippi, USA. A prominent feature of the aquifer is a paleochannel that crosses through two test sites. Key aspects related to the pumping test analysis are large-scale variations in the transmissivity field, preferential flow paths through high-K deposits/lenses and well screens, locally confined to unconfined aquifer conditions, and positive skin effects. Analysis of field data shows a fundamental connection among sedimentological features,  $\log(K)$  data, large-scale tracer test results, large-scale pumping test results, and ambient groundwater flow patterns. By detailing the characterization of the test site, paradigms different from those traditionally used for homogeneous aquifers are established to guide field tests and remediation efforts in similarly heterogeneous fluvial aquifers.



## **ACKNOWLEDGMENTS**

**Nancy, Amanda, and Shane.**

## TABLE OF CONTENTS

AUTHOR'S DECLARATION .....	ii
BORROWER'S PAGE .....	iii
ABSTRACT .....	iv
ACKNOWLEDGMENTS .....	v
TABLE OF CONTENTS .....	vi
LIST OF TABLES .....	xiii
LIST OF FIGURES .....	xv
1. INTRODUCTION .....	1
1.1 BACKGROUND .....	1
1.2 SCOPE OF WORK .....	2
1.3 OBJECTIVES .....	5
1.4 PRESENTATION OF INFORMATION .....	6
1.4.1 Important Issues .....	6
1.4.2 Chapter Overviews .....	8
1.4.3 Chapter Summaries .....	9
2. OVERVIEW OF PROJECTS AND TEST SITES AT COLUMBUS AFB, MISSISSIPPI .....	13
2.1 GENERAL SITE DESCRIPTION .....	13
2.2 THE MADE SITE .....	15
2.3 THE 1-Ha TEST SITE .....	17
3. GEOLOGICAL INVESTIGATION AT COLUMBUS AIR FORCE BASE .....	20
3.1 FLUVIAL DEPOSITION .....	20
3.2 BRAIDED RIVER SYSTEM .....	23
3.2.1 Braided Rivers .....	23
3.2.2 Longitudinal Bars .....	24
3.2.3 Transverse Bars .....	25
3.2.4 Summary .....	26
3.3 MEANDERING RIVER SYSTEMS .....	26
3.3.1 Meandering Rivers .....	26
3.3.2 Channel Abandonment .....	28
3.3.3 Point Bars .....	30
3.3.4 Summary .....	32

3.4 GEOLOGICAL DATA FROM COLUMBUS AFB .....	33
3.4.1 Information Sources .....	33
3.4.2 Archeological Study in the Tombigbee River Valley .....	34
3.4.3 Aerial Photographs of Test Site .....	35
3.4.4 Facies Mapping of Outcrops .....	37
3.4.5 Soil Logs from Well Boreholes .....	37
3.4.6 Continuous Soil Logs .....	39
4. CHARACTERIZATION OF HIGH-K PATHWAYS AT THE 1-Ha TEST SITE ...	55
4.1 INTRODUCTION .....	55
4.2 BRIEF DESCRIPTION OF THE 1-Ha TEST SITE AT COLUMBUS AFB	56
4.3 BOREHOLE FLOWMETER TESTS .....	56
4.3.1 The Cooper-Jacob Approach .....	57
4.3.2 K/ Profile Approach .....	58
4.4 BOREHOLE FLOWMETER DATA ANALYSIS FOR COLUMBUS AFB	59
4.4.1 Hydraulic Tests at the 1-Ha Test Site .....	59
4.4.2 Selection of an Analysis Approach .....	60
4.5 BOREHOLE FLOWMETER HYDRAULIC CONDUCTIVITY VALUES	61
4.6 EVALUATION OF THE TRENDS IN THE HYDRAULIC CONDUCTIVITY VALUES .....	62
4.6.1 Results from Geological Investigations .....	62
4.6.2 Results from Large-Scale Recirculating Tracer Test .....	64
4.7 EVALUATION OF THE MAGNITUDE OF THE K VALUES .....	65
4.7.1 Results from Large-Scale Aquifer Pumping Tests .....	65
4.7.2 Results from Small-Scale Recirculating Tracer Tests .....	67
4.8 CONCLUSIONS .....	71
5. POSITIVE SKIN EFFECTS .....	78
5.1 INTRODUCTION .....	78
5.2 BRIEF DESCRIPTION OF SITE CONDITIONS .....	79
5.2.1 The CAFB Aquifer .....	79
5.2.2 Test Sites .....	80
5.3 INVESTIGATIVE APPROACH .....	80
5.3.1 Previous Investigations .....	80
5.3.2 Vertical Heterogeneity Influence on Positive Skin Effects .....	81
5.3.3 Positive Skin Effects Impact on Calculated Transmissivity Values .....	82
5.4 BOREHOLE FLOWMETER TESTS AT THE SEVEN PAIRED WELLS .	83
5.4.1 Drawdown Responses .....	83
5.4.2 Vertical Flow Distributions .....	83
5.4.3 Calculated Transmissivity Values .....	85
5.4.4 Discussion of Results .....	86
5.5 WELL TEST RESULTS FROM THE 1-Ha TEST SITE .....	88
5.5.1 Approach to Identifying Positive Skin Effects .....	88

5.5.2 Large-Scale Aquifer Tests .....	89
5.5.3 Evaluation of Drawdown Data .....	90
5.5.4 Statistical Properties of the Borehole Flowmeter K Values .....	92
5.5.5 Transmissivity Values From Slug Tests .....	93
5.5.6 Discussion of Results .....	94
5.6 CONCLUSIONS .....	94
6. IMPACTS OF PUMPING TEST DURATION ON TRANSMISSIVITY VALUES	108
6.1 INTRODUCTION .....	108
6.2 A SEDIMENTOLOGICAL MODEL .....	109
6.3 LARGE-SCALE TRANSMISSIVITY VARIATIONS .....	110
6.3.1 Borehole Flowmeter Tests .....	110
6.3.2 Tracer Tests .....	111
6.4 DESCRIPTION OF LARGE-SCALE PUMPING TESTS .....	113
6.5 CONSIDERATIONS FOR ANALYZING THE PUMPING TEST DATA	115
6.6 NUMERICAL INVESTIGATION OF TRANSMISSIVITY CHANGES AND DELAYED DRAINAGE ON PUMPING TEST RESULTS .....	117
6.6.1 Numerical Model .....	117
6.6.2 Numerical Simulations .....	117
6.6.3 Analysis of Numerical Simulations .....	119
6.6.4 Summary of Relevant Impacts .....	121
6.7 ANALYSIS OF CAFB PUMPING TEST DATA USING THE CJSL METHOD .....	122
6.8 ANALYSIS OF CAFB PUMPING TEST DATA USING DELAYED GRAVITY DRAINAGE .....	124
6.8.1 Theoretical Considerations .....	124
6.8.2 Type-Curve Matching .....	124
6.8.3 Evaluation .....	125
6.9 SUMMARY .....	126
7. IMPACTS OF PUMPING RATE ON TRANSMISSIVITY VALUES .....	139
7.1 INTRODUCTION .....	139
7.2 BRIEF DESCRIPTION OF SITE CONDITIONS .....	140
7.2.1 Site Description .....	140
7.2.2 Well Network .....	141
7.3 RESULTS FROM SINGLE-WELL PUMPING TESTS AT THE 1-Ha TEST SITE .....	143
7.3.1 Description .....	143
7.3.2 Results .....	144
7.4 CONSIDERATIONS FOR NUMERICAL SIMULATIONS OF SINGLE- WELL PUMPING TESTS .....	146
7.4.1 Numerical Flow Code .....	146
7.4.2 Hydraulic Properties of Modeled Aquifer .....	146
7.4.3 Numerical Model .....	147

7.4.5 Pumping Rate and CJS� Transmissivity Values .....	148
7.5 SIMULATIONS OF PUMPING TESTS IN AN AQUIFER WITH A TREND OF INCREASING K WITH DISTANCE .....	148
7.5.1 Selection of Trend in the Transmissivity Field .....	148
7.5.2 Sensitivity of CJS� Transmissivity Values to Pumping Rates ...	148
7.5.3 Importance $R_i$ to Calculated CJS� Transmissivity Values .....	149
7.5.4 Factors Affecting the Sensitivity of CJS� Transmissivity Values to Pumping Rate .....	151
7.5.5 Summary .....	155
7.6 SIMULATIONS OF PUMPING TESTS IN AN AQUIFER WITH A TREND OF DECREASING K WITH DISTANCE .....	156
7.6.1 Selection of Trend in the Transmissivity Field .....	156
7.6.2 Pumping Test Results for Aquifer with Only Radial K Variations .....	157
7.6.3 Pumping Test Results for Aquifer with Radial and Vertical K Variations .....	159
7.6.4 Summary .....	160
7.7 CONCLUSIONS .....	160
8. IMPACTS OF VERTICAL HETEROGENEITY AND WELL SCREENS ON PUMPING TEST RESULTS .....	176
8.1 INTRODUCTION .....	176
8.2 TEST SITE .....	177
8.2.1 Site Description .....	177
8.2.2 Well Network .....	178
8.2.3 Vertical Heterogeneity at the Site .....	179
8.3 FIELD TEST RESULTS .....	180
8.3.1 Borehole Flowmeter Measurements .....	180
8.3.2 Small-Scale Pumping Tests .....	182
8.3.3 Small-Scale Recirculating Tracer Tests .....	184
8.3.4 Summary .....	185
8.4 MODEL RESULTS FOR A VERTICALLY HETEROGENEOUS CONFINED AQUIFER .....	186
8.4.1 Model Set-up .....	186
8.4.2 Pumping Test Simulation with Two High-K Lenses .....	187
8.4.3 Effect of Multi High-K Lenses on Aquifer Response .....	190
8.4.4 Summary .....	191
8.5 MODEL RESULTS FOR A VERTICALLY HETEROGENEOUS UNCONFINED AQUIFER .....	192
8.5.1 Model Set-up .....	192
8.5.2 Pumping Test Simulation with Two Lenses .....	194
8.5.3 Simulations with Multiple Lenses and Large-Scale Transmissivity Variations .....	195
8.5.3.1 K fields .....	195

8.5.3.2 Impact of Observation Wells .....	196
8.5.3.3 Reciprocity .....	200
8.5.4 Summary .....	201
8.6 CONCLUSIONS .....	201
9. FEASIBILITY OF DETRENDING LOG(K) DATA AT CAFB .....	223
9.1 INTRODUCTION .....	223
9.2 SITE DESCRIPTION .....	224
9.2.1 Geology .....	224
9.2.2 Test Sites .....	225
9.2.3 Hydraulic Gradients .....	227
9.3 HYDRAULIC PROPERTIES .....	228
9.4 DETRENDING LOG(K) DATA FROM CAFB .....	228
9.4.1 Approach to Detrending .....	228
9.4.2 The 1-Ha Test Site Log(K) Field .....	229
9.4.2.1 Trend identification .....	229
9.4.2.2 Detrending .....	231
9.4.2.3 The log(K) residuals from detrending .....	234
9.4.2.4 Comments regarding detrending the MADE Log(K) field .....	235
9.4.2.5 The feasibility of detrending log(K) data at CAFB .....	237
9.5 SUMMARY .....	238
10. CONTRIBUTION TO SCIENCE .....	251
10.1 OVERVIEW .....	251
10.2 CHARACTERIZATION OF THE CAFB AQUIFER .....	251
10.3 BOREHOLE FLOWMETER TESTS .....	253
10.4 POSITIVE SKIN EFFECTS .....	254
10.5 SINGLE-WELL AND MULTI-WELL TESTS IN UNCONFINED AQUIFERS .....	255
11. LESSONS LEARN AT CAFB AND THEIR APPLICATION TO INVESTIGATIONS OF SIMILAR FIELD SITES .....	258
11.1 THE KEY TO CAFB .....	258
11.2 ASSESSMENT OF THE FIELD INVESTIGATIONS .....	259
11.2.1 Geologic Structure .....	260
11.2.1 Transmissivity Field .....	263
11.2.2 Hydraulic Conductivity Distribution .....	264
11.2.3 Preferential Flow Paths .....	266
11.3 BOREHOLE FLOWMETER TESTS .....	268
12. REFERENCES .....	271

**APPENDIX A**

**DESIGN AND INSTALLATION OF THE INITIAL 37 WELLS AT THE  
1-HA TEST SITE ..... 295**

**A.1 DESIGN OF THE WELL NETWORK ..... 295**

**A.2 WELL INSTALLATION, CONSTRUCTION, AND DEVELOPMENT . 297**

**A.2.1 Well Construction Method ..... 299**

**A.2.2 Well Development ..... 302**

**APPENDIX B**

**LARGE-SCALE PUMPING TESTS AT THE 1-Ha TEST SITE ..... 307**

**B.1 GENERAL APPROACH ..... 307**

**B.2 PROGRAM WELLTEST ..... 308**

**B.3 AQUIFER TEST 1 ..... 310**

**B.3.1 Test Description ..... 310**

**B.3.2 WELLTEST Transmissivities and Storage Coefficients ..... 313**

**B.3.3 Transmissivities by the Cooper-Jacob Straight-Line Method ... 316**

**B.4 AQUIFER TEST 2 ..... 318**

**B.4.1 Test Description ..... 318**

**B.4.2 Transmissivities and Storage Coefficients From Program  
        WELLTEST ..... 320**

**B.5 AQUIFER TEST 3 ..... 328**

**B.5.1 Test Description ..... 328**

**B.5.2 Transmissivities and Storage Coefficients From Program  
        WELLTEST ..... 331**

**B.5.3 Transmissivities by the Cooper-Jacob Straight-Line Method ... 334**

**APPENDIX C**

**THE ELECTROMAGNETIC BOREHOLE FLOWMETER:  
DESCRIPTION AND APPLICATION ..... 353**

**C.1 INTRODUCTION ..... 353**

**C.2 THE ELECTROMAGNETIC FLOWMETER ..... 354**

**C.2.1 Description ..... 354**

**C.2.2 Laboratory Calibration ..... 356**

**C.2.3 Field Use ..... 358**

**C.3 COMPARISONS WITH OTHER FLOWMETERS ..... 359**

**C.3.1 Impeller Flowmeters ..... 359**

**C.3.2 Comparison Between the EM and Impeller Flowmeters ..... 360**

**C.3.3 The Thermal-Pulse Flowmeter ..... 361**

**C.3.4 Comparison Between the EM and Thermal-Pulse Flowmeters . 362**

**C.3.5 Final Assessment ..... 363**

**C.4 FIELD STUDIES INVOLVING THE ELECTROMAGNETIC  
FLOWMETER ..... 364**

**C.4.1 Measurement of the Hydraulic Conductivity(K) Values ..... 365**

**C.4.2 Preferential Groundwater Flow in Granular Aquifers ..... 366**

C.4.3 Preferential Groundwater Flow in Bedrock Aquifers .....	367
C.4.4 Monitoring of Preferential Groundwater Flow Zones .....	370
C.5 SUMMARY .....	371

**APPENDIX D**

BOREHOLE FLOWMETER K PROFILES FROM COLUMBUS AFB .....	378
---	-----

**APPENDIX E**

RECIRCULATING TRACER TESTS AT THE 1-Ha TEST SITE .....	382
E.1 CONCERNS WITH PERFORMING RECIRCULATING TRACER TESTS .....	382
E.2 TRACER TEST SET-UP .....	382
E.2.1 Tracer(s) .....	382
E.2.2 The Flow Field .....	383
E.2.3 Monitoring Approach and Equipment .....	383
E.2.4 The Location and Number of Tracer Tests .....	384
E.2.5 Type of Tracer Injection .....	384
E.2.6 Surface Piping Network .....	385
E.3 DESCRIPTION OF FIVE RECIRCULATING TRACER TESTS .....	385
E.3.1 Tracer Test 1 .....	385
E.3.2 Tracer Test 2 .....	386
E.3.3 Tracer Test 3 .....	386
E.3.4 Tracer Test 4 .....	387
E.3.5 Tracer Test 5 .....	388
E.4 RESULTS FROM TRACER TESTS 1 TO 4 .....	388
E.4.1 Data Presentation .....	388
E.4.2 Tracer Test 1 .....	389
E.4.2 Tracer Test 2 .....	390
E.4.3 Tracer Test 3 .....	392
E.4.9 Tracer Test 4 .....	393
E.5 RESULTS FOR TRACER TEST 5 .....	394
E.5.1 Data Presentation .....	394
E.5.2 Water Table Elevations .....	396
E.5.3 Tracer Concentrations .....	396



## LIST OF TABLES

Table 1.1 Pumping Test Data from Columbus AFB .....	4
Table 1.2 Tracer Test Data from Columbus AFB .....	5
Table 1.3 Various Issues Addressed in Chapters 4 to 8 .....	9
Table 2.1 Results of Pumping Tests in Reconnaissance Wells .....	17
Table 3.1 Classification of river types (modified after Miall, 1977) .....	22
Table 3.2 Information Used to Construct the Depositional Environment of the CAFB Terrace Aquifer .....	34
Table 3.3 The Homeostatic and the Heterostatic Periods Associated with the Development of the Tombigbee River Valley (after Muto and Gunn, 1986) .....	36
Table 4.1 Description of Tracer Tests .....	68
Table 4.2 Magnitudes and Arrival Times of Peak Tracer Concentrations for Tracer Tests 1 to 3 .....	69
Table 5.1 Drawdown Results from Each Well Pair .....	84
Table 5.2 Summary of Drawdown Results From the Well Pairs .....	84
Table 5.3 Chronology of Different Pumping Tests at the 1-Ha Test Site during 1989 .....	89
Table 6.1 Vertical Profile of Flow into Sand-Packed Wells Measured by a Borehole Flowmeter .....	111
Table 6.2 Pumping Tests Conducted at the Two Test Sites .....	115
Table 6.3 Parameters for Estimating Unsaturated Properties .....	118
Table 6.4 CJS� Transmissivity Values for AT4 .....	123
Table 6.5 CJS� Transmissivities for MADE1, MADE2, AT3, AT4 and AT8 .....	123
Table 7.1 Chronology of Pumping Tests Performed at the 1-Ha Test Site in 1989 .....	142
Table 7.2 CJS� Transmissivities from the Drawdown Data Collected from Aquifer Tests MADE1, MADE2, AT3, AT4, and AT8 .....	143
Table 7.3 Percentage Change in the CJS� Transmissivity Caused by Changes in the Specific Storage and Aquifer Unsaturated Properties .....	154
Table 7.4 Expected Effect on S, R <sub>p</sub> , and CJS� Transmissivities Caused by Model Parameter Changes for a Basecase Pumping Scenario that has K Increase with Distance from the Pumping well .....	156
Table 8.1 Maximum Value of Groundwater Flow Measured at Each Well During April 1989 .....	181
Table 8.2 Calculated Storage Coefficients for 4-m Observation Wells for the Aquifer Configuration in Figure 8.14 .....	188
Table 8.3 Calculated Storage Coefficients from Aquifers with Randomly Distributed Lens of High-K .....	191
Table 9.1 Results of ANOVA for Using Polynomials to Detrend the Borehole Flowmeter K Values at the 1-Ha Test Site .....	233

Table 11.1 Relative Importance of Different Information Sets for Defining Aquifer Properties at CAFB .....	261
Table 11.2 Major Tasks associated with Implementing the Borehole Flowmeter Tests .....	270
Table A.1 Well Specifications .....	300
Table A.2 Benefits of Well Development (from Driscoll, 1986) .....	303
Table A.3 Procedures for Well Development at CAFB .....	304
Table B.1 Measurements of the discharge rate for Aquifer Test 1 .....	311
Table B.2 Calculated storage coefficients and transmissivities for Aquifer Test 1 at 10,000; 50,000; and 100,000 seconds .....	315
Table B.3 Transmissivities calculated by the Cooper-Jacob Straight-line Method for Aquifer Test 1 .....	317
Table B.4 Pumping schedule and location of transducer for Aquifer Test 2 .....	319
Table B.5 Calculated storage coefficients and transmissivities for Aquifer Test 2 for Pulses 1 to 6 .....	321
Table B.6 Calculated Storage Coefficients and Transmissivities for Aquifer Test 2 for Pulses 8 to 13 .....	322
Table B.7 Calculated storage coefficients and transmissivities for Aquifer Test 2 for Pulses 15 to 20 .....	324
Table B.8 Observations from the from experimental and WELLTEST drawdown data sets Aquifer Test 2 .....	325
Table B.9 WELLTEST calculated storage coefficients and transmissivities for Aquifer Test 2 .....	327
Table B.10 Measurements of the discharge rate for Aquifer Test 3 .....	329
Table B.11 Calculated storage coefficients and transmissivities for Aquifer Test 3 at 10,000; 50,000; 100,000; and 250,000 seconds .....	333
Table B.12 Transmissivities Calculated by the Cooper-Jacob Straight-Line Method for Aquifer Test 3 .....	335
Table C.1 Calibration Factors (Liter/min/volt) from a regression of discharge versus voltage for electromagnetic flowmeter data from Young et al., (1995a) .....	357
Table C.2 Groundwater issues that borehole flowmeter data can help resolve .....	365
Table E.1 Comparison of hydraulic conductivity values from the borehole flowmeter and Tracer Test 1 .....	391
Table E.2 Comparison of hydraulic conductivity values from the borehole flowmeter and tracer test 2 .....	392
Table E.3 Comparison of hydraulic conductivity values from the borehole flowmeter and tracer test 3 .....	393
Table E.4 Comparison of hydraulic conductivity values from the borehole flowmeter and tracer test 4 .....	395
Table E.5 Hydraulic gradients calculated between the monitoring well and the injection well .....	397

## LIST OF FIGURES

Figure 2.1	Location Map for Columbus AFB, TVA Macrodispersion Experimental Site, and approximate location of the 1-Ha Test Site. . . . .	19
Figure 3.1	Schematic diagram showing multiple longitudinal bars (1st order) which commonly are themselves dissected into smaller bars and shallower channels (2nd and 3rd order). Diagram represents one braided-river reach or compound channel (within which all three bars roders are migrating; 0th order) of which a braidplain is composed of many (modified after Williams and Rust, 1969). . . . .	42
Figure 3.2	Schematic of the Complex Relationships among the different facies in a braided stream environment (after Williams and Rust, 1969). . . . .	42
Figure 3.3	Block diagram showing the major morphological elements of a meandering river system (after Walker, 1979, p. 23). . . . .	43
Figure 3.4	Meandering river flow pattern and channel cross sections (from Allen, 1985). . . . .	44
Figure 3.5	Modes of channel shifting in meandering systems; A=chute cutoff, B=neck cutoff, C=avulsion (from Collinson, 1986; after Allen, 1965). . . . .	44
Figure 3.6	Physiographical units recognized from air photographs and sampling sites selected by the Corps of Engineers near the CAFB aquifer (after Muto and Gunn, 1986). . . . .	45
Figure 3.7	Evolution of the Tombigbee River Valley in the Columbus, Mississippi area (after Muto and Gunn, 1986). . . . .	46
Figure 3.8	Test sites overlaid on a 1956 aerial photograph that shows the location of a paleochannel. . . . .	47
Figure 3.9	Geologic cross section of a textural facies map at a CAFB gravel pit (after Rehfeldt et al., 1989). . . . .	48
Figure 3.10	Field -averaged grain-size distribution for the CAFB aquifer (after Boggs et al., 1990). . . . .	49
Figure 3.11	Elevation of top of Eutaw Formation (contour in meters MSL -- after Boggs et al., 1990). . . . .	49
Figure 3.12	Photograph of 76-cm (~2.5 ft) long core sections from the location of Well 72. (Depths are referenced to below ground surface). . . . .	50
Figure 3.13	Photograph of 76-cm(~2.5 ft) core sections from the location of Well 73. (Depths are referenced to below ground surface). . . . .	51
Figure 3.14	Vertical profiles of mean grain-size at the continuous coring locations. . . . .	52
Figure 3.15	Vertical profile of grain-size standard deviations at the continuous coring locations. . . . .	53

Figure 3.16	Vertical profile of borehole flowmeter K values at the continuous coring locations. ....	54
Figure 4.1	Network of 37 fully-penetrating wells at the 1-Ha test site at Columbus AFB, Mississippi (see Figure 3.8 for location at CAFB). ...	72
Figure 4.2	Application of the Cooper-Jacob (CJ) equation and the Cooper-Jacob Straight-Line (CJSL) method for calculating transmissivity values for two sets of single-well drawdown data. ....	72
Figure 4.3	The effect pumping well location on the calculated transmissivity at four observation wells. Data from Young (1991a,b). Calculated transmissivity values are from Theis type-curve matching for multi-well pumping tests and from Cooper-Jacob Straight-Line (CJSL) analyses for the single-well pumping tests. ....	73
Figure 4.4	Depth-averaged log(K) cross sections based on the 881 borehole flowmeter hydraulic conductivity values. Circles denote well locations. ....	74
Figure 4.5	Measured and predicted times for peak chloride concentrations across the well network for Tracer Test 5, a large-scale recirculating tracer test with a central injection well and four withdrawal wells. Chloride data collected from multi-level samplers installed at all well locations. Potentiometric contours represent steady-state conditions during Tracer Test 5. ....	75
Figure 4.6	Profiles of the steady-state horizontal flow as measured by the electromagnetic borehole flowmeter at injection well 16 and the four withdrawal wells during the recirculating Tracer Test 1. ....	75
Figure 4.7	Examples of tracer breakthrough data collected with multi-level samplers in withdrawal wells for Tracer Tests 1, 2, and 3. ....	76
Figure 4.8	Lower estimate of hydraulic conductivity based on tracer test data compared to borehole flowmeter hydraulic conductivity values for selected aquifer intervals of rapid tracer transport between wells observed during Tracer Tests 1-3. ....	77
Figure 5.1	Aerial photograph of CAFB site showing locations of the 1-Ha test site and seven well pairs relative to the paleochannel. ....	97
Figure 5.2	Schematic of the regional features associated with the sedimentological model. ....	97
Figure 5.3	Coarse-grained point bar, showing sediment bodies and related features (after McGowen and Garner, 1970). ....	98
Figure 5.4	(a) Vertical sequence that characterized coarse-grained point bars. The four units represent scour pool deposits (1), lower point bar (2), chute bar (3), and floodplain (4) (Modified from McGowen and Garner, 1970.) (b) Generalized cross section shows a transverse profile across the coarse-grained point bar. (Modified from Brown et al., 1973.) ....	99
Figure 5.5	Average borehole flowmeter K values for the interval of 60 to 62 m MSL at the 1-Ha test site (from Chapter 4). ....	100

Figure 5.6	Location of 37 wells at the 1-Ha test site. ....	100
Figure 5.7	Drawdown results for gravel-packed and naturally-backfilled wells at locations 41 and 72 inside the paleochannel (see Figure 5.1 for well placement). ....	101
Figure 5.8	Drawdown results for gravel-packed and naturally-backfilled wells, the locations 76 and 78 outside the paleochannel (see Figure 5.1 for well placement). ....	101
Figure 5.9	Borehole flowmeter profiles at gravel-packed and naturally-backfilled wells that intersect the paleochannel shown in Figure 5.1. ....	102
Figure 5.10	Borehole flowmeter profiles for gravel-packed and naturally-backfilled wells located outside the paleochannel boundaries shown in Figure 5.1. ....	103
Figure 5.11	Comparison of flowmeter K values from gravel-packed and naturally-backfilled wells at location 73 inside the paleochannel (see Figure 5.1). ....	104
Figure 5.12	Time-drawdown responses at five observation wells during Aquifer test AT3. ....	105
Figure 5.13	Application of Theis type-curve fits, the Cooper-Jacob (CJ) equation, and the Cooper-Jacob straight-line (CJSL) method for calculating transmissivity values for two single-well pumping test performed in the 1-Ha test site. ....	105
Figure 5.14	Frequency distribution of the ratio between the CJ and Theis transmissivity values to the CJSL transmissivity values calculated for 115 single-well pumping tests at the 1-Ha test site. ....	106
Figure 5.15	Comparison of the arithmetic and harmonic means for 668 CJ and for 668 CJSL K values with results of a large-scale pumping test. ....	106
Figure 5.16	Slug-test results from fully-penetrating wells at the 1-Ha test site that illustrate a classical Hvorslev response. ....	107
Figure 6.1	Location of two test sites at Columbus AFB, MS, superimposed on a 1956 aerial photograph that reveals a paleochannel. ....	127
Figure 6.2	Well network for 1-Ha test site with location paleochannel estimated by dotted line. ....	128
Figure 6.3	Schematic of the regional features associated with the sedimentological model. ....	128
Figure 6.4	Vertical profile of grain-size distributions at Well 73 (ground surface is at 64.9 m MSL). ....	129
Figure 6.5	Areal profile of borehole flowmeter K values for the uppermost 2 m of the saturated aquifer at the 1-Ha test site (from Chapter 4). ....	130
Figure 6.6	Vertical cross section of tritium plume at the MADE site for 27, 132, and 224 days after injection (modified from Boggs et al., 1993). ....	131

Figure 6.7	Observation well time-drawdown response from large-scale aquifer tests with different pumping wells (see Figure 6.1 for location of pumping well). . . . .	132
Figure 6.8	Drawdown responses in a hypothetical aquifer with hydraulic properties that vary with radial distance from the pumping well. . . . .	132
Figure 6.9	Comparison of results from FRAC3DVS and the analytical solution of Kroszynski and Dagan (1975). . . . .	133
Figure 6.10	Comparison of results from FRAC3DVS and the numerical results of Akindunni and Gillham (1992). . . . .	133
Figure 6.11	K values used in the numerical simulations to represent aquifer properties for a vertical cross section through the paleochannel. . . . .	134
Figure 6.12	Areal changes in transmissivity for three hypothetical aquifers used to simulate pumping tests with FRAC3DVS. . . . .	134
Figure 6.13	Simulated pumping test drawdowns for hypothetical unconfined aquifer based at the pumping well and an observation well at a radial distance of 2.5 m. Time-drawdown response at the pumping well and an observation well (radial distance of 2.5m) for numerical simulated pumping tests in an hypothetical unconfined aquifer. . . . .	135
Figure 6.14	Theis type curve fit to data from Aquifer test 2, which includes a cyclic pumping schedule at Well 5. . . . .	135
Figure 6.15	Time-drawdown response at the pumping well and five observation wells during AT4. . . . .	136
Figure 6.16	Time-drawdown data from the pumping wells used in the large-scale pumping test designated as MADE1, MADE2, AT3, and AT8 (see Figure 6.15 for results from AT4). . . . .	136
Figure 6.17	Neuman type-curve fits to the simulated pumping tests for the benchmark and linear strip cases shown in Figure 6.12. . . . .	137
Figure 6.18	Values for transmissivity, specific storage, and specific yield from application of Neuman curve fits to seven pumping tests located in the paleochannel. . . . .	138
Figure 7.1	Location of two test sites at CAFB, MS superimposed on a 1956 aerial photograph that reveals a paleochannel. . . . .	162
Figure 7.2	Schematic of the regional features associated with the sedimentological model. . . . .	162
Figure 7.3	Vertical profile of grain-size distributions at Well 73 (ground surface is at 64.9 m MSL). . . . .	163
Figure 7.4	Well network for 1-Ha test site with location of the paleochannel estimated by dotted line. . . . .	164
Figure 7.5	Areal profile of borehole flowmeter K values for the uppermost 2 m of the saturated aquifer at the 1-Ha test site (from Chapter 4). . . . .	164
Figure 7.6	Effect of pumping rate on drawdown response (normalized by the pumping rate) and the CJSL transmissivity values for Wells 2 and 4 at the 1-Ha test site. . . . .	165

Figure 7.7	Trends in the CJS� transmissivity at selected wells. . . . .	165
Figure 7.8	Regions of high and low transmissivity inferred from the effects of pumping rate on the CJS� transmissivity at all 37 wells. . . . .	166
Figure 7.9	Unsaturated hydraulic properties used in numerical simulations. . . . .	167
Figure 7.10	Numerically simulated single-well pumping test results for aquifers with K values that increase with radial distance from the pumping well. . . . .	168
Figure 7.11	Sensitivity of CJS� transmissivity values to vertical anisotropy ( $0.01 < K_z/K_h \leq 1$ ) and pumping rate for an aquifer with K values that increase with radial distance from the pumping well. . . . .	169
Figure 7.12	Specific capacitance as a function of pressure for the baseline moisture retention curves described in Figure 7.9. . . . .	169
Figure 7.13	Sensitivity of CJS� transmissivity values to vertical anisotropy ( $10 \leq K_z/K_h \leq 1000$ ) and pumping rate for a hypothetical aquifer with K value that increases with radial distance from the pumping well. . . . .	170
Figure 7.14	The effect of vertical anisotropy on the location of the phreatic surface near the well at elapsed time of 60 minutes for the withdrawal and injection of $0.02 \text{ m}^3/\text{min}$ . . . . .	170
Figure 7.15	Response from Well 14 during an injection test in April 1989 and a pumping test in June 1989. . . . .	171
Figure 7.16	The June 1989 ambient water table superimposed on the borehole flowmeter K values for Well 2. . . . .	171
Figure 7.17	Numerically simulated single-well pumping test results for aquifers with K values that decrease with radial distance from the pumping well. . . . .	172
Figure 7.18	Sensitivity of CJS� transmissivity to pumping rate for a hypothetical aquifer with a K trend that increases with radial distance for the cases where $0.01 \leq K_z/K_h \leq 1000$ . . . . .	173
Figure 7.19	Numerically simulated single-well pumping tests results for hypothetical aquifers with K values that decrease with radial distance from the pumping well and with a high-K layer in the upper aquifer. . . . .	174
Figure 7.20	Sensitivity of CJS� transmissivity values to pumping rate and to anisotropy values for an hypothetical aquifer that has K values that decrease with radial distance from the pumping well and with a high-K layer in the upper aquifer. . . . .	174
Figure 7.21	CJS� transmissivity values as a function of the maximum drawdown in the pumping well at 60 minutes for an hypothetical aquifer that has K values that decrease with radial distance from the pumping well and with a high-K layer in the upper saturated aquifer. . . . .	175
Figure 8.1	Location of two test sites at CAFB, MS superimposed on a 1956 aerial photograph that reveals a paleochannel. . . . .	203

Figure 8.2	Schematic of the regional features associated with the sedimentological model. . . . .	204
Figure 8.3	Well network for 1-Ha test site with location of the paleochannel estimated by dotted line. . . . .	204
Figure 8.4	Vertical profile of grain-size distributions at location $x=65\text{m}$ and $y=35\text{m}$ at the 1-Ha test site (ground surface is at 64.9 m MSL and location is shown in Figure 8.3). . . . .	205
Figure 8.5	Facies map of soil outcrop at a gravel pit near the test sites at CAFB (from Rehfeldt et al., 1989b). . . . .	206
Figure 8.6	Borehole flowmeter K profiles at four well locations that illustrate the wide range of K values for aquifer deposits near the water table. . . . .	207
Figure 8.7	Comparison of the ambient vertical flow in Well 26 during April 1989 and the borehole flowmeter K profile from Well 26. . . . .	208
Figure 8.8	Comparison of the vertical flow in Wells 13 and 16 before and after the large-scale Aquifer test AT3. . . . .	208
Figure 8.9	Transmissivity (a) and storage coefficients (b) calculated from Theis fits to drawdown data from pumping tests with durations between 2 and 3 hours with the same observation well but different pumping wells. . . . .	209
Figure 8.10	Drawdown responses at well pairs Wells 16 and 19 and Wells 12 and 24 that illustrate that reciprocity is not valid at CAFB. . . . .	210
Figure 8.11	(a) Calculated transmissivity and (b) storage coefficients for small-scale pumping tests plotted as a function of distance. . . . .	210
Figure 8.12	Comparison of storage coefficients and K values for well pairs in Tracer Tests 1 and 2. . . . .	211
Figure 8.13	Predicted drawdown in a confined aquifer using an analytical and a numerical model. . . . .	212
Figure 8.14	Schematic of two high-K lenses located near the pumping well with the pumping well intersecting the lower lens and the observation well intersecting the lower and upper lens: (a) Partial vertical cross-section along the positive x axis; and, (b) Areal cross-section centered on pumping well. . . . .	212
Figure 8.15	Drawdown curves predicted at radial distances of 4 m and 16 m in the direction of the two lenses (along the positive x axis) for the cases with and without the effect of the high-K wellbore associated with the observation wells. Where wellbore effects are included the drawdown is nearly identical throughout the entire well so only one drawdown response is included. For comparison, drawdown results are provided for homogeneous aquifer. . . . .	213
Figure 8.16	Drawdown curves predicted at radial distances of 4 m and 16 m in the direction opposite of the two lenses (along the negative x axis) for the cases with and without the effect of the high-K wellbore associated with the observation wells. Where wellbore effects are	



	included the drawdown is nearly identical throughout the entire well so only one drawdown response is included. For comparison, drawdown results are provided for homogeneous aquifer. ....	214
Figure 8.17	Numerically simulated drawdown responses at observation wells located on the x and y axes at radial distances of 4 m and 32 m for four realizations of randomly distributed high-K lenses in a confined aquifer. ....	215
Figure 8.18	Numerically simulated drawdowns for an unconfined homogeneous aquifer with a K of 0.024 m/min for: (a) changes in the vertical anisotropy with S <sub>s</sub> set to 0.00005; and, (b) changes in specific storage with the vertical anisotropy set to 0.01. ....	216
Figure 8.19	Simulated drawdowns for an unconfined homogeneous aquifer with a K of 0.024 m/min and a lens with a K of 0.24 m/min located near the aquifer base and an upper lens located directly below the initial water table. ....	217
Figure 8.20	Storage coefficients (obtained from type-curve matches to numerically simulated drawdown responses) plotted as a function of radial distance to the observation well. ....	217
Figure 8.21	Temporal variations in the hydraulic head field along a vertical cross section of the aquifer aligned with the x axis for the three numerical simulations discussed in Figure 8.19. The unconfined aquifer has a K of the 0.024 m/min and a lens with a K of 0.24 m/min at the aquifer base. The hypothetical aquifers varied in the uniform values for S <sub>s</sub> , K <sub>z</sub> /K <sub>H</sub> , and the K of the upper lens. The values for these properties are (a) S <sub>s</sub> =5x10 <sup>-4</sup> , K <sub>z</sub> /K <sub>H</sub> =1, K <sub>upperlens</sub> =0.24 m/min, (b) S <sub>s</sub> =5x10 <sup>-5</sup> , K <sub>z</sub> /K <sub>H</sub> =0.1, K <sub>upperlens</sub> =0.024 m/min, (c) S <sub>s</sub> =5x10 <sup>-6</sup> , K <sub>z</sub> /K <sub>H</sub> =0.01, K <sub>upperlens</sub> =0.0024 m/min. ....	218
Figure 8.22	(a) Monitoring well network for the 298,265-node numerical model used to simulate pumping tests in hypothetical heterogeneous aquifers, and (b) the thickness variation of the high-K linear strip incorporated in one of the models. ....	219
Figure 8.23	Drawdown responses for pumping tests with and without observation wells for: (a) a K field consisting of multiple lens of different Ks.; and, (b) K field with large-scale transmissivity variation. ....	220
Figure 8.24	Observation-well drawdown responses for pumping Well 12 at 0.06 m <sup>3</sup> /min in the K field consisting of multiple lens of different Ks. ....	221
Figure 8.25	Temporal variation of vertical fluxes in the observation wells shown in Figure 8.24. ....	221
Figure 8.26	Drawdown responses showing reciprocity for well pairs in: (a) the K field consisting of multiple lens; and, (b) the K field with a large-scale transmissivity variations. ....	222

Figure 8.27	Drawdown responses showing non-reciprocity for well pairs in: (a) the K field consisting of multiple lens; and, (b) the K field with a large-scale transmissivity variations. . . . .	222
Figure 9.1	Location of two test sites at CAFB, MS superimposed on a 1956 aerial photograph that reveals a paleochannel. . . . .	240
Figure 9.2	Schematic of the regional features associated with the sedimentological model. . . . .	241
Figure 9.3	Well network for 1-Ha test site with location of the paleochannel estimated by dotted line. . . . .	241
Figure 9.4	Depth-averaged log(K) cross sections for the upper and lower 2 meter interval of the saturated aquifer at the 1-Ha test site based on borehole flowmeter meter tests. . . . .	242
Figure 9.5	Vertical cross sections of a tritium plume at the MADE site for 27, 132 and 224 days after injection (modified from Boggs et al., 1992). . . . .	243
Figure 9.6	Averaged vertical hydraulic gradients for paired piezometers plotted in reference to the paleochannel in Figure 1 and a scour channel filled with marine sands from the Eutaw Formation. . . . .	244
Figure 9.7	Experimental vertical and horizontal global semivariogram for Log(K) data fitted to an exponential semivariogram model. . . . .	244
Figure 9.8	Experimental directional semivariograms for log(K) data. Search angle is along a horizontal plane and measured clockwise from north. . . . .	245
Figure 9.9	Experimental regional semivariogram for log(K) data. . . . .	245
Figure 9.10	Depth-averaged cross sections for 60-62 m MSL based for log(K) values at flowmeter locations generated by the polynomials used for detrending. Circles denote well locations. . . . .	246
Figure 9.11	Depth-averaged cross sections for 54-56 m MSL based for log(K) values at flowmeter locations generated by the polynomials used for detrending. Circles denote well locations. . . . .	247
Figure 9.12	Experimental global variograms for the log(K) residuals. . . . .	248
Figure 9.13	Experimental directional variograms for the log(K) residuals. . . . .	249
Figure 9.14	Vertical and Horizontal correlation lengths determined by fitting an exponential semivariogram model to the log(K) residuals. . . . .	250
Figure A.1	The location of the initial 37 wells at the 1-Ha Test Site. . . . .	305
Figure A.2	Number of well pairs for each lag distance. . . . .	305
Figure A.3	Example of a typical well installation at the 1-Ha test site. . . . .	306
Figure B.1	WELLTEST Maps of the cumulative residual (as a percentage) for an pumping test with constant pumpage in an idealized homogeneous aquifer with a transmissivity and a storage coefficient of 30 cm <sup>2</sup> /s and 0.03, respectively. . . . .	336
Figure B.2	WELLTEST Maps of the cumulative residual (as a percentage) for an pumping test with pumpage at regulated intervals in an idealized	

	homogeneous aquifer with a transmissivity and a storage coefficient of 30 cm <sup>2</sup> /s and 0.03, respectively. ....	337
Figure B.3	The cone-of-depression for an Aquifer Test 1 at different times. ....	338
Figure B.4	WELLTEST Fits to Aquifer Test 1 drawdowns for Wells 2, 4, and 6. ....	339
Figure B.5	WELLTEST Fits to Aquifer Test 1 drawdowns for Wells 8, 15, and 17. ....	340
Figure B.6	WELLTEST Fits to Aquifer Test 1 drawdowns for Wells 18, 25, and 30. ....	341
Figure B.7	WELLTEST Fits to Aquifer Test 2 drawdowns for Pulses 1 through 7 at Wells 2, 4, 6, 8, 14, and 15. ....	342
Figure B.8	WELLTEST Fits to Aquifer Test 2 drawdowns for Pulses 1 through 7 at Wells 17, 19, 20, 25, 26, and 30. ....	343
Figure B.9	WELLTEST Fits to Aquifer Test 2 drawdowns for Pulses 8 through 14 at Wells 1, 9, 10, 11, 12, and 13. ....	344
Figure B.10	WELLTEST Fits to Aquifer Test 2 drawdowns for Pulses 8 through 14 at Wells 16, 18, 21, 24, 31, and 32. ....	345
Figure B.11	WELLTEST Fits to Aquifer Test 2 drawdowns for Pulses 15 through 21 at Wells 3, 7, 10, 11, 12, and 13. ....	346
Figure B.12	WELLTEST Fits to Aquifer Test 2 drawdowns for Pulses 15 through 21 at Wells 16, 18, 21, 24, 32, and 32. ....	347
Figure B.13	The cone-of-depression for an Aquifer Test 3 at different times. ....	348
Figure B.14	WELLTEST Fits to Aquifer Test 3 drawdowns for Wells 1, 2, and 4. ....	349
Figure B.15	WELLTEST Fits to Aquifer Test 3 drawdowns for Wells 6, 8, and 14. ....	350
Figure B.16	WELLTEST Fits to Aquifer Test 3 drawdowns for Wells 17, 20, and 25. ....	351
Figure B.17	WELLTEST Fits to Aquifer Test 3 drawdowns for Wells 26, 30, and 31. ....	352
Figure C.1	Illustrations of the electromagnetic flowmeter probe. ....	372
Figure C.2	Pre- and post-calibration data associated with field testing of the electromagnetic flowmeter in a 5.25-cm well: (a) flowmeter with 1.27-cm ID; and, (b) flowmeter with 2.54-cm ID (from Young et al., 1995) ....	372
Figure C.3	Measured frictional losses caused by channeling flow from a 5.25-cm ID well into EM flowmeters. ....	373
Figure C.4	Illustrations of flow probes used in: (a) impeller flowmeters; and, (b) thermal-pulse flowmeters. ....	373
Figure C.5	Impeller flowmeter calibration before and after field testing five well at Columbus AFB, Mississippi. ....	374
Figure C.6	Measured discharges by the electromagnetic and the impeller flowmeters at two wells located in a sand-and-gravel aquifer at Columbus AFB, Mississippi (from Young, 1990). ....	374

Figure C.7	Depth-averaged hydraulic conductivity values for the lowermost (left) and the uppermost (right) 2 meters of an fluvial aquifer at a 1-Ha test site at Columbus AFB, Mississippi (from Young, 1995). . . . .	375
Figure C.8	Net differential flow distributions from pumping in glacial till and stratified drift deposits at the Sylvester hazardous waste site in Nashua, NH (from Young et al., 1994). . . . .	375
Figure C.9	Ambient and pumping flow distributions for borehole FSE-6 installed a granitic dike near Mirror Lake, New Hampshire (from Young et al., 1994). . . . .	376
Figure C.10	Incremental flow distributions induced by pumping wells screened across limestone bedrock and a weathered zone above bedrock at TVA's Environmental Research Center in Muscle Shoals, Alabama (from Julian et al., 1993). . . . .	376
Figure C.11	Fluid resistivity and EM flowmeter logs for a borehole screened across shale at the Oak Ridge National Laboratory, Oak Ridge, TN (from Dreier and Caldanaro, 1994). . . . .	377
Figure D.1	Vertical profiles of hydraulic conductivity for Wells 1 - 15. . . . .	379
Figure D.2	Vertical profiles of hydraulic conductivity for Wells 16 - 30. . . . .	380
Figure D.3	Vertical profiles of hydraulic conductivity for Wells 31 - 36. . . . .	381
Figure E.1	Potential for mixing of concentration fronts in the annulus of multilevel samplers. . . . .	399
Figure E.3	Multilevel sampler for collecting groundwater samples from inside the injection wells. . . . .	400
Figure E.2	Borehole flowmeter and tracer concentration measurements at the injection and withdrawal wells. . . . .	400
Figure E.4	Multilevel sampler for collecting groundwater samples from inside the withdrawal wells. . . . .	401
Figure E.5	Location of the small-scale recirculating tracer tests at the 1-Ha test site. . . . .	401
Figure E.6	Setup for the tracer injection and recirculation of groundwater from the withdrawal well(s) to the injection well(s). . . . .	402
Figure E.7	Groundwater flow patterns at Wells 16, 13, 14, 19, and Well 5 during tracer Test 1. . . . .	403
Figure E.8	Tracer concentration patterns at Wells 13, 14, 19, and Well 5 during Tracer Test 1. . . . .	403
Figure E.9	Groundwater flow patterns at Wells 8, 10, 12, 24, and 25 during Tracer Test 2. . . . .	404
Figure E.10	Tracer concentration patterns at Wells 8, 10, 24, and 25 during Tracer Test 2. . . . .	404
Figure E.11	Groundwater flow patterns at Wells 2, 11, 17, 18, 20, and 21 during Tracer Test 3. . . . .	405
Figure E.12	Tracer concentration patterns at Wells 2, 11, and 17 during Tracer Test 3. . . . .	405

Figure E.13	Groundwater flow patterns at Wells 1, 3, 7, 9, 26, and 30, 31, and 32 during Tracer Test 4. ....	406
Figure E.14	Tracer concentration patterns at Wells 3, 7, and 9 during Tracer Test 4. ....	406
Figure E.15	Examples of vertical groundwater flow in wells during Tracer Test 5. ....	407

# **1. INTRODUCTION**

## **1.1 BACKGROUND**

Inadequate delineation of aquifer heterogeneity has significantly contributed to the improper design and, consequently, the inadequate performance of groundwater remediation systems. As aquifer hydrogeologic becomes more complex, so does the difficulty of effecting proper groundwater remediation. Fluvial aquifers (i.e., deposited by alluvial fans, braided rivers, meandering rivers, and/or anastomosing rivers) are among the most heterogeneous aquifers and, are therefore, difficult to properly characterize, monitor, and remediate.

Fluvial aquifers include abrupt lateral and vertical changes in hydraulic properties as a result of changing depositional environments such as channels and overbanks. As a result, calculated hydraulic conductivity (K) values depend on the scale (i.e., large or small sample) and orientation (e.g., vertical versus horizontal) of the test; the type of test (i.e., in-situ versus laboratory); and the location of the test. The sensitivity of calculated K to these factors makes the measurement of K values in fluvial deposits considerably more difficult than in aquifers formed of less variable depositional environments such as a lacustrine or near shore marine environments. Moreover in a fluvial aquifer, the generation of a K field from K data may be difficult because the K field is not expected to resemble a random field because of the different depositional environments.

Partly because of the cost of field work and the prudence to build on the simple to understand the complex, limited field data are available from fluvial aquifers. As a result,

geohydrologists are in the precarious position of extrapolating field tests and theories developed for homogeneous and moderately heterogeneous aquifers to highly heterogeneous aquifers. Pumping Tests (including multi-well, single-well, and borehole flowmeter tests) are potentially effective methods for measuring in-situ aquifer hydraulic properties. However, if pumping tests are to be diagnostic in fluvial aquifers, both theoretical and field studies are needed to address the problems/limitations of using conventional well hydraulics equations developed for homogeneous aquifers to characterize heterogeneous aquifers.

## **1.2 SCOPE OF WORK**

The dissertation focuses on interpreting pumping and tracer test results from two adjacent test sites at Columbus Air Force Base (CAFB) in Mississippi, USA. The two field sites are designated as the 1-Ha and the MADE test sites and are part of the research facility created by the Tennessee Valley Authority (Young, 1991a, b; Young et al., 1995; Boggs et al., 1992; Boggs et al., 1990; Rehfeldt et al., 1992). The author was closely involved with all field tests and was the primary geohydrologist who designed and conducted field tests at the 1-Ha test site. Tables 1.1 and 1.2 list some of the field tests that will be described in the dissertation. Because of the complexities associated with interpreting the field tests, numerical and analytical modeling is performed to help explain concepts and justify conclusions. This modeling focuses on simulating pumping-test results in confined and unconfined heterogeneous aquifers.

Considerable work has been performed at CAFB and this dissertation represents only a portion of the work performed at CAFB. The extensive field studies at CAFB have been funded by numerous agencies. The author began work at CAFB in 1982 with a project funded by the Electric Power Research Institute. From 1982 to 1988, the author performed field work at the MADE site related to solute transport and macrodispersion theory. In 1989, the author separated from the MADE site to create a 1-Ha test site with funding from the U.S. Air Force. After assembling an extensive field data set from the 1-Ha test site, the author began studies at the University of Waterloo in 1991. As a student at the University of Waterloo, the author was employed by the Tennessee Valley Authority and work on an EPA project to develop and analyze electromagnetic borehole flowmeter tests. After performing preliminary numerical simulations for the dissertation in 1992, the need for more field data related to sedimentology and positive skin effects was evident. In 1993, the author returned to CAFB to perform continuous aquifer coring and investigate positive skin effects with funding from the U.S. Corps of Engineers and the U.S. Air Force. Additional grant from the U.S. Corps of Engineers was provided to the author to help characterize and numerically simulate tracer and pump tests results at CAFB in 1996.



**Table 1.1 Pumping Test Data from Columbus AFB**

1	3-Day Large-Scale Aquifer Test with $Q = 62$ L/min at MADE's PW1 well	T at 12 wells S at 5 wells
2	3-Day Large-Scale Aquifer Test With $Q = 208$ L/min at MADE's PW2 well	T at 16 wells S at 13 wells
3	5-Day Large-Scale Aquifer Tests With a $Q = 68$ L/min at Well 5	T at 27 wells S at 9 wells
4	5-Day Pulsing Large-Scale Aquifer Tests With Average $Q = 68$ L/min at Well 5	T at 27 wells S at 26 wells
5	8-Day Large-Scale Aquifer Tests With $Q = 110$ L/min at Well 5	T at 27 wells S at 12 wells
6	Series of 12-hour Aquifer Tests at Well 16 a. $Q = 34.8$ L/min b. $Q = 11.5$ L/min c. $Q = 34.8$ L/min(injection) d. $Q = 11.5$ L/min(injection)	T at 6 wells, S at 5 wells T at 6 wells, S at 5 wells T at 6 wells, S at 5 wells T at 6 wells, S at 5 wells
7	Seven Small-Scale Aquifer Tests (1 hour to 3 hours) With Pumping Rates From 34 to 81 L/min	T at 35 wells S at 35 wells
8	34-Liter Slug Tests	T at 37 wells
9	2-Minute 34 L/min Pumping Tests	T at 37 wells
10	Single-Well Injection Tests at 22 L/min	T at 37 wells
11	115 Single-well Pumping Tests at rate (6 L/min to 80 L/min)	T at 37 wells
12	Borehole Flowmeter Tests at 37 wells with 22 L/min Injection	881 K values
13	Borehole Flowmeter Tests at 21 wells with 30 L/min Withdrawal	362 K values
14	Borehole Flowmeter Tests at 21 wells with 15 L/min Withdrawal	380 K values
15	Mini-Aquifer Tests at well cluster 38-39-40 and at cluster 41-42-43. Pump well and monitor 2 nearby wells. a. Pump near 8 L/min b. Inject near 8 L/min c. Pump near 22 L/min	18 T values, 12 S values 18 T values, 12 S values 18 T values, 12 S values

**Table 1.2 Tracer Test Data from Columbus AFB**

1	8-hour five-spot tracer test for wells spaced 3.6 to 4.6 meters apart with a 31 L/min injection rate	Breakthrough curves at 4 wells
2	25-hour five-spot tracer test for wells spaced 3.6 to 6.3 meters apart with a 38 L/min injection rate	Breakthrough curves at 4 wells
3	Three 36-hour doublet tracer tests conducted at 3 well pairs with spacings of 5.2, 6.7, and 6.2 meters with injection rates between 11.5 and 14.2 L/min	Breakthrough curves at 3 wells
4	Four 70-hour doublet tracer tests conducted at 4 well pairs with spacings of 7.3, 8.9, 15.2, and 15.8 meters with injection rates between 15.1 and 34.1 L/min	Breakthrough curves at 4 wells
5	One 168-hour five-spot tracer test with injection and pumping wells 31 meters apart and with 27 monitoring wells at distances from 4.8 to 31.1 meters from the injection well with an injection rate of 106 L/min	Breakthrough curves at 27 wells
6	Large-scale natural gradient tracer tests with tritium as a tracer and 350 multilevel samplers.	Several three-dimensional snapshots of the tritium plume during the first 300 days of transport

### 1.3 OBJECTIVES

The emphasis of the dissertation is the interpretation and evaluation of pumping test and borehole flowmeter data from Columbus AFB. As will be shown, proper data analysis requires assimilating data sets from several independent sources to demonstrate the correctness associated with a particular interpretation or analysis. By detailing the characterization of the Columbus AFB test site, paradigms different from those established for homogeneous aquifers are established to guide field tests and remediation efforts in

similarly heterogeneous fluvial aquifers. By example with the Columbus AFB data sets, the dissertation will:

- Demonstrate the significant effect that fluvial heterogeneity can have on multi-well and single well pumping test results;
- Develop an useful method for analyzing multi-well and single well pumping tests for aquifers with large-scale heterogeneity;
- Develop a methodology to assess the significance of positive skin effects;
- Develop an improved method for collecting and analyzing borehole flowmeter data;
- Identify and evaluate the effects that preferential flow paths can have on solute transport in a fluvial aquifer;
- Assess the potential impact of pumping rates and test duration on calculated transmissivity values;
- Evaluate the feasibility of using polynomials fitted by ordinary least squares regression to detrend a K field in a heterogeneous fluvial aquifer;
- Demonstrate the benefits of a site-wide depositional model for interpreting results from pumping tests and tracer tests; and
- Demonstrate the utility of a newly developed electromagnetic borehole flowmeter.

## **1.4 PRESENTATION OF INFORMATION**

### **1.4.1 Important Issues**

Traditional pumping test analyses involve type-curves derived for solutions to radial flow in homogeneous aquifers. Since the 1940's, radial flow in homogeneous aquifers has been the primary foundation on which geohydrologists have developed approaches for pump-test analyses. An important discussion lacking in the pumping-test literature is that although

type-curve matching is usually a reliable criteria for estimating hydraulic parameters for homogeneous aquifers, type curve matching can be unreliable criteria for highly heterogeneous aquifers.

Implicit to traditional type-curve matching is that calculated storage and transmissive parameters represent effective aquifer properties. Among the issues requiring consideration when interpreting pumping test data from highly heterogeneous aquifers are that: spatial heterogeneity in one aquifer property can significantly affect the calculation of the effective value of another aquifer property; and the effective value of an aquifer property can vary with both the location and the scale of the test.

This dissertation has been structured to address the numerous issues affecting pump-test interpretation at CAFB in a piecewise manner. The first several chapters toward show that highly heterogeneous conditions should and do exist at CAFB. The last several chapters demonstrate that unless a reasonable sedimentological model is used to guide the application of traditional pump-test analyses, significant error can exist with calculated values for effective aquifer parameters. The appendices document field methods and important field data.

Although the dissertation's nine chapters and five appendices are interrelated, each is structured to be relatively independent of the other chapters/appendices. This approach provides a straight-forward menu for dissecting and examining complex field issues and supports a format useful for readers who wish to read portions of the dissertation. A disadvantage of this approach is that some figures and text will appear more than once.

### 1.4.2 Chapter Overviews

Chapter 1 introduces the dissertation's objectives, test site, and data sets. Chapter 2 overviews the history and characteristics of the test sites at CAFB. Chapter 3 briefly describes the type of deposits associated with meandering and braided rivers to support possible sedimentological models, plausible  $K$  patterns, and effective aquifer parameters for the CAFB aquifer. Chapter 4 provides results from borehole flowmeter tests and geological investigations to demonstrate a fundamental connection between sedimentological features and large-scale patterns in the  $K$  field. Chapters 5, 6, 7, and 8 demonstrate that unrepresentative and/or misleading aquifer parameters can result from applications of traditional pumping test analyses to highly heterogeneous aquifers. A key point emphasized in these chapters is that although pumping-test analyses do not always produce representative estimates of effective aquifer parameters, the set of calculated hydraulic parameters contains useful information. The challenge in a highly heterogeneous aquifer is discovering how best to interpret the results of pump-test analyses.

The descriptions of pumping tests data in the dissertation has been organized primarily according to the aquifer heterogeneity of concern. Alternative organization schemes could have focused on hydraulic tests or hydraulic parameters of concern. To help direct readers to the material covered in each chapter, Table 1.3 lists the issues addressed in Chapters 4 to 8. Chapter 9 investigates the issue of the feasibility of detrending the  $K$  data sets at CAFB to produce the parameters necessary to support stochastic groundwater theories based a second-order stationary  $K$  field.

**Table 1.3 Various Issues Addressed in Chapters 4 to 8**

	Chapter				
	4	5	6	7	8
<b>Aquifer Heterogeneity of Primary Concern</b>					
Skin effects caused by well installation and/or drilling		✓			
Areal changes in the aquifer K field			✓	✓	
Vertical changes in the aquifer K field				✓	✓
<b>Hydraulic Test of Primary Concern</b>					
Borehole Flowmeter	✓	✓			
Single-Well Pumping Test		✓	✓	✓	
Multi-Well Pumping Test			✓		✓
Slug Test		✓			
<b>Aquifer Hydraulic Property of Primary Concern</b>					
Vertical Profile of K	✓	✓			
Effective Transmissivity		✓	✓	✓	
Effective Storage Parameters					✓

### 1.4.3 Chapter Summaries

Listed below are brief summaries for selected chapters. These summaries are provided to aid the reader in understanding where data and/or results can be found.

**Chapter 2** documents the funding sources for the work performed at CAFB and provides a general description of the CAFB aquifer, the MADE test site, and the 1-Ha test site.

**Chapter 3** briefly describes the characteristics of meandering, braided, straight, and anastomosing river types. Because the CAFB aquifer consists of meandering and braided deposits, the deposits typically associated with these two river environments are explained. Useful geological information from CAFB such as soil logs, aerial photographs, and facies maps are briefly discussed with respect to a sedimentological model for the site.

**Chapter 4** presents a borehole flowmeter testing approach suitable for CAFB along with an extensive set of K values for the 1-Ha test site. Validation of the K values is performed with results from tracer tests and the geological investigation. The results show a fundamental connection between sedimentological features and large-scale patterns in the K field. Among the important findings is that the channel lag deposits associated with a paleochannel represent a zone of high-K deposits that intersects both the MADE and 1-Ha test sites.

**Chapter 5** demonstrates that positive skin effects significantly affect both the total drawdown and the distribution of flow at wells that intersect the paleochannel. The probable cause of the skin effects is the mixing of low-K material from the clayey overburden into underlying high-K coarse-grained deposits during well installations. Various analyses of slug tests and pumping tests are provided to strengthen the argument for positive skin effects and to demonstrate the need for careful interpretation of hydraulic tests in highly heterogeneous aquifers. An important finding is that for wells with significant positive skin effects, a representative transmissivity can be calculated by prudent application of the Cooper-Jacob straight-line method.

**Chapter 6** presents several independent field data sets to demonstrate that large-scale transmissivity variations exist at CAFB and the location of the pumping wells greatly affects the shape of drawdown curves. Data analysis suggests that the major slope changes in the semilog time-drawdown plots associated with large-scale pumping tests are controlled primarily by the trends in the aquifer transmissivity field and not by unconfined or leaky aquifer conditions. Numerical simulations are presented to illustrate key relations among the location of the radius-of-influence, large-scale transmissivity patterns, and the change in the semilog time-drawdown slope at the pumping well.

**Chapter 7** expands on the results in Chapter 6 and illustrates that the location of the radius-of-influence depends not only on time but also on the pumping rate at CAFB. Field data as well as numerically simulated pumping test results show that pumping rates can significantly affect the transmissivity calculated with the Cooper-Jacob straight-line method. At the 1-Ha test site, large-scale trends in the transmissivity field were properly inferred by mapping the effect that pumping rate had on calculated transmissivity values.

**Chapter 8** demonstrates that significant preferential flow occurs through interconnected high-K deposits and open well screens at CAFB and that these flow patterns can be considerably different for ambient and pumping conditions. Analysis of field and numerically simulated pumping-test data show that significant error can occur with storage parameters calculated from type-curve fitting when preferential flow occurs. The three crucial issues that affect the error with the calculated storage parameters are the distribution of high-K deposits in the entire aquifer, the distribution of low-K deposits near the water



table, and the hydraulic connections between non-adjacent high-K deposits provided by the observation well screens.

**Chapter 9** investigates the feasibility and utility of calculating macrodispersivity parameters from the heterogeneous K field at CAFB. Important conclusions are that a large paleochannel controls the evolution of the MADE tracer plume and that for many fluvial aquifers where large-scale trends exist in the K field, groundwater theories based on stationary K fields have little, if any, practical applications.

## **2. OVERVIEW OF PROJECTS AND TEST SITES AT COLUMBUS AFB, MISSISSIPPI**

### **2.1 GENERAL SITE DESCRIPTION**

Since 1982, the Tennessee Valley Authority (TVA) has been leasing 25 hectares in the northeastern corner of CAFB from the United States Air Force. The leased area originally contained no known groundwater contaminants and was selected to perform field studies for the Electric Power Research Institute (EPRI). The first EPRI project led to the installation of a large-scale well network, henceforth designated as the MADE site (see Figure 2.1). Since 1982, two large-scale tracer tests have been performed at the MADE site and a third test began in September 1995. Work at the MADE site has been funded by the United States Air Force (USAF), EPRI, the Army Corp of Engineers (USCOE), and the TVA. To the northeast of MADE resides a 1-Ha test site that has been the focus of electromagnetic borehole flowmeter and recirculating tracer tests funded by the USAF and the United States Environmental Protection Agency (EPA) from 1988 to 1991.

As shown in Figure 2.1, the test sites are located approximately 6 km east of the Tombigbee River and 2.5 km south of the Buttahatchee River. The aquifer of concern is the uppermost aquifer and is composed of approximately 11 meters of terrace deposits composed primarily of poorly-sorted to well-sorted, sandy gravel and gravelly sand that often occur in irregular lenses and layers. The terrace deposits are unconformably underlain by the Cretaceous Age Eutaw Formation, which consists of marine clay, silt, and sand (Kaye, 1955).

The sand and gravel components of the aquifer are composed of quartz, feldspar, and mica. Fine-grained materials (i.e. those passing the 0.074-mm sieve) consist of quartz,

potassium feldspar, muscovite, and clay minerals. Clay minerals are predominantly kaolinites and illites with minor amounts of montmorillonites and vermiculites. Soil particles are commonly coated with iron oxides. Measurements of free iron oxides range from 2.0 to 3.9 percent by weight for particles less than 2 mm in diameter, and from 0.5 to 0.8 percent for particles larger than 2 mm (Boggs et al., 1990).

Near the MADE test site, seasonal water table fluctuations range from 2 to 3 meters. The magnitude of the horizontal hydraulic gradient changes from approximately 0.2 percent, when the water table is low, to 0.5 percent when the water table is high (Boggs, et al., 1990). Vertical hydraulic gradients several orders of magnitude larger than horizontal hydraulic gradients exist upgradient and downgradient of a paleochannel (to be discussed later) that intersects the MADE site. These vertical gradients can be attributed to the complex flow patterns produced by the heterogeneities in the hydraulic conductivity field.

Boggs et al., (1995) summarize the chemical characteristics of the groundwater from the terrace aquifer. The groundwater has a low total dissolved solids content averaging 43 mg/L. The ionic composition of the groundwater is dominated by sodium, silica, and chloride. Total acidity averages 71 mg/L (as  $\text{CaCO}_3$ ). Alkalinity averages 10 mg/L and is mainly in the form of bicarbonate. The average pH and mean Eh are 4.8 and 543 mV, respectively.

Rainfall at CAFB averages approximately 144 cm annually and is fairly uniform in distribution throughout the year. Most precipitation generally occurs during the winter and early spring, with the driest seasons being summer and early fall. The climate is temperate

with a mean annual air temperature of 17°C. The mean maximum daily temperature in July is 33°C, and the mean minimum daily temperature in January is 3°C (USAF, 1982).

## **2.2 THE MADE SITE**

Several projects have been performed at the MADE site. The first experiment, referred to as MADE-1, had the principal objectives of: (1) developing a data base for validating the advection-dispersion component of solute transport models; (2) developing practical methods of measuring hydraulic conductivity variability; and, (3) estimating macrodispersivity using the methods of Gelhar and Axness (1983). Primary components of MADE-1 included numerous borehole flowmeter tests to define a three-dimensional horizontal K field and a natural-gradient tracer test involving bromide and three fluorobenzoate tracers.

Boggs et al., (1990) describe the test site, experimental design and procedures, and present qualitative observations regarding the tracer plume behavior. The plume was monitored with an array of 258 multilevel samplers (MLS) each equipped with 20 to 30 sampling ports spaced approximately 0.38-m apart. A significant plume feature was its asymmetry in the longitudinal direction. After 250 days of tracer transport, the most concentrated region of the plume was approximately 20 m downgradient of the injection location while the advancing portion of the plume extended downgradient a distance in excess of 260 m. Adams and Gelhar (1992) provide spatial moments analysis of the bromide data for the MADE-1 field experiment. Their analysis indicates that the bromide mass recovery decreased to approximately 50 percent by the end of the study due to the combined

effects of plume truncation, sampling bias, and sorption. Their application of a non-uniform advection-dispersion model to bromide plume moments provided an estimate of longitudinal dispersivity of 5 to 10 m at a scale of 260 m.

Boggs et al., (1990) and Rehfeldt et al., (1992) performed numerous borehole flowmeter tests near and within the MADE well network. Hydraulic conductivity profiles measured at 0.5-foot intervals typically range between two- to four-orders of magnitude at each well. Rehfeldt et al., (1992) assimilated all 2187 borehole flowmeter K values and performed geostatistical analyses on them. They calculated a mean  $\log(K)$  of -2.25, a variance of  $\log(K)$  of 0.848, a horizontal correlation length of 12.8 m, and a vertical correlation length of 1.6 m. A main objective of Rehfeldt et al., (1992) was to separate the  $\log(K)$  data set into a deterministic and stochastic component to calculate a macrodispersivity. After performing this separation, Rehfeldt et al., (1992) calculate a macrodispersivity of 1 m using the method of Gelhar and Axness, 1983).

The MADE-1 tracer experiment occurred between October 1986 and June 1988. In June 1990, the MADE-2 tracer experiment began using the same injection wells used for the MADE-1 experiment. The primary purpose of MADE-2 was to resolve concerns with the MADE-1 plume data and to investigate biodegradation of selected organic components. Boggs et al., (1992) describe the experimental set-up and data analysis for the MADE-2 experiment. Tritium was used as the conservative tracer and the MLS sampling network was expanded by 70 MLS to improve the definition the plume configuration. Tracer sampling ended in September 1991. As stated by Boggs et al., (1992) the MADE-2 tritium plume was quite similar to the MADE-1 bromide plume.

### 2.3 THE 1-Ha TEST SITE

In 1988, TVA with funding from the USAF initiated a study to improve the methodology for the hydraulic design of pump-and-treat systems supporting bioremediation. The five reconnaissance wells in Figure 2.1 were installed and pump tested to help locate a test site approximately the site of a 'typical' gasoline spill, which was assigned a dimension of 1-Ha. Because Well R05 had the highest K value, the new test site was centered on Well R05.

**Table 2.1 Results of Pumping Tests in Reconnaissance Wells**

Reconnaissance Well	Number of Well Tests	Arithmetic Avg of K (cm/s)
R01	2	0.0010
R02	5	0.0005
R03	2	0.0045
R04	2	0.0070
R05	3	0.0200

During 1988 and 1989, an initial network of 37 wells was installed as described in Appendix A. At the onset of USAF bioreclamation project, the philosophy was to perform site characterization in the same manner as at the MADE site and to focus primarily on performing recirculating tracer tests. However, shortly after the testing of the reconnaissance wells, the author had concerns regarding the borehole flowmeter procedure and refocused the project toward analysis of pumping test data. As a result of the refocusing effort, the

author and other TVA employees performed several large-scale pumping tests (Appendix B) and developed the electromagnetic (EM) borehole flowmeter, which is described in Appendix C.

Borehole flowmeter testing at the 1-Ha test site was similar to that at the MADE site except: 1) a sensitive EM flowmeter replaced an impeller flowmeter; 2) drawdown measurements were taken at 1-second intervals with a pressure transducer instead of at 1- to 10-minute intervals using an electric tape; and, 3) a different analysis method was used to help correct for positive-skin effects.

To resolve differences between in the K values calculated using different data collection and analysis methods, a series of pumping and tracer tests was designed and implemented. An important consequence of the refocusing effort on site characterization was a reevaluation of the geological data. Based on facies mapping at nearby terrace outcrops, Rehfeldt et al., (1989a) state that the aquifer is "clearly a braided-stream deposit." As will be discussed in the next section, evidence of paleochannels in several aerial photographs strongly suggest that meander deposit compose some if not most of the aquifer.

Soon after the completion of the USAF bioreclamation projects, funding was obtained from the EPA to demonstrate and improve methods associated with performing EM flowmeter tests. Included as part of this project (Young et al., 1995) was the addition of six wells at the 1-Ha test site to help evaluate well development effects on flowmeter K values.

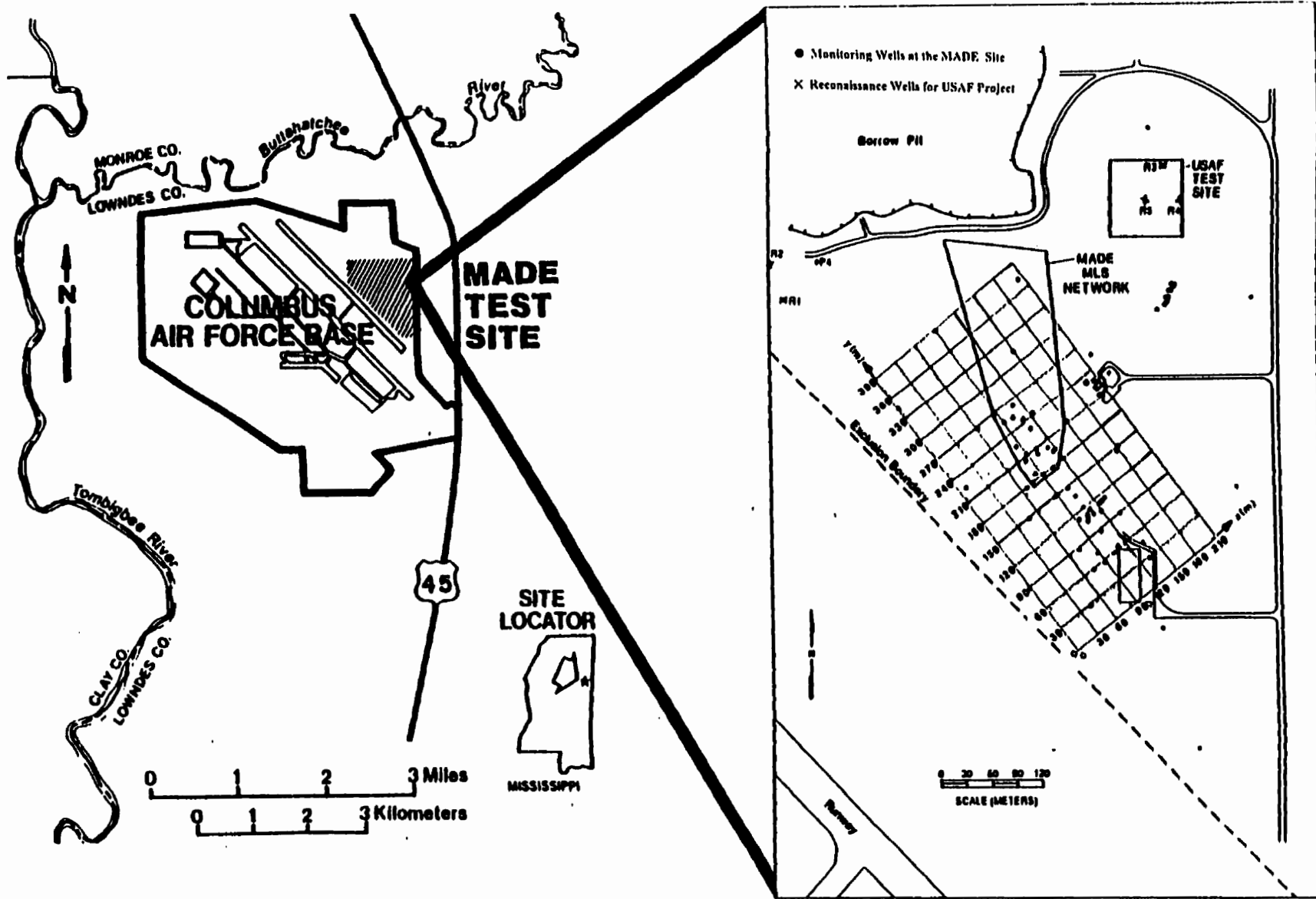


Figure 2.1 Location Map for Columbus AFB, TVA Macrodispersion Experimental Site, and approximate location of the 1-Ha Test Site.



### **3. GEOLOGICAL INVESTIGATION AT COLUMBUS AIR FORCE BASE**

#### **3.1 FLUVIAL DEPOSITION**

Channels within fluvial systems are the main focus of sediment transport and deposition (Galloway and Hobday, 1983). Influences on channel morphology are manifold and because the different influencing variables are interrelated, this topic is complicated (Leopold and Wolman, 1957; Miall, 1982). Variables that influence channel morphology encompass the amount and the variability with time of water discharge; the amount and nature (grain size) of the sediment load; the slope, width, and depth of the alluvial channel; the velocity with which water moves through the channel; the nature of the channel bottom (degree of smoothness/roughness); and, the stability of the channel banks. The latter is governed by the sediment type of the channel banks (more stable if the bank is made up of cohesive material) and the density of the vegetation (the more vegetation, the more stable) (Miall, 1982). Overriding influences are exerted by geology and climate. Geology determines the regional slope of the fluvial system and the nature of the source rocks supplying the sediment for the channel system (for example: sediment load of a river will consist of suspended load only, if mud and/or mudstone is the exclusive source material). Climate governs amount and temporal distribution of rainfall, temperature changes and, in part, the nature of weathering in the source region (for example: physical weathering can provide coarser material in the source area for erosion).

Rust (1978a, b) and Miall (1977) describe the general characteristics of and the broad differences among rivers. Meandering rivers display a single channel commonly on gentle

slopes with sinuosity values of  $>1.5$  and braiding values  $<1.0$ . They are dominated by suspended-and mixed-load and possess width/depth ratios of  $<40$ . Straight rivers are rarely encountered in nature. They possess a single channel with sinuosity values  $<1.5$  and braiding values  $<1.0$ .

The sediment load carried by the river can be either bedload, suspended load or any combination thereof. Braided rivers are dominated by bedload and display two or more channels separated by bars and islands. They possess a high width-to-depth ratio of up to  $>40$  (Schumm, 1977). The braiding parameter is  $>1.0$ , whereas the sinuosity is typically  $<1.5$ . Anastomosing rivers are multiple-channel rivers, which carry predominantly suspended-load in the water column. The channels are relatively stable and are separated by large, stable islands. The sinuosity of each separate channel is high ( $>2.0$ ) and the braiding parameter (of the whole system) is  $>1.5$ . Table 3.1 summarizes the characteristics among the four main types of rivers as based on channel morphology.

Different channel patterns are transitional to each other and form the continuum of channel patterns (Leopold and Wolman, 1957). The type of fluvial system can change in a vertical stratigraphic section, as measured, for example, in an outcrop. Different fluvial systems grading into each other laterally at a given instant in time will be found superimposed on each other when observations are conducted over longer time periods. The different systems shifted laterally with time due to changes in boundary conditions. The stratigraphic record, then shows one system overlying the other. A change in fluvial systems might occur following the shifting (with time) of environmental conditions following changes in local or regional base level, or it might be due to local changes in influencing factors determining the style of the fluvial system.

**Table 3.1 Classification of river types (modified after Miall, 1977)**

Type	Morphology	Braiding	Sinuosity	Load Type	Bedload Percent (of total load)	Width/depth ratio	Erosive Behavior	Depositional Behavior
Meandering	single channels	<1	>1.3	Suspension or mixed load	<11	<40	channel incision, meander widening	point-bar formation
Braided	two or more channels with bars and small islands	>1	<1.3	Bedload	>11	>40	channel widening	channel aggradation, mid-channel bar formation
Straight	single channel with pools and riffles, meandering thalweg	<1	<1.5	Suspension, mixed or bedload	<11	<40	minor channel widening and incision	side-channel bar formation
Anastomosing	two or more channels with large, stable islands	>1	>2.0	Suspension load	<3	<10	slow meander widening	slow bank accretion

Of the four categories of fluvial systems, the two most likely to have formed the terrace deposits at Columbus, Mississippi, are meandering and braided systems.

## **3.2 BRAIDED RIVER SYSTEM**

### **3.2.1 Braided Rivers**

A braided river is defined as one in which the channel repeatedly divides and rejoins around fluvial islands or bars (Leopold and Wolman, 1957) on a length scale of one to a few times the channel width. Braided rivers form most commonly in a transition zone between high gradient mountainous streams/fluvial fans and relatively low gradient rivers/lakes/deltas/oceans (LeBlanc, 1972).

Aquifers composed of braided river deposits accumulate as multi-story lenses and layers that are a product of rapid lateral migration and vertical aggradation of broad, shallow (5 cm to 0.5 m average depth) channels (Williams and Rust, 1969). Wherever braided rivers are developed, their most common characteristic is the presence of longitudinal bars separated by channels containing migrating transverse bars. The occurrence, geometry, and proportion of these bar types varies in different tectonic and climatic settings, and commonly varies in the same river along its course. The continuous branching and rejoining of channels with longitudinal bars between them gives rise to a braided river pattern (Figures 3.1 and 3.2).

Lateral and vertical changes in braided river deposits are abrupt due to variable preservation of channel and bar forms (Miall, 1987). Deposits tend to be lenses and discontinuous horizontal beds. Erosion, transport and deposition in the braided river

environment are controlled largely by flashy, turbulent flood events (e.g., Ferguson et al., 1992). Sediment is in transport across the braidplain during floods when gravel bars are submerged within the composite channel. Braided river sediment is characterized as being poorly to moderately sorted. Commonly, sand and pebbles are dominant (e.g., Campbell 1976). Boulders, common in most fluvial fans, are uncommon to absent in braided rivers. Clay and silt are not abundant in braided river deposits. Among the reasons for this is that clay and silt generally remain suspended in the high velocity flows or are reworked and carried farther downgradient downstream.

### **3.2.2 Longitudinal Bars**

Longitudinal bars (long dimension-flow parallel) are diamond-shaped accumulations of coarser sediment (commonly gravel) between channels. Their dimensions range from 25 m to several hundred meters in downstream length, by 5 to 100 m in flow-perpendicular width. They commonly are between 0.5 and 1 m high (Williams and Rust, 1969; Rust, 1972). Longitudinal bars are formed primarily during flooding events from gravelly material. As flood flow wanes, longitudinal bars are commonly dissected by small channels and finer sediments (sand and silt) are deposited on the bartop in thin horizontal beds and laminae.

Because they are primarily a flood stage phenomenon, longitudinal bars are typically internally massive or have or crude horizontally stratified, clast-supported gravel, which is commonly imbricated and rarely cross-stratified. Small-scale (a few meters), crudely developed, coarsening-upward or fining-upward sequences may be present. Downstream migration of longitudinal bars generally produces a coarsening-upward gravel sequence as

coarser, upbar gravel migrates over finer, downbar gravel (Hein and Walker, 1977). Crudely developed fining-upward sequences may arise as high-energy flood surge wanes, promoting aggradation and allowing progressively smaller clasts to be deposited on the bar top. Longitudinal bar gravel sequences may also possess thin (a few centimeters), impersistent sand lenticles and laminae deposited as flow competency over the bar top decreases further (Rust, 1972; Miall, 1977).

### 3.2.3 Transverse Bars

During the low stages of the river, sedimentation on the longitudinal bars becomes negligible but transport and redeposition of sand-sized material continues in the channels and forms transverse bars. Forming largely within broad channels (0.1 to 1 m deep x 4 m width; Bull, 1964; Miall 1977), transverse bars behave more like a migrating bedform (e.g., dune) than do longitudinal bars. Sand and gravel migrate up the lee side, then slide down the flow-perpendicular slipface that slopes downcurrent. This process forms planar cross-stratification, commonly defined by alternating foreset beds of sand and fine gravel, or just sand of varying sizes. As compared to longitudinal bars, transverse bars include: (1) relatively smaller mean grain size; (2) relatively better sorting; and, (3) a preponderance of high-angle planar cross-stratification topped by small-scale trough cross-stratification (Matthew, 1974).

### **3.2.4 Summary**

Gravel, sand, and silt lenses are deposited as migrating longitudinal, transverse bars; and in channels as sand sheets and overbank deposits of braided rivers. Braidplains form in relatively high-gradient regions under conditions of voluminous, coarse-grained bedload. Sand and gravel are derived from upgradient glacial systems or from fluvial fans, which in turn, receive debris from high relief mountainous areas. As basin flanks are uplifted, relative to the adjacent subsiding sedimentary basin, braidplain deposits are preserved, creating the heterogeneous aquifer.

## **3.3 MEANDERING RIVER SYSTEMS**

### **3.3.1 Meandering Rivers**

A meandering river is a single, markedly sinuous ( $S > 1.5$ ; Leopold and Wolman, 1957) channel that migrates laterally and downgradient within a meanderbelt (Matthes, 1941). The meanderbelt is approximately 15 to 20 times the width of the channel (LeBlanc, 1977) and is defined as part of the floodplain between two tangents to the outer bends of meanders (American Geological Institute, 1962). A floodplain commonly contains more than one meanderbelt, only one of which is dominantly active at any time. Meanderbelts become inactive through the process of avulsion, discussed later.

Aquifers composed of meandering river deposits accumulate as multi-story sand (some gravel) lenses and channel forms commonly encased in fine-grained mud. The single channel is generally much deeper than the shallow, shifting channels of braided rivers, and occupies only a narrow strip of the floodplain. Instead of midchannel bars, such as occur in

braided rivers, meandering rivers contain one major bar type (point bars), which are the focus of deposition. Point bars are connected to the river bank and develop on the convex side of each meander bend (see Figure 3.3). They are of relatively simple cross-sectional geometry in small rivers, but commonly are of a more complex double-tiered nature in medium and large meandering rivers, where point bars also differ in their upstream and downstream areas (e.g., Bluck, 1971; Jackson, 1975, 1976a).

The deepest part of the channel (thalweg) occurs on the concave side of each bend, forming a pool opposite the point bar, that slopes gently down into the channel (Figure 3.4). The outer concave bank (cutbank) is the focus of erosion. Much of the sediment eroded from the cutbank is deposited on the next point bar downstream, on the same side of the river (Matthes, 1941). As the cutbank is degraded, the point bar aggrades and migrates toward the cutbank. In this way the entire river migrates laterally, yet channel width remains constant (Matthes, 1941; Leopold et al., 1964).

Sediment within a meanderbelt undergoes a high rate of reworking as the channel migrates laterally and erodes previous deposits. Meandering systems, therefore, generally contain a much higher proportion of mud compared to braided systems (Pettijohn et al., 1987) due to the high rate of reworking of floodplain mud, higher amounts of bank-stabilizing vegetation, and the more distal position of meandering rivers with respect to the source terrain. Grain size generally ranges from clay to small pebble, and the degree of sorting is much higher than that of fluvial fans and braided rivers, unless the river flows through poorly-sorted sediment such as glacial till. Granule to pebble gravel is common as a thin lag at the channel base. Cobbles and boulders are rare.



Generally, the channel deposits are the coarse gravel on channel floor. The inner bend (point bar) consists of coarse sands close to the channel bottom (lower point bar) to fine sands on the upper part of the point bar. On the lower point bar (close to the channel) a bedform of sinuous crested dunes develops with a height ranging from 15 to 70 cm. These dunes, called crossbeds or foresets, can be used as an indicator of the local flow direction of the channel. As the main channel is migrating in the direction of its outer bend, the point bar on the inner bend is building itself outward, a process called lateral accretion. As a result, the point bar develops into a half-circular shaped sand body. This migration also results in regular vertical sequence sediments, overlying each other, successively deposited at a larger distance from the main channel. Therefore, a gradually fining upwards sequence can be expected.

Crevasse splay and overbank sands are deposited outside the main channel. The first category is originated by a break in the natural channel levee. The deposits are lobe-shaped sheets, generally fine sands and silts, coarser towards the feeding point. The overbank deposits occur from flooding at a high stage. Because all coarse material is transported along the bottom of the channel, the overbank deposits consist mainly of silt and clay. Oxbows occur when a meander is cut-off and the main channel takes a shorter track. The old meander, only fed at high flood stage, is filled with fines and clay.

### **3.3.2 Channel Abandonment**

Periodically the sinuous course of the meandering channel is shortened due to different rates and directions of erosion in adjacent meanders. The channel is straightened

and a former meander is abandoned or partially abandoned, thereby only accommodating flow during flood times. Meander cutoff is necessary to increase local river gradient and maintain a relatively constant flow velocity (Reineck and Singh, 1986). The two most common types of meander cutoff are neck cutoff and chute cutoff (Figure 3.5). The third mechanism for channel cutoff is avulsion.

Neck cutoff occurs as two concave banks erode toward one another producing a narrow neck of land. The neck is breached either during flood or during normal base flow. The meander loop is abandoned rather abruptly, and is plugged at both ends by sediment deposited from separated flow eddies (Collinson, 1986). The abandoned channel becomes a strongly curved lake called an oxbow lake. Following from the large angular difference between the old and new channels after neck cutoff, bedload sediments form plugs only at the immediate ends of the abandoned channel and contribute little to the total volume of the complete fill. Once the ends of the channel are sealed, the remaining fill enters as overbank flows (Allen, 1965).

Chute cutoff normally occurs during flood times when a new channel is cut and deepened along a swale or chute channel (see Section 3.3.4 below) on the point bar. They usually occur more gradually, over successive floods, as chutes are deepened, thereby causing progressively decreased flow in the main channel. Bedload sediments make important contributions to channel-fills following from chute cutoff. Because of the small angular difference between old and new channels, the river continues for a long time to flow through the old channel, depositing bedload sediment at the upstream and downstream ends

and on the floor and side until abandonment of the channel is complete. Once the ends of the channel are sealed, the remaining fill enters as overbank flows (Allen, 1965).

Once a portion of the channel is abandoned, it becomes a very low energy lake or swamp and is only affected by overbank floodwaters. It eventually is filled with laminated to massive overbank mud and dead organic matter. This curved, impermeable channel-fill deposit is termed a clay plug. Clay plugs that fill neck-cutoff oxbows are thicker and contain little to no sand or silt compared to clay plugs of chute cutoffs, because complete abandonment is more immediate during neck cutoff (Allen, 1965).

Entire stretches (10's to 100's km long) of river may be abandoned by the process of avulsion (Figure 3.5). Most sedimentation occurs within the active meanderbelt, thereby constructing a fluvial ridge, and raising the river above the level of the distal floodplain (Fisk, 1952). The ridge-building process tends to lower the river gradient over time but also retains the river in a kinetically unstable position. To relieve this condition and increase river gradient, the river periodically avulses, that is, breaches the channel bank and forms a new course flowing to the lowest elevations of the floodplain (Speight, 1965). The new course commonly is initiated by crevasse splay development, which is triggered during flooding or, in some cases, by ice or log jams damming the main channel (Smith et al., 1989).

### **3.3.3 Point Bars**

Point bars are the major depositional feature in meandering systems developed over a wide range of grain sizes, slopes, sinuosities, and discharges. Consequently, point bar formations display considerable variability from the simple classical fining-upward sequence

described above in section 3.2.1. In this classical sequence, the planar top of the bar slopes downward into the thalweg (see Figure 3.4) and serves as the surface of deposition. Grain size fines along this surface from the channel base to the point bar top. Several significant variations from the classic point bar sequence are documented in the literature. For simplicity, they will be grouped into three categories called complex point bar, coarse-grained point bar, and fine-grained point bar.

The classical point bar sequence is based on the location of the thalweg near the outer bend of meander. Jackson (1975, 1976) discovered that across the Wabash River the maximum depth, velocity, and grain size only occurred at the exit of bends. Within the entrances and medial portions of bends, the velocity profile was still in transition from the previous bend and thus was more evenly developed across the river (i.e. the fastest current may be in the middle to the river or nearer the inside of the bank). As a result, depth and grain size are relatively constant across the river instead of decreasing and fining, respectively, from the cutbank to the top of the point bar. The resulting vertical section, therefore, will not display the classic fining-upward sequence. Instead, it may coarsen upward or coarsen and then fine upward and form a complex point bar.

Some coarse-grained, bedload-dominated rivers are meandering instead of braided in plan view. Though they are of higher than normal gradient for a meandering stream (e.g., 0.6 m/km; Amite River, LA), their muddy, cohesive, vegetated banks serve to contain the channel (McGowen and Garner, 1970). Coarse-grained meandering rivers are also of lower sinuosity ( $S = 1.3$  to  $2.3$ ) than most meandering rivers, and their water level and velocity fluctuates strongly (Nijman and Puigdefabregas, 1978; Forbes, 1983; Arche, 1983).

Similar to mixed-load meandering rivers, coarse-grained meandering rivers migrate over the floodplain and deposit sediment in point bars. These point bars, however, are composed of gravel (pebble to cobble), are two-tiered (upper and lower point bar), and contain chute bars and chute channels on the upper tier (McGowen and Garner, 1970; Nijman and Puigdefabregas, 1978; Gustavson, 1978).

Fine-grained meandering rivers, containing little to no gravel, are not greatly different in process from normal, mixed-load rivers. Stewart (1983) characterized these rivers as having distinct channels with low width/depth ratios and very high sinuosities. Point-bar sequences are similar to the classic point bar, in that they fine upward. They are, however, finer-grained overall and fine upward from fine sand to clay, instead of from gravel to clay. They are also composed of smaller-scale bedforms (Steinmetz, 1967; in Reineck and Singh, 1986). In very fine-grained rivers, such as the Gomti River of India, even the coarsest grains are carried in suspension. Grain settling from graded suspension is the dominant depositional process. Horizontal lamination of very fine sand and mud, therefore, is most abundant, with some ripple and climbing ripple cross-lamination. Because of the uniformity of grain size, point bar sequences do not fine upward and are very similar to levee and overbank deposits (Kumar and Singh, 1978).

#### **3.3.4 Summary**

Meandering rivers commonly form down gradient from low-sinuosity braided rivers and slightly upgradient from more stable anastomosing river systems and deltas. Creation and maintenance of a meandering river pattern is favored by low slope, cohesive bank

material, vegetation-stabilized banks, relatively steady discharge, and a high suspended/bedload ratio (Leopold and Wolman, 1957; Reineck and Singh, 1986). The subtle interrelation among these characteristics are not fully understood as meandering rivers also form in areas of relatively high slope, coarse grain size (higher bedload) and more seasonal discharge (i.e. coarse-grained meandering rivers). Point bars are the major depositional feature in meandering systems developed over a wide range of grain sizes, slopes, sinuosities, and discharges. Consequently, point bar formations displays considerable variability from the simple classical fining-upward sequence.

Point bars accrete both laterally and vertically as the channel migrates over the floodplain. Meandering rivers change their course by neck cutoff, chute cutoff, and by avulsion in order to shorten channel length and increase gradient. Floodplain sediments accumulate due to overbank flooding and are deposited as natural levees, crevasse splays, and in oxbow lakes, bayous, abandoned channels, marshes, and swamps.

### **3.4 GEOLOGICAL DATA FROM COLUMBUS AFB**

#### **3.4.1 Information Sources**

The proximity of CAFB to the Tombigbee River and Buttahatchee rivers (see Figure 2.1) strongly suggest that either braided and/or meandering rivers were responsible for the aquifer deposits. To construct a viable depositional model for the aquifer, the sources of information in Table 3.2 were reviewed.

**Table 3.2 Information Used to Construct the Depositional Environment  
of the CAFB Terrace Aquifer**

Type of Information	Source
Aerial Maps of the Test Site	Columbus AFB, MS
Regional Aerial and Topographical Maps	U.S. Geological Survey
Thesis on Geology of County	Mississippi State University
Facies Mapping of CAFB Gravel Pits	EPRI-MADE Reports
CAFB Grain-Sizes from Well Boreholes	EPRI-MADE Reports
Study of Depositional Trends in the Tombigbee River Valley	U.S. Army Corps of Engineers
Examples of Modern Braided and Meandering Stream Sediments	Journal Articles and Text Books
Continuous Soil Logs	U.S. Army Corp of Engineers Field Data

#### **3.4.2 Archeological Study in the Tombigbee River Valley**

Under the supervision of the Army Corps of Engineers (ACE) an archeological study was carried out in the Tombigbee River valley for the purpose of identifying former living sites of ancient man (Muto and Gunn, 1986). It was recognized that the different elements of the surface physiography, as distinguishable from air photographs, were excellent first indicators for selecting the sampling sites. These sampling sites were approximately 50 by 150 meters and several were located in Columbus, Mississippi. Figure 3.6 shows the numerous oxbows, recognized from the air photographs, and the selected sampling sites near Columbus, Mississippi. This sampling included auger drilling to sample and describe the soils and depositional history altered and unaltered by human activity.

Figure 3.7 and Table 3.3 provide an interpretation of the river valley development from the early Pleistocene to modern times. During the Pleistocene, braided streams dominated the area, eroding the Cretaceous bedrock. The main topography (the Uplands, marked U in Figure 3.7) was shaped during this period. At the end of the Pleistocene (12,000 years B.P.), following an erosional phase, deposits from braided streams and coarse-grained meandering streams are found. Remnants of the Pleistocene have been found in terraces (marked T1 and T2 in Figure 3.7) higher up in the valley. During the Holocene, uplift continues and terraces were found (EHT and LHT). The Tombigbee River remained metastable until an erosional period began shaping the current physiography in modern times (4,000 years B.P.). During this metastable meandering environment, extensive overbank deposits were generated. Also remnants of oxbows (abandoned meanders, clay plugs) are found for this whole period.

### **3.4.3 Aerial Photographs of Test Site**

As shown in Figure 3.6, numerous outlines of river meanders are visible in aerial photographs near the CAFB. Figure 3.8 shows an aerial photograph of CAFB made in 1956. Aerial photographs taken several years previous show a recently leveled area that lacks any physiographical indication of a river meander. In 1956, however, differences in the growth patterns of newly developed vegetation outline a former river meander. Photographs taken after 1956 do not show the paleochannel because of dense vegetative cover.



**Table 3.3 The Homeostatic and the Heterostatic Periods Associated with the Development of the Tombigbee River Valley (after Muto and Gunn, 1986)**

<b>SCENARIO 1. PREBRAIDED STREAM PERIOD (&gt; 16,000 years B.P.)</b>
<p>I. Homeostatic environment periods</p> <p style="padding-left: 40px;">A. From 19,200 to 18,200 years</p> <p style="padding-left: 40px;">B. From 17,300 to 15,800 years</p> <p>II. Heterostatic environment periods</p> <p style="padding-left: 40px;">A. From 20,000 to 19,200 years</p> <p style="padding-left: 40px;">B. From 18,200 to 17,300 years</p>
<b>SCENARIO 2. BRAIDED STREAM OR COARSE-GRAINED MEANDER BELT PERIOD (16,000 - 8,000 years B.P.)</b>
<p>I. Homeostatic environment periods</p> <p style="padding-left: 40px;">A. From 12,500 to 9,600 years</p> <p>II. Heterostatic environment periods</p> <p style="padding-left: 40px;">A. From 15,800 to 12,500 years</p> <p style="padding-left: 40px;">B. From 9,600 to 6,400 years</p>
<b>SCENARIO 3. MEANDER BELT PERIOD (8,000 - 4,000 years B.P.)</b>
<p>I. Homeostatic environment periods</p> <p style="padding-left: 40px;">A. From 6,400 to 5,000 years</p> <p>II. Heterostatic environment periods</p> <p style="padding-left: 40px;">A. From 5,000 to 4,000 years</p>
<b>SCENARIO 4. RECENT PERIOD (4,000 years B.P. - Present)</b>
<p>I. Homeostatic environment periods</p> <p style="padding-left: 40px;">A. From 4,000 to 3,100 years</p> <p style="padding-left: 40px;">B. From 2,100 to 1,500 years</p> <p>II. Heterostatic environment periods</p> <p style="padding-left: 40px;">A. From 3,100 to 2,100 years</p> <p style="padding-left: 40px;">B. From 1,500 to Present</p>

#### **3.4.4 Facies Mapping of Outcrops**

Approximately 1 km northeast of the test site, Rehfeldt et al., (1989b) mapped sedimentary features observed in gravel-pit exposures. Four major sedimentary facies were observed in the gravel-pit exposures: (1) sandy gravel with bimodal mixtures of sand and gravel; (2) well-sorted sand; (3) a highly variable sandy, clayey gravel facies with substantial amounts of clay in pore spaces; and (4) open-work gravel facies of relatively limited horizontal and vertical extend. The sandy gravel facies appears to be a matrix in which the other facies were embedded. Dimensions of the other facies ranged up to 8 m horizontally and less than 0.5 m vertically. Figure 3.9 shows the map of the facies at the gravel exposures.

It is not clear how representative these facies at the gravel pit are of the conditions at the MADE and the USAF test sites. The gravel pit exposures that were mapped included only the upper three meters of the terrace deposits that lie above the water table. However, similar materials are found in soil cores at the test site with the exception of the open-work gravels. This may be due either to the scarcity of the open-work gravels or failure to recognize these features in disturbed soil cores. Rehfeldt et al. (1989), apparently had difficulty in interpretation of the facies as they state: "Based on unclear criteria the sands are interpreted as deposited by braided streams."

#### **3.4.5 Soil Logs from Well Boreholes**

During the installation of the 1-Ha network, split-spoon samples were collected at 0.61-m intervals for 10 wells. The samples were collected primarily for locating gravel and

clay lenses and for evaluating the ease of sampling using different drilling methods. Because of a lack of resources, grain-size analyses were not performed on any of these samples. Although descriptive field logs were made, these descriptions are too subjective and vague for critical evaluation.

Near the MADE MLS well network, 214 sediment samples from 7.6-cm OD split spoons were analyzed for grain-size information. From a geologic viewpoint, the data are of poor quality. The sample locations are very sporadic and are composite samples of vertical lengths of approximately 0.5 m. These samples are too mixed to investigate depositional environments and too widely distributed to map spatial trends. In addition, the churning of gravels in the split spoon samples destroyed potentially useful bedding or layering structure. To analyze the sediment data, Boggs et al., (1990) generated Figure 3.10, which shows a composite profile of the grain size from 38 coreholes near the MADE site.

In defense of classifying the paleochannel in Figure 3.8 as a surficial feature, Rehfeldt et al., (1992) cite the lack of distinguishable transitions in the profile of the average grain-size data in the upper aquifer (Figure 3.10). However, because only 3 of the 38 boreholes are located within the paleochannel at the MADE site (see Figure 3 in Rehfeldt et al. 1992) this argument is not a valid one.

Based on the soil sampling and drilling activities for the MADE project, a contour map (Figure 3.11) of the top of the Eutaw clay formation was constructed. Figure 3.11 shows the elevation of the erosion surface upon which the terrace sediments are deposited. Marine sands with traces of glauconite indicate that an ancient river and not the Tombigbee River scoured the Eutaw sand formation. Over most of the study area, the Eutaw clay

surface is composed of a dense clay, which forms an aquitard beneath the terrace deposits. However, fine-grained marine sands, frequently containing thin interbedded clay and silt laminations, form the upper Eutaw clay in one subregion of the site. This sand unit ranges up to approximately 3 m in thickness, and exhibits physical and hydraulic properties similar to those of the terrace deposits.

#### **3.4.6 Continuous Soil Logs**

During the Summer of 1994, continuous aquifer cores were taken at 9 locations shown in Figure 3.12. The cores were collected in 8.3-cm ID, 76-cm long, polycarbonate sleeves with a 10.8-cm ID hollow-stem auger. At the 7 locations near the MADE site, aquifer coring began at ground surface. At the 2 locations in the 1-Ha test site, sampling began approximately 2 m below ground surface. All soil cores except those from well location 74 were cut open, visually inspected, and photographed. To help illustrate the coarseness of the majority of the deposits, photographs of the deposits from the location of Well 72 and Well 73 are shown in Figures 3.11 and 3.12, respectively. Composite samples of 100 to 400 grams were made at intervals of approximately 25 cm. Grain-size analyses were performed at  $0.5\phi$  intervals over the range of  $-6.5\phi$  (90 mm) to  $+3.7\phi$  (0.075 mm). Shown in Figures 3.12 and 3.13 are the means and standard deviations for the composite samples.

Although dependent on the supply of particles available for transport, mean grain size serves as a general indicator of the energies associated with sediment transport in an environment. In general, coarser mean grain sizes are representative of higher depositional energies. The standard deviation (sorting) is a measure of how often and greatly the energy

changes. Sorting represents the balance between entry of sediment into the system and reworking or removal of sediment fine enough to be transported by the prevalent velocity of the water. A large standard deviation implies that sediment enters the system faster than currents can segregate it into different populations. A low standard deviation implies either a slow rate of deposition, which allows time for reworking, or that the sediments' source is already well sorted (Middleton and Southard, 1984).

In Figures 3.14 and 3.15, shading has been used to divide the aquifer thickness into three zones. The interval from 62 to 64 m MSL represents a fine-grained overburden that is normally unsaturated and has a mean grain size greater than  $2\phi$ . At high water-table conditions, these fine-grained deposits may lead to semi-confined to confined conditions in some areas such as near well location 76. The interval from 58 to 62 m MSL represents the upper half of the saturated aquifer. The mean and standard deviations for this interval are  $-2\phi$  and  $2\phi$ , respectively. These values suggest a high energy and chaotic depositional environment similar to that for a coarse-grained meandering river with frequent floods. The interval from 54 to 58 m M.S.L. represents the lower half of the saturated aquifer. Over this interval at every well location except Well 76, the mean grain size varies from  $-3\phi$  to  $2\phi$ . This wide range suggests that the deposits were formed by environments with very different modes of sediment transport.

At the seven core locations at the MADE site, 5-cm ID fully-screened wells were installed with gravel packs via a 10.8-cm ID hollow-stem auger. At the two core location at the 1-Ha test site, no wells were installed because the corings were within 1.5 m of

existing gravel-packed wells. Results from borehole flowmeter tests from the gravel-packed wells are shown in Figure 3.16.

Spatial variability is a dominant feature in all of the K profiles. Except at intervals where low-K, fine-grained deposits exist, K values typically fluctuate 1 to 2 orders of magnitude. Less variation is shown at the 1-Ha test site because at the two well locations, a larger vertical interval was used for averaging the flow measurements. Because of the highly heterogeneous conditions at the site, groundwater flow is likely controlled by preferential flow paths formed by a convoluted network of interconnected high-K deposits.

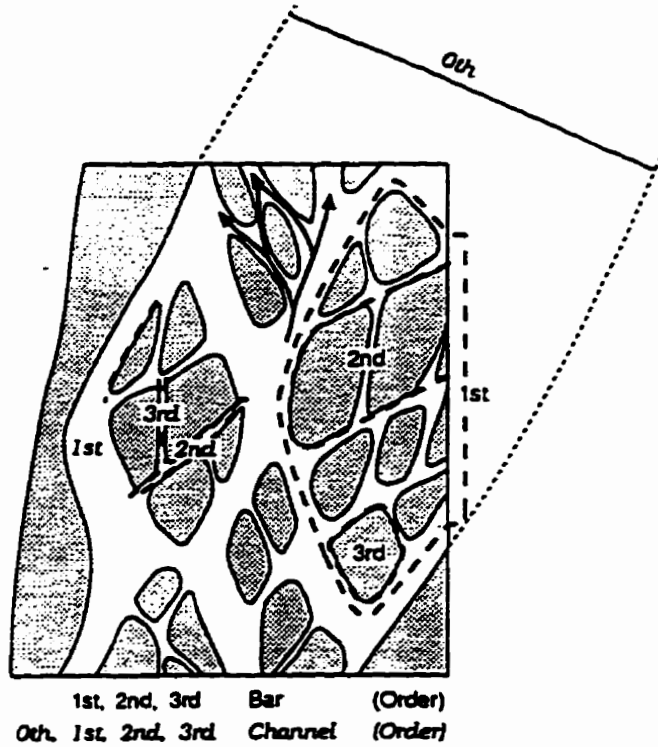


Figure 3.1 Schematic diagram showing multiple longitudinal bars (1st order) which commonly are themselves dissected into smaller bars and shallower channels (2nd and 3rd order). Diagram represents one braided-river reach or compound channel (within which all three bars orders are migrating; 0th order) of which a braidplain is composed of many (modified after Williams and Rust, 1969).

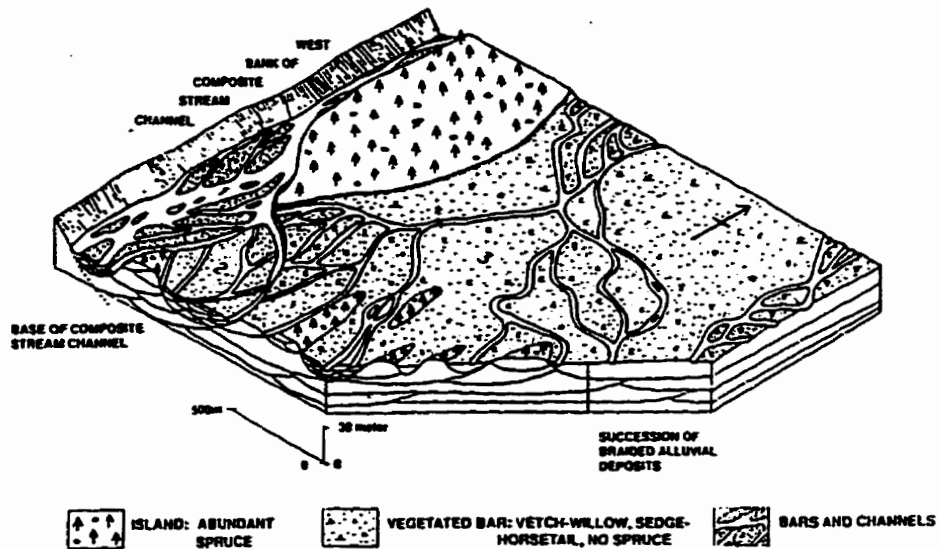


Figure 3.2 Schematic of the Complex Relationships among the different facies in a braided stream environment (after Williams and Rust, 1969).

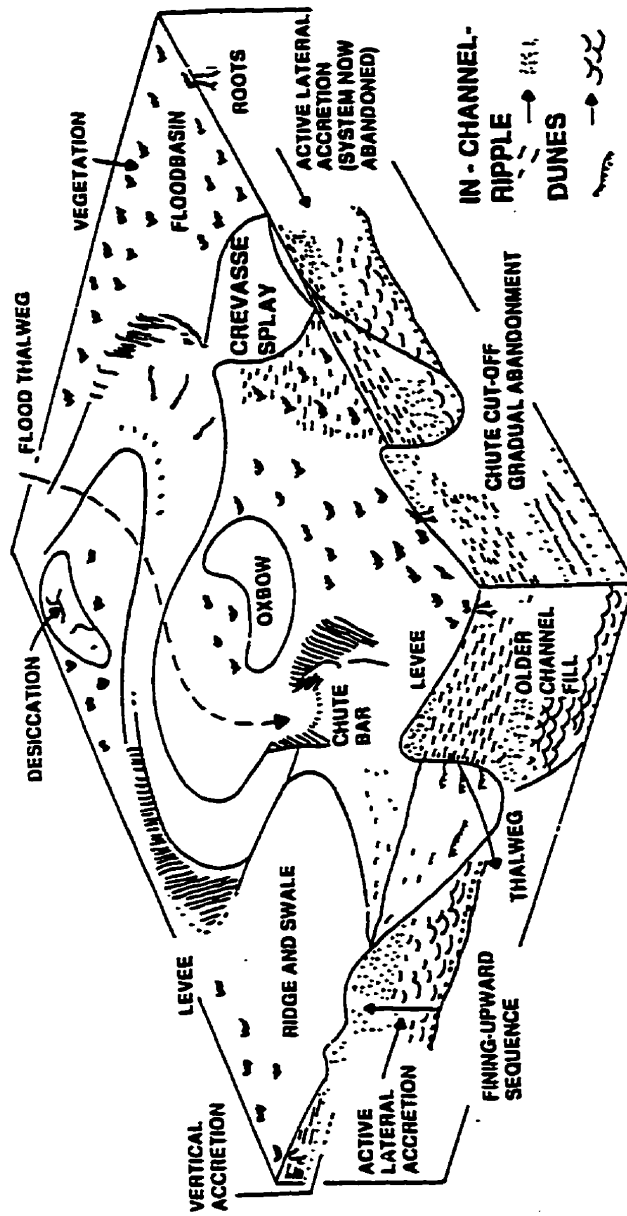


Figure 3.3 Block diagram showing the major morphological elements of a meandering river system (after Walker, 1979, p. 23).



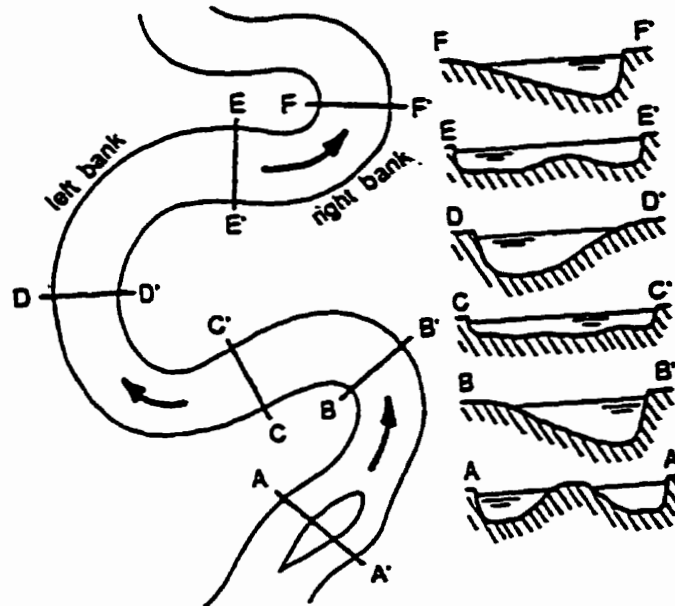


Figure 3.4 Meandering river flow pattern and channel cross-sections(from Allen, 1985).

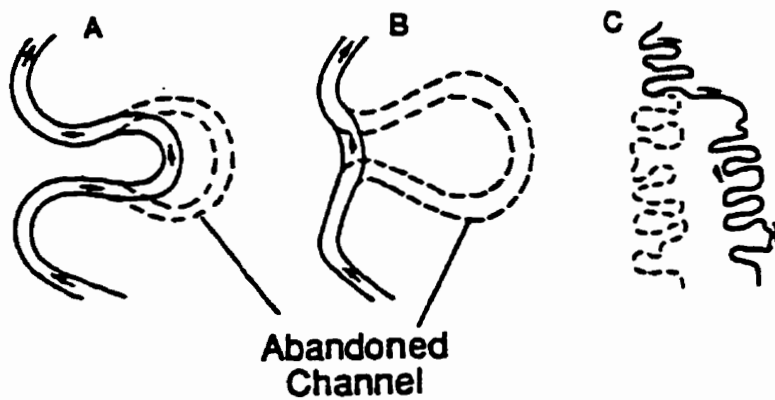


Figure 3.5 Modes of channel shifting in meandering systems; A=chute cutoff, B=neck cutoff, C=avulsion(from Collinson, 1986; after Allen, 1965).



Figure 3.6 Physiographical Units recognized from air photographs and sampling sites selected by the Corps of Engineers near the CAFB aquifer (after Muto and Gunn, 1986).

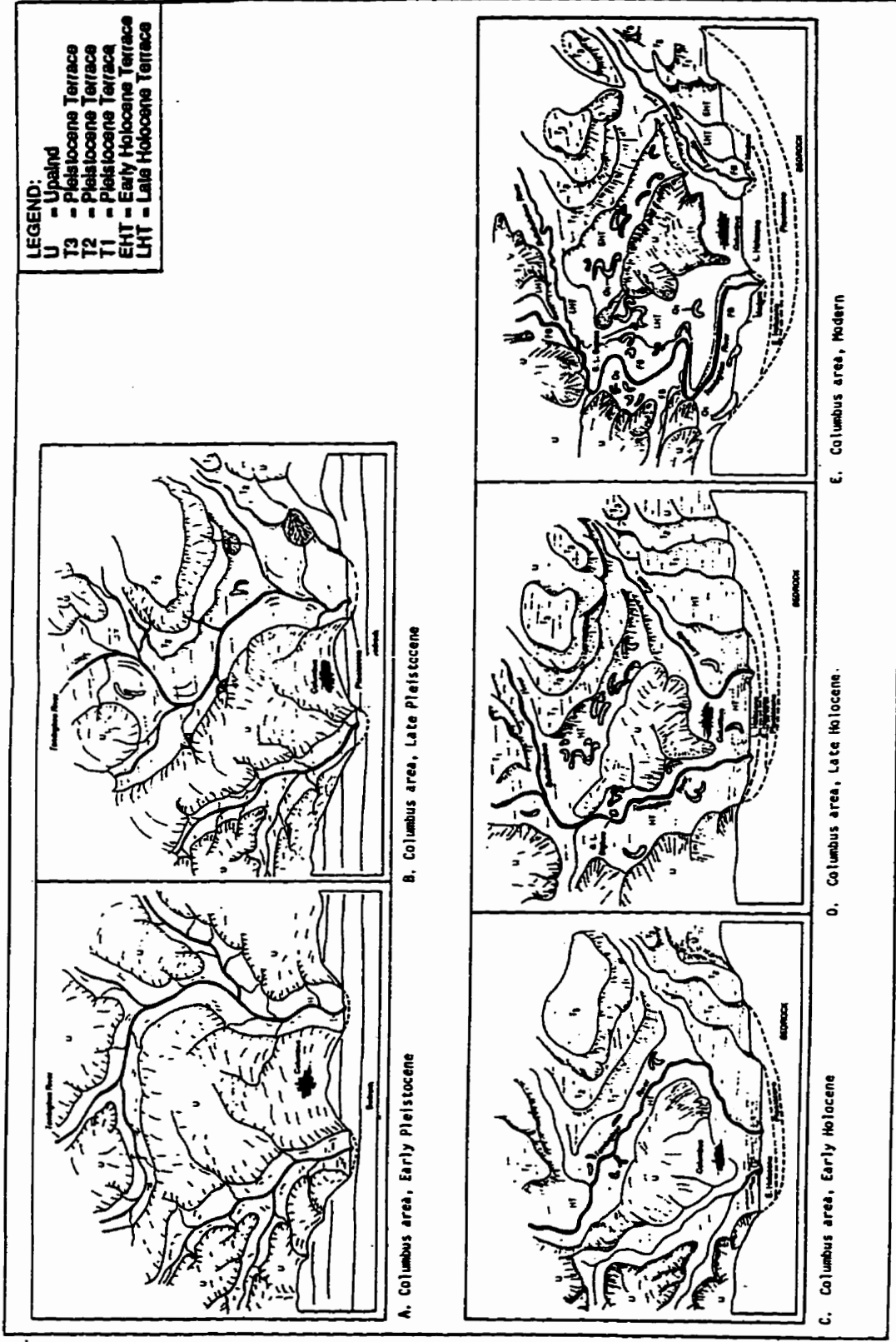


Figure 3.7 Evolution of the Tombigbee River Valley in the Columbus, Mississippi area (after Muto and Gunn, 1986).

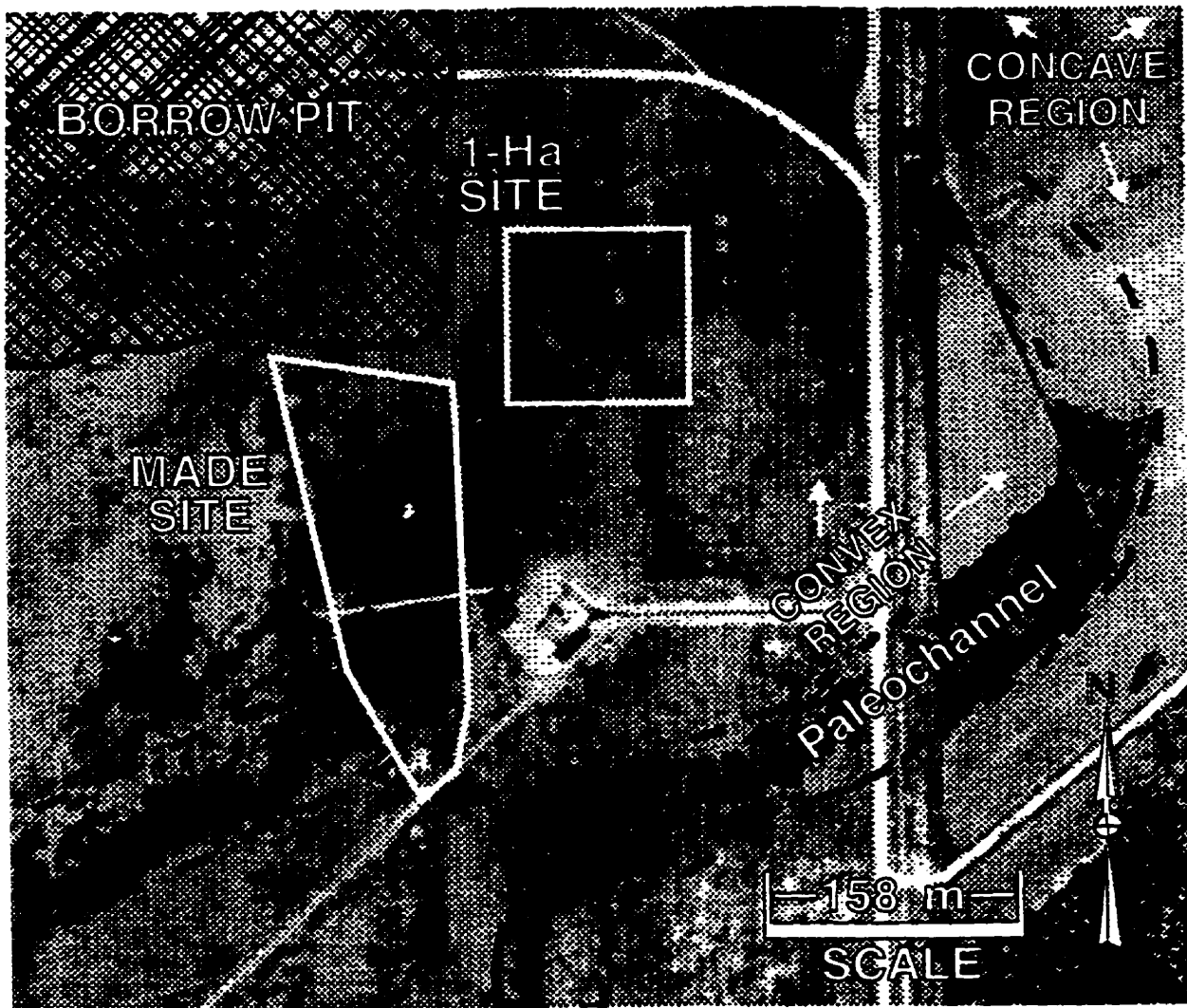


Figure 3.8 Test sites overlaid on a 1956 aerial photograph that shows the location of a paleochannel.

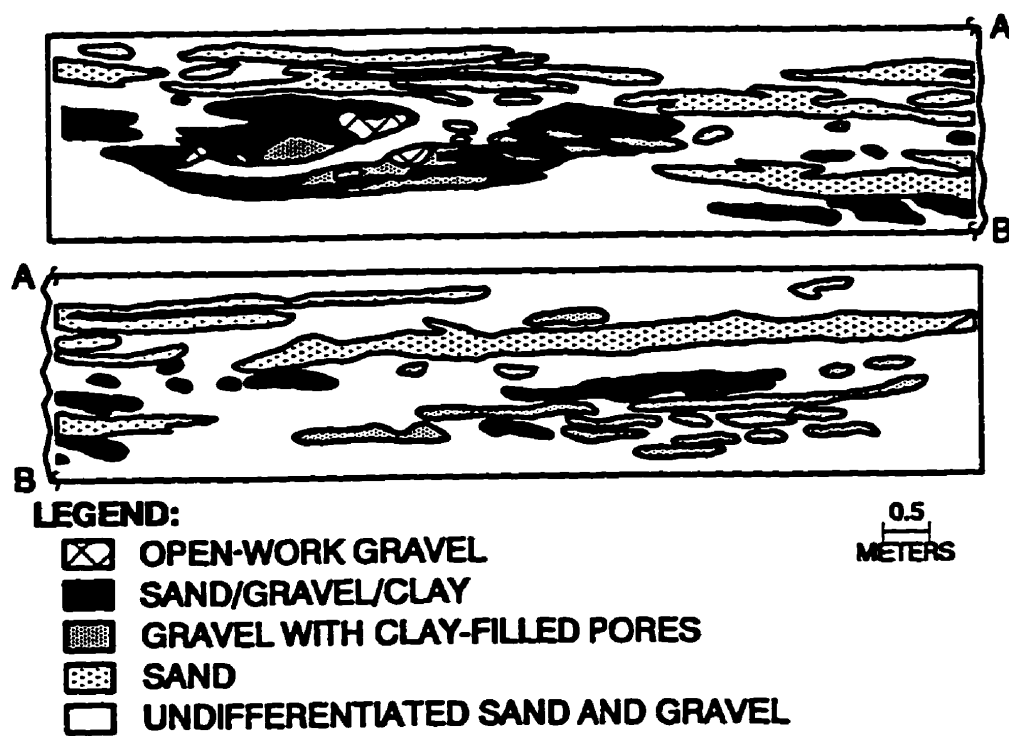


Figure 3.9 Geological cross-section of a textural facies map at a CAFB gravel pit (after Rehfeldt et al., 1989).

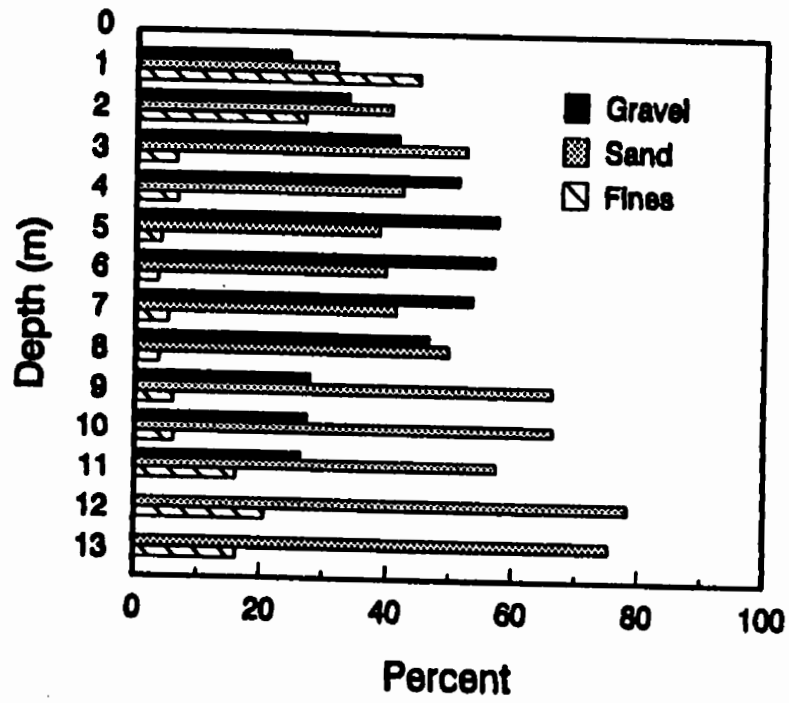


Figure 3.10 Field -averaged grain-size distribution for the CAFB aquifer (after Boggs et al., 1990).

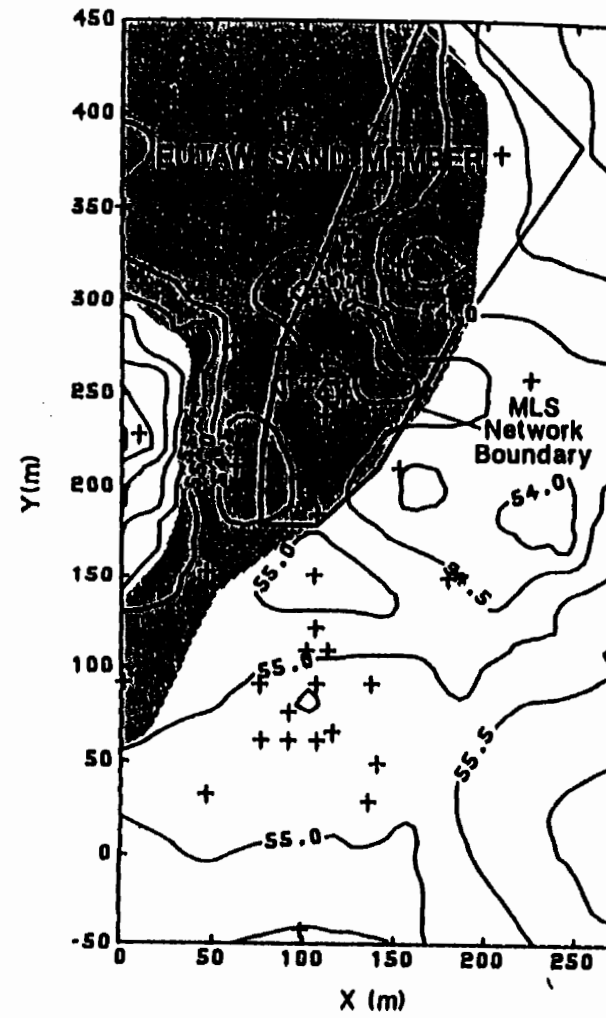


Figure 3.11 Elevation of top of Eutaw Formation (contour in meters MSL -- after Boggs et al., 1990).

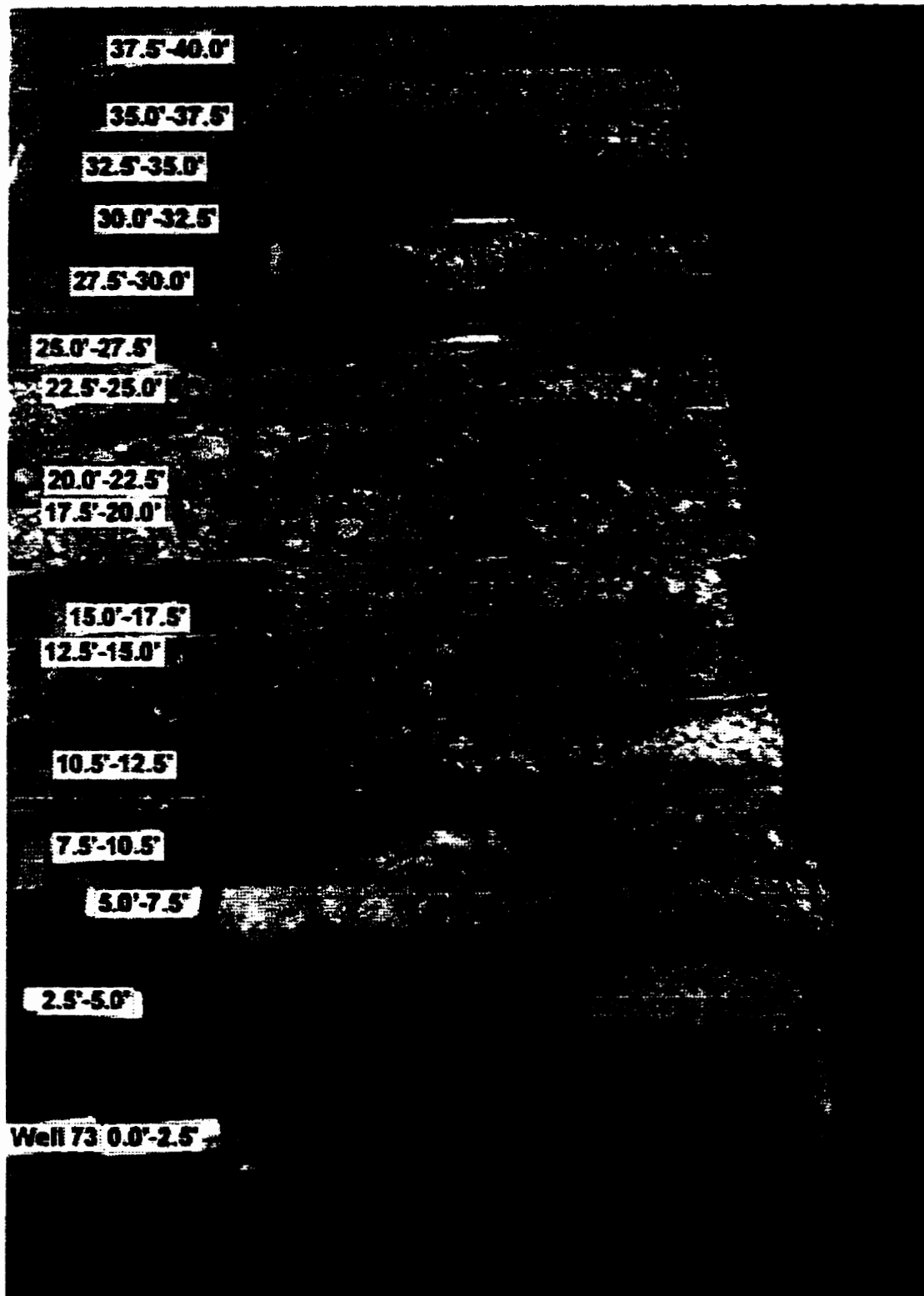


Figure 3.12 Photograph of 76-cm (~2.5 ft) long core sections from the location of Well 72. (Depths are referenced to below ground surface).

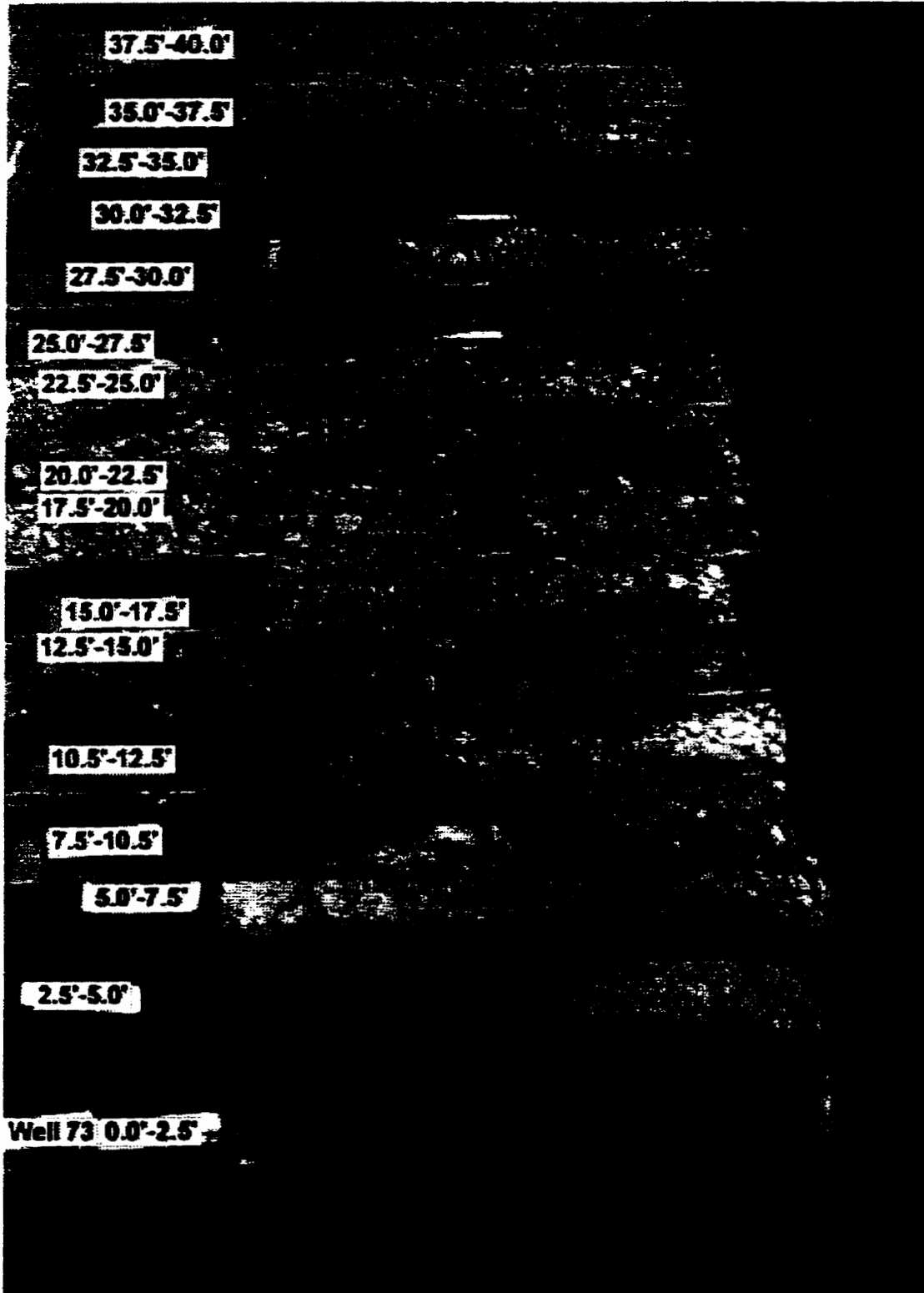


Figure 3.13 Photograph of 76-cm (~2.5 ft) core sections from the location of Well 73. (Depths are referenced to below ground surface).



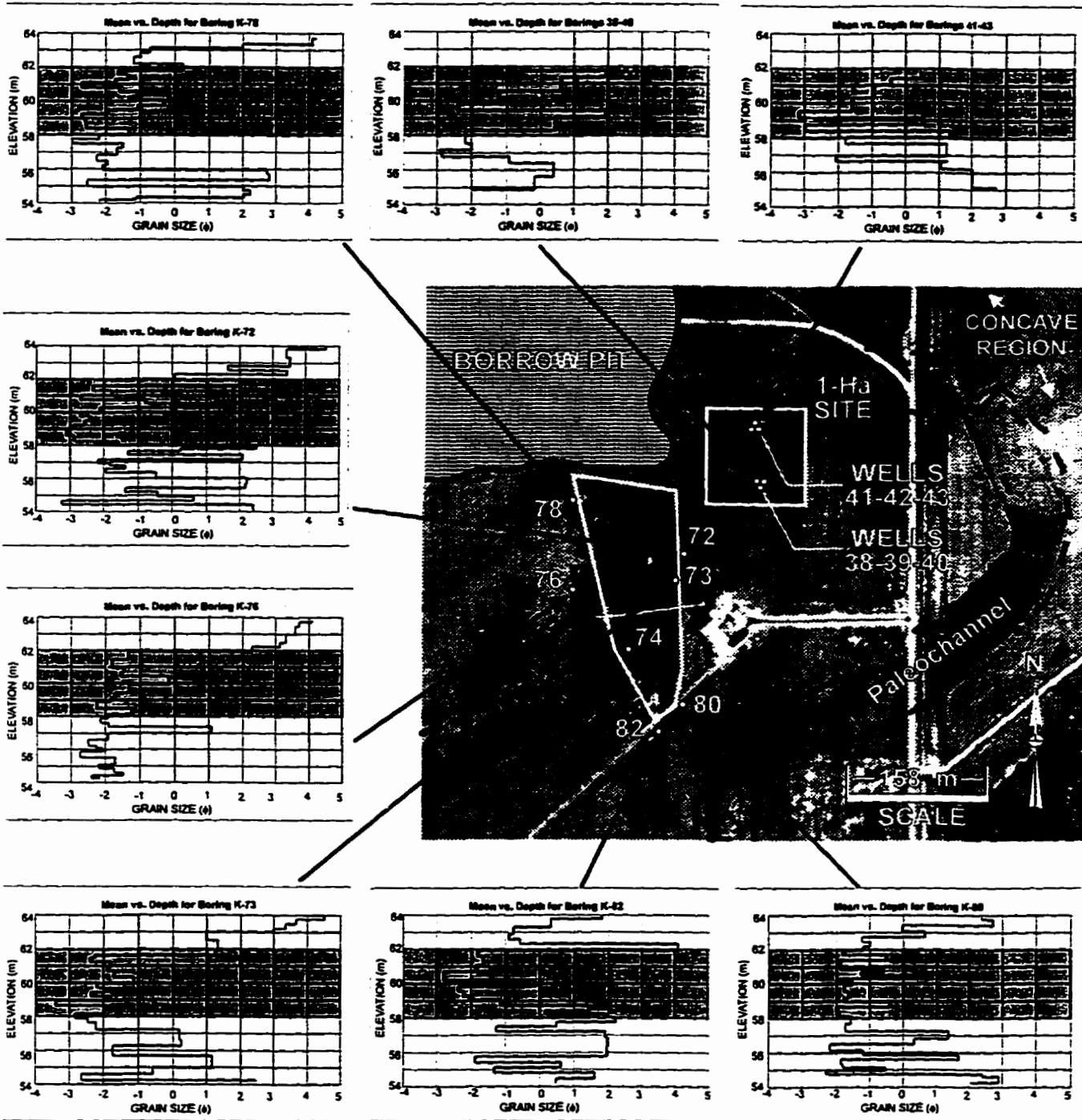


Figure 3.14 Vertical profiles of mean grain-size at the continuous coring locations.

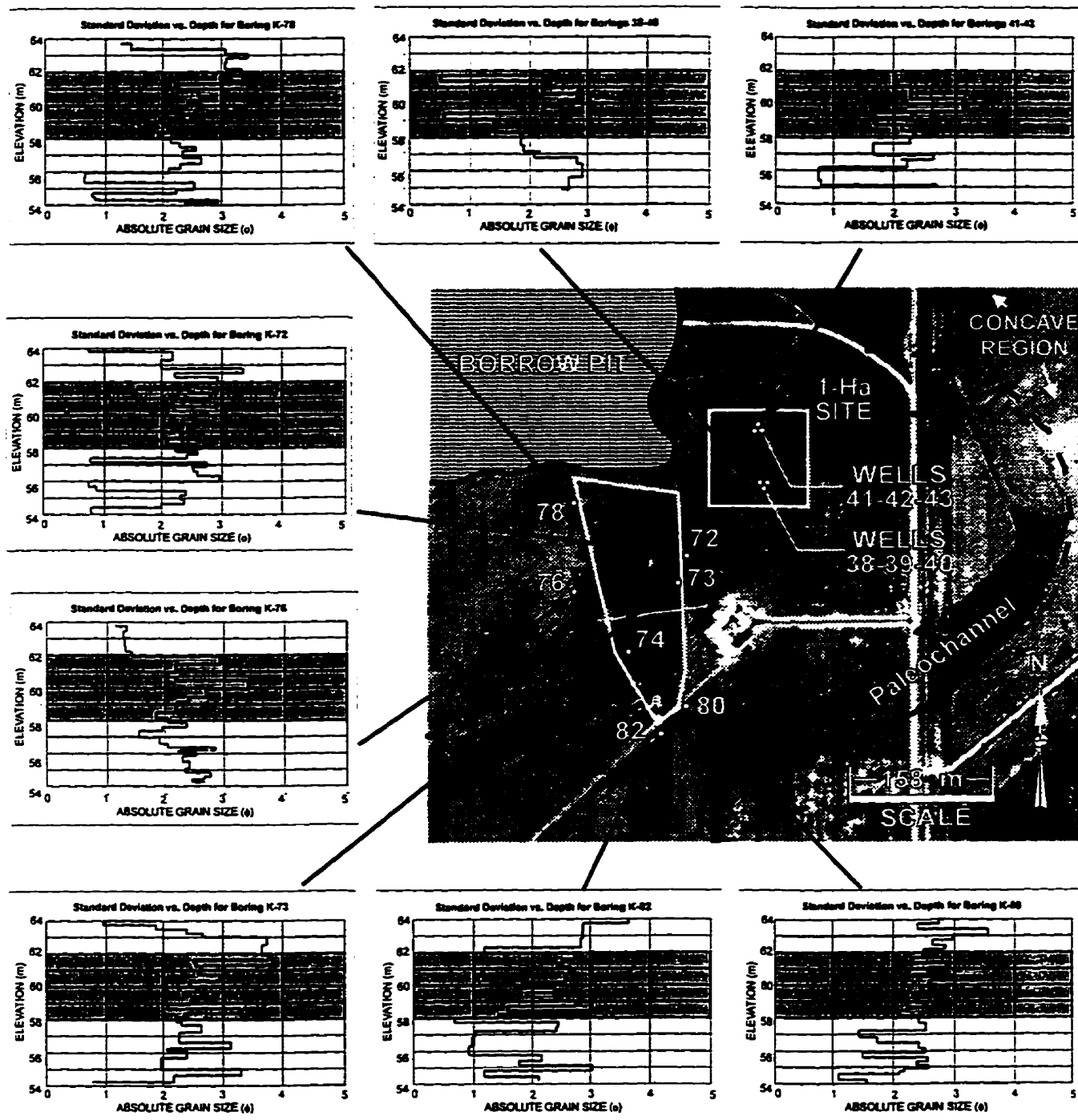


Figure 3.15 Vertical profile of grain-size standard deviations at the continuous coring locations.

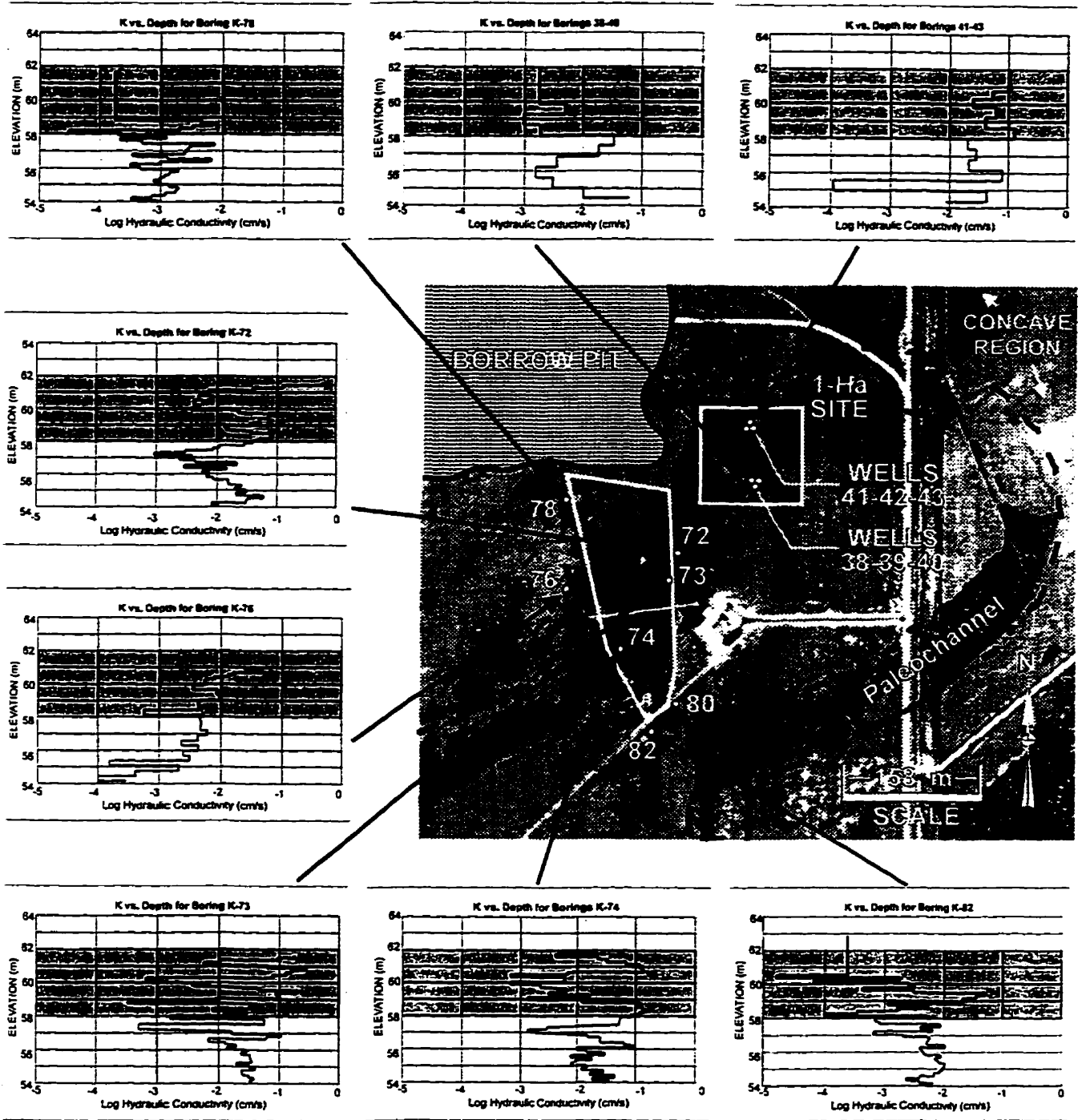


Figure 3.16 Vertical profile of borehole flowmeter K values at the continuous coring locations.

## **4. CHARACTERIZATION OF HIGH-K PATHWAYS AT THE 1-Ha TEST SITE**

### **4.1 INTRODUCTION**

Proper aquifer characterization in support of aquifer remediation activities requires delineating the hydraulic conductivity (K) field. Borehole flowmeter tests are a promising method for effectively measuring horizontal K. Several recent papers (Hufschmied, 1986; Hess, 1986; Hess et al., 1992; Morin et al. 1988; Molz et al., 1989, 1990; Rehfeldt et al., 1989; 1992; Molz and Young, 1993; and Young et al., 1993a, b) describe borehole flowmeter tests. Among these applications, differences exist regarding data collection and/or analysis.

Aquifer and tracer testing from a 1-Ha test site composed of fluvial deposits have produced independent data sets that indicate the aquifer is highly heterogeneous. The 1-Ha test site is located at CAFB Columbus, Mississippi. The test results indicate that alternative methods for analyzing flowmeter data, which may be equivalent in relatively homogeneous aquifers (see Molz et al., 1989), can produce significantly different K values at Columbus AFB. The most promising approach for flowmeter data analysis is a slightly modified method discussed by Molz et al., (1990). Using this method, 881 borehole flowmeter K values were calculated for the 1-Ha test site. To demonstrate the reliability of this method, the magnitude and trends in the K values are shown to be consistent with results from geologic investigations, recirculating tracer tests, and large-scale multi-well pumping.

#### **4.2 BRIEF DESCRIPTION OF THE 1-Ha TEST SITE AT COLUMBUS AFB**

The test site occupies approximately 1 of 25 hectares of TVA's Groundwater Research Area at Columbus AFB, Mississippi. The 1-Ha test site is within 50 m of the EPRI **MA**cro**D**ispersion **E**xperiment (MADE) site (Boggs et al., 1992; Rehfeldt et al., 1992). The Columbus aquifer is composed of approximately 10 meters of fluvial deposits consisting of interfingering, lozenge-shaped lenses of poorly- to well-sorted sandy-gravel and gravelly-sand. Of the 10 meters, the saturated thickness seasonally varies between 6.5 and 7.5 meters. The aquifer overlies the Eutaw Formation consisting of clay and silt that serves as an aquitard (Boggs et al., 1992). An aerial photograph (see Figure 3.8) shows a paleochannel crossing the 1-Ha test site.

The 1-Ha test site (Figure 4.1) includes thirty-seven 5.25-cm ID fully-screened wells constructed from schedule 40 PVC pipe with 0.025-cm slots at spacings of 0.318 cm. All wells were installed through either a 19.4-cm OD hollow stem auger or a 11.4-cm OD driven casing. After well installation, the annulus was allowed to backfill and auger cuttings were used to complete the backfill to ground surface. Each well was developed for approximately 3 hours using overpumping, backwashing, and mechanical swabbing (Young, 1991a; Young et al., 1993a). After well development, borehole flowmeter tests were performed.

#### **4.3 BOREHOLE FLOWMETER TESTS**

Borehole flowmeter tests involve measuring vertical flow in a well during ambient and pumping conditions after the water-table level has stabilized. Data analysis includes calculating K values based on borehole flowmeter and pressure measurements at designated

aquifer intervals. Within the refereed literature two approaches to borehole flowmeter analysis have been presented. They will be referred to as the Cooper-Jacob and the  $K_i/K$  profile approaches.

#### 4.3.1 The Cooper-Jacob Approach

The assumptions of horizontal flow and an infinite aquifer permit using the Cooper-Jacob (CJ) equation (Cooper and Jacob, 1946) to calculate horizontal  $K$  values for selected aquifer layers after an appropriate time interval. Application of the CJ equation requires values for the drawdown,  $\Delta H_i$ , and the storage coefficient,  $S_i$ , for each  $I^{\text{th}}$  aquifer layer. If the well losses are negligible, then the value of  $\Delta H_i$  for each aquifer layer can be assumed equal to the measured drawdown. If the well losses are not negligible, then values of  $\Delta H_i$  will need to be measured or estimated using a program such as KPFLOW3 (Young et al., 1993b).

In contrast to the relatively straight-forward methods for determining the  $\Delta H_i$  values, the  $S_i$  values can be difficult to select. Within the refereed literature, the following two methods have been used: (1) the specific storage,  $S_s$ , is constant so that  $S_i = S_s \times \Delta z_i$  (Morin et al., 1988; Molz et al., 1989); and, (2)  $S_i$  varies with  $K_i$  such that the hydraulic diffusivity (i.e.,  $T_i/S_i$ ) remains constant for each  $I^{\text{th}}$  layer (Rehfeldt et al., 1989; Hess et al., 1992; Hufschmied, 1986). Applying the Cooper-Jacob approximation for flow to a well in a confined aquifer (Cooper and Jacob, 1946) to represent flow from a single-aquifer layer,

the first and the second assumptions lead to Equations 4.1 and 4.2, respectively, where:  $\Delta H_i$  = drawdown from  $I^{\text{th}}$  layer;  $\Delta Q_i$  = total flow from  $I^{\text{th}}$  layer into the well;  $\Delta q_i$  = ambient flow from  $I^{\text{th}}$  layer;  $K_i$  = horizontal hydraulic conductivity of the  $I^{\text{th}}$  layer;  $S_i$  = storage coefficient for the  $I^{\text{th}}$  layer;  $\Delta z_i$  =  $I^{\text{th}}$  layer thickness;  $r_e$  = effective well radius; and,  $t$  = time since pumping started.

$$K_i = \frac{(\Delta Q_i - \Delta q_i)}{2\pi\Delta H_i\Delta z_i} \ln \left[ \frac{1.5}{r_e} \sqrt{\frac{Tt}{S}} \right] \quad (4.1)$$

$$K_i = \frac{(\Delta Q_i - \Delta q_i)}{2\pi\Delta H_i\Delta z_i} \ln \left[ \frac{1.5}{r_e} \sqrt{\frac{K_i\Delta z_i t}{S_i}} \right] \quad (4.2)$$

#### 4.3.2 $K_i/\bar{K}$ Profile Approach

Molz et al., (1989) cite the work of Javandel and Witherspoon (1969) to justify an alternative method to the CJ equation for borehole flowmeter data analysis. Javandel and Witherspoon (1969) numerically modeled the pumping well for an idealized, layered aquifer with a constant  $S_i$  and with  $K_i$  contrasts of up to 100. The modeling results showed that at steady-state conditions (defined when  $r_e^2 S_i / 4Tt \leq 0.01$ ) the flow to the pumping well becomes horizontal and the incremental induced discharge,  $(\Delta Q_i - \Delta q_i)$ , for any layer is directly proportional to  $T_i$  (i.e.,  $K_i \times \Delta z_i$ ).

From the modeling results of Javandel and Witherspoon (1969), Molz et al., (1989, 1990) developed Equation 4.3 so a dimensionless  $K_i/\bar{K}$  profile could be calculated with flowmeter data, where  $\bar{K}$  represents a vertical averaged  $K$ . A  $K_i$  profile is obtained by

multiplying the  $K_i/K$  values by  $K$ . Molz et al., (1989, 1990) suggest that  $K$  be obtained from a fully-penetrating pumping test. In applying Equation 4.3, they used the same  $K$  to calculate the  $K_i$  profiles for three flowmetered wells.

$$\frac{K_i}{K} = \frac{(\Delta Q_i - \Delta q_i) / \Delta z_i}{Q / Z} \quad (4.3)$$

#### 4.4 BOREHOLE FLOWMETER DATA ANALYSIS FOR COLUMBUS AFB

##### 4.4.1 Hydraulic Tests at the 1-Ha Test Site

Hydraulic testing at the 1-Ha test site included several 20-minute pumping tests at each well. For each pumping test, transmissivity values were calculated using the CJ equation and the Cooper-Jacob Straight-Line (CJSL) method (Cooper and Jacob, 1946). CJ transmissivity values were calculated with the drawdown at 20 minutes and an estimated storativity of 0.03 obtained from several large-scale pumping tests, which Appendix B describes in detail. CJSL transmissivity values were calculated using drawdown data of between approximately 3 and 20 minutes. For the majority of the pumping tests the CJSL transmissivity was typically 5 to 10 times higher than the CJ transmissivity. Figure 4.2 illustrates results for two pumping tests.

A likely explanation for the large discrepancy between the CJ and CJSL transmissivity values is positive (low-K) skin effects, which are described in Chapter 5. Evidence of low-K skin effects exists in the drawdown curves, which have considerably steeper semi-log slopes at early times (between 1 and 3 minutes) than at late times (between 3 and 20 minutes). Additional evidence of low-K skin effects are low transmissivity values



calculated from slug tests. Prior to each pumping test, slug tests were performed and analyzed using a modified Hvorslev method as coded by Thompson (1987). Slug test transmissivities averaged  $3.5 \text{ cm}^2/\text{s}$  and were much closer to the CJ transmissivity values, than to the CJSL transmissivity values from the pumping tests (Young, 1991a).

#### **4.4.2 Selection of an Analysis Approach**

Based on the analysis of the pumping tests and slug tests, low-K skin effects appear to exist at all wells. A possible cause of the low-K skin effects is backfill partially blocking the connection between one or more permeable aquifer layers and the well screen. Because of the likely existence of low-K skin effects (to be discussed in detail in Chapter 5), equations 4.1 or 4.2 should not be used to calculate borehole flowmeter  $K_f$  values.

Use of Equation 4.3 is straight-forward except for the selection of  $K$ . Approaches for calculating  $K$  include slug tests, multi-well tests, and single-well tests. Because of low-K skin effects at the wells, slug tests will not provide a  $K$  representative of the undisturbed aquifer material. The option of fully-penetrating multi-well pumping tests would help avoid skin-effects and has been successfully used by Molz et al., (1989; 1990).

The study of Molz et al., (1989, 1990) was performed in a more homogenous site than CAFB. A measure of aquifer heterogeneity is the difference observed among transmissivities obtained from multi-well and single-well pumping tests. Molz et al., (1990) obtained a maximum difference of 40 percent between transmissivity values calculated from fully-penetrating multi-well and single well tests. The calculated percent was based on a ratio of the difference the lower of the two values. A similar comparison at Columbus, MS,

for wells spaced about 5 meters apart produces differences greater than a 1000% (see Figure 4.3).

Figure 4.3 indicates that  $K$  values obtained from single-well and multi-well tests at Columbus are not close enough to be considered interchangeable. Because borehole  $K$  values should reflect aquifer heterogeneity at the local scale, a selected value for  $K$  should be calculated with drawdown data from when the cone-of-influence is near the pumping well. The average duration of the single-well and multi-well tests was about 0.3 and 3.0 hours, respectively. Because of this time difference, the  $K$  values from the single-well test should be more reflective of aquifer at the local scale than  $K$  values from the multi-well tests. Based on the available data at Columbus, AFB the best method for calculating borehole flowmeter  $K_i$  values is to use the  $K_i/K$  profile approach with the  $K$  values obtained from a CJSL analysis of a short-duration single-well pumping test.

#### **4.5 BOREHOLE FLOWMETER HYDRAULIC CONDUCTIVITY VALUES**

Borehole flowmeter flow profiles were made using a 0.1-m long electromagnetic (EM) borehole flowmeter, which is described in Appendix C. Flow measurements were made at 0.3-m intervals prior to and while injecting approximately 22 L/min into each well. Injection tests were used instead of pumping tests to maximize the saturated aquifer thickness. However, because of problems with the quality the injection test drawdown data, reliable  $K$  values could not be calculated for all wells. To process the borehole flowmeter data,  $K$  values were obtained from pumping tests performed at each well. These pumping tests included drawdown data at 1-second intervals for a 20-minute period.

Because of differences in the saturated aquifer thicknesses during the pumping tests (used for the  $K$  values) and the injection tests (used for  $K_i/K$  profiles), the  $K_i$  values were calculated in two steps. First, the  $K_i$  values were calculated for aquifer layers saturated during the pumping tests using Equation 4.3 and the  $K$  value from the pumping test. Second,  $K_i$  values were calculated for the remaining aquifer layers, which were saturated during the injection but not the pumping tests, using the linear relation between the induced incremental discharge and  $K_i$  values in Equation 4.3.

The borehole flowmeter tests at the 37 wells produced 881  $K$  values with an arithmetic mean, a geometric mean, and a  $\sigma^2_{\log(K)}$  of 0.26 cm/s, 0.032 cm/s, and 0.92, respectively. Appendix D presents the individual  $K$  profiles for each well. Figure 4.4 shows areal plots of the  $\log(K)$  field-based depth-averaged values for 2-m intervals. The 54 to 56 m MSL cross section has only a partial  $\log(K)$  field because of a 0.5 to 1-m depression in the middle of the test site. In generating the 54 to 56 m MSL cross section, only  $\log(K)$  values from wells with  $K_i$  values below 55 m MSL were used.

## **4.6 EVALUATION OF THE TRENDS IN THE HYDRAULIC CONDUCTIVITY VALUES**

### **4.6.1 Results from Geological Investigations**

The location of the paleochannel in Figure 3.8 coincides with high  $\log(K)$  values in the 60 to 62 m MSL cross section in Figure 4.4. An explanation for this alignment is that high  $\log(K)$  values represent the bedload deposits associated with the paleochannel shown in Figure 3.8. This explanation is consistent with the relation between depth and width in

Equation 4.4 that Leeder (1973) observed in 57 modern meandering rivers. Based on a meander width of 70 m from Figure 3.8, the depth of the river meander would be about 5.7 m and have a base near 59 m MSL. This elevation agrees with the lower boundary for the high values of  $\log(K)$  values in Figure 4.4 that coincide with the location of the meander.

$$w = 6.8 h^{1.34} \quad (4.4)$$

where:  $w$  = bankfull width (m)

$h$  = bankfull depth (m)

Preservation of a fluvial channel at the top of the aquifer occurred because no other channels could have subsequently truncated or eroded its boundaries. Within the middle of the aquifer, preservation of continuous portions of substantial bedload deposits would be less likely because multiple channels may have reworked the deposits. At the base of the scour in the Eutaw Formation, preservation of a bedload deposits could have, and appears to have, occurred. Within the middle of the scour (area in Figure 4.4 that includes  $K$  values at 54 to 56 m MSL) the aquifer is characterized by high  $\log(K)$  values. By analog with the paleochannel and the  $\log(K)$  values for the 60 to 62 m MSL cross section, the high  $\log(K)$  values are presumed to be associated with bedload deposits from a fluvial channel.

In short, the trends in the high values of  $\log(K)$  values are consistent with the presumed bedload deposits associated with fluvial channels as mapped from the aerial photograph and a scour in an underlying clay aquitard. The direct connection between inferred geological features and trends in the high  $\log(K)$  supports the results of the borehole flowmeter tests.

#### **4.6.2 Results from Large-Scale Recirculating Tracer Test**

In September 1989, a flow field for a recirculating tracer test was established by pumping wells 1, 3, 7, and 9 at 26.5 L/min and injecting the total 106 L/min discharge into well 5 (Figure 4.1). Once the water table stabilized, a 21200-liter chloride solution was injected into Well 5 and monitored for 170 hours by a network of multi-level samplers installed in selected wells. At each sampling well, groundwater samples were taken simultaneously at 0.6-m vertical increments using a network of peristaltic pumps connected to the sampling tubes (Young, 1991b). Appendix E provides additional information regarding this large-scale tracer test.

An objective of the chloride monitoring was to map the elevation and the arrival time of peak concentrations at each sampling well. The wells were sampled at intervals inversely proportional to their distance from the injection well. Sampling intervals varied from <1 hour for wells 13 and 16 to every 4 to 6 hours at wells 1 and 9. The exceptions were wells 32 and 7, which were inadvertently removed from the sampling schedule after 60 hours.

Figure 4.5 shows the steady-state water-table configuration and the times of the peak tracer concentrations across the test site. All of the peak tracer concentrations, and almost all the chloride mass, was detected above 58 m MSL. The mapped arrival times in Figure 4.5 suggest that preferential tracer transport occurred toward well 3. Included on Figure 4.5 are numerically simulated arrival times for peak concentrations for a homogeneous aquifer with a porosity of 0.3 and a saturated aquifer thickness of 6.5 m. The numerical model (see Linderfeldt and Wilson, 1993) generated a steady flow field based on the Theim equation (Davis and DeWiest, 1966) and used random-walk particle tracking to simulate groundwater

transport. The simulations included a longitudinal and a transverse dispersivity of 20 and 2 cm, respectively.

In the northwest quadrant, the predicted arrival times are about ten times greater than the measured arrival times. This large difference confirms and helps to quantify that preferential tracer transport occurred through the upper aquifer toward well 3. The observed preferential transport is consistent with Figure 4.4, which shows that the region of the most prevalent high  $\log(K)$  values is in the upper aquifer between wells 5 and 3.

#### **4.7 EVALUATION OF THE MAGNITUDE OF THE K VALUES**

##### **4.7.1 Results from Large-Scale Aquifer Pumping Tests**

Without imposing any constraints of the hydraulic conductivity field, Cardwell and Parsons (1945) show that for radial flow, the effective hydraulic conductivity,  $K_{\text{eff}}$  of a heterogeneous aquifer is bounded by the harmonic and arithmetic spatial averages of hydraulic conductivity weighted by the inverse square of their radial distance from the pumping well. Cardwell and Parsons (1945) define  $K_{\text{eff}}$  of the aquifer as the  $K$  that gives the same flux under the mean spatial gradient between the well and the radius-of-influence. Using results from multi-well pumping tests, a  $K_{\text{eff}}$  can be calculated and compared to the weighted harmonic and arithmetic averages of the borehole flowmeter  $K$  values.

During June and July 1989, Aquifer tests AT1, AT2, and AT3 were performed at the 1-Ha test site (see Appendix B for a detailed description of the field test and data analysis). Each pumping test included pumping Well 5 (the center well in Figure 4.1) for 6 days, manually monitoring drawdown in the remaining 36 wells, and automatically monitoring

drawdown in 7 of the 36 wells with pressure transducers (Young, 1991a). AT1 and AT3 had constant but different pumping rates. AT2 had a cyclic pumping rate. At late times ( $> 100,000$  s) all three tests provided an effective transmissivity estimate between 32 and 36  $\text{cm}^2/\text{s}$ .

Based on the Theis type-curve fitting in Young (1991a), the arithmetic average of the calculated transmissivities from observation well data from AT1 and AT3 at times 10000, 50000, 100000, and 250000 s are 81, 44, 39, and 36  $\text{cm}^2/\text{s}$ . The decreasing trend in transmissivity values over time occurs because the cone-of-influence started within the highly permeable channel deposits and then gradually expanded into less permeable deposits.

For a saturated aquifer thickness of 6.5 m, the results of the large-scale pumping tests provide a lower value of 0.05 cm/s (i.e.  $32 \text{ cm}^2/\text{s} \div 650 \text{ cm}$ ) and an estimated upper value of 0.125 cm/s (i.e.  $81 \text{ cm}^2/\text{s} \div 650 \text{ cm}$ ) for the  $K_{\text{eff}}$  of the 1-Ha test. Using the weighting scheme of Cardwell and Parsons (1945), the range of 0.0048 to 0.1785 cm/s is calculated for the  $K_{\text{eff}}$  of the 1-Ha test site using the borehole flowmeter K values (based on K values below the 61.0 m MSL water table level for AT1, AT2, and AT3). Because this range includes the range calculated from the large-scale pumping tests, the magnitude of the flowmeter K values appear reasonable.

Using K values from CJ transmissivities from the low-rate single-well pumping tests, an equivalent set of CJ-flowmeter K values were generated. Using the weighting scheme of Cardwell and Parsons (1945), the CJ-flowmeter K values have a range of 0.0003 to 0.0278 cm/s for  $K_{\text{eff}}$ . Because the upper limit of this range lies below the lower limit of the range from the large-scale pumping test, the CJ-flowmeter K values are too low—a result

consistent with the presumption that low-K skin effects exist and cause problems with using the CJ equation for flowmeter analysis.

#### **4.7.2 Results from Small-Scale Recirculating Tracer Tests**

Tracer tests 1 to 3 (Table 4.1) were designed to collect concentration breakthrough data from the most contiguous permeable zone between wells. Each test included establishing a steady flow field, introducing a tracer slug in the injection well, and monitoring tracer breakthrough at the observation wells. Appendix E provides a detailed description of the field test and data analysis. Table 4.2 lists the arrival times and magnitudes of the peak concentrations predicted using the numerical model and aquifer conditions described previously. The predicted values are compared to values obtained from the tracer concentrations in the total discharge from the withdrawal wells. The order-of-magnitude differences between the predicted and the measured arrival times suggests preferential flow paths between wells.

Evidence of preferential groundwater flow exists in both the flowmeter and concentration profiles taken during the tracer tests. As an example, Figure 4.6 provides the flowmeter profiles for Tracer Test 1. The data indicates that the two main intervals of groundwater transport are located near 56 and 59 m MSL. To monitor the tracer breakthrough at selected aquifer zones, multi-level samplers were installed in the wells and sampled with a network of peristaltic pumps.

Figure 4.7 shows examples of tracer breakthrough data for Tracer Tests 1 to 3 at selected wells. The results indicate that the tracer moved preferentially through laterally



contiguous zones of high-K material. At the zones of preferred tracer movement, sufficient data exists to estimate a minimum K value required to produce the observed tracer breakthrough times. To estimate this K value, horizontal groundwater flow is presumed. With this presumption, Equation 4.5 can be used to calculate a lower K value for the aquifer intervals with the tracer breakthrough data.

**Table 4.1 Description of Tracer Tests**

Test	Tracer Volume (liters)	Tracer Conc. (mg/L)	Injection Well	Pumping Well(s)
1	1744	800	16 @ 37.8 L/min <sup>1</sup>	5, 13, 14, 19
2	4077	800	12 @ 30.9 L/min <sup>1</sup>	10, 8, 24, 25
3a	1218	800	21 @ 11.4 L/min	17
3b	3247	800	18 @ 18.9 L/min	2
3c	3247	800	20 @ 18.9 L/min	11
5	21200	1500	5 @ 106 L/min <sup>1</sup>	1, 3, 7, 9

<sup>1</sup> Pumping wells supplied equal amounts to meet the injection rate.

- Notes: a) Bromide was tracer for tests 1 - 3.  
 b) Chloride was tracer for test 5.  
 c) Tracer Test 4 not discussed in dissertation  
 d) For Tracer Tests 1 to 3, no monitoring wells were located between the injection and the withdrawal well.  
 e) Radial distance from injection well to withdrawal well varied from 3.5 to 6.75 m for tests 1 - 3.

**Table 4.2 Magnitudes and Arrival Times of Peak Tracer Concentrations for Tracer Tests 1 to 3**

Tracer Test	Withdrawal Well (radial distance from injection well)	Predicted for a Homogeneous Aquifer <sup>1</sup>		Measured in the Total Discharge <sup>2</sup>	
		Hours	mg/L	Hours	mg/L
1	5 (r = 4.6 m)	44	18	3.2	13
	13 (r = 3.86 m)	27	25	<1.3	>56
	14 (r = 3.61 m)	23	31	1.5	122
	19 (r = 3.66 m)	23	31	<1.0	>148
2	8 (r = 6.25 m)	97	25	8.1	59
	10 (r = 4.39 m)	41	64	<2.6	>163
	24 (r = 3.64 m)	26	70	16.0	59
	25 (r = 6.13 m)	74	20	2.1	63
3	2 (r = 6.72 m)	86	20	9.8	4.0
	11 (r = 6.15 m)	71	23	2.9	62
	17 (r = 5.16 m)	89	12	25.6	14

<sup>1</sup> Based on 15-minute averages.

<sup>2</sup> Sampling frequency was approximately one sample per hour.

In Equation 4.5,  $R$  is easily measured and  $t_p$  is estimated from the tracer breakthrough curves. The value of  $J_t$  cannot be measured. However, because a tracer particle spends proportionally more time in the regions of low gradients (near the midpoint of two wells) than of high gradients (near each well), an upper bound for  $J_t$  is  $J_s$ . In solving Equation 4.5,  $J_s$  was used for  $J_t$ . The value for  $J_s$  was calculated from the constant water table elevations at the injection well and at the appropriate withdrawal well. The effective porosity  $\eta$  was set

to 0.3 based on results of 84 minimally-disturbed soil cores from the nearby MADE site (Boggs et al., 1992).

$$K = \frac{R \cdot \eta}{t_p \cdot J_t} \quad (4.5)$$

- where:
- K** = lower value for the average hydraulic conductivity of the aquifer zone of tracer transport
  - R** = distance between the wells
  - t<sub>p</sub>** = time of peak tracer concentration (note: t<sub>p</sub> is greater than the time required for a tracer particle to move between the two wells along the shortest streamline)
  - η** = effective porosity
  - J<sub>t</sub>** = the average spatial horizontal hydraulic gradient, J<sub>s</sub>, experienced by a tracer particle. In a uniform flow field, J<sub>t</sub> = J<sub>s</sub>. For a converging or diverging flow field, an upper bound for J<sub>t</sub> is J<sub>s</sub>.

In Figure 4.8, the tracer-based K values are compared with the borehole flowmeter K values at corresponding elevations at the injection and withdrawal wells. In general, the tracer-based K values are within a factor of 2 of the borehole flowmeter K value at the withdrawal well. Given the large horizontal and vertical variability in the aquifer's physical parameters, the comparisons in Figure 4.8 are very good. The tracer breakthrough data illustrates the need for three-dimensional K values and also supports the magnitudes of the borehole flowmeter K values.

#### **4.8 CONCLUSIONS**

Results of recirculating tracer tests at Columbus AFB demonstrate that the arrangement of high-K deposits greatly impact groundwater flows at the scales of 3 to 50 meters. Results of field tests show that the borehole flowmeter method is effective for identifying regions of high-K deposits. Because the aquifer is highly heterogeneous and the low-K skin effects exist at the wells, alternative methods for analyzing flowmeter data can lead to very different K values. At Columbus, the  $K_1/K$  profile approach is used with  $K$  determined from a Cooper-Jacob Straight-Line (CJSL) analysis of a short-term pumping test. An implication of the field tests is that because preferential flow in high-K deposits can significantly impact groundwater transport, borehole flowmeter data or some type of comparable data would help improve the design of groundwater remediation systems in heterogeneous fluvial aquifers.

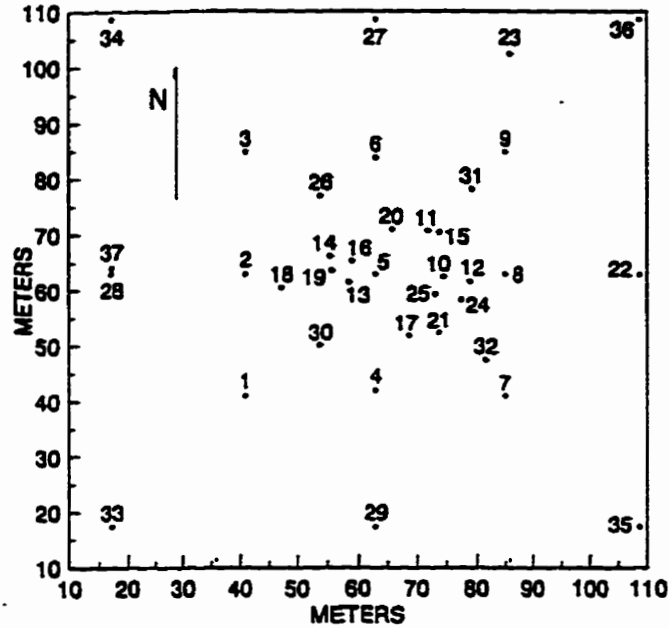


Figure 4.1 Network of 37 fully-penetrating wells at the 1-Ha test site at Columbus AFB, Mississippi (see Figure 3.8 for location at CAFB).

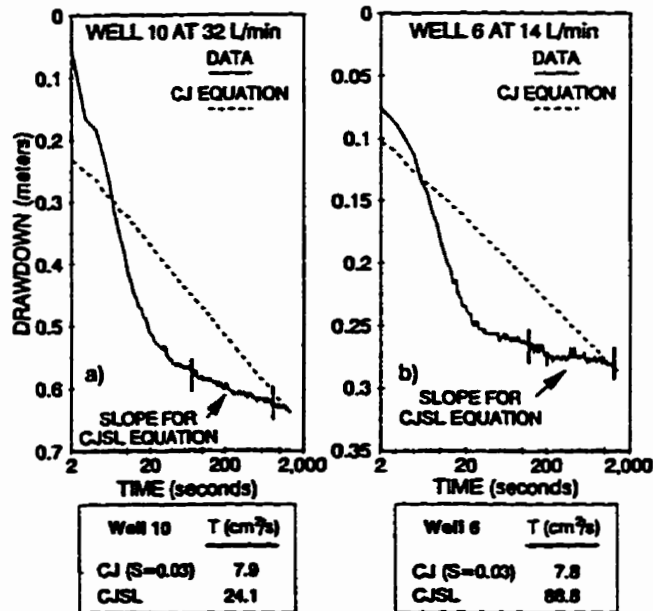


Figure 4.2 Application of the Cooper-Jacob (CJ) equation and the Cooper-Jacob Straight-Line (CJSJ) method for calculating transmissivity values for two sets of single-well drawdown data.

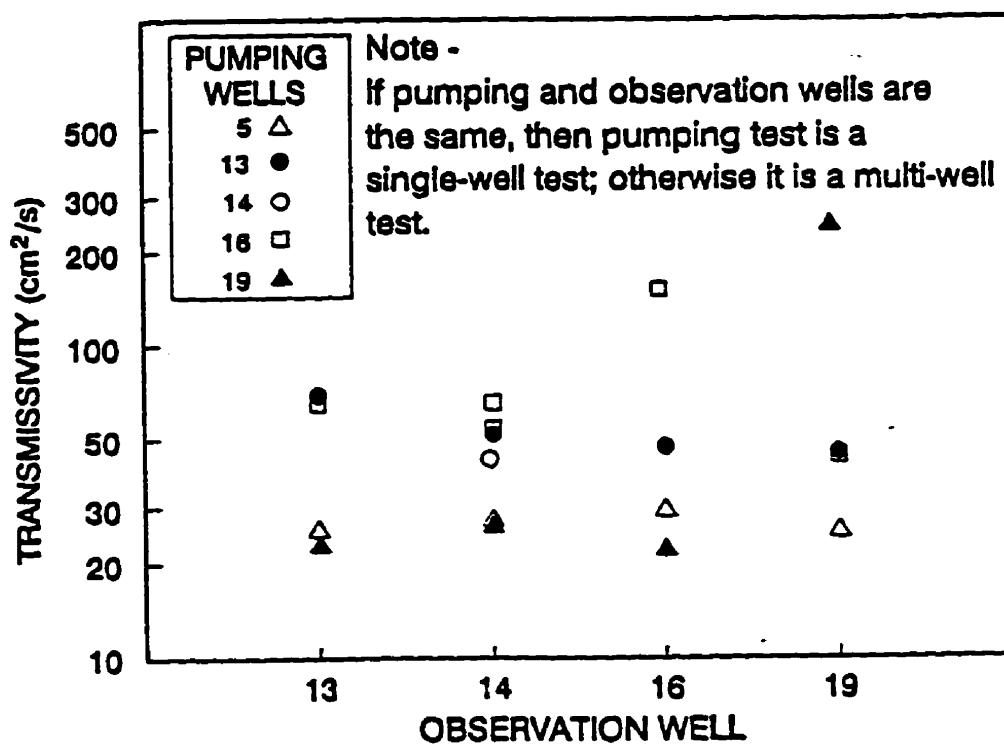


Figure 4.3 The effect pumping well location on the calculated transmissivity at four observation wells. Data from Young (1991a,b). Calculated transmissivity values are from Theis type-curve matching for multi-well pumping tests and from Cooper-Jacob Straight-Line (CJSL) analyses for the single-well pumping tests.

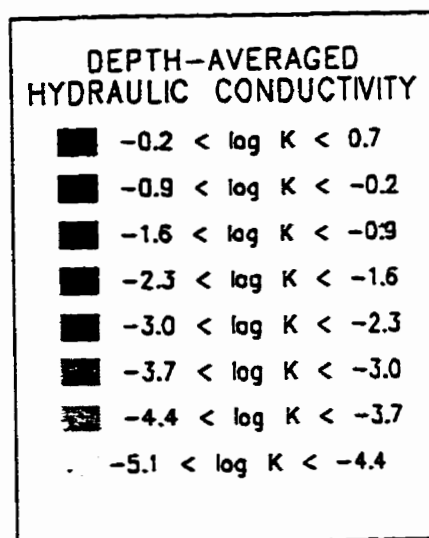
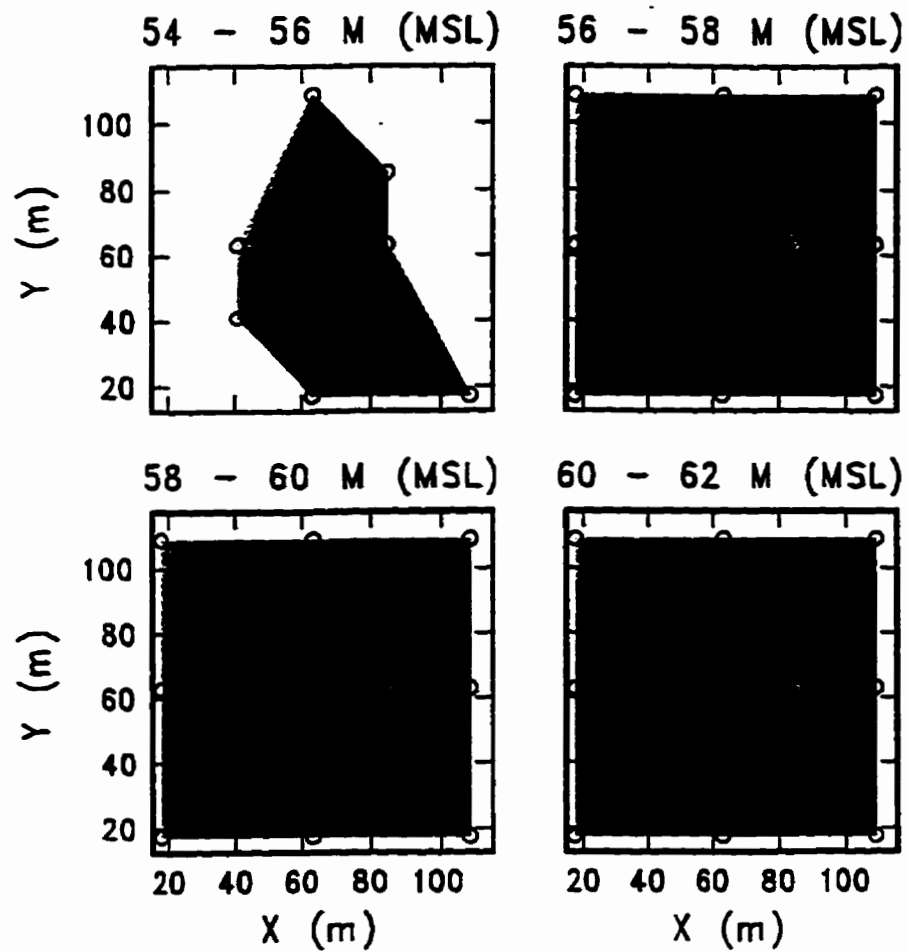
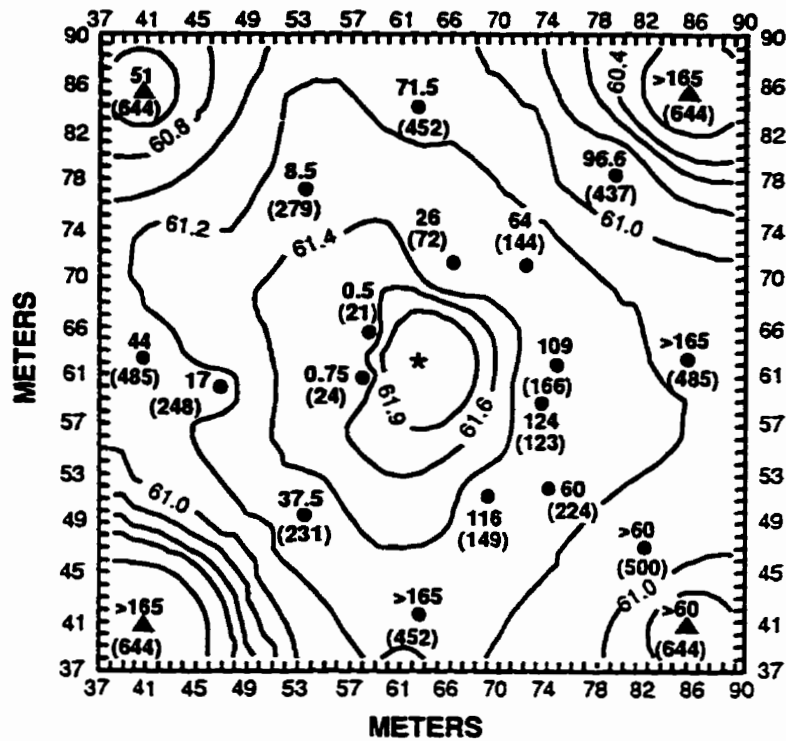


Figure 4.4 Depth-averaged  $\log(K)$  cross sections based on the 881 borehole flowmeter hydraulic conductivity values. Circles denote well locations.



- \* INJECTION SITE (Q = + 106 Liters/Min.)
- ▲ WITHDRAWAL WELL (Q = -26.5 Liters/Min.)
- MONITORING WELLS WITH MULTI-LEVEL SAMPLERS
- ~61~ POTENTIOMETRIC CONTOUR (m MSL)
- NOT IN ( ) - ARRIVAL TIME MEASURED IN FIELD
- IN ( ) - ARRIVAL TIME PREDICTED FOR HOMOGENEOUS AQUIFER

Figure 4.5 Measured and predicted times for peak chloride concentrations across the well network for Tracer Test 5, a large-scale recirculating tracer test with a central injection well and four withdrawal wells. Chloride data collected from multi-level samplers installed at all well locations. Potentiometric contours represent steady-state conditions during Tracer Test 5.

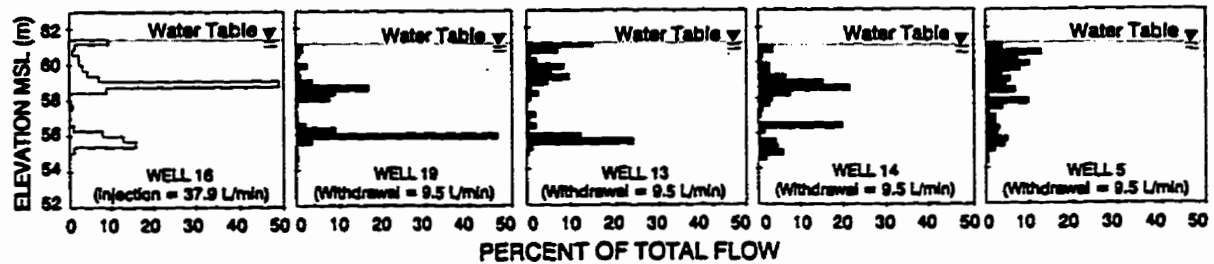


Figure 4.6 Profiles of the steady-state horizontal flow as measured by the electromagnetic borehole flowmeter at injection well 16 and the four withdrawal wells during the recirculating Tracer Test 1.



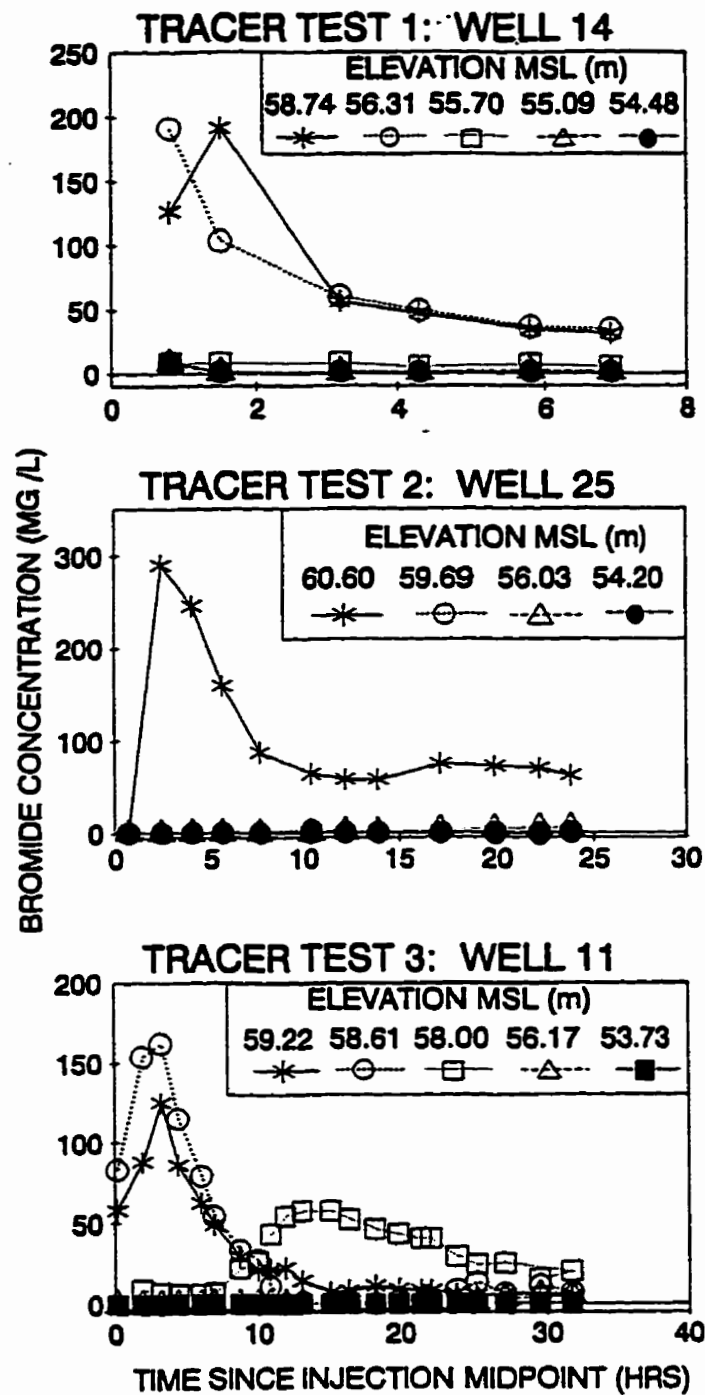


Figure 4.7 Examples of tracer breakthrough data collected with multi-level samplers in withdrawal wells for Tracer Tests 1, 2, and 3.

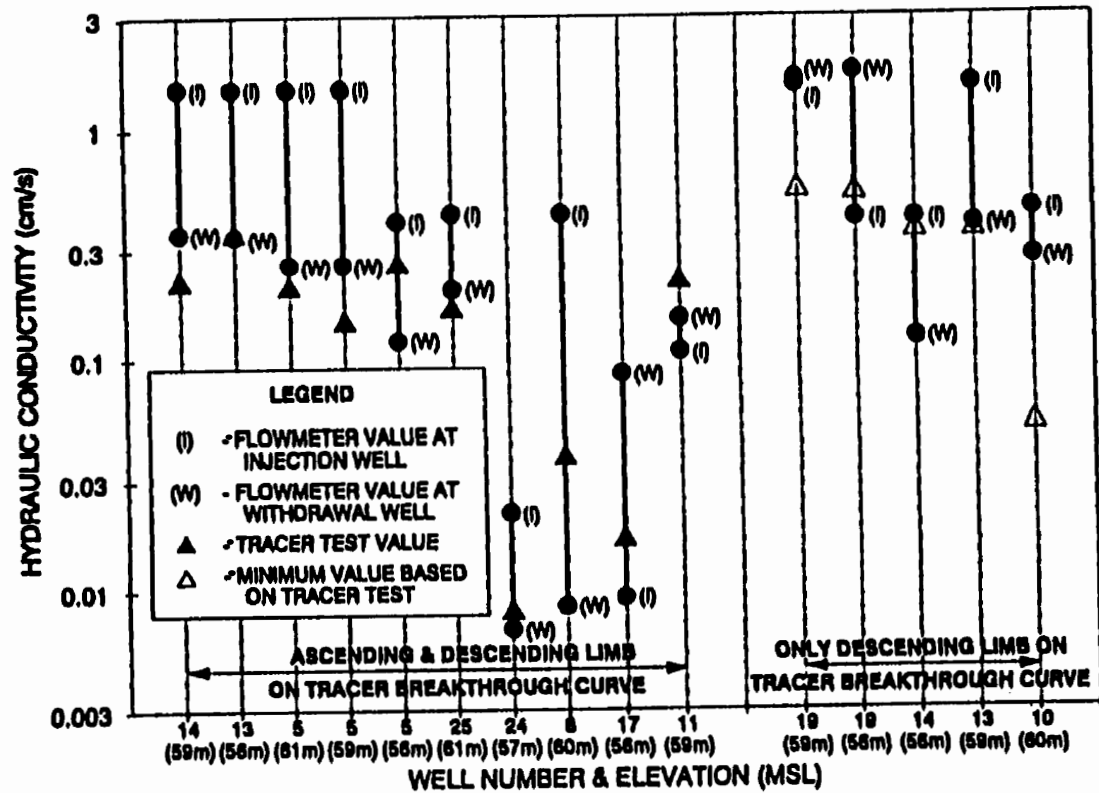


Figure 4.8 Lower estimate of hydraulic conductivity based on tracer test data compared to borehole flowmeter hydraulic conductivity values for selected aquifer intervals of rapid tracer transport between wells observed during Tracer Tests 1-3.

## **5. POSITIVE SKIN EFFECTS**

### **5.1 INTRODUCTION**

An important assumption regarding the analysis of slug tests, pumping tests, and borehole flowmeter tests is a good hydraulic connection between the well and the adjacent aquifer. Positive skin effects are the result of a reduction in hydraulic conductivity,  $K$ , near a well caused by drilling and/or well installation. If positive skin effects are not identified or minimized, then errors may be introduced in the analysis of field data.

The chapter focuses on the impacts that positive skin effects have on hydraulic well tests at Columbus Air Force Base (CAFB), Mississippi. Field data were collected from two sets of wells. One well set included 37 wells scattered across a 1-Ha test site intersected by a paleochannel. The other well set included seven pairs of closely-spaced wells located within and near a 300-m long section of the paleochannel. Before presenting well test results, the paper provides a general overview of the CAFB aquifer and the well installations. These overviews are provided because aquifer characteristics as well as drilling methods, backfill materials, and well development procedures contribute to the formation of positive skins. Well test results are then presented to illustrate approaches for detecting positive skin effects and to demonstrate that unrepresentative aquifer  $K$  values can be calculated from well test data if positive skin effects are ignored.

## **5.2 BRIEF DESCRIPTION OF SITE CONDITIONS**

### **5.2.1 The CAFB Aquifer**

Shown in Figure 5.1 is a paleochannel that intersects two tests sites at CAFB. Based on information in chapters 3 and 4, the simple sedimentological model in Figure 5.2 is proposed for the CAFB aquifer. At the base of the paleochannel are coarse-grained channel lag, scour pool, and chute bar deposit, whose location in a coarse-grained meandering system are shown in Figures 5.3 and 5.4. Above these deposits are fine-grained flood deposits that filled the meander channel after its abandonment. Associated with the convex regions of the paleochannel are pointbar deposits. Associated with the concave regions of the paleochannel are floodplain and backwater deposits. Based on borehole flowmeter tests and geometric relationships for meander channels provided by Leeder (1973), the base of the paleochannel has been estimated near 59 m MSL in Chapter 4. Below 59 m MSL, the aquifer is presumed to be a mixture of braided and/or meandering river environments.

The effective transmissivity of the CAFB at the regional scale has been estimated at  $30 \text{ cm}^2/\text{s}$  using the late-time results of drawdown responses from large-scale pumping tests discussed in Appendix B. Large-scale trends in aquifer properties inferred from early-time drawdown responses from the pumping tests in Chapter 6 and from borehole flowmeter tests in Figure 5.5 suggest a correlation between large-scale  $K$  patterns and the paleochannel. Specifically, high  $K$  values (e.g. 1.0 to .1 cm/s) are associated with the paleochannel coarse-grained deposits, low  $K$  values (e.g.  $\leq 0.001$  cm/s) are associated with the fine overbank deposits in the concave region of the paleochannel, and moderate  $K$  values (0.02 to 0.002 cm/s) are associated with point bar deposits in the convex region of the paleochannel.

### **5.2.2 Test Sites**

The 37 wells at the 1-Ha test site (Figure 5.5) were installed in 1988 and 1989. Rotary wash, air percussion, cable tool, and hollow stem auger drill methods were used to install 11, 14, 7, and 5 of the wells, respectively. All wells were constructed from schedule 40 PVC pipe with 0.025-cm slots at 0.318-cm spacings and backfilled with disturbed aquifer material (e.g. natural backfill). Each well was developed for approximately 3 hours using over pumping, back washing, and mechanical flushing (Young, 1991a; Young et al. 1993a; Rehfeldt et al. 1989). All wells were constructed from schedule 40 PVC pipe with 0.025-cm slots at 0.318-cm spacings.

Analyses of borehole flowmeter tests performed at the MADE site (Rehfeldt et al., 1992) and the and 1-Ha test site (Young, 1995) produced different conclusions regarding the importance of positive skin effects and the hydrological significance of the paleochannel. To help resolve the cause for the differences, seven pairs of closely-spaced wells were located at positions shown in Figure 5.1. For each well pair, a well was installed through a 15.2-cm OD hollow-stem auger and backfilled with disturbed aquifer material and another well was installed through a 30.5-cm OD hollow-stem auger and backfilled with pea-gravel.

## **5.3 INVESTIGATIVE APPROACH**

### **5.3.1 Previous Investigations**

Previous investigations concerning positive skin effects at CAFB have focused on well development (Rehfeldt et al., 1989; Young et al., 1993a). Field tests included performing flowmeter tests after well installation, after initial well development, and after

additional cycles of well development. At most of the wells, large differences were observed between flowmeter profiles for no well development and for 1-hour of well development. The differences observed among the sequences of flowmeter profiles suggest that well development is achieved with a three-hour protocol involving over pumping, back flushing, and mechanical surging. Result of the investigations indicate that well development beyond the protocol had only a minimal impact on borehole flowmeter profiles. Because of concerns regarding positive skin effects, the author has performed additional well development studies involving hydraulic jetting. These test results indicate that minor benefits, if any, would be gained by the addition of hydraulic jetting to the well development protocol. An important conclusion from these investigation is that wells at CAFB have been properly developed.

### **5.3.2 Vertical Heterogeneity Influence on Positive Skin Effects**

In heterogeneous aquifers similar to the CAFB aquifer, the K for the backfill material should be greater than the K of the most permeable aquifer deposits near the well. If this not be the case, the backfill material will partially obstruct the hydraulic connection between the aquifer's permeable zones and the well screen. If sufficient low-K material is relocated between the aquifer's high-K zones and the well screen, then a positive skin effect will be produced.

Because natural backfills were used at CAFB, positive skins are likely to form where thick zones of low-K material overlie high-K deposits. A location where this situation is prevalent is in the paleochannel. In the paleochannel, high-K channel-lag deposits directly underlie several meters of low-K channel-fill deposits. As part of the data analysis, the well

location relative to the paleochannel will be considered as a factor that affects the formation of positive skin effects.

### **5.3.3 Positive Skin Effects Impact on Calculated Transmissivity Values**

Three approaches commonly used to calculate transmissivity values are the Cooper-Jacob (CJ) equation (Cooper and Jacob, 1946), the Cooper-Jacob straight line (CJSL) method (Cooper and Jacob, 1946), and type-curve matching with the Theis solution (Theis, 1935). For an ideal pumping test response from a homogeneous aquifer, the calculated CJ, Theis, and CJSL transmissivity values should be the same because they are based on the Theis (1935) well solution. As discussed by Butler (1990), transmissivity values calculated from these methods can differ in a non-uniform transmissivity field because the approaches weight portions of the drawdown data differently. For instance, the CJ equation includes total drawdown but ignores the rate of change in drawdown whereas the CJSL methods includes the rate of change in drawdown but ignores the total drawdown.

A consequence of positive skins are head losses near the well during pumping conditions. Because the CJ equation determines transmissivity based primarily on drawdown, a CJ transmissivity based on data from a well with positive skin effect should be lower than the actual aquifer transmissivity. However, because the CJSL method is sensitive to the rate of change in drawdown, which is unaffected by the skin effect at late times, a CJSL transmissivity should be reflective of the aquifer actual transmissivity in spite of positive skin effects. Because it includes both the total drawdown and the rate of change in

the drawdown, This curve-matching should provide transmissivity values between those estimated using the CJ equation and the CJSJ method.

## **5.4 BOREHOLE FLOWMETER TESTS AT THE SEVEN PAIRED WELLS**

### **5.4.1 Drawdown Responses**

Figures 5.7 and 5.8 illustrate pumping test results for two well pairs located inside and two well pairs located outside the paleochannel, respectively. Tables 5.1 and 5.2 summarize the flow rates, total drawdowns, and specific capacities for all of the pumping tests. At the well outside the paleochannel boundaries (well pairs 76 and 78), the backfilled and gravel-packed wells have similar drawdown curves and specific capacities. At the wells that intersect the paleochannel (wells 41 and 72), the natural backfilled wells had more drawdown and 50% lower specific capacities than the gravel-packed wells.

### **5.4.2 Vertical Flow Distributions**

Shown in Figures 5.9 and 5.10 are flow distributions for six of the seven well pairs. Consistent with the drawdown results is that the paired well outside of the paleochannel have similar flow distributions but the paired wells in the paleochannel have different flow distributions. For the paired wells in the paleochannel, the greatest difference in flow between the backfilled and gravel-packed wells occur above the elevation of 60 m MSL—a region associated with the high-K channel lag deposits in the sedimentological model. At the four well pairs located in the paleochannel, the gravel-packed wells had an average of 5.5 times more flow above 60 m MSL than did the naturally backfilled wells.



**Table 5.1 Drawdown Results from Each Well Pair**

Well	In Paleochannel	Flow Rate (lpm)	Drawdown (m) <sup>1</sup>	Specific Capacity (lpm/m)	Transmissivity (cm <sup>2</sup> /s)		
					CJ <sup>2</sup>	CJSL <sup>3</sup>	$\frac{CJ}{CJSL}$
41-gravel pack	Yes	31.1	0.67	107.2	15.6	42.3	0.37
41-backfill	Yes	30.4	0.29	45.6	6.2	32.3	0.19
72-gravel pack	Yes	29.3	0.39	74.6	10.5	51.7	0.20
72-backfill	Yes	26.9	1.76	15.3	2.0	49.1	0.04
73-gravel pack	Yes	30.4	0.38	80.4	11.2	39.1	0.29
73-backfill	Yes	29.8	0.60	49.7	6.8	50.0	0.14
74-gravel pack	Yes	10.3	0.27	38.4	11.2	34.9	0.32
74-backfill	Yes	9.9	0.36	27.5	3.45	38.9	0.09
76-gravel pack	No	20.5	0.65	31.4	3.3	5.3	0.62
76-backfill	No	20.5	0.65	31.3	3.3	5.3	0.62
78-gravel pack	No	14.0	1.65	10.2	1.2	0.92	0.77
78-backfill	No	14.0	1.65	8.5	1.0	0.95	1.05
82-gravel pack	No	18.4	1.21	15.2	1.9	4.7	0.49
82-backfill	No	17.7	1.06	16.7	2.1	4.9	0.43

<sup>1</sup> at 1800 seconds.<sup>2</sup> Cooper-Jacob equation.<sup>3</sup> Cooper-Jacob straight line method.**Table 5.2 Summary of Drawdown Results From the Well Pairs**

	Average Specific Capacity (lpm/m)	Average Transmissivity (cm <sup>2</sup> /s)		
		CJSL	CJ	$\frac{CJ}{CJSL}$
<i>Outside Paleochannel</i>				
Gravel pack	18.9	3.1	2.1	0.68
Backfill	18.8	3.1	2.1	0.68
<i>Within Paleochannel</i>				
Gravel pack	75.2	42.0	12.1	0.29
Backfill	34.5	42.6	4.6	0.11

### 5.4.3 Calculated Transmissivity Values

For all of the 14 wells at well pair locations, CJ and CJS� transmissivity values were calculated from the drawdown data. The CJ transmissivity values were calculated with drawdown values measured at 1800 seconds and an assumed storage coefficient of 0.1 (based on the assumption of Rehfeldt et al., 1992). The CJS� transmissivity values were calculated using the rate of drawdown change for data after an elapsed time of 200 seconds. All pumping-test analyses were performed on drawdown data corrected for dewatering of the unconfined aquifer by applying the Jacob correction factor (Jacob, 1963).

Similar CJS� transmissivity values are calculated at the paired wells in spite of large differences in drawdowns between some of the wells. An extreme instance occurs at well pair 72 where the specific capacity is 5 times greater for the gravel-pack well, but the CJS� transmissivity values near  $50 \text{ cm}^2/\text{s}$  were calculated for both the natural backfilled and gravel-packed wells. As shown in Tables 5.1 and 5.2, the CJS� transmissivities values are near  $3 \text{ cm}^2/\text{s}$  for the wells outside the paleochannel and near  $42 \text{ cm}^2/\text{s}$  for the wells inside the paleochannel. The nearly 15 fold difference in the average CJS� transmissivity values is attributed to the 1- to 2- meter layer of high-K ( $> 0.1 \text{ cm/s}$ ) channel-lag deposits in the paleochannel.

At well pair locations outside the paleochannel, the CJ transmissivity values are about  $1 \text{ cm}^2/\text{s}$  less than the CJS� transmissivity values at both the gravel-packed and naturally backfilled wells. For the wells in the paleochannel, the CJ transmissivity values are about  $30 \text{ cm}^2/\text{s}$  less than the CJS� transmissivity values with greater differences occurring at the naturally backfilled wells.

#### **5.4.4 Discussion of Results**

The possibility that natural backfills promote positive skins was investigated by comparing well responses at closely spaced wells that differed in their backfill material. A premise for the investigation was that if low-K material in the natural backfill partially obstructed flow to the well, then different well responses should occur if the natural backfill was replaced with a high-K gravel pack.

At the well pairs located outside the paleochannel boundaries and thus in a region of relatively low transmissivity, no systematic differences in well responses were evident between the wells with a natural backfill and with a gravel-pack. The similar well responses suggest that the natural backfill has sufficient permeability to avoid contributing to positive skin effects.

At the well pairs located within the paleochannel boundaries and thus in the aquifer's highest transmissivity regions, systematic differences occurred between wells with a natural backfill and with a gravel-pack. At all four well pair locations, the gravel-packed wells had significantly lower total drawdown and higher flows from the channel lag deposits than did the backfilled wells during pumping conditions. Positive skin effects are believed to have been caused during the formation of the natural backfills when low-K, fine-grained deposits from the upper aquifer moved downward into the well annulus where they partially obstruct the hydraulic connection between the high-K channel lag deposits and the well screen.

To help quantify the possible errors to borehole flowmeter K values that positive skin effects could cause, two sets of flowmeter K profiles were calculated using data from wells

at location 73. One K data set is based on the CJ equation and flowmeter data from the naturally backfilled well. The other K data set is based on the CJSL method and flowmeter data from the gravel-packed well. As shown in Figure 5.11, the two data sets differ the most above 59 m MSL. Above 59 m MSL, the CJ K values are often 100 and are occasionally 1000 times smaller than the CJSL K values. Among the implications of such large differences is the representativeness of the borehole flowmeter K values and conclusions presented by Rehfeldt et al., (1992) for the MADE site. The flowmeter K values presented by Rehfeldt et al., (1992) are based on data collected in augured wells with natural backfills and analyzed with the CJ equation. Among the conclusions of Rehfeldt et al., (1992) is that the paleochannel is only a surficial feature.

Although the investigation indicates that the replacement of natural backfill with a gravel-pack reduces positive skin effects, the investigation falls short of indicating that augured wells with gravel packs are free of positive skin effects. The large differences between the CJ and CJSL transmissivity values calculated for the gravel-pack wells in the paleochannel suggest that positive skin effects exist in spite of the gravel-pack. Additional causes for positive skin effects besides backfill material are: 1) head losses associated with groundwater flow through disturbed aquifer material beyond the gravel-pack; and, 2) head losses associated the converging flowpaths required to direct groundwater through the 4% open area of the 0.025-cm slotted PVC well pipe.

With regard to all sources of head losses during pumping, future studies focused on minimizing positive skin effects at CAFB and other tests sites should extend beyond backfill type and include the drilling method and well screen type. Compared to drilling methods that

involve the advancement of a protective casing, auguring causes greater aquifer disturbance (Morin et al., 1988; Keely and Boateng, 1987a,b). Hence, head losses associated with disturbed aquifer material beyond the gravel-pack should be less if wells are installed through a protective casing than through a hollow stem auger. Discroll (1986, pg 405) states that the percentage of open area in a well screen should be at least equal to aquifer porosity, which at CAFB is greater than 30% (Boggs, et al., 1990). Headlosses that occur in and near the well screens in the coarse paleochannel deposits would be reduced by replacing the .25-mm slotted PVC pipe with a .50-mm continuous slotted pipe with an open area of 30%.

## **5.5 WELL TEST RESULTS FROM THE 1-Ha TEST SITE**

### **5.5.1 Approach to Identifying Positive Skin Effects**

In the previous section, positive skin effects were identified by comparing changes in flowmeter test caused by changes in well construction at closely spaced well pairs. In this evaluation, an evaluation was performed on the effect of changes in well construction affects the calculated  $K$  values. An alternative approach to identify positive skin effects is to evaluate how the values of  $K$  associated with a well (or a series of wells) is affected by changes in the well test or by the method of calculating  $K$ . This latter approach includes comparing results from different well tests and/or different analysis methods. An example of the former would be comparing results from slug tests to pumping tests whereas as example of the latter would be comparing results from Theis type-curve matches to Cooper-Jacob straight line fits. The numerous well locations and well tests performed at the 1-Ha test site (see Table 5.3) provides ample opportunity to evaluate whether positive skin effects

are significant by comparison of the trends and statistics associated with different K data sets. Among the most important of the K data sets are those from large-scale pumping tests because these provide the best estimate of the effective K for the 1-Ha test site.

**Table 5.3 Chronology of Different Pumping Tests at the 1-Ha Test Site during 1989**

Well Testing Activity	Dates	Saturated Aquifer Thickness
Slug Tests	April 18	7.2 m
Borehole Flowmeter Measurements	April 20-28	7.1 m
Multi-well Pumping Tests		
AT1	May 18-23	6.7 m
AT2	June 1-6	6.6 m
AT3	June 30-July 7	6.5 m
Multi-rate Single-Well Pumping Tests		
Phase 1	June 13-29	6.6 m
Phase 2	July 14-28	6.5 m

### 5.5.2 Large-Scale Aquifer Tests

During June and July 1989, Aquifer tests AT1, AT2, and AT3 were performed at the 1-Ha test site (see Appendix B). Each pumping test included pumping Well 5 (the center well in Figure 5.6) for 6 days, manually monitoring drawdown in the remaining 36 wells, and automatically monitoring drawdown in 7 of the 36 wells with pressure transducers (Young, 1991a). AT1 and AT3 had constant but different pumping rates. AT2 had a cyclic pumping

rate. At late times ( $> 100,000$  s) all three tests provided an effective transmissivity estimate between  $32$  and  $36$   $\text{cm}^2/\text{s}$ .

Based on the Theis type-curve fitting in Young (1991a), the arithmetic averages of the calculated transmissivities from observation well data from AT1 and AT3 at times 10000, 50000, 100000, and 250000 s are 81, 44, 39, and 36  $\text{cm}^2/\text{s}$ . The decreasing trend in transmissivity values over time is attributed to the cone-of-influence beginning in the highly permeable channel deposits and then extending to less permeable deposits. Figure 5.12 illustrate these slope changes for AT3. A detailed explanation for the slope changes is provided by Young(1991b), who discusses the effects of transmissivity variations at CAFB on observed changes in drawdown slope for several pumping tests. For a saturated aquifer thickness of 6.5 m at the test site, the results of the large-scale pumping tests provide a lower value of 0.05 cm/s (i.e.  $32 \text{ cm}^2/\text{s} \div 650 \text{ cm}$ ) and an estimated upper value of 0.125 cm/s (i.e.  $81 \text{ cm}^2/\text{s} \div 650 \text{ cm}$ ) for the  $K_{\text{eff}}$  of the 1-Ha test site.

### 5.5.3 Evaluation of Drawdown Data

In an effort to evaluate the sensitivity of calculated hydraulic parameters to pumping rates (to be discussed in Chapter 7), approximately 3 pumping tests were completed at each of the 37 wells. For the 115 pumping tests, transmissivity values were calculated using the CJ equation (Cooper and Jacob, 1946), the CJSL method (Cooper and Jacob, 1946), and curve matching with the Theis solution (Theis, 1935). The CJSL method was applied to between 200 seconds and 1000 seconds. The CJ-equation was applied with the drawdowns at 1200 seconds and a storage coefficient of 0.03, which was calculated from large-scale

pumping tests at the 1-Ha test site (Young, 1991a,b). The Theis equation was fitted to the drawdown curve from 10-30 seconds (time after which wellbore storage effects should be negligible) to 1000 seconds. For completeness, Theis type-curve matching was performed on a linear as well as on a logarithmic time scale. The linear scale has the effect of weighting late-time data more than the logarithmic scale. Figure 5.13 illustrates the results produced by applying these techniques to example drawdown curves.

For a homogeneous aquifer, a semilog plot of the time-drawdown response should plot as a straight line after an elapsed time greater than  $r^2S / .04T$ , where  $r$  is the well radius,  $S$  is the storage coefficient, and  $T$  is the transmissivity (Cooper and Jacob, 1946). However, for almost all of the pumping tests the actual time before the drawdown data approximates a straight-line is 10 to 1000 times greater than the theoretical time as determined from the values of  $S$  and  $T$  calculated from the Theis curve matches. This delay suggests that a low- $K$  region exists near the well.

Figure 5.14 compares the CJ and Theis transmissivity values to the CJSL transmissivity values. As may be expected for wells with positive skin effects, the CJ and the CJSL transmissivity values had the lowest and highest averages, respectively. On average, the CJSL transmissivity values were about 8 times greater than the CJ transmissivity values. Based on the results from the closely spaced well pairs, the greatest differences between the CJ and CJSL transmissivities should occur in the paleochannel. The test results confirm this expectation as the wells with the largest differences were all located in the paleochannel.

The geometric means for the transmissivity values calculated from the lowest-rate pumping test data are 37, 11, 10, and 7  $\text{cm}^2/\text{s}$  for analyses based on the CJSL method, log-



Theis type matching, linear-Theis type matching, and the CJ equation, respectively. Given a lower bound of  $33 \text{ cm}^2/\text{s}$  for the average transmissivity of the 1-Ha test site based on large-scale pumping test at the site (Young, 1995a, 1991a,b), the CJ and Theis transmissivity values appear too low whereas the CJSL transmissivity values appear reasonable. These results support the hypothesis that at wells with positive skin effects, the CJSL transmissivity values are more representative of the actual aquifer transmissivity values than CJ transmissivity values.

#### **5.5.4 Statistical Properties of the Borehole Flowmeter K Values**

Without imposing any constraints on the hydraulic conductivity field, Cardwell and Parsons (1945) show that for radial flow, the effective hydraulic conductivity,  $K_{\text{eff}}$  of a heterogeneous aquifer is bounded by the harmonic and arithmetic spatial averages of conductivity weighted by the inverse square of their radial distance from the pumping well. Cardwell and Parsons (1945) define  $K_{\text{eff}}$  of the aquifer as the K that gives the same flux under the mean spatial gradient between the well and the radius-of-influence. Using results from large-scale pumping tests, a  $K_{\text{eff}}$  can be calculated and compared to the weighted harmonic and arithmetic averages of the borehole flowmeter K values. For this comparison, a set of borehole flowmeter K values were calculated based on the CJ and CJSL transmissivities from the low-rate pumping tests.

Figure 5.15 shows the range for  $K_{\text{eff}}$  calculated from the large-scale pumping test data and from the weighting scheme of Cardwell and Parson (1945) for the CJ-flowmeter K and the CJSL-flowmeter K values. The data shows that with respect to the results from the large-

scale pumping tests, the CJSL K values appear reasonable but that the CJ K values appear too low. This result indicates that positive skin effects are introducing a low bias into the CJ borehole flowmeter K values.

### 5.5.5 Transmissivity Values From Slug Tests

Slug tests were conducted by injecting 23 liters of water into a well and monitoring the water-level changes with a pressure transducer. Figure 5.16 provides example well responses. The responses in Figure 5.16 are typical of those predicted by Hvorslev (1951), who assumed negligible aquifer storage and a finite radius-of-influence. Given the good agreement between theory and observation, a Hvorslev solution from Thompson (1987) was used to calculate a transmissivity value from the slug-test data. The arithmetic and geometric mean for the transmissivity values are 3.5 and 3.2 cm<sup>2</sup>/s, respectively. These values are approximately 10 times less than the effective transmissivity values from the pumping tests.

A possible cause for the straight-line responses in Figure 5.16 are positive skins effects. Using a solution by Cooper et al., (1967) that accounts for aquifer storage and has an infinite radius-of-influence, Chirlin (1989) shows that for a fully-penetrating well in an unconfined isotropic aquifer with a storage coefficient greater than 0.001, slug test responses should plot with a concave curvature. Hyder et al., (1994) and Hyder and Butler (1994) show that a straight-line slug test response for a well fully penetrating an unconfined aquifer can be caused by a positive skin effect characterized by a small finite radius with negligible storage properties. Hyder et al., (1994) suggest that indicators of positive skin effects are a good

Hvorslev fit and a systematic deviation between the Cooper et al., (1967) model and the slug test data.

The conclusion that the slug test transmissivity values are more reflective of a low-K zone near the wells than the natural aquifer can be explained by the numerical simulations of Faust and Mercer (1984). These simulations show that if positive skin effects exist at the well, then the transmissivity calculated from a slug test is more likely to reflect the properties of the disturbed rather than the undisturbed aquifer.

#### **5.5.6 Discussion of Results**

Evidence that positive skin effects exist at most, if not all, of the 37 wells at the 1-Ha test site include: 1) slug-test transmissivity values that typically range from 1 to 3  $\text{cm}^2/\text{s}$ ; 2) good matches between the Hvorslev solution and slug-test data; 3) delays in the linear behavior of the semilog time-drawdown plot of the pumping test data; 4) CJ transmissivity values from pumping tests that are typically below 10  $\text{cm}^2/\text{s}$ ; 5) an unreasonably low values of  $K_{\text{eff}}$  based on CJ borehole flowmeter K values; 6) order of magnitude differences between CJ and CJSL transmissivity values calculated from the same data; 7) CJSL transmissivity values from pumping test that are typically above 30  $\text{cm}^2/\text{s}$ ; and, 8) a reasonable range for  $K_{\text{eff}}$  based on CJSL borehole flowmeter K values.

#### **5.6 CONCLUSIONS**

Significant positive skin effects exist at some of the naturally backfilled wells at CAFB. Notable impacts that are caused by positive skin effects at CAFB include the reductions in

specific capacity values, low transmissivity values from slug tests, differences between CJ and CJSJL transmissivity values, and changes in the borehole flowmeter flow profiles. Well development studies suggest that over pumping, mechanical surging, back flushing or hydraulic jetting can not totally remove the skin effect caused by a natural backfill.

Two factors that contributed to the formation of positive skin effects were the site location and the material used to backfill the well. Outside of the paleochannel boundaries, the aquifer permeability is sufficiently low and/or uniform so that positive skin effects do not appear to exist at wells with either a natural backfill or a gravel-pack. Within the paleochannel boundaries, positive skin effects occurred at the natural backfilled wells. A cause for these positive skin effect appears to be partial blockage of the hydraulic connection between high-K channel lag deposits and the well screen by low-K material in the backfill that was relocated during well installation. Within the paleochannel, the replacement of the natural backfill with a gravel pack reduced the positive skin effects.

One impact from positive skins is an increased drawdown during pumping. If not recognized, the increased drawdowns will cause the aquifer transmissivity to be underestimated if the CJ equation is used to calculate transmissivity. As shown with field data in this paper, an appropriate method for calculating transmissivity from drawdown at wells with positive skin effect is the CJSJL method. At both the MADE and 1-Ha test site, the CJSJL method was successfully used to negotiate positive skin effects and produce a representative transmissivity for the undisturbed aquifer material.

A second impact of positive skin effects is changes in the distribution of horizontal flow to a well during pumping. At CAFB, this impact cannot be quantified but is known to

preferentially hinder flow from the aquifer's most permeable layers. Because this second impact cannot be properly negotiated with any analysis technique, proper well installation and development is a prerequisite for representative borehole flowmeter results. Methods useful for detecting positive skin effects at CAFB that may prove useful at other sites include: comparison of transmissivity values calculated from different methods from the same drawdown curve; comparison of well responses from closely spaced wells of different well construction; and, comparison of well responses from hydraulic tests with different volumes of influence.

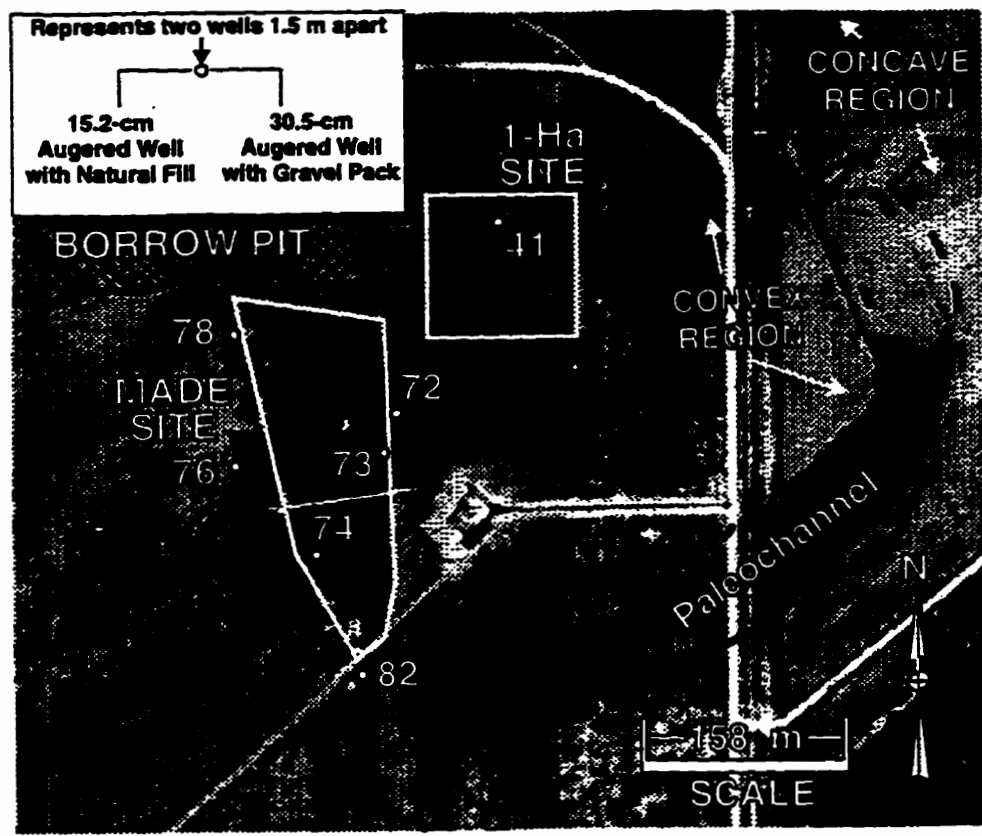


Figure 5.1 Aerial photograph of CAFB site showing locations of the 1-Ha test site and seven well pairs relative to the paleochannel.

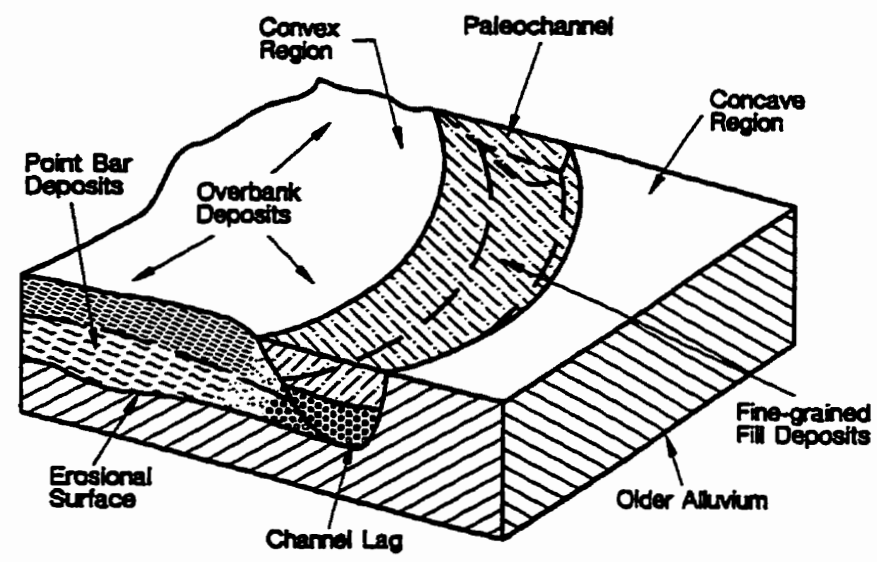


Figure 5.2 Schematic of the regional features associated with the sedimentological model.

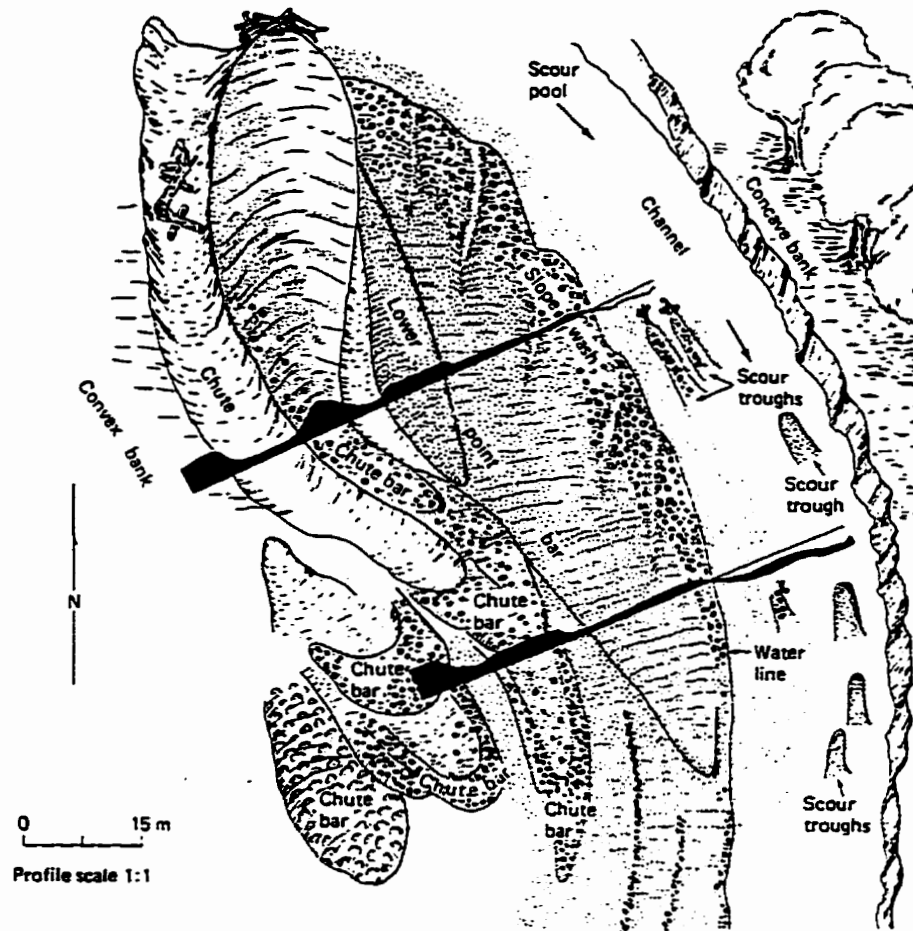


Figure 5.3 Coarse-grained point bar, showing sediment bodies and related features (after McGowen and Garner, 1970).

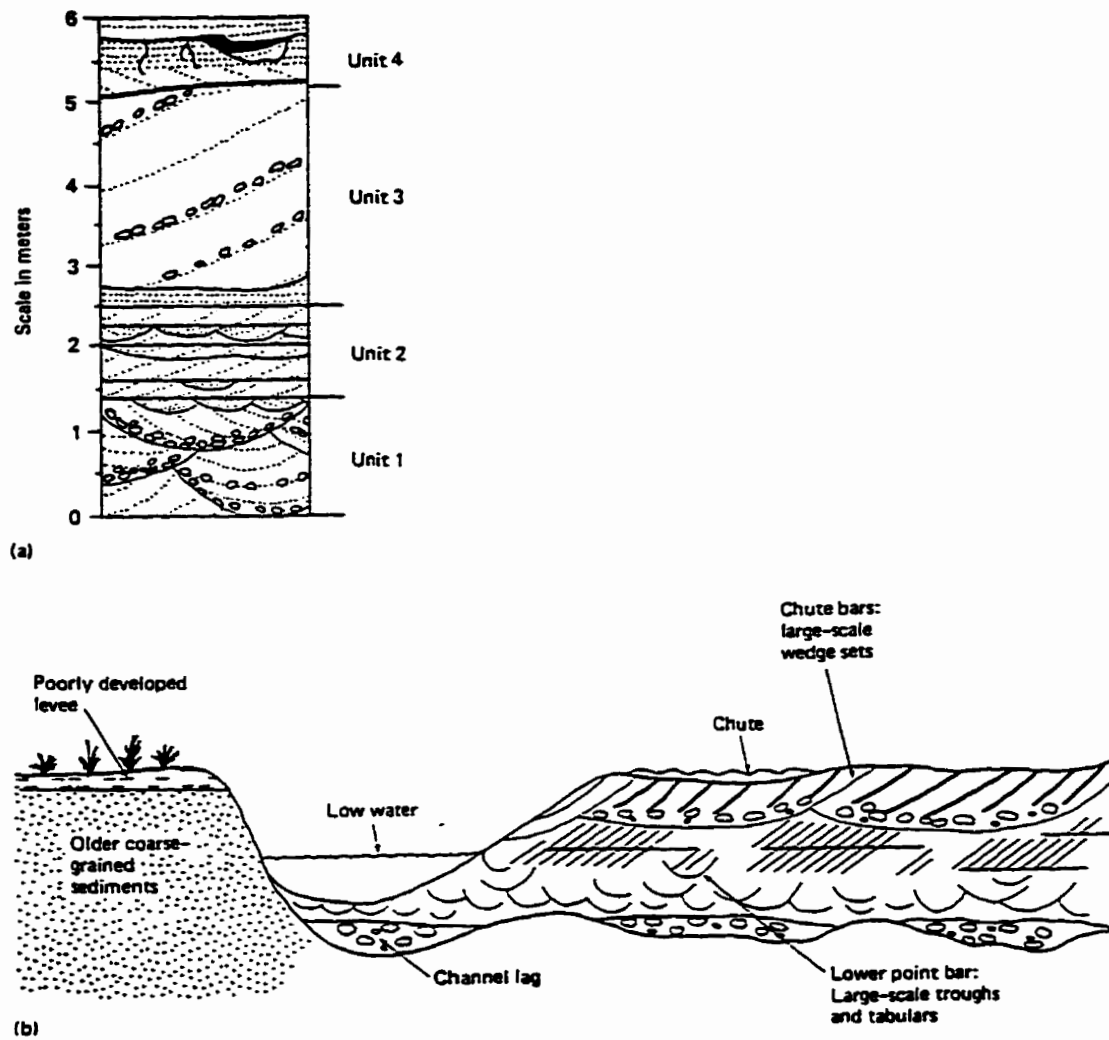


Figure 5.4 (a) Vertical sequence that characterized coarse-grained point bars. The four units represent scour pool deposits (1), lower point bar (2), chute bar (3), and floodplain (4) (Modified from McGowen and Garner, 1970.)  
 (b) Generalized cross section shows a transverse profile across the coarse-grained point bar. (Modified from Brown et al., 1973.)



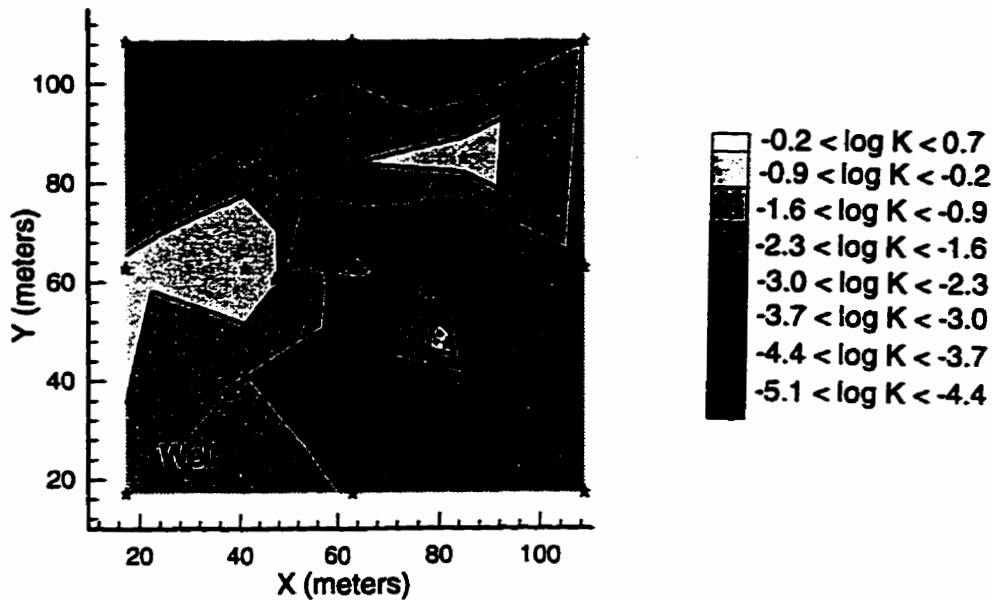


Figure 5.5 Average borehole flowmeter K values for the interval of 60 to 62 m MSL at the 1-Ha test site (from Chapter 4).

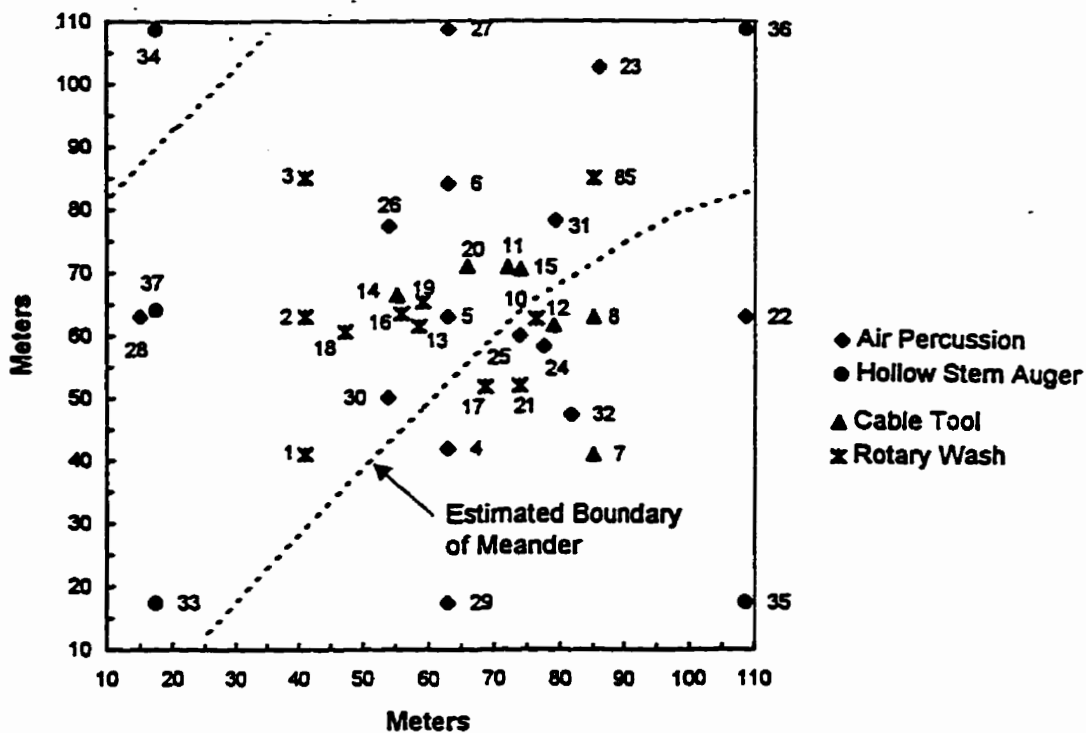


Figure 5.6 Location of 37 wells at the 1-Ha test site.

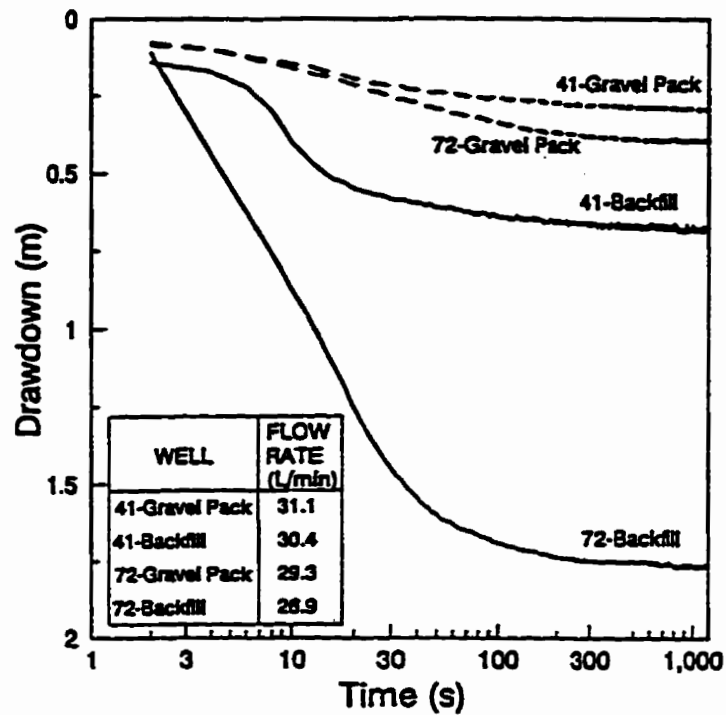


Figure 5.7 Drawdown results for gravel-packed and naturally-backfilled wells at locations 41 and 72 inside the paleochannel (see Figure 5.1 for well placement).

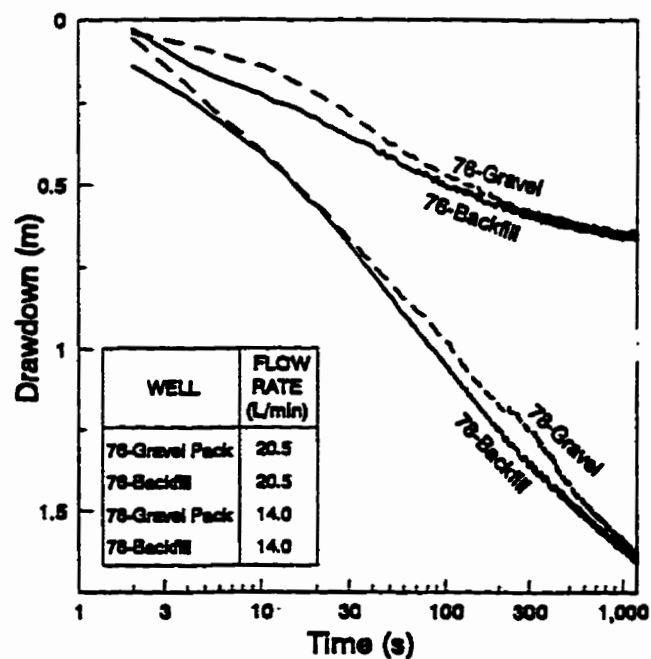


Figure 5.8 Drawdown results for gravel-packed and naturally-backfilled wells, the locations 76 and 78 outside the paleochannel (see Figure 5.1 for well placement).

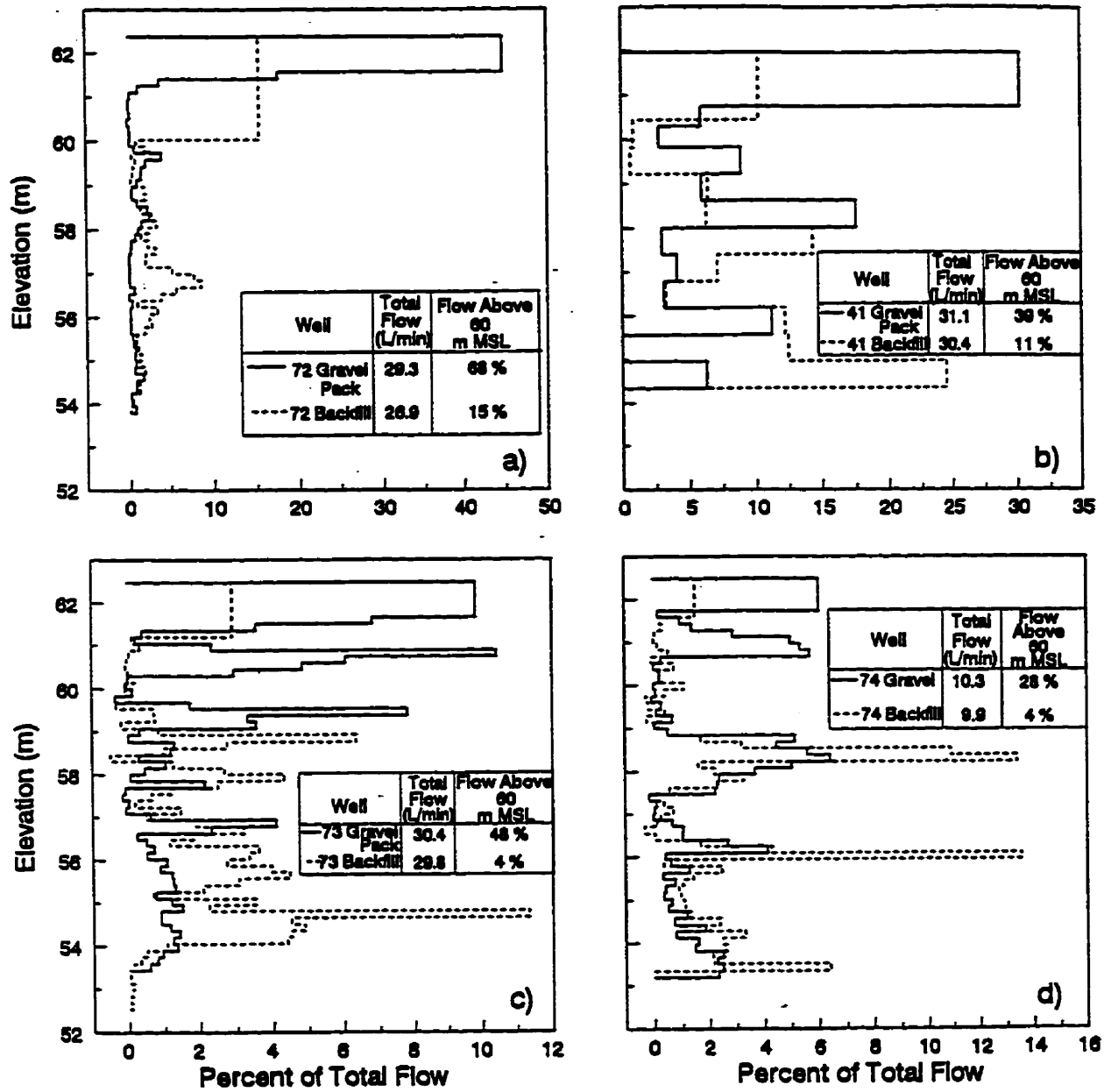


Figure 5.9 Borehole flowmeter profiles at gravel-packed and naturally-backfilled wells that intersect the paleochannel shown in Figure 5.1.

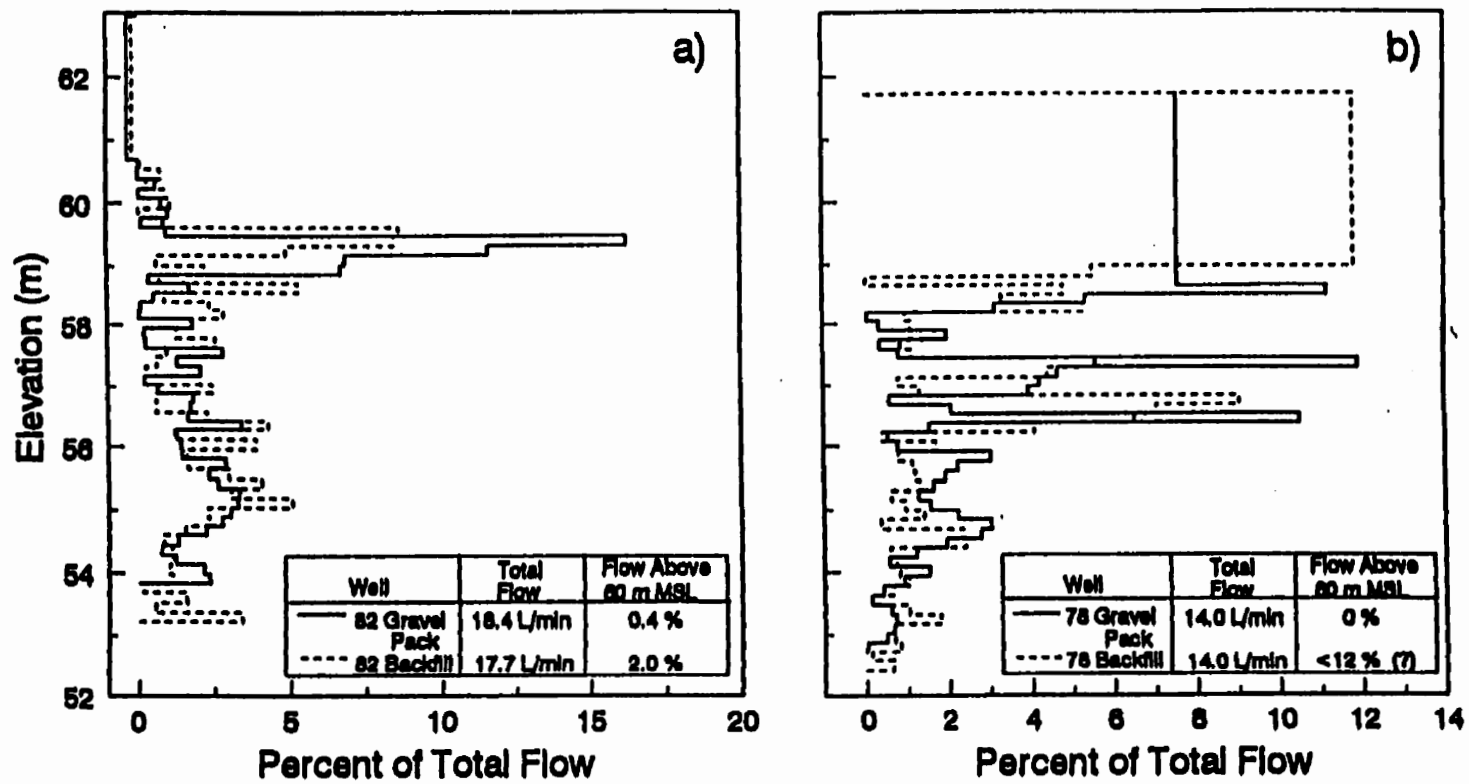


Figure 5.10 Borehole flowmeter profiles for gravel-packed and naturally-backfilled wells located outside the palechannel boundaries shown in Figure 5.1.

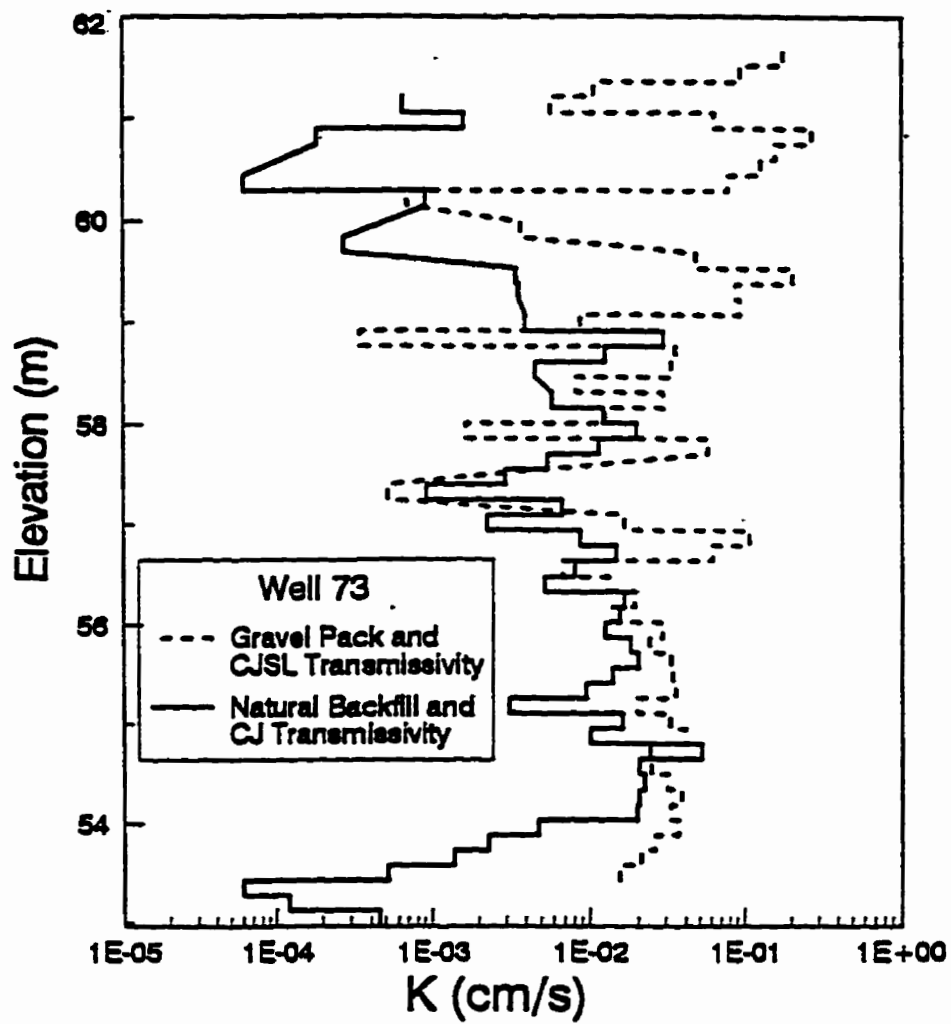


Figure 5.11 Comparison of flowmeter  $K$  values from gravel-packed and naturally-backfilled wells at location 73 inside the paleochannel (see Figure 5.1).

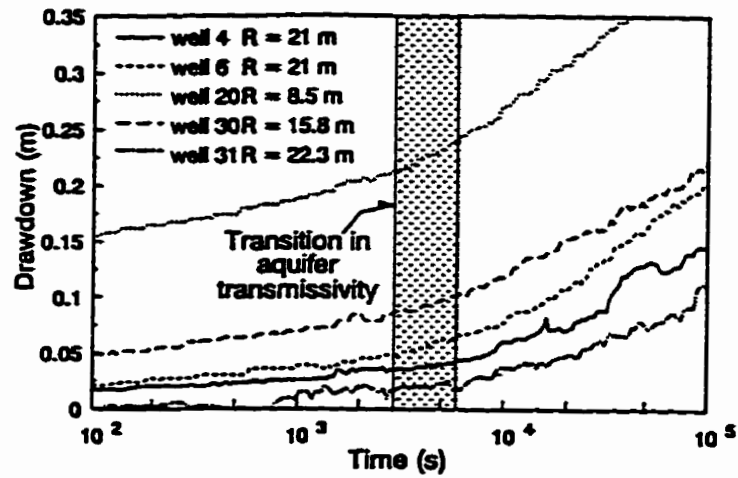


Figure 5.12 Time-drawdown responses at five observation wells during Aquifer test AT3.

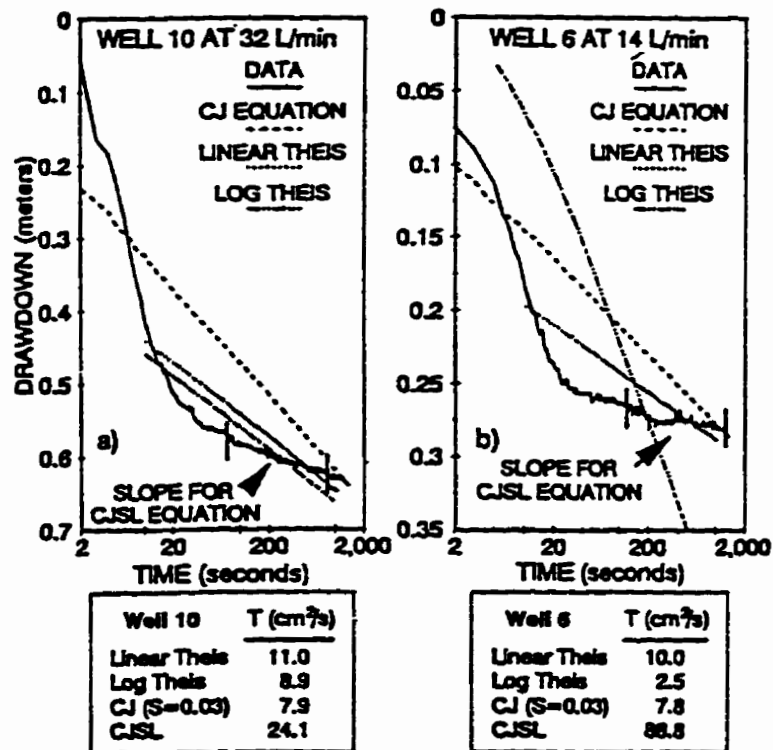


Figure 5.13 Application of Theis type-curve fits, the Cooper-Jacob (CJ) equation, and the Cooper-Jacob straight-line (CJSL) method for calculating transmissivity values for two single-well pumping tests performed in the 1-Ha test site.

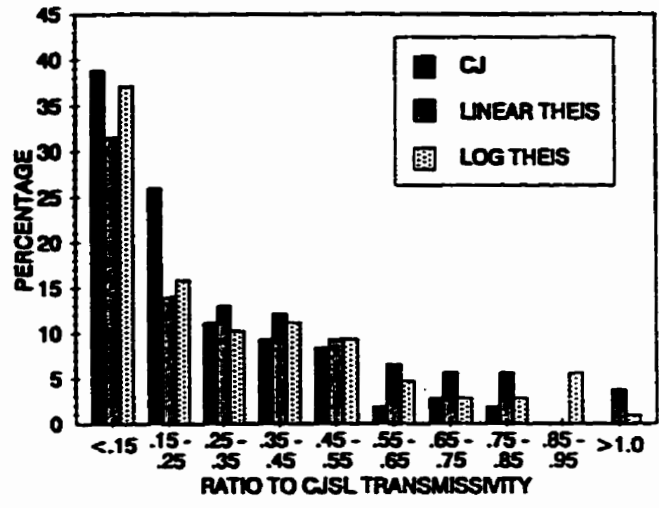


Figure 5.14 Frequency distribution of the ratio between the CJ and Theis transmissivity values to the CJSL transmissivity values calculated for 115 single-well pumping tests at the 1-Ha test site..

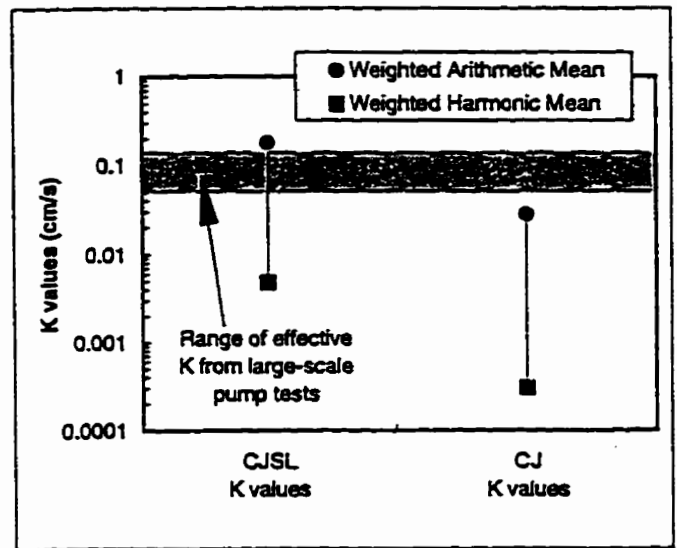


Figure 5.15 Comparison of the arithmetic and harmonic means for 668 CJ and for 668 CJSL K values with results of a large-scale pumping test.

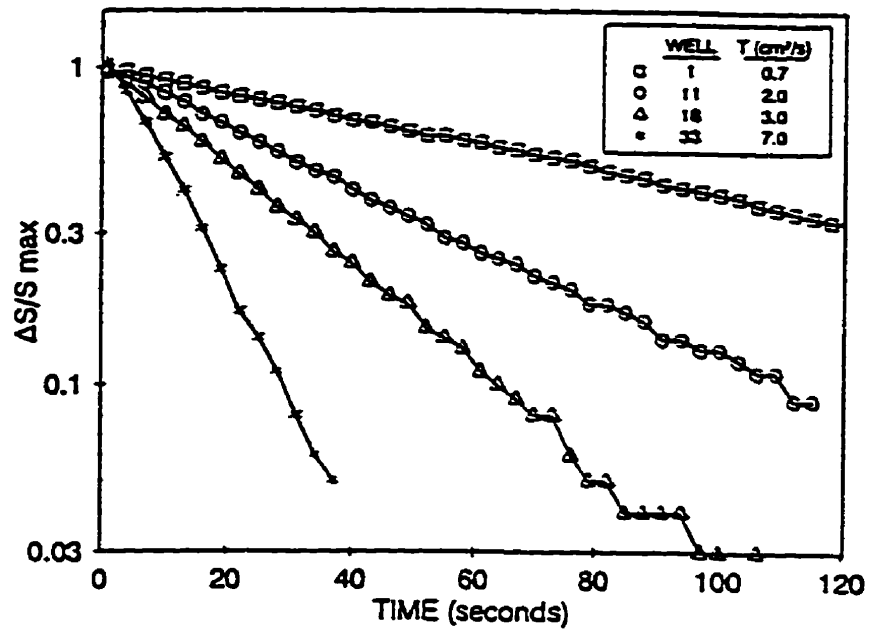


Figure 5.16 Slug test results from fully-penetrating wells at the 1-Ha test site that illustrate a classical Hvorslev response.



## **6. IMPACTS OF PUMPING TEST DURATION ON TRANSMISSIVITY VALUES**

### **6.1 INTRODUCTION**

Fluvial aquifers consist of sediments deposited in a wide range of depositional environments. As a result, fluvial aquifers are heterogeneous and can be viewed in a hierarchical scale according to their spatial architecture (Miall, 1988a,b; 1989; 1990). The possibility that many, if not most, fluvial aquifers have large-scale trends/patterns in their hydraulic conductivity (K) fields is significant to many field characterization activities, including the design and analysis of pumping tests.

This chapter primarily concerns the analysis of pumping test data from an unconfined, fluvial aquifer underlying the Columbus Air Force Base (CAFB) in Mississippi. Results from large-scale pumping tests show that the location of the pumping well relative to a preserved paleochannel (see Figure 6.1) affects both the calculated hydraulic properties (e.g., transmissivity and storage coefficients) as well as the aquifer structure (e.g., unconfined, confined, leaky) inferred from the time-drawdown data. Flowmeter and tracer test results from the MADE and the 1-Ha (see Figure 6.2) test sites indicate that the paleochannel represents a zone of high transmissivity. The complexity of the aquifer transmissivity field requires that the pumping test analyses extend beyond conventional type-curve matching and include: 1) a sedimentological model to help delineate plausible transmissivity patterns; and, 2) the Cooper-Jacob straight line (CJSL) analysis method (Cooper and Jacob, 1946) to estimate changes in the transmissivity field from the pumping test data.

Before presenting the pumping test data, the large-scale transmissivity variations at CÁFB are described and numerical simulations involving the potential impact of delayed gravity drainage and transmissivity changes are presented. Following this background material, the pumping test data are analyzed using two approaches. The first approach accounts for a simplified form of unsaturated flow but ignores transmissivity variations. The second approach accounts for a simplified form of transmissivity variations but ignores unsaturated flow.

## **6.2 A SEDIMENTOLOGICAL MODEL**

A simple but reasonable sedimentological model for the CAFB aquifer described in Chapter 5 is illustrated in Figure 6.3. At the base of the paleochannel shown in Figure 6.1 are coarse-grained channel lag, scour pool, and chute bar deposits. Above these deposits are fine-grained sediments that filled the meander channel after the channel was abandoned. Associated with the convex and concave regions of the paleochannel are pointbar and cutback\overbank deposits, respectively.

Based on an equation from Leeder (1973) and a 70-m width for the paleochannel, a base elevation near 59 m MSL is estimated for the channel lag deposits. Below 59 m MSL, the aquifer is presumed to be a mixture of coarse-grained fluvial deposits from braided and/or coarse-grained meandering rivers. Shown in Figure 6.4 are results of a continuous core from a borehole that intersects the paleochannel. The vertical profile of grain-size distribution shows that the coarse-grained deposits are interlayered between fine-grained sediments associated with the channel-fill and the Eutaw Formation. Near 59 m MSL in Figure 6.4

there is no obvious changes in grain-size distributions to mark an erosional surface associated with the paleochannel. The lack of a definable transition between channel lag deposits and older alluvium is attributed to the channel lag representing reworked alluvium best differentiated from other alluvium by its sedimentary structures.

### **6.3 LARGE-SCALE TRANSMISSIVITY VARIATIONS**

#### **6.3.1 Borehole Flowmeter Tests**

Shown in Figure 6.5 is the log (K) field based on these borehole flowmeter K values for the upper portion of the saturated CAFB aquifer from 60 to 62 m MSL. The high-K zone coincides with the location of the paleochannel channel lag deposits. On the convex and concave regions of the paleochannel are areas of moderate K values and low K values, respectively. With respect to the sedimentological model, the low K values are associated with overbank/flood deposits and the moderate K values are associated point bar deposits.

To support the continuation of the high-K channel-lag deposits from the 1-Ha site to the MADE site, borehole flowmeter tests performed at gravel-packed wells at well pair locations 72 and 73 are shown in Table 6.1. Consistent with the presumption of high-K channel lag deposits above 59 m MSL is that the majority of inflow at the two gravel-packed wells occurred above 59 m MSL. Analysis of this and other flowmeter data confirms that K values near 0.5 cm/s consistently exist above 59 m MSL within the paleochannel at both the 1-Ha and the MADE site.

**Table 6.1 Vertical Profile of Flow into Sand-Packed Wells Measured by a Borehole Flowmeter**

Elevation (m MSL)	Well 72 <sup>1</sup>	Well 73 <sup>1</sup>
52-54	1.2%	3.8%
54-56	8.1%	15.3%
56-58	3.6%	11.2%
58-60	18.8%	21.4%
60-62	68.3%	48.3%

Note: Constant pumping rate at Well 72 was 111 L/min  
Constant pumping rate at Well 73 was 115 L/min

<sup>1</sup> see Figure 6.1 for well locations

### 6.3.2 Tracer Tests

To investigate the effect of the heterogeneous K field on groundwater flow at the 1-Ha test site, a five-spot tracer test was performed and is described in Appendix E, Section 5. The flow field was created by pumping equal amounts from Wells 1, 3, 7, and 9 while injecting the total amount into Well 5. Once the flow field stabilized, a tracer slug was injected into Well 5 and monitored for several days using multilevel sampling devices at selected wells. Analysis of the tracer data revealed a strong preferential flow in the upper aquifer toward the north west. At wells located in the northwest quadrant of the site (e.g., Wells 6, 26, 3, 2, and 18 in Figure 6.2), significant tracer concentrations were measured above 58 m MSL but no tracer was detected below 58 m MSL. Tracer breakthroughs occurred at all seven wells at about ten times sooner than expected for a homogeneous

aquifer. The skewed vertical distribution of tracer and the rapid tracer breakthrough at wells in the northwest quadrant is consistent with high K values above 59 m MSL in the paleochannel.

To help investigate hydrodynamic dispersion in heterogeneous aquifers, Boggs et al., (1993) performed a natural gradient test at the MADE site. The tracer slug was injected at the designated location in Figure 6.1 along the cross section A-A'. The sampling network consisted of 328 multi-level sampling wells. Figure 6.6 shows a vertical profile of tritium concentrations through the MADE sampling network for three times. At 27 and 132 days, the plume occupied the entire aquifer thickness between the injection location and a longitudinal distance of 20 m. At 132 days, the portion of the plume downgradient of 20 m was confined to the upper aquifer above 58 m MSL. At 224 days, the plume was above 58 m MSL within the paleochannel boundaries but occupied the entire aquifer thickness outside of the paleochannel's boundaries.

An interesting feature of the tritium plume is the skewed tracer concentration field. At 224 days, although the plume front has advanced 225 meters, the majority of the plume mass remains near the injection location. Beyond longitudinal distances of 20 m and 50 m, the maximum concentrations are 1.0% and 0.1% of the injected concentration, respectively. The skewed tracer profiles suggests that a non-uniform velocity field exists along the longitudinal cross section. Support for large-scale differences in the groundwater flow pattern is given by Boggs et al., (1993), who provides an estimated near-field velocity of 5 m/yr and a mid- to far-field velocity of 128 m/yr for the tritium plume.

A possible explanation for the skewed tracer plume is aquifer heterogeneity. In light of the K patterns implicit in the sedimentological model, most of the major plume features can be explained. The slowest tritium movement occurred near the injection location because the tracer was injected into low-K cutbank/overbank deposits in the concave region near the paleochannel. Approximately 25 m downgradient of the injection location, the tritium plume moved toward the upper aquifer and became more dilute because groundwater converged toward and flowed through the permeable channel lag deposits. Once in the permeable channel lag deposits, the tritium remained in the upper aquifer until the plume reached the paleochannel boundary at a longitudinal distance of 150 m, at which point a vertical diverging flow spread the tritium plume across the entire aquifer depth.

#### **6.4 DESCRIPTION OF LARGE-SCALE PUMPING TESTS**

To help design and interpret the tracer test and borehole flowmeter tests at CAFB, the ten large-scale pumping tests listed in Table 6.2 have been performed. Eight of the tests were conducted in the 1-Ha test site (see Figure 6.2). Three of the pumping tests involved pumping Well 5 (AT1 to AT3) for about 6 days and monitoring all 37 wells in the 1-Ha test site (Appendix B). For AT1 and AT3, nine observation wells had pressure transducers and the remaining wells were monitored manually with an electric tape. For AT2, nine pressure transducers were shifted every two days. The pumping tests at Well 16 (AT4 to AT7) included monitoring the four closest wells with pressure transducers. The pumping test at Well 12 (AT8) included monitoring the six closest wells with pressure transducers.

At the MADE site, two pumping tests (see Figure 6.1 for location) had durations greater than 12 hours. The MADE1 pumping test included 12 partially-penetrating observation wells along three rays extending outward from well PW1. Four of the wells were monitored with pressure transducers; the remaining wells were monitored manually with an electric tape. The MADE2 aquifer test included 15 partially-penetrating observation wells. Five of the wells were monitored with pressure transducers, two of the wells were monitored with chart recorders, and the remaining wells were monitored manually with an electric tape (Boggs et al., 1990, 1992).

Figure 6.7 shows drawdowns caused by pumping tests at five different pump well locations (see Figure 6.1). The variations among the shapes of the drawdown curves suggest different aquifer models (i.e., confined, unconfined, leaky) and a range of transmissivity values. If each pumping test was analyzed independently by different professionals, an inconsistent set of aquifer structures and parameters would be generated.

Geohydrologists analyzing data from pumping tests at Wells 5, 16 and PW2 likely would use type curves for unconfined aquifers (Neuman, 1972, 1974, 1975) because of the sigmoidal-shaped drawdown curves. Geohydrologists analyzing data from the pumping test at well PW1 likely would use type curves for a leaky aquifer (Hantush, 1956) because of the flat drawdown response at late time. Finally, geohydrologists analyzing data from the pumping test at Well 12 likely would use type curves for a confined aquifer (Theis, 1935) because of the constant semi-log slope at intermediate and late times.

**Table 6.2 Pumping Tests Conducted at the Two Test Sites**

Test	Pump Well	Rate (L/min)	Duration (hour)	Date	Remark
AT1	5	68	144	5/89	
AT2	5	68	144	6/89	Cyclic Pumping
AT3	5	112	144	7/89	
AT4	16	36	12	10/91	
AT5	16	12	12	10/91	
AT6	16	35	12	10/91	Injection
AT7	16	12	12	10/91	Injection
AT8	12	24	12	6/92	
MADE1	PW1	62	72	3/85	
MADE2	PW2	208	192	7/85	

### 6.5 CONSIDERATIONS FOR ANALYZING THE PUMPING TEST DATA

Based on the sedimentological model, tracer test data, and borehole flowmeter data, significant transmissivity variations exist in the aquifer. Consequently, an important consideration in the analysis of pumping test data is the location of the wells with respect to the regions of high and low transmissivity.

Because Well PW1 is located on the concave side of the paleochannel—a region associated with overbank and cutbank deposits of low transmissivity—the apparent leaky aquifer response from the PW1 pumping test in Figure 6.7 may have occurred because the cone-of-influence started in an area of low transmissivity and spread into regions of high transmissivity associated with the paleochannel. Similarly, sigmoidal-shaped aquifer



response for the pumping tests involving Wells PW2, 5, and 16 in Figure 6.7 may have occurred because of aquifer heterogeneity. In these instances, the cone-of-influence would have started in a high transmissivity region associated with the paleochannel and then spread into regions of lower transmissivity associated with point bar and cutbank deposits.

The effect of transmissivity changes on drawdown responses can be demonstrated analytically. Figure 6.8 shows drawdown curves from wells in a hypothetically, confined aquifer consisting of three concentric rings of different transmissivity and storage properties (Liu and Butler, 1990). The changes in the semi-log slope occur when the radius of influence approaches and leaves a boundary between zones of differing hydraulic properties. A constant slope indicates that one zone is contributing the majority of flow to the well. Using the guidelines provided by Butler (1990), CJSJL method can be used to estimate variations in the transmissivity field.

Assuming that the CAFB aquifer is unconfined and is heterogeneous, a paramount question affecting data analysis is whether the most representative transmissivity values are obtained with an analytical solution that ignores transmissivity variations but can account for a simplified form of unsaturated flow [i.e., delayed gravity drainage theory by Neuman (1972, 1974, 1975)] or with an analytical solution that ignores unsaturated flow but can account for simple transmissivity variations [i.e., CJSJL method by Cooper and Jacob, (1946)]. Because of the complexity of this issue, the numerical simulations were performed to help guide and support the analysis of the pumping test data.

## **6.6 NUMERICAL INVESTIGATION OF TRANSMISSIVITY CHANGES AND DELAYED DRAINAGE ON PUMPING TEST RESULTS**

### **6.6.1 Numerical Model**

The numerical code selected for simulating the pumping test was the finite difference/finite element code FRAC3DVS (Therrien and Sudicky, 1996). An attractive feature of FRAC3DVS is the use of line elements to accurately and effectively represent pumping wells as described by Sudicky et al. (1995). Several data sets have been used to check the numerical schemes employed by FRAC3DVS. With respect to unconfined flow, the FRAC3DVS code has been verified using the analytical results of Kroszynski and Dagan (1975) and the numerical simulations of Akindunni and Gillham (1992) (see Figures 6.9 and 6.10). With respect to transmissivity variations, the FRAC3DVS code has been verified using the analytical solutions for pumping tests in aquifers with transmissivity patterns involving concentric rings (Liu and Butler, 1990) and linear strips (Butler and Liu, 1991).

### **6.6.2 Numerical Simulations**

To investigate the cause for the sigmoidal-shape drawdown response, aquifer parameters reflective of conditions at the paleochannel were used in the numerical simulations. Based on sediment descriptions (Figure 6.4) and flowmeter K values (Figure 6.5), a representative three-layered aquifer model was used (Figure 6.11). The top model layer represents the 2-m thick, low-K, clayey material associated with overbank and channel fill deposits. The middle model layer represents a 1.5-m thick, high-K, well-connected, coarse-grained channel lag deposits within the paleochannel. The bottom model layer represents a 6.5-m thick, moderate-K gravelly material that represents a mixture of fluvial deposits from several

fluvial subenvironments. Based on field measurements, an initial water table depth of 2.5 m was used. A horizontal K of 0.042 cm/s was assigned to the mixture of fluvial deposits based on the arithmetic and geometric mean of 881 flowmeter K values at the 1-Ha test site (Young, 1995a) and the late-time, depth-averaged K calculated from large-scale pumping tests (to be discussed later). A horizontal K of 0.83 cm/s was assigned to the channel lag deposits based on the most permeable 1.5-m zone in the upper aquifer at 13 wells (e.g., Wells 1, 2, 3, 5, 6, 9, 11, 19, 26, 28, 30, 33, and 36). A horizontal K of .000016 cm/s was assigned to the clayey material based on grain-size data and a limited number of laboratory permeameter tests. For all model layers, the vertical K was set to 25% of the horizontal K.

To calculate unsaturated flow, the van Genuchten parameters in Table 6.3 were used to describe the pressure head-saturation and saturation-relative K relation for the different model layers. The parameters for the clayey deposits are those provided by van Genuchten (1978) for a Beit Netofa Clay. The van Genuchten parameters for the CAFB fluvial deposits estimated by running the code SOILPROP (Mishra et al., 1989) with CAFB grain-size data and by reviewing moisture retention relation for sandy and/or gravelly material like those provided by Akindunni and Gillham (1992).

**Table 6.3 Parameters for Estimating Unsaturated Properties**

Layer	$\theta_s$	$\theta_r$	$\alpha$	n
1 - Top Layer	.446	.286	0.2	1.59
2 - Middle Layer	.35	.05	2.2	1.85

$\theta_s$  = total porosity ( $m^3/m^3$ ).

$\theta_r$  = residual moisture content ( $m^3/m^3$ ).

$\alpha$  =  $\alpha$  value for van Genuchten function (van Genuchten, 1978).

n = n value for van Genuchten function (van Genuchten, 1978).

To minimize the required computer resources by 75%, the numerical mesh for the pumping test represented only the northeast quadrant of the hypothetical aquifer. A 0.25-m ID fully-screened pumping well with a constant pumping rate of 120 liters/min was located at the origin ( $x=0, y=0$ ). A variable finite-difference mesh was used. Horizontal grid spacing was 0.05 m near the well but increased to 100 m near the model boundaries at 1300 m. Vertical spacing was 0.125 m near top of the saturated aquifer but increased to 1 m near the base of the aquifer. The finite difference grid had a total of 34425 elements. No-flow boundaries were set at all six sides of the model domain to ensure that all pumpage originates from storage. A specific storage of  $.0005 \text{ (m}^{-1}\text{)}$  was used throughout the model and is based on the range of compressibilities provided by Freeze and Cherry (1979) for sand.

Numerical simulations were performed for three different transmissivity fields. The benchmark simulation represents the layered aquifer system shown in Figure 6.11 that has a transmissivity of  $112.5 \text{ cm}^2/\text{s}$ . The benchmark system was modified to create the linear and radial changes in transmissivity shown in Figure 6.12 by changing the K assigned to the middle model layer from  $0.83 \text{ cm/s}$  to  $0.042 \text{ cm/s}$  at linear and radial distances of 25 m from the pumping well, respectively.

### 6.6.3 Analysis of Numerical Simulations

The simulated drawdowns for the three transmissivity patterns are plotted on semi-logarithmic axes in Figure 6.13. For the benchmark case (layered aquifer in Figure 6.11), the drawdown plots for the pumping and observation wells are straight-lines after 300 and 900 s, respectively. Application of the CJSL method to the pumping well data from 600 to 6000 s

produces a transmissivity of  $112.6 \text{ cm}^2/\text{s}$ , which is within 0.1% of the  $112.5 \text{ cm}^2/\text{s}$  transmissivity of the hypothetical aquifer. The lack of a sigmoid-shape drawdown response indicates that delayed gravity drainage occurs rapidly enough such that, for all practical purposes, the data can be analyzed with the Theis solution. As shown in Figure 6.13, this conclusion is still valid for the case reducing the pumping rate and K values by 75%. A ramification of the benchmark simulations is that because of the high permeability of the channel lag deposits and the other fluvial deposits, delayed gravity drainage would not be sufficient to produce the sigmoidal-shape drawdown responses for pumping tests performed in the paleochannel.

Unlike the effects of unsaturated flow, the effects of areal heterogeneity are readily shown in the drawdown plots. For both the linear and radial case, the transmissivity reduction at 25 m produces a significant slope increase at approximately 1800 s. For the radial case, the slope of the drawdown response gradually increases after 1800 s until approximately 18000 s, at which time the drawdown response begins to plot again as a straight line. Application of the CSJL method from 1800 to 180000 s produces a transmissivity of  $32.7 \text{ cm}^2/\text{s}$ , which is within 2% of the low transmissivity shown in Figure 6.12.

For the radial case, a straight-line response does not exist between 1800 and 18000 s because the predominant source of well discharge is changing from the high to the low transmissivity zone. Because the linear case has a significantly greater area associated with the high transmissivity zone than does the radial case, the transition period is longer and the slope change is more gradual. Although visual inspection of Figure 6.11 suggests that a

straight-line response exists after 60000 s for the linear case, the slope is slowly changing over time. Because the radius-of-influence can not leave the high transmissivity zone, the slope for the linear case will asymptotically approach the slope for the radial case. A regression analysis of the drawdown data between 150000 and 180000 s for the linear case produces a transmissivity of  $43.8 \text{ cm}^2/\text{s}$ . This transmissivity represents a weighted average of the transmissivity for the two zones from which well pumpage originated during the 300000-s period.

#### **6.6.4 Summary of Relevant Impacts**

Based on aquifer parameters that characterize the highly transmissive deposits in and near the paleochannel, delayed gravity drainage does not have a significant effect on drawdown response. This conclusion is consistent with the numerical simulations of Akindunni (1987) for a hypothetical sandy aquifer with an average  $K$  of  $0.06 \text{ cm/s}$ . For all practical purposes, he demonstrated the Theis solution was appropriate because of the quick release of drainage from the unsaturated zone.

Because delayed drainage effects are negligible, the Theis solution is appropriate to analyze the CAFB the pumping test data collected in and near the paleochannel. Field evidence that supports applying the CJSL method and the Theis solution to pumping tests at CAFB are excellent Theis type curve matches for the cyclic pumping test AT2 (Figure 6.14) in the paleochannel and the Theisian drawdown responses for the pumping test at Well 12 (Figures 6.7 and 6.16) near the paleochannel boundary.

## 6.7 ANALYSIS OF CAFB PUMPING TEST DATA USING THE CJSJL METHOD

Shown in Figure 6.15 are results for a pumping test at Well 16. A reasonable explanation for the non-Theisian drawdown response is that the slope changes are caused by a decrease in the aquifer transmissivity beyond the paleochannel boundary. The slope of the first linear segment suggests that during the initial 3000 s, the radius-of-influence passes through aquifer material with an effective transmissivity of near  $65 \text{ cm}^2/\text{s}$  (Table 6.4). After 3400 s, the rate of change in the drawdown response suggests that the radius-of-influence is passing through aquifer material with an effective transmissivity near  $30 \text{ cm}^2/\text{s}$ .

In order to determine whether there are correlations between the transmissivity trends and the paleochannel location, drawdown responses from the other four pumping wells were analyzed with CJSJL method. Figure 6.16 shows the drawdown curves for the other pumping wells, and Table 6.5 provides the results of the CJSJL analysis. On close examination, one can deduce that the location of the pumping well relative to the paleochannel affects the shape of the drawdown curve and the calculated transmissivity trends.

Table 6.5 shows that the CJSJL analysis produces a transmissivity near  $25 \text{ cm}^2/\text{s}$  at late times for all pumping test data. At early times, however, the highest transmissivity values are calculated at the three wells located in the paleochannel and the lowest transmissivity values are calculated for the two wells located outside the former river channel. These results are consistent with the premise that the transitions in the semi-log plots of the drawdown data are caused by the radius-of-influence entering and leaving the permeable sediments in the former river channel. The difference in the results for Wells PW1 and 12 are attributed to their geological setting. Well PW1 is on the concave side of the paleochannel and therefore

more likely to be located in low K deposits than is Well 12, which is on the convex side of the paleochannel and therefore likely located in moderately permeable pointbar deposits.

**Table 6.4 CJSJL Transmissivity Values for AT4**

Well ID	Radius (m)	200 - 1000 seconds			3400 to 34000 seconds		
		Slope	R	T	Slope	R	T
16	.03	.16E-1	.98	69	.33E-1	.98	29
14	3.61	.14E-1	.97	79	.27E-1	.97	39
19	3.66	.15E-1	.98	74	.44E-1	.99	25
13	3.86	.18E-1	.98	62	.39E-1	.99	28
5	4.6	.17E-1	.98	65	.45E-1	.99	25
26	12.76	N/A			.42E-1	.99	26

Note: Slope = semilog slope of a line segment in Figure 6.16  
 R = regression coefficient for the calculated slope  
 T = transmissivity (cm<sup>2</sup>/s) calculated from the CJSJL equation  
 N/A = not applicable beside of low drawdown measurements

**Table 6.5 CJSJL Transmissivities for MADE1, MADE2, AT3, AT4 and AT8**

Well	Test Name	Rate (L/min)	Early times			Late times		
			Duration (s)	T*	R*	Duration (s)	T*	R*
PW1	MADE1	62	100-1800	2	1.0	2000-250000	21	.93
PW2	MADE2	208	100-8700	102	.96	33000-500000	17	.97
5	AT3	112	100-2500	99	.94	5600-100000	23	.99
16	AT4	35	100-2500	63	.98	3400-35000	29	.98
12	AT8	24	171-30000	27	.95	171 - 30000	27	.95

\* T - Transmissivity (cm<sup>2</sup>/s); R - regression coefficient



## **6.8 ANALYSIS OF CAFB PUMPING TEST DATA USING DELAYED GRAVITY DRAINAGE**

### **6.8.1 Theoretical Considerations**

A criterion associated with pumping test analyses is minimizing the residual between the type curve and the field data. Care needs to be taken in that the correct type of model has been selected before optimizing a type-curve fit. A concern with using complex aquifer solutions such as Neuman type curves is that they can accurately reproduce non-Thessian drawdowns caused by aquifer heterogeneity. For example, the simulated drawdown at the 2.5-m observation well for the benchmark and linear strip case has been satisfactorily fitted by Neuman type curves in Figure 6.17.

Good curve matches such as those in Figure 6.17 could erroneously lead hydrogeologists into thinking that the simple aquifer model used to develop the analytical solution curve may sufficiently represent the real-world setting. During type-curve matching, one needs be mindful that a type-curve match only defines aquifer parameters that simulate a drawdown response according to the assumptions embedded in the analytical solution. Before assigning the type-curve parameters to an aquifer, one needs to evaluate the defined parameters for consistency with other field data, a sedimentological model, an assessment of important flow processes, and consistency with results from other type-curve fits.

### **6.8.2 Type-Curve Matching**

The matching of Neuman type curves to pumping test data from the 1-Ha test was performed with AQTESOLV (Duffield, 1994). For most instances, the responses like those in Figures 6.7 and 6.15 were well matched by a type curve. Results for the PW2 pumping test

at the MADE site were taken from Boggs et al., (1990). A summary of the calculated hydraulic parameters is shown in Figure 6.18. Although a consistent set of transmissivity values is presented, there is considerable variability in the calculated values for storage coefficient,  $S$ , and specific yield,  $S_y$ . The two-order magnitude range for both storage parameters, the unrealistic low values near 0.007 for  $S_y$ , and the unrealistic high values near 0.01 for  $S$ , suggest the delayed yield model has limited application at CAFB. Evidence that areal trends may exist in the transmissivity field lies with the MADE2 results that show decreases in  $S$  and  $S_y$  with radial distance—a result that can be partially explained by a decrease in transmissivity with distance. Additional concerns with the general applicability of the Neuman theory arise when pumping test data from outside the paleochannel are included. When this is done, the range of transmissivity,  $T$ , increases from a factor of 4 to 100.

### 6.8.3 Evaluation

The consistency and reasonableness of the hydraulic parameters from type-curve analysis is an indicator of the appropriateness of the analytical solution. If a wide-range or an unreasonable set of values are obtained for any model parameter, the applicability of the analytical solution should be questioned. For instance, in order to obtain the good type-curve fits in Figure 6.17, unreasonable values were required for the storage coefficient (e.g., values greater than 0.01) and for the ratio  $K_v/K_h$  (e.g., values greater than 10). Similarly, the wide range of hydraulic parameters from the Neuman type-curve analysis for the CAFB data

suggest that site conditions such as heterogeneity preclude the reliable characterization of aquifer storage parameters by fitting pumping test data to Neuman type curves.

## 6.9 SUMMARY

Multi-well pumping tests were performed in a highly heterogeneous fluvial aquifer at Columbus AFB, MS. Results from geological investigations, large-scale tracer tests, and borehole flowmeter tests indicate that transmissivity variations are fundamentally connected to the location of a paleochannel. Pumping test data show that the location of the pump well can greatly affect not only the calculated hydraulic properties but also the inferred aquifer structure (e.g. confined, leaky, and unconfined). Drawdown results from tests with the pumping well intersecting the former paleochannel exhibit the characteristic sigmoidal shape associated with delayed gravity drainage in unconfined aquifers. Near perfect Neuman type-curve matches are misleading, as aquifer heterogeneity is the major cause of the sigmoidal drawdown responses at CAFB. Application of the Cooper-Jacob straight-line (CJSL) method to different segments of drawdown data from different pump locations provide transmissivity values, at early and late times, that are consistent transmissivity changes inferred from field data. These results demonstrate that comprehensive pumping test analyses should include investigating whether areal heterogeneity is partially responsible for non-Theisian drawdown behavior.

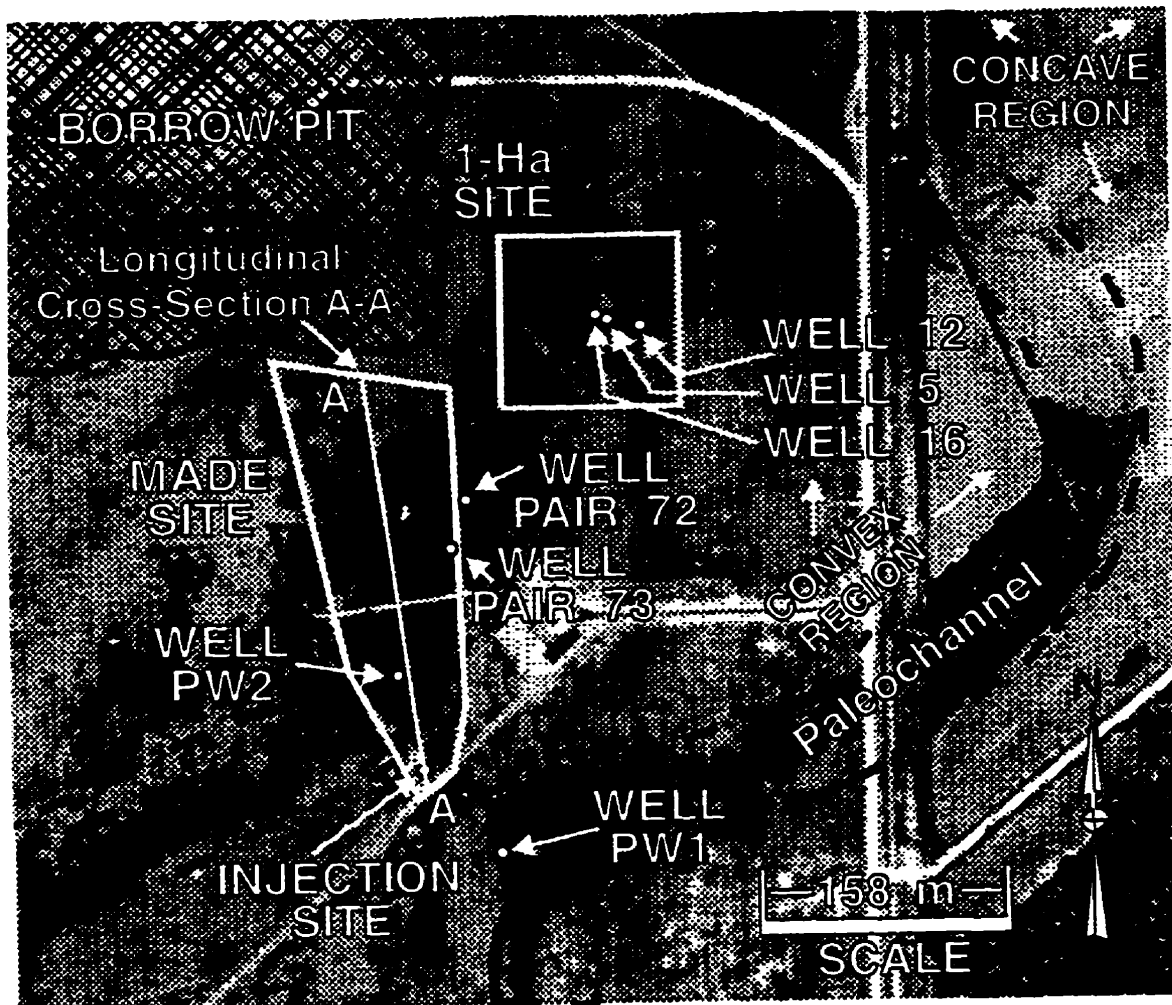


Figure 6.1 Location of two test sites at Columbus AFB, MS, superimposed on a 1956 aerial photograph that reveals a paleochannel.

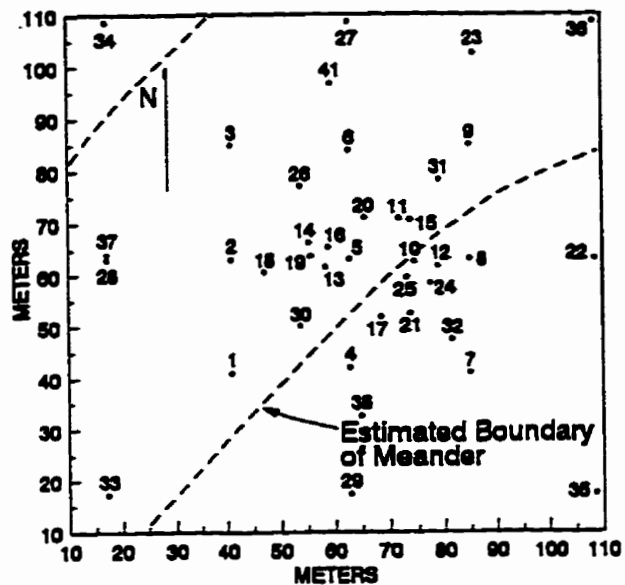


Figure 6.2 Well network for 1-Ha test site with location paleochannel estimated by dotted line.

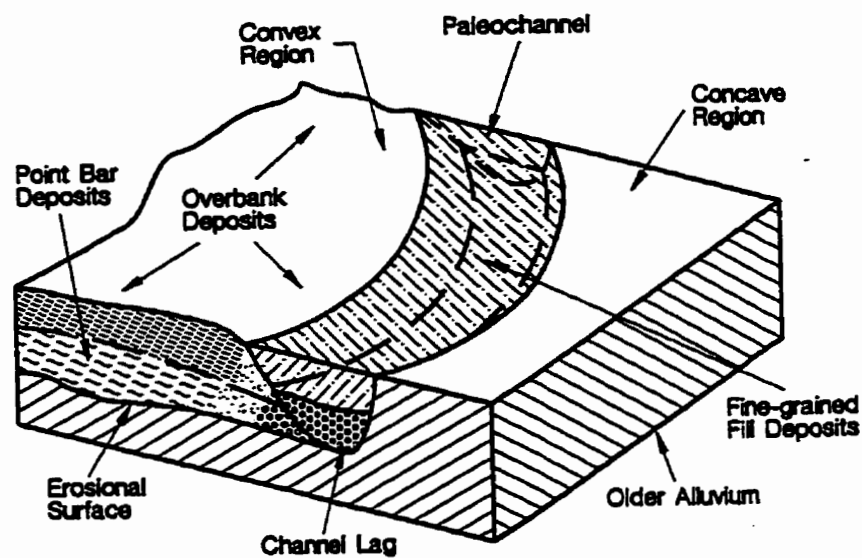


Figure 6.3 Schematic of the regional features associated with the sedimentological model.

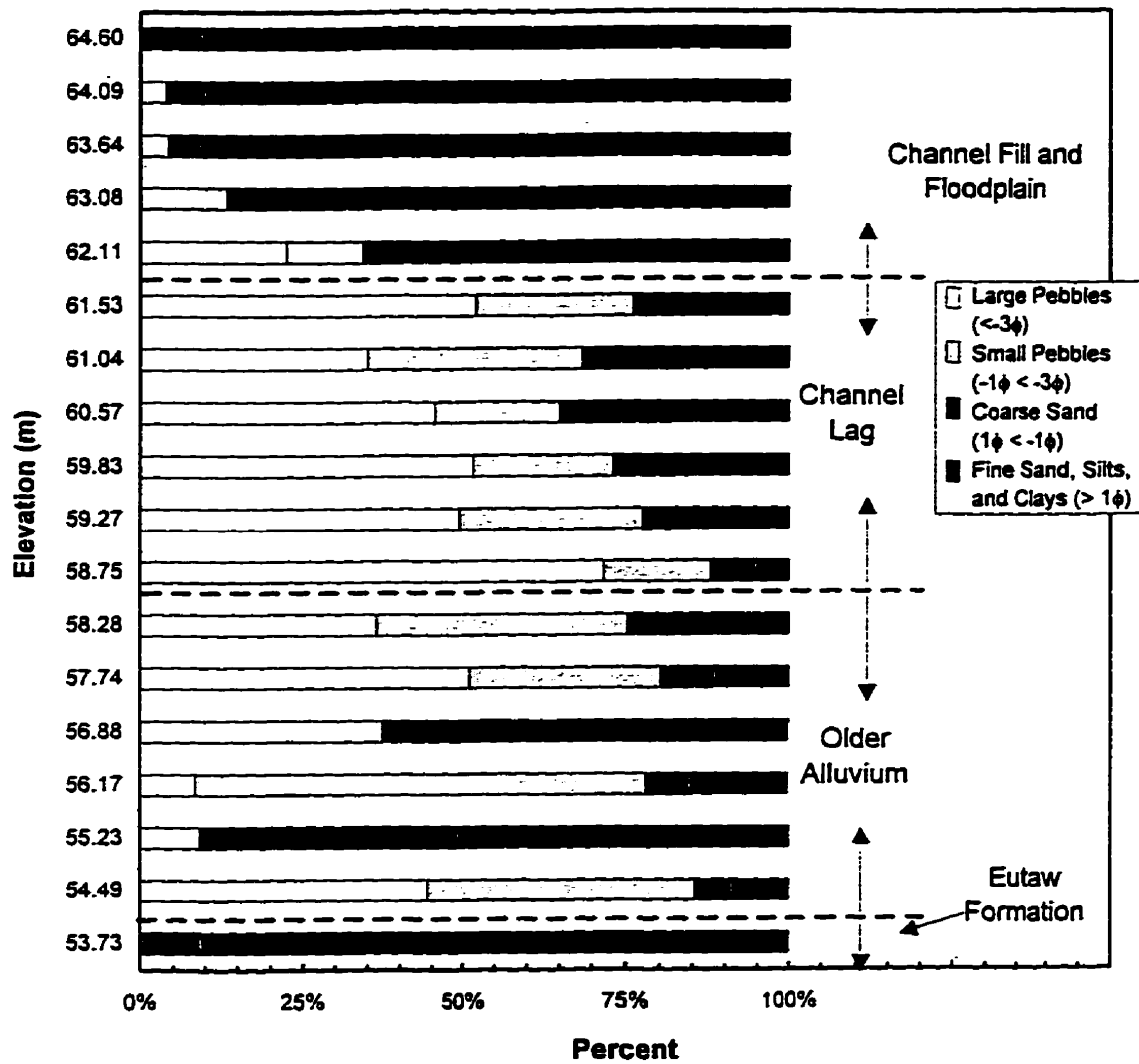


Figure 6.4 Vertical profile of grain-size distributions at Well 73 (ground surface is at 64.9 m MSL).

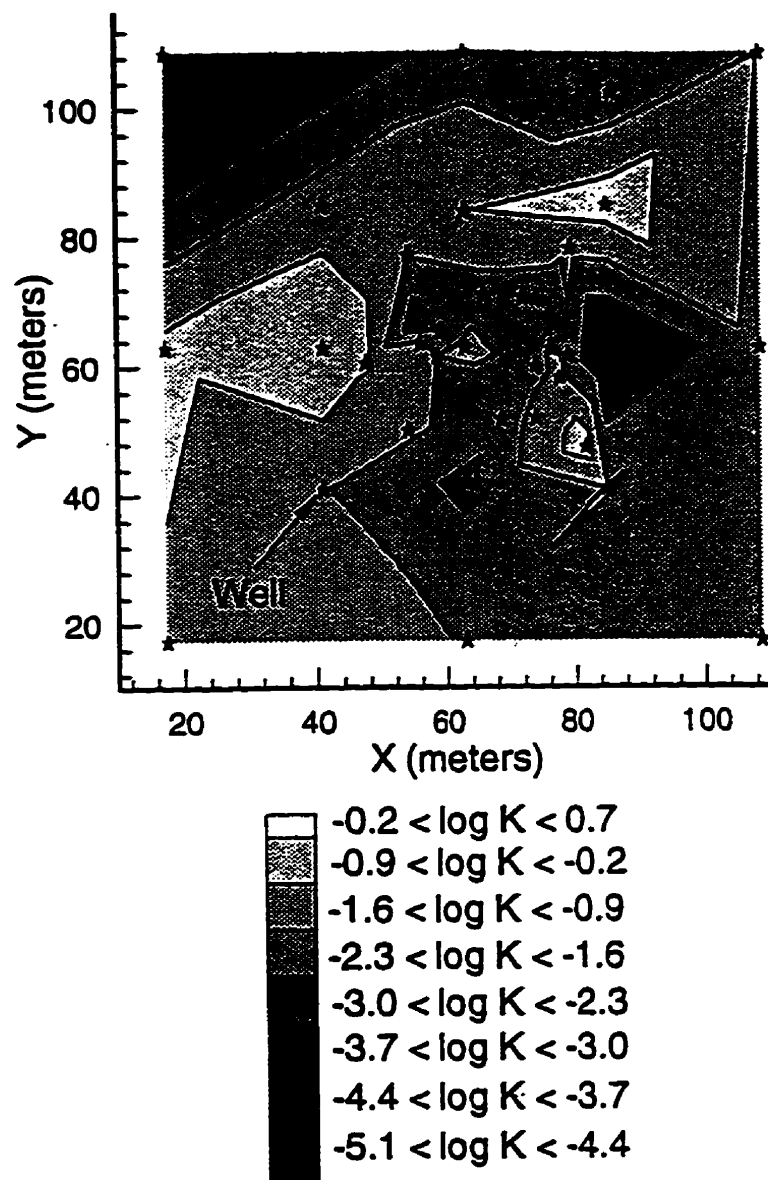


Figure 6.5 Areal profile of borehole flowmeter K values for the uppermost 2 m of the saturated aquifer at the 1-Ha test site (from Chapter 4).

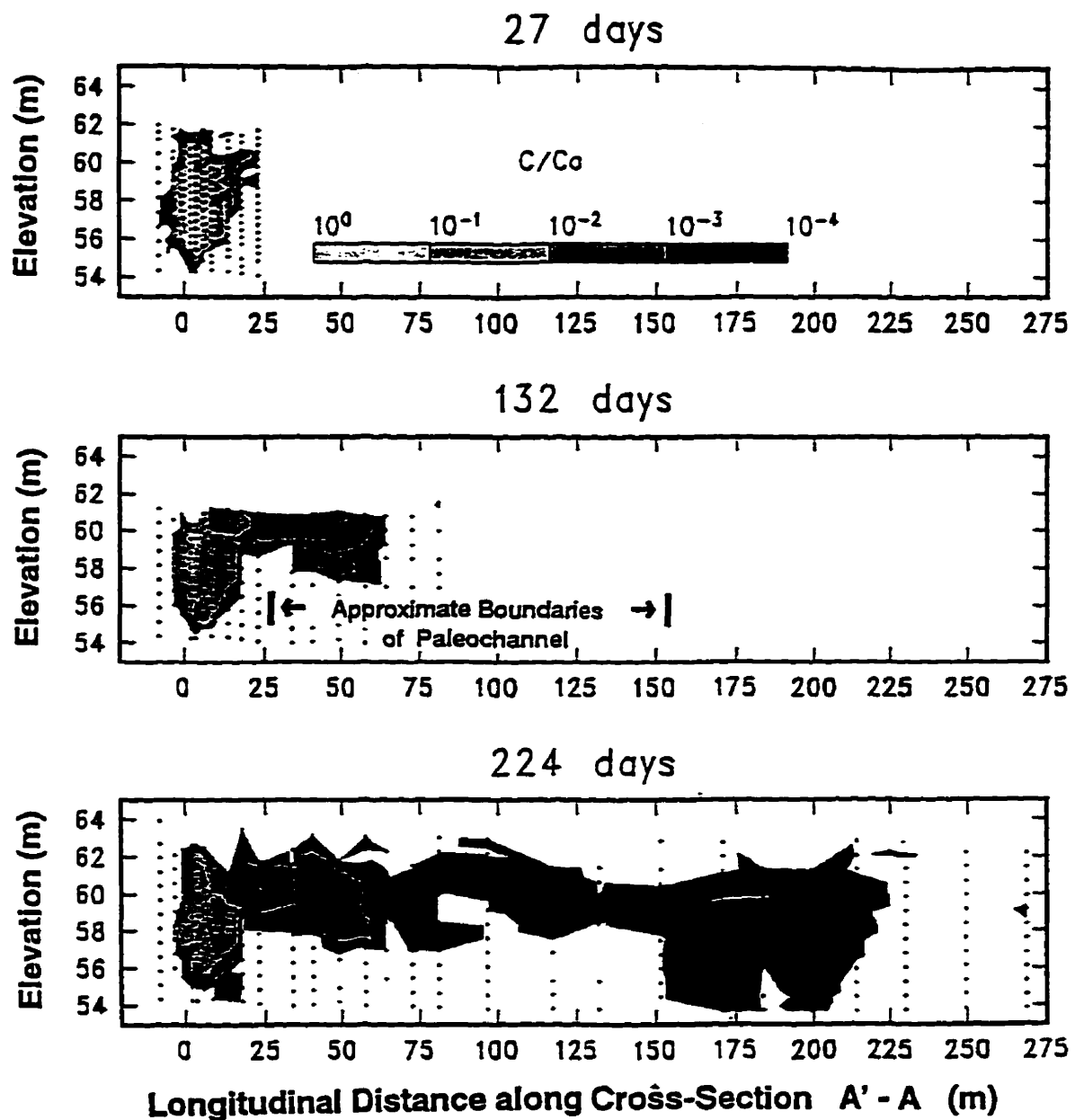


Figure 6.6 Vertical cross-section of tritium plume at the MADE site for 27, 132, and 224 days after injection (modified from Boggs et al., 1993).



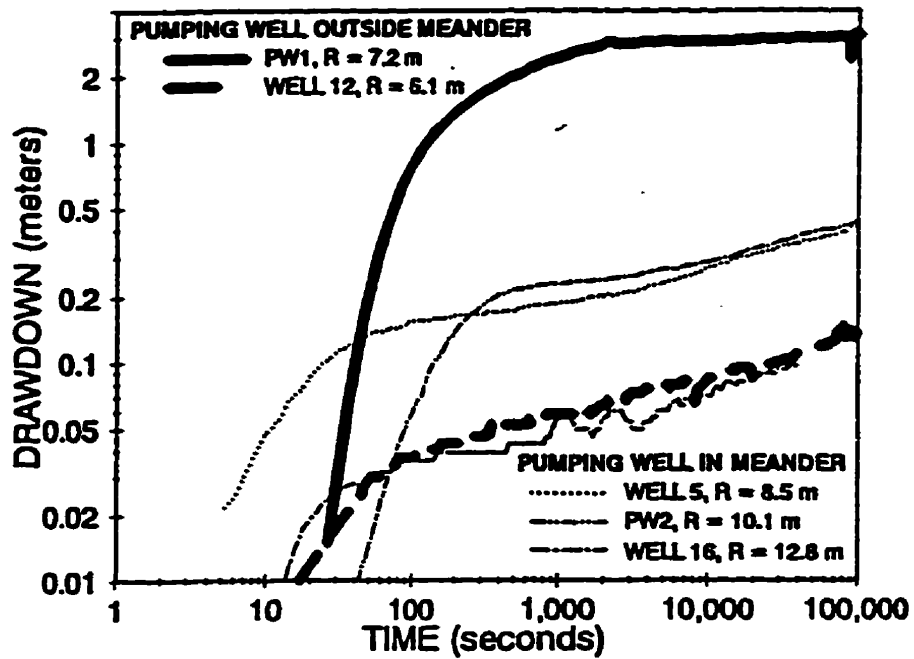


Figure 6.7 Observation well time-drawdown response from large-scale aquifer tests with different pumping wells (see Figure 6.1 for location of pumping well).

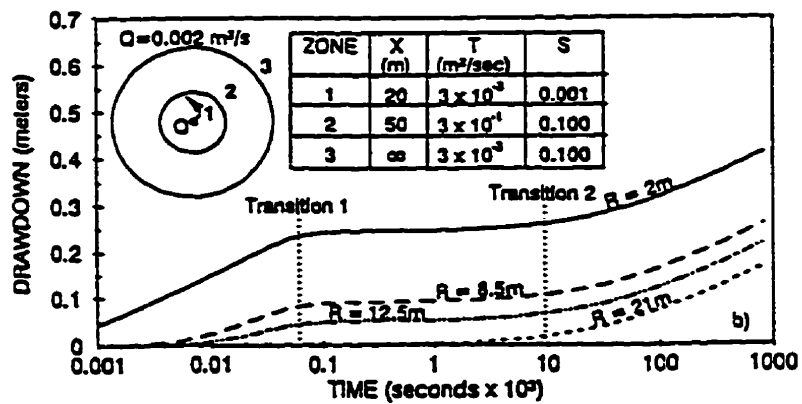


Figure 6.8 Drawdown responses in a hypothetical aquifer with hydraulic properties that vary with radial distance from the pumping well.

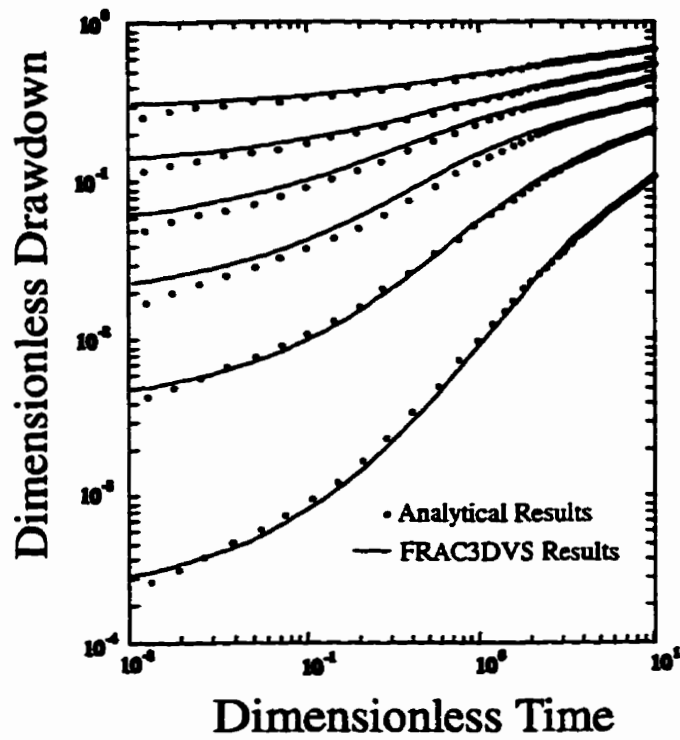


Figure 6.9 Comparison of results from FRAC3DVS and the analytical solution of Kroszynski and Dagan (1975).

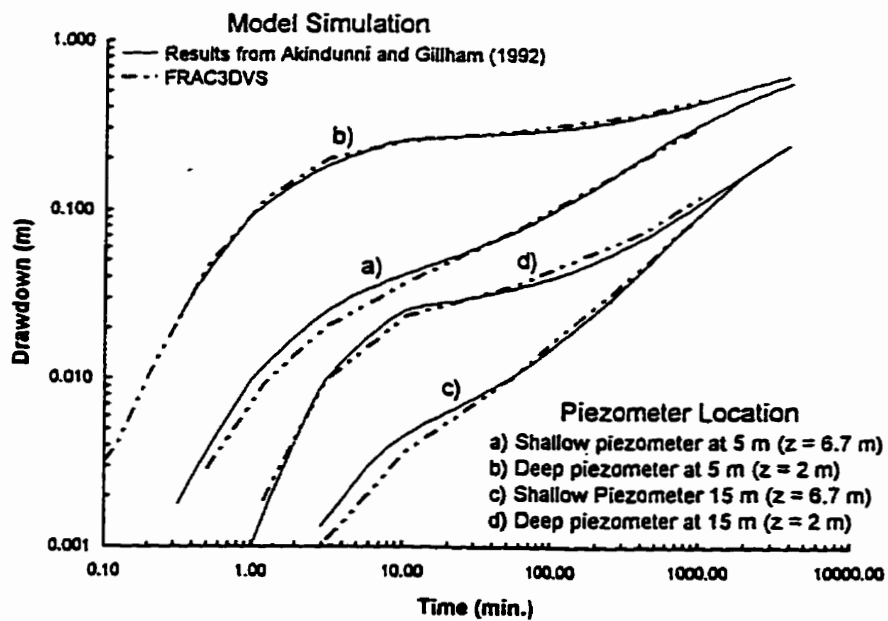


Figure 6.10 Comparison of results from FRAC3DVS and the numerical results of Akindunni and Gillham (1992).

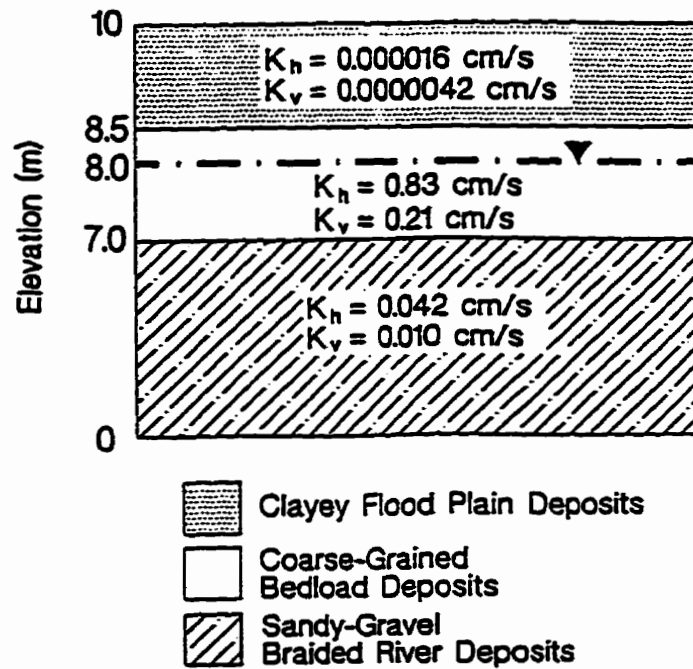


Figure 6.11 K values used in the numerical simulations to represent aquifer properties for a vertical cross section through the paleochannel.

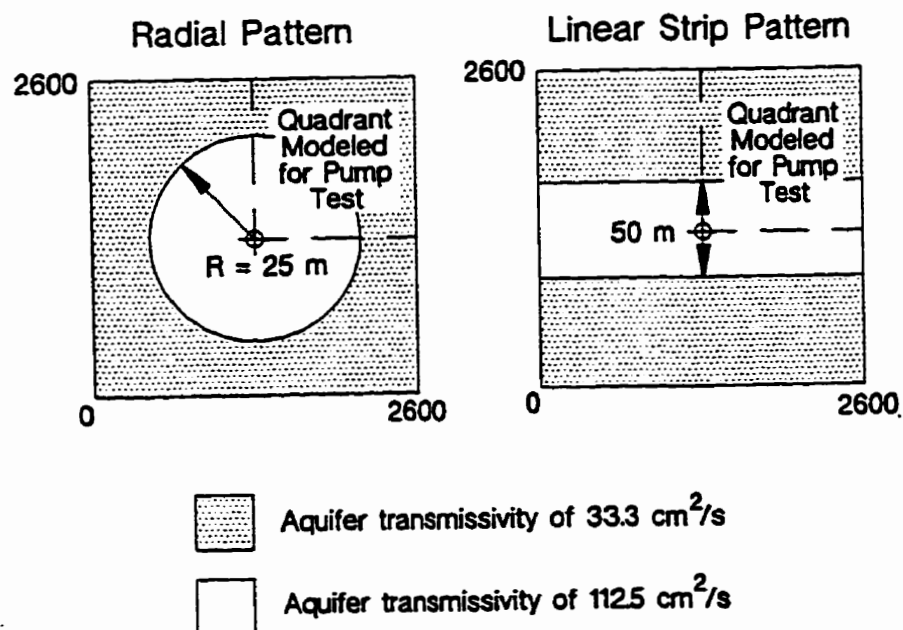


Figure 6.12 Areal changes in transmissivity for three hypothetical aquifers used to simulate pump tests with FRAC3DVS.

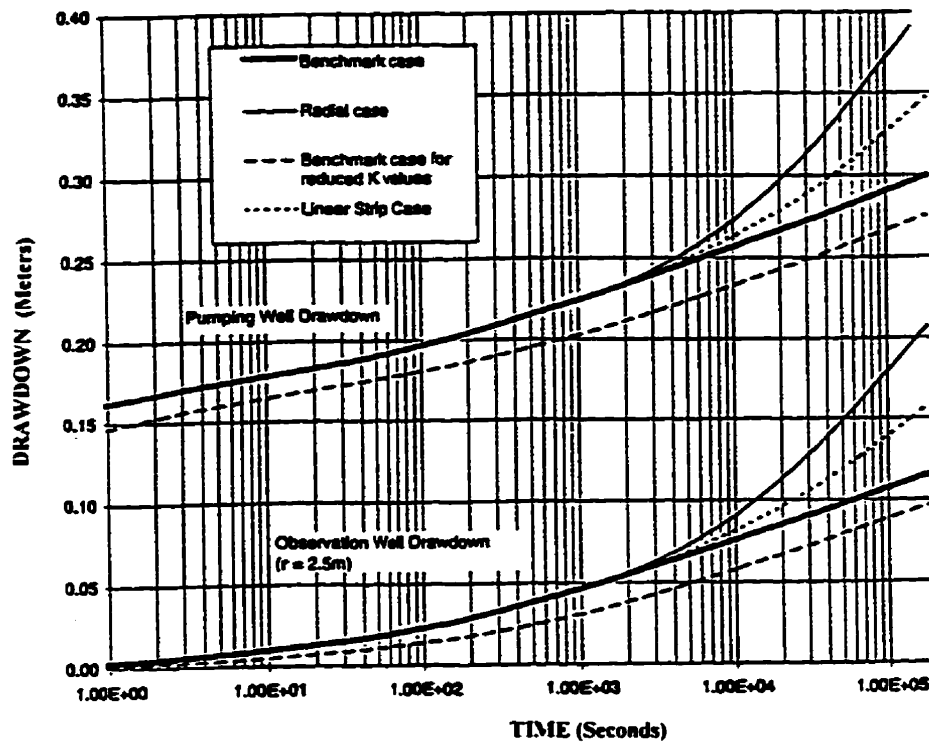


Figure 6.13 Simulated pump test drawdowns for hypothetical unconfined aquifer based at the pumping well and an observation well at a radial distance of 2.5 m. Time-drawdown response at the pumping well and an observation well (radial distance of 2.5m) for numerical simulated pump tests in an hypothetical unconfined aquifer.

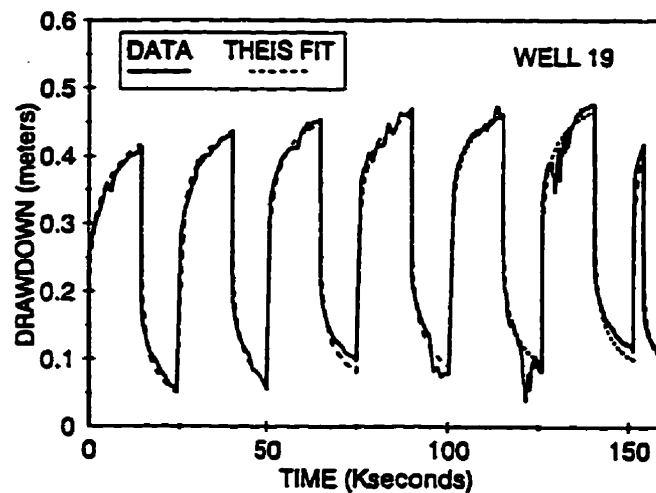


Figure 6.14 Thisis type curve fit to data from aquifer test 2, which includes a cyclic pumping schedule at Well 5.

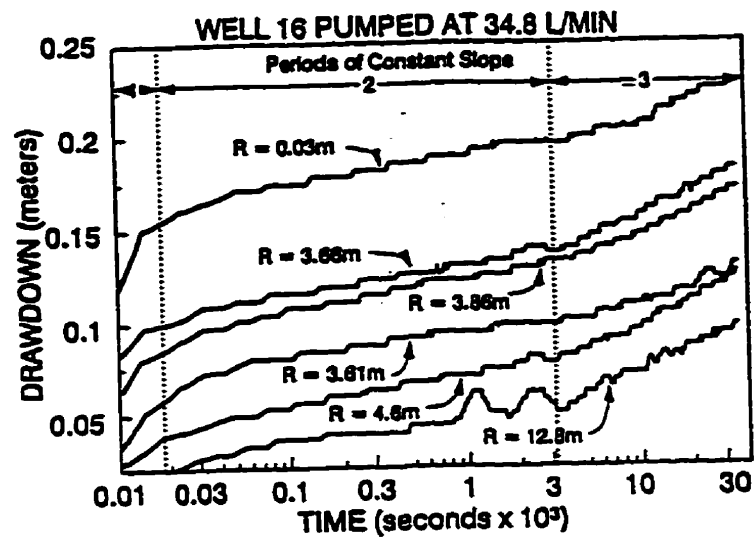


Figure 6.15 Time-drawdown response at the pumping well and five observation wells during AT4.

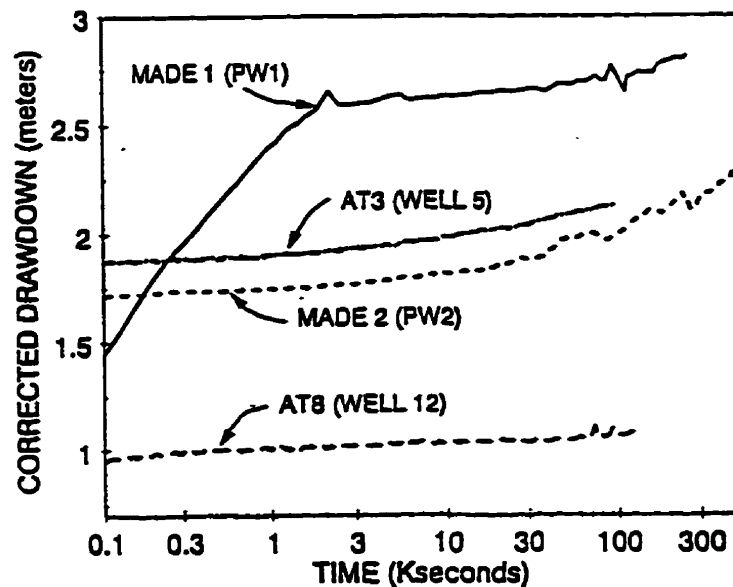


Figure 6.16 Time-drawdown data from the pumping wells used in the large-scale pumping test designated as MADE1, MADE2, AT3, and AT8 (see Figure 6.15 for results from AT4).

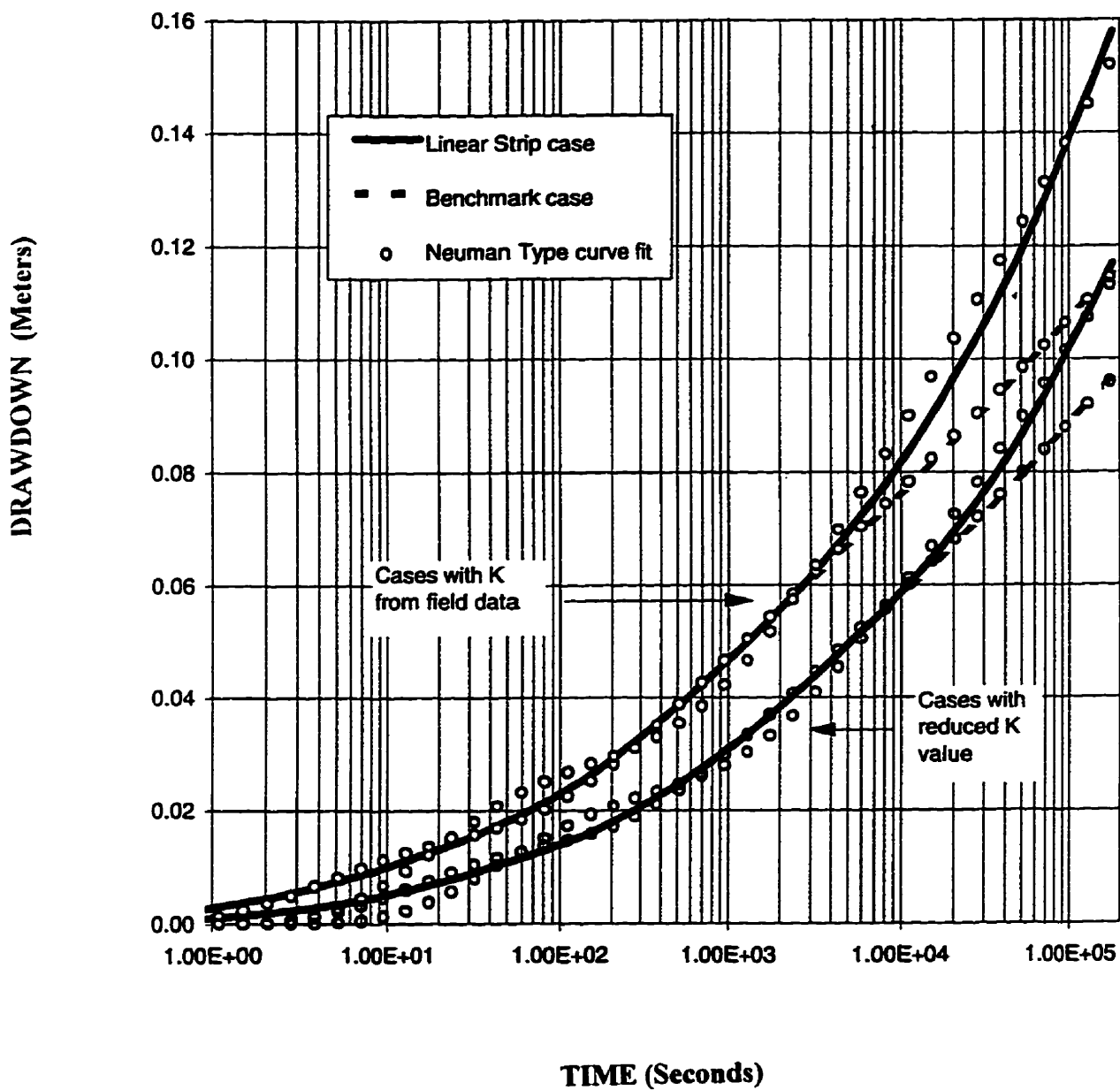


Figure 6.17 Neuman type-curve fits to the simulated pump tests for the benchmark and linear strip cases shown in Figure 6.12.

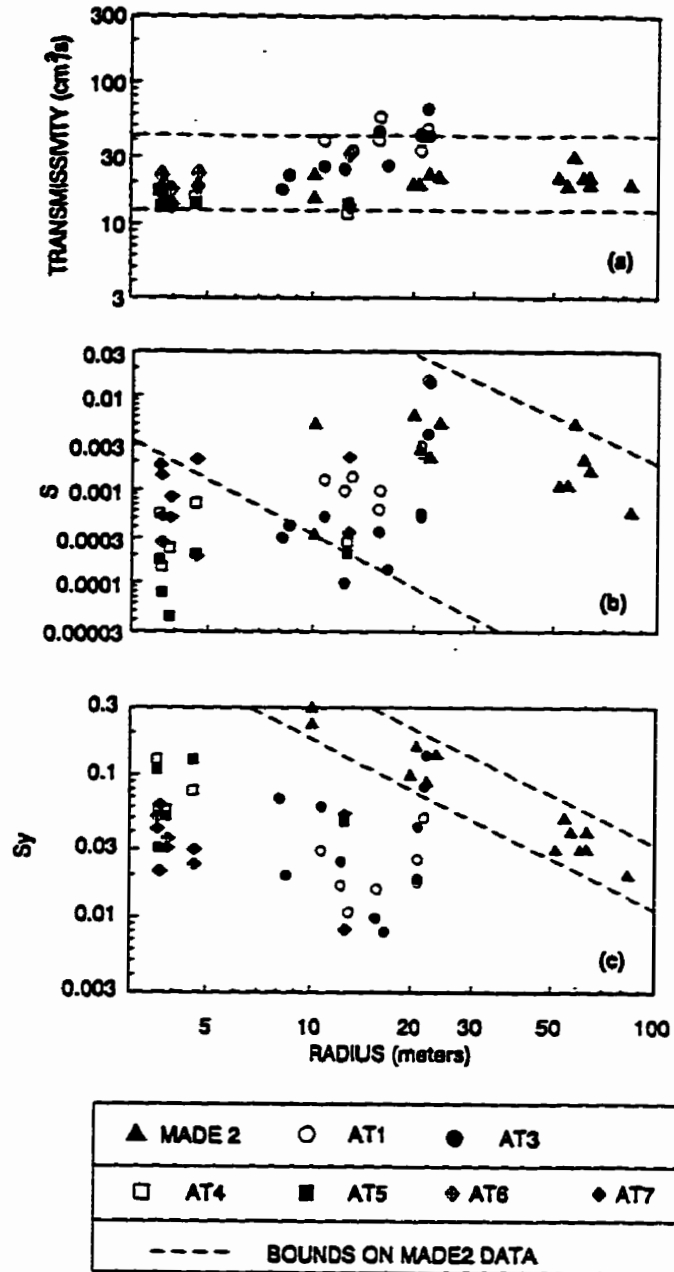


Figure 6.18 Values for transmissivity, specific storage, and specific yield from application of Neuman curve fits to seven pumping tests located in the paleochannel.

## 7. IMPACTS OF PUMPING RATE ON TRANSMISSIVITY VALUES

### 7.1 INTRODUCTION

Traditional objectives for conducting/analyzing pumping tests have focused mainly on effective hydraulic properties at the regional scale in support of water-supply studies. Issues of scale and heterogeneity have been secondary. Over the last decade, pumping tests have focused increasingly on characterizing aquifer spatial variability, mostly with a majority of testing performed in support of groundwater remediation. If pumping tests are to become effective methods for characterizing aquifer variability, both theoretical and field studies are needed to investigate prudent application of pumping tests in heterogeneous aquifers.

This chapter describes results from single-well pumping tests in an unconfined, heterogeneous aquifer underlying the Columbus Air Force Base (CAFB) in Mississippi. At the 1-Ha test site, which is intersected by a paleochannel, several single-well pumping tests were performed at 37 wells. Based on the trends in the transmissivity values calculated from the Cooper-Jacob straight-line (CJSL) method, the wells were divided into two groups. One group was characterized by CJSL transmissivity values that decreased with higher pumping rates. The other group was characterized by CJSL transmissivity values that increased with higher pumping rates. For both well groups, order-of-magnitude changes in the CJSL transmissivity values occurred at several wells in response to changes in the pumping rate. Analysis of the field data and complementary numerical simulations show that CJSL transmissivity values can be sensitive to pumping rates for pumping tests in heterogeneous unconfined aquifers.



This chapter contains three main sections. The first section describes the 1-Ha test site and large-scale transmissivity trends at CAFB. The second section summarizes results of 115 single-well pumping tests at 37 wells in the 1-Ha test site. The third section presents results from numerical simulations of single-well pumping tests to help explain some of the trends observed in the field data. The intent of the paper is to demonstrate, using field and numerical results, that pumping rate can have a significant effect on CJSL transmissivity calculated from pumping test data in a heterogeneous, unconfined aquifer.

## **7.2 BRIEF DESCRIPTION OF SITE CONDITIONS**

### **7.2.1 Site Description**

The CAFB aquifer is composed of 10 to 12 m of fluvial Quaternary-age deposits, which consist primarily of highly heterogeneous coarse-grained deposits in the lower 8 to 10 m and fine-grained deposits in the upper 2 to 3 m. Based on 881 borehole flowmeter K values, Young (1995) estimated an arithmetic mean, a geometric mean, and a  $\sigma^2_{\log(K)}$  of 0.26 cm/s, 0.032 cm/s, and 0.92, respectively, for the deposits. The Quaternary deposits conformably overlie the Cretaceous Eutaw Formation, which consists primarily of marine clay and silt. Seasonal effects cause the water table to vary from 1 to 3 m below ground surface. Regional geological information for the Columbus aquifer was obtained from an Army Corps of Engineers archaeological study within the Tombigbee valley (Muto and Gunn, 1988). The study suggests that braided streams and coarse-grained meandering streams formed the Columbus aquifer. Shown in Figure 7.1 is a 1956 USAF aerial

photograph that outlines a paleochannel that intersects test sites designated as the MADE (Boggs et al., 1992) and the 1-Ha (Young, 1995) test sites.

A simple sedimentological model for the CAFB aquifer proposed in previous chapters is illustrated in Figure 7.2. At the base of the paleochannel are coarse-grained channel lag, scour pool, and chute bar deposits. Above these deposits are fine-grained sediments that filled the meander channel after it was abandoned. Associated with the convex and concave regions of the paleochannel are point bar and cutback/overbank deposits, respectively.

Based on an equation from Leeder (1973) and a 70-m width for the paleochannel, a base elevation near 59 m MSL for the channel lag deposits was estimated (Chapter 4). Below 59 m MSL, the aquifer is presumed to be a mixture of coarse-grained fluvial deposits from braided and/or coarse-grained meandering rivers. Shown in Figure 7.3 are results of a continuous soil core from a borehole that intersects the paleochannel. The vertical profile of grain-size distribution shows that the coarse-grained deposits are sandwiched between fine-grained sediments associated with the channel-fill and the Eutaw Formation. The lack of a definable transition between channel lag deposits and older alluvium near 59 m MSL in Figure 7.3 is attributed to the channel lag representing reworked alluvium that is best differentiated from other alluvium by its sedimentary structures.

### **7.2.2 Well Network**

The primary focus of this chapter is the 1-Ha test site, which includes thirty-seven 5.0-cm ID fully-screened PVC wells (Figure 7.4). All wells were constructed from schedule

40 PVC pipe with 0.01-in slots and 0.125-in spacers (see Appendix A). Each well was developed for approximately 3 hours using overpumping, backwashing, and mechanical flushing (Young, 1991a; Young et al., 1993a). Table 7.1 lists hydraulic tests performed at the 1-Ha test site in 1989.

**Table 7.1 Chronology of Pumping Tests Performed at the 1-Ha Test Site in 1989**

Well Testing Activity	Dates	Saturated Aquifer Thickness
Slug Tests	April	7.2 m
2-minute Single-well Pumping Tests	April	7.2 m
Borehole Flowmeter Measurements	April	7.1 m
Multi-well Pumping Tests		
AT1 at well 5	May	6.7 m
AT2 at well 5	June	6.6 m
AT3 at well 5	June-July	6.5 m
Multi-rate Single-Well Pumping Tests		
Phase 1	June	6.6 m
Phase 2	July	6.5 m

Shown in Figure 7.5 is the  $\log(K)$  field from 60 to 62 m MSL for the upper portion of the 1-Ha test site, as determined from borehole flowmeter K values (Young, 1995). The high-K zone coincides with the location of the paleochannel channel lag deposits. In the convex and concave regions of the paleochannel are areas of moderate K values and low K values, respectively. Shown in Table 7.2 are changes in CJS� transmissivity values over time calculated from pumping test data collected from the pumping wells shown in Figure 7.1. The data show that the highest CJS� transmissivity values are from early-time

drawdown data collected from the three pumping wells located within the paleochannel. At these well locations, the CJS� transmissivity decreases over time. At the two wells located outside the paleochannel, the CJS� transmissivity values remain constant or increase with time. At late times, the CJS� transmissivity values are similar for all wells, irrespective of their location. As shown in Chapter 6, the changes in the CJS� transmissivity values over time are caused by the expansion of radius-of-influence,  $R_i$  (to be discussed later), into or beyond the high-K deposits associated with the paleochannel.

**Table 7.2 CJS� Transmissivities from the Drawdown Data Collected from Aquifer Tests MADE1, MADE2, AT3, AT4, and AT8**

Well	Test Name	Rate (L/min)	Early times			Late times		
			Duration (s)	T*	R*	Duration (s)	T*	R*
PW1	MADE1	62	100-1800	2	1.0	2000-250000	21	.93
PW2	MADE2	208	100-8700	102	.96	33000-500000	17	.97
5	AT3	112	100-2500	99	.94	5600-100000	23	.99
16	AT4	35	100-2500	63	.98	3400-35000	29	.98
12	AT8	24	171-30000	27	.95	171-30000	27	.95

\* T - Transmissivity ( $\text{cm}^2/\text{s}$ )  
R - regression coefficient

## 7.3 RESULTS FROM SINGLE-WELL PUMPING TESTS AT THE 1-Ha TEST SITE

### 7.3.1 Description

During stable water conditions in the summer of 1989, single-well pumping tests targeted at high (~60 L/min), moderate (~30 L/min), and low (~15 L/min) pumping rates

were performed at each of the wells in the 1-Ha test site. A total of 115 successful pumping tests were conducted. Reproducibility of the tests was checked by duplicating several pumping tests. Each pumping test lasted approximately 20 minutes. Drawdown values were measured with a pressure transducer at 1- to 2-second intervals. A problem encountered during testing was maintaining a constant pumping rate at wells where large drawdowns occurred. At these wells, a constant pumping rate was typically established after 20 to 60 seconds.

### 7.3.2 Results

For each single-well test, transmissivity values were calculated using the CJS� method after the Jacob correction factor (Jacob, 1963) had been applied for dewatering effects. For most of the drawdown curves, the time interval for the CJS� method began between 100 and 200 seconds and ended between 900 and 1200 seconds. The CJS� method was applied in a manner to account for wellbore storage (Cooper et al., 1967), aquifer storage effects (Cooper and Jacob, 1946), and positive skin effects (Young, 1996).

Plots similar to those in Figure 7.6 show that the slope of late-time semilog time-drawdown data varied with the pumping rate in some nonlinear manner at all 37 wells. At approximately half of the wells, the transmissivity values decreased with increased pumping. This trend can be partly explained by the desaturation of the aquifer. At the remaining half of the wells, however, the reverse occurred—the transmissivity values increased with increased pumping.

The sensitivity of the calculated CJSL transmissivity values to the pumping rate varied considerably among the well locations. At several wells, the CJSL transmissivity values varied less than 10%, but at some well locations, the CJSL transmissivity values varied over 10-fold. Figure 7.7 shows the effect of the pumping rate on the CJSL transmissivity for several of the most sensitive wells. A mapping of the CJSL trends in Figure 7.8 shows that the CJSL trends are not random. By assuming that increases in the pumping rate accelerated the expansion of the  $R_1$  one can delineate regions of relatively high and relatively low transmissivity from the trends in the CJSL transmissivity values (Figure 7.8). A notable feature of the region of inferred high transmissivity is that it corresponds to the mapped locations of the paleochannel in Figure 7.1 and the high-K zone in Figure 7.5.

The field results show that an increase in the pumping rate can have a major impact on the calculated CJSL transmissivity values causing them to either increase or decrease. To help identify the reasons CJSL transmissivity values are sensitive to the pumping rate, numerical simulations are presented in the next section. To reduce the complexity and uncertainty associated with simulating and interpreting pumping-test results, model simulations were performed with a two-dimensional axisymmetric model. A premise for the simulations is that the transmissivity field at CAFB contains large-scale trends. To investigate the decreased CJSL transmissivity values with increased pumping rate for wells intersecting the paleochannel, model simulations were performed with a transmissivity field that has K decrease with radial distance from the well. To investigate the increased CJSL transmissivity with increased pumping rate for wells outside but near the paleochannel,

model simulations were performed with a transmissivity field that has  $K$  increase with radial distance from the well.

#### **7.4 CONSIDERATIONS FOR NUMERICAL SIMULATIONS OF SINGLE-WELL PUMPING TESTS**

Important issues associated with simulating pumping tests in an unconfined, heterogeneous aquifer are: 1) the selection of the numerical groundwater flow code, 2) the hydraulic properties of the modeled aquifer, 3) the pumping rates, and 4) the numerical discretization.

##### **7.4.1 Numerical Flow Code**

Among the desired capabilities of the numerical code is the ability to accurately represent unsaturated processes and well hydraulics in a heterogeneous aquifer. Though numerous codes exist, only a few codes have these two capabilities. One of these codes is FRAC3DVS (Therrien and Sudicky, 1996), which solves Richard's equation with a robust Newton-Raphson iteration scheme and solves flow to a well using line-elements, as described by Sudicky et al., (1995). FRAC3DVS has been successfully used to reproduce published analytical, numerical, and field data for pumping tests in unconfined aquifers.

##### **7.4.2 Hydraulic Properties of Modeled Aquifer**

All model simulations were for a 10-m thick aquifer with an initial saturated thickness of 6.5 m. No field data have been collected at CAFB to determine aquifer storage properties. For simplicity, the aquifer was assumed to have uniform storage properties. The

specific storage coefficient was set to 0.00005, which is consistent with the range provided by Freeze and Cherry (1979) for sands and gravel. Unsaturated hydraulic properties were calculated based on the van-Gentuchen parameters in Chapter 6 to simulate large-scale pumping tests at CAFB. These parameters are illustrated in Figure 7.9.

As previously mentioned, model simulations were performed using data sets based on a  $K$  field that increased and a  $K$  field that decreased with distance from the pumping well. Based on the range of transmissivity values in Figure 7.7, transmissivity varied 100 fold within each data set. To account for the effects of vertical heterogeneity, different values of vertical anisotropy ( $K_z/K_h$ ) were used.

### 7.4.3 Numerical Model

All pumping tests were performed with an axisymmetric 2-dimensional grid with 7800 elements and 8003 nodes. In the vertical direction, 53 elemental layers had variable thicknesses that ranged from 0.125 m near the initial water table to 0.5 m at the base of the aquifer. In the radial direction, the element lengths varied from 0.02 m at the well to 10 m at the aquifer boundary at 400 m. No-flow conditions were imposed at the aquifer top, bottom, and sides. Model simulations began with an initial time step of 0.0005 minutes and ended with a maximum time step of 5 minutes over a period of 60 minutes. Model output included a vertical profile of groundwater flow into the well at each time step. Examination of these profiles showed that wellbore storage effects had dissipated after 40 s for all model runs.



#### **7.4.5 Pumping Rate and CJS� Transmissivity Values**

For each transmissivity field, pumping tests were performed at three pumping rates and one injection rate. The pumping rates were selected to cover a 10-fold range with the largest pumping rate producing a maximum drawdown of about 3 m. The injection rate was set to the magnitude of the pumping rate that would produce a head build-up of about 1 m. For every simulated pumping test, CJS� transmissivity values were calculated with drawdown data for a period of 40 to 60 minutes. To correct for dewatering effects, all drawdown data was adjusted by the Jacob correction factor (Jacob, 1963) .

### **7.5 SIMULATIONS OF PUMPING TESTS IN AN AQUIFER WITH A TREND OF INCREASING K WITH DISTANCE**

#### **7.5.1 Selection of Trend in the Transmissivity Field**

Based on the borehole flowmeter K values from the 1-Ha test site (Young , 1995) and transmissivity values in Figure 7.7, wells outside the paleochannel intersect aquifer material that is approximately 100 times less transmissive than the paleochannel bedload deposits. To represent a trend of increasing transmissivity with distance, a hypothetical aquifer was constructed with K values that increased linearly from 0.04 cm/s at the well to 0.4 cm/s at a radial distance of 37.5 m. These K values produced transmissivity values from 2.6 cm<sup>2</sup>/s to 260 cm<sup>2</sup>/s.

#### **7.5.2 Sensitivity of CJS� Transmissivity Values to Pumping Rates**

Figure 7.10 presents example simulations of drawdown responses for unconfined aquifers with vertical anisotropies (Kz/Kh) of 1 and 0.01. The pumping test responses are

plotted with drawdown normalized to the pumping rate. For reference, the simulated drawdown obtained for a confined case is presented. Although it may appear that only one drawdown curve is provided for the confined case, numerous runs were made with different pumping rates and anisotropy values, but they all matched the result provided in Figure 7.10. Figure 7.11 provides the CJSJL transmissivity values for simulated pumping tests in Figure 7.10 and for cases of different anisotropy values. These results show that an increase in the pumping rate leads to an increase in the CJSJL transmissivity values similar to that shown in Figure 7.7b. This result is contrary to what is expected in a homogeneous aquifer where increased pumping would cause a decrease in the transmissivity for the saturated aquifer. To help explain the physical processes that cause the trends in Figures 7.7b and 7.11, one needs to understand the sensitivity of CJSJL transmissivity values to the rate of expansion of  $R_1$  in a heterogeneous aquifer.

### **7.5.3 Importance $R_1$ to Calculated CJSJL Transmissivity Values**

According to Butler (1990), CJSJL transmissivity values primarily reflect the transmissivity of the aquifer material from which water is being released for the time period of the drawdown data. As a result, during the late times of a pumping test, the CJSJL transmissivity value is relatively insensitive to the total drawdown and the aquifer transmissivity near the well, but very sensitive to the aquifer transmissivity away from the well (Oliver, 1990; Butler, 1988, 1990; Butler and Liu, 1991). Because CJSJL transmissivity values primarily reflect the transmissivity of the aquifer material away from the well at late

times, a major factor affecting CJSJL transmissivity values in aquifers with radial trends in the K field is the rate that  $R_i$  passes through aquifer material with different K values.

Numerous definitions for  $R_i$  have been proposed. Streltsova (1988) states that these definitions can be written as  $R_i = A * (C * T * t / S)^{-0.5}$  where A and C are coefficients; t is time; S is the effective storage coefficient; and T is transmissivity. Implicit in this relation is that the expansion of  $R_i$  is proportional to T and inversely proportional to S. Because the pumping rate affects neither T nor S in an confined aquifer, CJSJL transmissivity values in a confined aquifer should not be affected by the pumping rate—a finding confirmed by results in Figures 10 and 11. However, because the pumping rate indirectly affects T and S in an unconfined aquifer, the pumping rate will affect the rate of expansion of  $R_i$ .

The relation between pumping rate and transmissivity is relatively straightforward in an unconfined aquifer. An increased pumping rate reduces the saturated aquifer thickness and aquifer transmissivity near the well and thereby slows the expansion rate of  $R_i$  away from the well. Although desaturation and resaturation can be important in vertical heterogeneous material, as will be shown later, changes in the transmissivity of the aquifer saturated thickness cannot cause the trends observed in Figures 7.10 and 7.11. For increased pumping to cause the higher CJSJL transmissivity values in Figure 7.11, it must decrease the value of S near the well so that an increase in the CJSJL transmissivity can be realized by an increase in the expansion rate of  $R_i$  into the higher K materials away from the well.

In an unconfined aquifer, the value of S represents an effective storage coefficient that accounts for the water released from drainage and elastic storage. Because elastic storage contributes much less to the total water released from storage than does drainage,

drainage principally determines the value of  $S$ . Key model parameters associated with drainage are fluxes at the aquifer boundaries (e.g. pumping rate, recharge distribution), the amount of water available from storage (e.g., moisture retention curves, specific storage coefficients), and the energy required to cause groundwater to flow (e.g., unsaturated  $K$  functions, anisotropy).

#### **7.5.4 Factors Affecting the Sensitivity of CJSL Transmissivity Values to Pumping Rate**

An important relation that affects the relation between the pumping rate and  $S$  is specific moisture capacity, which is the first derivative of the moisture content change with respect to pressure change. Figure 7.12 shows that specific moisture capacity increases from 0 to  $-0.31$  m pressure but decreases steadily for pressures below  $-0.31$  m and becomes less than 0.01 at about  $-3$  m. Because of the non-linearity in the pressure-moisture content relation, the amount of drainage released from the unsaturated zone (e.g., from the water table to 10-m elevation) per unit drop in pressure will decrease with increased drawdown. Thus, at higher pumping rates, a reduction in  $S$  and an increased expansion rate of  $R_i$  should be expected. If increased pumping causes lower  $S$  values, one should expect that increased pumping should cause an increase in the transmissivity values—a trend shown in Figures 7.11 and 7.7b.

Because drainage travels partially downward along a flowpath toward the well during pumping, changes in  $K_z$  should affect the temporal and spatial variability in the drainage patterns. As shown in Figures 7.11 and 7.13, an increase in  $K_z$  causes a decrease in the CJSL transmissivity for a particular pumping rate and also reduces the range of CJSL

transmissivity among different pumping rates. These results are consistent with an increased  $K_z$  leading to improved drainage and thus higher values of  $S$  near the pumping well at early times.

The phreatic surface near the well for injection and withdrawal scenarios is presented in Figure 7.14 for anisotropy values of 0.01 and 100. Differences in the vertical distance between the phreatic surface and the initial head elevation of 6.5 m provide a measure of the value of  $S$  and  $T$  as a function of distance. For the withdrawal scenarios, an increased anisotropy from .01 to 100 caused a general trend of smaller  $T$  values and larger  $S$  values near the well. Both of these changes promote a reduced expansion rate of  $R_e$ . Hence, the trend of lower CJSL transmissivity values with lower anisotropy values shown in Figures 7.11 and 7.13 for the withdrawal scenarios, is consistent with the fact that an increase in anisotropy tends to decrease  $T$  but increase  $S$  near the well. For the injection scenarios, an increased anisotropy from .01 to 100 caused smaller values for both  $T$  and  $S$  near the well. The fact that  $S$  and  $T$  change in the same direction makes CJSL transmissivity values less sensitive to changes in anisotropy for the injection than for the withdrawal scenarios. As a result, the range for CJSL transmissivity values from the injection simulations is approximately one-seventh the range for the CJSL transmissivity values from the withdrawal simulations .

Because the CJSL transmissivity values for the injection and withdrawal scenarios have different sensitivities to changes in the anisotropy, the ratio of the injection to the withdrawal CJSL transmissivity values should be sensitive to the anisotropy value. This sensitivity is shown in Figures 7.11 and 7.13. For the case of high anisotropy (e.g.,  $K_z/K_h$

>10), the CJSL transmissivity values are higher for injection than for withdrawal of 0.02 m<sup>3</sup>/min. However, for the case of low anisotropy values (e.g.  $K_z/K_h < 1$ ), the CJSL transmissivity values are lower for injecting than for withdrawing 0.02 m<sup>3</sup>/min.

Figure 7.15 shows results from withdrawal and injection tests performed at well 14, which according to Figures 7.4 and 7.8 is located in a region where a radial increase in  $K$  with distance is presumed to exist. For the case of  $K$  increase with radial distance and low anisotropy (i.e.  $K_z/K_h < 1$ ), the results of the numerical simulations indicate that higher CJSL transmissivity values should be obtained for pumping than for injection. Analysis of the data in Figure 7.15 supports the findings of the numerical results as the CJSL transmissivity values for the injection and withdrawal tests are 12 cm<sup>2</sup>/s and 81 cm<sup>2</sup>/s, respectively. In evaluating this comparison, one should note that the injection test was performed in April 1989 when the ambient water table was 0.5 m higher than in June 1989 when the pumping test was performed. As a result of the high water table in April, the CJSL transmissivity value for the injection test would likely have been lower if the test were performed at the time of the pumping test. Hence, the field data are consistent with the results of the numerical simulations of injection and withdrawal scenarios in Figure 7.10.

Drainage, and thus the value of  $S$  near the well, are affected by aquifer unsaturated soil-moisture characteristics. With regard to the baseline conditions shown in Figure 7.9, the drainage rate near the well can be slowed by maintaining the baseline pressure- $K$  function while slightly increasing the capacity of the aquifer to retain moisture according to the modified moisture-pressure function in Figure 7.9. As shown in Table 7.3, a reduced

capability of the aquifer to retain water leads to higher CJSL transmissivity values, which is consistent with an accelerated growth rate of  $R_i$  caused by a reduction in the value of  $S$ .

Drainage near the well can be changed not only via the moisture retention curve but also via the pressure- $K_{\text{unsaturated}}$  relation. A simple approach to increase  $S$  near the well is to make  $K$  unaffected by decreased pressure (Figure 7.9). The impact of improving drainage near the well by increasing the values of  $K_{\text{unsaturated}}$  cause lower CJSL transmissivity values, which is consistent with a reduced growth rate of  $R_i$  caused by an increase in the value of  $S$  near the well.

**Table 7.3 Percentage Change in the CJSL Transmissivity Caused by Changes in the Specific Storage and Aquifer Unsaturated Properties**

Anisotropy $K_z/K_h$	Pumping Rate ( $\text{m}^3/\text{min}$ )	Modified Unsaturated Functions *		Baseline Unsaturated Functions *	
		Theta Change	K Change	$S_s = .0005$	$S_s = .000005$
1.0	+0.02	-11.1	12.9	-1.4	1.6
	-0.005	-13.9	31.1	-1.5	1.7
	-0.02	-15.5	34.5	-1.7	2.1
	-0.04	-18.5	41.7	-2.4	2.9
0.1	+0.02	-25.6	37.2	-2.5	2.8
	-0.005	-57.7	155.0	-3.8	4.4
	-0.02	-63.9	196.5	-5.2	6.0
	-0.04	-69.6	258.7	-7.9	9.1
0.01	+0.02	-38.8	53.5	-3.4	3.7
	-0.005	-80.4	438.2	-6.8	7.5
	-0.02	-87.3	692.4	-13.5	16.1
	-0.04	-91.4	1050	-25.0	34.2

\* see Figure 7.12 for baseline and modified unsaturated relations

Although the value of  $S$  is dominated by drainage, elastic storage should affect CJSL values. As shown in Table 7.3, an increase in  $S_s$  caused a reduction in the CJSL value, which is consistent with a slower expansion rate for  $R_i$  caused by a higher  $S$  value. Similarly, a decrease in  $S_s$  caused an increase in the CJSL value, which is consistent with an accelerated expansion rate for  $R_i$  caused by a lower  $S$  value. As with changes in the aquifer unsaturated properties, changes in  $S_s$  have a greater effect on the CJSL values at higher pumping rates and at lower anisotropy values.

#### 7.5.5 Summary

Results from numerically simulated pumping tests are presented for the case where  $K$  increases with distance from the pumping well. These results show that CJSL transmissivity values for late times are sensitive to model parameters that affect drainage processes near the well. Table 7.4 summarizes some of the major results. Among the interesting findings are that: (1) the value of  $S$  near the well can have a greater effect on the CJSL transmissivity values than does the value of  $T$  near the well; and, (2) an increased pumping rate can lead to an increase in the CJSL transmissivity value calculated from the semilog slope of the time-drawdown data.



**Table 7.4 Expected Effect on S,  $R_i$ , and CJSL Transmissivities Caused by Model Parameter Changes for a Basecase Pumping Scenario that has K Increase with Distance from the Pumping well**

Parameter Change	Effect on S	Reason for Change in S	Effect on $R_i$	Effect on CJSL T
Increase in Pumping Rate	Decrease	Trend for specific moisture capacity to decrease with increased drawdown (see Figure 7.12)	Accelerate rate of expansion	Increase
Injection instead of Pumping	Increase	Trend for specific capacitance to increase with decreased drawdown (see Figure 7.12)	Reduce rate of expansion	Decrease for $K_z/K_h < 1$ . Increase for $K_z/K_h > 10$ .
Lower Anisotropy	Decrease	Increased resistance to vertical flow	Accelerate rate of expansion	Increase
Change Aquifer Unsaturated Properties	Decrease or increase	Greater retention capability of soil would decrease S. Higher values for $K_{unsaturated}$ would increase S.	Reduce or accelerate rate of expansion	Increase or Decrease
Increase Specific Storage	Increase	Release of additional elastic storage per unit drop in pressure	Reduce rate of expansion	Decrease

## 7.6 SIMULATIONS OF PUMPING TESTS IN AN AQUIFER WITH A TREND OF DECREASING K WITH DISTANCE

### 7.6.1 Selection of Trend in the Transmissivity Field

Based on K values from borehole flowmeter tests described in Chapter 4 and transmissivity values from single-well pumping tests (Figure 7.7), the paleochannel has transmissivity values that are approximately 100 times greater than the deposits that lie 30 to 50 meters outside the paleochannel. Flowmeter data from the paleochannel indicate that

the upper aquifer has significantly higher  $K$  than does the lower aquifer. At most of the well locations in the paleochannel, permeable deposits with  $K$  values in the range of 0.5 to 1 cm/s can be found above 59 m MSL. To illustrate the significant vertical differences in the  $K$  values, the borehole flowmeter  $K$  values for Well 2 are presented in Figure 7.16. As shown in Figure 7.16, the ambient water table in June 1989 lies about 1.5 m above the base of the high- $K$  zone. Among the considerations of a low water table is that desaturation of the upper permeable layers could significantly affect the sensitivity of the CJSL transmissivity values to pumping rates.

To represent a trend of decreasing transmissivity with distance, a hypothetical aquifer was simulated with  $K$  values that decreased linearly from 0.04 cm/s at the well to 0.004 cm/s at a radial distance of 37.5 m. For the initial 6.5 m saturated aquifer thickness, these  $K$  values correspond to transmissivity values of 26 cm<sup>2</sup>/s and 2.6 cm<sup>2</sup>/s, respectively. To investigate the importance of the vertical variation in  $K$  near the well, the  $K$  field from the first hypothetical aquifer was modified by a highly permeable zone with a  $K$  of 4 cm/s between the elevations of 6.28 and 6.6 m. This additional  $K$  layer increases the near-field transmissivity of the saturated zone of the second hypothetical aquifer from 26 to 111 cm<sup>2</sup>/s.

### **7.6.2 Pumping Test Results for Aquifer with Only Radial $K$ Variations**

Figure 7.17 presents example simulations of drawdown responses for unconfined aquifers with anisotropies of 1 and 0.01. The pumping test responses are plotted with drawdown normalized to the pumping rate. For reference, the simulated drawdown obtained for a confined case is presented. Although it appears that only one drawdown curve is

provided for the confined case, numerous runs were made with different pumping rates and anisotropy values but they all matched the result provided in Figure 7.17. Figure 7.18 provides the CJSL transmissivity values for pumping tests simulated with different anisotropy values.

Given that the expansion rate for  $R_f$  increases with a higher pumping rate, a trend expected in Figure 7.18 is for the CJSL transmissivity values to decrease with increased pumping. This expected trend is evident for only the case where anisotropy is 0.01. For anisotropy values greater or equal to 0.1 the CJSL transmissivity values are relatively insensitive to the pumping rate. A key factor that reduced the sensitivity of CJSL transmissivity values in Figure 7.17 to changes in anisotropy and pumping rate is that decreasing transmissivity with distance buffers the expansion rate of  $R_f$ . As pumping conditions cause an increase in the expansion rate  $R_f$ , the migration of  $R_f$  into aquifer material of lower transmissivity throttles back the expansion rate and forces additional drawdown within the inner cone-of-influence. Thus the trend of decreasing transmissivity with distance produces a different effect than produced by an increasing transmissivity with radial distance, which serves to accelerate the expansion rate of  $R_f$ . An implication of the results in Figure 7.18 is that an increase in the pumping rate would cause a decrease in the CJSL transmissivity values only for anisotropy values less than 0.01, which is likely near the lower boundary for the field conditions at CAFB. Moreover, for the anisotropy value of 0.01, the range in the CJSL transmissivity values is much less than the range of values shown in Figure 7.7a. An implication of the low sensitivity of the CJSL transmissivity values in Figure 7.18 to pumping rates is that the trends observed in the CJSL transmissivity values

in Figure 7.7a may be partially caused by desaturation of high-K material in the upper aquifer.

### **7.6.3 Pumping Test Results for Aquifer with Radial and Vertical K Variations**

Figure 7.19 presents example simulations of drawdown responses for unconfined aquifers with anisotropies of 1 and 0.01 for a decreasing trend in K with radial distance that has a high-K layer placed in the upper aquifer. As in Figures 7.10 and 7.17, the pumping test drawdowns in Figure 7.19 have been normalized by the pumping rate. Shown in Figure 7.20 are the CJS� transmissivity values for the simulated pumping tests. Compared to the drawdown responses and CJS� transmissivity values in Figures 7.17 and 7.18, the drawdown responses and CJS� transmissivity values in Figures 7.19 and 7.20 are significantly more sensitive to the pumping rate.

The importance of the desaturation of the high-K layer to the CJS� trends in Figure 7.20 can be partially evaluated from a plot of CJS� transmissivity versus the maximum well drawdown for an anisotropy of 0.01. As shown in Figure 7.21, there is a non-linear relations between total drawdown and CJS� transmissivity values. For total drawdowns less than 0.07 or greater than 0.7 m, transmissivity values are less sensitive to changes in the drawdown (based on relative and not absolute differences) than transmissivity values for total drawdowns in the range of 0.07 to 0.7 m. For drawdowns that exceed 0.7 m (e.g., elevation less than 5.8 m), the transmissivity values are moderately sensitive to additional drawdown because the well is essentially hydraulically disconnected from the high-K zones away from the well as a result of the desaturation of the upper high-K zone

near the well. For drawdowns less than 0.07 m, the transmissivity values are moderately sensitive to drawdown increases because desaturation of the high-K layer has not been sufficient to significantly restrict the hydraulic connection between the well and the high-K material away from the well. Transmissivity values are strongly sensitive to drawdown changes in the range of 0.07 to 0.7 m because across this range of drawdown, the hydraulic connection between the high-K layer away from the well is dependent on the saturated thickness of the high-K layer near the well.

#### **7.6.4 Summary**

Results from numerically simulated pumping tests have been presented for the case where K decreases with distance from the pumping well. These results show that CJSL transmissivity values for late times are much less sensitive to anisotropy values and pumping rates than in the case where K increases with distance from the pumping well. For the situation where K decreases with distance from the well and also with depth, the CJSL transmissivity is strongly sensitive to both the pumping rate and the anisotropy value. This sensitivity occurs primarily because the aquifer saturated thickness near the well can significantly affect the hydraulic connection between the well and the higher K material in the upper aquifer away from the well.

### **7.7 CONCLUSIONS**

Based on a geological investigation and borehole flowmeter and pumping test results, a 1-Ha test site at Columbus Air Force Base (CAFB), Mississippi has significant large-scale

transmissivity variations caused by high-K bedload deposits associated with a paleochannel that crosses the site. Results from pumping test indicate that calculated CJSJ values can be very sensitive to the pumping rate. To help identify the reasons for this sensitivity, numerical simulations were performed with a two-dimensional axisymmetric model. Using simplistic K-field trends, numerical models simulated the trend of lower CJSJ values with increased pumping at wells that intersected the paleochannel and the trend of higher CJSJ values with increased pumping at wells outside the paleochannel. Among the important results from field and numerical results is that at CAFB the rate of expansion of the radius-of-influence,  $R_i$  has a significant effect on the calculated transmissivity value. Although  $R_i$  is not a function of the pumping rate,  $R_i$  is a function of aquifer storage and transmissive properties that are affected by the pumping rate in an unconfined aquifer. Hence, the pumping rate is a parameter that can indirectly have significant effect on the calculated CJSJ transmissivity values for unconfined aquifers where large-scale transmissivity values exists.

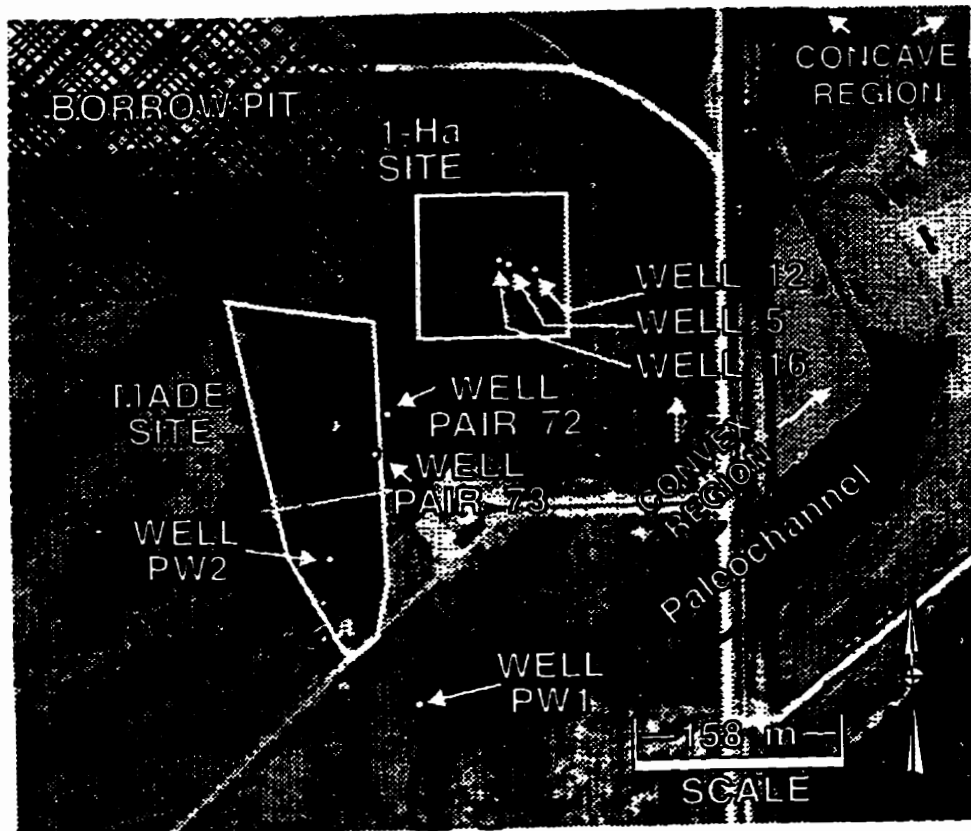


Figure 7.1 Location of two test sites at CAFB, MS superimposed on a 1956 aerial photograph that reveals a paleochannel.

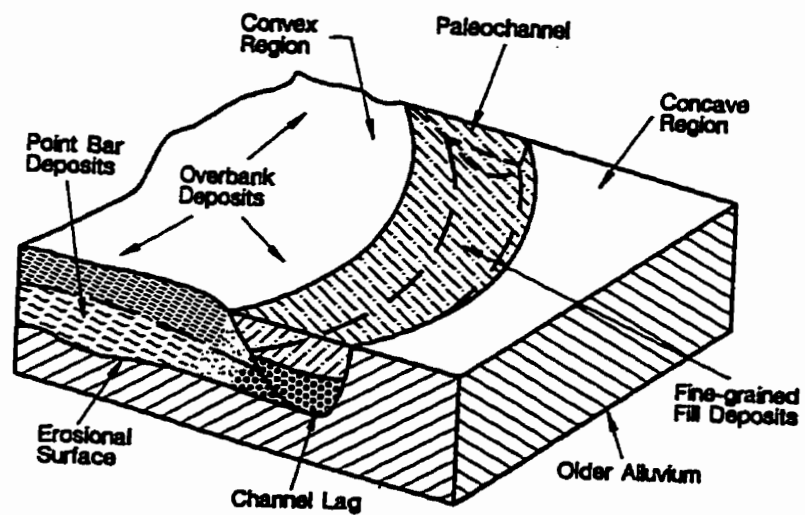


Figure 7.2 Schematic of the regional features associated with the sedimentological model.

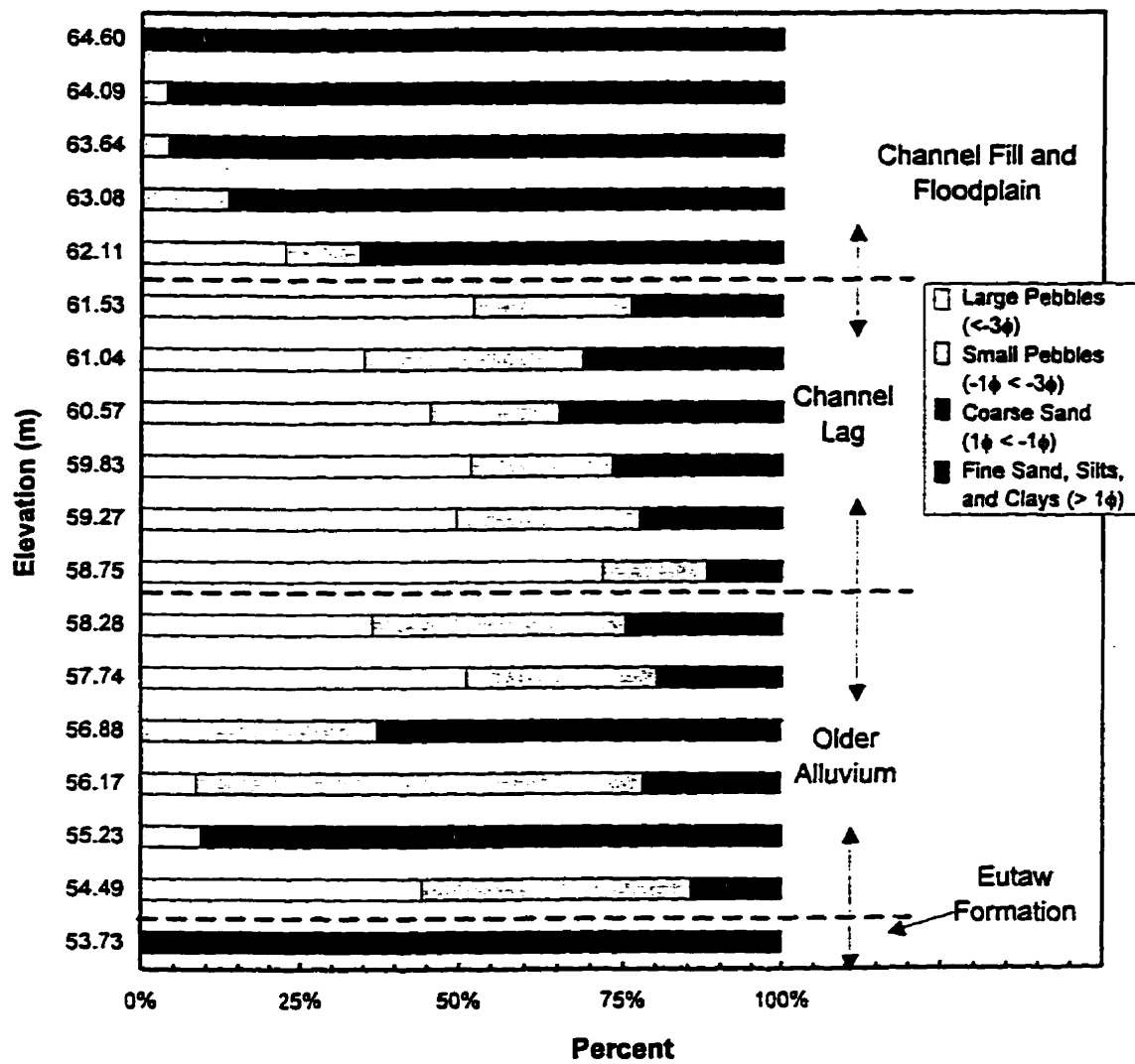


Figure 7.3 Vertical profile of grain-size distributions at Well 73 (ground surface is at 64.9 m MSL).



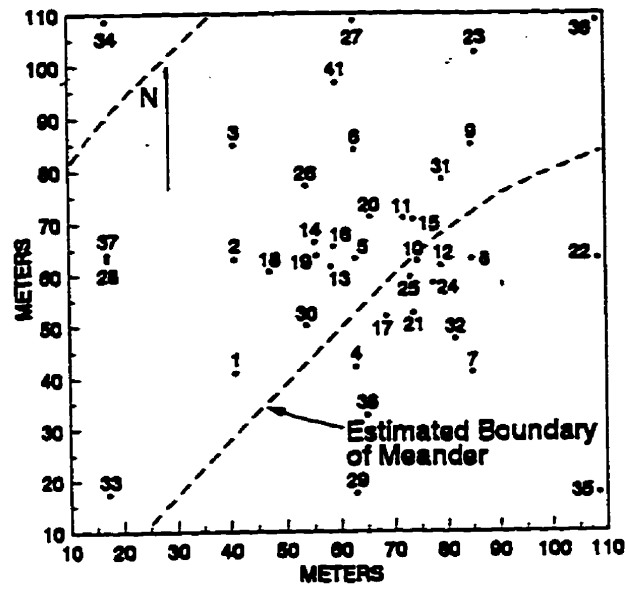


Figure 7.4 Well network for 1-Ha test site with location of the paleochannel estimated by dotted line.

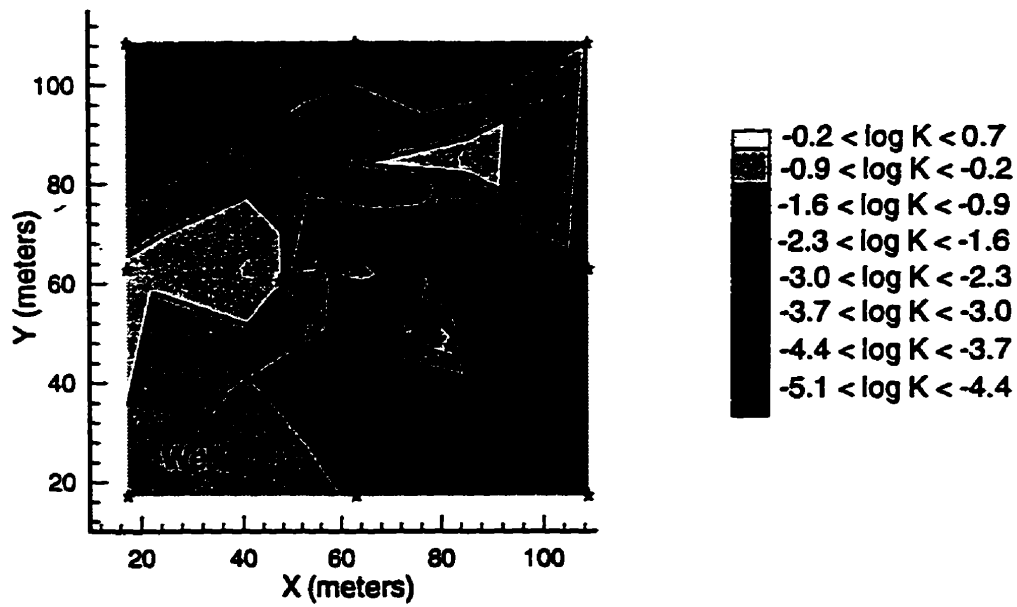


Figure 7.5 Areal profile of borehole flowmeter K values for the uppermost 2 m of the saturated aquifer at the 1-Ha test site (from Chapter 4).

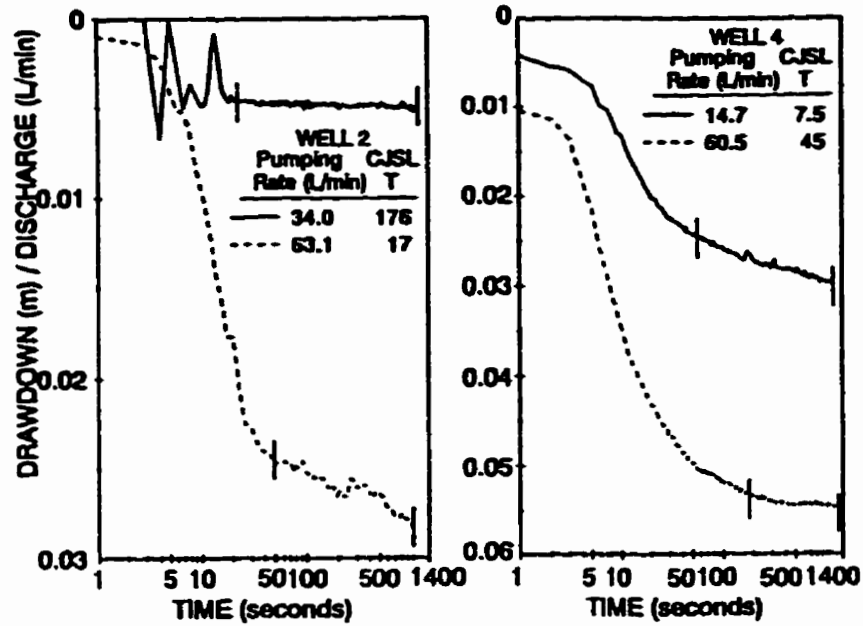


Figure 7.6 Effect of pumping rate on drawdown response (normalized by the pumping rate) and the CJSL transmissivity values for Wells 2 and 4 at the 1-Ha test site.

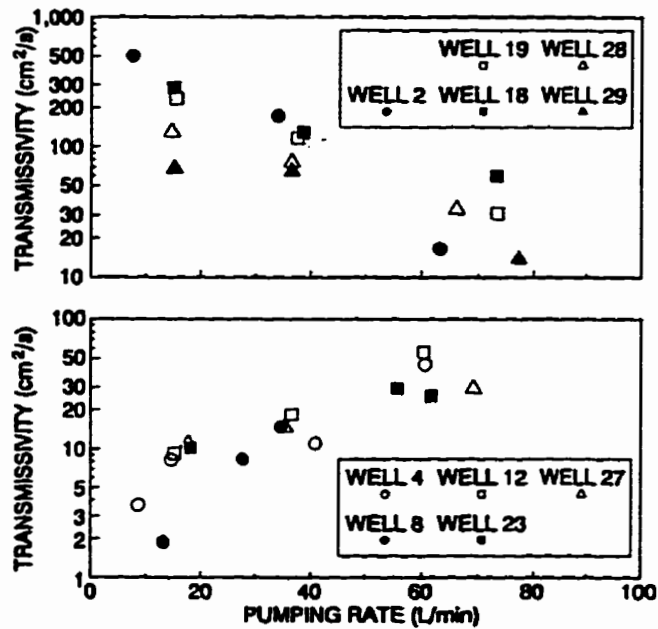


Figure 7.7 Trends in the CJSL transmissivity at selected wells.

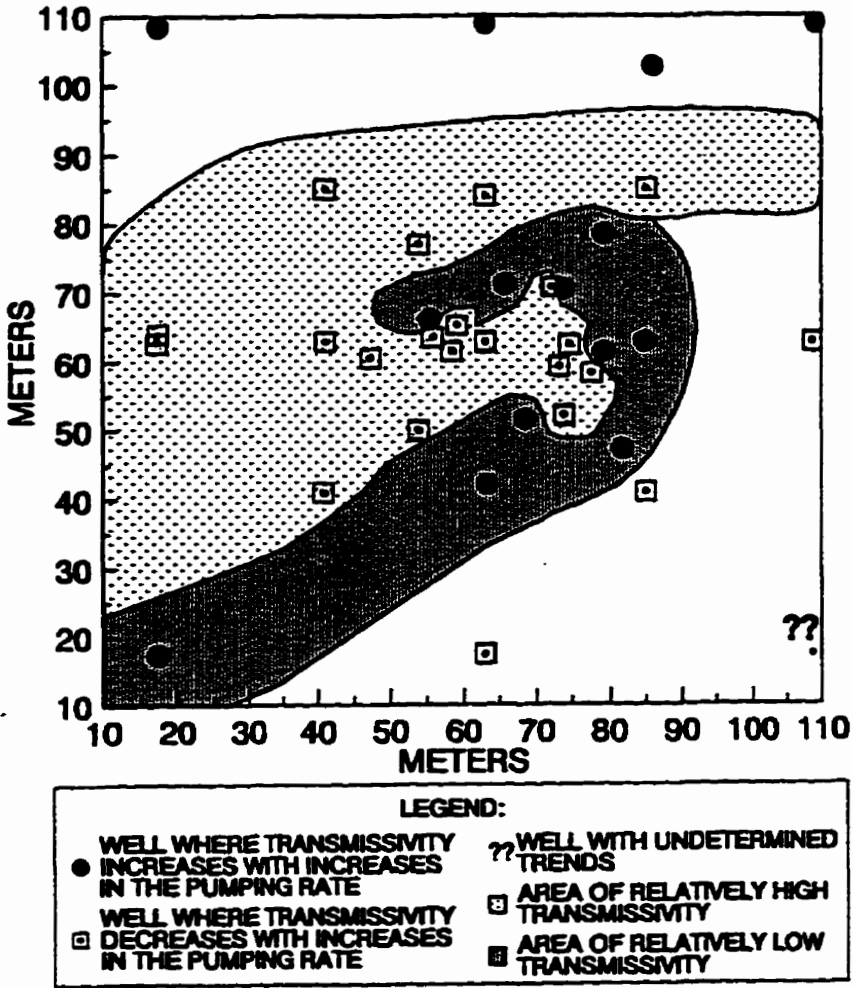


Figure 7.8 Regions of high and low transmissivity inferred from the effects of pumping rate on the CJSL transmissivity at all 37 wells.

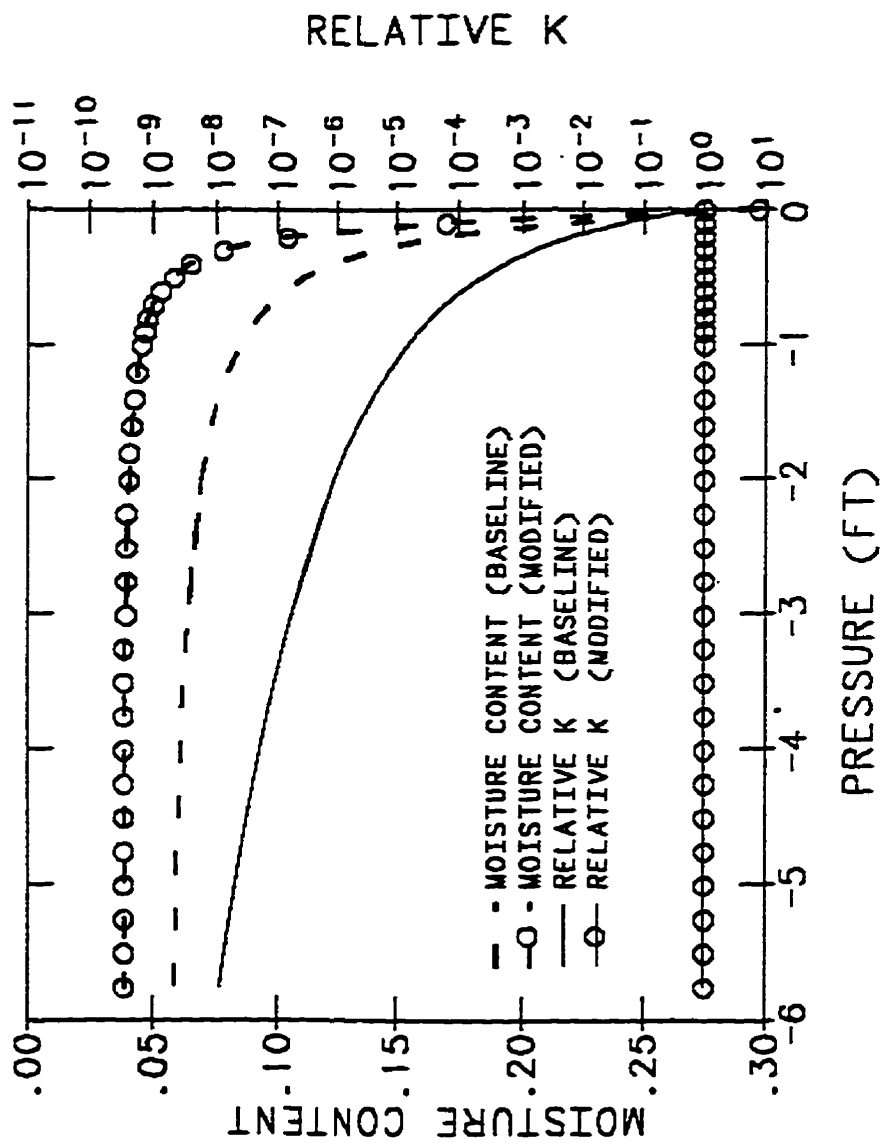


Figure 7.9 Unsaturated hydraulic properties used in numerical simulations.

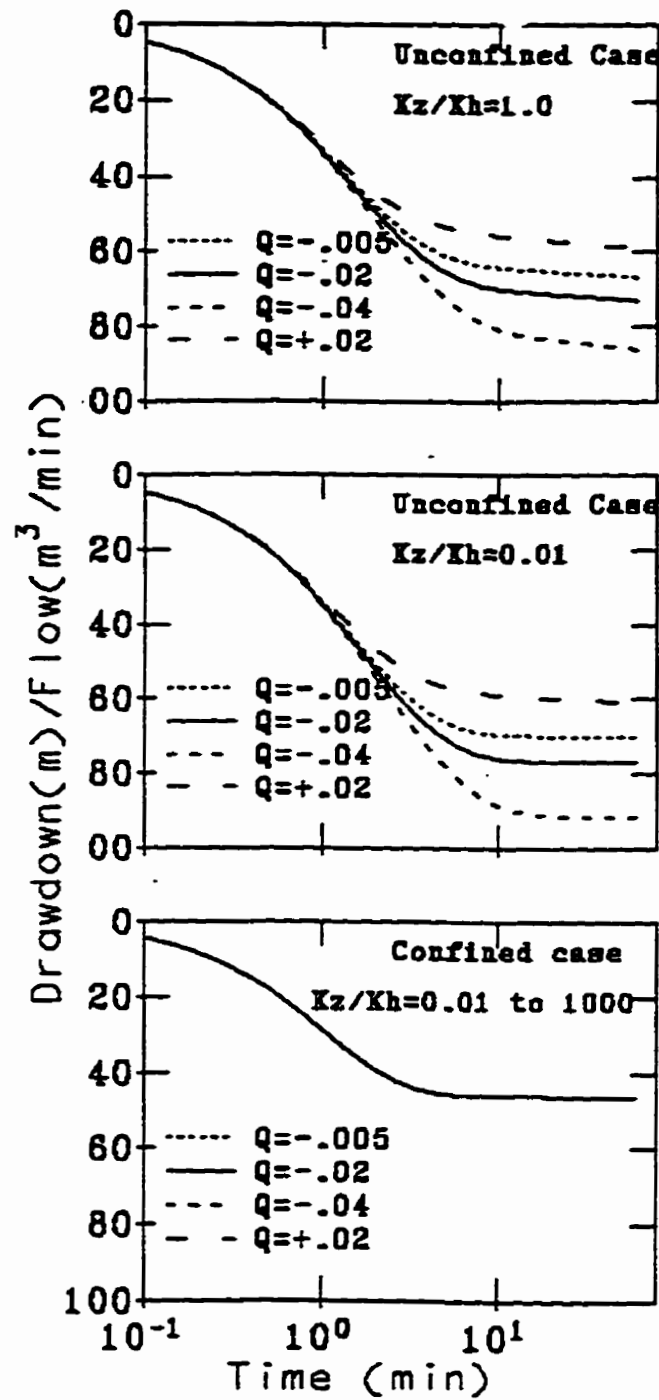


Figure 7.10 Numerically simulated single-well pumping test results for aquifers with  $K$  values that increase with radial distance from the pumping well.

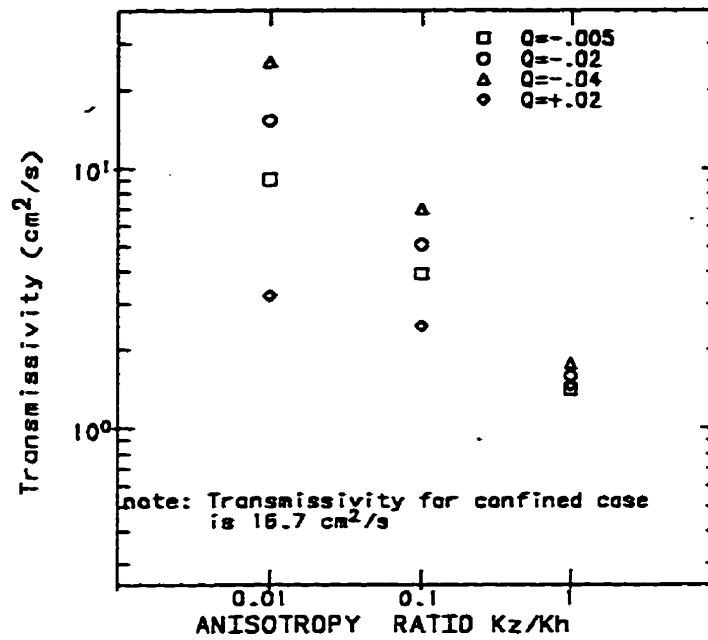


Figure 7.11 Sensitivity of CJSL transmissivity values to vertical anisotropy ( $0.01 < K_z/K_h \leq 1$ ) and pumping rate for an aquifer with K values that increase with radial distance from the pumping well.

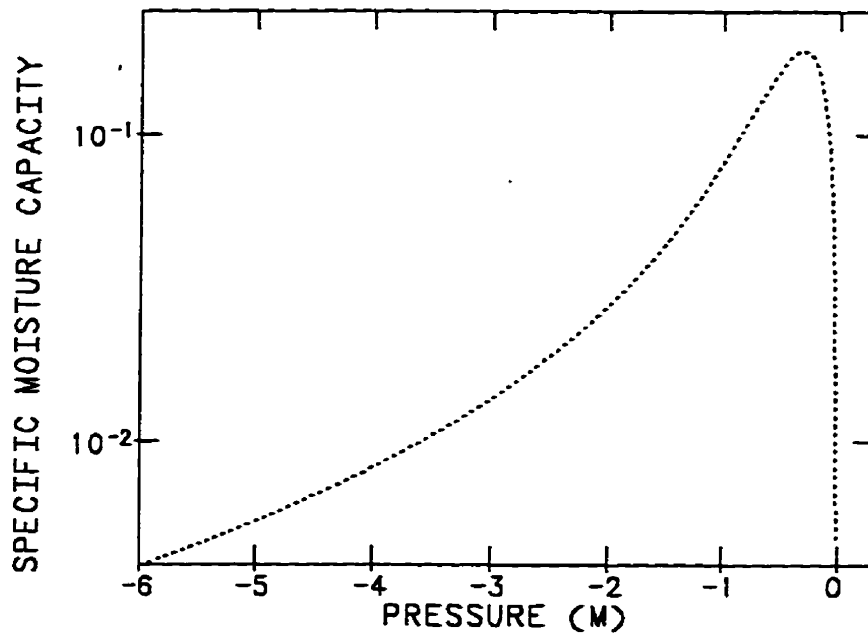


Figure 7.12 Specific capacitance as a function of pressure for the baseline moisture retention curves described in Figure 7.9.

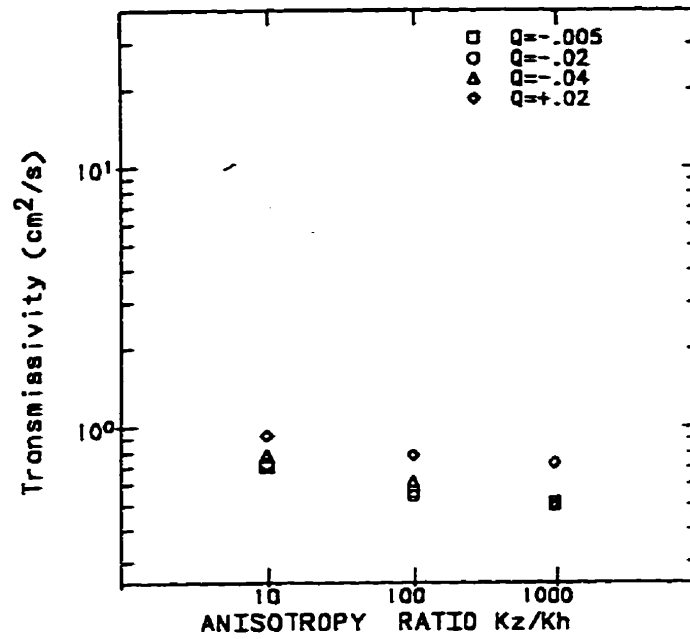


Figure 7.13 Sensitivity of CJSL transmissivity values to vertical anisotropy ( $10 \leq K_2/K_n \leq 1000$ ) and pumping rate for a hypothetical aquifer with  $K$  value that increases with radial distance from the pumping well.

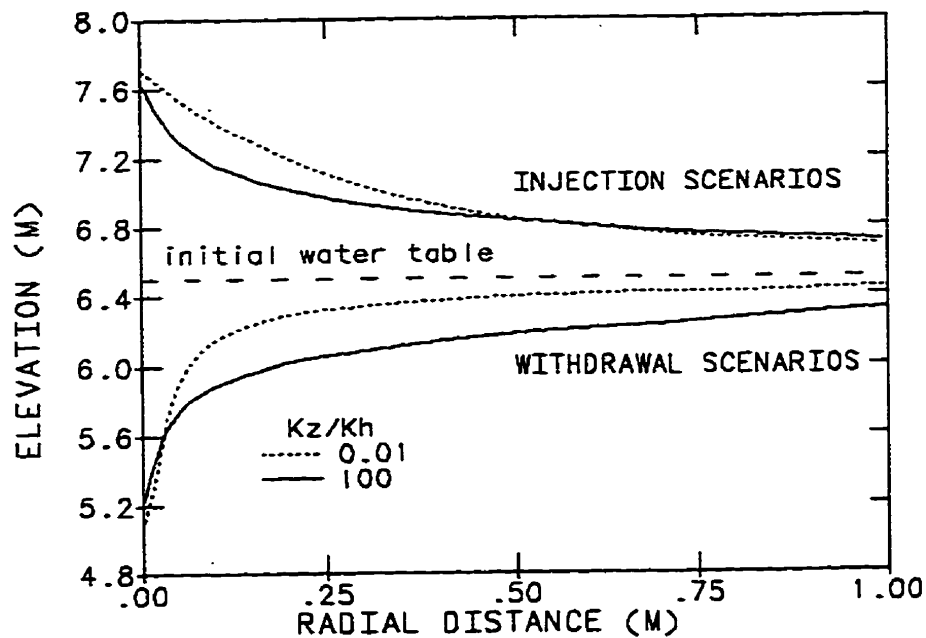


Figure 7.14 The effect of vertical anisotropy on the location of the phreatic surface near the well at elapsed time of 60 minutes for the withdrawal and injection of  $0.02 \text{ m}^3/\text{min}$ .

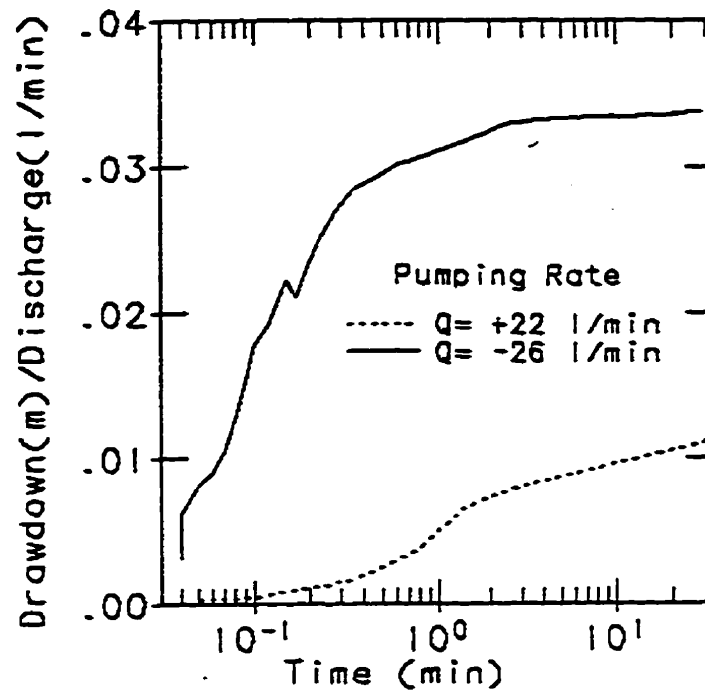


Figure 7.15 Response from Well 14 during an injection test in April 1989 and a pump test in June 1989.

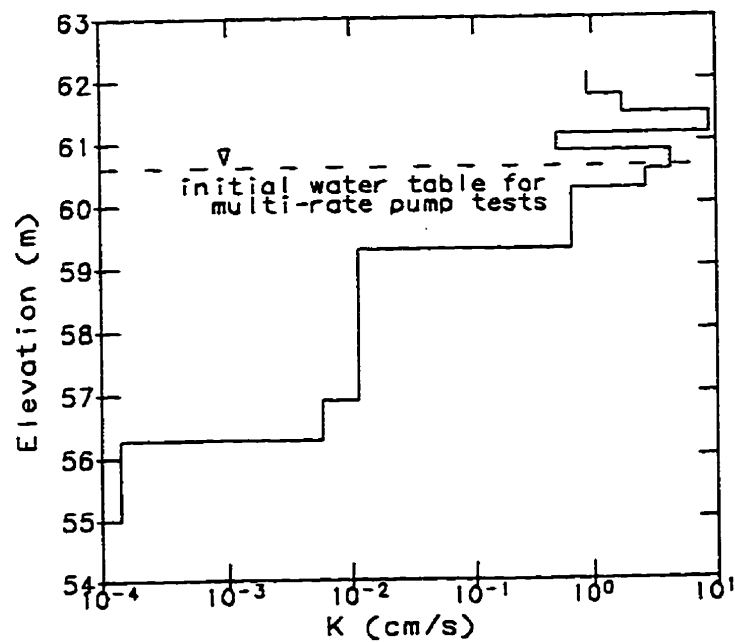


Figure 7.16 The June 1989 ambient water table superimposed on the borehole flowmeter K values for Well 2.



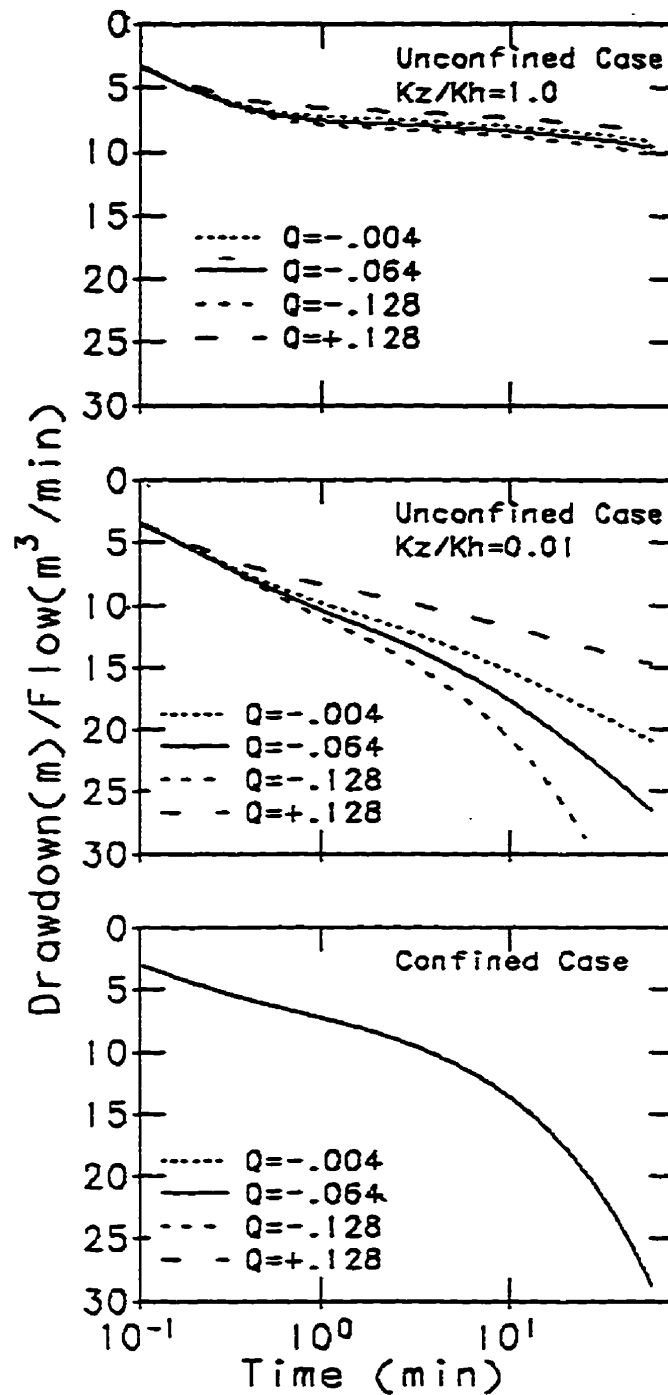


Figure 7.17 Numerically simulated single-well pumping test results for aquifers with K values that decrease with radial distance from the pumping well.

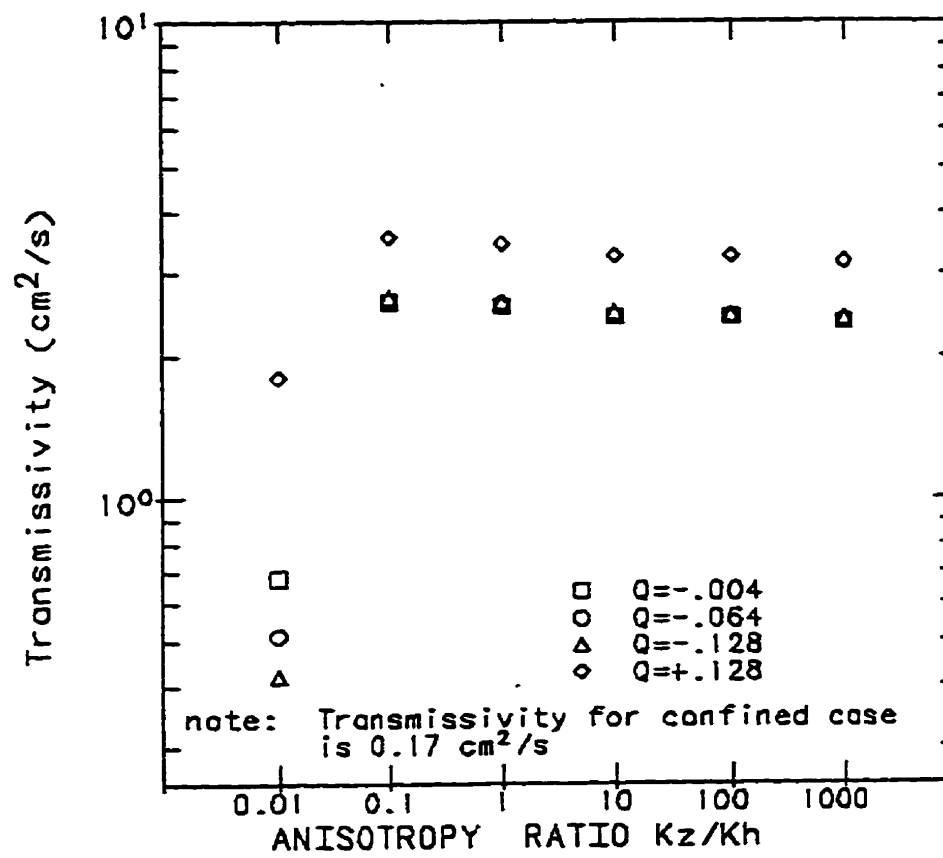
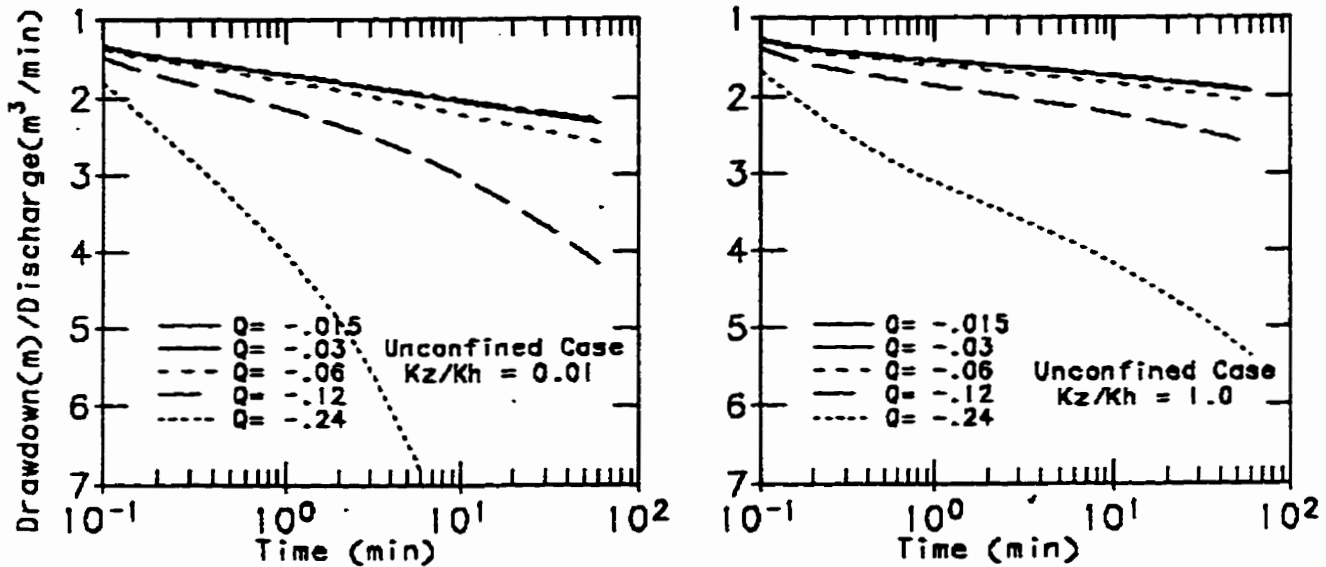


Figure 7.18 Sensitivity of CJSL transmissivity to pumping rate for a hypothetical aquifer with a  $K$  trend that increases with radial distance for the cases where  $0.01 \leq K_z/K_h \leq 1000$ .



7.19 Numerically simulated single-well pumping tests results for hypothetical aquifers with K values that decrease with radial distance from the pumping well and with a high-K layer in the upper aquifer.

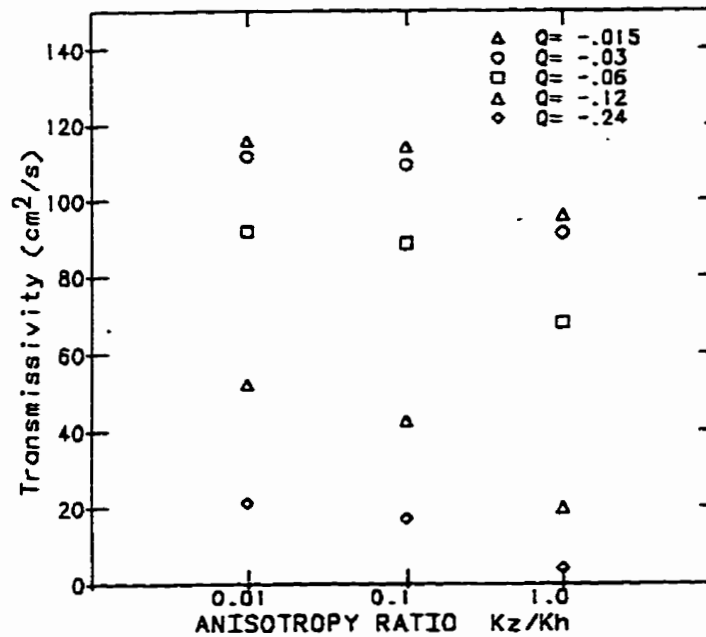


Figure 7.20 Sensitivity of CJSL transmissivity values to pumping rate and to anisotropy values for an hypothetical aquifer that has K values that decrease with radial distance from the pumping well and with a high-K layer in the upper aquifer.

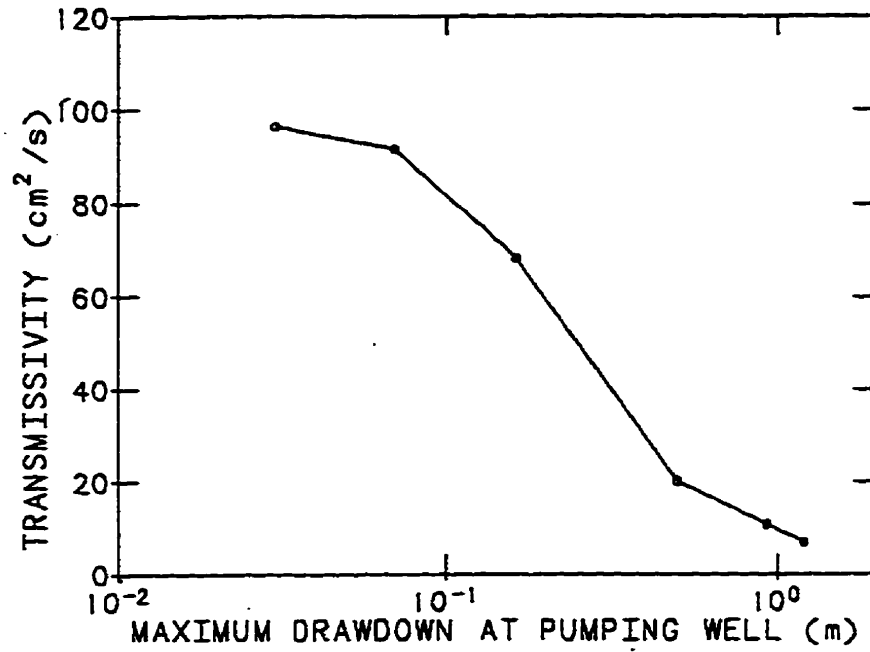


Figure 7.21 CJSJL transmissivity values as a function of the maximum drawdown in the pumping well at 60 minutes for an hypothetical aquifer that has K values that decrease with radial distance from the pumping well and with a high-K layer in the upper saturated aquifer.

## **8. IMPACTS OF VERTICAL HETEROGENEITY AND WELL SCREENS ON PUMPING TEST RESULTS**

### **8.1 INTRODUCTION**

Because of the wide range of depositional and erosional processes that contribute to their formations, fluvial aquifers can be highly heterogeneous. A concern with performing pumping tests in heterogeneous aquifers is that drawdown responses can significantly deviate from type curves based on homogeneous aquifer models. Primary causes for deviations are preferential flowpaths associated with interconnected high-K aquifer deposits, well screens, and/or well annuluses. If preferential flowpaths are ignored, then the analysis of pumping test data from highly heterogeneous aquifers can lead to unrepresentative values for calculated hydraulic parameters.

This chapter discusses pumping test results from a highly heterogeneous unconfined aquifer underlying the Columbus Air Force Base (CAFB) in Mississippi. The field site of primary concern is the I-Ha test site where numerous borehole flowmeter, single-well, and multi-well pumping tests have been performed. Field data indicate that significant preferential flow occurs through interconnected high-K deposits and well screens during both ambient and pumping conditions. The purpose of the chapter is to identify, using field and numerical results, some of the problems and uncertainties associated with interpreting pumping-test data from aquifers that are highly heterogeneous. Potential issues of concern are accelerated propagation of pressure change through high-K lenses and vertical groundwater flow in well screens.

This chapter is organized into two main sections. The first section describes the 1-Ha test and provides results from field investigations. The second section presents numerical simulations from hypothetical confined and unconfined aquifers. Results from the numerical simulations are used to support the analysis of the field data and to illustrate some of the significant problems associated with monitoring and analyzing pump-test data from heterogeneous aquifers such as CAFB.

## **8.2 TEST SITE**

### **8.2.1 Site Description**

The CAFB aquifer is composed of 10 to 12 m of fluvial Quaternary-age deposits. These primarily consist of coarse-grained deposits in the lower 8 to 10 m and fine-grained deposits in the upper 2 to 3 m. The coarse-grained deposits are highly heterogeneous. The Quaternary deposits conformably overlie the Cretaceous Eutaw Formation, which consists primarily of marine clay and silt. Seasonal effects cause the water table to vary from 1 to 3 m below ground surface. Regional geological information for the Columbus aquifer was obtained from an Army Corps of Engineers archaeological study within the Tombigbee valley (Muto and Gunn, 1988). The study suggests that braided streams and coarse-grained meandering streams formed the Columbus aquifer. Shown in Figure 8.1 is a 1956 USAF aerial photograph that outlines a paleochannel that intersects the MADE and the 1-Ha test sites.

A simple but reasonable sedimentological model for the CAFB aquifer has been suggested in Chapters 5, 6, and 7 and is illustrated in Figure 8.2. At the base of the

paleochannel are coarse-grained channel lag, scour pool, and chute bar deposits. Above these deposits are fine-grained sediments that filled the paleochannel before it was abandoned. Associated with the convex and concave regions of the paleochannel are pointbar and cutback/overbank deposits, respectively. Below the paleochannel are deposits from coarse-grained meandering and/or braided stream deposits.

### **8.2.2 Well Network**

The 1-Ha test site includes thirty-seven 5.0-cm ID fully-screened PVC wells (Figure 8.3). All wells were constructed from schedule 40 PVC pipe with 0.01" slots and 0.125" spacers. Each well was developed for approximately 3 hours using overpumping, backwashing, and mechanical flushing (Young, 1991a; Young et al., 1993a). Numerous hydraulic well tests have been performed at the 1-Ha test site.

The majority of the field tests at the 1-Ha test site were performed during 1989. In the Spring of 1989, borehole flowmeter tests included measuring the profile of vertical flow at each well for ambient and pumping conditions. In the Summer of 1989, three large-scale aquifer tests (> 5 days pumping) were performed using Well 5 as the pumping well and eight small-scale pumping tests (< 3 hours pumping) were performed using different pumping wells located across the test site ( see Appendix B). In late Summer 1989, five-spot recirculating tracer tests were performed at the two well clusters shown in Figure 8.3 (see Appendix E).

### 8.2.3 Vertical Heterogeneity at the Site

At the 1-Ha test site, detailed grain-size data have been collected from two locations. At these locations cores were retrieved with a 8.26-cm ID polycarbonate sleeve inserted into a hollow-stem auger. Visual inspection and grain-size analysis of soil cores reveal fining upward cycles common to fluvial systems (Allen, 1964). Figure 8.3 provides the grain-size data from one of these two locations. The figure illustrates sequences of fining upward cycles about every 2 meters. Evaluation of comparable grain-size data from the MADE site suggest that these cycles vary widely in their dimensions, composition, and preservation. No grain-size data are shown between 61.3 m MSL and ground elevation at 64 m MSL because no cores were taken within this vertical interval. Previous split-spoon samples and visual inspection of the deposits indicate that the upper 2.5 m zone is characterized by fine-grained deposits with more than 80% of the grains finer than  $1\phi$ .

The limited grain-size data prevents estimating the horizontal dimension and continuity of the sedimentary structures. Fortunately, sedimentary structures are exposed at nearby gravel pits. At a gravel pit approximately 1 km northeast of the test site, Rehfeldt et al., (1989) mapped sedimentology features. They provide aspect ratios of length to width ranging from nearly 1 to more than 20 (see Figure 8.5) for lenses with a variety of different physical characteristics.

Besides grain-size data and facies maps, borehole flowmeter K values (Young, 1995) indicate highly heterogeneous conditions at CAFB. Illustrated in Figure 8.6 are borehole flowmeter K values from four wells. At each well location, vertical variations of several orders of magnitude typically occur over distances of a few tenths of meters. Statistical



analysis of the 881 borehole flowmeter K values provide an arithmetic mean, a geometric mean, and a  $\sigma^2_{\log(K)}$  of 0.26 cm/s, 0.032 cm/s, and 0.92, respectively, for the deposits (Young, 1995). Geostatistical analysis of the K values provide horizontal and vertical correlation lengths of 10.0 and 1.75 m, respectively (Young, 1991a,b).

Because of the highly heterogeneous conditions at CAFB, the K values for the aquifer deposits near the water table varies significantly. In Figure 8.6, for example, the average K near the water table for Wells 16 and 7 is approximately 100 times less than for Wells 2 and 9. Using data from Figures 8.4 and 8.3 one can visualize how water table variations of 1-2 meters could change the average K near the water table at a well 10 to 100 fold. As will be discussed later, an important aspect related to aquifer analysis at CAFB is whether the water table is located in a region of low-K or high-K deposits.

### **8.3 FIELD TEST RESULTS**

#### **8.3.1 Borehole Flowmeter Measurements**

In a highly heterogeneous aquifer like CAFB, groundwater flow includes converging and diverging flowpaths that direct groundwater through the high-K deposits and around the low-K deposits. As a result of the convoluted flowpaths, the CAFB aquifer has vertical gradients that are occasionally 10 times greater than horizontal hydraulic gradients. A concern with fully penetrating wells at CAFB is that their annuluses and open screens are potential high-K pathways between non-adjacent high-K deposits.

A measure of the amount of disturbance caused by a well is the vertical flow in the well. Shown in Table 8.1 are the maximum vertical discharges measured with the

electromagnetic flowmeter (Young and Pearson, 1995) at the 37 wells in April 1989. The relatively high values of the discharges suggest that the fully-penetrating wells disrupt groundwater flow patterns at CAFB. Shown in Figure 8.7 are the profiles of ambient vertical flow and the borehole flowmeter K values for Well 26. Examination of both data sets reveal that Well 26 disrupts natural groundwater flow by accelerating groundwater flow from the high-K deposits in the middle of the aquifer to high-K deposits near the top and the bottom of the aquifer.

**Table 8.1 Maximum Value of Groundwater Flow Measured at Each Well During April 1989**

Well	Flow (L/min)	Well	Flow (L/min)	Well	Flow (L/min)	Well	Flow (L/min)
1	-0.261	11	+0.193	21	-0.322	31	+0.742
2	-0.428	12	+0.322	22	-0.223	32	+0.208
3	-1.529	13	-0.840	23	+0.950	33	-0.000
4	+0.496	14	-0.159	24	+0.473	34	-0.246
5	-0.129	15	+0.136	25	+1.200	35	+0.261
6	+0.061	16	+1.230	26	-0.681	36	-0.848
7	+0.216	17	-0.173	27	+2.945	37	-0.322
8	+0.201	18	-0.352	28	-0.481		
9	+0.360	19	-0.397	29	-0.511		
10	+0.367	20	+1.317	30	-0.129		

Notes: negative sign indicates downward flow  
positive sign indicates upward flow

Shown in Figure 8.8 are vertical flow profiles at two wells before and during the Aquifer Test 3 (AT 3), which included pumping Well 5 at a constant rate of 62 L/min. As in all wells that were monitored for changes in vertical flow during AT3, the vertical flow greatly increased during the pumping test. At Well 16, which is approximately 4.6 m from the pumping well, the maximum vertical flow is about 5% of the total pumping rate throughout the entire test. Examination of all of the well data indicate that the artificial high-K conduit provided by the well screens enhances flow through high-K deposits, and consequently reduces flow through low-K deposits, during a pumping test.

### 8.3.2 Small-Scale Pumping Tests

The small-scale pumping tests consisted of pumping a well at a constant rate between 2 and 3 hours and measuring the drawdown in nearby wells with pressure transducers. Seven small-scale pumping tests were conducted from April to July 1989, with pumping rates near 60 L/min. Most of the wells associated with the tests were at one of two well clusters in the 1-Ha test site. One well cluster (Wells 5, 13, 14, 16, and 19) is located 5 meters northwest of the center of the well network. The other well cluster (Wells 8, 10, 12, 24, and 25) is located about 10 meters east of the center of the well network (see Figure 8.3).

To determine bulk transmissivity and storage parameters, the drawdown data were corrected for desaturation effects using the Jacob correction (Jacob, 1963) and then fitted to Theis type-curves automatically using conventional curve-fitting routines. Figure 8.9 shows calculated transmissivity and storage coefficient values at selected observation wells for different pumping tests. The transmissivity and storage coefficient values calculated using

data from the same observation well but for different pumping tests typically varied by a factor of two and several orders of magnitude, respectively. Similarly, the calculated hydraulic parameters were sensitive to the selection of which well was selected for pumping in a well pair. Shown in Figure 8.10 are examples of drawdown curves from the two well clusters.

The relatively small variability in transmissivity in Figure 8.9 can be partly explained by the known large-scale trends in transmissivity caused by the wide range of sedimentary deposits that compose a fluvial aquifer. To investigate the cause for the wide range of values for the storage parameters, the storage coefficient values were plotted as a function of the radial distance between the pumping and observation well. Figure 8.11 shows that as the radial distance increases, the variability decreases in the calculated storage coefficients. Although delayed gravity theory (Neuman, 1972; 1975) and the delayed yield theory (Bolton, 1954; 1963) can partially account for the increase in the mean storage coefficient with distance, these theories cannot account for the differences in the range of storage values associated each the radial distances.

Among the reasons for the wide range of storage coefficients at short radial distances is spatial variability in the K field near the water table. Relatively high storage coefficients can be envisioned near Well 2 in Figure 8.6, for example, because of the high-K material near the water table. In this example, the high-K deposits promote drainage and provide a preferential flowpath for drainage to reach the well. Similarly, relatively low storage coefficients can be envisioned at small radial distances for the case of low-K material near the water table and high-K lens at depth as shown for Well 16 in Figure 8.6. In this instance,

semi-confined conditions at the well hinder drainage and promote the preferential removal of water from the high-K lens at early time. Because the cone-of-influence will eventually expand beyond and/or below the low-K deposits in the upper aquifer near Well 16 and because high-K deposits have finite dimensions, the trend of higher storage coefficients at larger radial distance in Figure 8.11b appears plausible.

### **8.3.3 Small-Scale Recirculating Tracer Tests**

To help interpret the results of the small-scale pumping tests, Tracer Tests 1 and 2 were conducted near the two well clusters shown in Figure 8.3 with the specific purpose of investigating the impact that high-K lenses have on groundwater flow. Both tracer tests involved pumping equal amounts of water from four observation wells and injecting the combined flow into the injection well. After stable hydraulic gradients were established, a bromide tracer pulse was uniformly injected into each injection well. During the tracer tests, tracer breakthrough curves were developed for selected vertical aquifer zones using multi-level samplers located at 0.61-meter intervals inside the pumping and observations well (Chapter 4, Appendix E).

Tracer Test 1 involved injecting a tracer at Well 16 and observing tracer breakthroughs at pumping wells 5, 13, 14, and 19. Tracer Test 2 involved injecting a tracer at Well 12 and observing tracer breakthrough at pumping wells 8, 10, 24, and 25. The tracer monitoring confirmed preferential flow patterns along thin horizontal layers as significant differences were observed in the tracer breakthrough curves measured at vertical intervals of 0.6 m inside the well. Using the travel distance, the time of the peak tracer concentration,

an estimate of the porosity for the high hydraulic conductivity lenses, and the measured average spatial hydraulic gradient between the injection and observation wells, a lower value for the average K was calculated for each breakthrough curve in Chapter 4. From these calculations, a vertical profile of tracer-based K values was constructed for the aquifer materials between a paired pumping and observation well. Figure 8.12 shows the highest value of the tracer-based K value and the storage coefficient for each pumping-observation well pair from the tracer tests. For each tracer test, higher K values are associated with lower storage coefficients. This correlation can be explained if the aquifer is visualized as a layered media with high-K lenses acting as “mini” confined aquifer layers that hydraulically connect an observation well and a pumping well.

#### **8.3.4 Summary**

As a result of highly heterogeneous conditions at CAFB, preferential flowpaths at CAFB promote channeling of groundwater flow through a network of interconnected high-K deposits. Field evidence suggest that high-K deposits near the pumping and observation wells cause biases in the calculated storage coefficients. Direct measurement of vertical flow inside wells indicate that well screens can significantly disrupt groundwater flow patterns by providing good hydraulic connection among non-adjacent high-K deposits. To help evaluate the potential impact that vertical heterogeneity and open well screens can have on pumping-test results, model simulations were performed for both confined and unconfined aquifers.

## **8.4 MODEL RESULTS FOR A VERTICALLY HETEROGENEOUS CONFINED AQUIFER**

### **8.4.1 Model Set-up**

To demonstrate several fundamental issues associated with impact of high-K lens on drawdown responses, pumping tests were simulated in a confined aquifer using the integrated finite-difference code WELL3D (Lacombe et al., 1995). A reason for selecting WELL3D is that it represents well screens via line elements in the manner described by Sudicky et al., (1995). All numerical simulations were based on a hypothetical 4-m thick square aquifer with side lengths of 400 m and a uniform specific storage coefficient of  $5 \times 10^{-6} \text{ m}^{-1}$  with no-flow boundaries along the perimeter. A pumping well with a constant discharge of 0.6 L/min ( $10^{-5} \text{ m}^3/\text{s}$ ) was located in the center ( $x=y=0$ ) of the aquifer. Observation wells were placed along the x and y principal axes at radial distances of 4, 16, and 32 m. The pumping well and the 12 observation wells were fully penetrating with a pipe radius of 0.025 m. Based on a modified form of the Hagen-Poiseuille equation (Sudicky et al., 1995), a K of 2400 m/s was assigned to each well screen. Because the aquifer is confined, the storage assigned to the open well screen is based on the compressibility of water and thus is essentially equal to zero.

A baseline simulation was performed for an aquifer with a uniform K of  $10^{-4} \text{ cm/s}$ . The numerical discretization was constant at 1 m in the vertical and varied in the horizontal from 0.05 m, which was near the well locations, to a maximum of 4 m, which existed at the outer boundaries. Figure 8.13 shows that the numerical solution accurately matches an analytical solution for the Theis Equation (Theis, 1935). As should be expected, no vertical

flow occurred in the observation wells because pressure changes moved uniformly outward from the pumping well.

#### **8.4.2 Pumping Test Simulation with Two High-K Lenses**

Results from the small-scale pump and tracer tests shown in Figure 8.12 indicate that calculated storage coefficients are sensitive to the location of high-K lens. The limited field data indicate that calculated storage coefficients are biased if a high-K lens intersect the pumping and the observation well. To evaluate this hypothesis, the hypothetical aquifer with a uniform  $K$  of  $10^{-4}$  cm/s was modified by the addition of two high-K lenses aligned with the positive  $x$  axis. As shown in Figure 8.14, the high-K lens at the base of the aquifer intersects the pumping well and the 4-m observation well on the positive  $x$  axes. The high-K lens at the top aquifer intersects only the 4-m observation well on the positive  $x$  axis.

Using the simple two-lens model, a sensitivity study was performed to evaluate the following three model parameters: 1) the  $K$  of the lenses; 2) the vertical anisotropy (i.e.,  $K_v/K_h$ ); and, 3) the dimension of the lenses. By considering two values for the  $K$  of the lens, three different values for anisotropy, and two values for the dimension of the high-K lenses, 12 pumping tests were numerically simulated. For each of the 4-m observation wells located on the  $x$  and  $y$  axes (see Figure 8.14), the simulated drawdown responses were matched to a Theis type-curve. For all cases, the lowest and highest storage coefficients were calculated at the 4-m observation wells located along the positive and negative  $x$  axes, respectively. Listed in Table 8.2 is the lowest storage coefficient calculated and the ratio of the highest to lowest storage coefficient for each of the 12 simulations. No statistics are provided for



calculated transmissivity values because these values remained relatively constant. For all 12 cases, the transmissivity values were within 5% of the true value of  $0.04 \text{ m}^2/\text{min}$ .

**Table 8.2 Calculated Storage Coefficients for 4-m Observation Wells for the Aquifer Configuration in Figure 8.14**

Ratio of $K_{\text{lens}}$ $K_{\text{matrix}}$	Vertical Anisotropy $K_z/K_h$	Dimension of lenses			
		8m x 4m x 1m		8m x 2m x .4m	
		Lowest S	$S_{\text{max}}/S_{\text{min}}$	Lowest S	$S_{\text{max}}/S_{\text{min}}$
100	1	1.6E-5	3.6	9.6E-6	4.4
100	0.1	1.3E-5	4.5	5.4E-6	7.8
<b>100*</b>	<b>0.01*</b>	<b>1.2E-5*</b>	<b>5.2*</b>	3.2E-6	12.5
1000	1	1.3E-5	4.9	5.6E-6	7.6
1000	0.1	4.8E-6	10.6	2.9E-6	16.7
1000	0.01	3.4E-6	14.1	1.1E-6	46.1

\*Drawdown curves for this example are shown in Figures 8.14 and 8.15.

Table 8.2 illustrates that vertical heterogeneity can cause significant bias in calculated storage coefficients. Conditions that promote the calculation of low storage coefficients are high K values for the lens, low vertical anisotropy for the aquifer, and small dimensions of the lens. Some of the reasons for these trends are: 1) higher K values enhance the lens' capacity to propagate pressure change; 2) lower vertical anisotropy decreases vertical cross-flow (i.e. flow vertically perpendicular to radial flow toward the well) that helps dampen the propagation of pressure change in a high-K lens; and, 3) decreases in the lens' thickness and

width provide less surface area for lateral and vertical cross-flows to dampen the propagation of pressure change in the lens.

For all of the pumping-test simulations, the observation well intersected by the two high-K lenses had downward flows of about 35% of the total pumped discharge. Because of the high-K of the well screen, the value of hydraulic heads within each well screen varied by only a few percent. For the purpose of calculation of aquifer parameters, only a single hydraulic head value is assigned to the well screen. To help illustrate the significant impact that the well screen has on the aquifer response, Figures 8.15 and 8.16 show predicted drawdown curves with and without observation wells for the case highlighted by bold print in Table 8.2. For comparison, the drawdown curves for a homogeneous aquifer from Figure 8.13 are included.

For the case of no observation well, different drawdown curves are produced for each vertical aquifer interval. Because of the high-K values associated with the open well screen, the drawdown response is nearly identical in the observation well. As a result of less vertical connection among the aquifer layers, a greater range of storage coefficients is calculated at each radial distance when fully-penetrating wells are ignored than if they are included in the numerical simulations. For the case of no fully-penetrating wells, the calculated storage coefficients vary from  $3.3 \times 10^{-6}$  to  $7.6 \times 10^{-5}$ . These values provide a value of 23 for  $S_{\max}/S_{\min}$ , which is much greater than the range of 5 obtained when fully-penetrating observation wells are included in the numerical simulations.

As a result of lateral and vertical cross flows, all the drawdown responses are converging toward the homogeneous case over time. Because cross flows dampen pressure

changes along preferential flowpaths, the range of drawdown responses is considerably less at radial distances of 16 m than 4 m. For the case of no observation well, the calculated storage coefficients vary between  $1.1 \times 10^{-5}$  to  $2.7 \times 10^{-5}$  for the distance of 16 m. These values have a range that is approximately one-tenth the range of the storage coefficients for the radial distances of 4-m. Among the implications of Figures 8.15 and 8.16 is that vertical heterogeneity causes problems with calculating storage coefficients whether or not fully-penetrating for partially-penetrating wells are used.

#### **8.4.3 Effect of Multi High-K Lenses on Aquifer Response**

To more thoroughly evaluate the effect of vertical heterogeneity on calculated S values, numerical pumping tests were performed in synthetic aquifers created by randomly aligning 8 m long, 4 m wide, 2 m thick high-K lenses alternately in the x and y directions until they occupied 20% of the aquifer volume. The aquifer matrix was assigned a uniform K of  $10^{-6}$  m/s and vertical anisotropy of 0.1. The K value for each lens was randomly generated from a Gaussian distribution with a  $\log(K)$  mean of -4 (i.e.  $10^{-4}$  m/s) and a  $\log(K)$  standard deviation 0.5. Figure 8.17 shows the drawdowns for the 4-m and the 32-m observation wells generated by simulating four pumping tests in synthetic aquifers. Table 8.3 provides the range of calculated storage coefficients based on a 2000-s analysis period for the three sets of observation wells at different radial distances.

The results in Table 8.3 show that in a vertically heterogenous aquifer the range of calculated storage coefficients decrease with radial distance. A decreased range with distance is expected based on the trends in Figure 8.11b and lower probabilities of high-K

pathways intersecting the pumping and observation well at greater distances. However, although the range for the storage coefficients decreases with radial distance in Table 8.3, the mid-point of the range appears independent of distance as it remains near  $2.0 \times 10^{-5}$ , which is the storage coefficient assigned to the aquifer. For the field results in Figure 8.11b, the upper boundary and not the midpoint for the range of S values remained nearly constant with distance. As will be shown in the next section, simulations for an unconfined model are required to reproduce the general trends in the bulk storage coefficients shown in Figure 8.10b.

**Table 8.3 Calculated Storage Coefficients from Aquifers with Randomly Distributed Lens of High-K**

Radial Distance (m)	Calculated S Values	$S_{\max}/S_{\min}$
4	5.8E-5 to 4.8E-6	12.1
16	3.2E-5 to 8.5E-6	3.8
32	3.5E-5 to 1.9E-5	1.8

#### 8.4.4 Summary

Numerical simulations for confined aquifer conditions demonstrate that the arrangement and properties of high-K lenses can cause significant bias calculated storage coefficients obtained from curve matching. Field data indicated that the higher the K of a lens intersecting the observation and pumping wells, the lower the calculated storage coefficient. Numerical simulations confirm this trend and showed that calculated storage coefficients are less sensitive to vertical heterogeneity with increases in radial distance. The

latter result can be also inferred from a plot of calculated storage coefficients from field data as a function of the distance between the pumping and observation well. A likely reason for the decreased sensitivity with distance is that the greater the distance traveled by a pressure change, the more tortuous (and therefore less permeable) the flowpath becomes and the more time cross flows have to dampen the pressure change in a high-K pathway. Among the important results from the field and numerical results is that fully-penetrating wells are important regions where significant vertical flow may occur between non-adjacent high-K deposits.

## **8.5 MODEL RESULTS FOR A VERTICALLY HETEROGENEOUS UNCONFINED AQUIFER**

### **8.5.1 Model Set-up**

FRAC3DVS (Therrien and Sudicky, 1996) was selected to numerically simulate pumping tests in hypothetical unconfined aquifers. These simulations were performed to help explain CAFB field data and to illustrate the significant impacts that vertical heterogeneity and wells screens can have on drawdown results. FRAC3DVS was selected because it solves Richard's equation with a robust Newton-Raphson iteration scheme and solves flow to a well uses line-elements as described by Sudicky et al., (1995).

Different numerical grids were used in the simulations but all had relatively small vertical grid spacing near the water table and small horizontal spacing near wells. Uniform specific storage was used in the entire aquifer domain except at the well locations where the value was set to 1. For simplicity, the same unsaturated property relations were used for all

K values and were based on the van Genuchten parameters (van Genuchten, 1978) used in Chapters 5, 6, and 7. The van Genuchten parameters were as follows: the total porosity is 0.446; the residual moisture content is 0.286;  $\alpha$  is set to 0.2; and,  $n$  is set to 1.59.

Values considered for  $S_s$  were  $5 \times 10^{-4}$ ,  $5 \times 10^{-5}$ , and  $5 \times 10^{-6}$ . These values were calculated from the range of bulk compressibilities provide by Freeze and Cherry (1979) for clayey, sandy, and gravelly deposits. Because of the very gravelly nature of CAFB deposits, the most representative value for  $S_s$  would appear to be near the lower limit of the range. However, because of the possibility that unconfined sediments may be more loosely compacted than confined deposits, a  $S_s$  of  $5 \times 10^{-4}$  was considered. Values considered for  $K_z/K_h$  were 1.0, 0.1 and 0.01. These values reflect the vertical anisotropy caused by vertical stacking of aquifer deposits of different  $K_s$ . Because the aquifer is not a perfectly stratified medium, the opportunity for preferential vertical pathways through the entire aquifer thickness, and thus the effective value for vertical anisotropy, is scale dependent. With regard to pump-test analysis, anisotropy values less than 0.01 will not be considered for observation wells at a radial distance of 32 m.

Several baseline numerical simulations were performed with a homogeneous aquifer for a uniform  $K$  of 0.04 cm/s (0.024 m/min) and an initial saturated thickness of 8 m. These model inputs were selected based on the borehole flowmeter  $K$  values and borehole logs from CAFB. Nine simulations were performed based on the permutations of three values for  $S_s$  and three values for  $K_z/K_h$ . Although unsaturated flow occurs in all simulations, the drawdown responses more closely resemble classical Theis type-curves than classical Neuman type-curves. A primary reason for the minor effects of delayed drainage is the high-

K of the aquifer, which tends to quicken and minimize the effects of unsaturated flow on drawdown responses (Akindunni ,1989; Chapter 6). As shown in Figure 8.18, changes in the values of  $Kz/Kh$  and  $Ss$  have a small but measurable impact on the drawdown curves.

### 8.5.2 Pumping Test Simulation with Two Lenses

Besides delayed drainage, another concern associated with analysis of short-term pumping tests at CAFB is aquifer heterogeneity. To illustrate this concern, a K field was created by modifying the homogenous K field of 0.04 cm/s with two lenses. One lens had a K of 0.4 cm/s and was 10 m long, 2 m wide, and 0.5 m thick . This lens was located near the base of the aquifer and intersected both the pumping and a 4-m observation well. The other lens was 20 m long, 20 m wide, and 0.5 m thick and was assigned different but uniform K values. This second lens was located at the top of the saturated aquifer just below the initial water table and will be used to represent the different K values in the upper aquifer as shown near Wells 2 and 6 in Figure 8.6.

Numerical simulations were performed with the top lens assigned K values of 0.004, 0.04, and 0.4 cm/s for the cases where: 1)  $Ss$  equaled  $5.0 \times 10^{-4}$  and  $Kz/Kh$  equaled 1.0; 2)  $Ss$  equaled  $5.0 \times 10^{-6}$  and  $Kz/Kh$  equaled 0.01; and, 3)  $Ss$  equaled  $5.0 \times 10^{-6}$  and  $Kz/Kh$  equaled 0.01. Figure 8.19 illustrates the wide range variations in the simulated drawdowns. Of these three cases, the effects of delayed yield are most important for cases for low values of  $Kz/Kh$ ,  $Ss$ , and K for the top lens.

Figure 8.20 shows the storage calculated from 12 homogeneous scenarios and from the 9 two-lens scenarios coefficients as a function of radial distance to the observation well.

The trend is similar to that obtain from field data from CAFB. Examination of all the data reveals that: 1) high-K layers near the initial water table lead to high storage coefficients for short and large radial distances; and, 2) low-K layers near the initial water table combined with a high-K lens at depth lead to low S values at short radial distances. A primary cause for the trend in storage coefficients values shown in Figures 8.11 and 8.20 is the impact that vertical heterogeneity has on producing preferential flow paths at depths and localized semi-confined and confined aquifer conditions. Implicit in this finding is that not only does the aquifer heterogeneity affect calculated storage coefficients but also the selected wells and the location of the water table.

A notable feature in Figure 8.20 is the wide range of storage coefficient values from the 4 m observation wells. As noted above, a primary contributing cause for the wide range is the large the variation of K values near the water table near the pumping well. The propagation of the drawdown into the aquifer is shown in Figure 8.21 for the three hypothetical aquifers used to produce the drawdown responses in Figure 8.19. The hydraulic head contours illustrate that as conditions for drainage become less favorable, the advancement of the pressure drop into the aquifer increases.

### **8.5.3 Simulations with Multiple Lenses and Large-Scale Transmissivity Variations**

#### **8.5.3.1 K fields**

A concern with highly heterogeneous conditions is the applicability of type-curves based on homogeneous aquifer models to estimate aquifer parameters. To investigate this concern, Pumping tests were simulated for two different aquifers. One aquifer had a large-



scale transmissivity trend and the other consisted of multiple lenses of different K. The numerical grid for the simulations included the well network shown in Figure 8.22. The aquifer was represented as a 8-m thick, 400 x 400 m square with an initial water table at 6.5 m.

For the case of multiple lenses, the numerical model included 298,265 nodes with 16 nodal layers spaced at 0.5 m intervals. The K field was established by continually inserting 12 m long, 3 m wide, and 0.5 m thick lenses of different K into the model until the lenses occupied 90% of the aquifer volume. The K for each lens was assigned randomly from a normal distribution of  $\log(K)$  with a mean of -2.6 (0.0025 m/min) and a standard deviation of 1. For the entire aquifer the storage coefficients, the vertical anisotropy, and the K value for the matrix, were set to  $5E-5$ , 0.01, and 0.0025 m/min, respectively.

To create a large-scale transmissivity trend, a linear strip with a K of 0.25 m/min was placed into a uniform aquifer with a K of 0.0025 m/min. The linear strip was aligned with the vertical axis between the x values of -1 and 8 with a variable thickness as shown in Figure 8.21. For this aquifer scenario, the storage coefficient was set to  $5 \times 10^{-5}$  and the vertical anisotropy was set to 0.1. Because of the symmetry of the K field with respect to the x axis, the number of nodes required to represent the transmissivity trend was approximately half the nodes used for the K field consisting of multiple lenses.

### **8.5.3.2 Impact of Observation Wells**

Observation wells modify local aquifer conditions by providing vertical high-K pathways among non-adjacent aquifer deposits and increasing the amount of water available

from storage. Simulations were performed with fully-screened wells at the locations shown in Figure 8.22 and with only a fully-screened well at the pumping well location. For simulations without observation wells, the drawdown in the aquifer at an elevation of 2 m was recorded at the location shown in Figure 8.22. The drawdowns represent values from a partially-penetrating well. For the K field with a large-transmissivity trend, simulations were performed for pumping at locations 1, 2, and 3. For the K field with multiple lenses, simulations were performed for pumping at locations 1, 8, 12, and 13. At each pumping well location, pumping tests were simulated for three pumping rates in the range of 0.0075 to 0.12 m<sup>3</sup>/min.

For all simulations, drawdown in the pumping well was less for the case of fully-penetrating than without fully-penetrating observation wells. This effect is consistent with the additional storage and vertical flow pathways added by the fully-penetrating observation well. Shown in Figure 8.23 are selected drawdown responses performed with the two K fields. The effects of the observation wells on drawdown results are very different for the two K fields. Whereas the observation wells significantly affect drawdown responses for the K field with large transmissivity trends, they have only a minor affect on drawdown responses for the K field with multiple lenses.

Figure 8.23 shows drawdowns caused by pumping Well 12 at 0.06 m<sup>3</sup>/min in the K field with multiple lenses. For simulations with no observation wells, drawdown curves strongly mimic the sigmoidal-shaped drawdown curves associated with delayed gravity theory (Neuman, 1972; 1975) and/or delayed yield theory (Bolton, 1954; 1963). However, for simulations with observations wells, drawdown curves closely resemble those from the

This solution (Theis, 1935) for a confined aquifer. The different drawdown patterns occur because the open channel of the observation well essentially eliminates the pressure differences between the upper and lower aquifer near the observation well.

The maximum vertical discharge at all seventeen observation wells ranged between 2% and 9% of the pumpage at well 12. Variations in the magnitude and pattern of vertical flow is caused by variations in the K of the deposits adjacent to the observation wells. At fifteen of the 17 observation wells, only downward flow occurred. The prevalence of downward flow is consistent with delayed gravity theory and delayed yield theory where water released from drainage causes the drawdown in the upper aquifer to lag behind drawdown in the lower aquifer. Shown in Figure 8.24 is the temporal variation of vertical flow for the set of observation wells shown in Figure 8.23.

Among the important variables that affect the temporal variations in vertical flow is the location of the water table relative to the zone providing water into the observation well. At Wells 3 and 4, the drawdown is not great enough to partially desaturate the primary water bearing zones during the pumping test. As a result, the vertical flow gradually increases until about 2000 minutes, at which time flow stabilizes. However, at Well 7 increased desaturation of the primary water bearing zones occurs over time. As a result, the vertical flow in the observation well gradually decreases over time.

To quantify the impacts of preferential flowpaths through observation wells and through high-K deposits, hydraulic parameters were calculated from the drawdown curves produced for the case of pumping well 12 at  $0.06 \text{ m}^3/\text{min}$ . For the scenario with observation wells, type curves from the Theis solution (Theis, 1935) and the Neuman solution (Neuman,

1972, 1975) were fitted to the simulated drawdown curves. For the scenario with no observation wells, only the Neuman solution (Neuman, 1972, 1975) was used. For all three of these curve fits, the calculated transmissivity values varied over the relatively narrow range from 0.05 to 0.1 m<sup>2</sup>/min. However, the calculated storage parameters varied approximately four orders of magnitude. The Neuman type-curve fits for cases with observation wells produced values from .00001 to .01 and from .001 to .02 for the specific storage and specific yield,  $S_y$ , respectively (the lower limit for  $S_y$  was set to 0.001). The Neuman type-curve fits for no observation wells produced values that ranged from 0.0006 to .003 and from 0.001 to 0.26 for  $S_s$  and  $S_y$ , respectively. The Theis type-curve fits produced storage coefficients that varied over the narrow range of .00001 to .00006.

Analysis of the numerical simulations suggest that in a vertically heterogeneous aquifer with high-K lens type curve-matching may be useful only for determining bulk transmissivity of the aquifer. For the case of fully- or partially-penetrating observation wells, preferential flowpaths distort drawdown curves so that biases are introduced into calculated storage parameters. In cases where a large range is calculated for either  $S_s$  or  $S_y$ , the range should be reviewed with regard to aquifer heterogeneity and grain-size characteristics.

As shown in Figure 8.22 vertical flow through observation wells is not necessarily a problem at all heterogeneous aquifers. For the cause of large-scale transmissivity trends, the vertical discharge in the observation wells reached a maximum of about 1% of the total pumpage and had negligible impacts on drawdowns throughout the entire aquifer. Among the reasons for minimal vertical flow for this K field is that high-K deposits exist in the upper

aquifer but not in the lower aquifer. The former reason accelerates drainage and the latter reason greatly limits the rate at which water can exit (and thus flow through) the borehole.

### **8.5.3.3 Reciprocity**

Based on results in Figures 8.8 and 8.9, reciprocity does not appear to be valid for the unconfined conditions at CAFB. The law of reciprocity (Deng and Horne, 1993; also see Maxwell, 1864) which was derived for confined aquifer conditions, states that the drawdown response measured at well A while well B is pumped should be identical to the drawdown response measured at well B while well A is pumped. Implicit in reciprocity is that the same hydraulic parameters calculated for the drawdown data from Well A and Well B when well B and Well A are pumped, respectively. As shown in Figures 8.8 and 8.9 reciprocity did not hold true for Wells 12 and 24 and Wells 16 and 19.

Shown in Figure 8.25 are drawdown responses for different observation and pumping well pairs. The results suggest that for small drawdowns and the same pumping rate, reciprocity can be valid for unconfined aquifers. For both K fields, drawdown plots for higher pumping rates indicate that deviations from reciprocal drawdown responses for observation-pumping well pairs become greater with increases in the pumping rate and aquifer desaturation. Shown in Figure 26 are drawdown responses for the case where different pumping rates are used. For both K fields, the drawdown responses for the paired wells are not reciprocal. As should be expected in an unconfined aquifer, reciprocity is not necessarily a valid principle for the design well testing strategies in unconfined aquifers.

#### **8.5.4 Summary**

Numerical simulations for unconfined aquifers condition demonstrate that preferential groundwater flow in vertically heterogenous aquifers bias calculated storage parameters. Because of the importance of drainage in unconfined flow, the effect of high-K lens and preferential pathways between pumping and observation wells is sensitive to the K of the material near the water table. In vertically heterogeneous aquifers were local conditions can range from confined to unconfined, the calculated storage coefficients can be highly dependent on the location of the well, the water table, and well screen.

#### **8.6 CONCLUSIONS**

Field data from CAFB indicate that significant preferential flow occurs through interconnected high-K deposits and open well screens. Numerical simulations illustrate that preferential flow paths can lead to significant errors with calculated storage parameters based on type-curve fits. Three crucial issues that affect the error with the calculated storage parameters are: (1) the distribution of high-K deposits in the entire aquifer, (2) the distribution of low-K deposits near the water table, and (3) the hydraulic connections between non-adjacent high-K deposits provided by observation well screens. These three issues strongly impact the non-uniform propagation of pressure change from the pumping well and drainage in the vicinity of the observation and pumping wells. Unlike storage coefficients, transmissivity values appear to be reliability estimated (within a factor of 2) with type-curve matching using data from both the CAFB site and the numerical simulations.

**This discrepancy occurs because transmissivity values are much less sensitive to the early time responses than are storage coefficients.**

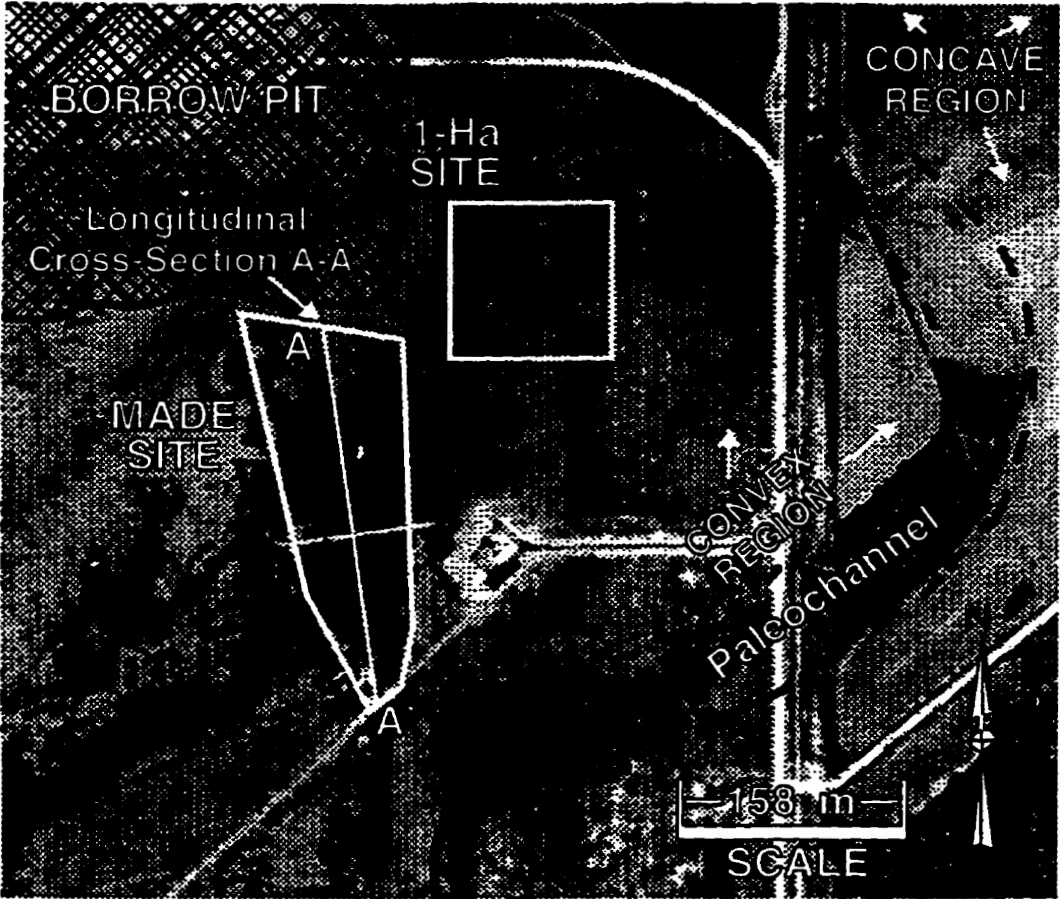


Figure 8.1 Location of two test sites at CFB, MS superimposed on a 1956 aerial photograph that reveals a paleochannel.



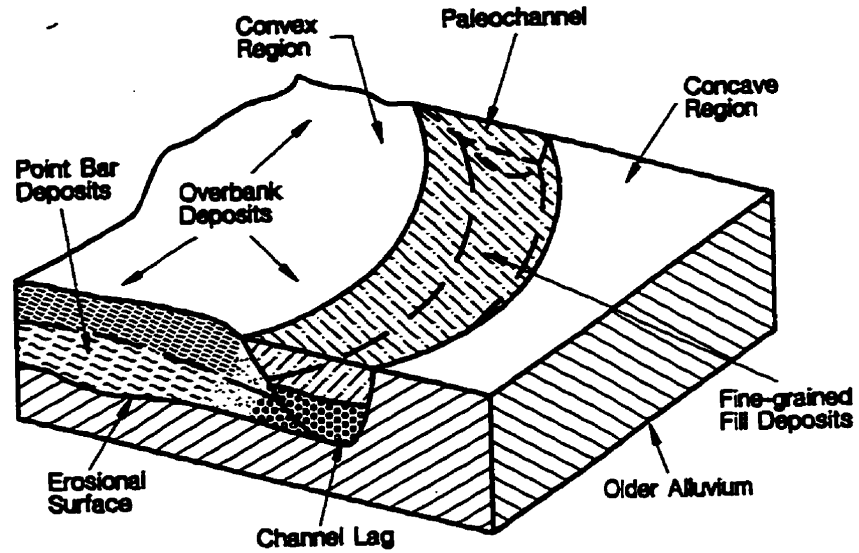


Figure 8.2 Schematic of the regional features associated with the sedimentological model.

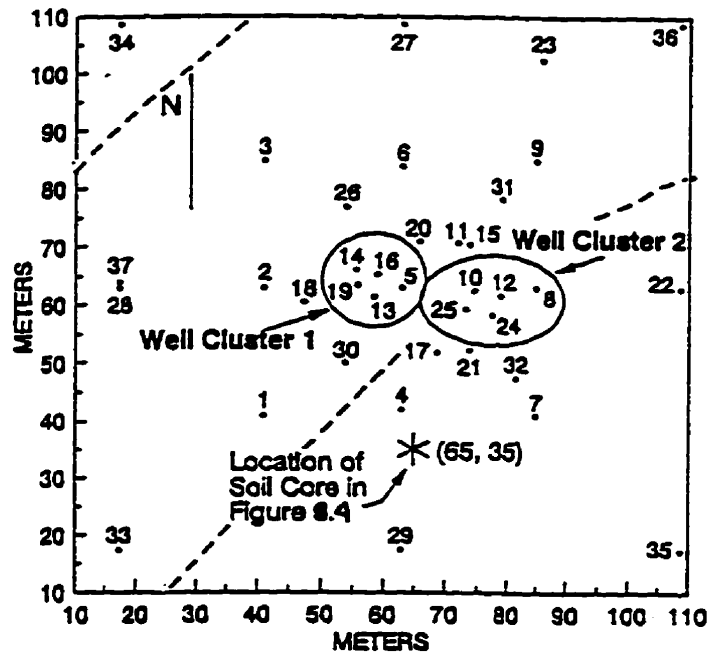


Figure 8.3 Well network for 1-Ha test site with location of the paleochannel estimated by dotted line.

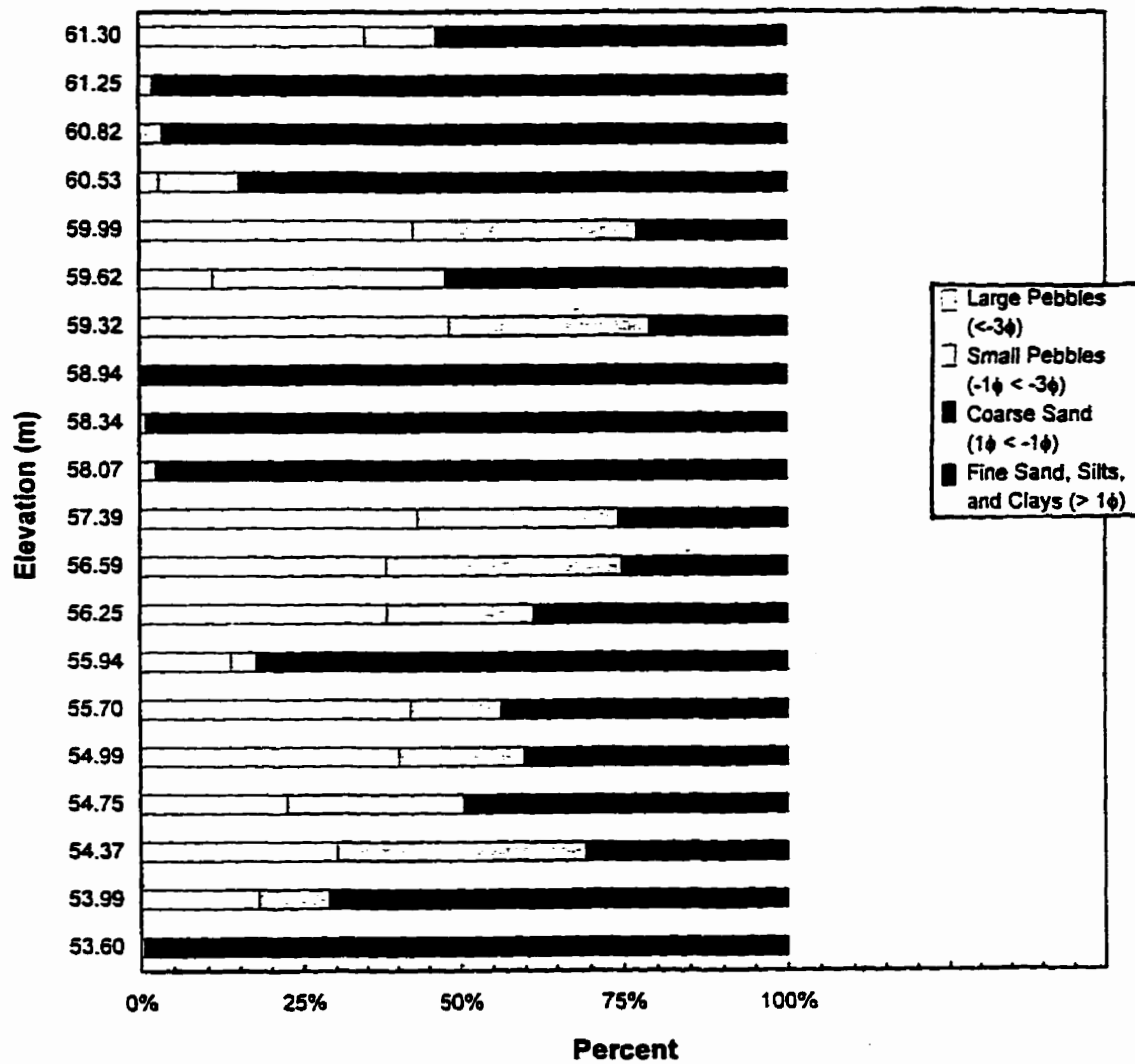


Figure 8.4 Vertical profile of grain-size distributions at location  $x=65\text{m}$  and  $y=35\text{m}$  at the 1-Ha test site (ground surface is at  $64.9\text{ m MSL}$  and location is shown in Figure 8.3).

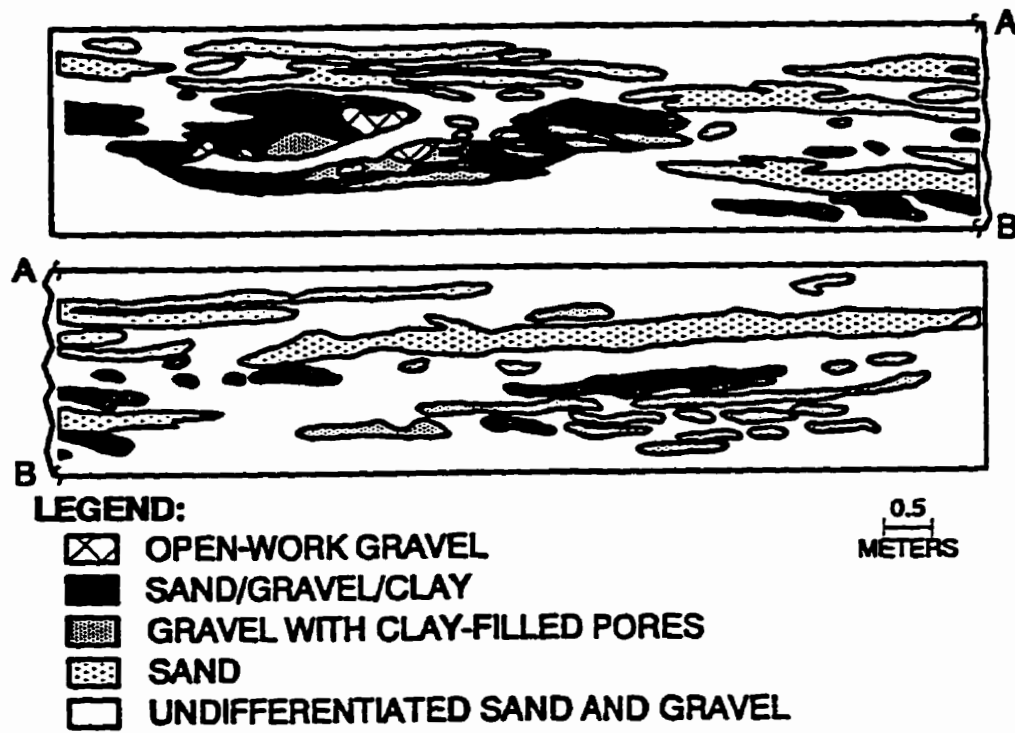


Figure 8.5 Facies map of soil outcrop at a gravel pit near the test sites at CAFB (from Rehfeldt et al., 1989b).

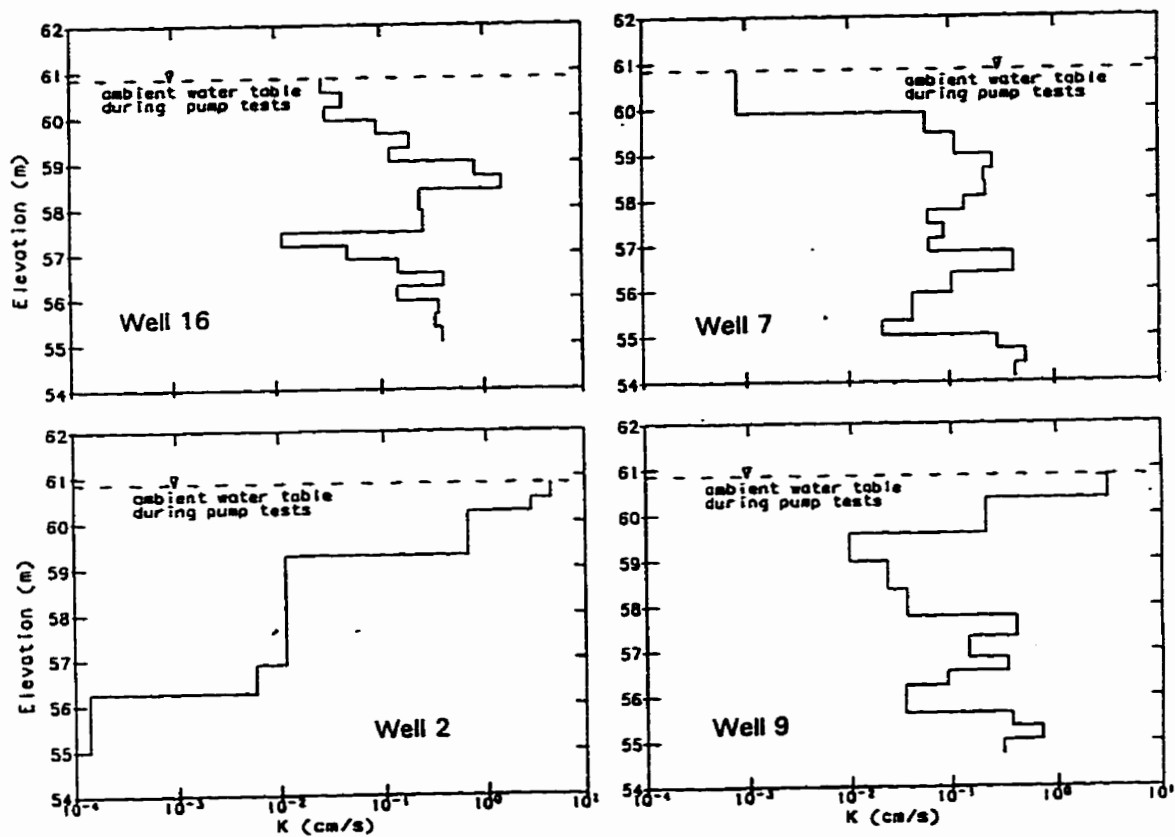


Figure 8.6 Borehole flowmeter K profiles at four well locations that illustrate the wide range of K values for aquifer deposits near the water table.

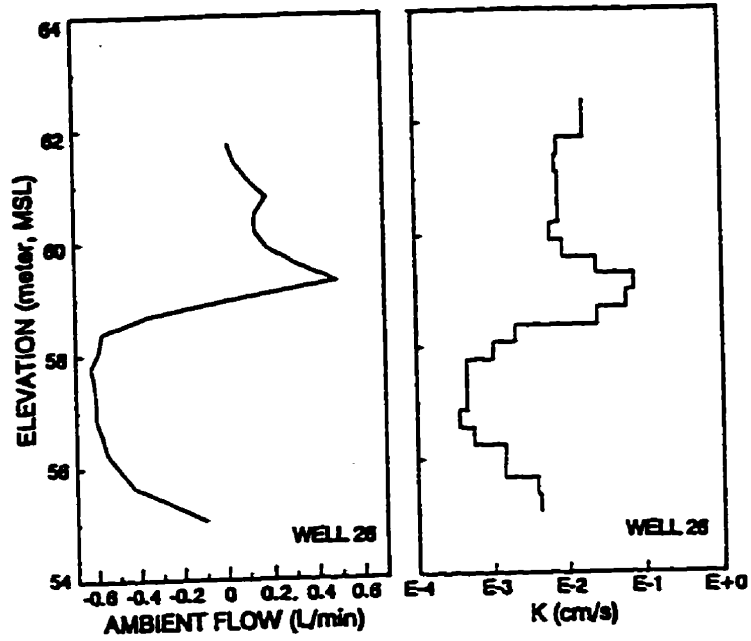


Figure 8.7 Comparison of the ambient vertical flow in Well 26 during April 1989 and the borehole flowmeter K profile from Well 26.

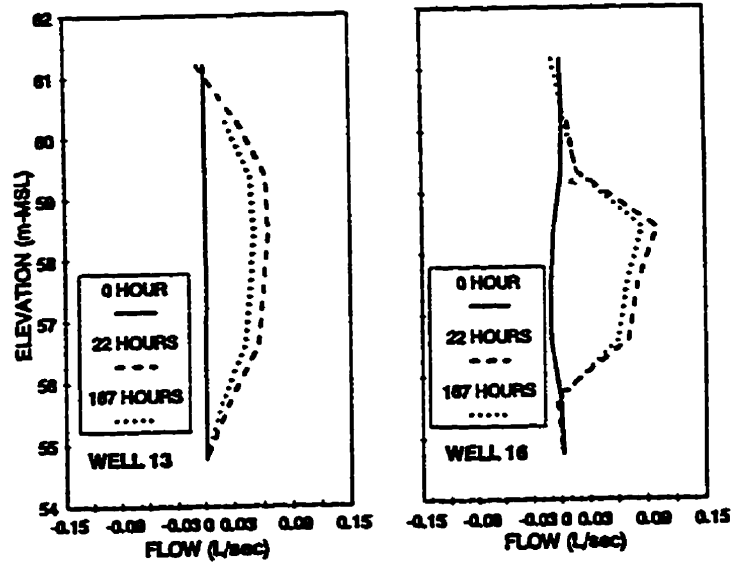


Figure 8.8 Comparison of the vertical flow in Wells 13 and 16 before and after the large-scale aquifer test AT3.

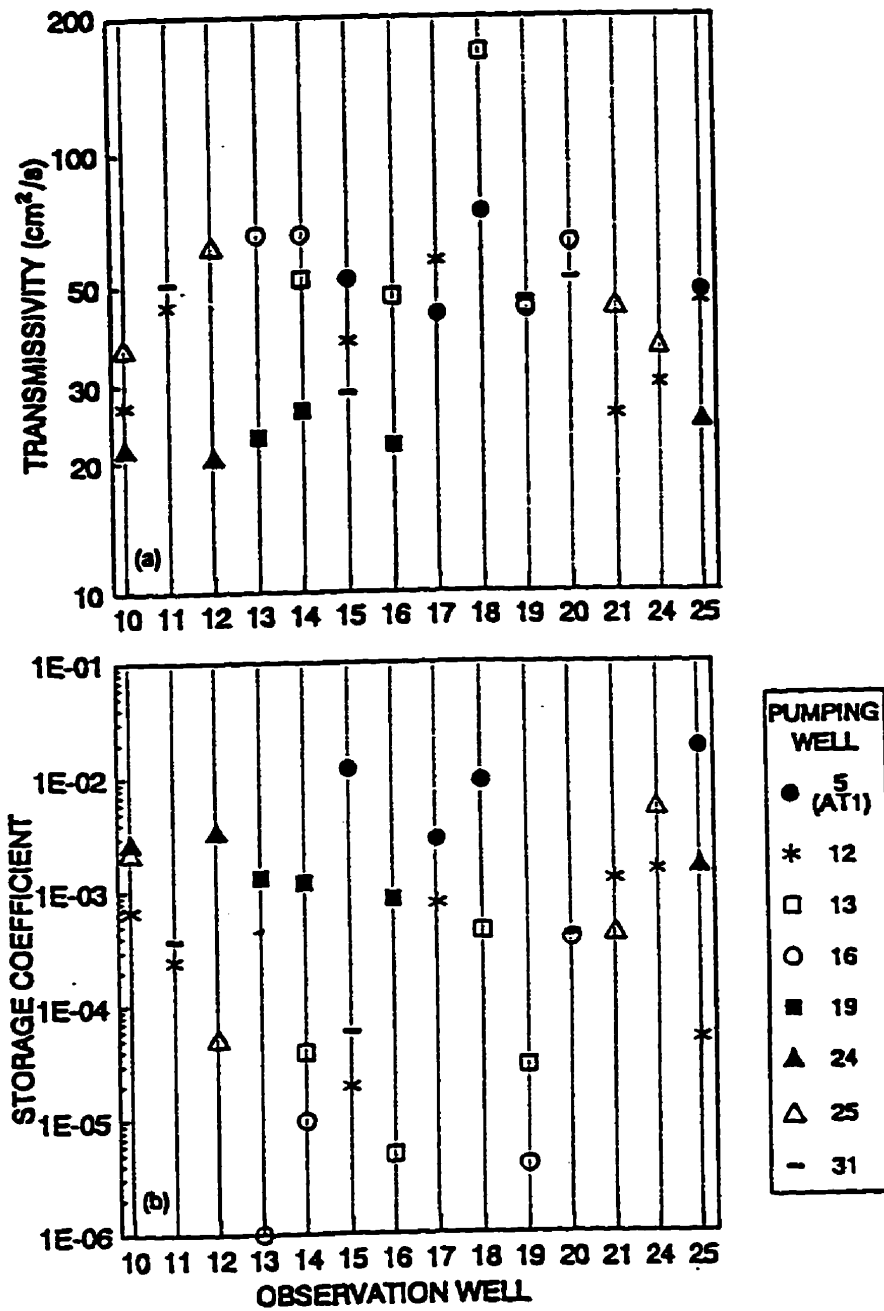


Figure 8.9 Transmissivity (a) and storage coefficients (b) calculated from Theis fits to drawdown data from pumping tests with durations between 2 and 3 hours with the same observation well but different pumping wells.

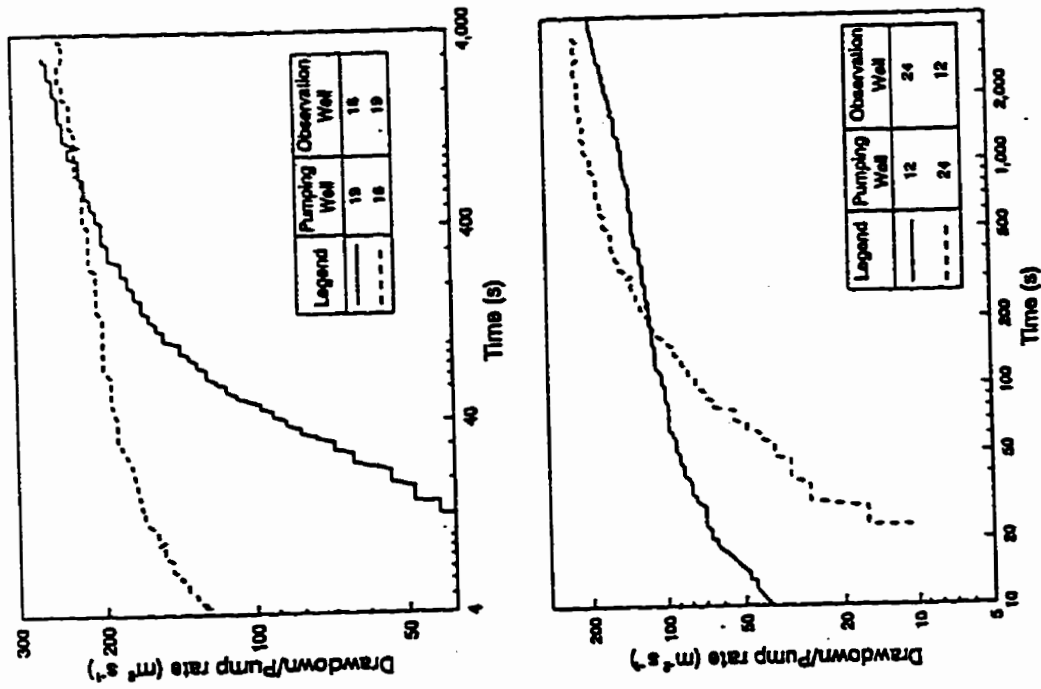


Figure 8.10 Drawdown responses at well pairs Wells 16 and 19 and Wells 12 and 24 that illustrate that reciprocity is not valid at CAFB.

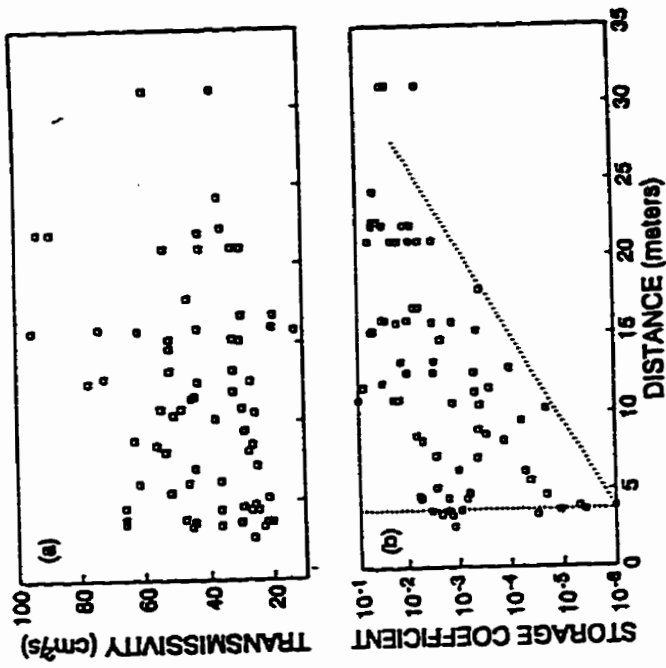
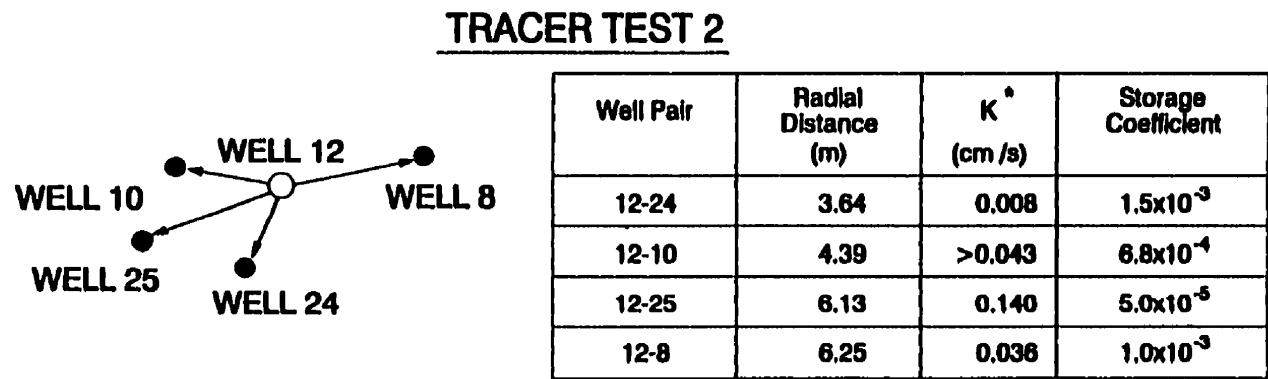
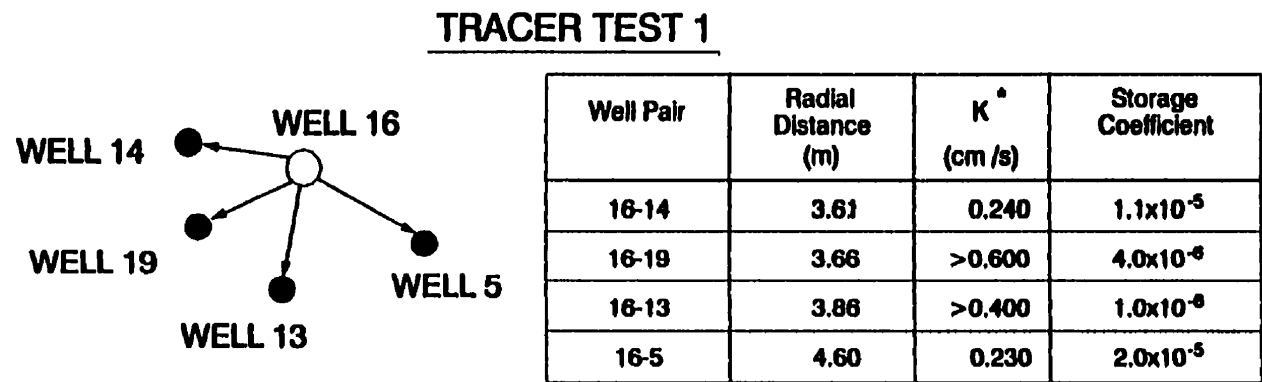


Figure 8.11 (a) Calculated transmissivity and (b) storage coefficients for small-scale pumping tests plotted as a function of distance.



\* Calculated from Tracer Test Data and Equation 3

Figure 8.12 Comparison of storage coefficients and K-values for well pairs in Tracer Tests 1 and 2.



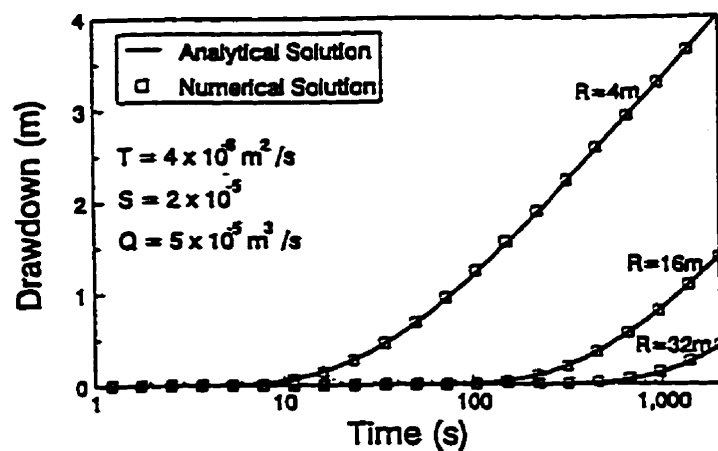


Figure 8.13 Predicted drawdown in a confined aquifer using an analytical and a numerical model.

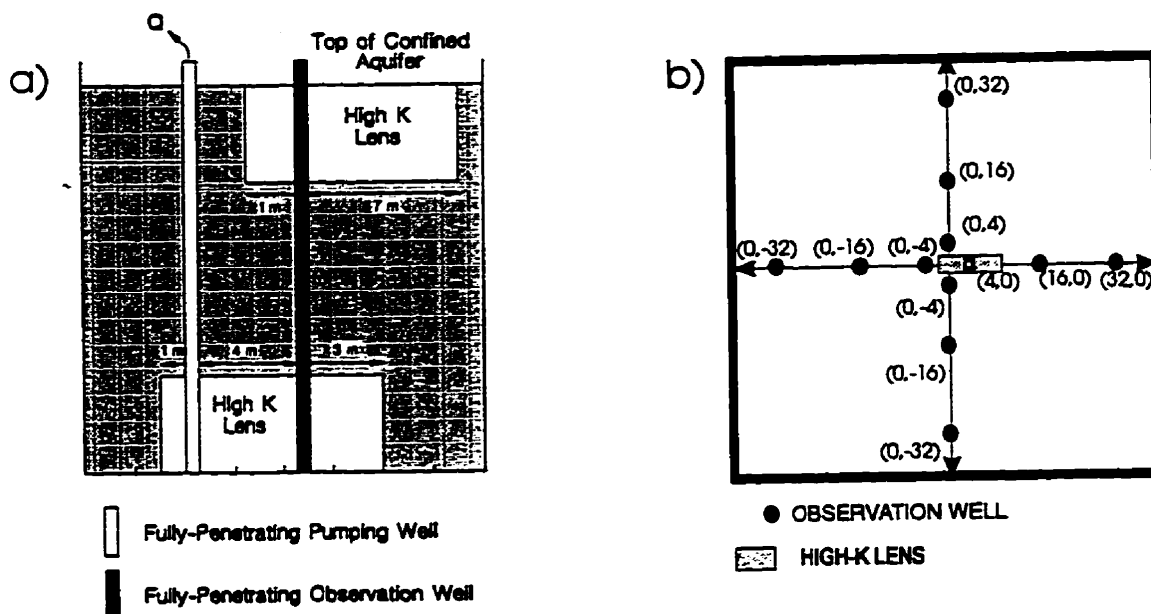


Figure 8.14 Schematic of two high-K lenses located near the pumping well with the pumping well intersecting the lower lens and the observation well intersecting the lower and upper lens: (a) Partial vertical cross-section along the positive x axis; and, (b) Areal cross-section centered on pumping well.

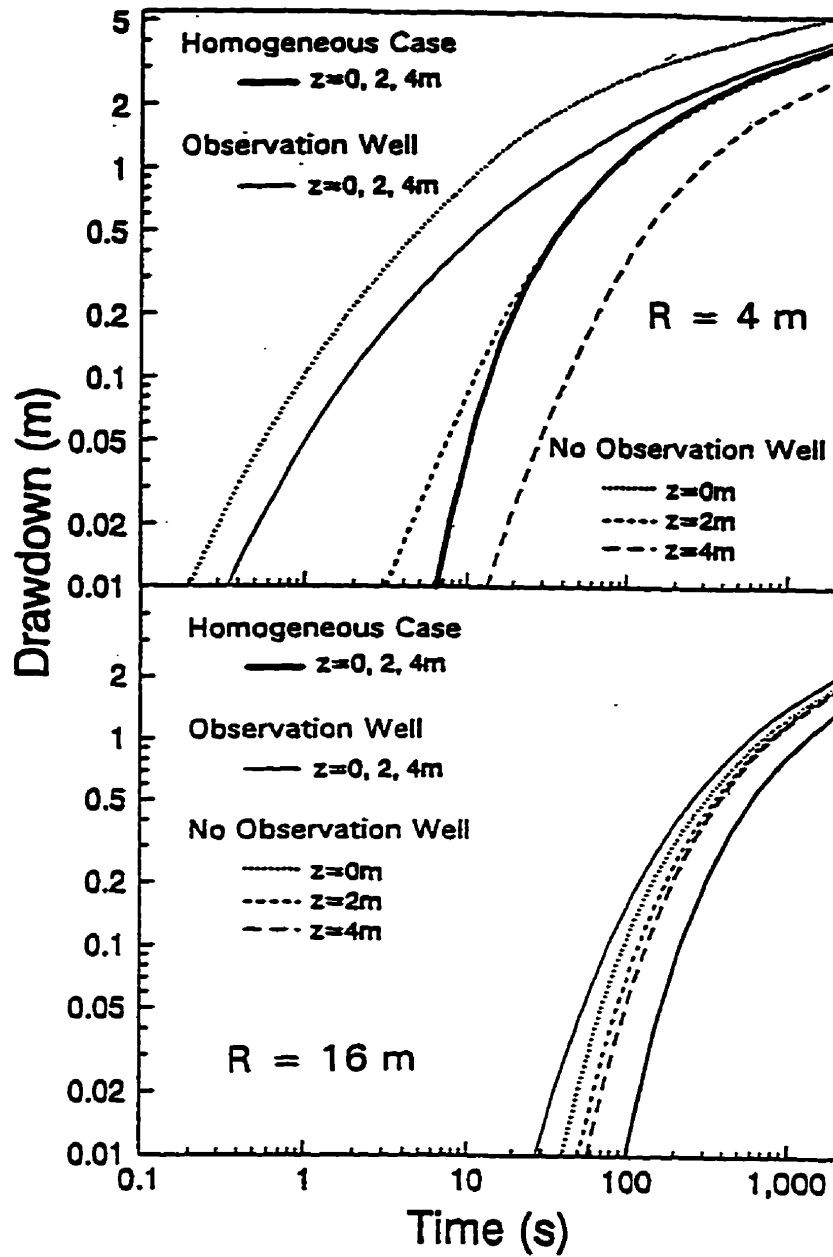


Figure 8.15 Drawdown curves predicted at radial distances of 4 m and 16 m in the direction of the two lenses (along the positive x axis) for the cases with and without the effect of the high-K wellbore associated with the observation wells. Where wellbore effects are included the drawdown is nearly identical throughout the entire well so only one drawdown response is included. For comparison, drawdown results are provided for homogeneous aquifer.

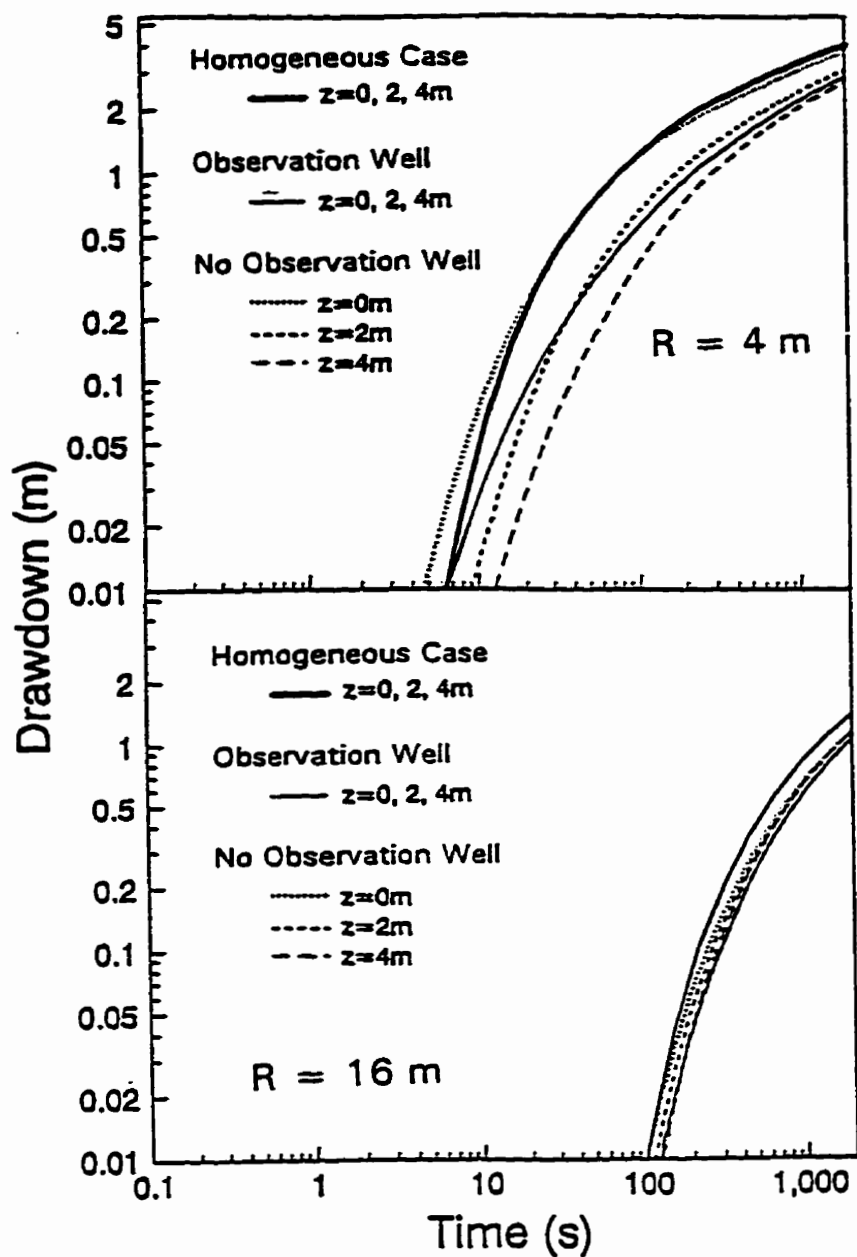


Figure 8.16 Drawdown curves predicted at radial distances of 4 m and 16 m in the direction opposite of the two lenses (along the negative x axis) for the cases with and without the effect of the high-K wellbore associated with the observation wells. Where wellbore effects are included the drawdown is nearly identical throughout the entire well so only one drawdown response is included. For comparison, drawdown results are provided for homogeneous aquifer.

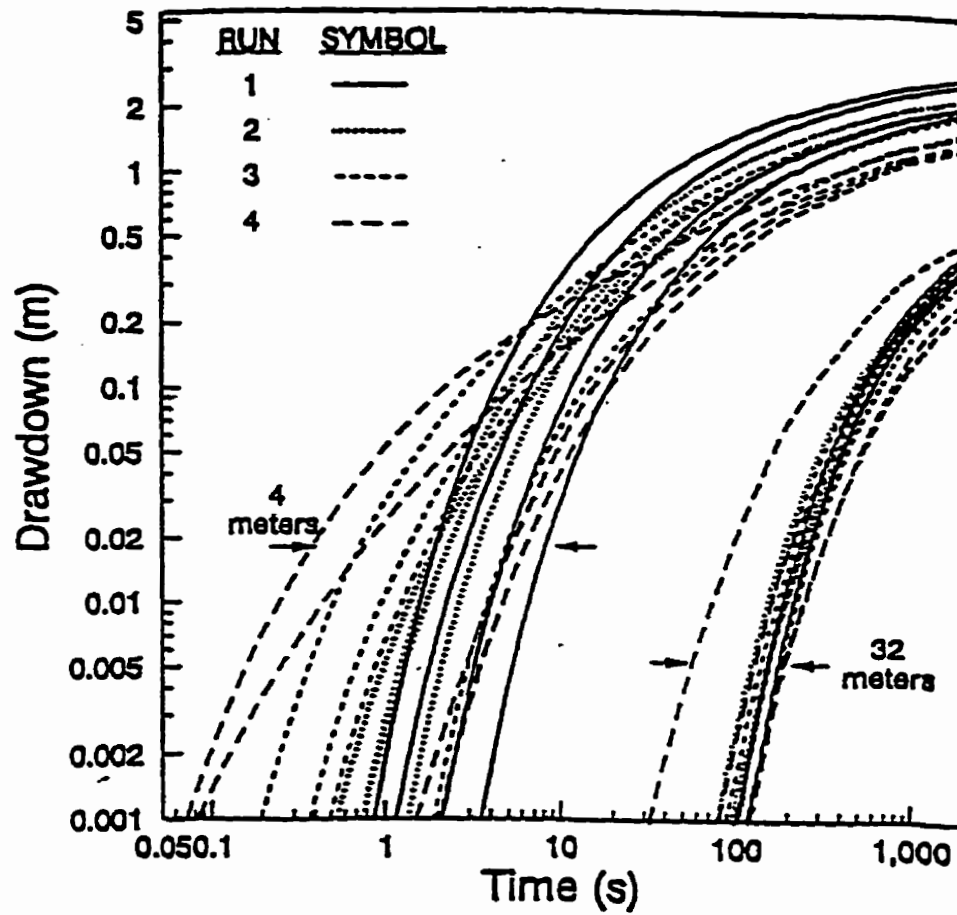


Figure 8.17 Numerically simulated drawdown responses at observation wells located on the x and y axes at radial distances of 4 m and 32 m for four realizations of randomly distributed high-K lenses in a confined aquifer.

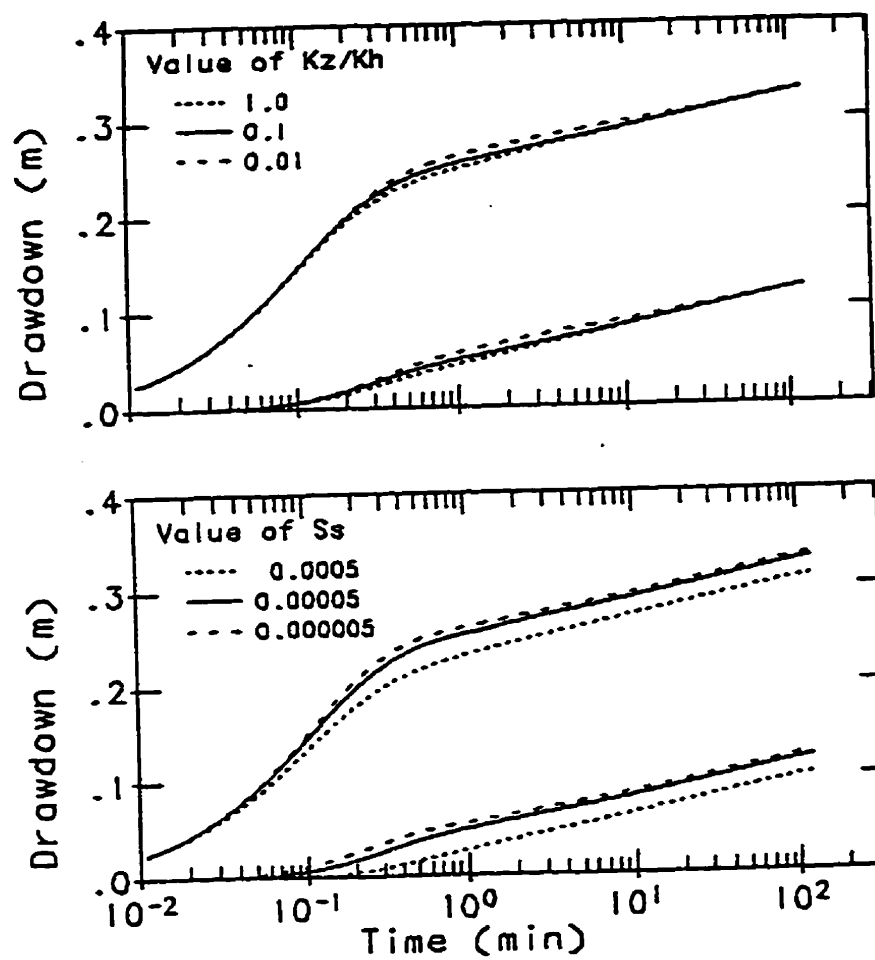


Figure 8.18 Numerically simulated drawdowns for an unconfined homogeneous aquifer with a  $K$  of 0.024 m/min for: (a) changes in the vertical anisotropy with  $S_s$  set to 0.00005; and, (b) changes in specific storage with the vertical anisotropy set to 0.01.

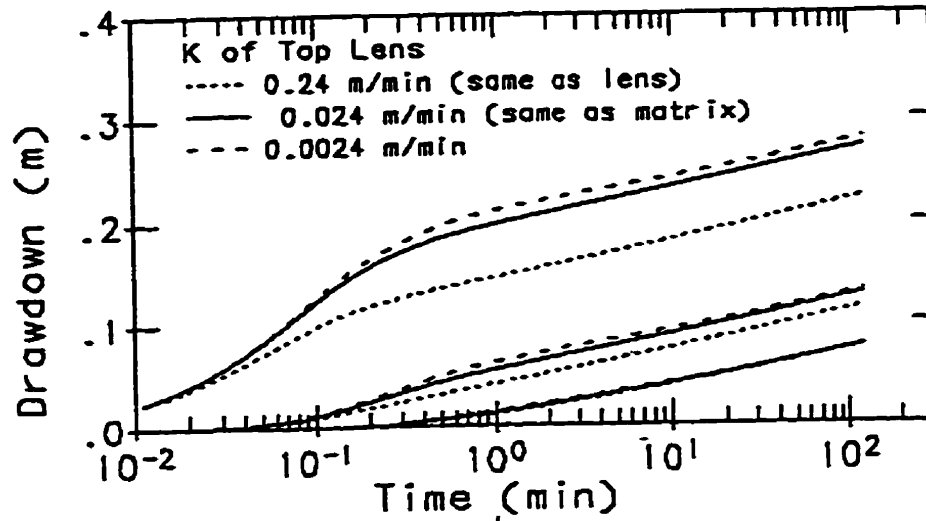


Figure 8.19 Simulated drawdowns for an unconfined homogeneous aquifer with a K of 0.024 m/min and a lens with a K of 0.24 m/min located near the aquifer base and an upper lens located directly below the initial water table.

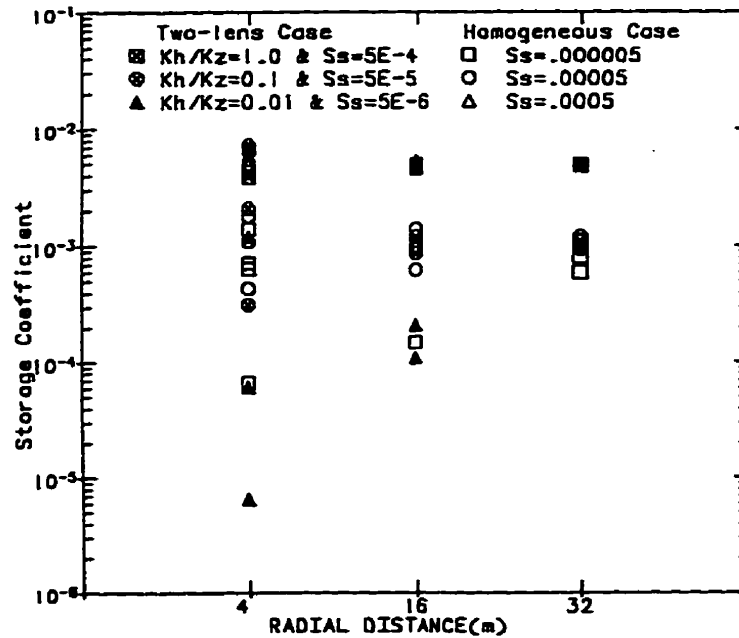


Figure 8.20 Storage coefficients (obtained from type-curve matches to numerically simulated drawdown responses) plotted as a function of radial distance to the observation well.

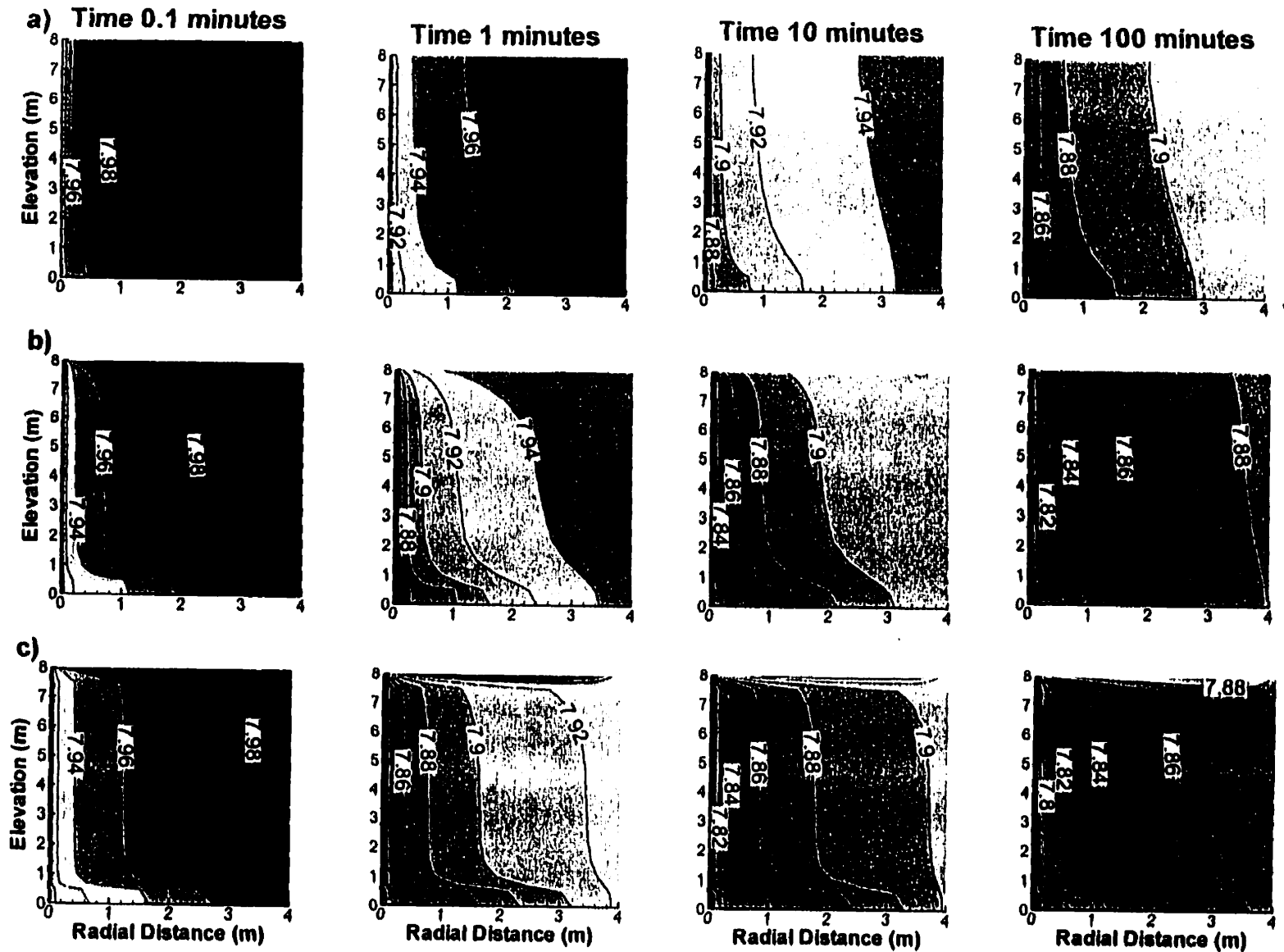


Figure 8.21 Temporal variations in the hydraulic head field along a vertical cross section of the aquifer aligned with the x axis for the three numerical simulations discussed in Figure 8.19. The unconfined aquifer has a K of the 0.024 m/min and a lens with a K of 0.24 m/min at the aquifer base. The hypothetical aquifers varied in the uniform values for  $S_s$ ,  $K_z/K_{ll}$ , and the K of the upper lens. The values for these properties are (a)  $S_s=5 \times 10^{-4}$ ,  $K_z/K_{ll}=1$ ,  $K_{upperlens}=0.24$  m/min, (b)  $S_s=5 \times 10^{-5}$ ,  $K_z/K_{ll}=0.1$ ,  $K_{upperlens}=0.024$  m/min, (c)  $S_s=5 \times 10^{-6}$ ,  $K_z/K_{ll}=0.01$ ,  $K_{upperlens}=0.0024$  m/min.

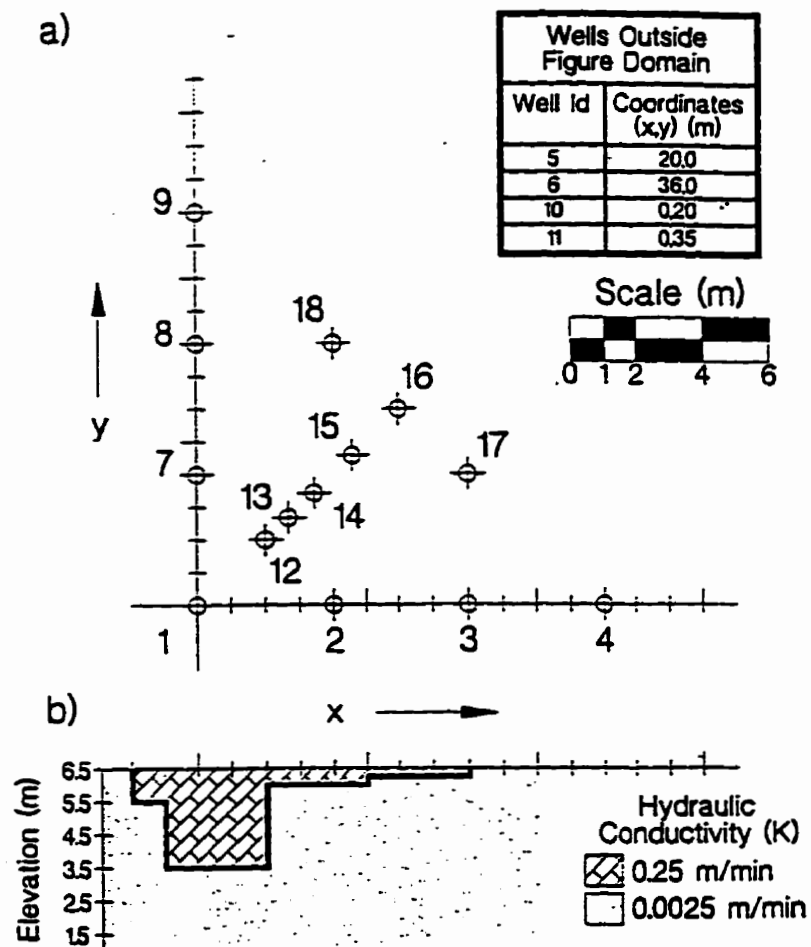


Figure 8.22 (a) Monitoring well network for the 298,265-node numerical model used to simulate pumping tests in hypothetical heterogeneous aquifers, and (b) the thickness variation of the high-K linear strip incorporated in one of the models.



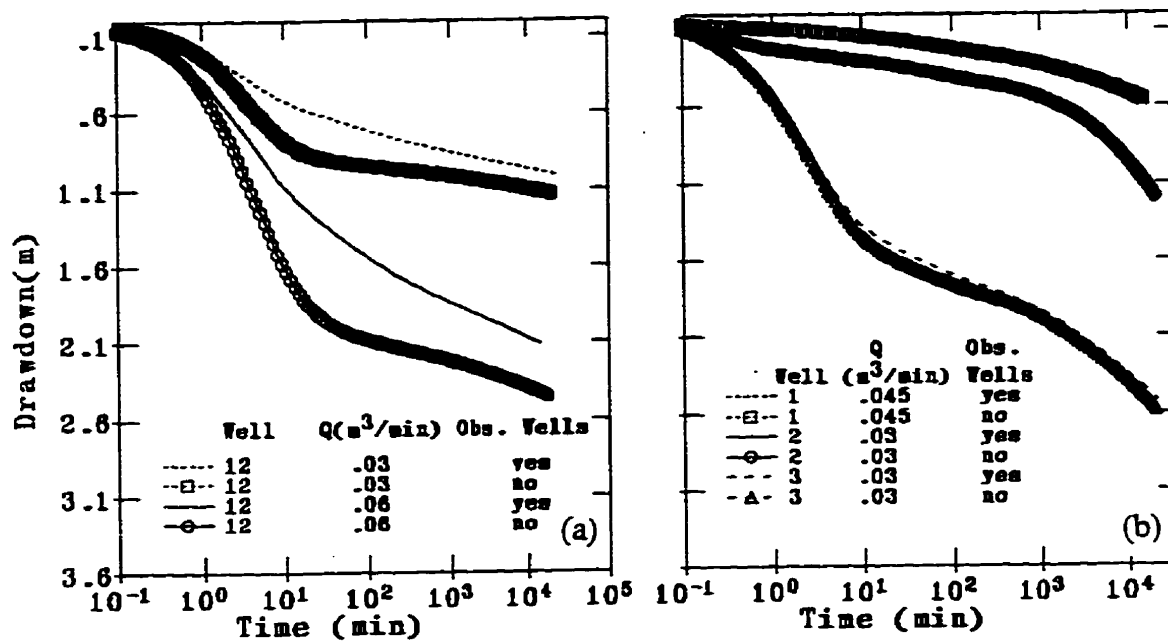


Figure 8.23 Drawdown responses for pump tests with and without observation wells for: (a) a K field consisting of multiple lenses of different Ks.; and, (b) K field with large-scale transmissivity variation.

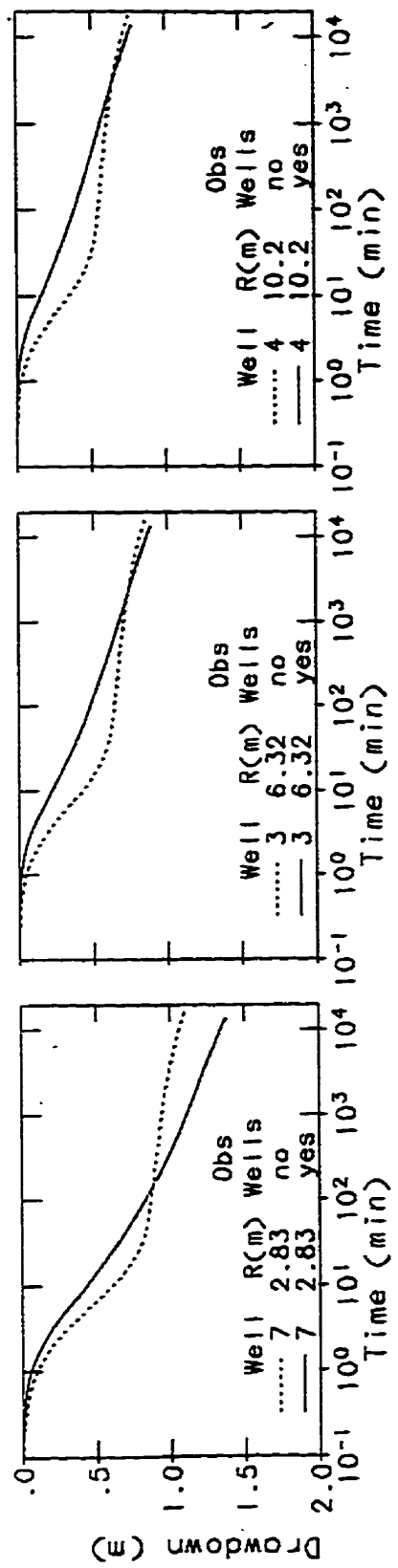


Figure 8.24 Observation-well drawdown responses for pumping Well 12 at 0.06 m<sup>3</sup>/min in the K field consisting of multiple lens of different Ks.

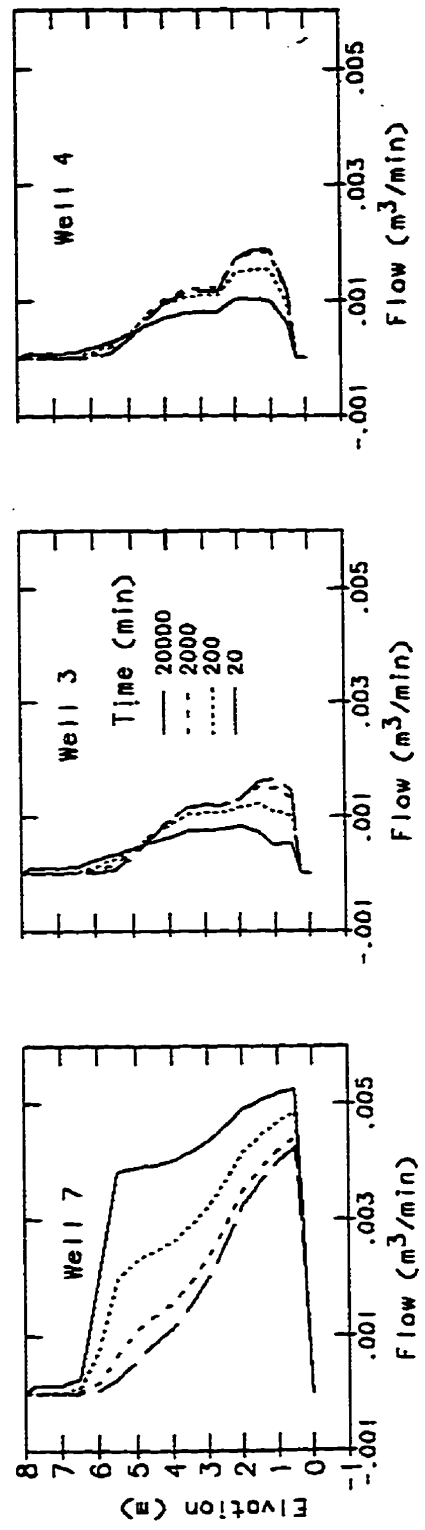


Figure 8.25 Temporal variation of vertical fluxes in the observation wells shown in Figure 8.24.

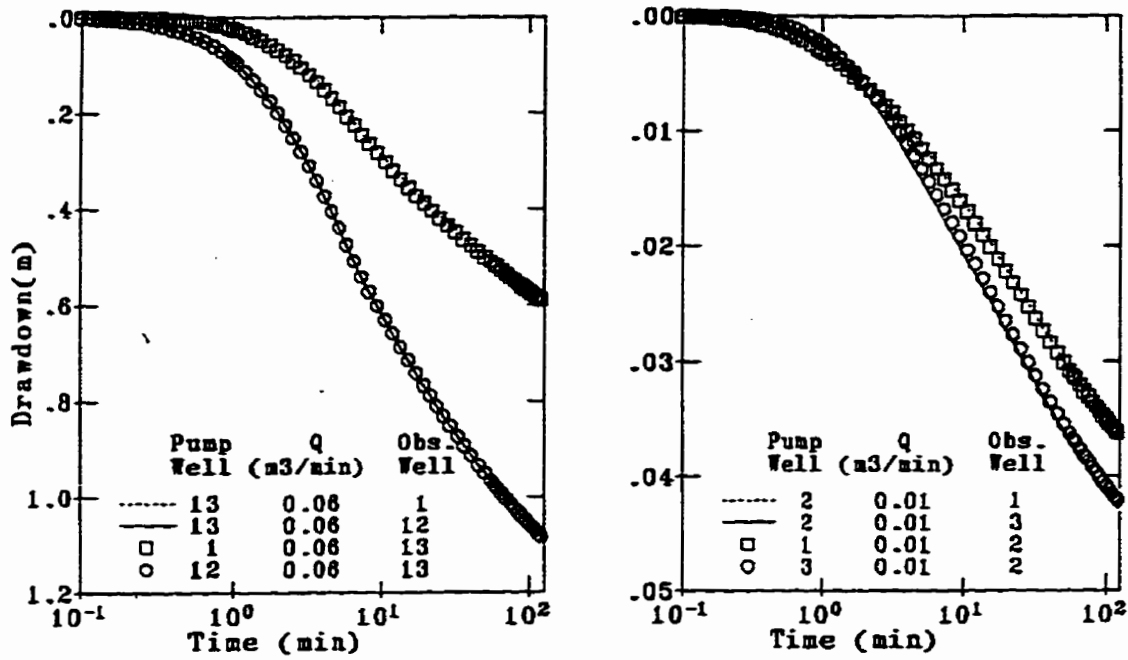


Figure 8.26 Drawdown responses showing reciprocity for well pairs in: (a) the K field consisting of multiple lens; and, (b) the K field with a large-scale transmissivity variations.

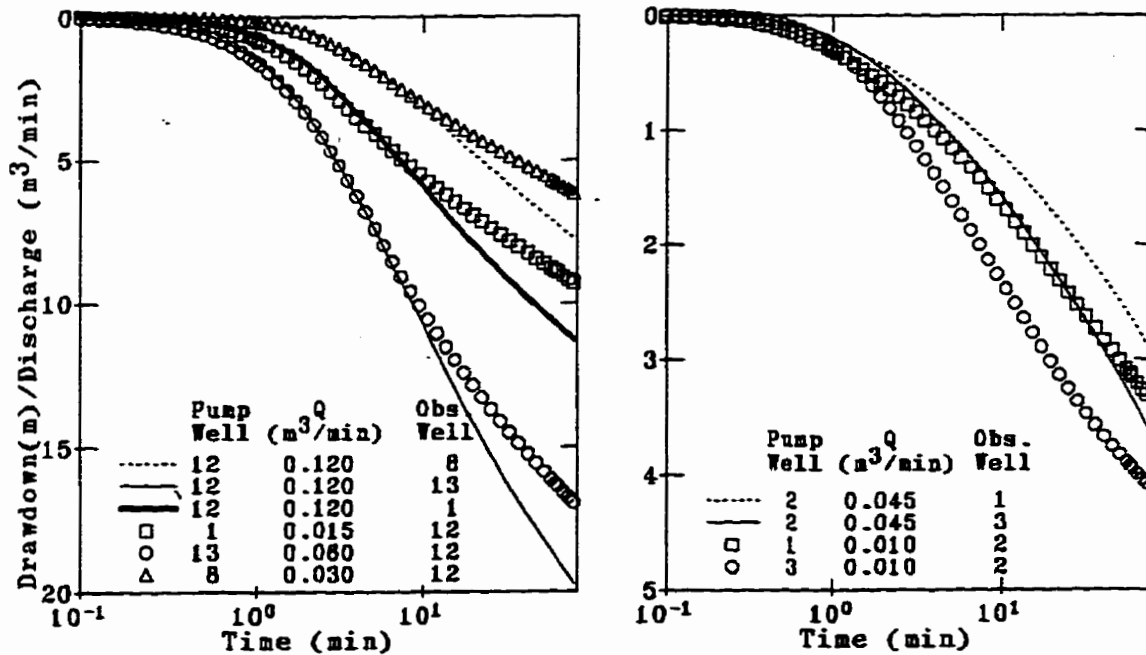


Figure 8.27 Drawdown responses showing non-reciprocity for well pairs in: (a) the K field consisting of multiple lens; and, (b) the K field with a large-scale transmissivity variations.

## **9. FEASIBILITY OF DETRENDING LOG(K) DATA AT CAFB**

### **9.1 INTRODUCTION**

At Columbus Air Force Base (CAFB), Mississippi, large-scale natural gradient experiments have been performed at the MADE site (Boggs et al. 1992; 1993). Similar natural gradient tracer experiments have been performed at the Borden site (Freyberg, 1986; Sudicky, 1986), the Cape Cod site (LeBlanc et al. 1991; Garabedian et al. 1991), and the Twin Lakes site (Killey and Moltyaner, 1988; Moltyaner and Killey, 1988a,b). Compared to tracer plumes at the other field sites, the tracer plumes are highly skewed at CAFB.

Previous to the tracer tests at CAFB, stochastic macrodispersion theory had been successfully applied at Borden, Cape Cod, and Twin Lakes sites. Unlike the field data from these three sites, field data from CAFB indicate that the  $\log(K)$  field has significant large-scale trends in the  $\log(K)$  field. Because a prerequisite of stochastic macrodispersion theory is a second-order stationary  $\log(K)$  field, the CAFB  $\log(K)$  data set must be separated into deterministic and stochastic components before macrodispersivities can be calculated. To detrend the CAFB  $\log(K)$  data set, Rehfeldt et al., (1992) used polynomials fitted by ordinary least squares.

The objective of this chapter is to demonstrate, using field data from two sites at CAFB, that although detrending is conceptually appealing to apply stochastic groundwater theories, problems with implementing detrending are formidable and perhaps intractable. Before problems associated with detrending are discussed, this chapter briefly describes the CAFB aquifer, the tests sites, and results of a large-scale tracer test at the MADE test site.

Detailed site information is provided so that criteria can be established for evaluating results of detrending. Detrending focuses primarily on the log(K) test site from the 1-Ha test site adjacent to the MADE site. Emphasis is on the log(K) data because it has been shown in Chapter 5 to be more representative of site conditions than the MADE log(K) data set.

## **9.2 SITE DESCRIPTION**

### **9.2.1 Geology**

The Columbus aquifer is composed of 10 to 12 m of fluvial Quaternary-age deposits. These deposits primarily consist of coarse-grained deposits in the lower 8 to 10 m and fine-grained deposits in the upper 2 to 3 m. The Quaternary deposits unconformably overlie the Cretaceous Eutaw Formation, which consists primarily of marine clay and silt. Seasonal effects cause the water table to vary 1 to 3 m below ground surface.

Regional geological information for the Columbus aquifer was obtained from an Army Corps of Engineers archaeological study within the Tombigbee valley (Muto and Gunn, 1988). The study suggests that braided streams and coarse-grained meandering streams formed the Columbus aquifer. Shown in Figure 9.1 is a 1956 USAF aerial photograph that outlines a paleochannel that intersects both test sites.

Besides aerial photographs, contour maps of the underlying Eutaw Formation are useful indicators of sedimentological features at CAFB, MS. In the vicinity of the MADE site (see Figure 9.5), there is a 1-m to 3-m deep scour filled with marine sands, which are part of the Eutaw Formation (Boggs et al., 1992). At the 1-Ha test site there is a 0.5- to 1-meter

deep scour at the base of the terrace aquifer filled with high-K deposits (to be discussed later).

A simple sedimentological model for the CAFB aquifer has been advocated in Chapters 2 through 8 and is illustrated in Figure 9.2. At the base of the paleochannel are coarse-grained channel lag deposits. Above these deposits are fine-grained sediments that filled the paleochannel after its abandonment. Based on an equation from Leeder (1973) and a 70-m width for the paleochannel, a base elevation near 59 m MSL was estimated for the channel lag deposits in Chapter 4. Below 59 m MSL and above the Eutaw Formation, the aquifer is presumed to be a mixture of coarse-grained fluvial deposits from braided and/or coarse-grained meandering rivers. Associated with the convex and concave regions of the paleochannel are pointbar and cutback\overbank deposits, respectively.

### 9.2.2 Test Sites

At CAFB, two test sites lie within 50 m of each other (see Figure 9.1). The MADE test site includes over 300 multilevel samplers and over 70 piezometers. At this test site, two large-scale natural gradient tracer tests have been performed (Boggs et al., 1992; Boggs et al., 1993). The 1-Ha test site includes 37 fully-screened wells that were used to support extensive borehole flowmeter tests (Chapter 4 and Appendix C), pumping tests (Chapters 5, 6, and 7), and forced gradient tracer tests (Appendix E). In order to illustrate that large-scale trends in the log(K) field exist at CAFB, results will be presented from the tracer tests from the MADE site and from borehole flowmeter tests from the 1-Ha test site.

Figure 9.3 shows the 37 well network at the 1-Ha test. Based on borehole flowmeter K values at 0.3-m intervals at each well location, the K field shown in Figure 9.4 was created for the upper and lower 2-m zones of the saturated aquifer. The figure shows that high-K values in the upper aquifer are aligned with the location of the paleochannel in Figure 9.1. In addition, zones of moderate K values and low K values in the upper aquifer correspond to the convex and concave regions of the paleochannel, respectively. With respect to the sedimentological model, the low K values are associated with the overbank/flood deposits and the moderate K values are associated with pointbar deposits. At the base of the aquifer, an incomplete  $\log(K)$  field is shown because of the uneven surface of the underlying Eutaw clay. Presumably, the high-K deposits in the scour are bedload deposit from the river that incised the channel.

Shown in Figure 9.5 is a vertical cross section of a tritium plume formed when a  $9.7 \text{ m}^3$  tritium solution was injected at the MADE site. The cross section is aligned with the segment A-A shown in Figure 9.1. At 27 and 132 days, the plume occupied the entire aquifer thickness between the injection location and a longitudinal distance of 20 m. At 132 days, the portion of the plume downgradient of 20 m was confined to the upper aquifer above 58 m MSL. At 224 days, the plume resided above 58 m MSL within the paleochannel boundaries but occupied the entire aquifer thickness outside of the paleochannel's boundaries. Based the complete tritium data set, Boggs et al., (1993), estimated near-field velocity of 5 m/yr and a mid- to far-field velocity of 128 m/yr for the tritium plume. Consistent with the increase in groundwater velocity downgradient and flow convergence

to the upper aquifer at a downgradient distance of about 25 m are the locations of the high-K deposits associated with the paleochannel shown in Figure 9.1.

### 9.2.3 Hydraulic Gradients

Historic and detailed water table data have been collected only at the MADE site. Seasonally, the water table fluctuates 2 to 3 meters and the mean horizontal hydraulic gradient varies between 0.002 and 0.005 and has an estimated maximum variation in direction of 44 degrees (Boggs et al., 1990). Considerable seasonal and spatial variability exists in the vertical hydraulic gradients. Typically, the vertical hydraulic gradients are 5 to 50 times greater than the horizontal gradients (Boggs et al. 1990).

Figure 9.6 shows the average vertical hydraulic gradients from monthly data for 1988 to 1991 (using data from Boggs (1991, 1992) in piezometer pairs immediately southeast and in the MADE MLS network. Approximately 60 m upgradient of the paleochannel in the MADE MLS well network, the vertical gradients are strongly downward (3 to 11%). Near the upgradient and southern boundary of the paleochannel, the average hydraulic gradients are slightly upward (as high as 2%). In the middle and toward the downgradient boundary of the paleochannel the average vertical gradients are consistently small (less than 0.5%). Between 10 and 100 meters downgradient of the paleochannel, the average gradients are strongly downward (2 to 8%). The general trends in the vertical hydraulic gradients are consistent with groundwater converging upward and diverging downward as it enters and exits a the high -K region associated with paleochannel bedload deposits.



### **9.3 HYDRAULIC PROPERTIES**

The effective transmissivity of the CAFB at the regional scale has been estimated at  $30 \text{ cm}^2/\text{s}$  based on the late-time results of drawdown responses from five large-scale aquifer tests discussed in Chapter 6. Large-scale trends in aquifer properties inferred from early-time drawdown responses from the pumping tests in Chapter 6 and from borehole flowmeter tests in Chapters 4 and 5 suggest a correlation between large-scale K patterns and the paleochannel. Specifically, high K values (e.g. 1.0 to 0.1 cm/s) are associated with paleochannel coarse channel lag deposits, low K values (e.g.  $\leq 0.001 \text{ cm/s}$ ) are associated with the fine overbank deposits in the concave region of the paleochannel, and moderate K values (0.02 to 0.002 cm/s) are associated with point bar deposits in the convex region of the paleochannel.

### **9.4 DETRENDING LOG(K) DATA FROM CAFB**

#### **9.4.1 Approach to Detrending**

Based on the results of Russo and Jury (1987), Rehfeldt et al., (1989a, 1992), and Davis et al., (1991), ordinary least square (OLS) regression appears to be as good, if not better, than other more complicated methods for detrending nonstationary fields. Following the example of Rehfeldt et al., (1992) and Davis et al., (1991), the OLS method will be used with polynomial expressions to detrend the 881 log(K) values from the 1-Ha test site.

Of interest to detrending the 1-Ha log(K) data set are the following four issues:

- (1) The density of log(K) values at the 1-Ha site is relatively high and is not likely to be exceeded at many groundwater test sites. As a result, detrending

at other sites may not be an option because of insufficient data to define trend(s).

(2) The objective of detrending the  $\log(K)$  data from CAFB is to remove deterministic patterns or inhomogeneities in the  $\log(K)$  data associated with large-scale sedimentological features. In this paper, a "trend" is a pattern in the  $\log(K)$  data related to a large-scale sedimentological feature and "detrending" is the removal of a  $\log(K)$  pattern associated with a large-scale sedimentological feature.

(3) Because of its large dimensions and its high- $K$  bedload deposits, the paleochannel in Figure 9.1 is the sedimentological feature of most concern.

(4) Because there are no physical or geological reasons why the deterministic  $\log(K)$  patterns should be reproduced by low-order polynomials, a priori constraints will not be placed on the maximum polynomial order available for detrending.

## **9.4.2 The 1-Ha Test Site Log(K) Field**

### **9.4.2.1 Trend identification**

Results from borehole flowmeter, pumping and tracer tests demonstrate that the aquifer deposits associated with the paleochannel in Figure 9.1 are responsible for a region of high  $\log(K)$  values in the upper aquifer. It is of interest to determine whether semivariograms, from which key parameters are derived to calculate macrodispersivity values, can be used to identify and quantify trend(s) in the  $\log(K)$  data.

Global and directional semivariograms are provided in Figures 9.7 and 9.8. For comparison, an exponential semivariogram model with a variance equal to the sample variance has been visually fitted to the global semivariogram. (An approximate 95 percent confidence region is given for each sample variance, according to a method explained by Rehfeldt et al. (1992)). The global semivariograms closely match the exponential model and

provide no evidence of a trend. The inability to detect the known trends in global semivariograms has been reported also by Russo and Jury (1987), Rehfeldt et al.,(1989a), and Desbarats and Srivastava (1991). The directional horizontal semivariograms are similar to the global horizontal semivariograms for lag distances of less than 40 meters. The variability among the directional semivariograms at lag distances beyond 50 meters is not known. The variability may be related to  $\log(K)$  trends and/or to the biases introduced by the large lag distances compared to the site dimensions.

The lack of evidence for a trend in the cumulative distribution or global and directional semivariograms prompted analysis of regional subsets of the  $\log(K)$  data. The rationale for regional subsets is that fluvial aquifers have deposits from a wide variety of depositional environments such as point bars, channels, and cut banks that have different  $\log(K)$  structures. To discover any differences among these deposits, the  $\log(K)$  data were used to generate six subsets to represent the upper, lower, eastern, western, northern, and southern regions of the aquifer. No geological information was used to guide the selection process. The  $\log(K)$  data for each group is as follows: Upper - values above 58.5 meters MSL; Lower - values below 58.5 meters MSL; East - values from wells east of well 5, West - values from wells west of well 5; North - values from wells north of well 5; South - values from wells south of well 5 (see Figure 9.2). Each of these subsets contain between 320 and 470  $\log(K)$  values and represent an area with at least one dimension greater than 90 meters.

Shown in Figure 9.9 are the semivariograms for the six  $\log(K)$  subsets. For mutually exclusive data sets, similar results were obtained for the upper and lower regions but large differences were obtained for the west and east regions. Based strictly the properties of the

semivariograms shown in Figure 9.9, one could infer that a trend in the vertical is not as important as a trend in the east-west direction. However, other statistical measures provide a different picture. For instance, comparison of the mean values among the mutually exclusive subsets indicates that the largest difference occurs between the upper and lower regions, with the former having more than double the mean  $\log(K)$  value than the latter. The Kolmogorov-Smirnov limiting distribution test (Feller, 1948; Smirnov, 1948) also suggests differences exist among the  $\log(K)$  subsets. The test provides less than a .0001% chance for the upper and lower  $\log(K)$  subsets to be realizations of the same population and for the west and east  $\log(K)$  subsets to be realizations of the same population. In short, although regional variograms and the statistics of their respective data sets provide qualitative insight into whether trends exist in the  $\log(K)$  data, they cannot provide sufficient information to identify, much less delineate, trends in the  $\log(K)$  data.

In the final analysis, the first step towards applying stochastic macrodispersion theory at CAFB, and perhaps most heterogeneous fluvial aquifers, includes the highly subjective process of interpreting field data for identification of  $\log(K)$  trends. This process can be partially successful at CAFB because of an 10-year field effort involving numerous tracer tests, pumping tests, and a geological investigations. However, even with the extensive data set available at CAFB, significant differences will exist among hydrogeologists.

#### **9.4.2.2 Detrending**

The  $\log(K)$  field was detrended by polynomial expressions of orders one to six. The approach and the program used for the exercise is similar to Rehfeldt et al. (1992).

Figures 9.10 and 9.11 show the calculated trends for the uppermost and lowermost 2 meters of the saturated aquifer, respectively. Selection of the most approximate trend based solely on visual observation (as proposed and done by Rehfeldt et al., (1992)) has problems and uncertainty. Some of the uncertainty is caused by the unequal development of the high  $\log(K)$  regions associated with the paleochannel and the scour channel. Because the paleochannel is larger and contains higher  $\log(K)$  values than the lower river channel, the high  $\log(K)$  region associated with the paleochannel evolves ahead of the high  $\log(K)$  region associated with the lower river channel. Another problem is the gradual refinement of the high  $\log(K)$  region with increases in the order of the polynomial. In Figure 9.10, for instance, the high  $\log(K)$  region associated with the paleochannel appears to begin with a second order polynomial but is not defined across the site until a fifth order polynomial is attained. Because of a lack of an objective criteria, an appropriate polynomial to detrend the  $\log(K)$  data is hard to justify based on visual observations.

Among the classical methods for evaluating detrending method are F-tests (Davis, 1986). F-tests values for evaluating the appropriateness of increasing the order of the polynomials to detrend the 881  $\log(K)$  values are in Table 9.1. The results indicate that at least a fifth order polynomial is required to explain 50% (e.g.  $R^2$  is 0.5) of the variance and that the difference between the regression effect and a random effect (at a 1% confidence level) does not occur until after a sixth order polynomial. The F-test results indicate that there is no justification for using less than a sixth order polynomial to divide the  $\log(K)$  data into a deterministic component and a stochastic component. The F-test results for 307  $\log(K)$

values from a regular grid are presented in Table 9.1 to show that any clustering in the 881 log(K) data set is not sufficient to affect the selection of a sixth order polynomial trend.

**Table 9.1 Results of ANOVA for Using Polynomials to Detrend the Borehole Flowmeter K Values at the 1-Ha Test Site**

Polynomial Fit	Number of Terms	881 Log(K) values <sup>A</sup>			307 Log(K) values <sup>B</sup>		
		R <sup>2</sup> <sup>C</sup>	Vital Terms <sup>D</sup>	F Test <sup>E</sup>	R <sup>2</sup> <sup>C</sup>	Vital Terms <sup>D</sup>	F Test <sup>E</sup>
1 <sup>ST</sup> Order	4	0.07	4	N/A	0.13	4	N/A
2 <sup>ND</sup> Order	10	0.18	10	19	0.39	10	21
3 <sup>RD</sup> Order	20	0.26	15	9.5	0.52	19	7.9
4 <sup>TH</sup> Order	35	0.33	34	5.8	0.66	35	7.7
5 <sup>TH</sup> Order	56	0.50	53	13	0.72	56	2.3
6 <sup>TH</sup> Order	84	0.63	81	10	0.77	83	1.7

<sup>A</sup> Log(K) values generated from borehole flowmeter tests at all 37 wells.

<sup>B</sup> Log(K) values generated from borehole flowmeter tests at 13 wells on a regular grid (e.g. wells 1, 3, 5, 7, 9, 22, 27, 33, 34, 35, 36, 37).

<sup>C</sup> R<sup>2</sup> is calculated by dividing the sum of the squares due to regression by the total sum of the squares and represents a measure of goodness-of-fit.

<sup>D</sup> The F-test was applied to determine which polynomial coefficients are not zero by chance given a 1.0% confidence limit (see Davis (1986) pg 423 for detailed explanation).

<sup>E</sup> Values calculated shows that incremental increases in the order of the polynomial equation up to a sixth order are justified by on a ANOVA analysis at a 1.0% confidence limit except for the 6<sup>TH</sup> order fit for the 307 log(K) values, which is justified at a 1.5% confidence limit. (see Davis (1986) pg 72 for critical values for the F-test).

Table 9.1 also provides the results of F-tests to evaluate the contribution of the partial regression coefficients for each of the polynomials. The results indicate that almost every term in the polynomial, even at the higher orders, is justified.

#### 9.4.2.3 The $\log(K)$ residuals from detrending

For each polynomial expression, a set of residuals was calculated by subtracting the value of the trend from the measured  $\log(K)$  value. If detrending has been properly accomplished then the residuals represent the stochastic (i.e., random) component of the  $\log(K)$  data required to calculate macrodispersivity values. Figure 9.12 shows that increases in the order of the polynomial cause decreases in the variance and the correlation scale in the global semivariograms. The decreases continue until little, if any, correlation exists among the residuals. Although there are noticeable differences among the semivariograms for the original  $\log(K)$  data and for the residuals, there is no indication that any of these differences reflect the removal of trend(s).

Unlike the global semivariograms, the directional semivariograms (Figure 9.13) provide evidence that trend removal occurs. In particular, a third-order polynomial appears to remove enough of a trend to greatly improve the similarity among the directional semivariograms. The question remains, however, whether this third-order polynomial has properly detrended the data set.

For the west and east subsets of the residuals from the third-order polynomials, the Kolmogorov-Smirnov limiting distribution test (Feller, 1948; Smirnov, 1948) provides less than a 2.3% chance that the two subsets could be realizations of the same population. A

increase from 0.0001% in the  $\log(K)$  data to 2.3% is very significant but the probability increases to more than 20% for the fourth-order polynomial. This 10 fold increase in the probability and the wide range of horizontal correlation lengths among the regional subset of third-order residuals in Figure 9.14 indicate that complete detrending does not occur with a third order polynomial.

Potential problems with detrending are further reflected in the probability distribution of the residuals. Ideally, the residuals should have a normal distribution because this is distribution created if a random deviation existed at each measurement point. A test for normality is the Kolmogorov-Smirnov test (see Davis, 1986). For this application, however, standard tables for the test such as those in Davis (1986) are not applicable because the parameters for the specified distribution are estimated from the sample data (Liffiefors, 1967; Davis, 1986). Using the appropriate tables developed by Liffiefors (1967), the null hypothesis of normality is rejected with at a 99% confidence limit for every set of residuals produced by detrending with polynomials of order one through six.

#### **9.4.2.4 Comments regarding detrending the MADE Log(K) field**

Rehfeldt et al., (1992) indicate detrending the  $\log(K)$  data at the MADE site is possible and successfully accomplished with a third-order polynomial. This result contrasts with the results above for the  $\log(K)$  data from the 1-Ha site. Given the proximity of the two test sites and the use of the same numerical code for polynomial regression, the very different outcomes require an explanation. The reasons for the different results include the method



of calculating  $K$  from borehole flowmeter tests, the depositional model for CAFB, and the lack of an objective criteria to evaluate trends.

The majority of the work associated with detrending the  $\log(K)$  at the MADE site (see Boggs et al., 1990) was performed when the CAFB aquifer was thought to be braided-river deposits. As a result, little, if any, concern was given to the possible importance of the paleochannel. The set of field tests with which the detrending results were primarily evaluated were the snapshots from the first MADE tracer test (Boggs et al., 1992). Thus, the information used to evaluate the detrending results from the MADE site is significantly less than that for the 1-Ha test site.

The primary criteria for evaluating the MADE detrending results used by Rehfeldt et al., (1992, 1989b) and Boggs et al. (1990) is visual comparison of plotted  $\log(K)$  trends and field data. Objective criteria involving ANOVAs and F-tests, which are traditionally important aspects to regression analysis (Davis, 1986) were ignored. Application of the F-test to the MADE  $\log(K)$  data provided in Boggs (1992) provides results similar to those obtained for the 1-Ha test site: namely, there is no justification for using a polynomial less than a sixth order polynomial to divide the  $\log(K)$  data into a deterministic component and a stochastic component.

In evaluating the residuals, Rehfeldt et al., (1992) limit the examination to global and directional semivariograms. At CAFB, the trends in the  $\log(K)$  values are not expected to be aligned along pathways across the entire site because of the location of deposits of different depositional environments such as point bars, channels, and cutbanks. As result,

regional semivariograms should be considered as part of a detailed analysis at the CAFB site.

#### **9.4.2.5 The feasibility of detrending $\log(K)$ data at CAFB**

Analysis of the 1-Ha  $\log(K)$  data set illustrates that trends are difficult to detect in semivariograms. The best method for detecting the presence of a trend is large-scale pumping or tracer tests. Justification of a polynomial selection to detrend the  $\log(K)$  by visual inspection is highly subjective and involves considerable uncertainty. At the 1-Ha test site, F-tests justify the use of sixth order polynomials with more than 80 terms. From a conceptual viewpoint, one should question detrending with a sixth order polynomial that includes many terms with no physical relevance. Given the task of detrending with polynomials, there is sufficient justification to use high-order polynomials. Hence, the methodology for detrending and the rationale for detrending requires scrutiny.

At least two problems exist with detrending using polynomial expressions and the OLS fitting criteria. First, the method cannot equally or independently remove multiple  $\log(K)$  trends of different magnitudes with the same efficiency. Second, the form of polynomials is not analogous to the sedimentological features at CAFB. A fundamental difference between the polynomial functions and sedimentological features is that the former are continuous throughout the field, whereas the latter are limited in their areal extent. It is doubtful that polynomials can remove a trend from one  $\log(K)$  region without introducing a trend or noise into another  $\log(K)$  region.

The mapping of several former river channels at CAFB was performed without using any detailed sedimentological data. Proper sampling and analysis of the fluvial deposits

should help to define the architectural elements and the internal structures of the sedimentological features. With this type of information, it may seem appealing to partition according to sedimentological facies and then detrend. However, it is unlikely that additional data would be sufficient to construct a deterministic sedimentological model on which to base detrending. Moreover, the elusive criteria required to evaluate detrending remain.

## 9.5 SUMMARY

At Columbus AFB, Mississippi, a fundamental connection among sedimentological features,  $\log(K)$  data, large-scale tracer test results, large-scale pumping tests, and ambient groundwater flow patterns exists. This connection is most evident between high  $K$  values and the deposits associated with a paleochannel shown in an aerial photograph. The data clearly shows that the paleochannel is not a surficial feature as suggested as Rehfeldt et al. (1992). The heterogeneous conditions at CAFB require a stochastic approach. It is clear that the trends in the  $\log(K)$  are the major causes for the highly skewed tracer plumes and the non-classical pumping-test results.

Advocates of stationary stochastic theories suggest that these theories are applicable to nonstationary fields after deterministic features (e.g. trends, inhomogeneities) have been removed. Yet, at Columbus and at other fluvial aquifers, the primary reason for a stochastic model is the uncertainty with defining the deterministic features. For many fluvial aquifers where  $\log(K)$  trends are likely to exist (Neton et al. in press; Young et al., 1993b,c), an essential ingredient for the use of stochastic models is missing; namely, a method to remove

deterministic trends. The chapter shows that the assumptions and procedures required to separate the Columbus  $\log(K)$  data into a deterministic and stochastic component are highly subjective and uncertain.

If stochastic models are to be used at CAFB, it seems logical that they should be aimed at quantifying the effect of the uncertainty in the  $\log(K)$  trend and not the effect of the uncertainty in the  $\log(K)$  residuals. Because  $\log(K)$  trends cannot be defined accurately and they have a first-order effect on contaminant transport at CAFB, application of nonstationary models, which permit multiple realization of possible trends, would appear more useful and applicable than stationary models, which are based on an invariant and assumed known trend. As a result, at CAFB, considerable attention should be given to nonstationary models that can include geological information such as architectural models (Haldorsen and Damsleth, 1990; Haldorsen and MacDonald, 1988) and sequential indicator simulations (SIS) techniques (Journel and Alabert, 1990; Gomez-Hernandez and Srivastava, 1990). By performing multiple condition simulations with nonstationary models, an assessment can be made of how the uncertainty in the deterministic features of the aquifer affects the aspect of the groundwater flow of interest.

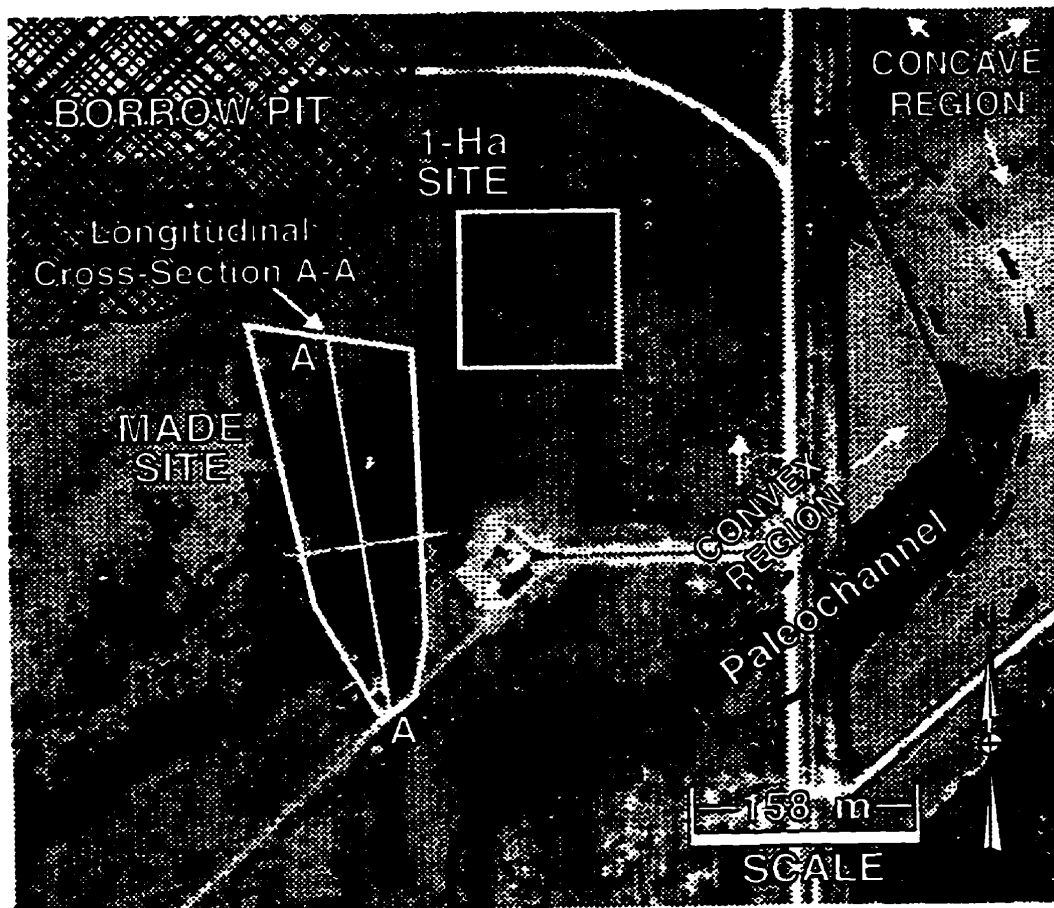


Figure 9.1 Location of two test sites at CFB, MS superimposed on a 1956 aerial photograph that reveals a paleochannel.

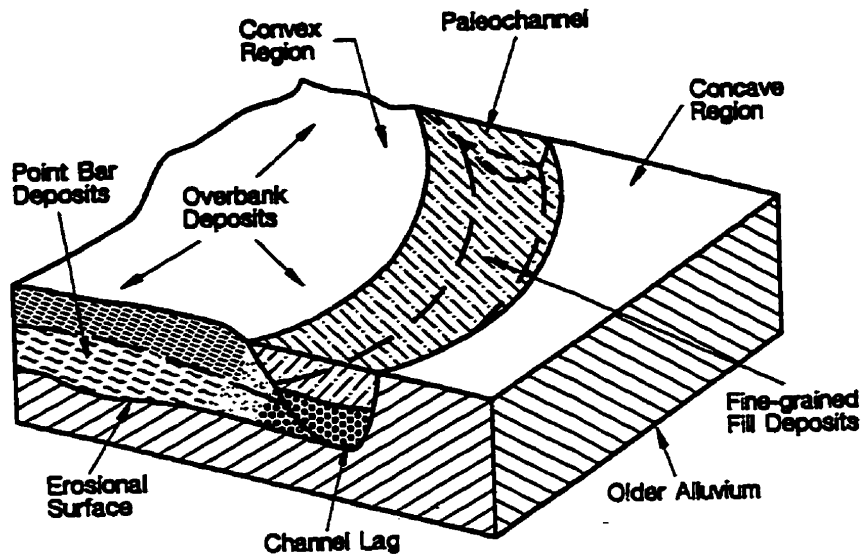


Figure 9.2 Schematic of the regional features associated with the sedimentological model.

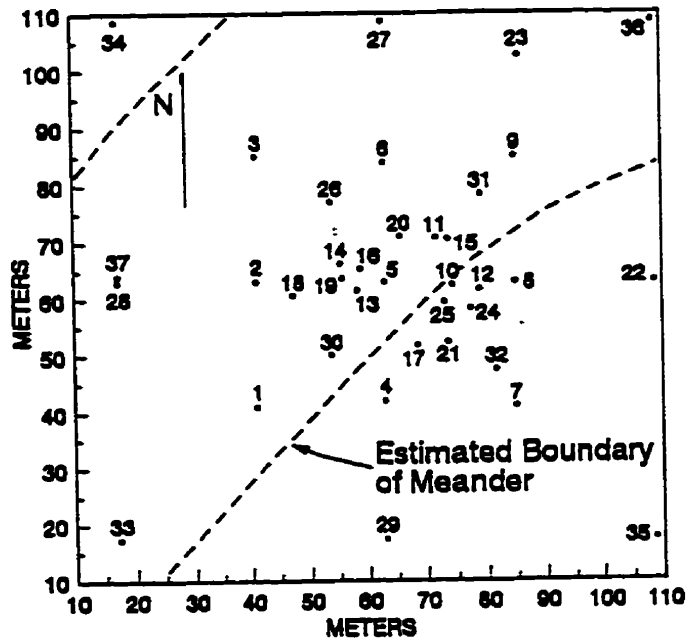


Figure 9.3 Well network for 1-Ha test site with location of the paleochannel estimated by dotted line.

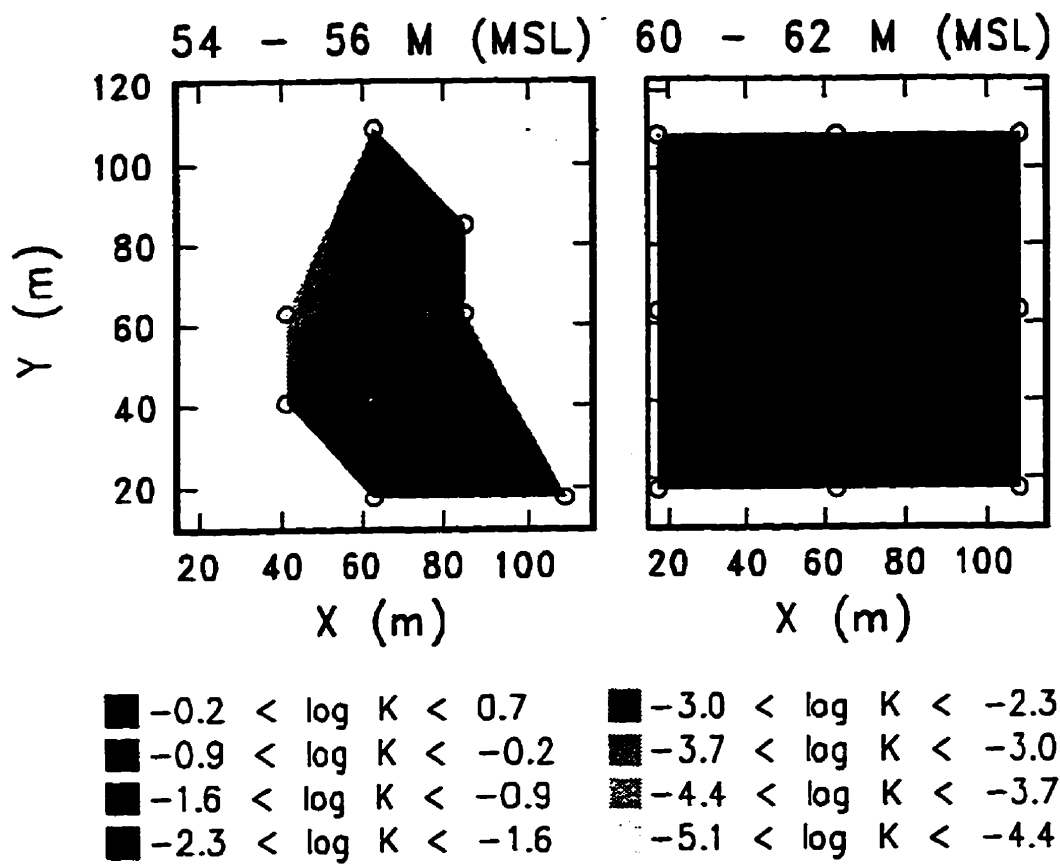


Figure 9.4. Depth-averaged  $\log(K)$  cross sections for the upper and lower 2 meter interval of the saturated aquifer at the 1-Ha test site based on borehole flowmeter tests.

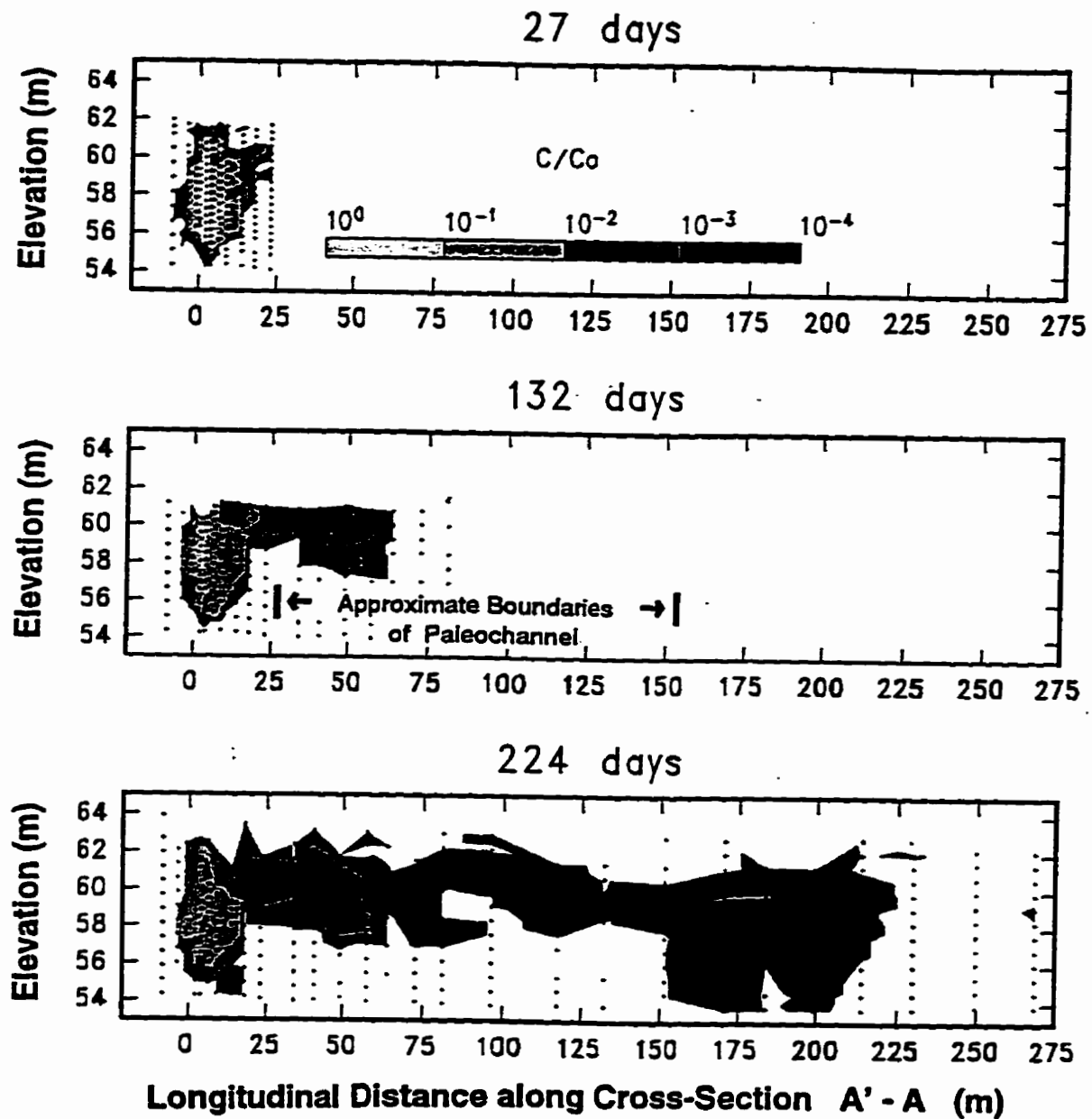


Figure 9.5 Vertical cross-sections of a tritium plume at the MADE site for 27, 132 and 224 days after injection (modified from Boggs et al., 1992).



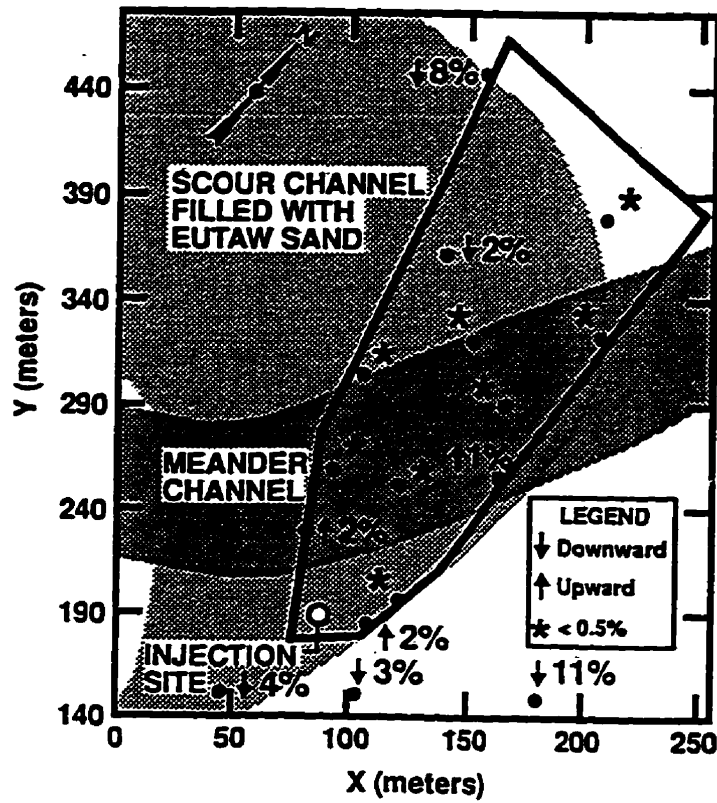


Figure 9.6. Averaged vertical hydraulic gradients for paired piezometers plotted in reference to the paleochannel in Figure 1 and a scour channel filled with marine sands from the Eutaw Formation.

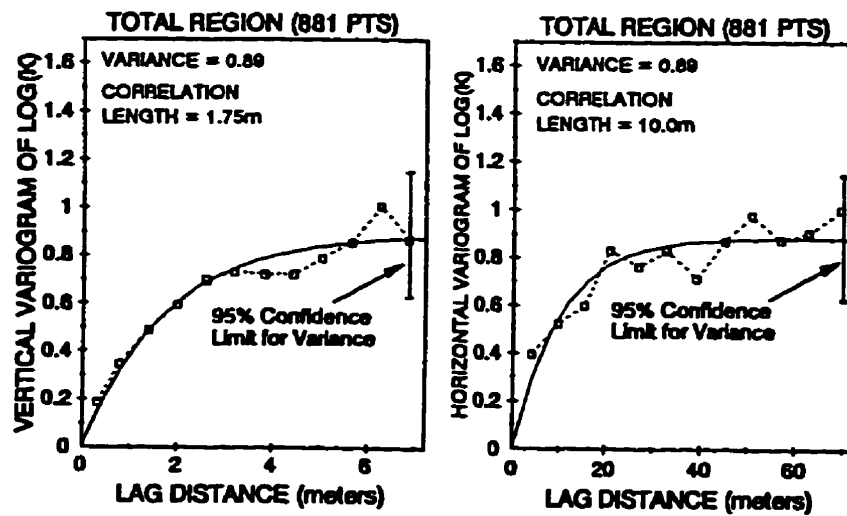


Figure 9.7 Experimental vertical and horizontal global semivariogram for Log(K) data fitted to an exponential semivariogram model.

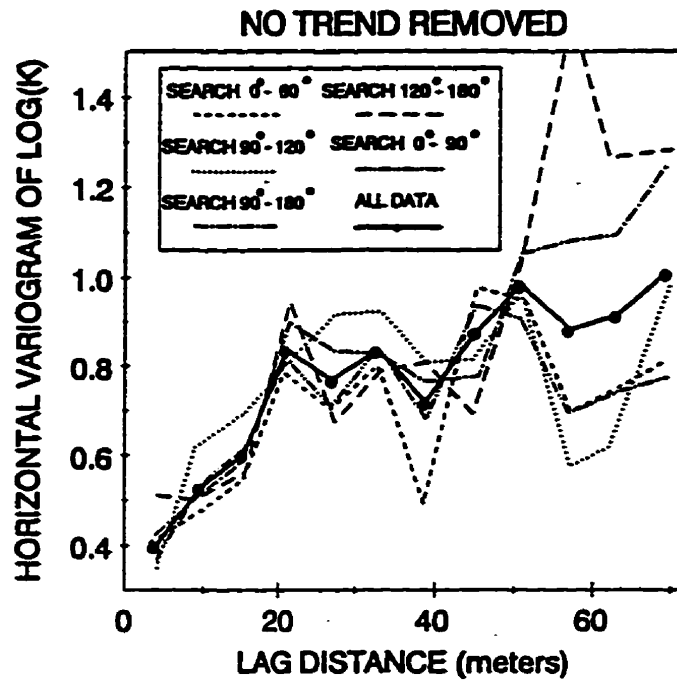


Figure 9.8 Experimental directional semivariograms for log(K) data. Search angle is along a horizontal plane and measured clockwise from north.

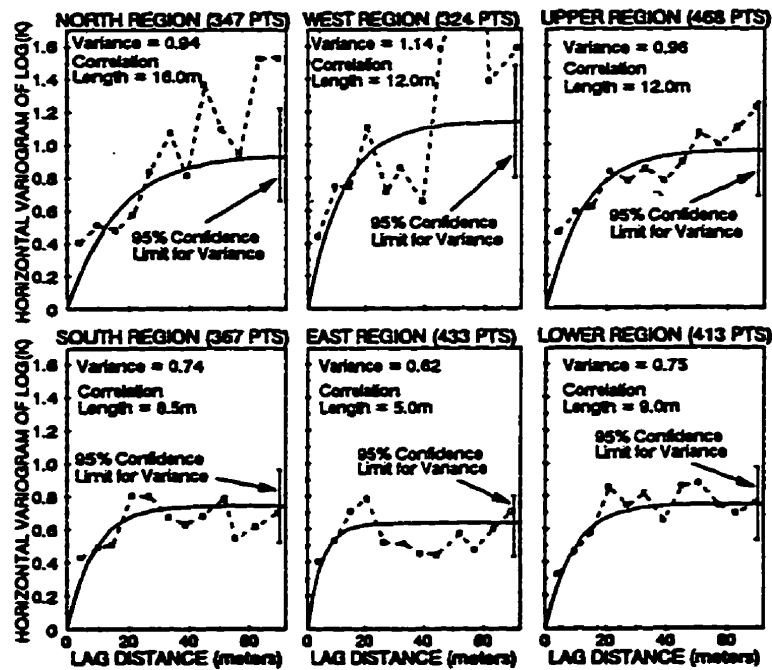


Figure 9.9 Experimental regional semivariogram for log(K) data.

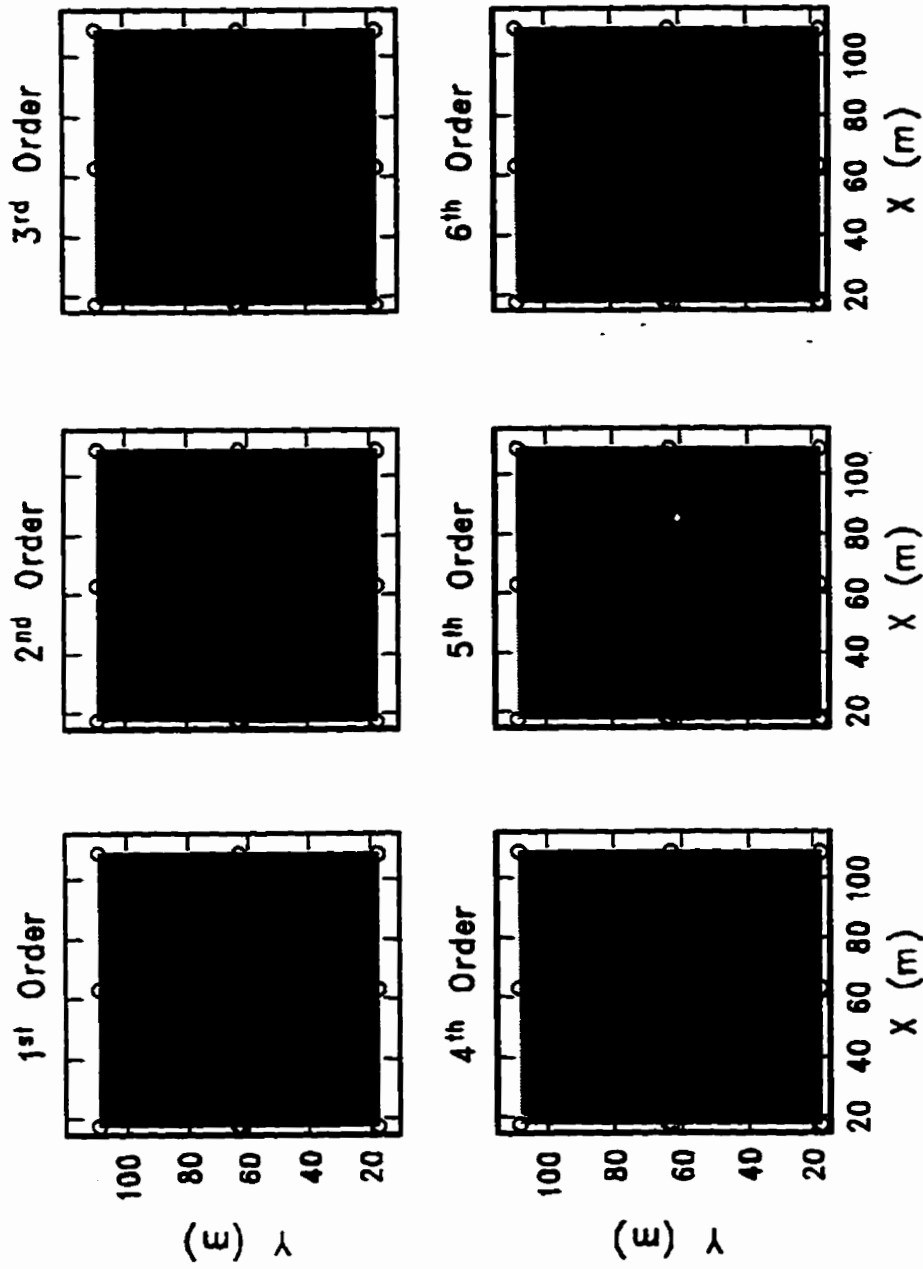


Figure 9.10 Depth-averaged cross sections for 60-62 m MSL based for log(K) values at flowmeter locations generated by the polynomials used for detrending. Circles denote well locations.

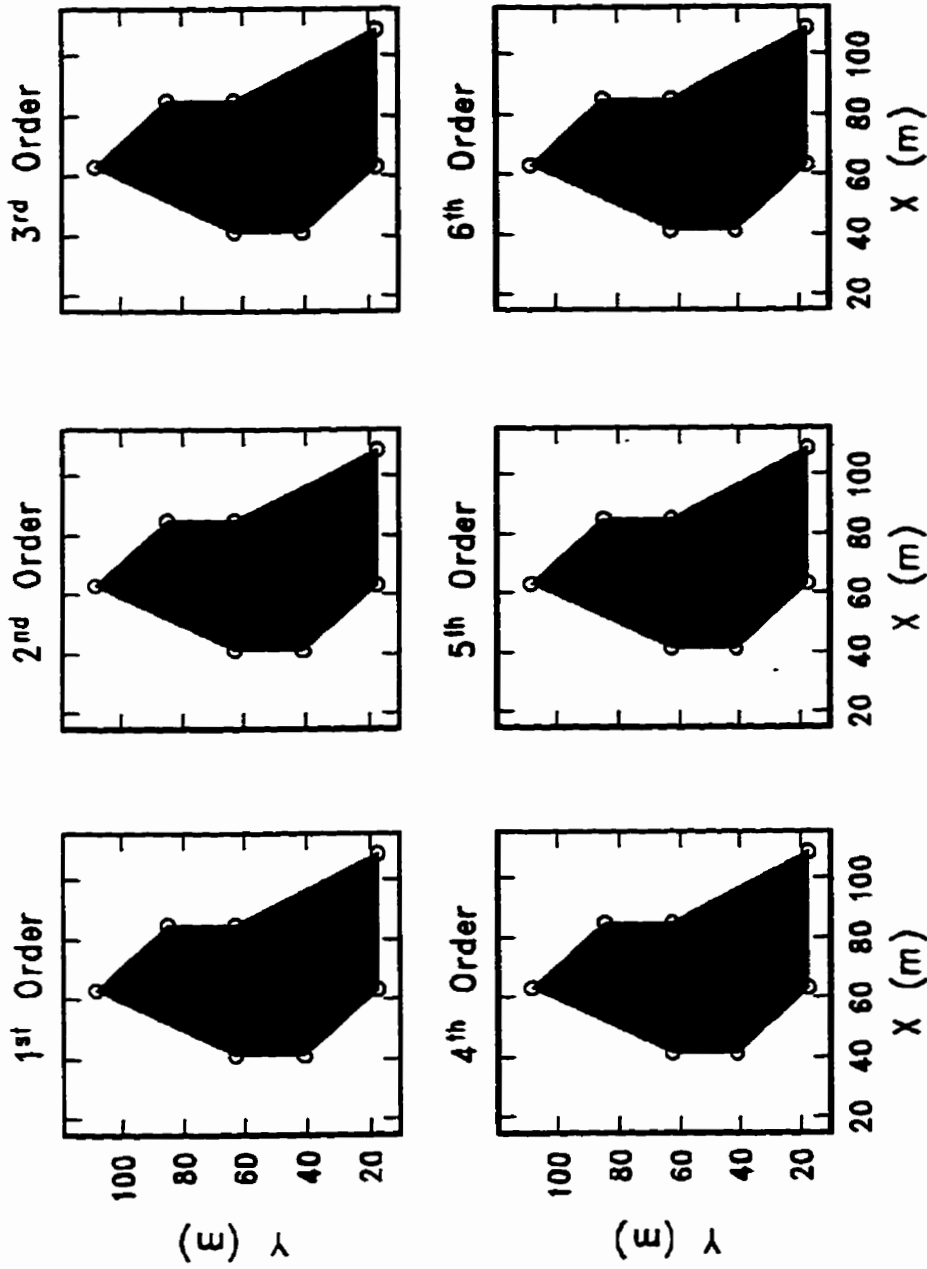


Figure 9.11 Depth-averaged cross sections for 54-56 m MSL based for  $\log(K)$  values at flowmeter locations generated by the polynomials used for detrending. Circles denote well locations.

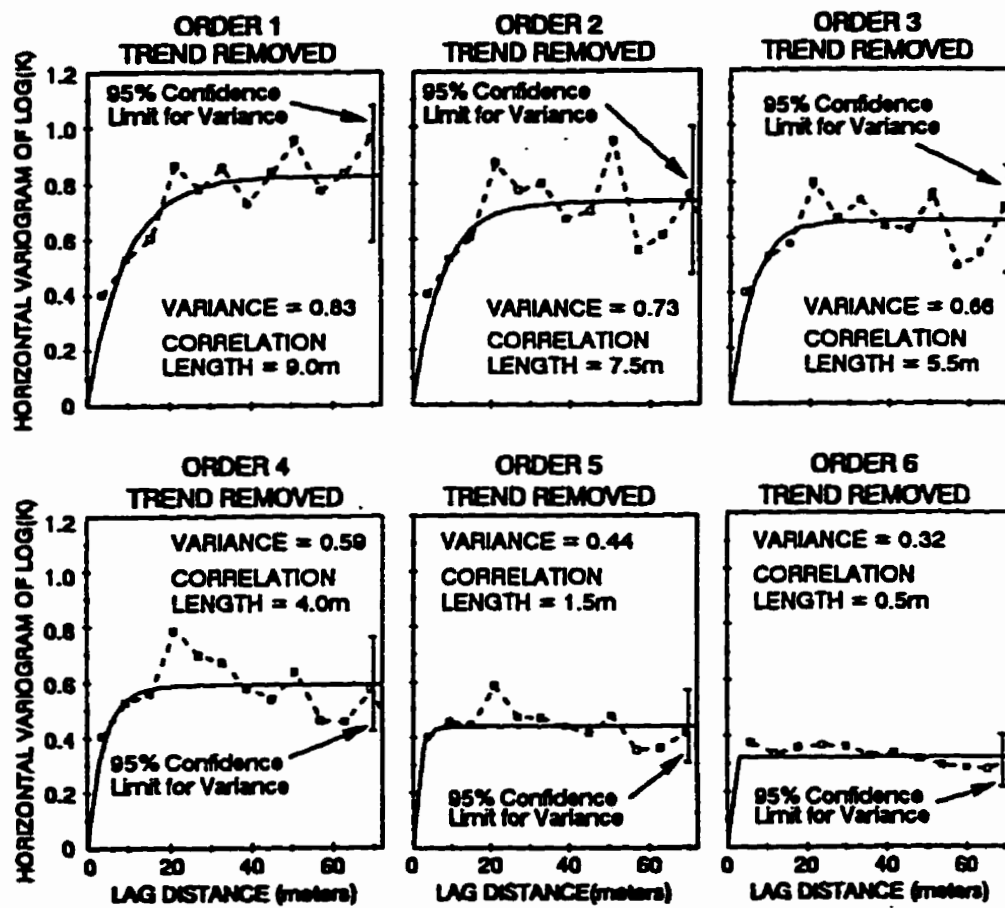


Figure 9.12 Experimental global variograms for the  $\log(K)$  residuals.

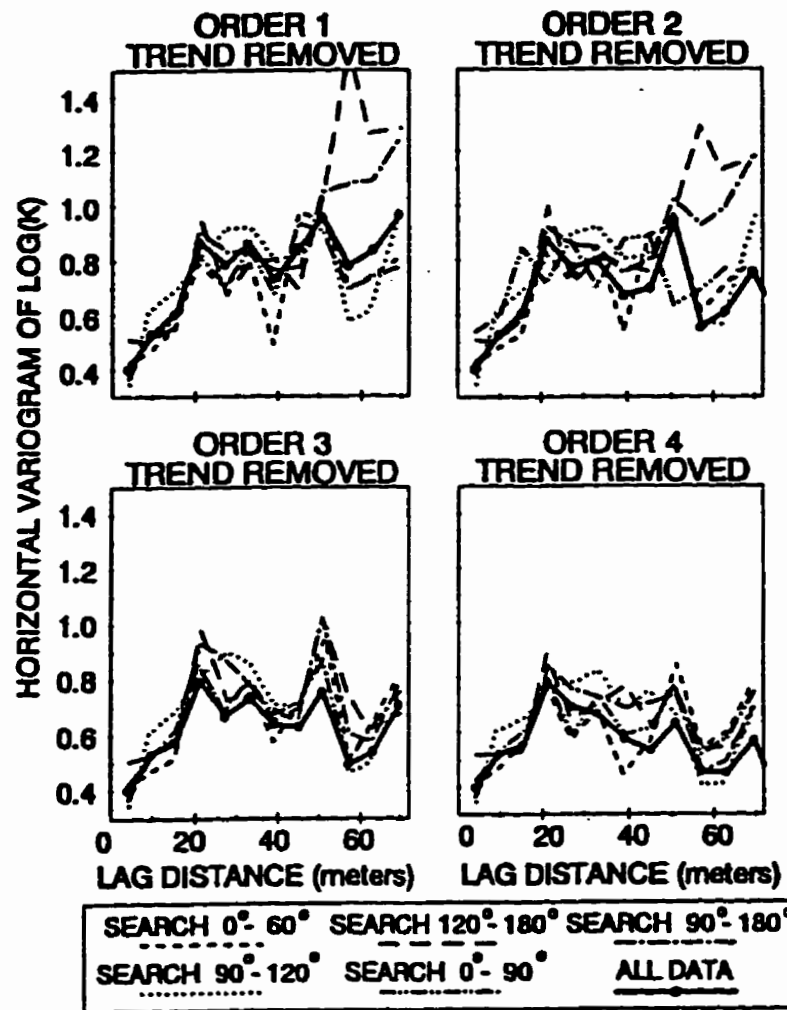


Figure 9.13 Experimental directional variograms for the log(K) residuals.

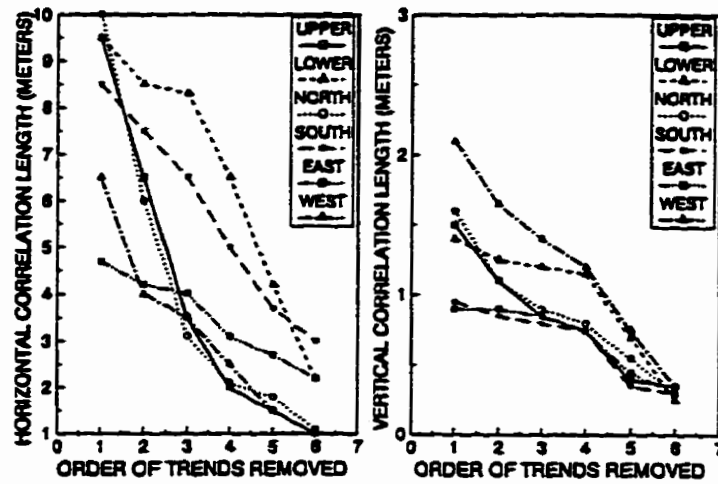


Figure 9.14 Vertical and Horizontal correlation lengths determined by fitting an exponential semivariogram model to the  $\log(K)$  residuals.

## **10. CONTRIBUTION TO SCIENCE**

### **10.1 OVERVIEW**

No matter the technology used to remediate groundwater, a key ingredient for success is characterization of aquifer heterogeneity. In the United States, inadequate delineation of aquifer heterogeneity has significantly contributed to the improper design, and consequently, the inadequate performance of many groundwater remediation systems (Haley et al., 1991). At many, if not most, groundwater remediation sites, pumping tests are an integral part of the site characterization program. At many test sites, a contributing cause for inadequate aquifer characterization is that insufficient and/or improper pump testing and analyses have been performed.

The primary contribution of this dissertation to the groundwater community is a set of ideas, tools, methodologies, and data that geohydrologists can use to help guide the characterization of heterogeneous aquifers. For discussion purposes, contributions will be discussed with regard to the following four topics: 1) Characterization of the CAFB Aquifer; 2) Borehole Flowmeter Tests, 3) Positive Skin Effects, and , 4) Single-well and Multi-well Tests in Unconfined Aquifers.

### **10.2 CHARACTERIZATION OF THE CAFB AQUIFER**

The CAFB aquifer is important to the groundwater community for two reasons. First, approximately \$10 million has been spent at CAFB on groundwater research focused on macrodispersion and biodegradation during the last 14 years. Second, the CAFB aquifer is one of the few highly heterogeneous unconsolidated aquifers whose K field as been



thoroughly studied. For these two reasons, site specific results from CAFB directly impacts the groundwater community perception of geohydrological processes.

During the first six years of the work at the MADE site, geological investigations performed by Rehfeldt et al., (1989) had not identified the paleochannel shown in Figure 1.1 and had concluded the CAFB aquifer was composed primarily of braided river deposits. As part of this dissertation, references and collected field data demonstrate the CAFB aquifer is composed principally of coarse-grained meandering river deposits. Among the most revealing information is a 1956 aerial photograph that shows a 70-m wide paleochannel crossing through the 1-Ha and the MADE test sites.

Examination of the borehole flowmeter K values from the 1-Ha test site indicate that the bedload deposits associated with the paleochannel represent a zone of interconnected high-K deposits. Contour maps of these K values in the upper aquifer provide a strong correlation between high-K values and the paleochannel's location. The correlation between high-K values and the paleochannel, however, is not well defined using the published borehole flowmeter K values from the MADE site (Rehfeldt et al., 1992; Boggs, 1991; 1993). The lack of correlation at the MADE site should be questioned because patterns in both the hydraulic head field and the tritium tracer concentrations are consistent with the paleochannel containing high-K material. As demonstrated in this dissertation, the strong correlation between the paleochannel and high K values did not exist at the MADE site because positive skin effects were ignored in the collection and analysis of borehole flowmeter data. To help illustrate and quantify the error associated with positive skin effects, borehole flowmeter tests were performed at the MADE site in wells backfilled with different

materials. Results of these tests, shows that the MADE flowmeter K values (Rehfeldt et. al., 1992; Boggs , 1991; 1993) significantly underestimate the K values in the paleochannel.

With the discovery of significant biases in the K data sets and the paleochannel at the MADE site, key relations and modeling approaches advocated by earlier MADE papers (Boggs et al., 1992; Adams and Gelhar, 1992; Rehfeldt et al., 1992) should be revisited. A specific issue addressed by this dissertation is the utility and appropriateness of stochastic macrodispersion theory. A problem with applying this theory to CAFB is the presumption of a second-order stationary K field. Patterns in the K, hydraulic head, and tracer concentration data indicate that the K field contains significant trends. Thus, in order to apply macrodispersion theory as attempted by Rehfeldt et al., (1992), the K field needs to be separated into a deterministic and stochastic component. Extensive analysis of CAFB field data in the dissertation demonstrates that this separation was not performed properly by Rehfeldt et al., (1992) and is likely not possible. Close examination of the data sets reveals that temporal variations in the hydraulic head field have a much greater potential for producing dispersion than does the estimated macrodispersivities at the CAFB site. Hence, from the viewpoints of both feasibility and utility, macrodispersion theory has little practical value for characterizing hydrodynamic dispersion at the CAFB site.

### **10.3 BOREHOLE FLOWMETER TESTS**

Borehole flowmeter tests have the potential for being effective for characterizing K spatial variability. This dissertation has helped improved these tests with respect to data collection and data analysis. A key component of flowmeter testing is the flowmeter tool.

Appendix C documents the development and demonstration of the electromagnetic flowmeter, which provides significant advantages over conventional impeller and heat-pulse flowmeters.

Numerous referred articles proposed and practiced an analysis of borehole flowmeter tests that ignored positive skin effects. As demonstrated in this dissertation, positive skin effects can be significant in highly heterogeneous aquifers. A contribution of the dissertation is to demonstrate that skin effects can be minimized by using gravel-packs during well installation and by using the Cooper-Jacob straight-line method during data analyses.

Using the borehole flowmeter K field at the 1-Ha test site, the dissertation illustrated fundamental relations among sedimentological features, K values and patterns, and preferential flow paths inferred from tracer tests. These results provide a foundation on which flowmeter investigations can be effectively incorporated into studies focusing on delineating K fields. In addition, the field work associated with large-scale pumping tests and the small-scale tracer tests at the 1-Ha test site provide a basis for using borehole flowmeters to investigate short-circuiting in observation wells during pumping tests and to delineate concentration profiles during recirculating tracer tests.

#### **10.4 POSITIVE SKIN EFFECTS**

Although positive skin effects can adversely impact conventional aquifer testing and sampling methods, most field studies assume that positive skin effects are negligible after conventional well development procedures. Among the reasons for this practice is that there are no guidelines in the groundwater literature or requirements in regulatory field practices

for evaluating positive skin effects. This dissertation shows that significant positive skin effects still exist at CAFB after extensive well development. An implication of this discovery is that unknown, and potentially significant, biases exist with some of the tracer sampling and hydraulic testing in the paleochannel at the MADE site.

Several approaches are demonstrated in the dissertation for identifying and assessing the impacts of positive skin effects. Documented positive effects in the paleochannel include biasing borehole flowmeter K values by factors up to 1000 and transmissivity values by factors up to 10. The most reliable and thorough method for identifying skin effects includes comparing results from borehole flowmeter tests in wells of different well construction. A simple, but less reliable method, involves comparing the hydraulic response of pumping and slug tests.

#### **10.5 SINGLE-WELL AND MULTI-WELL TESTS IN UNCONFINED AQUIFERS**

A standard component to site characterization programs are single-well and multi-well pumping tests. Results from these pumping tests are usually the basis for quantifying aquifer structure and hydraulic properties. A concern with pump tests in heterogeneous aquifers is that conventional analyses methods are premised on paradigms associated with homogenous aquifers. At heterogeneous site, conventional pump-test analyses involving type-curve matching should be enhanced to include a simple sedimentological model and complementary numerical simulations. The purpose of the sedimentological model is to help delineate plausible areal and vertical aquifer heterogeneities. The purpose of numerical

simulations is to investigate and/or confirm the potential impact of aquifer heterogeneity on aquifer drawdown response.

As demonstrated in the dissertation, areal heterogeneity in the CAFB transmissivity field greatly impacts drawdown responses. With respect to numerous large-scale pumping tests, changes in the location of the pumping well with respect to the paleochannel affect the shape of the drawdown curves. An important aspect with interpreting the large-scale pumping tests is the relations among the radius-of-influence, the sequence of the transmissivity changes radially outward from the pumping well, and the semilog slope of the time-drawdown responses.

Depending on the location of the pumping well, drawdown curves at CAFB vary considerably and can potentially resemble those associated with leaky aquifers, confined aquifers, or unconfined aquifers. At CAFB spatial variations in aquifer transmissivity field largely controls the shape of the time-drawdown response curve. Prudent use of the Cooper-Jacob straight line method was demonstrated to provide reasonable transmissivity values for early and late-times for all pumping test data. Because of the unconfined conditions and a really extremely transmissivity field at CAFB, the expansion rate of the radius-of-influence is affected by the pumping rate. As a consequence, the transmissivity value calculated from the Cooper-Jacob straight-line method can be significantly affected by the pumping rate. Thus, in heterogeneous and unconfined aquifers, pumping tests should be designed and analyzed with consideration of the sensitivity of effective transmissivity to elapsed time and the pumping rate.

Besides areal heterogeneity, an important consideration at CAFB is vertical heterogeneity. Primarily because of vertical heterogeneity, large vertical hydraulic gradients exist at CAFB and significant vertical flow can occur between non-adjacent high-K deposits via an open well screen. Results of borehole flowmeter and recirculation tracer tests show that high-K pathways between the pumping and observation wells can lead to unrealistic storage coefficients being calculated from type-curve analyses. In fact, because of the extremely heterogeneous conditions at CAFB, there is little, if any evidence, that representative values of specific storage could be gleaned from early time drawdown data at CAFB. Numerical simulations show that the well screen vertical and horizontal location impacts greatly the calculated storage coefficient.

## **11. LESSONS LEARN AT CAFB AND THEIR APPLICATION TO INVESTIGATIONS OF SIMILAR FIELD SITES**

### **11.1 THE KEY TO CAFB**

When field work was initiated at CAFB in 1981, the adopted paradigm for the K field was a second-order stationary field, which is presumed by many stochastic theories developed in the late 1970's. Fueled by successful demonstration of stochastic macrodispersion theory in the early 1980's at Borden, Cape Cod, and Twin Lakes, early field work at CAFB was performed with little consideration to the possibility that within the highly heterogeneous CAFB K field there were definable patterns that could greatly impact groundwater flow and transport.

From 1981 to 1989, millions of dollars was spent at CAFB applying numerous conventional field tests. During this time, none of the professionals examining the field data suspected that a major geohydrological control at the site were high-K channel lag deposits associated with a paleochannel. With regard to unlocking the geohydrologic structure of the CAFB aquifer, the single most important piece of information is the aerial photograph of the paleochannel. Without this photograph there would have been no basis for investigating the validity of the borehole K measurements at the MADE site, the application of conventional well analysis techniques to large-scale pumping tests, the sensitivity of calculated CJSI transmissivity values to the pumping rate, the importance of connectivity among high-K deposits, and whether significant positive skin effects exist at wells within the paleochannel. With knowledge of high-K deposits in the paleochannel, most of the non-classical responses from both large-scale tracer and pumping tests results at CAFB can be explained.

An important lesson learned at CAFB is that at sites where paleochannels might exist, field work and data analyses should not be geared toward developing effective properties of a presumed homogeneous media but rather toward identifying and quantifying the scale, the arrangement, and connectivity of aquifer heterogeneities. In investigating fluvial deposits in support of aquifer remediation, the mindset should be more toward assuming that preferential flow paths are important until proven otherwise than toward assuming that preferential flow paths are not important until proven otherwise. Given practical limitations of resource and time, a site characterization program cannot be geared toward delineating all, or even most, of the preferential flow paths. However, with prudent use of geological investigations, borehole flowmeter tests, small-scale multi-well pumping tests, and small-scale tracer tests a reasonable goal for a site characterization program to evaluate the potential importance of preferential flow paths in a fluvial aquifer.

## **11.2 ASSESSMENT OF THE FIELD INVESTIGATIONS**

Based on the data from CAFB, the author recommends that a site characterization program for meandering river deposits be structured to assess the potential for preferential flow paths to significantly impact groundwater flow and transport. In order to perform such an assessment several different types of information are required. Listed in Table 11.1 are the types of information sets collected at CAFB to help evaluate possible aquifer constructs and preferential flows that impact groundwater flow and transport. The various information sets are grouped within the following four general aquifer properties: 1) Geologic Structure; 2) Transmissivity Field; 3) Hydraulic Conductivity Distribution; and, 4) Preferential Flow



Paths. The information sets listed for each aquifer property are limited to only those that can be directly used to characterize the aquifer property of interest. For instance, although geology and hydraulic conductivity values indirectly help to assess the potential for preferential flow paths, it is the interpolation of these data that directly helps to assess the potential for preferential flow paths.

Besides each information set is a ranking that reflects the value of the information set for characterizing the aquifer property. Listed below are short explanations for the rankings. An understanding of the different data sets and their ranking is a prerequisite for the development of general site characterization strategy for aquifers with deposits similar to those at CAFB.

### **11.2.1 Geologic Structure**

A key to understanding the geohydrology at CAFB is the location of the high-K deposits associated with the paleochannel channel lag deposits. Consequently, aerial photographs received a high ranking of 10. A review of existing geological reports regarding Columbus, Mississippi produced very useful information including aerial photographs of ox bows and paleochannels within a few miles of CAFB. Based on these photographs and detailed stratigraphy of large-scale continuous coring, two references stated the much Columbus, Mississippi, is composed of meandering river deposits. Although the background literature survey did not specifically discuss the test site, it merits a ranking of 7 because it identified the depositional environments responsible for the CAFB aquifer.

**Table 11.1 Relative Importance of Different Information Sets for Defining Aquifer Properties at CAFB**

AQUIFER PROPERTY	INFORMATION SET	RANKING
1. Geologic Structure	a. Aerial Photographs	10
	b. Background Literature Survey	7
	c. Continuous Aquifer Cores (Includes Grain-Size Analyses)	5.5
	d. Facies Mapping of Outcrops	5.5
	e. Split-spoon Samples at 5-foot centers (Includes Grain-Size Analyses)	3
2. Transmissivity Field	a. Single-Well Pumping Tests	9
	b. Small-Scale Multi-Well Pumping Tests (< 3 hours)	6
	c. Large-Scale Multi-Well Pumping Tests (> 12 hours)	4
	d. Slug Tests	2
3. Hydraulic Conductivity Distribution	a. Borehole Flowmeter Tests	9
	b. Straddle-Packer Tests*	5
	c. Permeameter Tests*	3
	d. Grain-size Correlation*	1
4. Preferential Flow Paths	a. Small-scale Recirculation Tracer Tests	8
	b. Small-scale Recirculation tests	6
	c. Small-scale Multi-well Pumping Tests	4

Note: \*Data was not presented in dissertation.

Ranking is on a linear scale from 1 to 10 with 10 being the most useful.

Examination of the eight continuous aquifer cores and the facies map did not provide evidence of large-scale (> 50 m) trends in aquifer properties. A limitation of both the limited continuous cores and the single facies map was that some of the geological processes of interest occurred at much greater dimensions than the scale of the field measurements. For either the facies map or the continuous cores to be useful indicators of large-scale K trends, a prohibitive amount of data would be required. The primary value of the facies map and continuous cores lies in revealing some of the possible vertical sequencing of fine-grained and coarse-grained deposits. Both information sets show that abrupt changes in grain-size frequently occur over vertical distances as small as a few centimeters and that thin layers of fine-grain materials are often interbedded with coarse-grain deposits. The facies map showed that coarse-grained "stringer" could extend for distances 10 to 50 times their thicknesses. Examination of the grain-size analysis of the continuous cores suggest much of the aquifer was formed from a high energy and chaotic depositional environment similar to a coarse-grained meandering river or braided river with frequent floods. Trends in the grain-size distributions supported the division of the aquifer into the following three zones: 1) above 62 m MSL—the clayey overburden; 2) between 54 to 58 m MSL—the lower aquifer; and 3) between 58 and 62 m MSL—the upper aquifer. Because they both provide sound evidence that preferential flow occurs at the scale of 1 to 10 meters, the continuous cores and the facies map were assigned a ranking of 5.5.

During the first several years of drilling at CAFB, aquifer samples were primarily collected with a 45-cm long, 3.8-cm ID, split-spoon at 1.5-m centers. After approximately 70 borehole locations had been split-spooned, several attempts were made to construct aquifer cross-sections from the data. Construction of reliable cross-sections proved to be impossible with such a sparse data set. With hindsight, a better data set would have been constructed with continuous samples from perhaps 20 locations. However, there is some question on whether these 20 locations should be sampled with a 3.8-cm ID split spoon. Compared to the cores collected via the 3-foot long, 3.0-inch diameter, continuous core barrels, the deposits in the split spoons appear highly disturbed and biased with an undersampling of the coarsest materials. Because the split-spoon samples provided marginal information about the aquifer structure, a ranking of 3 was assigned to the split-spoon data set.

### **11.2.1 Transmissivity Field**

Pumping tests and slug tests are commonly used to determine aquifer transmissivity. At heterogeneous aquifers such as CAFB, definition of the scale effect on calculated transmissivity values at each well location would help to evaluate the potential for preferential flow. Theoretically, slug tests should provide the best estimate of transmissivity at the local scale. However, at CAFB significant positive skin effects occur at some wells without gravel packs. As a result, if slug tests are used in wells without gravel packs, positive skin effects will cause the calculated transmissivity values at some wells to be too low. If gravel packs are used, then slug-test transmissivity values will be too high at some

wells because of the region of high-K gravel-pack material. Consequently, slug tests received the low ranking of 1.

At CAFB, the results of the pumping-tests showed that measurement scale had a significant effect on the calculated transmissivity values. Both field and theoretical data show that the representative scale for the transmissivity values increased at later time and at higher pumping rates. The best method for defining a map of local-scale transmissivity was from single-well pumping tests performed at a low pumping rate. Results from these tests at the 1-Ha test site produced transmissivity values that ranged from 500 to 1 cm<sup>2</sup>/s and a transmissivity pattern that agreed with high-K deposits lying in the paleochannel. Analysis of the large-scale pumping tests at the 1-Ha tests site produced transmissivities that ranged from 40 to 20 cm<sup>2</sup>/s and a transmissivity pattern that was relatively uniform. Based on the variability illustrated in their respective transmissivity patterns, the single-well pumping tests and large-scale pumping tests were given a ranking of 9 and 4, respectively. The transmissivity values from the multi-scale pumping tests produced transmissivity values reflective of both the single-well and large-scale. A ranking of 6 was assigned to the multi-well pumping tests to reflect a utility that ranks in between the other two tests.

### **11.2.2 Hydraulic Conductivity Distribution**

Although the dissertation presented only borehole flowmeter K values, K values were calculated with several other methods. These values meet with varying degrees of success, but none were as effective as the borehole flowmeter method. An important consideration at CAFB is that K values are needed at a resolution and at a scale that supports

extrapolation to a continuous three-dimensional  $K$  field for predictive assessments of groundwater transport. Of the four  $K$  information sets listed in Table 11.1, borehole flowmeter tests provided the most useful  $K$  data to support groundwater modeling. At CAFB, borehole flowmeter tests were performed and analyzed differently at the MADE site and the 1-Ha test site. Based on the methodology used at the 1-Ha test site, borehole flowmeter tests were assigned a ranking of 9.

In a highly heterogenous aquifers with very coarse-grained deposits, the validity of many, if not all, predictive equations for  $K$  based on grain-size is questionable. A review of these grain-size methods reveal that most are based on data from significantly less coarse and better sorted aquifer deposits. Based on a limited evaluation of the grain-size equations involving both field data and theoretical considerations, these equations are given a ranking of 2.

Detailed permeameter tests were performed on eighty-seven 25-cm long sections of the 8.3-cm ID continuous aquifer cores according to a method described by Wolfe et al., (1991) (Ogden, 1994) The author supervised the collection and testing of these samples and has not reported the values because of concerns with the test results. One problem was the representativeness of the samples. Because of the relatively small sample diameter and coarseness of the aquifer deposits, most of the samples were highly disturbed. A not infrequent occurrence were gravels larger than 5 cm partially blocking the relatively small cross-sectional area of the sample. In one sample, over 90% of the cross-sectional area was blocked by a single stone. During many of the tests, significant channeling of water through the permeameter was evident but likely could have been eliminated if a pressurized

flexible sleeve was used to contain the sample. Because of poor sampling and instrumentation setup, the permeameter K values were not considered reliable and therefore were assigned a ranking of 3. If reliable K values could have been measurement, an useful comparison would have been among grain-size distributions, permeameter K values, and borehole flowmeter K values.

Straddle packer tests were performed at a few wells and their results were compared to results from the borehole flowmeter data (Boggs et al., 1990). The K values estimated from the packer tests were consistently higher than those obtained from the flowmeter measurements, and they showed less variation. This difference was attributed to artificial vertical movement of the injected water within the disturbed well annulus during the packer tests. Because the straddle packer tests is are less tolerant of positive skin effects and aquifer heterogeneity than borehole flowmeter tests, straddle tests were assigned a ranking of 5.

### **11.2.3 Preferential Flow Paths**

In a heterogeneous aquifer, the interpolation method for constructing a three-dimensional K field can be as important as the K values themselves. Without information regarding specific preferential flow paths as measured from tracer tests or patterns inferred from hydraulic testing, there is no data for rigorously evaluating the appropriateness of alternative K fields. Large-scale tracer tests are too expensive and time-consuming to consider as a part of a site characterization program. Though they can be relatively expensive, small-scale recirculating tests can be quickly completed. Because the the tracer breakthrough curves and flow distributions provide a relatively simple and direct method for

evaluating the connectivity among the aquifer high-K deposits at scales of 5 to 20 m, these tests were assigned a ranking of 8.

The primary cost factors associated with the small-scale tracer tests is the equipment and labor associated with the collection and analysis of the tracer data. Considerable cost can be omitted with a relatively small reduction in valuable data by eliminating all tracer work and focusing on borehole flowmeter measurements at the pumping and extraction wells.

Tests in which a steady flow field is established by a array of pumping and injection wells and quantified by borehole flowmeter tests at each well is designated as a "small-scale flow recirculation test." Because this type of flow data can be easily used to help evaluate alternative K fields, small-scale recirculation tests were assigned a ranking of 6.

Small-scale multi-well pumping tests involve pumping a well and analyzing the transient response at observation wells to calculate aquifer hydraulic parameters. If numerous tests are performed, the range in calculated storage coefficients can be used as a measure of the variability in the aquifer's flow paths. Although these results cannot be used to delineate particular high-K zones, they do provide useful qualitative data concerning aquifer variability. An aquifer with a large range for the calculated storage coefficients would have a much greater potential for preferential flow than an aquifer with a small range for the calculated storage coefficients. When combined with borehole flowmeter K values, information from these tests should help with selecting the most likely zones of high-K interconnectivity between selected well pairs. Because small-scale multi-well tests provide more qualitative than quantitative information, the tests were assigned a ranking of 4.



### **11.3 BOREHOLE FLOWMETER TESTS**

Borehole flowmeter tests represent a promising method for characterizing the K fields of heterogeneous aquifers. Like many types of field tests, borehole flowmeter tests are not failsafe and established guidelines are needed for properly collecting and analyzing the data. Table 11.2 lists the major tasks associated with flowmeter tests. Based on the field test program at CAFB, several lessons have been learned on how to implement each task.

Of the four drilling methods used at CAFB, hollow-stem augering produced the greatest aquifer disturbance. If gravel-packs are not to be used, then flowmeter wells should not be installed with hollow-stem augers because of concerns with positive skins. Two advantages of using augering methods are that they are cheaper than drilling with methods involving protective casings and they permit effective sampling of aquifer deposits. In order to maximize the number of well installations and the number of aquifer samples, auger well installations are recommended with the constraint that a gravel-pack is used.

Although not reported in the dissertation, extensive well development studies were performed at CAFB. These studies conclusively show that well development is essential to collecting representative flowmeter data. A reliable well development protocol at CAFB involved a sequence of pumping, mechanical surging, and back flushing that took approximately 3-hours to complete. At similar sites to CAFB, this protocol may be appropriate after being evaluated. Data for the evaluation could be collected by developing and flowmetering a well and then repeating the sequence. If the two borehole flowmeter profiles are very similar then the protocol can be adopted without any changes. If notable

difference exist between the two profiles, then additional field investigations are need to develop an appropriate well development protocol for that site.

Considerable field data is collected during a borehole flowmeter tests. Accurate and reliable field equipment is required. Automatic data logging is a required to ensure unbiased and accurate recording of all field data. Transducers and flowmeters should be of highest quality and subject to both pre- and post-testing calibrations. The flowmeter tool of choice is the electromagnetic(EM) flowmeter. Several field tests at CAFB have demonstrated that the EM flowmeter has significantly better performance characteristics with respect to measurement range and durability than does high-performance impeller meters.

The pumping rate for flowmeter tests should be as low as possible without adversely impacting the capability of the field equipment to accurately measure the drawdown versus time response and the cumulative flow versus depth profile. Low pumping rates help to minimize well head losses and the vertical groundwater flow near a well. In addition, if pumping rates affect the expansion rate for the radius-of-influence, a low pumping rate helps keep the calculated transmissivity value reflective of the local scale. Flowmeter measurements should not begin until the drawdown level starts to stabilize in the well. At a minimum, flowmeter measurements should be taken at intervals equal to one-tenth of the aquifer thickness. After an initial flowmeter measurements have been made, several should be checked and then additional measurements make where large changes in flow occur.

The recommended data analysis method is based involves a modified procedure developed by Molz et al., (1989) that is discussed in Chapter 4. This method requires a profile of borehole flowmeter measurements versus depth and a transmissivity value. For

aquifers composed of very permeable deposits such as those at CAFB, the best approach for calculating transmissivity is applying the CJSI method to drawdown data from a pumping test.

**Table 11.2 Major Tasks associated with Implementing the Borehole Flowmeter Tests**

<b>Task</b>	<b>Factors Affecting Result</b>
1. Well Installation	a. Drilling Method b. Backfill Material
2. Well Development	a. Conventional Techniques b. Hydraulic Jetting
3. Data Collection	a. Flowmeter b. Transducer c. Data Logger
4. Field Testing	a. Pumping Rate b. Measurement Frequency
5. Data Analysis	a. Method b. Transmissivity Calculation

## 12. REFERENCES

- Adams, E.E., and L.W. Gelhar, 1992. Field Study of Dispersion in a Heterogeneous Aquifer 2. Spatial Moments Analysis, Water Resources Research, v 28(12), pg 3293-3307.
- Akindunni, F.F., 1987. Effect of the Capillary Fringe on Unconfined Aquifer Response to Pump Numerical Simulations, M.S. Thesis, University of Waterloo, Waterloo, Ontario, Canada.
- Akindunni, F.F. and R.W. Gillham, 1992. Unsaturated Flow in Response to Pump of an Unconfined Aquifer: Numerical Investigation of Delayed Drainage, Ground Water, 30(6), pp. 873-884.
- Allen, J.R.L., 1965. A Review of the Origin and Characteristics of Recent Alluvial Sediments. Sedimentology. 5, pp 89-191.
- Arche, A., 1983. Coarse-grained meander lobe deposits in the Jarama River, Madrid, Spain. In: Modern and Ancient Fluvial Systems. Edited by J.D. Collinson and J. Lewin. International Association of Sedimentologists Special Publication 6, pp 313-321.

Betson, R. P., J. M. Boggs, S. C. Young, and L. W. Gelhar, 1985. Macrodispersion Experiment (MADE): Design of a field experiment to investigate transport processes in a saturated groundwater zone, Technical Report EA-4082, Electric Power Research Institute, Palo Alto, California.

Bluck, 1971. Sedimentation in the Meandering River Endrick. Scottish Journal of Geology, 7, pp 93-138.

Boggs, J.M., S.C. Young, D.J. Benton, and Y.C. Chung, 1990. Hydrogeologic Characterization of the MADE Site, Electric Power Research Institute Interim Report EN-6915, Palo Alto, California.

Boggs, J. M., 1991. Database for the First Macrodispersion Experiment (MADE-1). EPRI Final Report EN-7363, Electric Power Research Institute, Palo Alto, CA.

Boggs, J.M., S.C. Young, L.M. Beard, L.W. Gelhar, K.R. Rehfeldt, and E.E. Adams, 1992. Field Study of Dispersion in a Heterogeneous Aquifer, 1. Overview and Site Description, Water Resources Research, v.28, no 12, pp 3281-3291.

Boggs, J. M., 1993. Database for the First Macrodispersion Experiment (MADE-1). EPRI Project Report TR-102072, Electric Power Research Institute, Palo Alto, CA.

- Boggs, J.M., L.M. Beard, W.R. Waldrop, T.B. Stauffer, W.G. MacIntyre, and C.P. Antorith, 1993. Transport of Tritium and Four Organic Compounds During a Natural-Gradient Experiment (MADE-2), Electric Power Research Institute Final Report 2485-05, Palo Alto, California.
- Bull, W.B., 1964. Geomorphology of segmented alluvial fans in western Fresno County, California. U.S. Geological Survey Professional Paper 352-E, pp 89-129.
- Butler, J.J. Jr., 1988. "Pumping in Nonuniform Aquifers -- the Radially Symmetric Case." Journal of Hydrology, Vol. 101, pp 15-30.
- Butler, J.J. Jr., 1990. The Role of Pump Tests in Site Characterization: Some Theoretical Considerations, Ground Water, 28(3):394-402.
- Butler, J.J., Jr., and W. Liu, 1991. Pump Tests in Non-Uniform Aquifers - The Linear Strip Case, Journal of Hydrology, Vol. 128, pp. 69-99.
- Campbell, C.V., 1976. Reservoir geometry of a fluvial sheet sandstone. American Association of Petroleum Geologists Bulletin. 60, 1009-1021.
- Cardwell, W.T. and R.L. Parsons, 1945. Average Permeabilities of Heterogeneous Oil Sands. Trans. Am. Inst. Min. Metall. Pet. Eng., v. 160, pg 34-42.

Chirlin, G.R., 1989. Critique of the Hvorslev Method for Slug Test Analysis: the Fully Penetrating Well. Ground Water Monitoring Review, 9(2), pg 130-138.

Collinson, J.D., 1986. Alluvial sediments. In: *Sedimentary Environments and Facies*. Edited by H.G. Reading. Blackwell Scientific Publications, Oxford, 20-62.

Cooper, H.H. and C.E. Jacob, 1946. A Generalized Graphical Model for Evaluating Formation Constants and Summarizing Well-Field History. *Transaction of the American Geophysical Union*, Vol. 2, pp. 526-534.

Cooper, H.H., J.D. Bredehoeft, and I.S. Papadopoulos, 1967. Response of a Finite-diameter Well to an Instantaneous Charge of Water. Water Resources Research, 3(1), pp. 263-269.

Davis, J. M., S. J. Colarullo, R. C. Lohmann, and F. M. Phillips, 1991. Alluvial aquifer heterogeneities in the Rio Grande Valley: Implications for ground water contamination, Technical Report No. 256, New Mexico Water Resources Research Institute, Las Cruces, New Mexico, pp 111.

Davis, S.N. and R.J.M. DeWeist, 1966. *Hydrogeology*, John Wiley & Sons, Inc., New York, pp 463.

Deng, X., and R.N. Horne, 1993. Well Analysis of Heterogeneous Reservoirs. SPE Paper 26458.

Desbarats, A. J., and R. M. Srivastava, 1991. Geostatistical characterization of groundwater flow parameters in a simulated aquifer, Water Resources Research, 27(5), pp. 687-698.

Dreier, R.B., J. Switek, and B.A. Couzens, 1992. Construction and Installation Summary for Fiscal Year 1992 of the Hydraulic Head Monitoring Stations at Oak Ridge National Laboratory, Oak Ridge, Tennessee, Report ORNL, ER-125, Oak Ridge National Laboratory, Oak Ridge, TN.

Dreier, R.B. and A.J. Caldanaro, 1994. Installation Summary for the DNAPL Characterization Multiport Wells, GW-726, GW-727, GW-729, GW-730, Report Y/ER-117, Oak Ridge National Laboratory, Oak Ridge, TN.

Driscoll, F.G., 1986. Groundwater and Wells, Johnson Filtration Systems, Inc., St. Paul, MN, 1089 pp.

Dudgeon, C.R., M.J. Green, and J.W. Smedmore, 1975. Heat-pulse Flowmeter for Boreholes. Medmenham, Marlow, Bucks, England, Water Research Centre, Technical Report TR-4, 69 p.



Duffield, G.M., 1994. AQTESOLV, Aquifer Test Solver, Geraghty & Miller, Inc., Reston, VA.

Faust, C.R. and J.W. Mercer, 1984. Evaluation of Slug Tests in Wells Containing a Finite-Thickness Skin, Water Resources Research, 20(4):504-506.

Feller, W., 1948. On the Kolmogorov-Smirnov Limit Theorems for Empirical Distributions, Annals of Mathematical Statistics, 19, pp. 177-189.

Ferguson, R.I., P.E. Ashmore, P.J. Ashworth, C. Paola, D.M. Powell, and K.L. Prestegard, 1992. Measurements in a Braided River Chute and Lobe, 1, Flow Pattern, Sediment Transport, and Channel Change. Water Resources Research, 28. pp 877-886.

Fisk, 1952. Mississippi River Valley Geology Relation to River Regime. Transactions American Society of Civil Engineers. 117, pp 667-682.

Forbes, D.L., 1983. Morphology and Sedimentology of a Sinuous Gravel-bed Channel System: Lower Babbage River, Yukon Coastal Plain, Canada. In: Modern and Ancient Fluvial Systems. Edited by J.D. Collinson and J. Lewin. International Association of Sedimentologists Special Publication 6, pp 195-206.

Freeze, J. A. and J. A. Cherry, 1979. *Groundwater*. Prentice-Hall, Englewood Cliffs, NJ, p.604.

Freyberg, D. L., 1986. A natural gradient experiment on solute transport in a sand aquifer, 2, Spatial moments and the advection and dispersion of nonreactive tracers, Water Resources Research, 22(13), 2031-2046.

Galloway, W.E., and D.K. Hobday, 1983. *Terrigenous Clastic Depositional Systems*. Springer Verlag, New York, 423 p.

Garabedian, S. P., D. R. LeBlanc, L. W. Gelhar, and M. A. Celia, 1991. Large-scale natural gradient tracer test in sand and gravel, Cape Cod, Massachusetts, 2, Analysis of spatial moments for a nonreactive tracer, Water Resources Research, 27(5), 911-924.

Gomez-Hernandez, J. J., and R. M. Srivastava, 1990. ISIM3D: An ANSI-C three-dimensional multiple indicator conditional simulation program, Computers and Geosciences, 16(4):395-440.

Gustavson, T.C., 1978. Bed Forms and Stratification Types of Modern Gravel Meander Lobes, Nueces River, Texas. Sedimentology. 25, pp 401-426.

Haldorsen, H. H., P. J. Brand, and C. J. MacDonald, 1988. Review of the stochastic nature of reservoirs, Mathematics in Oil Production, S. Edwards and P. King (eds.), Oxford Science Publications, Clarendon Press, Oxford, pp 109-209.

Haldorsen, H. H., and E. Damsieth, 1990. Stochastic modeling, Society of Petroleum Engineers, pp 404-412, April.

Haley, J.L., B. Hanson, C. Enfield, and J. Glass, 1991. Evaluating the Effectiveness of Groundwater Extraction Systems, Ground Water Monitoring Review, Winter, pp 119-124.

Hantush, M.S., 1956. Analysis of Data from Pump Tests in Leaky Aquifers. Transactions, American Geophysical Union, 37(6), pp 702-714.

Hein, F.J. and R.G. Walker, 1977. Bar Evolution and Development of Stratification in the Gravelly, Braided Kicking Horse River, British Columbia. Canadian Journal of Earth Sciences. 14, pp 562-570.

Hess, A. E., 1982. A Heat-pulse Flowmeter for Measuring Low Velocities in Boreholes, Open Report 82-699, U.S. Geological Survey, Denver, CO.

Hess, A.E., 1986. Identifying Hydraulically Conductive Fractures with a Slow-velocity Borehole Flowmeter. Canada Geotechnical Journal. v. 23. pp 69-78.

Hess, A.E. and F.L. Paillet, 1989. Characterizing Flow Paths and Permeability Distribution in Fractured Rock Aquifers Using a Sensitive Thermal Borehole Flowmeter, in *Proceedings of the Conference on New Field Techniques for Quantifying the Physical and Chemical Properties of Heterogeneous Aquifers*, Molz, F. J., Guven, O., and Melville, J. G., ed., Water Resources Research Institute, Auburn University, AL.

Hess, A.E., 1990. Thermal-pulse Flowmeter for Measuring Slow Water Velocities in Boreholes, Open Report, 87-121, U.S. Geological Survey, Denver, CO.

Hess, K.M., H.W. Wolf and M.A. Celia, 1992. Large-scale Natural Gradient Tracer Test in Sand and Gravel, Cape Cod, Massachusetts, 3, Hydraulic Conductivity Variability and Calculated Macrodispersivities. Water Resources Research, v. 29(8), pp. 2011-2018.

Hufschmied, P., 1986. Estimation of Three-dimensional Statistically Anisotropic Hydraulic Conductivity Field by Means of Single Well Pumping Tests Combined with Flowmeter Measurements. Hydrogeologic, v. 10, pp 163-174.

Hvorslev, M.J., 1951. Time Lag and Soil Permeability in Groundwater Observations, U.S. Army Corps of Engineers Waterway Experiment Station Bulletin 36, Vicksburg, MS.

Hyder Z. and J.J. Butler, 1994. Slug Tests in Unconfined Formations: An Assessment of the Bouwer and Rice Technique, Ground Water, 33(1), pp 16-23.

Hyder, Z., J.J. Butler, C.D. McElwee, and W. Liu, 1994. Slug Tests in Partially Penetrating Wells, Water Resources Research, 30(11), pp 2945-2957.

Jackson, R.G. II, 1975. Hierarchical Attributes and a Unifying Model of Bed Forms Composed of Cohesionless Material and Produced by Shearing Flow. Geological Society of America Bulletin. 86, pp 1523-1533.

Jackson, R.G. II, 1976. Largescale Ripples of the Lower Wabash River. Sedimentology. 23, pp 593-623.

Jacob, C.E., 1963. Determining the Permeability of Water Table Aquifers, U.S. Geol. Surv. Water Supply Paper 1563-I.

Javandel, I., and P.A. Witherspoon, 1969. A Method of Analyzing Transient Flow in Multilayered Aquifers. Water Resources Research, v. 5. pp 856-869.

Journel, A. G., and F. G. Alabert, 1990. New methods for reservoir mapping, J. Pet. Technol., 42(2):212-218.

Julian, H.E., S.C. Young, C. Lu, J.C. Herweijer, and K.E. Richter, 1993. NFERC Regional Groundwater Investigation, Technical Report WR28-1-520-191, Tennessee Valley Authority, Norris, TN.

Kaye, J. M., 1955. "Certain Aspects of the Geology of Lowndes County, Mississippi," M.S. Thesis, Mississippi State University, Starkville, MS.

Keely, J.F. and K. Boateng, 1987a. "Monitoring Well Installation, Purging and Sampling Techniques - Part 1: Conceptualizations," Ground Water, 25: 300-314.

Keely, J.F. and K. Boateng, 1987b. "Monitoring Well Installation, Purging and Sampling Techniques - Part 2: Case Histories," Ground Water, 25: 427-439.

Killey, R. W. D., and G. L. Moltyaner, 1988. Twin Lake tracer tests: Setting, methodology, and hydraulic conductivity distribution, Water Resources Research, 24(10), 1585-1612.

Kroszynski, U.I. and G. Dagan, 1975. Well Pump in Unconfined Aquifers: the Influence of the Unsaturated Zone. Water Resources Research, 11(3), pp.479-490.

Kumar, S. and I.B. Singh, 1978. Sedimentological Study of Gomti River Sediments, Uttar Pradesh, India. Example of a River in Alluvial Plain. *Senckenbergiana Maritima*, 10, pp 145-211.

Lacombe, S., E.A. Sudicky, S.K. Frape, and A.J.A. Unger, 1995. Influence of Leaky Boreholes on Cross-formational Groundwater Flow and Contaminant Transport, Water Resources Research, Vol. 31, No. 8, pp 1871-1882, August.

LeBlanc, R.J. Sr., 1977. Distribution and Continuity of Sandstone Reservoirs - Part 1. Journal of Petroleum Geology, July, pp 776-804.

LeBlanc, D. R., S. P. Garabedian, K. M. Hess, L. W. Gelhar, R. D. Quadri, K. Gl. Stollenwerk, and W. W. Wood, 1991. Large-scale natural gradient tracer test in sand and gravel, Cape Code, Massachusetts, 1, Experimental design and observed tracer movement, Water Resources Research, 27(5), 895-910.

Leeder, M. R., 1973. Fluvialite Fining-Upward Cycles and the Magnitude of Paleochannels, Geol Mag., 110(3):265-76.

Leopold, L.B. and M.G. Wolman, 1957. River Channel Patterns: Braided, Meandering and Straight. Physiographic and Hydraulic Studies of Rivers. United States Geological Survey Professional Paper. 282-B, 144 p.

Leopold, L.B., M.G. Wolman, and J.P. Miller, 1964. *Fluvial Processes in Geomorphology*.

W.H. Freeman and Co., San Francisco. 522 p.

Liffiefors, H. W., 1976. "On the Kolmogorov-Smirnov Test for Normality With the Mean and Variance Unknown," *American Statistical Association Journal*, pp. 399-402.

Linderfelt, W.R. and J.L. Wilson, 1993. *Capture Zone Delineation: Models and Experiment*.

EPA Draft Report, US EPA Kerr Laboratory, Ada, OK.

Liu, W. and J.J. Butler, Jr., 1990. *Software for the Evaluation of Analytical and Semianalytical Solutions for Pump Induced Drawdown in Complex Geologic Settings*, KS Geo. Survey Computer Program Series 90-4, 52 pp.

Matthes, G.H., 1941. *Basic Aspects of Stream-Meanders*. *Transactions of the American Geophysical Union*, pp 632-636.

Matthews, R. K. 1974. *Dynamic Stratigraphy*. Prentice Hall, New Hall, New Jersey.

Maxwell, J. C., 1864. "On the calculation of equilibrium and stiffness of frames."

*Philosophical Magazine*, Series 4, Vol 27, pp 294.



McGowen, J.H. and L.E. Garner, 1971. "Physiographic Features and Stratification Types of Coarse-Grained Point Bars: Modern and Ancient Examples." Sedimentology. Vol. 14, pp 77-111.

Miall, A.D., 1977. A Review of the Braided-river Depositional Environment. Earth Science Reviews. 13, pp 1-62.

Miall, A.D., 1982. Analysis of Fluvial Depositional Systems. American Association of Petroleum Geologists Continuing Education Course Notes 20. Tulsa, 75 p.

Miall, A.D., 1987. Recent Developments in the Study of Fluvial Facies Models. In: Recent Developments in Fluvial Sedimentology. edited by F.G. Ethridge, R.M. Flores, and M.D. Harvey, Society for Sedimentary Geology (SEPM) Special Publication 39, pp 1-9.

Miall, A.D., 1988a. Alluvial Sedimentary Basins: Tectonic Setting and Basin Architecture. In: Sedimentation and Tectonics in Alluvial Basins. Edited by A.D. Miall. Geological Association of Canada Special Paper 23, pp 979-988.

Miall, A.D., 1988b. Facies Architecture in Clastic Sedimentary Basins. In: New Perspectives in Basin Analysis. Edited by K.L. Kleinspehn and C. Paola. Springer Verlag. New York, 668 p.

Miall, A.D., 1989. Architectural Elements and Bounding Surfaces in Fluvial Deposits: Anatomy of the Kayenta Formation (Lower Jurassic), Southwest Colorado. *Sedimentary Geology*. 55, pp 233-262.

Miall, A.D., 1990. Principles of Basin Analysis, Springer Verlag, New York, 668 p.

Mishra, S., J.C. Parker, and N. Singhal, 1989. Estimation of Soil Hydraulic Properties and Their Uncertainty From Particle Size Distribution Data, *J. of Hydrology*, Vol. 108, pp 1-18.

Moltyaner, G. L. and R. W. D. Killey, 1988a. Twin lake tracer tests: Longitudinal dispersion, *Water Resources Research*, 24(10), 1623-1627.

Moltyaner, G. L., and R.W.D. Killey, 1988b. Twin Lake tracer tests: Transverse dispersion coefficients, *Water Resources Research*, 24(10), 1613-1627.

Molz, F.J., R.H. Morin, A.E. Hess, J.G. Melville, and O. Guven, 1989. The Impeller Meter for Measuring Aquifer Permeability Variations: Evaluation and Comparison with Other Tests. *Water Resources Research*. v. 25. No. 7. pp 1677-1683.

Molz, F.J., O.K. Guven, J.G. Melville, I. Javandel, A.E. Hess, and F.L. Paillet, 1990. A New Approach and Methodologies for Characterizing the Hydrogeologic Properties of Aquifers, EPA Report/600-2-90/002, US EPA Kerr Laboratory, Ada, OK.

Molz, F.J. and S.C. Young, 1993. Development and Application of Borehole Flowmeters for Environmental Assessment. The Log Analyst, January-February, pp 13-23.

Molz, F.J., G.K. Bowman, S.C. Young, and W.R. Waldrop, 1995. Borehole Flowmeters: Field Application and Data Analysis, Journal of Hydrology, 163, pp 200-212.

Moore, G.K., and S.C. Young, 1992. Borehole Flowmeter Data and Interpretation, ORNL/ER-91, Oak Ridge National Laboratory, Oak Ridge, TN.

Morin, R.H., A.E. Hess, and F.L. Paillet, 1988. Determining the Distribution of Hydraulic Conductivity in Fractured Limestone Aquifers by Simultaneous Injection and Geophysical Logging. Ground Water. v. 26. pp 587-595.

Morin, R.H., D.R. LeBlanc, and W.E. Teasdale, 1988. "A Statistical Evaluation of Formation Disturbance Produced by Well/Casing Installation Method," Ground Water, 26:207-217.

Morrison, A., 1983. Arresting a Toxic Plume, Civil Engineering, ASCE, 53(8), pp 35-37.

Muto, G.R., and J. Gunn, 1986. "A Study of Late Quaternary Environments and Early Man," Phase I Final Report, Project Narrative and Appendices A-D, U.S. Army Corps of Engineers, Mobile and Nashville Districts, Appendix C, Geosciences Documentation.

Neton, M. J., J. Dorsch, C. D. Olson., and S. C. Young, in press. Architecture and directional scales of heterogeneity in alluvial-fan aquifers, *Journal of Sedimentary Research*, v. B64 (2).

Neuman, S.P., 1972. Theory of Flow in Unconfined Aquifers Considering Delayed Response of the Water Table, *Water Resources Res.*, 8(4):1031-1045.

Neuman, S.P., 1974. Effect of Partial Penetration on Flow in Unconfined Aquifers Considering Delayed Gravity Response, *Water Resource Res.*, 10(2):303-312.

Neuman, S.P., 1975. Analysis of Pump Test Data From Anisotropic Unconfined Aquifers Considering Delayed Gravity Response, *Water Resource Res.*, 11(2):329-342.

Nijman, W., and C. Puigdefabregas, 1978. Coarse-grained Point Bar Structure in a Molasse-type Fluvial System, Eocene Castisent Sandstone Formation, South Pyrenean Basin. In: *Fluvial Sedimentology*. edited by A.D. Miall, Canadian Society of Petroleum Geologists Memoir. 5, pp 487-510.

Ogden Environmental and Energy Services, 1994. TVA Columbus Air Force Base Laboratory Testing TVA Contract No. TV-92813V: Permeability Reports. prepared for TVA Engineering Laboratory, Norris, TN, Odgden File No. 4-4248-0000. Oak Ridge, TN.

Oliver, D., 1990. The Averaging Process in Permeability Estimation from Well-Test Data. SPE Evaluation, SPE Paper 19845, September 1990, pg 319-324.

Paillet, F.L., A.E. Hess, C.H. Cheng, and E. Hardin, 1987. Characterization of Fracture Permeability with High-resolution Flow Measurements During Borehole Pumping, Ground Water, v.25, no 1, pp 28-40.

Pettijohn, F. J., P.E. Potter, and R. Siever. 1987. Sand and Sandstone (2nd edition). Springer-Verlag. New York, 553. p

Rehfeldt, K.R., P. Hufchmied, L.W. Gelhar, and M.E. Schaefer, 1989a. Measuring Hydraulic Conductivity with the Borehole Flowmeter, Electric Power Research Institute Report EN-6511, Palo Alto, California.

Rehfeldt, K.R., L.W. Gelhar, J.B. Southard, and A.M. Dasinger, 1989b. "Estimates of Macrodispersivity Based on Analyses of Hydraulic Conductivity Variability at the

MADE Site." Electric Power Research Institute Interim Report EN-6405, Palo Alto, California.

Rehfeldt, K.R., J.M. Boggs, and L.W. Gelhar, 1992. Field Study of Dispersion in a Heterogeneous Aquifer 3. Geostatistical Analysis of Hydraulic Conductivity, Water Resources Research, v. 28(12), pp 3309-3324.

Reineck, H., and I.B. Singh, 1986. "Depositional Sedimentary Environments." Springer-Verlag. Berlin, 551 p.

Russo D., and W. A. Jury, 1987. A theoretical study of the estimation of the correlation scale in spatially variable fields; 2. Nonstationarity fields, Water Resources Research, 23(7):1269-1279.

Rust, B.R., 1972. Structure and Process in a Braided River. Sedimentology. 18, pp 221-245.

Rust, B.R., 1978a. A Classification of Alluvial Channel Systems. In: Fluvial Sedimentology. Edited by A.D. Miall. Canadian Society of Petroleum Geologists Memoir 5, pp 187-198.

Rust, B.R., 1978b. **Depositional Models for Braided Alluvium.** In: **Fluvial Sedimentology.** edited by A.D. Miall. **Canadian Society of Petroleum Geologists Memoir 5,** pp 605-625.

Schumm, S. A., 1977. **The Fluvial System.** John Wiley & Sons, New York, New York. 335p.

Smirnov, N., Table for estimating the goodness of fit to empirical distributions, **Annual of Mathematical Statistics,** 19, 279-281, 1948.

Smith, N.D., T.A. Cross, J.P. Dufficy, and S.R. Clough, 1989. Anatomy of an avulsion. **Sedimentology** 36, pp 1-23.

Speight, J.G., 1965. Flow and Channel Characteristics of the Angabunga River, Papua. **Journal of Hydrology.** 3, pp 16-36.

Stewart, D.J., 1983. Possible Suspended-load Channel Deposits from the Wealden Group (Lower Cretaceous) of Southern England. In: **Modern and Ancient Fluvial Systems.** Edited by J.D. Collinson and J. Lewin. International Association of Sedimentologists Special Publication 6, pp 369-384.

Streltsova, T.D., 1988. **Well Testing in Heterogeneous Formations: An Exxon Monograph.**

Sudicky, E. A., 1986. A natural gradient experiment on solute transport in a sand aquifer: Spatial variability of hydraulic conductivity and its role in the dispersion process, Water Resources Research, 22(13), 2069-2082.

Sudicky, E.A., A.J.A. Unger, and S. Lacombe, 1995. A Noniterative Technique for the Direct Implementation of Well Bore Boundary Conditions in Three-dimensional Heterogeneous Formations, Water Resources Research, 31(2), pp. 411 - 416.

Theis, C.V., 1935. The Relation Between the Lowering of the Piezometer Surface and the Rate and Duration of Discharge of a Well Using Ground-Water Storage, Transactions of the American Geophysical Union, Vol. 16, pp 519-524.

Therrien, R., and Sudicky, E.A., 1996, Three-dimensional analysis of variably-saturated flow and solute transport in discretely-fractured porous media, Journal of Contaminant Hydrology, 23, 1-44.

Therrien, R., E.A. Sudicky, and R.G. McLaren, 1994. *User's Guide for FRAC3DVS: An Efficient Simulator for Three-Dimensional Saturated-Unsaturated Groundwater Flow and Chain-Decay Solute Transport in Porous Formations*, Waterloo Groundwater Centre for Research, Waterloo University, Canada.



Thompson, D.B., 1987. Microcomputer Program for Interpreting Time-Lag Permeability Tests, Ground Water, 25(2):212-218, 1987.

U.S. EPA, 1990. Basics of Pump-and-Treat Ground-Water Remediation Technology, EPA/600/8-90/003, prepared by GeoTrans, Herndon, Virginia.

van Genuchten, R., 1978. Calculating the Unsaturated Hydraulic Conductivity with a New Closed Form Analytical Model. Dept. of Civil Engineering, Princeton University, NJ, Report 78-WR-08.

Wheatcraft, S. W., and S. W. Tyler, 1988. An explanation of scale-dependent dispersivity in heterogeneous aquifers using concepts of fractal geometry, Water Resources Res., 24(4):566-578.

Williams, P.F., and B.R. Rust, 1969. The Sedimentology of a Braided River. Journal of Sedimentary Petrology. 39, pp 649-679.

Wolfe, 1991. Evaluation of Hydraulic Conductivities Calculated from Multiport-Permeameter Measurements, Ground Water, Vol 29(4), pg 516-525.

Young, S.C., 1991a. A Site Characterization Methodology for Aquifers in Support of Bioreclamation Activities. Vol I: Well Network Design, Well Equation, and Aquifer

**Multiwell and Single-well Tests. Technical Report ESL-TR-90-19. USAF Engineering and Services Center, Tyndall AFB, FL. pp 178.**

**Young, S.C., 1991b. A Site Characterization Methodology For Aquifers in Support of Bioreclamation Activities, Vol. II: Borehole Flowmeter Technique, Tracer Tests, Geostatistics, and Geology, Technical Report ESL-TR-90-19, United States Air Force Engineering and Services Center, Tyndall AFB, Florida.**

**Young, S.C. and H. Julian, 1991. Assessment of Surface Water and Groundwater Impacts from Solid Waste Management Unit 108," Technical Report WR28-1-520-167, Tennessee Valley Authority, Norris, TN.**

**Young, S.C., H.E. Julian, H.S. Pearson, F.J. Molz, and J.K. Bowman, 1993a. User's Guide for the Application of the Electromagnetic Borehole Flowmeter, EPA Draft Report, US EPA Kerr Laboratory, Ada, OK, pp 126.**

**Young, S.C., M.J. Fraley, P. Hufschmied, M. Dillio, B.M. Thompson, J.M. Lavanchy, and S. Vomvoris, 1993b. Guidelines and Documentation of KPFLOW3 and KPFLOWIN: Programs to Analyze Borehole Flowmeter Data, EPA Draft Report, US EPA Kerr Laboratory, Ada, OK, pp 126.**

Young, S.C., 1995. Characterization of High-K Pathways using Borehole Flowmeter Method and Recirculating Tracer Tests, Ground Water, 33(2), 311-318.

Young, S.C., and H.S. Pearson, 1995. The Electromagnetic Borehole Flowmeter: Description and Application. Ground Water Monitoring and Remediation, Vol 4, pp 138-147.

Young, S.C., 1996. Positive Skin Effects in a Heterogeneous Granular Aquifer and their Impact on Borehole Flowmeter tests, in revision by Ground Water.

**APPENDIX A**  
**DESIGN AND INSTALLATION OF THE INITIAL 37 WELLS**  
**AT THE 1-HA TEST SITE**

**A.1 DESIGN OF THE WELL NETWORK**

Planning for the well network began in 1988 and included the following seven objectives:

1. Conduct a large-scale recirculation tracer test at the scale typical for bioremediation of jet-fuel spills;
2. Monitor the pathway of tracer transport between the injection and withdrawal wells during the large-scale tracer test;
3. Conduct a series of small-scale tracer tests at the scale of the averaged dimensions for the gravel and sand lenses;
4. Perform large- and small-scale pumping tests at the test;
5. Determine the geostatistical properties of the hydraulic conductivity field;
6. Determine values for hydraulic pressure and hydraulic conductivity fields so that two- and three-dimensional fields could be approximated; and
7. Maintain a reasonable cost for the well installation program.

Because of the complexities associated with optimizing the well locations with respect to the seven objectives, the author (as a TVA employee) and GeoTrans, Inc., a subcontractor,

developed the computer program WELPLAN. WELPLAN was used to help construct a well network given a set of constraints for the well locations and to help evaluate the merits of alternative well locations for calculating a semivariogram.

WELPLAN receives as input the number of existing wells, the number of new wells that are to be used to improve the data set for kriging, the number of wells to be used to improve the data set for the semivariogram, the boundaries for the well network location, the lag distance, and the weights assigned to the criteria on which the well locations are evaluated. For the test site, a unit lag distance of 3 meters was used in WELPLAN and the following three criteria were used to rank each well network configuration under consideration: (1) a sufficient number ( $>10$ ) of paired data points are available for every lag distance which is a multiple of 3 meters; (2) the actual average lag distance for each set of data points does not deviate more than 0.2 m from the desired lag distance for that set of data points; (3) the variance in the lag distance for each set of points is less than 0.5 m.

The author used WELPLAN interactively to develop the well network. The steps used to design the well network were as follows. The first 17 wells were selected to provide uniform coverage across the site and well locations suitable for conducting a large-scale four-well recirculating tracer test and for kriging. The next 10 well locations were selected primarily to improve the semivariogram calculations. The next 9 well locations were selected with considerations 2, 3, 4, and 5 listed above. The last well (Number 37) was located adjacent to Well 28 so that the effects of the well installation method on well performance could be investigated.

Figure A.1 illustrates the final well network. In designing the well network, WELPLAN was run approximately 600 times. The 37 wells provide for 666 well pairs (i.e.,  $37 \times 36/2$ ). Figure A.2 shows the distribution of the well pairs as a function of lag distances and the angles between the wells. The angles between the wells are measured clockwise from the north and are important with regard to Objectives 4 and 5 listed above.

## **A.2 WELL INSTALLATION, CONSTRUCTION, AND DEVELOPMENT**

Four well drilling methods were used to install the wells. The first 3 wells were installed in February 1988 by the air percussion method. The air compressor operated at 110 psi and at a flow rate of 20 m<sup>3</sup>/min. The drill casing was flush-jointed and had a 7.5-cm OD. During November and December 1988, Graves Well Drilling of Sylacauga, Alabama (AL), used a Bucyrus-Erie cable drill rig to install seven wells. The drill casing had a 10-cm OD but had casing couplings that were 11.5-cm OD. In December 1988, Law Engineering of Birmingham, AL, installed 11 wells by the rotary method with a Failing 1500 rotary wash drill rig. The drill casing was flush-jointed with a 10-cm OD. During April 1989, 11 additional wells by the air percussion method and Springer Engineering of Starkville, MS, installed 5 wells by the hollow-stem auger method with a CME 65 drill rig. The hollow-stem auger had a 9.0-cm ID and a 15-cm OD.

During the well drilling, major problems occurred at Wells 8, 4, 6, and 13. At Well 8 on 9 November 1988, the cable tool rig drove the drill casing to a depth of 39 feet but could not withdraw the drill casing. On 21 November 1988, a crane was mobilized to retrieve the

drill casing. The long delay in freeing the drill casing may have adversely affected the aquifer properties in the vicinity of the well.

On 11 November 1988, the drill casing broke during its retrieval at Well 13. A new location for Well 13 was selected; presently 6 meters of steel casing exists at the original location of Well 13. The breaking of the drill casing was attributed to drilling a crooked hole (Law, 1989).

In December 1988, a light- to medium weight mud ( $<150 \text{ lb/ft}^3$ ) was inappropriately used during a rotary wash well installation method at Well 4. The drilling mud, Super Gel X Extra High Yield Drilling Fluid, was a product of American Colloid Company and is nonbiodegradable. Law Engineering reported that their well development activities indicated that the introduction of the mud had no adverse effects on the hydraulics of the well (Law, 1989). In December 1988, the drilling mud was also inappropriately used at Well 6. At Well 6, the drilling and setting of the well progressed satisfactorily, but as the drill casing was retrieved from the hole, it was discovered that a 10-foot section of the casing had been lost down the hole. Law Engineering inserted the drilling mud to stabilize the borehole so that the lost casing could be retrieved and the well set. Law Engineering reported that their well development activities could not remove the apparent effects of the drilling mud. One week after the installation of Wells 4 and 6, TVA performed single-well pumping tests on the wells. TVA showed that both wells were irreversibly affected by the drilling mud. The decision was made to install new wells for 4 and 6 about 2 meters away from the original locations for Wells 4 and 6.

Table A.1 lists the coordinates, top of casing elevations, installation methods, installation date, and the drilling companies for the 37 wells in the well network. All of these wells were constructed and developed according to the procedures described in the following two sections.

#### **A.2.1 Well Construction Method**

All 37 wells are constructed from Schedule 40 5.08-cm Triloc PVC pipe. The screened sections of the pipe have 0.025-cm slots spaced at increments of 0.317 cm. The slotted pipe has an open area of about 5 percent. At its bottom, each well has a 14-cm unslotted section of pipe below about 9 meters of slotted pipe. Above these sections, the wells vary in their constructions; however, every well has slotted pipe up to at least 0.5 meters from the ground surface. During the construction of each well, the location of the slotted and unslotted sections of pipe were recorded.

During the construction of each well, four 0.06-cm OD plastic tubes were attached at designated locations on the well's exterior and extended to the top of the well. The tubes provide the capability for monitoring the hydraulic pressures during ambient conditions and during pumping by the method demonstrated by Young and Boggs (1988), and for obtaining groundwater samples during subsequent tracer tests. The plastic tubes were color-coded for ease of identification and attached in such a fashion as not to block any screened sections of the pipe.



**Table A.1 Well Specifications**

<b>Well</b>	<b>X (m)</b>	<b>Y (m)</b>	<b>Company</b>	<b>Well Type</b>	<b>Installation Date</b>	<b>TOC MSL (m)</b>
1	41	41	LAW	RW	11/23/88	65.18
2	41	63	LAW	RW	11/29/88	65.40
3	41	85	LAW	RW	12/02/88	65.51
4B	63	42	TVA	AP	4/11/89	65.38
5	63	63	TVA	AP	2/17/88	64.97
6B	63	84	TVA	AP	4/07/89	65.30
7	85	41	GRAVES	CT	11/09/88	65.12
8	85	63	GRAVES	CT	11/22/88	65.12
9	85	85	LAW	RW	12/04/88	65.36
10	74.59	62.52	LAW	RW	12/04/88	65.33
11	71.95	70.8	GRAVES	CT	11/15/88	65.01
12	78.9	61.66	GRAVES	CT	11/14/88	65.12
13	58.5	61.5	LAW	RW	12/06/88	65.15
14	55.52	66.17	GRAVES	CT	11/18/88	65.45
15	73.88	70.52	GRAVES	CT	11/15/88	65.02
16	59.03	65.32	LAW	RW	12/01/88	65.44
17	68.67	51.85	LAW	RW	12/06/88	65.05
18	47.28	60.61	LAW	RW	11/30/88	65.32
19	55.83	63.55	LAW	RW	12/01/88	65.52
20	65.81	71.05	GRAVES	CT	11/17/88	65.29
21	73.8	52.41	LAW	RW	12/05/88	65.09
22	108.7	63.0	TVA	AP	2/11/88	65.09
23	85.87	102.6	TVA	AP	2/18/88	65.01
24	77.5	58.3	TVA	AP	4/06/89	65.54

25	73.2	59.4	TVA	AP	4/06/89	64.87
26	53.93	77.05	TVA	AP	4/07/89	65.07
27	63.0	108.7	TVA	AP	4/05/89	65.58
28	17.3	63.0	TVA	AP	4/05/89	65.01
29	63.0	17.37	TVA	AP	4/05/89	64.92
30	53.88	50.16	TVA	AP	4/11/89	65.01
31	79.22	78.27	TVA	AP	4/10/89	65.47
32	81.60	47.44	TVA	AP	4/10/89	65.67
33	17.37	17.37	SE	HS	4/06/89	65.51
34	17.37	108.7	SE	HS	4/05/89	65.68
35	108.7	17.37	SE	HS	4/05/89	65.36
36	108.7	108.7	SE	HS	4/05/89	65.23
37	17.37	64.0	SE	HS	4/06/89	65.19

TVA - Tennessee Valley Authority    LAW - Law Engineering  
 SE - Springer Engineering            GRAVES - Graves Drilling

RW - Rotary Wash (10-cm OD); Number of RW wells = 11

AP - Air Percussion (9.0-cm OD); Number of AP wells = 14

CT - Cable Tool (11.5-cm OD); Number of CT wells = 7

HS - Hollow Stem Auger (15-cm OD); Number of HS wells = 5

TOC - Top of Casing

Figure A.3 is an example of a typical well installation. At each of the wells, the aquifer was permitted to collapse around the well and no extensive backing was performed with either the natural material or sand. In May 1989, all of the wells were grouted to ensure an adequate seal between the well and the ground surface. The grouting process included

centering a 75-cm square piece of 1.3-cm thick plywood over the well and adding concrete around the well.

### **A.2.2 Well Development**

Traditionally, well development has two broad objectives: (1) to repair damage done to the formation by drilling operations so that the natural hydraulic properties are restored, and (2) to alter the basic physical characteristics of the aquifer near the borehole so that water will flow more freely to a well (Driscoll, 1986). Well development methods rely on applying the necessary force to cause movement and transport of the aquifer material around a borehole. These methods include overpumping, backwashing, mechanical surging, and air development. Driscoll (1986) offers a thorough discussion for each of these methods. Table A.2 lists the benefits achieved by well development.

The goal of well development for our project is primarily to repair damage done to the aquifer during well installation and to avoid increases in the hydraulic conductivity of the aquifer. At the MADE site, Rehfeldt, et al. (1986), conducted a series of field tests to determine the optimum method for well development. Rehfeldt, et al. (1986), conclude that a scheme including overpumping, backflushing, and mechanical surging led to adequate well development. However, Rehfeldt, et al. (1986), do not provide a recommended protocol for the well development.

**Table A.2 Benefits of Well Development (from Driscoll, 1986)**

---

- (1) Reduce the compaction and intermixing of grain sizes produced during drilling by removing the fine material from pore spaces.
  - (2) Increase the natural porosity and permeability of the previously undisturbed formation near the [borehole] by selectively removing solids that have invaded the formation.
  - (3) Remove the filter cake or drilling fluid film that coats the borehole, and remove much or all of the drilling fluid and natural formation solids that have invaded the formation.
  - (4) Create a graded zone of sediment around the screen in a naturally developed well, thereby stabilizing the formation so that the well yields sand-free water.
- 

Working with Rehfeldt, the author developed the procedures list in Table A.3 for well development. The surge block used in the procedures was approximately 0.3-meter long and consisted of a string of alternating layers of rubber gaskets and metal washers with diameters slightly less than the ID of the 5.2-cm wells. A well typically took about 2 hours to develop. These procedures were used at all of the 37 wells and should be appropriate for wells in unconsolidated materials at other sites.

**Table A.3 Procedures for Well Development at CAFB**

---

- (a) Place 2.5-cm hose at the bottom of the well and run the pump at its maximum rate without drawing the water table down more than 5 feet;
  - (b) Continue step (a) until the effluent begins to clear;
  - (c) Once the effluent is clear, surge water into and out of the well by switching the pump on and off (notice no foot valves can be used) for about 5 minutes and then pump the well until it clears;
  - (d) Repeat step (c) at the middle and at the top of the well;
  - (e) Once the surging of the well is completed, lower the TVA surge block (weighs approximately 2 pounds) to the bottom of the well;
  - (f) Quickly pull the surge block up about 1 meter and then allow it to drop back to its original position. Work the surge block up and down through this 1-meter vertical interval for 5 cycles. Apply the surge block to each 1-meter vertical interval in the well until the water table is reached;
  - (g) Repeat steps (e) and (f);
  - (h) Repeat steps (a) through (g) two more times.
-

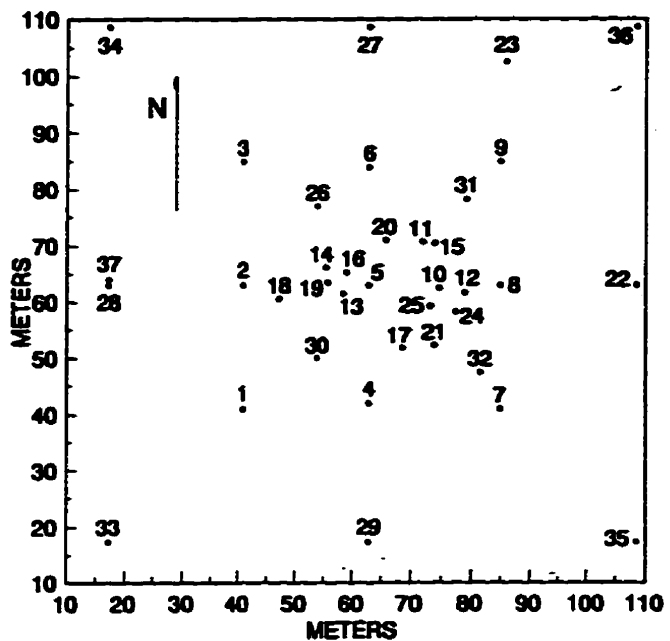


Figure A.1 The location of the initial 37 wells at the 1-Ha Test Site.

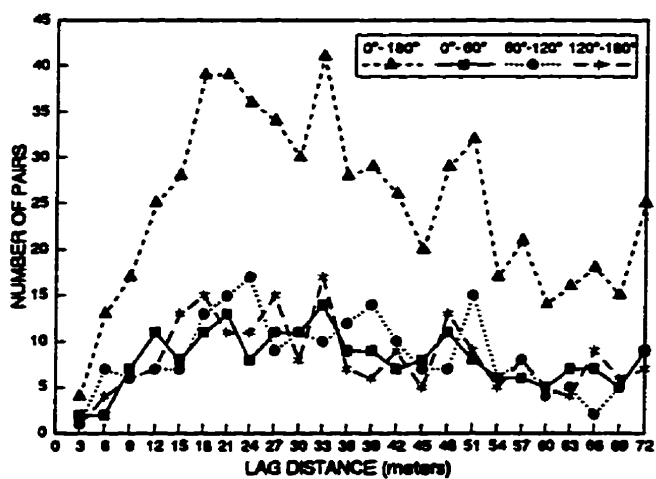


Figure A.2 Number of well pairs for each lag distance.

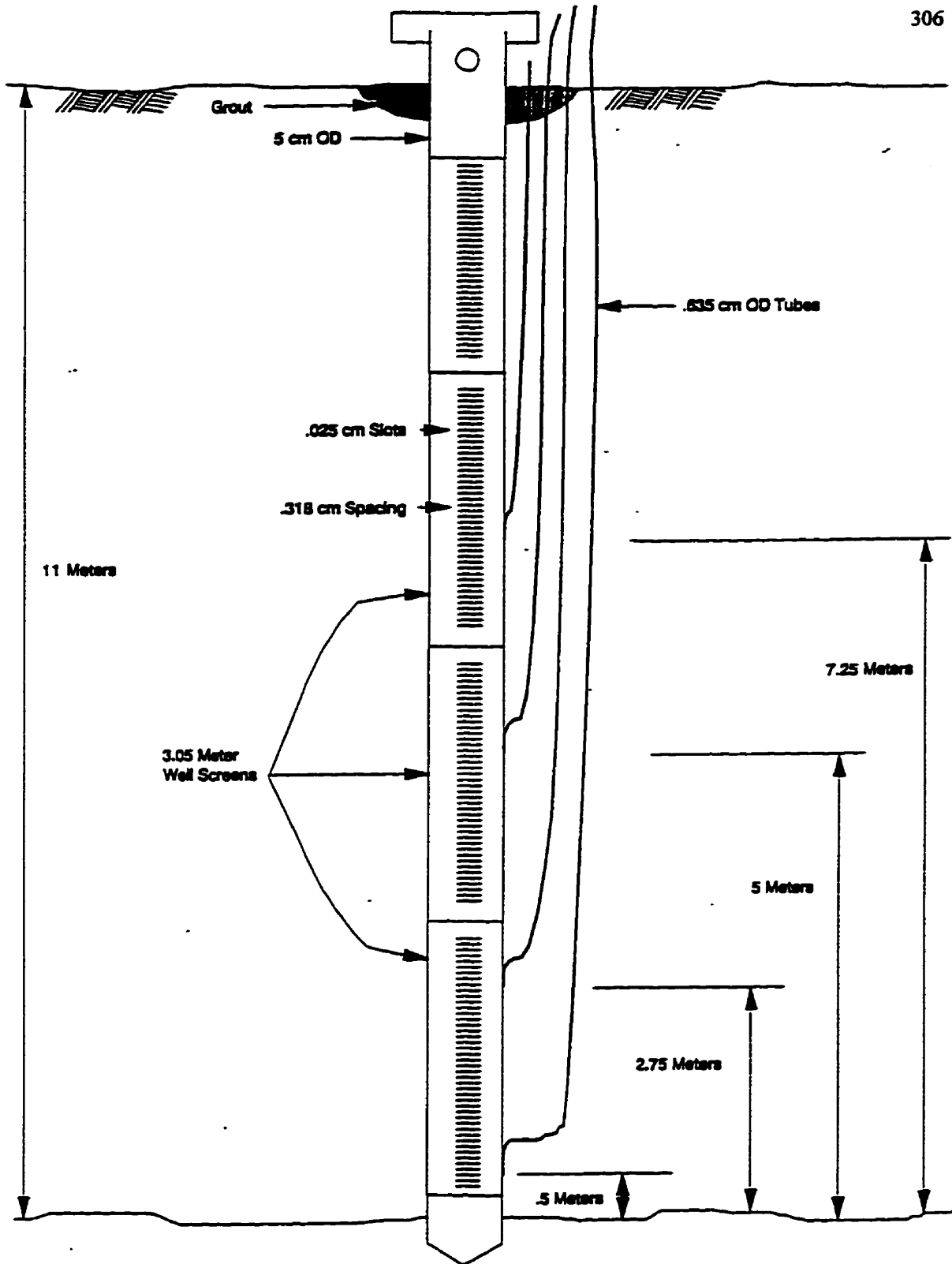


Figure A.3 Example of a typical well installation at the 1-Ha test site.

## **APPENDIX B**

### **LARGE-SCALE PUMPING TESTS AT THE 1-H<sub>a</sub> TEST SITE**

#### **B.1 GENERAL APPROACH**

Between June 1988 and August 1989, three large-scale aquifer tests were conducted. Each of the large-scale aquifer tests included pumping Well 5 (the center well) for about 6 days at a rate sufficient to produce measurable drawdowns at most, if not all, of the wells. Two important tasks associated with pumping tests are maintaining a constant pumping rate and collecting accurate drawdown data in a timely fashion. For all of the pumping tests, a positive displacement pump was used; and, the pumping rate was frequently measured. For each of the pumping tests, continuous values of drawdown were measured by Druck transducers and recorded by Telog data-logging systems. The Druck transducers are accurate to within 0.3 cm. The Telog data-logging systems permitted logging at intervals equal to or greater than 1 second and a graphical display of the data at any time.

Another important task associated with pumping tests is to systematically analyze the data in an unbiased manner. Traditionally the evaluation process has centered on visually matching the experimental pumping-test data to a theoretical drawdown curve to obtain values of transmissivity and storage coefficient. The manual method of curve matching can be cumbersome and labor intensive. Moreover, the method contains subjectivity that varies among geohydrologist. In order to improve the speed and the objectivity associated with pumping test analyses, the author and TVA employees developed the program WELLTEST.



## **B.2 PROGRAM WELLTEST**

WELLTEST is a computer program that automatically determines which values of transmissivity and storage coefficient produce a drawdown curve that best matches the experimental data set. Program WELLTEST uses the method of nonlinear least-squares regression to obtain the best match. The concept of applying a computerized analysis to determine the "best" transmissivity and storage coefficient was introduced by Vandenberg (1971). Vandenberg's (1971) program was specifically written for drawdown measurements in an observation well near a well pumping at a constant rate from a semi-infinite, nonleaky aquifer. An examination of the program reveals several potential problems among which is the inability to properly converge in some situations.

Since 1971, numerous programs (i.e., McElwee and Yukler, 1978; Chander, et al., 1981; Bardsley, et al., 1985) have been written to improve Vandenberg's approach. These programs differ in the type of well equations used and the speed and accuracy of the algorithms used to solve the nonlinear regression. In general, the logic and structure of these programs are very similar: the programs use partial derivatives of the well equations to drive the regression analysis. Because they use derivatives, each program is limited to a specific well equation and is computationally intensive when numerous experimental data points are used.

The WELLTEST program was written to solve for best values of transmissivity and storage coefficient for either a confined or an unconfined aquifer, for either leaky or nonleaky conditions, and for constant or variable pumping rates. WELLTEST does not account for any type of borehole storage or borehole skin effects. The WELLTEST program algorithms

are more computationally efficient than the algorithms used in the programs similar to Vandenberg's (1971). The modularity and speed of WELLTEST results by using Broyden's Method (Benton, 1990) to develop derivative-free algorithms for locating extreme of nonlinear equations.

The input requirements for WELLTEST include the experimental data, the distance to the observation well, the pumping schedule, the thickness of the aquifer, and whether the aquifer is confined or unconfined. The main output from WELLTEST is the "best" values for transmissivity and storage coefficient. Optional output from WELLTEST includes a sensitivity analysis for each parameter, a plot comparing the predicted and the observed pump- test curves, and/or a map of the residuals.

The map of the residuals provided by WELLTEST illustrates the sensitivity of the predicted time-drawdown response to transmissivity and the storage coefficient values. To create a map of the residuals, program WELLTEST generates a series of hypothetical time-drawdown aquifer responses for different sets of transmissivity and storage coefficient values. For each of these time-drawdown responses, program WELLTEST divides the difference in the areas between the predicted and the observed time- drawdown response by the total area beneath the observed time-drawdown curve. For convenience, the residual is expressed as a percentage. A residual of 0.10 means that the difference between area of the predicted and the observed time-drawdown curves is 10 percent of the total area beneath the observed time-drawdown curve. A residual of 0.0 means that the predicted and the observed time-drawdown curves are exactly the same.

Figures B.1 and B.2 show an application of WELLTEST and the importance of pumping test design. The figures illustrate the residuals created for observation wells at different distances from the pumping well for a hypothetical aquifer with a transmissivity and a storage coefficient of  $30 \text{ cm}^2/\text{s}$  and 0.03, respectively. Figure B.1 is for a constant pumping rate of 40 L/min for 24 hours, whereas Figure B.2 is for a 2-hour-on and 2-hour-off pumping rate of 80 L/min for 24 hours. Figure B.1 indicates that near the pumping well, the solution to the well equations are relatively insensitive to storage coefficient values. Similarly, for distances far from the pumping well, the solution to the well equations are relatively insensitive to transmissivity values. A comparison between Figure B.1 and B.2 shows, that at distances near the well, the sensitivities of the solution to the well equations to both storage coefficient and transmissivities are remarkably improved by pulsing the pumping well. This means that by pulsing the pumping well, the aquifer's hydrologic properties can be better defined.

### **B.3 AQUIFER TEST 1**

#### **B.3.1 Test Description**

Aquifer Test 1 consisted of pumping Well 5 at a constant rate and measuring the drawdown in all 37 wells. The pumping began on 18 May 1989 at 0800 hours and ended on 23 May 1989 at 0900 hours. The pump ran continuously for 435,587 seconds (5.04 days) except during a 6,075-second (1.69-hour) power outage that began 55,820 seconds (15.5 hours) into the test. Problems encountered with the flowmeter totalizer prevented an continuous record of pump discharge. Measurements of the discharge rate were taken with

a stopwatch and a calibrated 23.2-liter container. Table B.1 lists the measurements of the discharge rate.

**Table B.1 Measurements of the discharge rate for Aquifer Test 1**

<b>Date</b>	<b>Time</b>	<b>Cumulative Seconds</b>	<b>Flow (L/min)</b>
5/18/89	8:00	—	69.64
5/18/89	13:00	18,000	69.64
5/18/89	16:15	29,700	69.64
5/19/89	7:35	84,900	68.51
5/19/89	16:25	116,700	68.51
5/22/89	12:35	362,100	69.64
5/23/89	6:10	425,400	67.75

Drawdown measurements were made in all the wells with an electric tape during the pumping period. During the first several hours of pumping, the wells near the pumping well were intensively monitored. Approximately 4 hours into the test, the first set of measurements at all 37 wells was made. Subsequent surveys were made periodically throughout the test with at least one survey each day. During the test, measurements were taken at eight wells located several hundred meters away from the site in order to record the fluctuations in the water table caused by natural phenomena.

A total of ten pressure transducers were used for the pumping tests in order to get continuous drawdown measurements. These transducers were placed into Wells 2, 4, 6, 5, 8, 15, 17, 18, 25, and 30. For the first 3 hours of the pumping tests, transducer measurements

were recorded every 2 seconds. Thereafter measurements were recorded every 2 minutes until the pumping stopped. At the end of the pumping, measurements of the water table recovery were taken every 2 seconds for approximately 3 hours, after which measurements were taken every 2 minutes.

Figure B.3 shows contours of the cone-of-depression at elapsed times of 15,500 seconds (0.18 days); 82,400 seconds (0.95 days); 169,200 seconds (1.96 days); and 432,000 seconds (5.0 days). Figure B.3 shows: (1) at early times the drawdown cone is extended more in the westerly than easternly direction; (2) at late times the drawdown cone is extended more in the easternly direction than westerly direction; (3) the contours are very asymmetric; (4) the dimensions of the cone-of-depression change very little between 169,200 seconds and 432,000 seconds.

One explanation for the trends presented in Figure B.3 is that the western region has a higher diffusivity than the eastern region. In such a situation, the aquifer would have an asymmetrical response to the pumping well. At the early times, the cone-of-depression would penetrate farther into the western region than the eastern region. At intermediate times, the pressure gradients in the western region would approach some type of quasi-steady-state while the pressure gradients in the eastern region continue to increase. At late times, the pressure gradient in both the eastern and western regions would reach a quasi-steady-state but the gradients would differ. Because of its lower diffusivity, the cone-of-depression would extend farther into the eastern region.

Figure B.3 indicates that quasi-steady-state conditions over the total well network occurs around 169,200 seconds. After 169,200 seconds, the cone-of-depression is expanded

slowly enough that the plots do not show the changes in the cone-of-depression. In both the eastern and western regions, considerable asymmetry and differences in the horizontal hydraulic gradients exist. These variations are most likely caused by heterogeneity in the aquifer's hydraulic conductivity field.

### **B.3.2 WELLTEST Transmissivities and Storage Coefficients**

The WELLTEST program was used to determine the values for transmissivity and storage coefficient at the location of the nine observation wells with transducers. Input to WELLTEST included a pumping rate of 69.6 L/min before the power outage, a pumping rate of 68.5 L/min after the power outage, a saturated thickness of 7 meters, and an unconfined aquifer. WELLTEST was applied to drawdown values collected during the first 10,000; 50,000; and 100,000 seconds.

A comparison between the predicted and the observed drawdown curves for the nine wells for the three time periods is shown in Figures B.4 to B.7. These figures one show that the curve for each time period has been extrapolated to the end of the test to predict the final drawdowns.

Two trends should be noted in the figures. One trend is that the plotted data is nearly a straight line shortly after the pumping started and until the pump outage. This trend was present in almost all of the drawdown data taken manually at the 37 wells with the electric tape. As a result, the Cooper-Jacob straight-line analysis could be easily applied to the data sets. The other trend is that after 100,000 seconds, most of the drawdown curves flatten out and/or exhibit large fluctuation about a mean value.

An explanation for the trend in the data points after 100,000 seconds has not been sought by the author. Possible explanations include a region of high hydraulic conductivity near the boundary of the well network or delayed drainage from low permeability sediments within the well network. An investigation into the reason for the trend would include using image wells in WELLTEST and/or three-dimensional groundwater flow models. Such an investigation may lead to some interesting hypotheses, but it would be very time consuming and would not lead to any changes in the calculated values of transmissivities. As a result, such an investigation was not pursued.

Table B.2 lists the combination of transmissivity and storage coefficient values that provided the time-drawdown curve that best fit the observed time-drawdown curve as determined by the program WELLTEST. Included in Table B.2 are the factors by which the best value for either the transmissivity and the storage coefficient values can be multiplied or divided by so that the calculated residual is increased to 0.10 and to 0.20. These adjustment factors are a measure of the sensitivity of the final answer to both transmissivity and the storage coefficient. Table B.2 shows that the match between the observed and the predicted time-drawdown curves is more sensitive to the storage coefficient than to the transmissivity. No values are listed for a residual interval when the "best" set of transmissivity and storage coefficient values lead to a residual that is greater than the designated residual. No results are provided for Well 8 at 100,000 seconds because no set of transmissivity and storage coefficient values could produce a residual less than 20 percent.

**Table B.2 Calculated storage coefficients and transmissivities for Aquifer Test 1  
at 10,000; 50,000; and 100,000 seconds**

Well	Time Transmissivity (seconds)	Value	10%		20%		Storage Coefficient Value	10%		20%	
			10%	20%	10%	20%		10%	20%		
2	10K	92.90	*/1.20	*/1.58	.02818	*/1.17	*/1.38				
4	10K	42.46	*/1.17	*/1.48	.01413	*/1.15	*/1.41				
6	10K	53.46	*/1.17	*/1.41	.00832	*/1.26	*/1.58				
8	10K	104.24	*/1.05	*/1.38	.01072	*/1.10	*/1.62				
15	10K	52.24	*/1.12	*/1.32	.00282	*/1.45	*/2.14				
17	10K	43.45	*/1.15	*/1.32	.00295	*/1.45	*/2.09				
18	10K	73.79	*/1.15	*/1.35	.00955	*/1.32	*/1.82				
25	10K	48.75	*/1.15	*/1.38	.01862	*/1.29	*/1.66				
30	10K	61.38	*/1.15	*/1.32	.00302	*/1.41	*/2.04				
2	50K	57.28	*/1.15	*/1.41	.03802	*/1.23	*/1.55				
4	50K	44.46	*/1.15	*/1.38	.01413	*/1.29	*/1.66				
6	50K	36.98	*/1.12	*/1.35	.01349	*/1.26	*/1.66				
8	50K	64.27	NC	*/1.35	.02089	NC	*/1.58				
15	50K	39.63	*/1.12	*/1.29	.00575	*/1.48	*/2.24				
17	50K	36.14	*/1.12	*/1.29	.00447	*/1.51	*/2.34				
18	50K	51.05	*/1.12	*/1.32	.01660	*/1.32	*/1.78				
25	50K	36.14	*/1.15	*/1.35	.03020	*/1.32	*/1.78				
30	50K	45.50	*/1.12	*/1.29	.00603	*/1.45	*/2.14				
2	100K	46.56	*/1.10	*/1.29	.05623	*/1.23	*/1.66				
4	100K	43.45	*/1.15	*/1.32	.01514	*/1.35	*/1.91				
6	100K	37.85	*/1.15	*/1.32	.01230	*/1.35	*/1.91				
8	100K	-	NC	NC	-	NC	NC				
15	100K	28.71	NC	*/1.23	.01995	NC	*/1.95				
17	100K	25.59	*/1.02	*/1.26	.01698	*/1.17	*/2.04				
18	100K	48.75	*/1.12	*/1.32	.01862	*/1.38	*/2.00				
25	100K	39.63	*/1.15	*/1.32	.02512	*/1.45	*/2.14				
30	100K	35.32	*/1.02	*/1.26	.01698	*/1.20	*/2.00				

\*K = 1,000

NC = not calculated

\*/ = multiplied or divided by

Note: The pumped well, Well 5, is not listed because of the large uncertainty associated with determining its effective well radius (i.e., the distance from the point of pumping to the point of observation).



Table B.2 shows that as the time period increases, the range in the calculated variables decreases. For the 10,000-second period, the transmissivities vary from 40 to 100  $\text{cm}^2/\text{s}$  and the storage coefficients from .002 to .03. For the 100,000 second period, the transmissivities vary from 30 to 50  $\text{cm}^2/\text{s}$  and the storage coefficients from .01 to .05. This trend is expected, because as time increases equilibration processes in the aquifer (e.g., crossflows) will result in symmetry and smoothness in the hydraulic pressure field.

### **B.3.3 Transmissivities by the Cooper-Jacob Straight-Line Method**

The Cooper-Jacob approximation should be applied only when  $u$  (see list of symbols) is equal to or less than 0.07 (Cooper and Jacob, 1947). Using the range of parameters estimated from the Theis curve fitting analysis, the Cooper-Jacob analysis is appropriate 3 to 4 hours after the pumping begins for most of the wells.

Because of the concern of the pump outage at 15 hours and possible boundary effects at 1 day, the straight-line analyses were done cautiously. All of the slopes for wells near the pumping well were calculated from times less than 15 hours; and all the slopes for the wells far from the pumping well were calculated for times less than 1 day.

Calculations of the slopes were done with the aid of a computer program. The computer program graphically displays the drawdown data and permits the marking of any segment of the curve with cross-hairs. The best fit straight-line can be calculated by either a linear regression through the data points in the designated segment or by the slope between the designated endpoints of the segment. At wells where transmissivities were calculated using both transducer and manual measurements, the transducer-based transmissivity

estimate was considered the more accurate. Table B.3 lists the transmissivities calculated by the Cooper-Jacob straight-line method.

The arithmetic and geometric means for the 27 transmissivity values in Table B.3 are 38 and 37 cm<sup>2</sup>/s, respectively. The standard deviation for the transmissivities is 8.2 cm<sup>2</sup>/s and all except two of the transmissivities are within 35 percent of the arithmetic average. Within the transmissivity field, there appears a region of high transmissivity apparent in the west and northwest (Wells 1, 2, 3, 6, 18, 30) and a region of low transmissivity in the east (Wells 8, 12, 15).

**Table B.3 Transmissivities calculated by the Cooper-Jacob Straight-line Method for Aquifer Test 1**

Well	T (cm <sup>2</sup> /s)	Well	T (cm <sup>2</sup> /s)	Well	T (cm <sup>2</sup> /s)
1	57	13	33	25	37
2	50	14	36	26	36
3	56	15	29	27	-
4	40	16	27	28	-
5	34	17	31	29	-
6	49	18	46	30	43
7	42	19	34	31	34
8	27	20	38	32	35
9	35	21	40	33	-
10	36	22	-	34	-
11	38	23	-	35	-
12	29	24	38	36	-

## **B.4 AQUIFER TEST 2**

### **B.4.1 Test Description**

Aquifer Test 2 included cyclic pumping at Well 5 and measuring the drawdowns at the wells with pressure transducers. Cyclic pumping began on 1 June 1989, and ended on 6 June 1989. The targeted average pumping rate was 68 L/min (the constant pumping rate for Aquifer Test 1). The average pumping rate was achieved by a series of pulses. A pulse included a period during which the pumping rate was approximately 120 L/min and a period during which the pump rate was zero L/min. During the first 5 days of testing, a pulse included 4 hours of pumping and 3 hours of no pumping. For the last 2 days of testing, a pulse included 2 hours of pumping and 1- ½ hours of no pumping.

Immediately after the pump was turned on or turned off, the water level changed quickly in the observation wells. The relatively quick rate of change in water levels was measured by pressure transducers. Data was collected every 8 seconds throughout the duration of the test. Because of the limited number of transducers, the transducers were moved from well to well during the test. At the end of Pulse 7, 12 transducers were moved to new wells. At the end of Pulse 14, 3 of the 13 transducers were moved to new wells. The relocation of the transducers permitted data to be collected at all 28 wells within the interior of the well network.

The pump was automatically switched on and off with an electronic timing device. This device increased the consistency of the pulse cycles and eliminated the necessity for a night shift. Accurate measurements were made of the total discharge by a mechanical flowmeter (the flowmeter calibration was checked at the TVA Engineering Laboratory after

the test and found to be within 1 percent). Measurements of the total amount of groundwater discharged were taken only after Pulses 1, 3, 4, 5, 6, 7, 8, 9, 10, 14, 15, 19, 20, and 21. Table B.4 provides details on the actual pumping schedule and the location of transducers during Aquifer Test 2. The pumping rate gradually declined over the duration of the test. During Pulse 7, the pump prematurely stopped 48 minutes after start-up because of a power outage.

**Table B.4 Pumping schedule and location of transducer for Aquifer Test 2**

<b>Pulses</b>	<b>Start/End (date, time)</b>	<b>Pulse On/Pulse Off</b>	<b>Discharge Rates for Pulses (L/min)</b>	<b>Wells With Transducers</b>
1 - 7	6/1/89 12:30:00	4 hours	1 (121.1)	2 4 5 6 8 14
	6/3/89 8:02:15	3 hours	2 & 3 (119.2)	15 17 19 20
				4 to 7 (117.3)
8 - 14	6/3/89 12:30:00	4 hours	8 (117.3)	1 5 9 10 11
	6/05/89 13:30:00	3 hours	9,10 (116.2)	12 16 18 21
				11 to 14 (115.4)
15 - 21	6/05/89 13:30:00	2 hours	15 (116.2)	3 5 7 11 10 12
	6/06/89 14:00:00	1.5 hours	16 to 21 (115.4)	13 16 18 21 24 31 32

**Note:**

- A reading of the Cumulative Discharge was taken after Pulses 1, 3, 4, 5, 6, 7, 8, 9, 10, 14, 15, 19, 20, and 21
- Pulse 7 consisted of 48 minutes on and 4 hours 28 minutes off

During the test, manual drawdown measurements were made in all of the wells with an electric tape. These data provided a means to verify the accuracy of the transducer measurements and determine the amount of offset to be added to the transducer measurements at the second and third group of wells. As done in Aquifer Test 1, drawdown measurements were also taken at eight wells that were located several hundred meters away from the site in order to estimate the naturally occurring fluctuations in the water table. All the analysis was performed after the data had been detrended for these fluctuations.

#### **B.4.2 Transmissivities and Storage Coefficients From Program WELLTEST**

The WELLTEST program was used to determine the values of transmissivity and storage coefficient for each set of transducer measurements. The variable pumping rate listed in Table B.4 was used to generate the drawdown curves. The data sets were divided into 3 groups. The groups are Pulses 1-7, Pulses 8-14, and Pulses 15-21. For each series of pulses at a well, the drawdown data were analyzed with respect to the first 3 pulses, the second 3 pulses, and the first 6 pulses. The multiple analyses were performed to better detect any trends in the data.

Potential sources for trends in the drawdown data include the effects of the far-field boundary conditions and of the cyclic fluctuation of the water table. Aquifer Test 1 revealed that boundary conditions near the test site affected the drawdown at some of the wells 1 day after pumping. Thus, given the same average pumping rate at Aquifer Test 1, the potential existed for boundary conditions to affect the drawdown values after the third pulse.

Figures B.7 through B.12 show the match between the experimental data and the curves generated by WELLTEST. Tables B.5 to B.7 lists the calculated values of transmissivity and storage coefficients and their respective sensitivities at confidence limits of 10 percent and 20 percent. Several observations from the figures are listed in Table B.8.

**Table B.5 Calculated storage coefficients and transmissivities for  
Aquifer Test 2 for Pulses 1 to 6**

Well	Pulses		Transmissivity			Storage Coefficient		
	From	To	Value	10%	20%	Value	10%	20%
2	1	6	42.46	NC	*/1.26	.053703	*/1.00	*/1.55
2	1	3	39.63	NC	*/1.35	.063096	NC	*/1.58
2	4	6	46.56	NC	*/1.20	.041687	NC	*/1.51
4	1	6	29.38	NC	*/1.29	.040738	NC	*/1.78
4	1	3	28.06	NC	*/1.32	.050119	NC	*/1.55
4	4	6	31.48	*/1.05	*/1.29	.028840	*/1.10	*/2.09
6	1	6	32.21	NC	*/1.26	.020417	NC	*/1.95
6	1	3	33.73	NC	*/1.29	.023988	NC	*/1.74
6	4	6	33.73	*/1.07	*/1.29	.013804	*/1.20	*/2.34
8	1	6	20.80	NC	NC	.014125	NC	NC
8	1	3	22.29	NC	NC	.007079	NC	NC
8	4	6	15.42	NC	NC	.040738	NC	NC
14	1	6	27.42	*/1.07	*/1.26	.005248	*/1.41	*/3.02
14	1	3	26.79	*/1.07	*/1.26	.005623	*/1.38	*/2.69
14	4	6	27.42	*/1.10	*/1.26	.004571	*/1.55	*/3.47
15	1	6	32.21	NC	*/1.26	.012303	NC	*/2.40
15	1	3	35.32	NC	*/1.23	.011220	NC	*/2.14
15	4	6	31.48	*/1.10	*/1.26	.010965	*/1.45	*/2.88
17	1	6	26.79	NC	*/1.23	.008128	NC	*/2.45
17	1	3	27.42	NC	*/1.23	.009772	NC	*/2.04
17	4	6	26.79	*/1.10	*/1.26	.006026	*/1.48	*/3.09
19	1	6	25.00	*/1.10	*/1.23	.002570	*/1.62	*/3.63

19	1	3	24.44	*/1.10	*/1.23	.002818	*/1.70	*/3.47
19	4	6	25.59	*/1.07	*/1.23	.002188	*/1.62	*/3.98
20	1	6	26.18	*/1.10	*/1.26	.006026	*/1.58	*/3.24
20	1	3	27.42	*/1.10	*/1.26	.005888	*/1.51	*/2.88
20	4	6	26.18	*/1.10	*/1.26	.005495	*/1.74	*/3.63
25	1	6	29.38	NC	*/1.26	.093325	NC	*/1.74
25	1	3	30.76	NC	*/1.26	.100000	NC	*/1.55
25	4	6	31.48	NC	*/1.29	.064565	NC	*/2.09
26	1	6	29.38	*/1.05	*/1.26	.005754	*/1.17	*/2.45
26	1	3	30.06	*/1.07	*/1.26	.006310	*/1.32	*/2.34
26	4	6	30.06	*/1.05	*/1.26	.004571	*/1.23	*/2.69
30	1	6	12.53	NC	*/1.17	.014791	NC	*/1.48
30	1	3	11.70	NC	*/1.17	.013804	NC	*/1.41
30	4	6	12.25	NC	*/1.20	.020417	NC	*/1.70

NC = not calculated

\*/ = multiplied or divided by

**Table B.6 Calculated Storage Coefficients and Transmissivities  
for Aquifer Test 2 for Pulses 8 to 13**

Well	Pulses		Transmissivity			Storage Coefficient		
	From	To	Value	10%	20%	Value	10%	20%
1	8	13	70.47	NC	*/1.26	.017378	NC	*/2.29
1	8	10	58.62	*/1.10	*/1.29	.021380	*/1.38	*/2.45
1	11	13	82.80	*/1.05	*/1.29	.017378	*/1.26	*/2.88
9	8	13	41.50	*/1.07	*/1.29	.028184	*/1.23	*/2.24
9	8	10	37.85	*/1.12	*/1.29	.028184	*/1.35	*/2.19
9	11	13	42.46	*/1.12	*/1.29	.033884	*/1.45	*/2.34
10	8	13	57.28	NC	*/1.20	.038019	NC	*/2.14
10	8	10	44.46	*/1.07	*/1.26	.070795	*/1.23	*/2.51
10	11	13	67.30	NC	*/1.23	.031623	NC	*/2.69
11	8	13	33.73	*/1.10	*/1.26	.019953	*/1.45	*/3.02
11	8	10	32.21	*/1.10	*/1.26	.021380	*/1.41	*/2.82
11	11	13	35.32	*/1.10	*/1.26	.019953	*/1.51	*/3.24

12	8	13	21.28	NC	*/1.12	.026915	NC	*/1.51
12	8	10	19.86	NC	*/1.17	.029512	NC	*/1.66
12	11	13	22.29	NC	*/1.12	.028840	NC	*/1.51
13	8	13	26.79	*/1.10	*/1.23	.001445	*/2.29	*/6.46
13	8	10	25.59	*/1.10	*/1.23	.001778	*/2.19	*/5.89
13	11	13	28.06	*/1.10	*/1.23	.001288	*/2.51	*/7.41
13	8	13	26.79	*/1.10	*/1.23	.001445	*/2.29	*/6.46
13	8	10	25.59	*/1.10	*/1.23	.001778	*/2.19	*/5.89
13	11	13	28.06	*/1.10	*/1.23	.001288	*/2.51	*/7.41
16	8	13	31.48	*/1.10	*/1.23	.000457	*/2.63	*/8.51
16	8	10	29.38	*/1.10	*/1.23	.000603	*/2.57	*/7.76
16	11	13	32.21	*/1.10	*/1.23	.000380	*/2.82	*/9.55
18	8	13	47.64	*/1.07	*/1.26	.017378	*/1.29	*/2.88
18	8	10	43.45	*/1.10	*/1.26	.019953	*/1.38	*/2.75
18	11	13	52.24	*/1.10	*/1.26	.016596	*/1.55	*/3.31
21	8	13	32.96	*/1.10	*/1.29	.051286	*/1.38	*/2.51
21	8	10	30.06	*/1.12	*/1.29	.058884	*/1.38	*/2.34
21	11	13	35.32	*/1.12	*/1.29	.050119	*/1.55	*/2.75
24	8	13	33.73	*/1.10	*/1.29	.045709	*/1.38	*/2.57
24	8	10	32.21	*/1.10	*/1.29	.045709	*/1.38	*/2.45
24	11	13	34.52	*/1.12	*/1.29	.051286	*/1.51	*/2.69
31	8	13	39.63	*/1.05	*/1.29	.042658	*/1.15	*/2.29
31	8	10	35.32	*/1.12	*/1.29	.045709	*/1.38	*/2.24
31	11	13	42.46	*/1.10	*/1.29	.044668	*/1.45	*/2.51
32	8	13	37.85	*/1.07	*/1.29	.050119	*/1.26	*/2.24
32	8	10	36.14	*/1.10	*/1.29	.048978	*/1.32	*/2.14
32	11	13	39.63	*/1.10	*/1.29	.054954	*/1.38	*/2.34

NC = not calculated

\*/ = multiplied or divided by



**Table B.7 Calculated storage coefficients and transmissivities  
for Aquifer Test 2 for Pulses 15 to 20**

Well	Pulses		Transmissivity			Storage Coefficient		
	From	To	Value	10%	20%	Value	10%	20%
3	15	20	80.91	*/1.10	*/1.29	.034674	*/1.41	*/2.75
3	15	17	73.79	*/1.12	*/1.29	.034674	*/1.58	*/2.75
3	18	20	88.72	*/1.12	*/1.29	.036308	*/1.70	*/2.95
7	15	20	61.38	*/1.10	*/1.29	.021878	*/1.45	*/2.88
7	15	17	52.24	*/1.12	*/1.29	.025704	*/1.55	*/2.69
7	18	20	53.46	*/1.12	*/1.29	.036308	*/1.55	*/2.63
10	15	20	44.46	NC	NC	.077625	NC	NC
10	15	17	62.81	NC	*/1.26	.058884	NC	*/2.69
10	18	20	37.85	*/1.10	*/1.26	.064565	*/1.55	*/3.09
11	15	20	40.55	*/1.10	*/1.26	.012303	*/1.55	*/3.72
11	15	17	37.85	*/1.10	*/1.26	.015136	*/1.66	*/3.72
11	18	20	42.46	*/1.10	*/1.26	.012023	*/1.58	*/3.98
12	15	20	51.05	NC	NC	.008318	NC	NC
12	15	17	44.46	NC	NC	.014454	NC	NC
12	18	20	57.28	NC	NC	.004169	NC	NC
13	15	20	33.73	*/1.10	*/1.23	.000550	*/2.45	*/8.71
13	15	17	31.48	*/1.10	*/1.23	.000955	*/2.29	*/7.59
13	18	20	34.52	*/1.10	*/1.23	.000437	*/2.82	*/10.1
16	15	20	39.63	*/1.10	*/1.23	.000102	*/2.57	*/10.3
16	15	17	37.85	*/1.07	*/1.23	.000135	*/2.45	*/10.5
16	18	20	42.46	*/1.10	*/1.23	.000054	*/2.88	*/10.5
18	15	20	67.30	*/1.05	*/1.26	.009333	*/1.26	*/3.55
18	15	17	58.62	*/1.12	*/1.26	.011749	*/1.74	*/3.89
18	18	20	72.11	*/1.07	*/1.26	.008710	*/1.38	*/3.80
21	15	20	67.30	NC	NC	.031623	NC	NC
21	15	17	52.24	*/1.12	*/1.26	.035481	*/1.62	*/3.16
21	18	20	82.80	NC	*/1.23	.034674	NC	*/3.02
24	15	20	37.85	*/1.12	*/1.26	.038905	*/1.62	*/3.09
24	15	17	36.98	*/1.12	*/1.26	.039811	*/1.66	*/3.02
24	18	20	38.73	*/1.12	*/1.26	.040738	*/1.66	*/3.16

31	15	20	53.46	*/1.12	*/1.29	.037154	*/1.62	*/2.88
31	15	17	52.24	*/1.12	*/1.29	.038019	*/1.62	*/2.88
31	18	20	54.70	*/1.12	*/1.29	.037154	*/1.66	*/2.95
32	15	20	47.64	*/1.12	*/1.29	.038019	*/1.55	*/2.69
32	15	17	44.46	*/1.12	*/1.29	.039811	*/1.51	*/2.63
32	18	20	47.64	*/1.12	*/1.29	.044668	*/1.58	*/2.69

NC = not calculated

\* / = multiplied or divided by

**Table B.8 Observations from the from experimental and WELLTEST drawdown data sets Aquifer Test 2**

- 1 Although 7 pulses exist in each figure, only 6 pulses are used in the data analyses. For each of the three curve fits, the predicted well response is made for all 7 pulses.
- 2 Most of the cumulative drawdown measurements are less than 0.20 meter; for ten of the plots the greatest measured drawdown is less than 0.1 meter.
- 3 The water level responds almost immediately after a change in the pumping schedule.
- 4 A spike (an unexpectedly large recovery) in the drawdown values occurred at Well 30 after the fourth pulse.
- 5 The cyclic response at Wells 8, 10, and 12 has considerably more scatter than the patterns for the other wells.
- 6 The WELLTEST curve for the group of 6 pulses fits the experimental data acceptably for Pulses 1-7 and 15-20. For Pulses 8-14, the first 3 pulses match the WELLTEST curves but the last 4 pulses do not. In general, the observed drawdown response to the last 4 pulses is less than one would predict from the WELLTEST simulation.

Observation 1 is intended to clarify that the seventh pulse in each group of pulses was not used in the curve fitting procedure. Observations 2 and 3 demonstrate the necessity for reliable transducers and data logging equipment. Observation 4 relates to the diagnosis of

the spike after Pulse 4. The spike was caused by runoff from a rain event draining beneath faulty grout seals at Well 30. This discovery prompted the regrouting at Well 30 before Aquifer Test 3. Observation 5 indicates that natural phenomena or anthropogenic effects in the vicinity of Wells 8, 10, and 12 may have led to the nonclassical behavior at each of these wells.

Observation 6 indicates that sometime between the tenth and the eleventh pulse (3.1 days into the test), a change in the aquifer response occurred. The change may have been caused by the effects of boundary condition(s) or by the improper detrending of the experimental data. The latter reason, however, does not seem plausible because the detrending adjustment between the tenth and the eleventh pulse is less than 0.002 m/day. The reason for the change in the well responses has not been investigated, but is speculated to be caused either by an area of high hydraulic conductivity near the boundaries of the well network or by a delayed drainage from low permeability materials within the boundaries of the well network.

Because of the concern over the effects of boundary conditions after Pulse 11, none of the data after Pulse 11 is considered reliable. For the second set of pulses, only the hydraulic properties calculated for Pulses 8-10 are used. An examination of the data generated for Pulses 1-6 indicates a possible difference between Pulses 1-3 and Pulses 3-6. However, the importance of the trend does not seem significant because the transmissivities and storage coefficients calculated for Pulses 1-6 are typically within 10 percent of the values calculated for Pulses 1-3. Hence, the values calculated for Pulses 1-6 are used. Table B.9 lists the values calculated by the program WELLTEST for Aquifer Test 2.

**Table B.9 WELLTEST calculated storage coefficients and transmissivities for Aquifer Test 2**

Well	T (cm <sup>2</sup> /s)	S (-)	Well	T (cm <sup>2</sup> /s)	S (-)
1	58.6	0.0214	15	32.2	.0123
2	42.5	0.0540	16	29.4	.000603
3	NC	NC	17	26.8	.00813
4	29.4	0.0407	18	43.5	.0200
5	NC	NC	19	25.0	.00257
6	32.2	0.0204	20	26.2	.00603
7	NC	NC	21	30.1	.0589
8	20.8	0.0141	24	32.2	.0457
9	37.9	0.0282	25	29.4	.0933
10	44.5	0.071	26	29.4	.0575
11	32.2	0.021	30	12.3	.0148
12	19.9	0.030	31	35.3	.0457
13	25.6	0.00178	32	36.1	.0490
14	27.4	0.00525			

NC = not calculated

The arithmetic and the geometric means for the 24 transmissivity values in Table 16 are 32 and 30 cm<sup>2</sup>/s, respectively (within 27 percent of values from Test 1). In general, little variations exists among the different values; their standard deviation is 9.4 cm<sup>2</sup>/s and all except 4 values are within 35 percent of the arithmetic average. The variations in the transmissivities indicate high values in the western region (at Wells 1, 2, and 18) and low values scattered through the well network (at Wells 8, 30, 12, 16, and 19).

The arithmetic value for the storage coefficients is 0.030. The values of storage coefficients have considerable variability and range over approximately two orders of

magnitude. No clear trend seems to exist in the location of high storage coefficient values, but a trend exists with the low storage coefficient values. The lowest storage coefficient values ( $<0.01$ ) are found near Well 5.

## **B.5 AQUIFER TEST 3**

### **B.5.1 Test Description**

Aquifer Test 3 included pumping Well 5 at a constant rate and measuring the drawdown in all 37 wells. The pumping began on 30 June 1989 at 0936 and ended on 7 July 1989 at 1614. The pump ran continuously for 628,473 seconds (7.27 days). A mechanical flowmeter was used to measure the cumulative discharge during the test (the flowmeter's calibration was checked at the Engineering Laboratory after the test and found to be within 1 percent). Based on the flowmeter's readings, the pumping rate declined from an initial rate of 121 L/min to a final rate of 110.5 L/min. Table B.10 lists the history of the discharge rate.

Drawdown measurements were made in all wells with an electric tape during the pumping period. During the first several hours of pumping, the wells near the pumping well were intensively monitored. Approximately 5 hours into the test, the first set of measurements at all 37 wells were made. Subsequent surveys were made periodically throughout the test with at least one survey each day. During the test, measurements were taken at eight wells located several hundred meters away from the site to estimate the naturally occurring fluctuations in the water table.

**Table B.10 Measurements of the discharge rate for Aquifer Test 3**

<b>Date</b>	<b>Time</b>	<b>Cumulative Seconds</b>	<b>Average Discharge (L/min)</b>
6/30/89	9:36	16,080	121.1
6/30/89	14:04	95,940	121.1
7/1/89	12:15	197,220	117.0
7/2/89	16:23	280,380	113.6
7/3/89	15:29	364,620	111.7
7/4/89	14:53	397,440	110.9
7/5/89	12:55	443,940	110.9
7/6/89	14:38	536,520	110.5
7/7/89	10:31	608,100	110.5

A total of 13 pressure transducers were used for the pumping tests in order to get continuous drawdown measurements. These transducers were placed into Wells 1, 2, 4, 5, 6, 8, 14, 17, 20, 25, 26, 30, and 31. For the first 3 hours of the pumping tests, transducer measurements were recorded every 2 seconds. Thereafter measurements were recorded every 2 minutes until the pumping ceased. At the end of pumping, measurements of the water table recovery were taken every 2 seconds for approximately 3 hours, after which measurements were taken every 2 minutes.

Before the water table data was analyzed, the trend in the natural water table fluctuations was removed. As a check on the consistency between the transducer and the manual measurements, the two data sets were compared. The comparison showed good agreement between the data sets except for Well 6. At Well 6, the two data sets showed the

same slope but the transducer data had values that were 0.06 meters greater. The discrepancy is believed to have been caused by an incorrect initial manual measurement at Well 6.

Figure B.13 shows contours for the cone-of-depression at elapsed times of 19,500 seconds (0.22 days); 95,000 seconds (1.1 days); 190,600 seconds (2.2 days); and 438,600 seconds (5.1 days). The figure shows: (1) at early times the cone-of-depression extends the farthest in the west and southwest regions; (2) at late times the cone-of-depression extends appreciably farther in the east than to the west; (3) the configuration of the cone-of-depression changes slightly between 190,600 and 438,600 seconds; (4) between time 190,600 and 438,600 seconds, the cone-of-depression has increased in the eastern region of the well network but decreased slightly in the western region of the well network.

The trend in the pressure gradients in Figure B.13 agrees with the trends shown for Aquifer Test 1 in Figure B.3. As previously mentioned, one interpretation of this trend is that zones of highest diffusivities exist in the western region. The two figures show asymmetry contours that suggest large-scale heterogeneities in the aquifer. Unlike Figure B.3, Figure B.15 shows that at late times slight changes exist in the configurations of the cone-of-depression. One unexpected trend was the slight decrease in the drawdowns at Wells 1 and 3 between 190,600 and 438,600 seconds.

Several possible explanations exist for the slight decline in drawdowns at the western wells for late times. First, the decreases may have resulted from the gradual decrease in the pumping rate. However, the average pumping rate during this interval dropped only 3 percent. This change in pumping caused a 0.03-meter increase in the water table at the pumped well between 350,000 and 438,600 seconds. The predicted change at Wells 1 and

3 is negligible. Second, the decreases may have resulted from the method used to detrend the data. It is possible that less drawdown occurred at Wells 1 and 3, rather than at the other wells, because of natural temporal and spatial groundwater fluctuations. Third, the decreases may have resulted from equilibration processes acting within the aquifer. Over time, the hydraulic head gradients change which results in flow pattern changes to the pumped well.

### **B.5.2 Transmissivities and Storage Coefficients From Program WELLTEST**

The WELLTEST program was used to determine transmissivity and storage coefficient values at the locations of the twelve observation wells equipped with transducers. Input to WELLTEST included the pumping schedule in Table B.10, a saturated thickness of 7 meters, and an unconfined aquifer. WELLTEST was applied to data sets for 10,000; 50,000; 100,000; and 250,000 seconds in order to investigate the sensitivity of the calculated hydraulic parameters with respect to time.

A comparison between the predicted and the observed drawdown curves for all twelve wells for the four time periods is shown in Figures B.15 to B.18. For each of the figures, the predicted drawdown curve for each time period has been extrapolated to the end of the test to predict the final drawdowns. Several interesting features should be noted in the figures. First, as was true of Aquifer Tests 1 and 2, the drawdown response at Well 8 is very non-classical and cannot be adequately reproduced by WELLTEST. Second, the plotted data approximates a straight-line shortly after the pumping started to about 200,000 seconds. Third, after 200,000 seconds, some type of boundary condition, a delayed drainage



phenomena, and/or change in the pumping rate prevents additional drawdown at all of the wells.

Table B.11 lists the combination of transmissivity and storage coefficient values that provided the time-drawdown curve that best fit the observed time-drawdown curve as determined by the program WELLTEST. Included in Table B.11 are the factors by which the best value for either the transmissivity and the storage coefficient values can be multiplied or divided so that the calculated residual is increased to 0.10 and to 0.20. These adjustment factors are a measure of the sensitivity of the final answer to both transmissivity and the storage coefficient. No values are listed for a residual interval, when the "best" set of transmissivity and storage coefficient values lead to a residual that is greater than the designated residual. No results are provided for Wells 1 and 8 for times greater than 10,000 seconds because the residual calculated for the best set of transmissivity and storage coefficient values were greater than a residual of 20 percent.

The trends shown in Table B.11 are the same as those shown in Table B.2 for Aquifer Test 1. In general, as the time period increases the variability decreases, the average transmissivity decreases, and the average storage coefficient increases. For time periods of 10,000; 50,000; 100,000; and 250,000 seconds the average transmissivities (excluding Wells 1 and 8) are 102, 44, 40, and 36  $\text{cm}^2/\text{s}$ , respectively, and the average storage coefficients (excluding Wells 1 and 8) are 0.008, .029, .031, and .042, respectively. The trends in the transmissivities and storage coefficients are very similar to those observed for Aquifer Test 1.

**Table B.11 Calculated storage coefficients and transmissivities for Aquifer Test 3  
at 10,000; 50,000; 100,000; and 250,000 seconds**

Well	Time (seconds)	Transmissivity			Storage Coefficient		
		Value	10%	20%	Value	10%	20%
1	10K	345.16	*/1.10	*/1.29	.00537	*/1.35	*/2.24
2	10K	194.10	*/1.15	*/1.32	.01047	*/1.38	*/1.95
4	10K	203.24	*/1.12	*/1.29	.00288	*/1.62	*/2.57
6	10K	104.24	*/1.12	*/1.32	.00537	*/1.45	*/2.09
8	10K	88.72	*/1.15	*/1.32	.00776	*/1.35	*/1.91
14	10K	53.46	*/1.12	*/1.26	.00013	*/2.24	*/5.13
17	10K	77.27	*/1.12	*/1.26	.00048	*/1.86	*/3.63
20	10K	55.98	*/1.12	*/1.26	.00029	*/2.14	*/4.47
25	10K	54.70	*/1.15	*/1.32	.01413	*/1.41	*/2.00
26	10K	19.41	NC	*/1.29	.00708	NC	*/1.51
30	10K	95.06	*/1.12	*/1.29	.00126	*/1.70	*/2.95
31	10K	165.20	*/1.00	*/1.32	.03715	*/1.00	*/1.48
1	50K	-	NC	NC	-	NC	NC
2	50K	116.95	*/1.10	*/1.32	.01995	*/1.29	*/1.91
4	50K	29.38	NC	*/1.17	.07244	NC	*/1.15
6	50K	30.06	NC	*/1.32	.03715	NC	*/1.38
8	50K	-	NC	NC	-	NC	NC
14	50K	43.45	*/1.12	*/1.26	.00051	*/2.09	*/4.37
17	50K	35.32	*/1.07	*/1.29	.00912	*/1.29	*/2.09
20	50K	31.48	*/1.12	*/1.26	.00457	*/1.55	*/2.63
25	50K	36.14	*/1.12	*/1.32	.02884	*/1.29	*/1.82
26	50K	25.59	*/1.07	*/1.26	.00398	*/1.32	*/2.09
30	50K	43.45	*/1.10	*/1.29	.01318	*/1.29	*/1.86
31	50K	52.24	NC	*/1.35	.10000	NC	*/1.32
1	100K	-	NC	NC	-	NC	NC
2	100K	99.54	*/1.10	*/1.32	.03020	*/1.29	*/2.04
4	100K	36.14	*/1.07	*/1.32	.06026	*/1.12	*/1.55
6	100K	26.79	*/1.10	*/1.32	.04266	*/1.17	*/1.55
8	100K	-	NC	NC	-	NC	NC
14	100K	30.06	*/1.12	*/1.26	.00407	*/1.82	*/3.39

17	100K	23.34	*/1.07	*/1.26	.02512	*/1.17	*/1.86
20	100K	26.79	*/1.12	*/1.26	.00871	*/1.62	*/2.75
25	100K	42.46	*/1.12	*/1.29	.01995	*/1.48	*/2.29
26	100K	28.06	*/1.10	*/1.26	.00282	*/1.51	*/2.57
30	100K	37.85	*/1.12	*/1.29	.01862	*/1.38	*/2.09
31	100K	48.75	*/1.10	*/1.35	.10000	*/1.15	*/1.48
1	250K	-	NC	NC	-	NC	NC
2	250K	90.79	*/1.10	*/1.29	.03715	*/1.38	*/2.34
4	250K	32.96	*/1.12	*/1.32	.06761	*/1.32	*/1.82
6	250K	28.06	*/1.12	*/1.32	.03890	*/1.38	*/1.95
8	250K	-	NC	NC	-	NC	NC
14	250K	28.71	*/1.12	*/1.26	.00513	*/1.95	*/3.98
17	250K	17.30	*/1.10	*/1.26	.05370	*/1.32	*/2.00
20	250K	25.00	*/1.12	*/1.26	.01148	*/1.74	*/3.16
25	250K	21.28	*/1.05	*/1.29	.10000	*/1.15	*/1.95
26	250K	30.06	*/1.12	*/1.26	.00219	*/1.78	*/3.39
30	250K	38.73	*/1.12	*/1.29	.01738	*/1.58	*/2.57
31	250K	43.45	*/1.12	*/1.32	.09550	*/1.26	*/1.78

K = 1,000

NC = not calculated

\*/ = multiplied or divided by

### B.5.3 Transmissivities by the Cooper-Jacob Straight-Line Method

The slopes of the time-drawdown curves were calculated as described in the discussion of Aquifer Test 1 data. The slopes were evaluated using data taken between 70,000 seconds and 200,000 seconds. At wells where transmissivities were calculated using both transducer and manual measurements, the transducer-based transmissivity estimate was

considered more accurate. Table B.12 lists the transmissivities calculated by the Cooper-Jacob straight-line method for Aquifer Test 3.

The arithmetic and the geometric means for the 27 transmissivity values in Table B.12 are 33 and 31  $\text{cm}^2/\text{s}$ , respectively. The standard deviation for the transmissivities is 12.9  $\text{cm}^2/\text{s}$ . The variations in the transmissivity indicate a region of high values in the western region (at Wells 1, 2, 3, and 18). Values of low transmissivity appear to be scattered throughout the well network.

**Table B.12 Transmissivities Calculated by the Cooper-Jacob Straight-Line Method for Aquifer Test 3**

Well	T ( $\text{cm}^2/\text{s}$ )	Well	T ( $\text{cm}^2/\text{s}$ )	Well	T ( $\text{cm}^2/\text{s}$ )
1	62	13	26	25	25
2	60	14	29	26	33
3	56	15	28	27	-
4	32	16	34	28	-
5	20	17	17	29	-
6	31	18	46	30	36
7	36	19	26	31	32
8	30	20	24	32	34
9	38	21	28	33	-
10	24	22	-	34	-
11	26	23	-	35	-
12	27	24	25	36	-

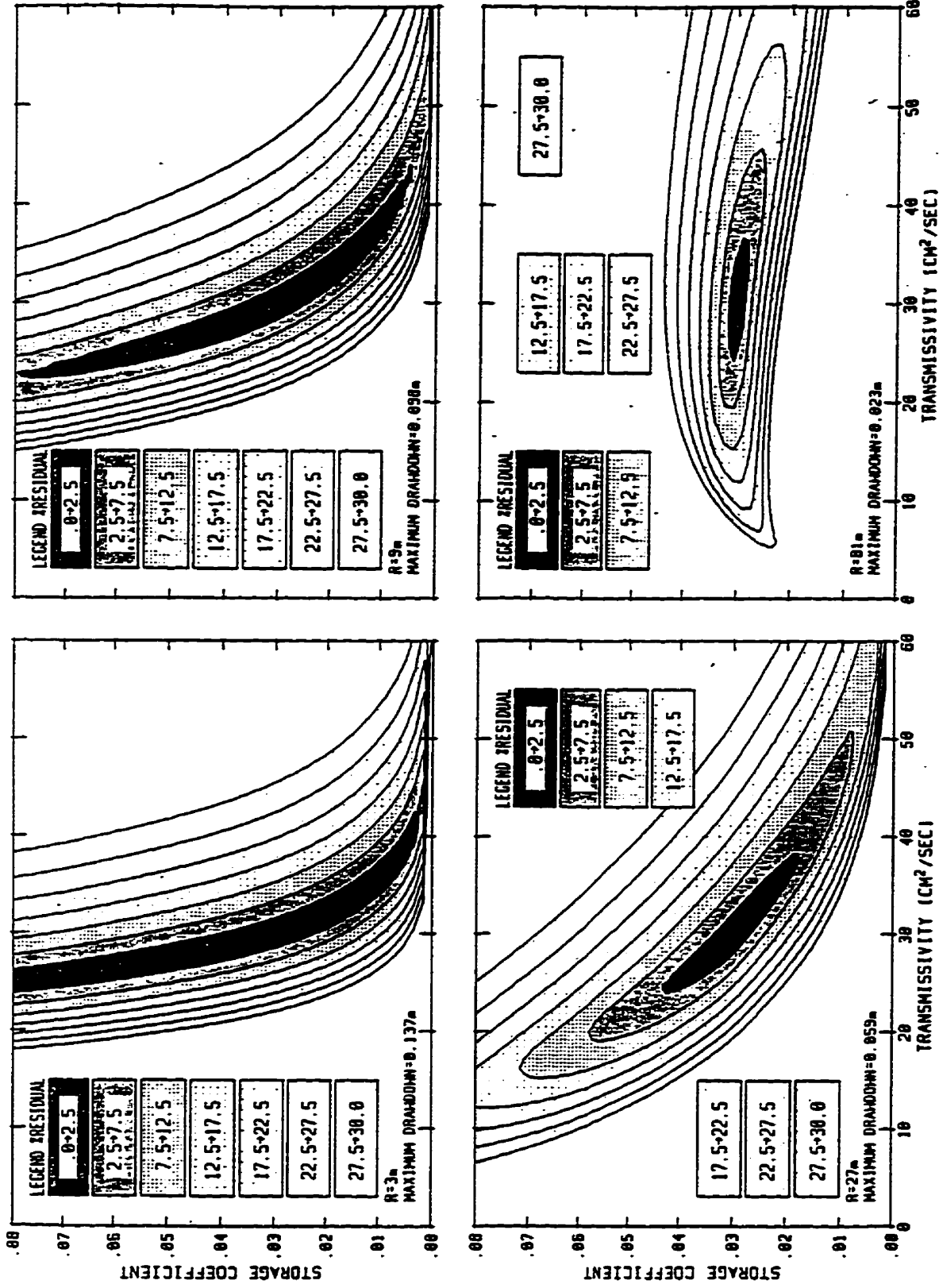


Figure B.1 WELLTEST Maps of the cumulative residual (as a percentage) for an aquifer test with constant pumpage in an idealized homogeneous aquifer with a transmissivity and a storage coefficient of 30 cm<sup>2</sup>/s and 0.03, respectively.

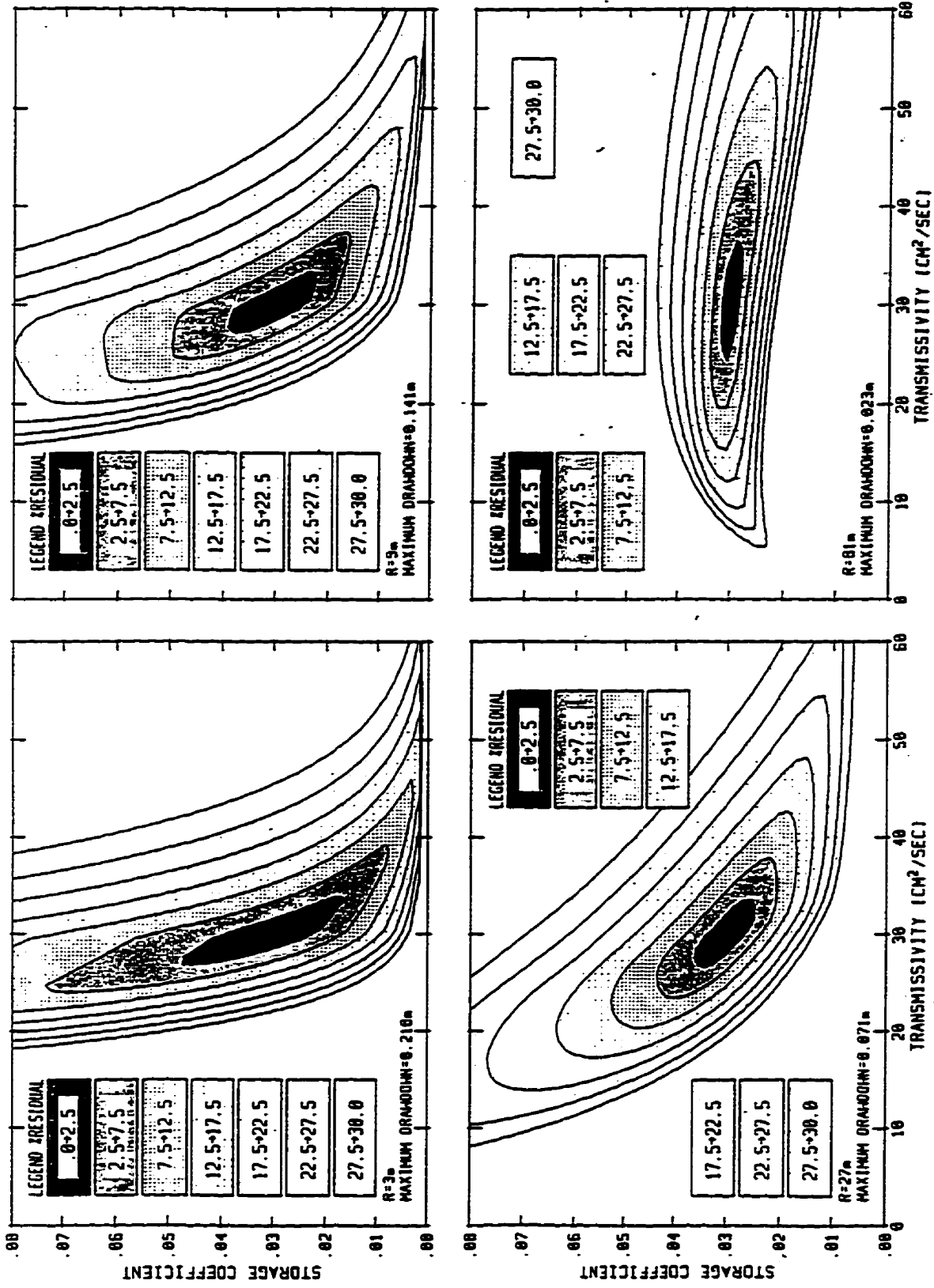


Figure B.2 WELLTEST Maps of the cumulative residual (as a percentage) for an aquifer test with pumpage at regulated intervals in an idealized homogeneous aquifer with a transmissivity and a storage coefficient of 30 cm<sup>2</sup>/s and 0.03, respectively.

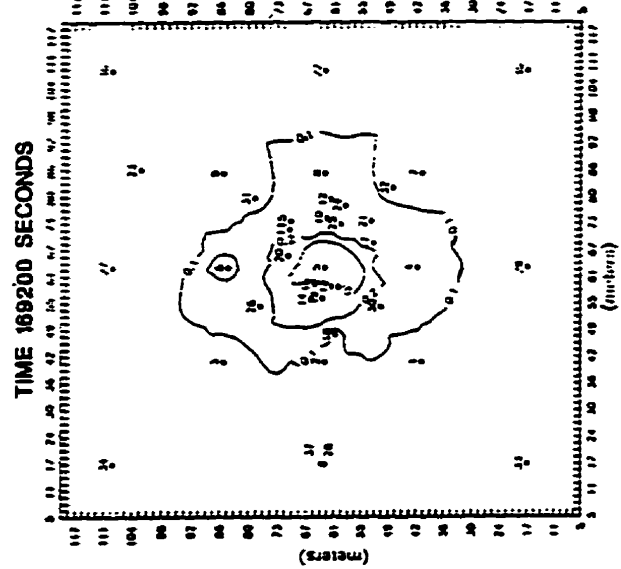
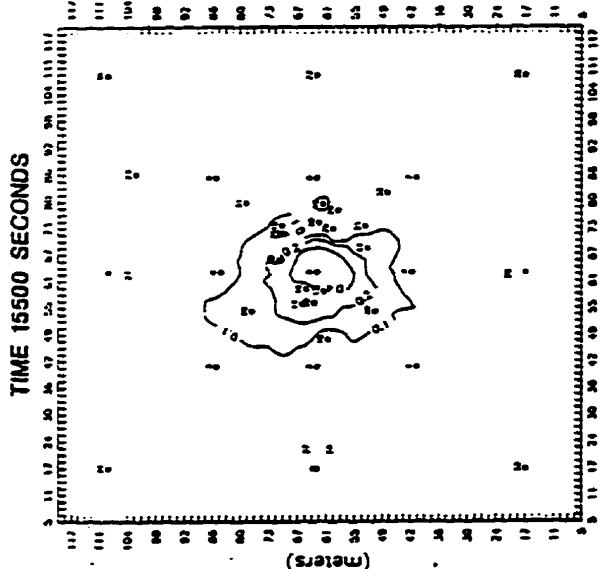
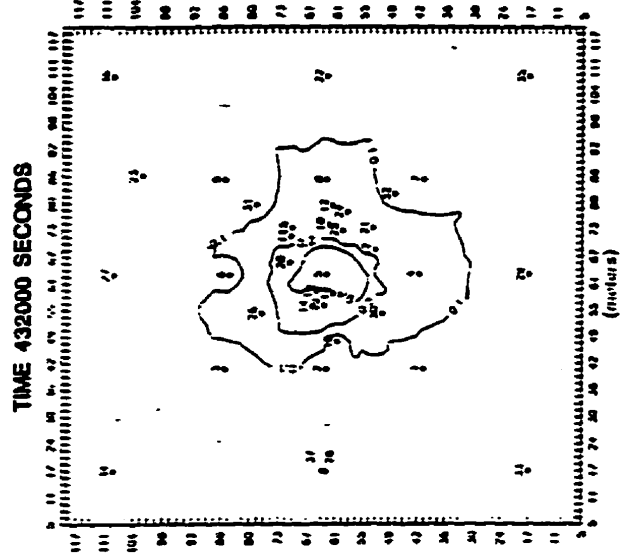
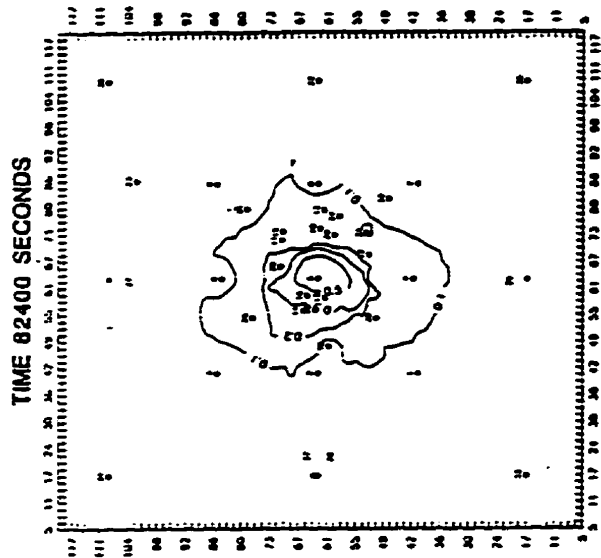


Figure B.3 The cone-of-depression for an Aquifer Test 1 at different times.

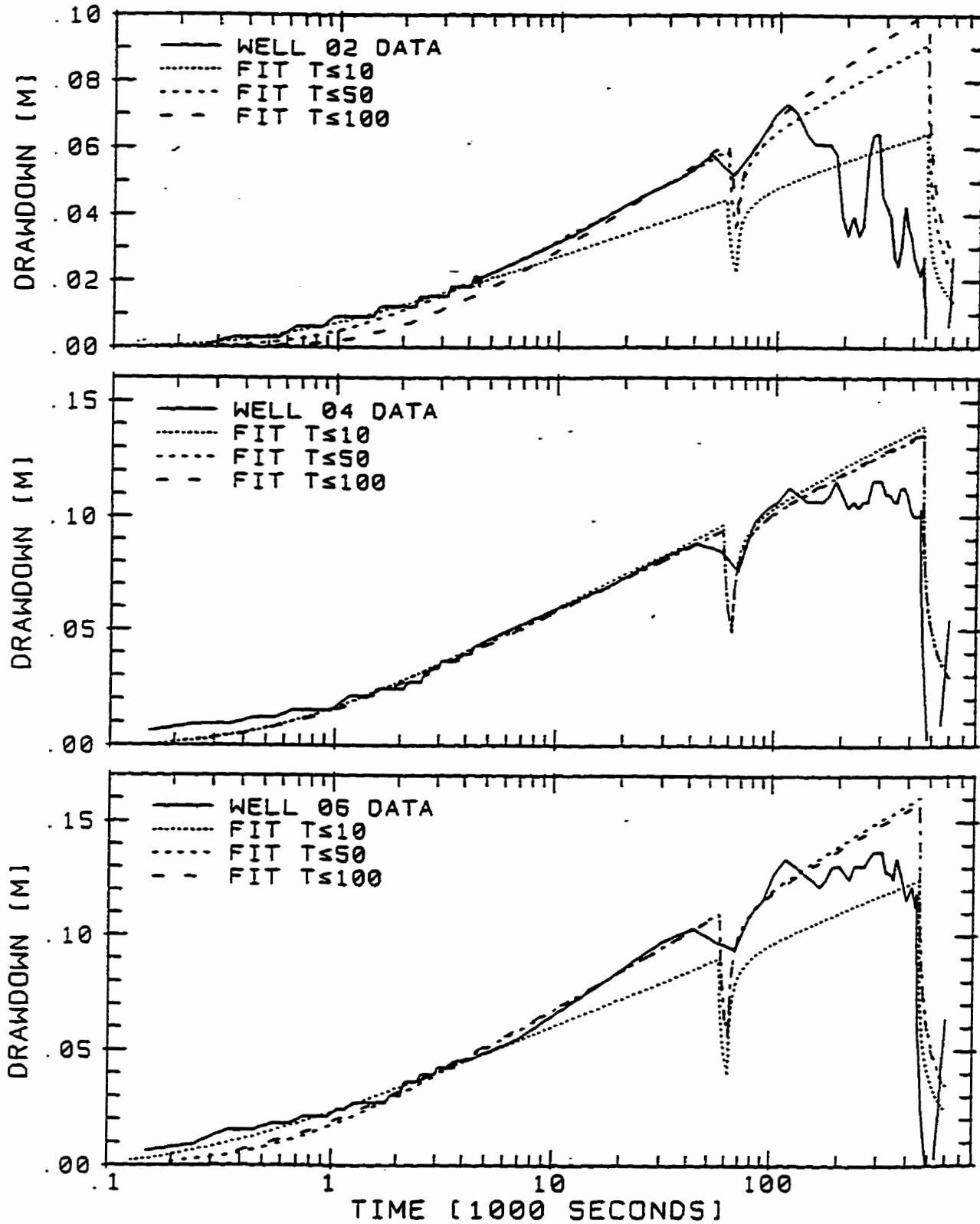


Figure B.4 WELLTEST Fits to Aquifer Test 1 drawdowns for Wells 2, 4, and 6.



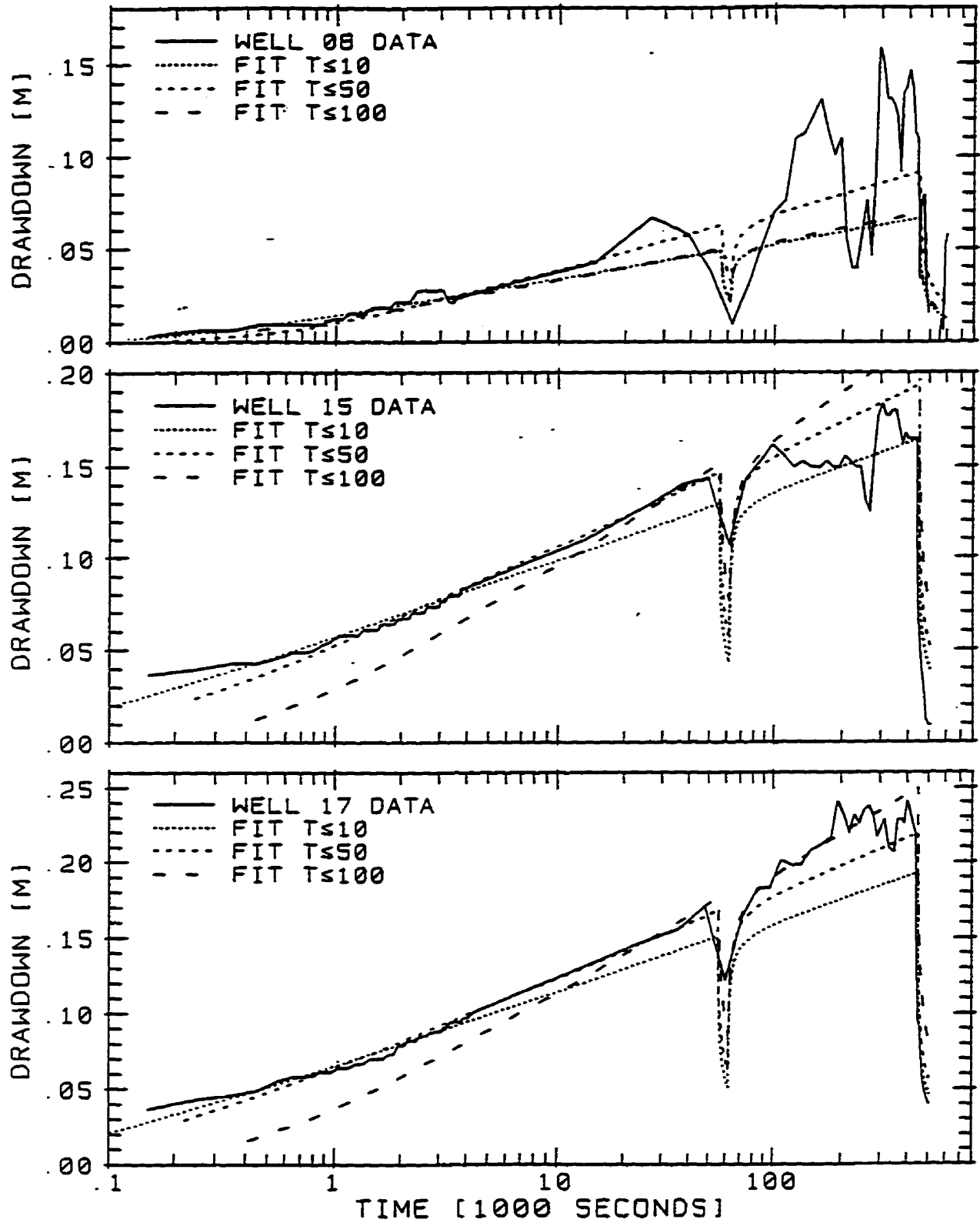


Figure B.5 WELLTEST Fits to Aquifer Test 1 drawdowns for Wells 8, 15, and 17.

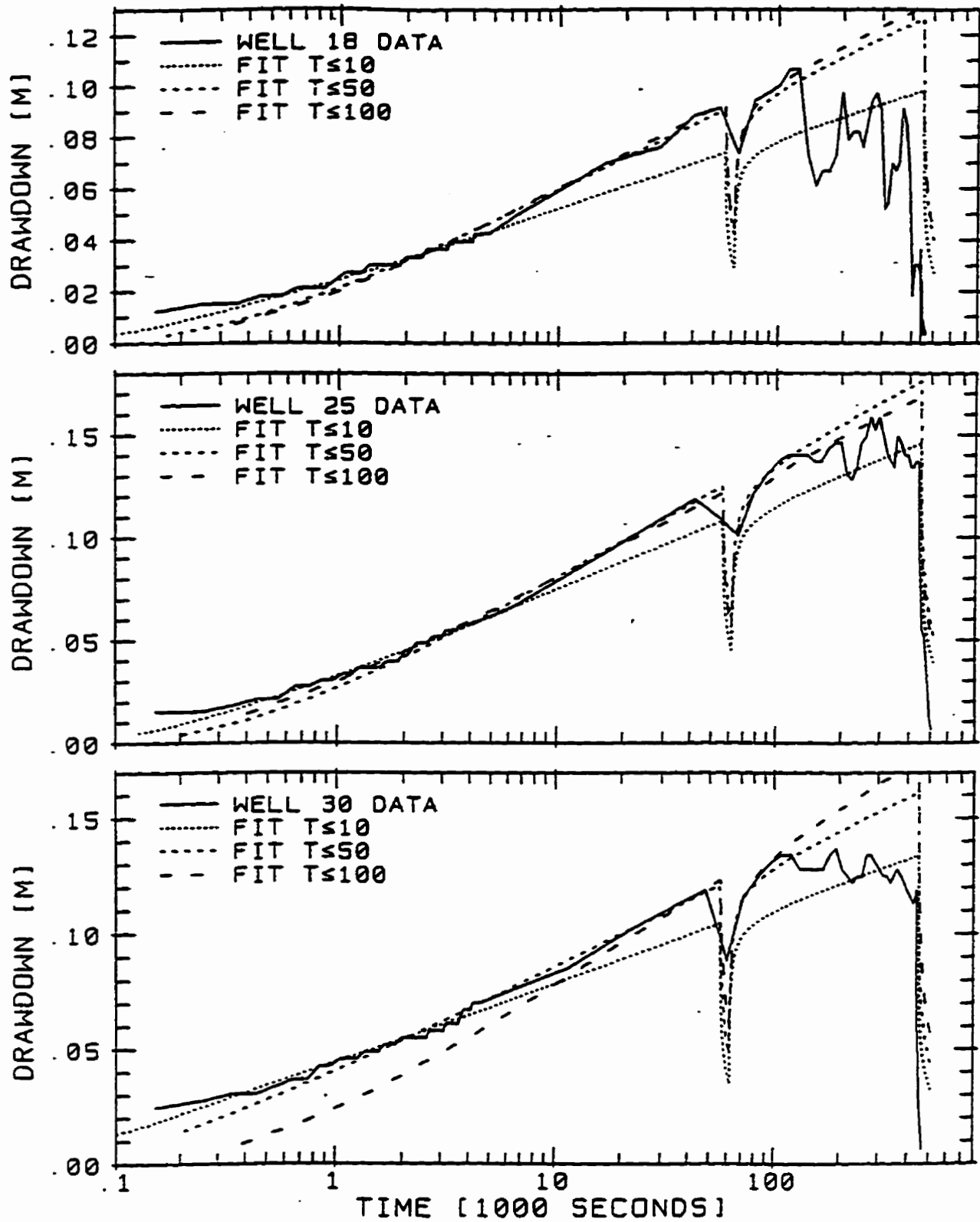


Figure B.6 WELLTEST Fits to Aquifer Test 1 drawdowns for Wells 18, 25, and 30.

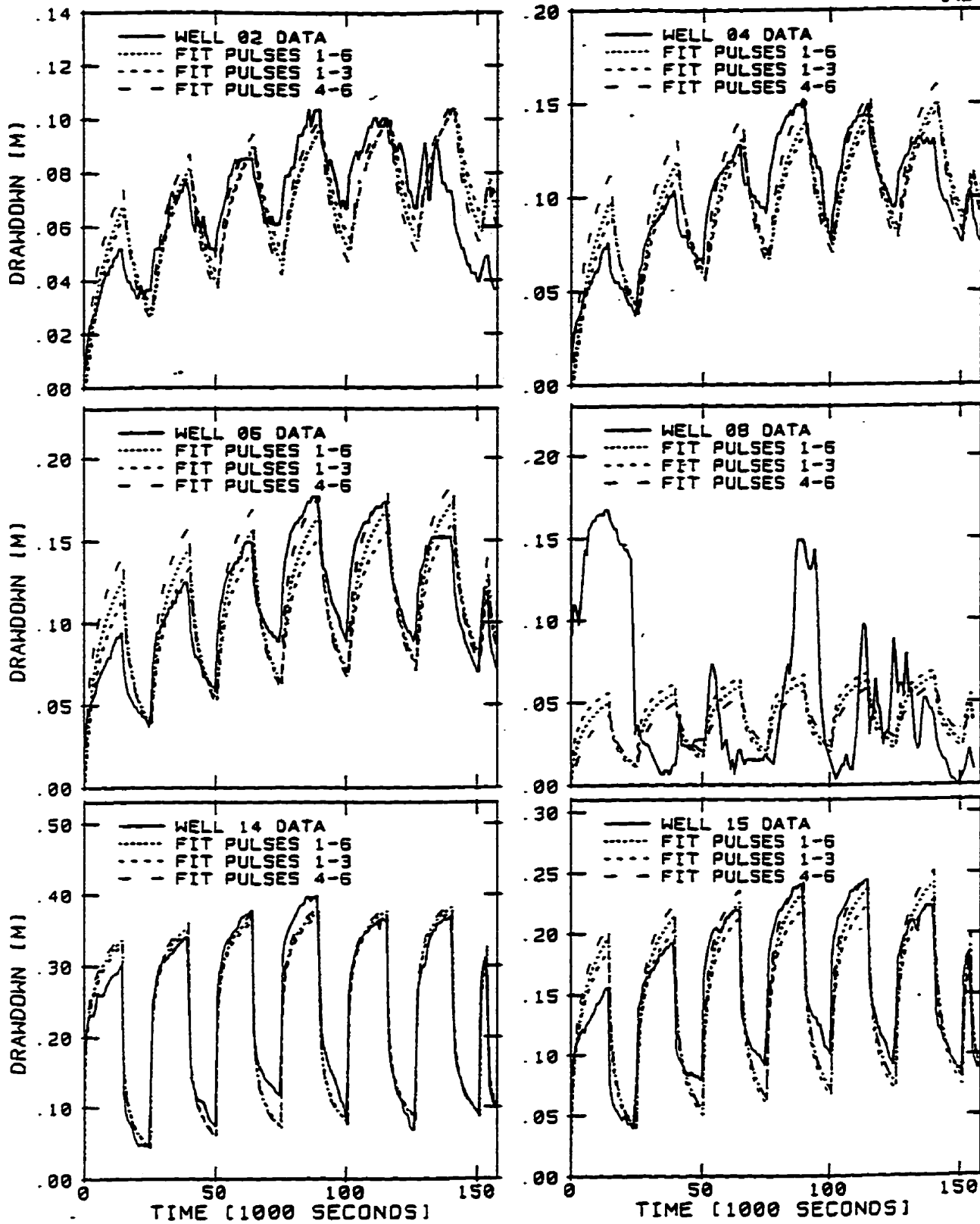


Figure B.7 WELLTEST Fits to Aquifer Test 2 drawdowns for Pulses 1 through 7 at Wells 2, 4, 6, 8, 14, and 15.

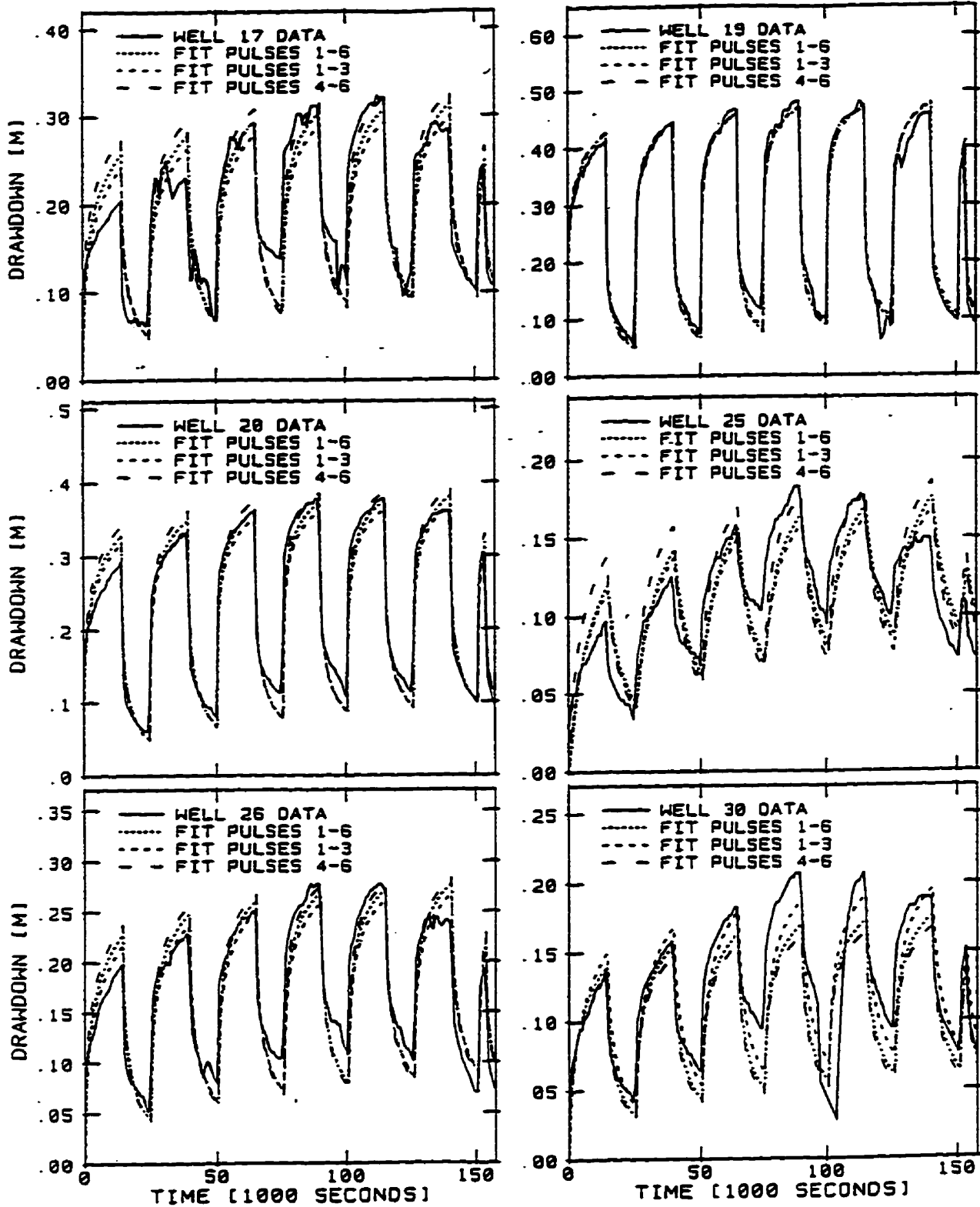


Figure B.8 WELLTEST Fits to Aquifer Test 2 drawdowns for Pulses 1 through 7 at Wells 17, 19, 20, 25, 26, and 30.

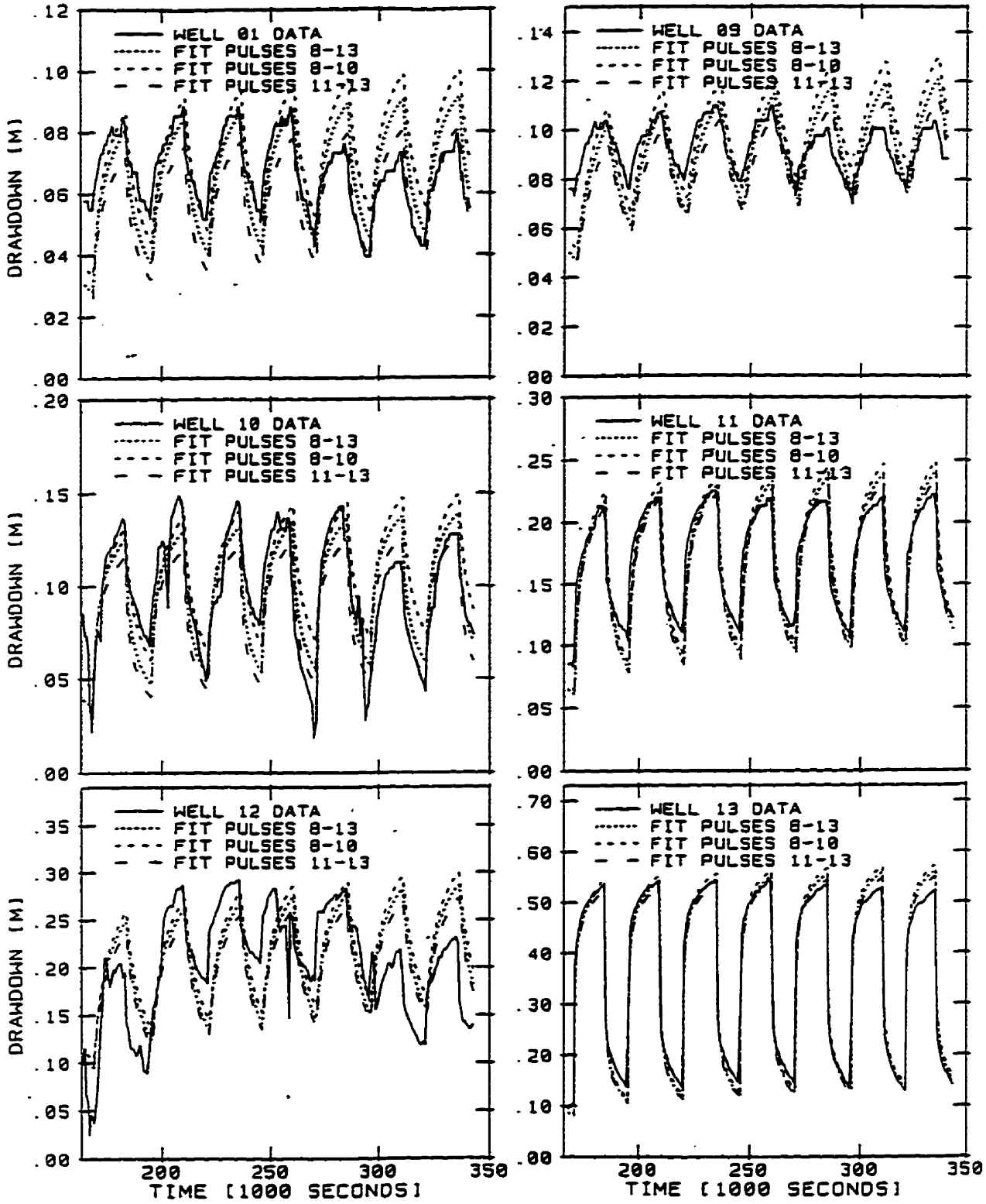


Figure B.9 WELLTEST Fits to Aquifer Test 2 drawdowns for Pulses 8 through 14 at Wells 1, 9, 10, 11, 12, and 13.

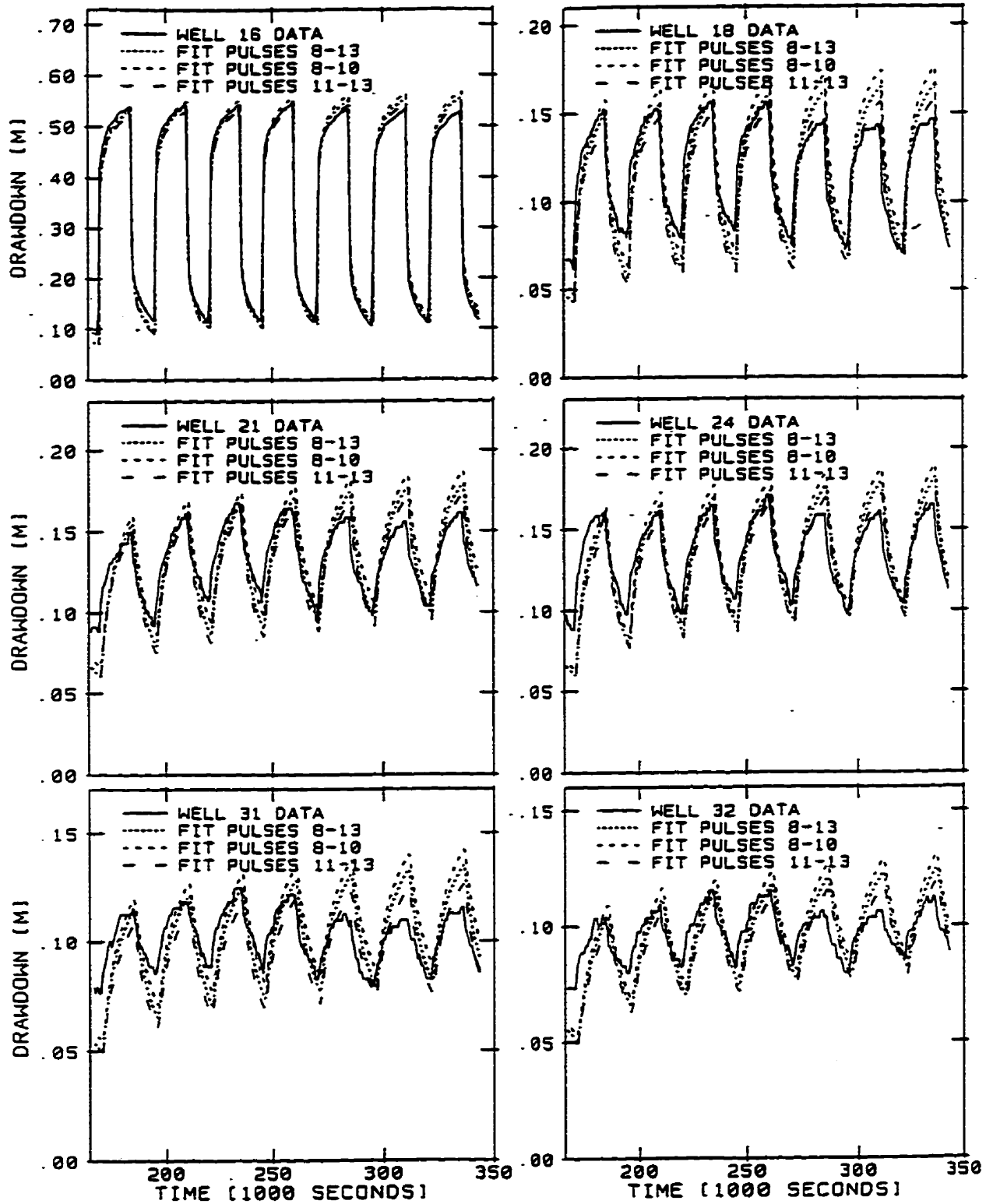


Figure B.10 WELLTEST Fits to Aquifer Test 2 drawdowns for Pulses 8 through 14 at Wells 16, 18, 21, 24, 31, and 32.

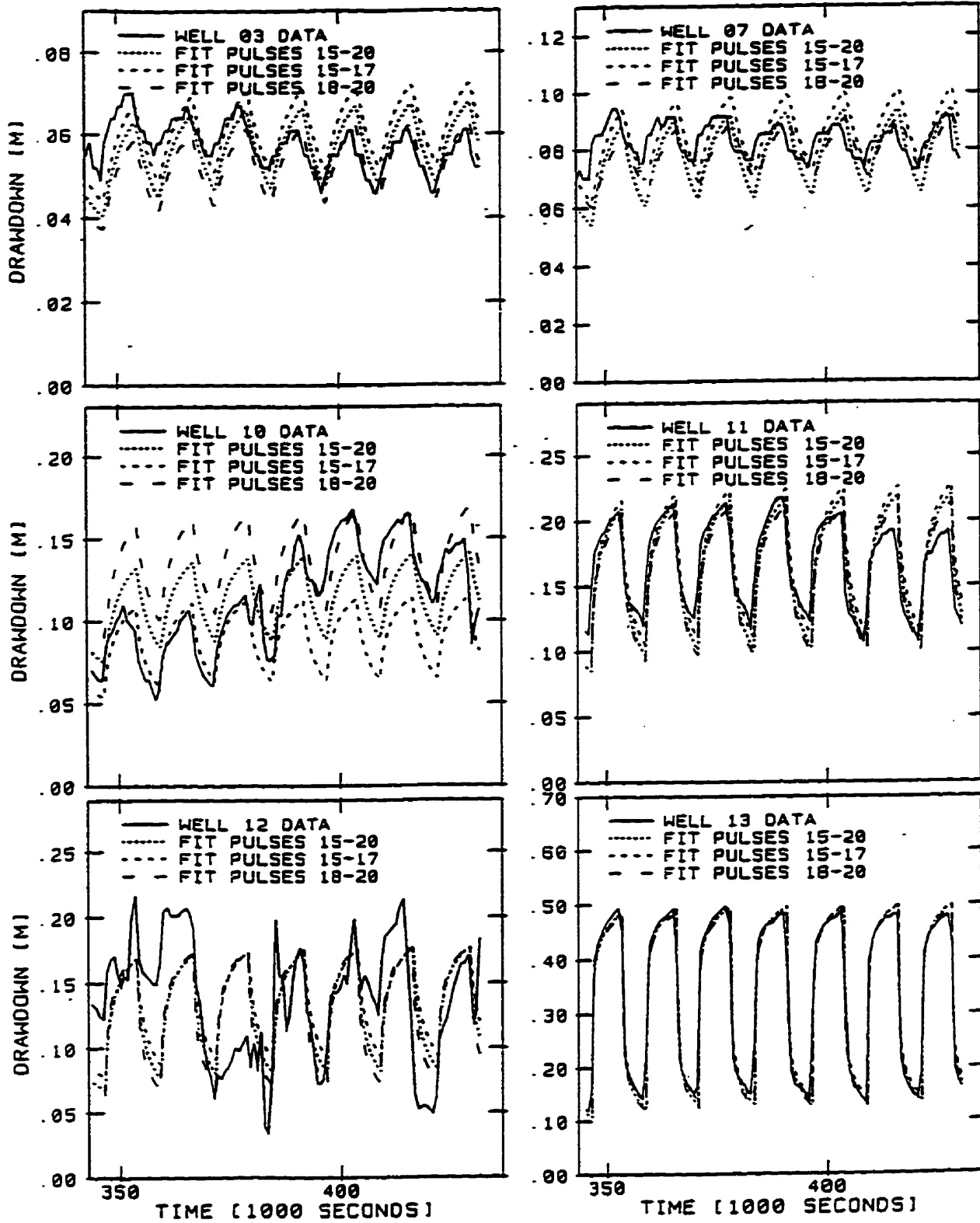


Figure B.11 WELLTST Fits to Aquifer Test 2 drawdowns for Pulses 15 through 21 at Wells 3, 7, 10, 11, 12, and 13.

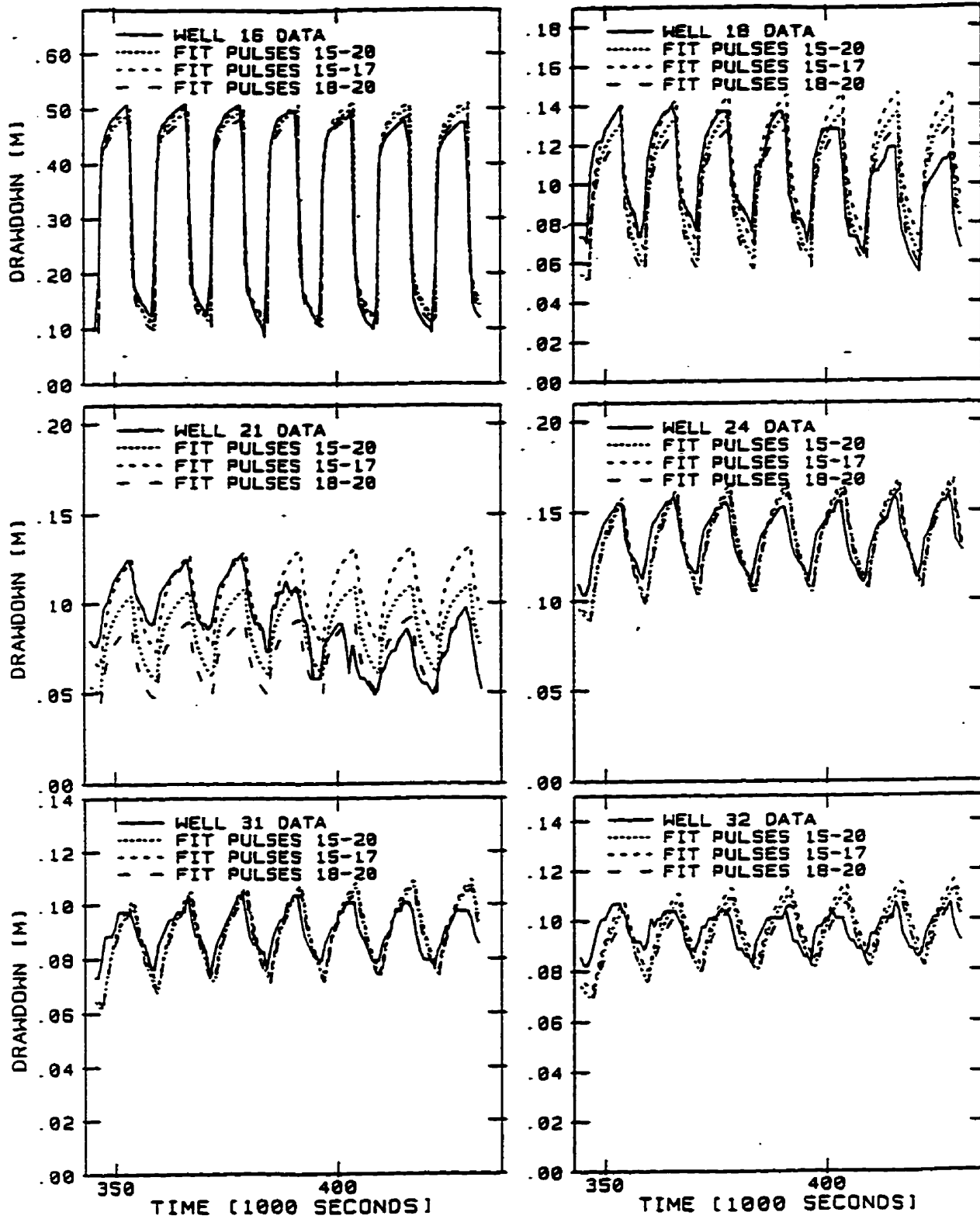


Figure B.12 WELLTST Fits to Aquifer Test 2 drawdowns for Pulses 15 through 21 at Wells 16, 18, 21, 24, 32, and 32.



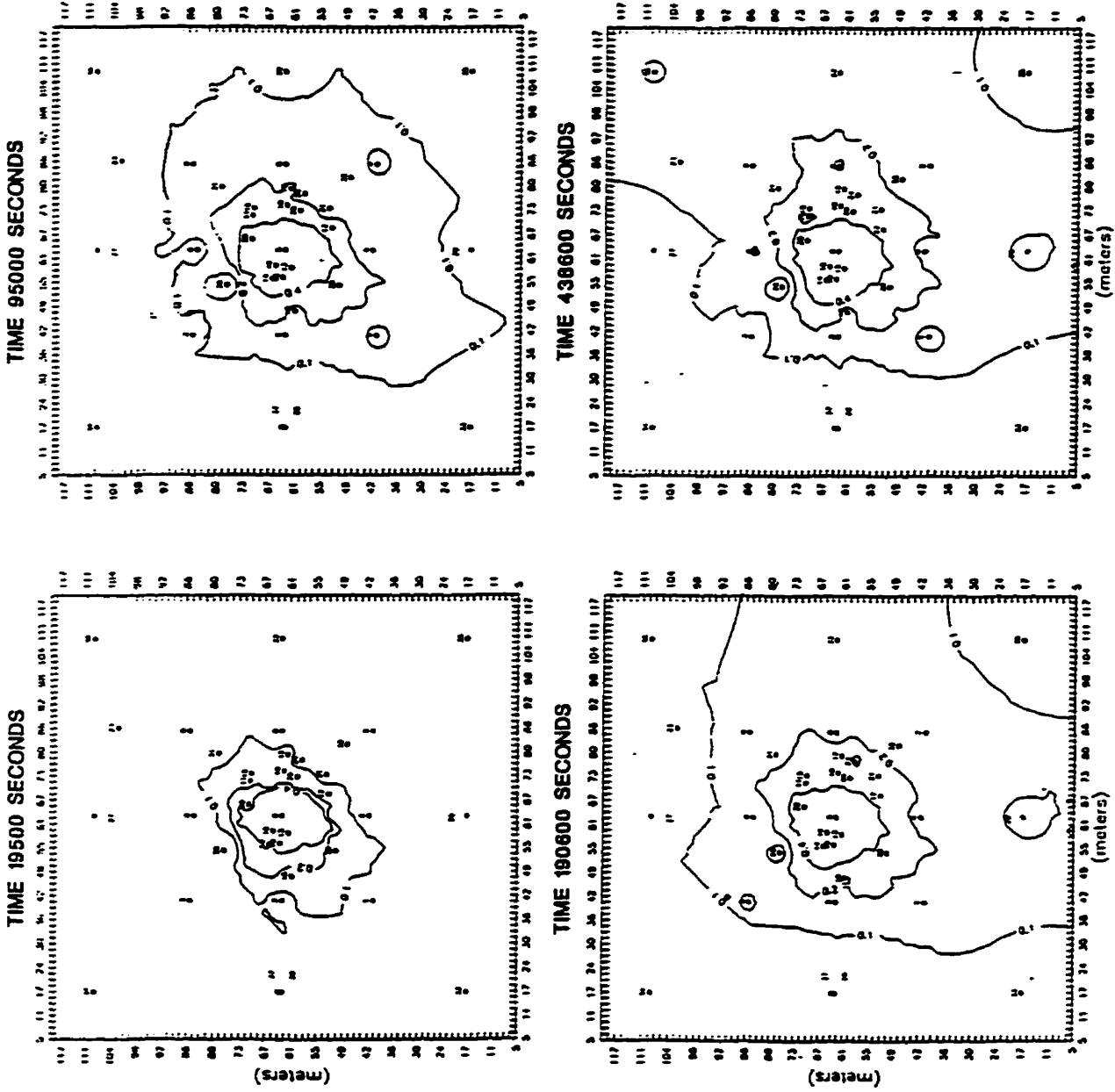


Figure B.13 The cone-of-depression for an Aquifer Test 3 at different times.

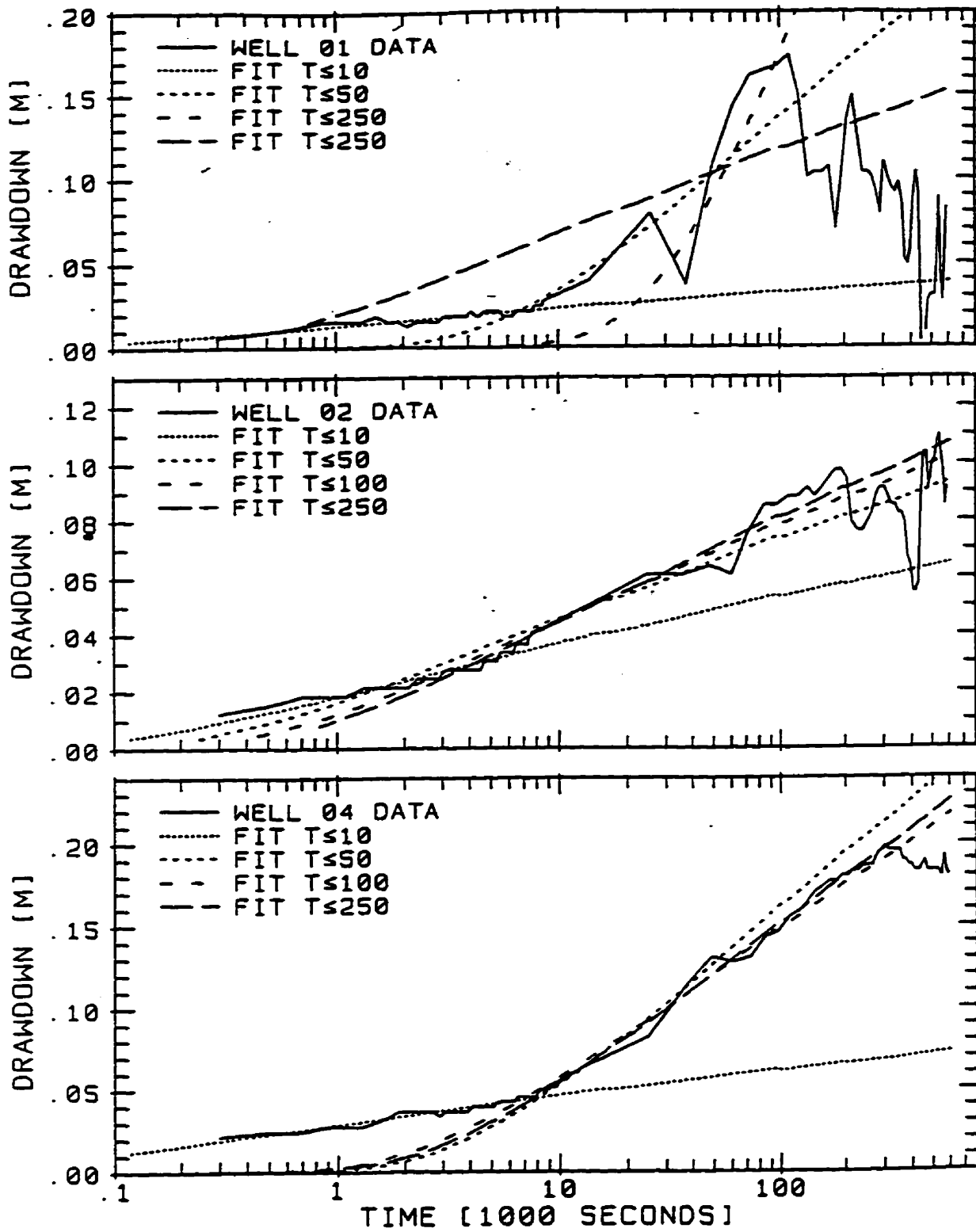


Figure B.14 WELLTST Fits to Aquifer Test 3 drawdowns for Wells 1, 2, and 4.

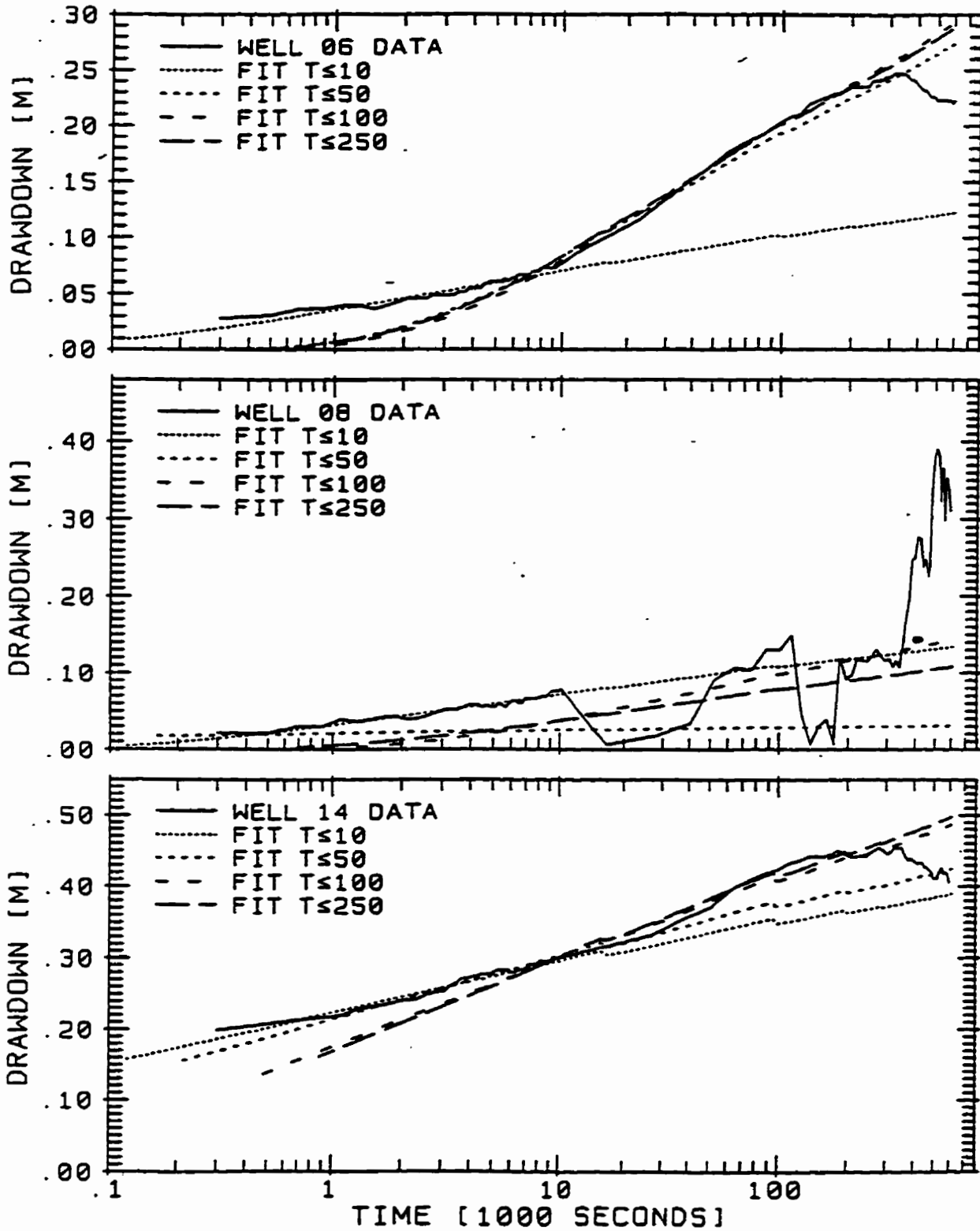


Figure B.15 WELLTEST Fits to Aquifer Test 3 drawdowns for Wells 6, 8, and 14.

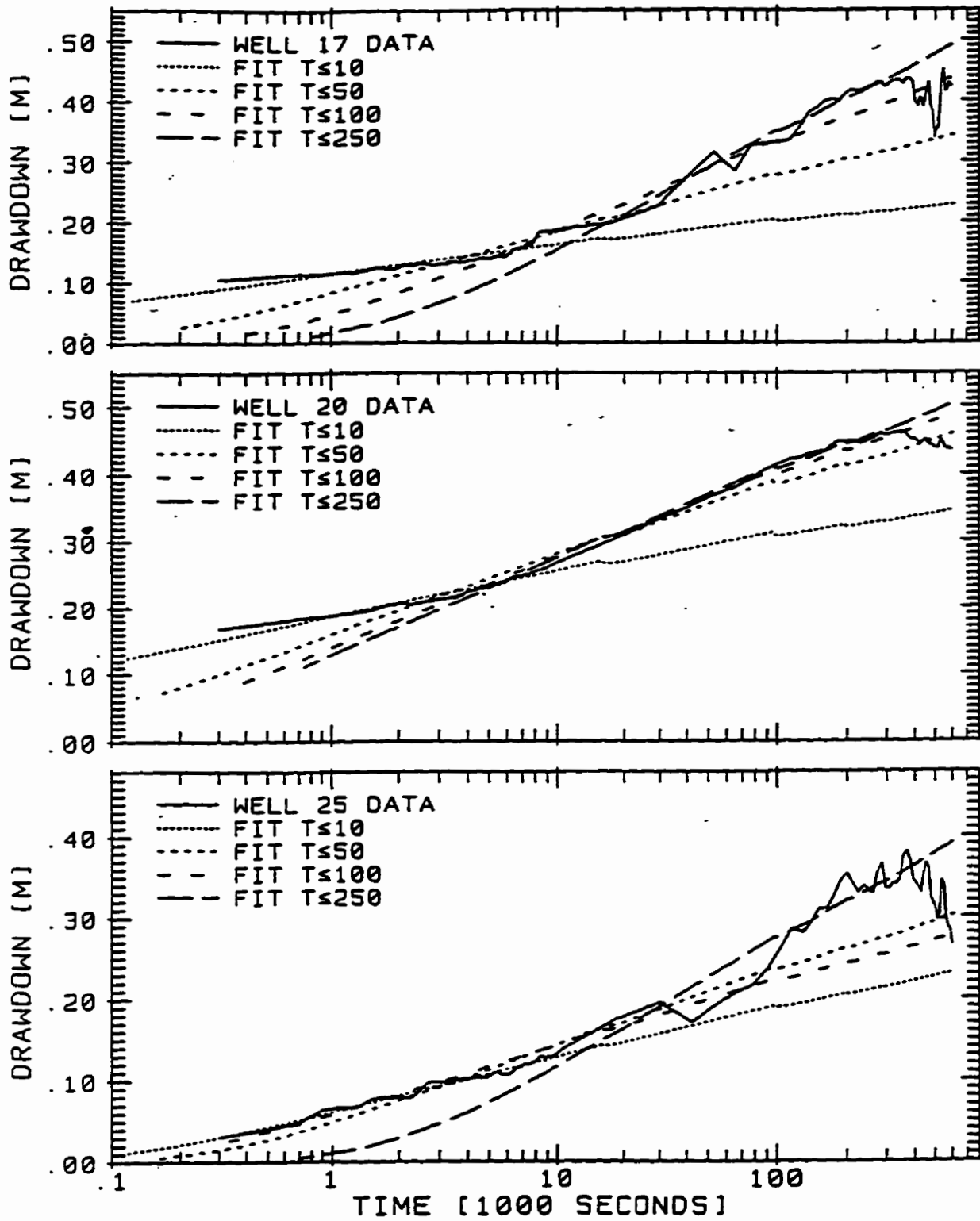


Figure B.16 WELLTTEST Fits to Aquifer Test 3 drawdowns for Wells 17, 20, and 25.

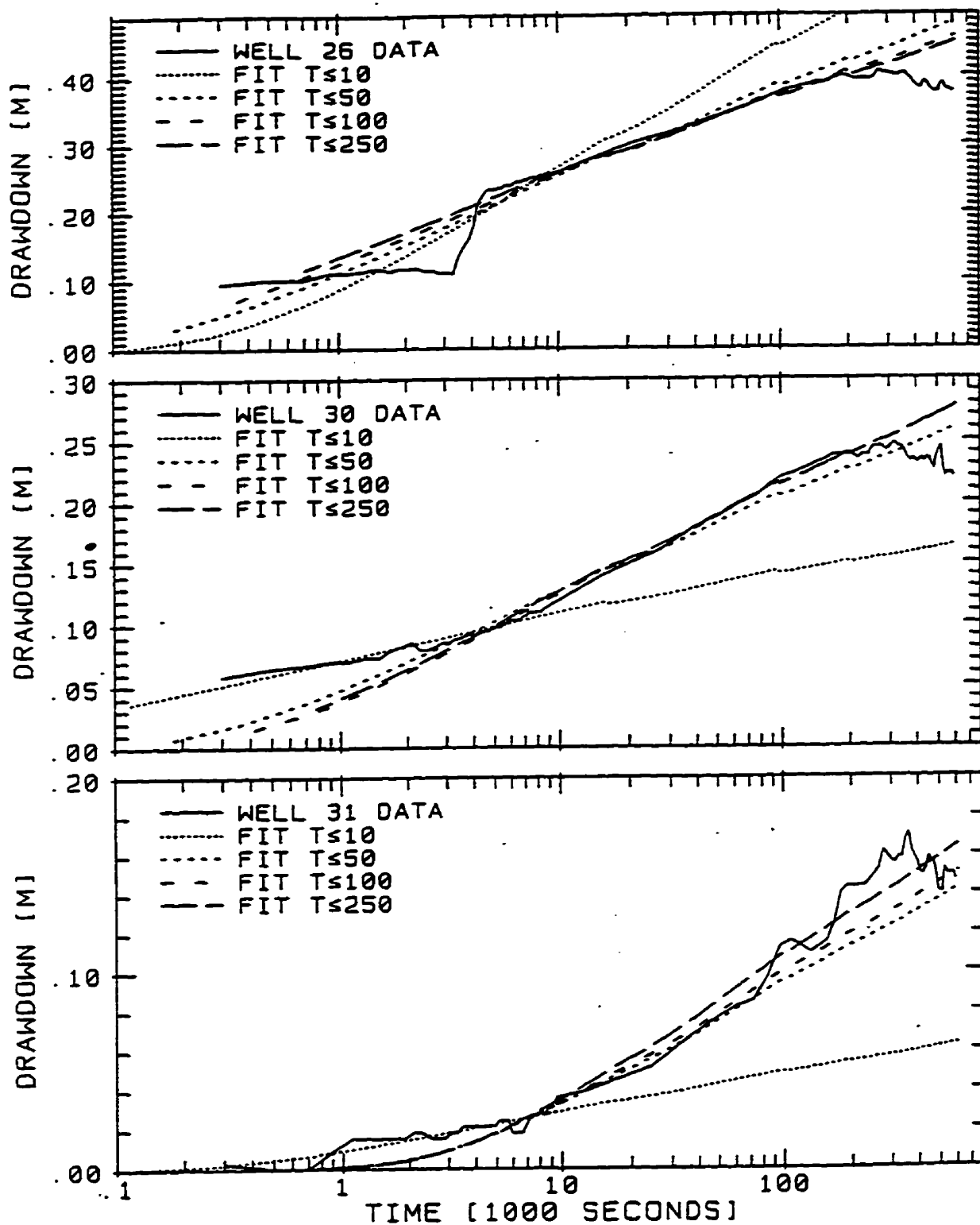


Figure B.17 WELLTST Fits to Aquifer Test 3 drawdowns for Wells 26, 30, and 31.

**APPENDIX C**  
**THE ELECTROMAGNETIC BOREHOLE FLOWMETER:**  
**DESCRIPTION AND APPLICATION**

**C.1 INTRODUCTION**

Borehole flowmeters are downhole tools that measure axial flow in a well or borehole. Profiles of axial flow during ambient conditions can help to determine the direction of the vertical hydraulic gradient, evaluate cross-communication among different geologic units, and locate hydraulically-active fractures. Profiles of axial flow during pumping conditions can help locate the vertical position of well screens, identify hydraulically-active fractures, and measure hydraulic conductivity profiles. Easy and simple to perform, borehole flowmeter tests provide, at a relatively low cost, three-dimensional information about subsurface conditions.

A primary reason for the lack of borehole flowmeter tests in the groundwater industry has been the lack of suitable flowmeters. Desirable flowmeter traits include a low detection limit, a wide range of operation, good accuracy, durability, reliable performance, and a small diameter and length. The petroleum industry has used impeller flowmeters for decades to measure flows typically with velocities greater than 2 m/min. For many groundwater applications, flows with average velocities below 2 m/min are of interest. These low flows cannot be accurately measured with impeller flowmeters typically available in the petroleum industry.

Primarily, because of the need to measure low flow velocities, the United States Geological Survey (USGS) developed a thermal-pulse flowmeter (Hess, 1982; 1986; 1990). The sensitivity of the USGS thermal-pulse flowmeter has made flowmeter testing possible

in fractured crystalline rocks with low permeabilities (Morin et al., 1988; Hess, 1986; Palliet et al., 1987). The thermal-pulse flowmeter however, has a narrow measurement range that limits its utility in some moderate to highly permeable aquifers.

In order to have both a low detection limit and a large range of operation, TVA developed the electromagnetic (EM) flowmeter (Young and Pearson, 1995). Since 1989, TVA has successfully applied EM flowmeters to numerous groundwater investigations. Partly because of the successful application of EM borehole flowmeter tests (Young and Pearson, 1990; Young, 1990; Molz and Young, 1993), EM borehole flowmeters are proven technology and are commercially available. The first portion of this appendix presents the EM flowmeter design, provides laboratory calibration data, and compares the performance characteristics of EM flowmeters to those of impeller and thermal-pulse flowmeters. The second portion of the appendix discusses applications of the EM flowmeter and several case studies.

## **C.2 THE ELECTROMAGNETIC FLOWMETER**

### **C.2.1 Description**

The EM flowmeter consists of a downhole probe and uphole electronics. The probe contains an electromagnet, two electrodes and a buffer amplifier that are cast in a ceramic epoxy within a stainless steel shell (Figure C.1). The flow passage through the probe is cylindrical. A water proof connector on the probe allows cables of various lengths to be attached.

During operation, the electromagnet creates a magnetic field across the flow passage. As water (the conductor) flows through the magnetic field a voltage gradient is generated. The voltage is proportional to the average velocity of the water across the magnetic field and is detected by the electrodes. Theoretically, and as verified by laboratory tests performed at the TVA Engineering Laboratory in Norris, TN, the magnitude of the voltage is unaffected by the electrical conductivity of the groundwater.

The uphole electronics provides excitation to the electromagnet, power to the amplifier, and converts the probe signal to a flow. Upward flow is generally designated as a positive voltage and downward flow as a negative voltage. Separate from the uphole electronics, appropriate computer software calculates the mean and standard deviation of the voltage measurements at the end of a preset time interval, or upon keyboard command. For most applications, an appropriate time interval is one minute, with readings taken every second.

EM flowmeters are constructed to fit snugly into 5.25-cm ID wells. A standard length is 25 cm, but flowmeters as short as 10 cm have been successfully used. Short flowmeters help to minimize the blockage of horizontal flow and are used where detailed measurements are desired. The longer flowmeters can support an inflatable packer assembly and are used for testing large-diameter boreholes.

For wells with inner diameters greater than 5.25 cm, a mechanical or inflatable packer can be used to help channel axial flow through the EM flowmeter probe. TVA's mechanical packer consists of a rubber gasket sandwiched between two plexiglass rings. In large-diameter boreholes whose diameter changes with depth, the EM flowmeter is most effective



when coupled with an inflatable packer. Packer inflation can be achieved by injecting water either with a pressurized chamber at the ground surface or with a submersible pump placed slightly above the flowmeter.

### **C.2.2 Laboratory Calibration**

EM flowmeter calibration involves plotting flowmeter voltage as a function of steady uniform flow in a vertically-oriented PVC pipe. For consistency, the voltage is corrected by an offset equal to the voltage at zero flow. Figure C.2 provides pre- and post-calibrations from several field tests. A desirable feature of the EM flowmeter calibration is linearity over a wide flow range. Linearity means that the flowrate is directly related to voltage through the equation:  $\text{flowrate} = (\text{calibration factor}) * (\text{voltage})$ .

The calibration factor and range of linearity for an EM flowmeter is affected by the flowmeter's size and magnetic field as well as the test configuration. Table C.1 provides calibration factors for combinations of two flowmeter sizes, and two packer types in differently sized pipes. The calibration factors in Table C.1 are based on data above 0.03 L/min and 0.1 L/min for the 1.27-cm and 2.54-cm flowmeters, respectively. Below these respective limits, the correlation between flow and voltage becomes non-linear. Laboratory testing has shown the detection limit — the flow at which a flowmeter provides a measurable response — is about 0.005 L/min and 0.03 L/min for the 1.27-cm and 2.54-cm flowmeters, respectively. However, TVA has not collected sufficient data to characterize the EM flowmeter capabilities near these very low flows.

**Table C.1 Calibration Factors (Liter/min/volt) from a regression of discharge versus voltage for electromagnetic flowmeter data from Young et al., (1995a)**

	<b>1.27-cm ID EM Flowmeter</b>	<b>2.54-cm ID EM Flowmeter</b>
Flowmeter in a 5.25-cm PVC pipe*	1.32	3.94
Flowmeter with a mechanical collar in a 10.2-cm PVC pipe*	1.38	3.95
Flowmeter with an inflatable packer in a 15.4-cm PVC pipe*	1.46	3.99

\* pipe is schedule 40

Because of the wide range over which the EM flowmeter provides a linear response between voltage and flow, most flowmeter calibrations can be performed quickly as they require only a few data points to check the calibration factor. Although an EM flowmeter's voltage caused by flow through the flowmeter should not change over time or with use, the percentage of flow around the outside of the flowmeter may change for different test set-ups. As a result, laboratory calibrations should reproduce the physical set-up of the field test as much as possible.

In Table C.1, the addition of a packer increases the calibration factor because a packer reduces, and possibly eliminates, flow around the flowmeter's exterior. The calibration factors are higher for the inflatable packers than for the mechanical packers (to be discussed in next section) because the former provides a better seal than the latter. Similarly, because the smaller ID flowmeter has more flow by-pass than the larger ID flowmeter for the no-packer condition, an inflatable packer has a greater effect on the calibration factor for the smaller than for the larger ID flowmeter.

### **C.2.3 Field Use**

Two concerns with using the EM flowmeter in the field are ambient EM currents and frictional losses through the flowmeter probe. Neither of these concerns pose a threat to the quality of the field data if field personnel take appropriate precautions.

High background EM currents lead to biased measurements that include unstable readings with high standard deviations. This problem has occurred at 2 out of approximately 150 wells tested by TVA with the EM flowmeter. At one of these wells, the problem was traced to heavy machinery operating in a nearby building. This problem was solved by testing the well when the machinery was not in use. For cases where this option would not exist, a modification to the existing TVA flowmeter design is required. Based on limited laboratory tests at the TVA Engineering Laboratory, placement of wire mesh across the openings of the flowmeter may help reduce or even eliminate problems associated with high background EM currents.

High frictional losses affect the hydraulic head distribution and, consequently, the distribution of flow in a well. Figure C.3 shows frictional losses associated with different EM flowmeters. The selection between EM flowmeters with different inner diameters involves a tradeoff between improved accuracy at low flows for increased frictional losses through the flowmeter. Electromagnetic flowmeters with small diameters are best for measuring ambient flows and for induced flows where large drawdowns are required to produce flow in the range of a few liters per minute.

### **C.3 COMPARISONS WITH OTHER FLOWMETERS**

#### **C.3.1 Impeller Flowmeters**

Impeller flowmeters have been used for several decades in the petroleum industry. These flowmeters are calibrated so that the number of impeller revolutions per time unit corresponds to a flow rate. The impeller is aligned by needles that fit snugly into bearings attached to the main shaft (Figure C.4a). Sensors located near the upper needle bearing track the rotation of the impeller. These sensors are typically optical or magnetic and detect the passing of markers positioned in the impeller.

Because of frictional forces associated with the impeller's rotation, there is a threshold velocity below which the impeller does not respond. Increased sensitivity of an impeller flowmeter is gained by decreasing frictional losses by using lightweight impellers, jeweled bearings, and magnetic forces to reduce the contact pressure between the needles and the bearings.

By convention, geophysical companies provide flowmeter specifications in units of velocity. The flow range provided by geophysical companies for impeller flowmeters is typically from 2 to 300 meters/min. Hess (1986) reports impeller flowmeters typically can measure velocities of 2 meters/min and greater although some impeller meters have stall velocities as low as 0.6 meters/min. Using the stall velocity and the cross sectional area of the well pipe, one can estimate 1.0 L/min as a lowest discharge measured by most impeller flowmeters in a standard 5.25-cm ID schedule 40 pipe.

### **C.3.2 Comparison Between the EM and Impeller Flowmeters**

To collect impeller flowmeter data, TVA used a flowmeter built by Haferland Geophysical, Hanover, Germany and used by Rehfeldt et al., (1989, 1992) and Hess et al., (1992). Rehfeldt et al., (1989) reported that the practical detection limit of the Haferland flowmeter was 0.3 L/min in a 5.25-cm well. A similar model was used by Hufschmeid (1986). In comparison, the Habert impeller flowmeter used by Molz et al., (1990) has a detection limit near 1 L/min in a 5.25-cm well.

In July 1988, TVA used the Haferland impeller flowmeter at five 5.25-cm wells while injecting or pumping water at rates of 7.5 to 26 L/min. Figure C.5 shows the pre- and the post-calibrations: a difference of about 1.0 L/min exists between the two calibrations. The shift occurred because of needle-point wear. The pre-test calibration results were reproduced after the needles were resharpened. Subsequent field testing with the impeller meter did not produce shifts as large as those shown in Figure C.5. Reduction in calibration degradation could be achieved by using lubricants and pumping at flows below 10 L/min. Even with these precautions, however, shifts in the flowmeter calibration during field use were enough to introduce major uncertainties with flow data below 5 L/min. Unlike an impeller flowmeter, an EM flowmeter has no moving or adjustable parts so its calibration does not shift during field testing.

Unlike typical laboratory calibration tests, field tests include horizontal inflows that produce a swirling/lateral component to the flow. Large lateral inflows can occur at hydraulically-active fractures or zones of high permeability. Laboratory tests show that when the top of an impeller flowmeter approaches a lateral inflow, an impeller flowmeter can

indicate flow rates as high as 50 percent of the inflow although no flow is moving vertically through the flowmeter. These and other similar tests at TVA show that when an impeller flowmeter is above and near a zone of lateral inflow, an impeller flowmeter can produce erroneous results that includes an oscillatory flow profile and flows greater than 200 percent of the actual flow. Laboratory tests with the EM flowmeter indicate that swirling flows and turbulence has no measurable effect on the EM flowmeter response. Field comparison between the Haferland impeller and the EM flowmeter has been performed at four wells in a gravel-and-sand aquifer at Columbus AFB, Mississippi. Young (1990) presents these flow profiles, of which one is shown in Figure C.6. In general, the flow profile for the impeller flowmeter included more spatial variability as a result of higher peak flows and regions of slightly negative flows. Based on the laboratory test results, the difference between the two sets of profiles were primarily caused by the adverse effects that lateral/swirling inflows have on the performance of the impeller flowmeter.

### **C.3.3 The Thermal-Pulse Flowmeter**

Thermal-pulse flowmeters use a tracer-time principal developed by Dudgeon et al., (1975) and enhanced by Hess (1982; 1986). The key components are a resistance-wire heating grid and thermistors within a hollow, vertically oriented tube (see Figure C.4b). Borehole fluid is heated by electrically pulsing the heating grid and groundwater flow and temperature changes are monitored at a thermistor. Flow rates are calculated based on the time between the trigger pulse and the peak response at the thermistors.

When combined with a wireline packer, Hess and Paillet (1989) report a measuring range between 0.04 to 8 L/min. Because the thermal-pulse flowmeter has an inner diameter of 4.1-cm (Hess, 1990), this flow range corresponds to a velocity range of 0.03 to 6 meters/min. This velocity range is also cited by Hess (1990), Hess and Paillet (1989), and Mount Sopris, a geophysical company that markets thermal-pulse flowmeters.

### **C.3.4 Comparison Between the EM and Thermal-Pulse Flowmeters**

To collect thermal-pulse flowmeter data, TVA selected a flowmeter built by Mount Sopris, Golden Colorado. The flowmeter was selected because its construction is similar to the USGS thermal-pulse flowmeter. The downhole portion of the flowmeter has a length of about 1.2 m and is constructed such that it cannot be effectively used in 5.02-cm PVC wells. The purpose for leasing the thermal-pulse flowmeter was to perform comparative logging in uncased boreholes.

Laboratory tests with the thermal-pulse flowmeter included a check on its sensitivity to horizontal inflow. Flow measurements were taken with the inlet of the thermal-pulse flowmeter at distances of 1, 5, 10, and 20 cm above horizontal inflows ranging from 1 to 4 L/min. For the flow rates tested, the thermal flowmeter provided the same flow (within TVA measurement error) at all distances from the horizontal inlet source. The test results indicated that like the EM flowmeter, the thermal-pulse flowmeter can accurately pinpoint horizontal inflows. The good performance of the flowmeter is attributed, in part, to a steel screen mesh that helps to straighten the flow before it contacts the heating grid.

A limitation with the Mount Sopris thermal-pulse flowmeter was the lack of an inflatable packer. Calibration tests in translucent PVC well pipe indicated significant flow by-pass and a relatively poor fit with the rubber-fingered type mechanical collar provided with the flowmeter. Replacement of this collar with a more rigid mechanical collar used by TVA significantly decreased the flow by-pass and caused an 40 percent increase in the calculated flow. A problem with the more rigid collar, however, is that although it performs adequately in a fixed-diameter pipe, it may not perform satisfactorily in a borehole with a variable diameter. In order to perform an accurate survey in a uncased borehole, an inflatable packer should be used. Because of a lack of a suitable inflatable packer for the Mount Sopris thermal flowmeter, no comparative field flowmeter tests were conducted with the two flowmeters.

The only set of comparable flow data from an borehole from a EM and a thermal-pulse flowmeter attached to an inflatable packer is from borehole FSE-6 at Mirror Lake, New Hampshire (Young et al., 1994). Although very similar, the flow profiles may not be directly comparable because they were performed at different times and for different pumping conditions. As should be expected based on the laboratory tests, however, the two sets of flow logs suggest that the thermal-pulse and EM flowmeter produce results of comparable quality.

### **C.3.5 Final Assessment**

EM flowmeters combine the lower detection limit of thermal-pulse flowmeters with the wide measurement range of impeller flowmeters. They have the desirable properties of



being insensitive to turbulence associated with horizontal inflow, and their calibrations are unaffected by field use. Because of their durable and simple design EM flowmeters can be easily decontaminated and adapted with mechanical collars or inflatable packers. In summary, the EM flowmeters provide the capabilities to make flowmeter tests possible in many aquifer and well types.

#### **C.4 FIELD STUDIES INVOLVING THE ELECTROMAGNETIC FLOWMETER**

Table C.2 includes important aspects of site characterization that can be partially addressed by flowmeter testing. Issues related to aquifer heterogeneity are particularly crucial at sites involving groundwater remediation because remediation systems are often based on improper and/or inadequate three-dimensional data (U.S. EPA, 1990; Haley et al., 1991). At sites where conditions permit single-well pump testing, EM flowmeters can be effective for obtaining three-dimensional data.

Although flowmeter testing appears straight-forward, collecting and analyzing flowmeter data has several potential problems. In most field situations, these problems can be avoided with proper field and analysis methods, which are discussed in reports focused on flowmeter testing (Rehfeldt et al., 1988; Molz et al., 1990; Young et al., 1995a,b). These reports explain the assumptions and theories associated with analyzing flowmeter data and provide field data and/or discussions associated with: drilling methods, well construction, well development, borehole flowmeter calibration, selection of pumps and pumping rate, measurement and analysis of well drawdown response, well storage effects, changes in ambient flow conditions, statistical analysis, and quality assurance.

**Table C.2 Groundwater issues that borehole flowmeter data can help resolve\***

<b>Measured Flow Log</b>	<b>Issues That Can be Investigated</b>
Ambient	<ul style="list-style-type: none"> <li>- direction of the vertical hydraulic gradient</li> <li>- cross-connection among geological units intersected by a well</li> <li>- fracture locations in bedrock</li> <li>- seepage pathways beneath dams in karstic terrain and/or through earthen dams</li> </ul>
Pumping	<ul style="list-style-type: none"> <li>- fracture locations in bedrock</li> <li>- horizontal hydraulic conductivity values</li> <li>- performance of underground injection wells</li> <li>- placement of multi-layer monitoring zones</li> <li>- zones of high contaminant transport</li> <li>- design of high-capacity water wells</li> </ul>

\*References documenting case studies involving these issues are provided in this article and by Young et al., (1995a)

The objective of presenting case studies is to demonstrate the utility of the EM flowmeter under a variety of field conditions, flow rates, and groundwater projects. The case studies do not explain the data collection and/or analysis methods. Such detailed is provided in the cited references, in Young et al., (1995a), and in recent articles focused on EM flowmeter data (Molz et al., 1995; Young, 1995).

#### **C.4.1 Measurement of the Hydraulic Conductivity(K) Values**

The first application of the EM flowmeter was in an 11-m unconfined sand-and-gravel aquifer at Columbus Air Force Base (CAFB), Mississippi. The EM flowmeter measured the flow profiles at 0.31-meter intervals at 37 wells across a 1-Ha test site to obtain 881 measurements of hydraulic conductivity (Young, 1995). Figure C.7 shows areal plots

of the depth-averaged  $\log(K)$  values for the uppermost and lowermost 2 meters of the saturated aquifer. The 54 to 56-m MSL cross section has an incomplete  $\log(K)$  field because of a 0.5 to 1 meter channel scour in the underlying clay aquitard.

The region of high  $\log(K)$  values in the upper aquifer coincides with the suspected base of an abandoned meander outlined in an aerial photograph. The region of high  $\log(K)$  values in the lower aquifer lie in a 0.5 to 1-m scour produced by a former fluvial channel. The flowmeter data at Columbus AFB provided sufficient  $K$  data to map coarse-grained bedload deposits associated with former river channels (Young, 1995). This type of detail  $K$  data is required in order to model solute transport in heterogeneous aquifers.

#### **C.4.2 Preferential Groundwater Flow in Granular Aquifers**

Extensive flowmeter testing performed at Columbus AFB (Young, 1995); Boggs et al., 1992); Rehfeldt et al., 1992)), is not possible at many sites. In fact, at the majority of EM flowmeter test sites less than seven wells have been tested. Even with flowmeter data from just a few wells, the data has been useful for identifying preferential flow zones, estimating the spatial variability in hydraulic conductivity, evaluating the site's conceptual aquifer model, and/or designing a monitoring and characterization program. A site where a few flowmeter tests have helped to improve aquifer characterization is the Sylvester Hazardous waste site.

In 1979, illegal dumping of hazardous waste off Gilson Road (a.k.a the Sylvester hazardous waste site) in Nashua, New Hampshire, lead to a leachate plume over 450-m wide and 33-m deep (Morrison, 1983). Remediation of the Gilson Road site included constructing

a bentonite slurry wall around the 8-Ha site, capping the surface with an impermeable liner, and installing a pump-and-treat system.

In June 1992, EM flowmeter tests were performed at monitoring wells (including Well 3S) and at the three shallow extraction wells that fully penetrate glacial deposits underlain by a biotite schist (Young et al., 1994). Figure C.8 suggests that a 0.5 to 1-m zone (possibly glacial drift) of high relative K exists above a 4 to 5-m zone (possibly glacial till) of significantly lower K. The flowmeter profiles indicate that the extraction wells may not be efficiently removing contamination if the majority of the contamination is in the lower aquifer. Clearly, the combination of flowmeter flow profiles along with chemical profiles would be valuable data prior to the design and operation of pump-and-treat recovery systems.

#### **C.4.3 Preferential Groundwater Flow in Bedrock Aquifers**

Groundwater flow in crystalline bedrocks and limestones/dolostones usually occurs primarily in fractures, bedding planes and solution cavities. EM borehole flowmeter tests have successfully identified these important flow zones in sandstone, gneiss, shale, limestone, schist, and granite. At many of these sites, the location of major fracture zones was apparent from the ambient flow logs.

A site where the ambient flow profile is an useful indicator of high permeability fracture zones is Mirror Lake, New Hampshire. Flowmeter measurements were made in three well with 55-m screens in a granitic bedrock. The flow profiles for ambient and for pumping conditions indicate that only 1 to 2 major flow zones exist at each of the three wells. Figure C.9 shows results for borehole FSE-06. During pumping, approximately 30

percent and 65 percent of the total flow originates from depths of 62 and 35 m, respectively. During ambient conditions, approximately 0.25 L/min enters the borehole at a depth of 35 m and travels downward to a depth of 62 m before exiting.

Although the flowmeter results only identified a few major flow zones at each borehole, acoustic televiewer images indicated that numerous fractures intersected the borehole. This observation suggests that only a few of the available fractures are responsible for the vast majority of groundwater flow. This observation is consistent with the finding of Paillet et al., (1987), who performed thermal-pulse flowmeter tests at the Mirror Lake site and the Arizona Fractured Rock Hydrology Research Site near Oracle, Arizona. They conclude that "televiewer logs and other geophysical data indicate that the fractures intersecting the borehole at the point where most water enters or exits during pumping or injection tests are similar to other prominent fractures that may be permeable, but that do not take part in the flow system."

Based on the analysis of Paillet et al., (1987), the best model for the fracture-flow system at Mirror Lake and the Oracle test sites are nearly horizontal zones of fracture permeability composed of intersecting fractures that have orientations far different than that of the fracture zone. This type of model would require that flowmeter tests be performed in order to properly characterize a site. Unlike crystalline bedrock, karstic bedrocks consisting of limestone/dolostone may have flow concentrated within a single solution cavity or weathered zone across very long distances.

At many of its facilities and also at the Oak Ridge National Laboratory (ORNL) (Moore and Young, 1992), TVA has discovered zones of relatively high permeability near

the contact between karstic bedrock and the overburden. These zones consist of a mixture of overburden material and highly weathered bedrock. A case study illustrating the importance of preferential flow in karstic bedrock involves the TVA's Environmental Research Center (ERC). ERC is located on a 1,050 Ha site between the northern city limits of Muscle Shoals, Alabama, and the Tennessee River. The reservation is approximately 6 km from a 1.8 m<sup>3</sup>/s spring that serves as a drinking water supply. Dye tracing studies across and southwest of ERC indicate groundwater velocities of up to 335 m/day and >1300 m/day (Julian et al., 1993).

Across the ERC site, flowmeter tests were performed in wells screened in the overburden, which is approximately 18 m thick, and in boreholes screened near the overburden/bedrock contact. At the five boreholes near the overburden/bedrock contact, the screened area included both the bedrock and a portion of the bedrock/overburden contact. Drilling conditions required that immediately above the top of rock (as established by auger refusal), solid casing and grout be used (see Figure C.10). EM flowmeter tests in the boreholes indicated that almost all of the water pumped from the wells originated from the weathered zone.

Figure C.10 provides EM flowmeter logs from three boreholes at ERC. Julian et al., (1993) and Young and Julian (1991) show that the weathered zone is at least 100 to 1000 times more permeability than either the residual clays above or the solid limestone bedrock below. The flowmeter tests indicate that the majority of regional flow toward the domestic spring may occur within a relatively narrow zone near the overburden/bedrock

contact. This observation has several implications including the prudence of monitoring groundwater quality below a possible weathered zone and only within solid bedrock.

#### **C.4.4 Monitoring of Preferential Groundwater Flow Zones**

At the Oak Ridge National Laboratory(ORNL) Reservation, ORNL/TVA has flowmetered boreholes up to 400 m deep to help locate multiport monitoring systems as described by Dreier et al., (1992) and Dreier and Caldanaro (1994). The boreholes intersect moderately to steeply dipping, fractured and faulted strata composed of dolostone, limestone, siltstone, or shale. On the basis of these flowmeter logs, geophysical logs, and visual inspection of continuous core samples, ORNL has selectively installed 8 to 12 sampling zones, 3 to 7.6 m long, in order to monitor: (1) fluids from hydraulically conductive fractures or fracture zones; (2) matrix fluids with long residence times, (3) fluids that may show water chemistry signatures with a particular rock type; and/or, (4) fluids that may show changes in water chemistry with depth.

At most of the boreholes, geophysical logging included caliper deviation, natural gamma, fluid resistivity, stream potential, long-short-normal resistivity, full waveform sonic, and temperature. Figure C.11 provides the results of the fluid resistivity and flowmeter logs—the most useful for identifying hydraulically active features according to Dreier and Caldanaro, (1994)—along with the selected zones for monitoring at one of the tested boreholes.

## **C.5 SUMMARY**

Knowledge of aquifer spatial variability is important to aquifer characterization and remediation. Borehole flowmeter tests can help identify preferential flow zones in granular and bedrock aquifers. A primary reason for the lack of borehole flowmeter tests in the groundwater industry has been the scarcity of suitable flowmeters. Desirable flowmeter characteristics include a low detection limit, a large dynamic range, good accuracy, and reliable performance. The recently developed EM flowmeter provides the capability to perform flowmeter tests in the vast majority of well types and geologic settings and should help improve the effectiveness of site characterization and remediation programs.



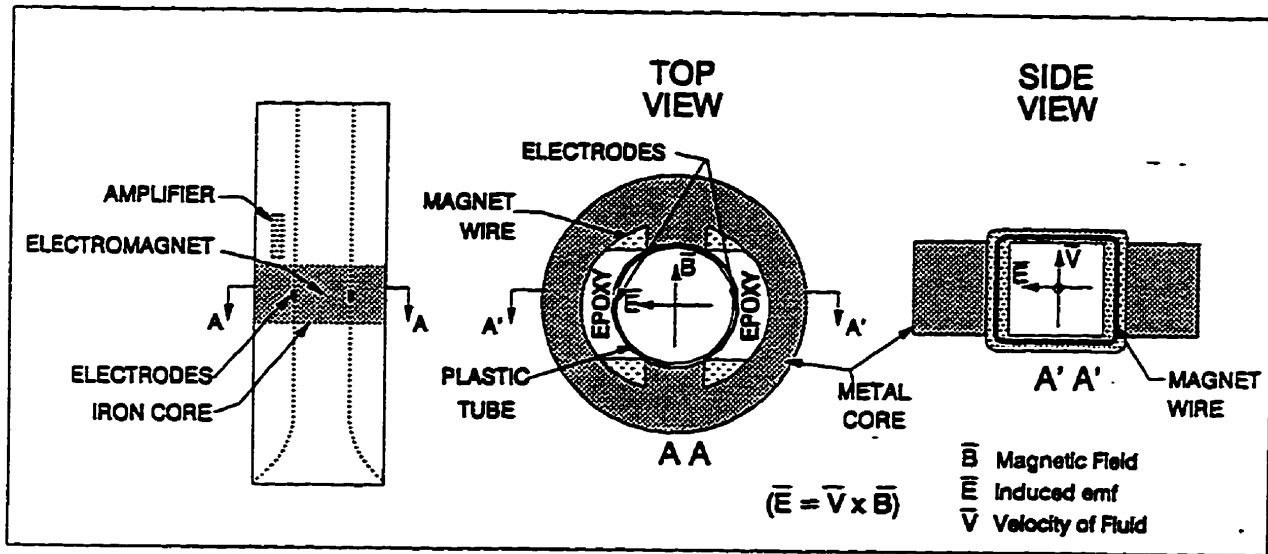


Figure C.1 Illustrations of the electromagnetic flowmeter probe:

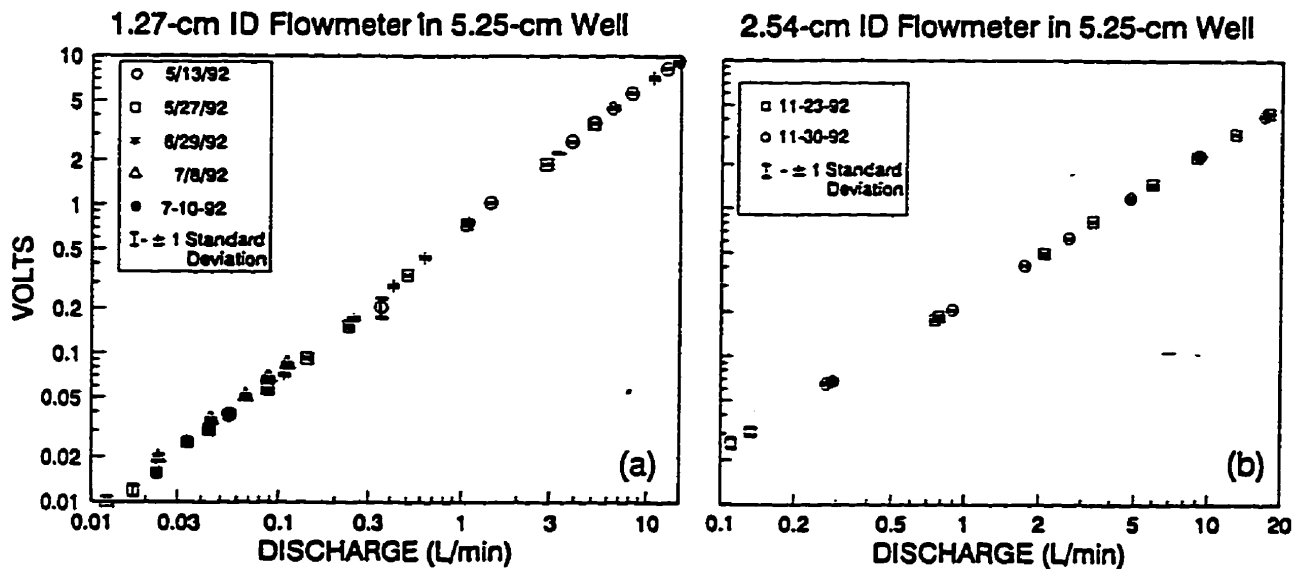


Figure C.2 Pre- and post-calibration data associated with field testing of the electromagnetic flowmeter in a 5.25-cm well: (a) flowmeter with 1.27-cm ID; and, (b) flowmeter with 2.54-cm ID (from Young et al., 1995)

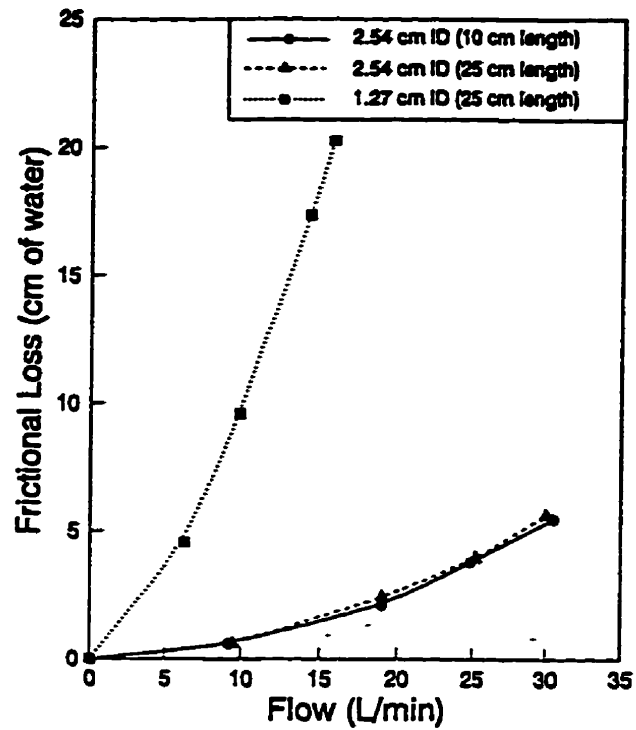


Figure C.3 Measured frictional losses caused by channeling flow from a 5.25-cm ID well into EM flowmeters.

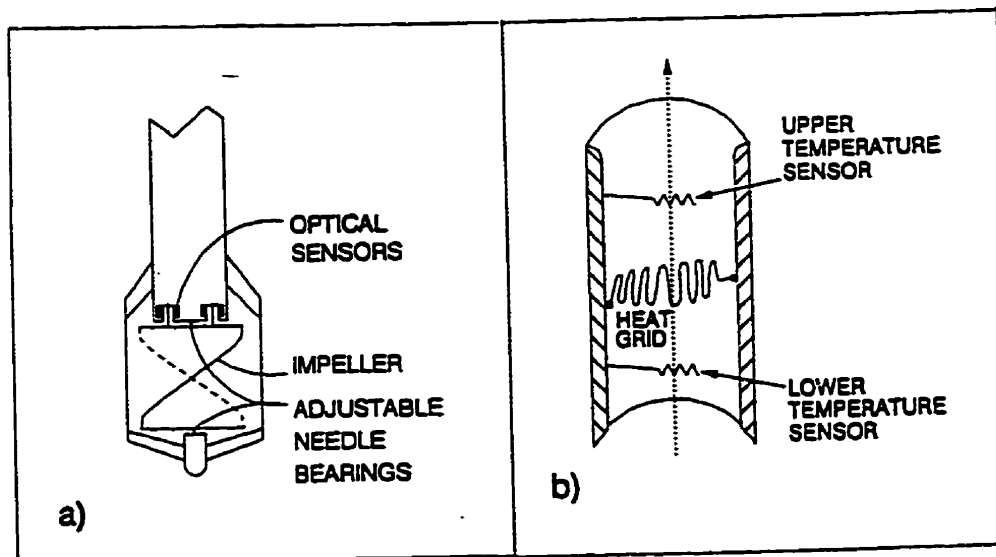


Figure C.4 Illustrations of flow probes used in: (a) impeller flowmeters; and, (b) thermal-pulse flowmeters.

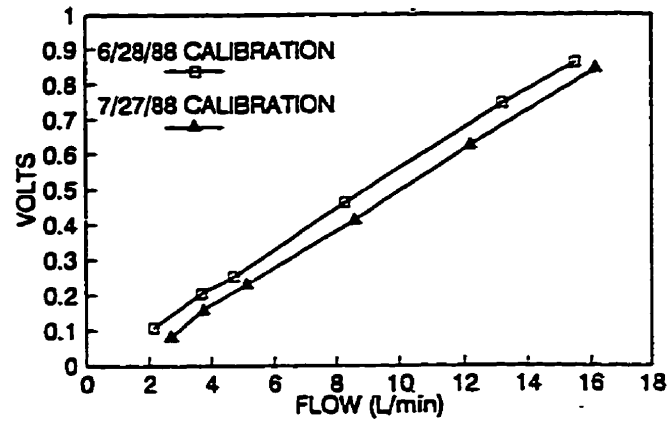


Figure C.5 Impeller flowmeter calibration before and after field testing five well at Columbus AFB, Mississippi (from Young and Waldrop, 1989).

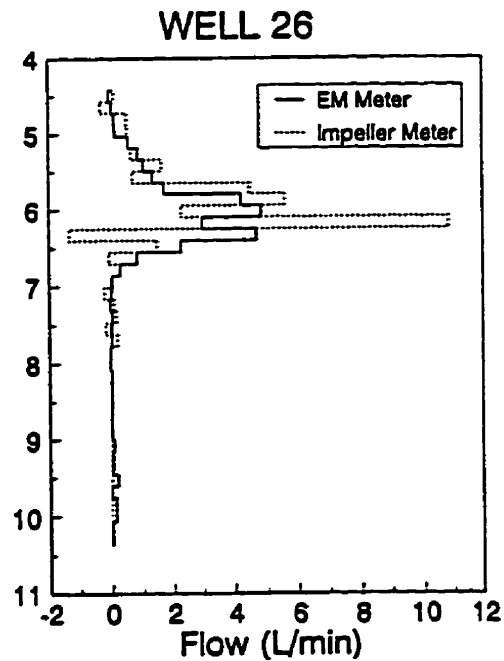


Figure C.6 Measured discharges by the electromagnetic and the impeller flowmeters at two wells located in a sand-and-gravel aquifer at Columbus AFB, Mississippi (from Young, 1990).

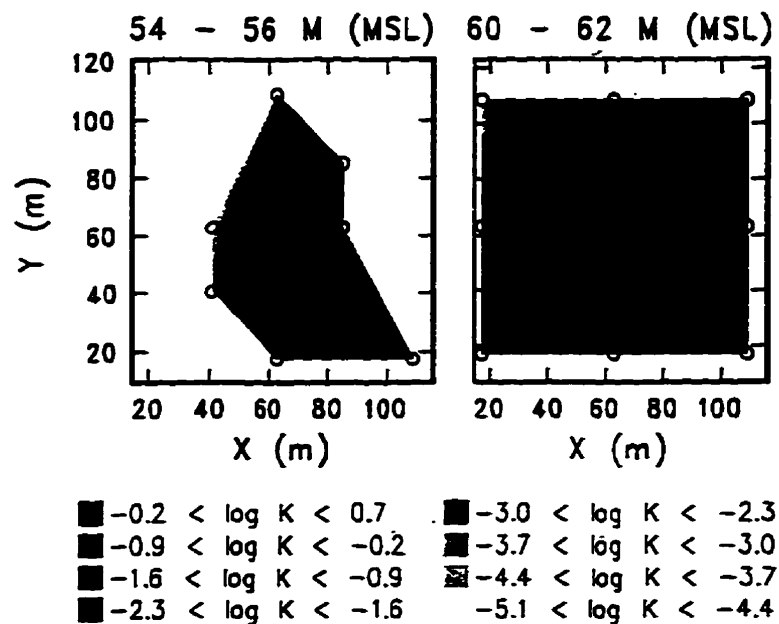


Figure C.7 Depth-averaged hydraulic conductivity values for the lowermost (left) and the uppermost (right) 2 meters of an fluviol aquifer at a 1-Ha test site at Columbus AFB, Mississippi (from Young, 1995).

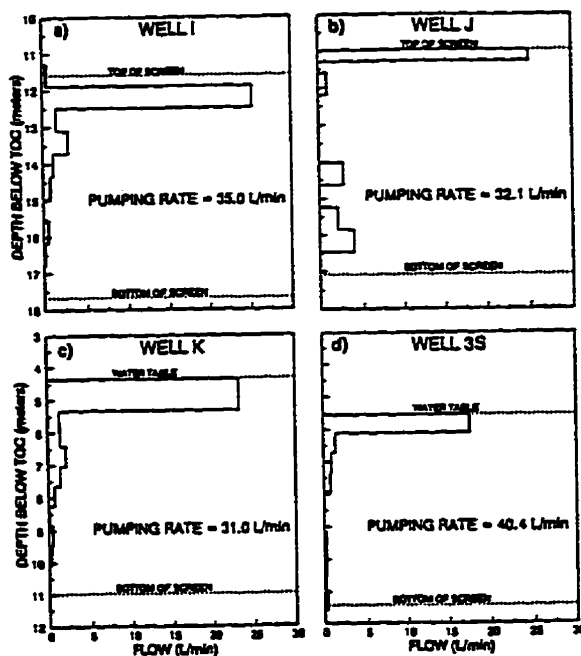


Figure C.8 Net differential flow distributions from pumping in glacial till and stratified drift deposits at the Sylvester hazardous waste site in Nashua, NH (from Young et al., 1994).

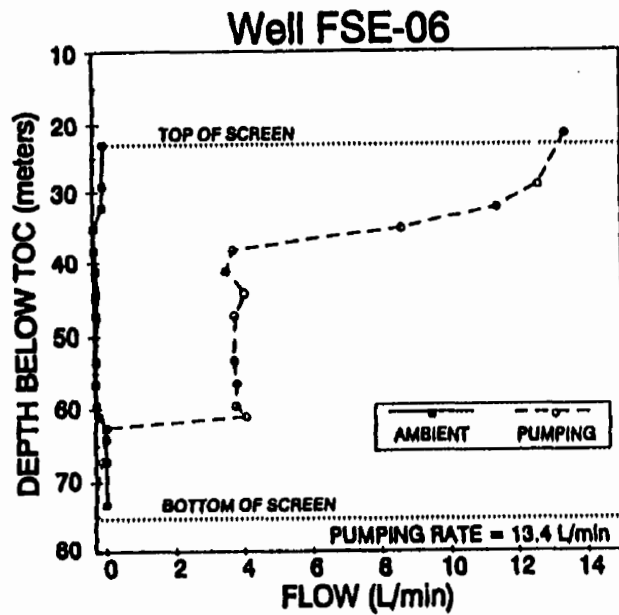


Figure C.9 Ambient and pumping flow distributions for borehole FSE-6 installed a granitic dike near Mirror Lake, New Hampshire (from Young et al., 1994).

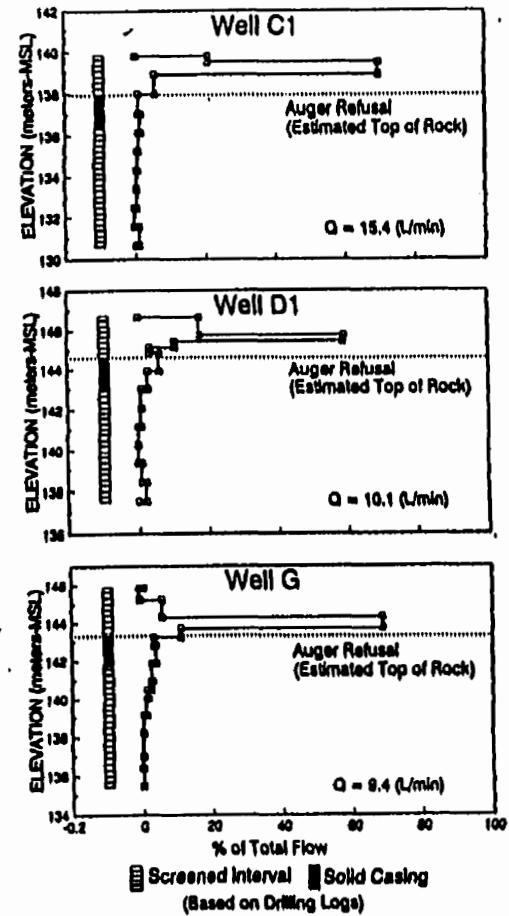


Figure C.10 Incremental flow distributions induced by pumping wells screened across limestone bedrock and a weathered zone above bedrock at TVA's Environmental Research Center in Muscle Shoals, Alabama (from Julian et al., 1993).

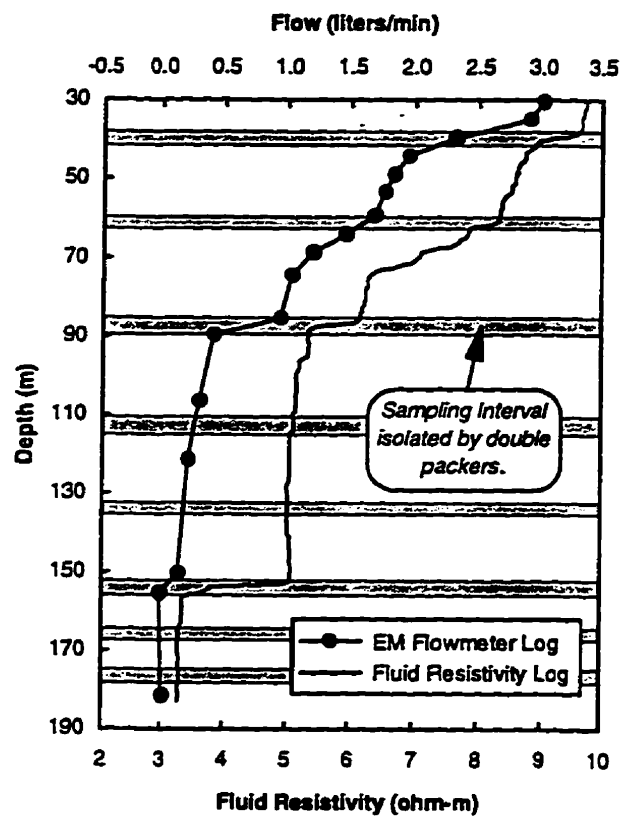


Figure C.11 Fluid resistivity and EM flowmeter logs for a borehole screened across shale at the Oak Ridge National Laboratory, Oak Ridge, TN (from Dreier and Caldanaro, 1994).

**APPENDIX D**  
**BOREHOLE FLOWMETER K PROFILES FROM COLUMBUS AFB**

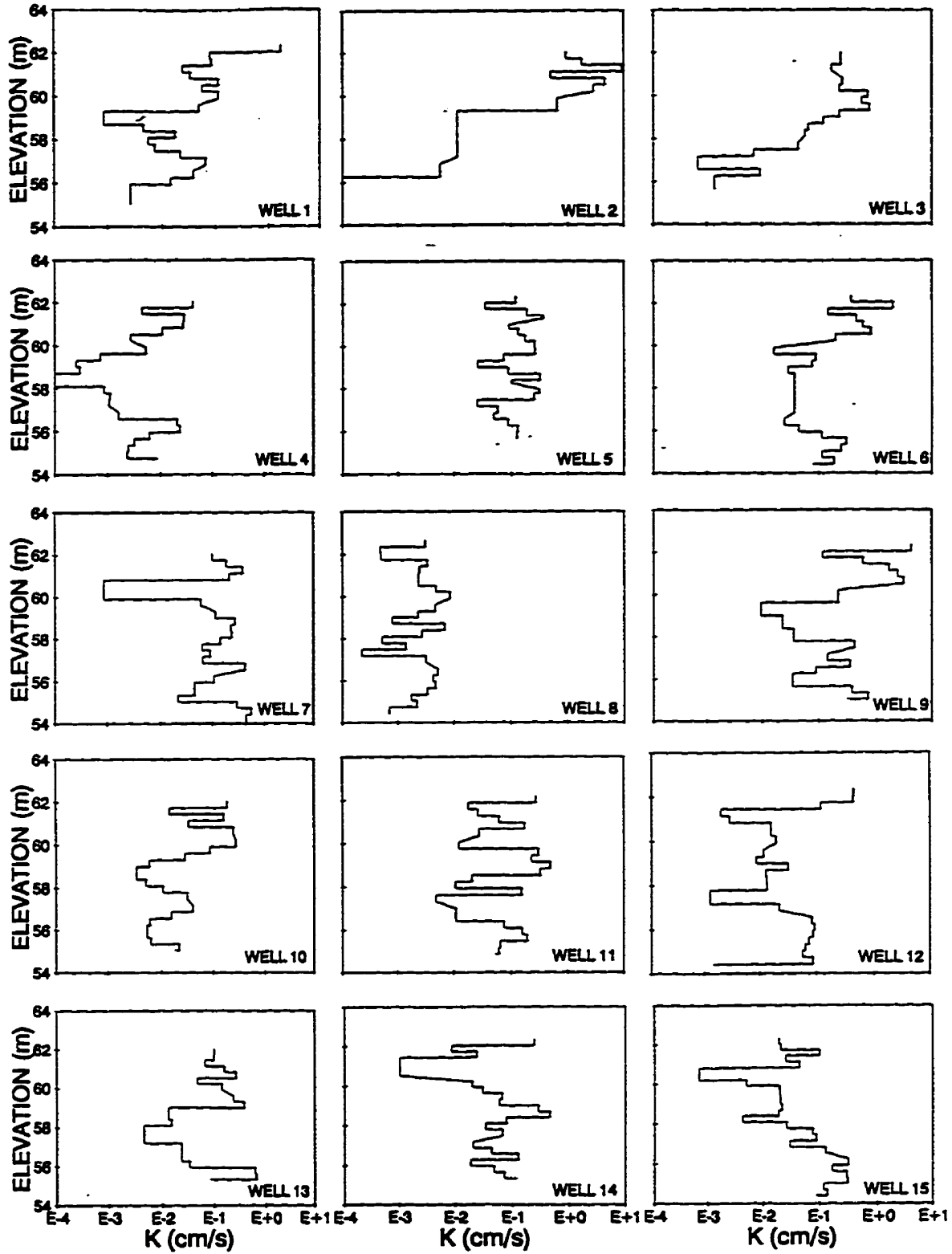


Figure D.1 Vertical profiles of hydraulic conductivity for Wells 1 - 15.



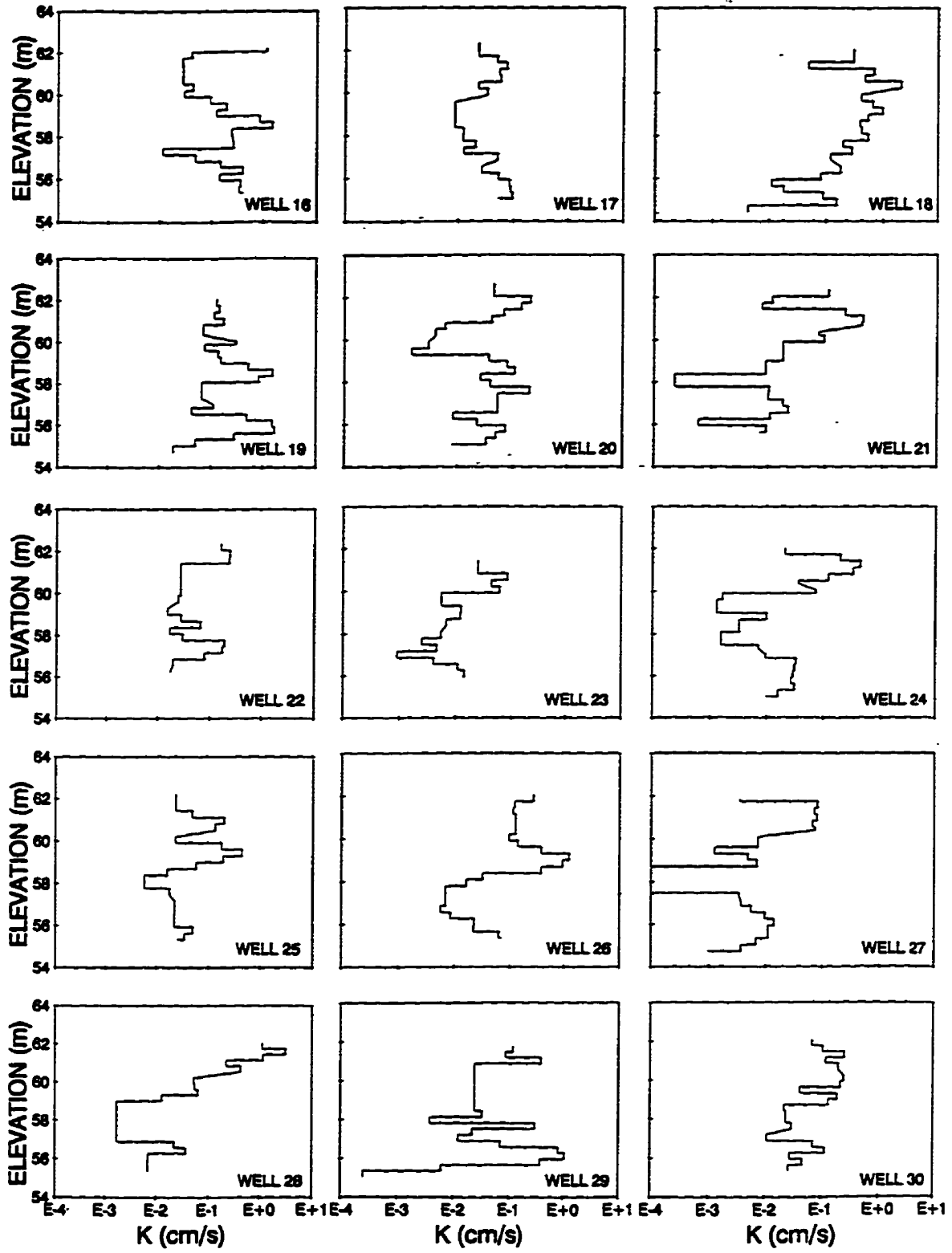


Figure D.2 Vertical profiles of hydraulic conductivity for Wells 16 - 30.

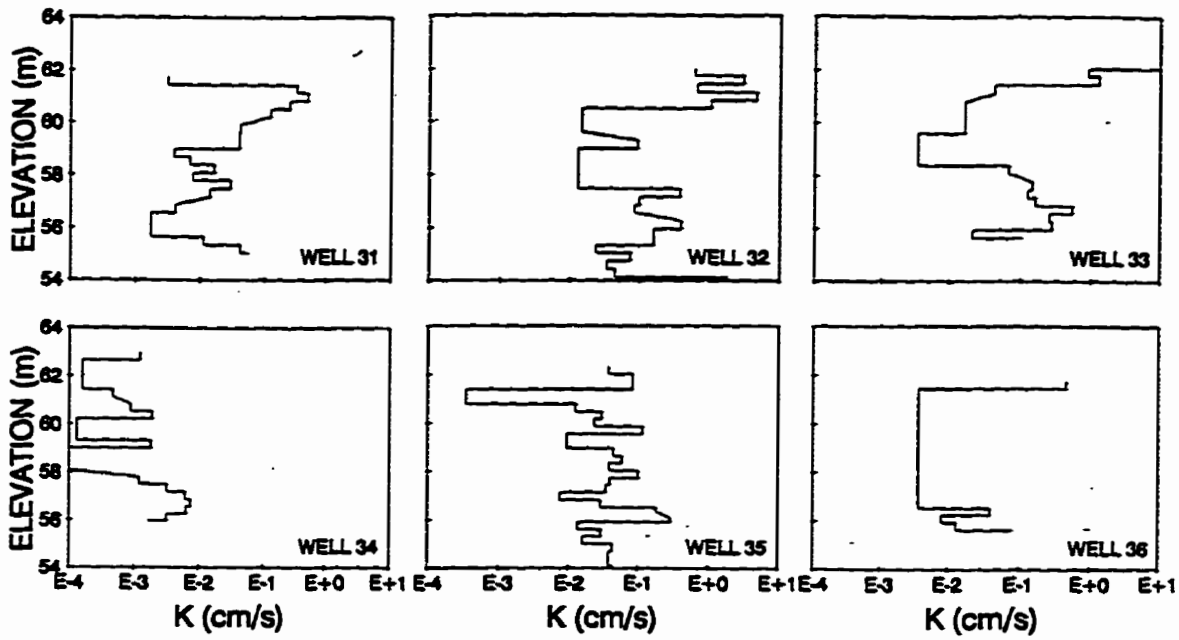


Figure D.3 Vertical profiles of hydraulic conductivity for Wells 31 - 36.

## **APPENDIX E**

### **RECIRCULATING TRACER TESTS AT THE 1-H<sub>a</sub> TEST SITE**

#### **E.1 CONCERNS WITH PERFORMING RECIRCULATING TRACER TESTS**

The complex and heterogeneous hydraulic conductivity field at the site poses several problems associated with the monitoring and the interpretation of the three-dimensional tracer concentration data. Monitoring of the three-dimensional tracer concentrations is complicated by the large vertical hydraulic gradients. These vertical gradients can cause mixing of the tracer concentration fronts near the well.

Figure E.1 illustrates how the disturbed zone around the multilevel samplers install at the MADE site could lead to mixing of the concentration fronts near the well installation. This mixing prevents multilevel samplers from obtaining representative groundwater samples from specific elevations in the aquifer. The fact that some type of vertical mixing could occur in the annulus of the wells was demonstrated by a series of small-scale tracer tests in the annulus of the wells by Boggs et al. (1989). As discussed by Young and Boggs (1989), mixing in the well annulus has adversely affected the representativeness of the groundwater samples from the multilevel samplers.

#### **E.2 TRACER TEST SET-UP**

##### **E.2.1 Tracer(s)**

Chloride and bromide were selected as tracers because: (1) they are believed to be conservative tracers (Betson et al., 1985); (2) their background concentrations are relatively low; (3) their relative concentrations can be measured quickly and accurately in the field with

an electrical conductivity meter; and, (4) their absolute concentrations can be measured relatively quickly and accurately in the laboratory with specific-ion probes.

### **E.2.2 The Flow Field**

For the tracer tests, the groundwater flow patterns were controlled by injection and withdrawal wells. In order to mimic flow fields used in bioreclamation activities, the groundwater was recirculated from the withdrawal wells to the injection well(s). For each tracer test, accurate measurements of water table levels and flow rates were made to determine when the hydraulic pressure field stabilized. Once quasi-steady-state flow conditions were achieved, the tracer solution was injected.

### **E.2.3 Monitoring Approach and Equipment**

Because of concerns about the performance of the MADE multilevel samplers, none of these type of samplers were installed around the wells. Instead, a procedure developed to monitor three-dimensional tracer flux inside the wells using the borehole flowmeter and multilevel samplers (Figure E.2). The procedure focuses on taking concentration and groundwater flow measurements at the same elevations in a well. Because both the tracer concentration and the vertical groundwater flow at designated elevations are known, the amount of tracer mass entering the designated layers can be calculated.

Figures E.3 and E.4 show the multilevel samplers placed inside the tracer injection wells and withdrawal wells, respectively. During the tracer test, groundwater samples were collected simultaneously from all sampling tubes by using peristaltic pumps. In order to

avoid problems with sample collection, all of the sample tubing and peristaltic pump connections were color coded. As shown in Figure E.4, two samples were collected at each elevation of the withdrawal wells. At the surface, these two samples were mixed into a single composite sample.

For each tracer test, two sets of borehole flowmeter measurements were taken. The first set of measurements was taken after the steady-state flow field had been established but before the tracer was injected. The second set of measurements was taken after the last set of groundwater samples was collected from the multilevel samplers. For the purpose of characterizing the flow field during the tracer test, the flow rates from the two data sets were averaged.

#### **E.2.4 The Location and Number of Tracer Tests**

Several tracer tests are required to independently evaluate the K profile from borehole flowmeter tests. In order to collect as much information as possible about solute transport in the aquifer, small-scale (3-5 meters), intermediate-scale (7-15 meters), and large-scale (31 meters) tracer tests were conducted. Figure E.5 shows the locations of the injection and the withdrawal wells for all of the tracer tests.

#### **E.2.5 Type of Tracer Injection**

In order to conduct all of the tracer tests in a timely and cost-effective manner, the tracer solutions were introduced as a pulse. The advantages of a finite duration instead of a continuous tracer injection include the following: (1) a better tracer breakthrough curve

for calculating the average velocity of the tracer; (2) lower costs; (3) minimum contamination of the aquifer; and (4) a lower risk of cross-contamination between the different tracer tests. A possible disadvantage of a finite duration test is that an inadequate amount of tracer may be added to provide a well-defined breakthrough curve.

### **E.2.6 Surface Piping Network**

Figure E.6 presents a general schematic of the piping system used to regulate the pumping of water from the withdrawal wells to the injection wells. The system is designed to accommodate up to four injection wells, four withdrawal wells, and three tracer tanks. The piping arrangement provided the capability to conduct several tracer tests simultaneously. In order to monitor the flow through the pipes, numerous rotameters were installed in-line to provide quick visual checks of the flow rates.

As shown in Figure E.6, the piping arrangement permits pumping from the tracer tank to the injection wells while another tracer tank is filled. During the start of the tracer tests, the tracer solution was pumped from the tracer tanks to the injection wells. After the tracer slug was injected, the groundwater was then pumped directly from the withdrawal wells to the injection wells.

## **E.3 DESCRIPTION OF FIVE RECIRCULATING TRACER TESTS**

### **E.3.1 Tracer Test 1**

Tracer Test 1 included pumping Wells 5, 13, 14, and 19 at approximately 9.5 L/min and injecting the total discharge into Well 16. The pumping began at 1552 on August 29 and

the initial borehole flowmeter survey was conducted at all of the withdrawal wells on August 30 from approximately 1050 to 1550. On August 31 from 0000 to 0047, a tracer slug of 1,781 liters of 800 ppm bromide solution was injected into Well 16. Groundwater samples were collected at 0.6-meter vertical intervals from the withdrawal wells for about 7 hours after the tracer mid-point of the tracer injection. A final borehole flowmeter survey of all the wells was conducted on August 31 from 1355 to 1740.

### **E.3.2 Tracer Test 2**

Tracer Test 2 included pumping Wells 8, 10, 24, and 25 at approximately 7.6 L/min and injecting the total discharge into Well 12. The pumping began at 0015 on September 1 and the initial borehole flowmeter survey was conducted at all of the withdrawal wells on September 1 from approximately 0840 to 1433. A slug of 4,077 liters of 800 ppm bromide solution was injected into Well 12 from 2330 on September 1 to 0145 on September 2. Groundwater samples were collected at 0.6-meter vertical intervals from the withdrawal wells for about 26 hours after the tracer mid-point of the tracer injection. A final borehole flowmeter survey of all the wells was conducted on September 2 from 0840 to 1650.

### **E.3.3 Tracer Test 3**

Tracer Test 3 was designed to simulate three recirculating doublet tests. The withdrawal wells were Wells 2, 11, and 17; the injection wells were Wells 18, 20, and 21. Figure E.6 shows the well locations and Table 14 provides the approximate pumping or injecting rates for each well. The initial borehole flowmeter survey was conducted at

Wells 2, 11, and 17 on September 4 from 0920 to 1415. A slug of 7,712 liters of 800 ppm bromide solution was partitioned into all three injection wells in amounts proportional to their respective flow rates between 2230 on September 4 and 0200 on September 5. Groundwater samples were collected at 0.6-meter vertical intervals from the withdrawal wells for about 34 hours. A final borehole flowmeter survey of all of the wells was conducted from 1115 to 2215 on September 6.

#### **E.3.4 Tracer Test 4**

Tracer Test 4 was designed to simulate four recirculating doublet tests. The withdrawal wells were Wells 1, 3, 7, and 9; the injection wells were Wells 30, 26, 32, and 31. Table 14 provides the approximate pumping or injection rate for each well. The pumping began at 0500 on September 8 and the initial borehole flowmeter survey was conducted at all of the withdrawal wells from 1805 to 2250 on September 8. A slug of 14,559 liters of 1200 ppm bromide solution was partitioned into all three injection wells in amounts proportional to their respective flow rates between 1840 and 2120 on September 9. Groundwater samples were collected at 0.6-meter vertical intervals from the withdrawal wells for about 50 hours. The final borehole flowmeter survey was conducted at Wells 3, 26, 32, 30, 31, and 7 on September 12 from 0905 to 1930. The final borehole flowmeter survey was conducted at Wells 9 and 1 from 0830 to 1026 on September 13.



### **E.3.5 Tracer Test 5**

Tracer Test 5 included pumping Wells 1, 3, 7, and 9 at approximately 26.5 L/min and injecting the total discharge of 106 L/min into Well 5. The pumping began at 1330 on September 13. The injection of 21,238 liters occurred between 1130 and 1450 on September 14. No initial borehole flowmeter survey was conducted before the tracer injection. Throughout the entire tracer test groundwater samples were taken from most of the 27 wells with the type of multilevel sampler shown in Figure E.5. During the tracer test, borehole flowmeter surveys were conducted in the monitoring wells. Tracer Test 5 lasted for approximately 170 hours and ended on September 21 at 0900.

## **E.4 RESULTS FROM TRACER TESTS 1 TO 4**

### **E.4.1 Data Presentation**

Important data for each tracer test includes the water table elevations, the vertical distribution of groundwater flow at the wells, and the vertical distribution of the tracer flux and concentration at each of the withdrawal wells. For purposes of data analysis, the time required to reach the peak concentration at a well represents the time for the middle of the tracer pulse to reach the well.

To estimate this  $K$  values from the tracer tests, horizontal groundwater flow is presumed. With this presumption, Equation E.1 can be used to calculate a lower  $K$  value for the aquifer intervals with the tracer breakthrough data. In Equation E.1,  $R$  is easily measured and  $t_p$  is estimated from the tracer breakthrough curves. The value of  $J_t$  cannot be measured. However, because a tracer particle spends proportionally more time in the regions

of low gradients (near the midpoint of two wells) than of high gradients (near each well), an upper bound for  $J_t$  is  $J_S$ . In solving Equation E.1,  $J_S$  was used for  $J_t$ . The value for  $J_S$  was calculated from the constant water table elevations at the injection well and at the appropriate withdrawal well. The effective porosity  $\eta$  was set to 0.3 based on results of 84 minimally-disturbed soil cores from the nearby MADE site (Boggs et al., 1992).

$$K > \frac{R \cdot \eta}{t_p \cdot J_t} \quad (5)$$

where:  $K$  = lower bound for the average hydraulic conductivity of the aquifer zone of tracer transport  
 $R$  = distance between the wells  
 $t_p$  = time of peak tracer concentration (note:  $t_p$  is greater than the time required for a tracer particle to move between the two wells along the shortest streamline)  
 $\eta$  = effective porosity  
 $J_t$  = the average spatial horizontal hydraulic gradient,  $J_S$ , experienced by a tracer particle. In a uniform flow field,  $J_t = J_S$ . For a converging or diverging flow field, an upper bound for  $J_t$  is  $J_S$ .

#### E.4.2 Tracer Test 1

In Figure E.7 all of the wells except for Well 5 have very similar vertical distributions of groundwater flows. The similar patterns indicate that Wells 13, 14, 16, and 19 intersect the interconnected lenses of relative high  $K$  at elevations near 56 and 59 m MSL. The profile for Well 5 provides no evidence of a high hydraulic conductivity lens at any depth. The two profiles most similar that are those for Wells 16 and 19. The high amount of similarity of

well locations 16 and 19 may have occurred because they are aligned along the lenses of high hydraulic conductivity.

Figure E.8 shows that for Wells 13, 14, and 19, the tracer slug was advected most rapidly two aquifer lenses located near 56 and 59 m MSL. At some locations the ascending portion of the breakthrough curve was missed. It is of interest to note that each of the wells show slightly different results. At Well 19, most of the tracer arrives from the lower lens. At Well 14, most of the tracer arrives from the higher lens. At Well 13, similar amounts of tracer arrives from the upper and the lower lenses.

Table E.1 compares these values and the borehole flowmeter results. Because the groundwater is traveling from the injection well to the withdrawal well, the hydraulic conductivity value calculated from the tracer test should be compared to both the borehole flowmeter results at the injection and the withdrawal well. In general, favorable agreement was obtained between the two sets of hydraulic conductivity values.

#### **E.4.2 Tracer Test 2**

Figure E.9 shows that each of the wells has a zone of relatively high hydraulic conductivity near elevation 61 m MSL. In general, all of the profiles, with the possible exception of Well 8, exhibit similar flow patterns. Figure E.10 shows that at for all of the wells, the majority of rapid tracer transport occurred above 58 m MSL. At Well 10, the zone of primary tracer transport is located at an elevation near 60 m MSL but a smaller amount of tracer transport did occur at the lower elevation of 57 m MSL. The profile for Well 24 does not show any tracer transport at elevations higher than 58 m MSL. Based on

Figure E.9, one might expect a zone of high tracer transport at an elevation of about 61 m MSL. However, the sampling ports were not positioned high enough in this well to confirm the expected trend. Table E.2 compares these values and the borehole flowmeter results.

**Table E.1 Comparison of hydraulic conductivity values from the borehole flowmeter and Tracer Test 1**

Withdrawal Well	ELEV (m)	R (m)	Time (min)	V (cm/min)	J	Tracer Test <sup>1</sup> K(cm/s)	Flowmeter <sup>2</sup>	
							Well W K(cm/s)	Well I K(cm/s)
19	58.5	4.18	60	6.97	.060	>0.58	1.6	1.5
19	56.1	4.18	60	6.97	.060	>0.58	1.7	0.4
14	58.7	4.12	80	5.15	.106	0.24	0.36	1.5
14	56.3	4.12	48	8.58	.106	>0.40	0.12	0.4
13	59.6	4.41	96	4.59	.058	0.40	0.38	1.5
13	56.0	4.41	96	4.59	.058	0.40	0.61	0.4
5	60.7	5.25	213	2.46	.054	0.23	0.26	1.5
5	59.5	5.25	306	1.72	.054	0.16	0.26	1.5
5	55.8	5.25	171	3.07	.054	0.28	0.12	0.4

<sup>1</sup>From Equation 5

<sup>2</sup>Well W is withdrawal well, Well I is injection Well 16, K is taken from Figures 30-32

**Table E.2 Comparison of hydraulic conductivity values from the borehole flowmeter and tracer test 2**

Withdrawal Well	ELEV (m)	R (m)	Time (min)	V (cm/min)	J	Tracer Test <sup>1</sup> K(cm/s)	Flowmeter <sup>2</sup>	
							Well W K(cm/s)	Well I K(cm/s)
25	60.6	6.13	144	4.26	.155	0.14	0.20	0.43
24	57.0	3.64	969	0.386	.249	.0078	0.0071	0.022
10	60.2	4.39	174	2.52	.292	>0.043	0.27	0.43
8	59.94	6.25	504	1.24	.175	0.036	0.0086	0.43

<sup>1</sup>From Equation 5

<sup>2</sup>Well W is withdrawal well, Well I is injection Well 12, K is taken from Figures 30-32

### E.4.3 Tracer Test 3

Figure E.11 shows the vertical distribution of groundwater flow for three doublet tests. All of the paired flow profiles show noticeable differences. Wells 2 and 18 have very different profiles below 59 m MSL. Whereas Well 21 has most of its flow located in zones above 59 m MSL, Well 17 has most of its flow located in zones below 59 m MSL. Below 61 m MSL, the high flow zones at Well 11 matches up with the low flow zones at Well 20. The differences in the flow profiles at the paired wells indicate that the transport of tracer between the wells did not occur within contiguous horizontal lenses.

Figure E.12 shows well defined tracer flux breakthrough curves for Wells 2, 11, and 17. For both Wells 2 and 11, the plots show that the primary zone of tracer transport is near 59 m MSL. For Well 17 no information is shown for elevations above 59 m MSL because above 59 m MSL there were problems with the tracer test data. Table E.3 shows an

agreement at Wells 17 and 11. At Well 2, the hydraulic conductivity values from the tracer test is about one-fourth of the hydraulic conductivity derived from the borehole flowmeter tests.

**Table E.3 Comparison of hydraulic conductivity values from the borehole flowmeter and tracer test 3**

Withdrawal Well	ELEV (m)	R (m)	Time (min)	V (cm/min)	J	Tracer Test <sup>1</sup> K(cm/s)	Flowmeter <sup>2</sup>	
							Well W K(cm/s)	Well I K(cm/s)
2	59.6	6.72	603	1.11	0.0376	0.148	0.645	0.955
11	58.6	6.15	153	4.02	0.274	0.073	0.148	0.107
17	55.61	5.16	1362	0.379	0.123	0.0154	0.085	0.0093

<sup>1</sup>From Equation 5

<sup>2</sup>Well W is withdrawal well, Well I is the respective injection well, K is taken from Figures 30-32

#### E.4.9 Tracer Test 4

Figure E.13 shows that the similar flow profiles were for Wells 26 and 3. The profile comparisons for the other well pairs, however, are poor and indicate that very few, if any, lenses are common to both the injection and the withdrawal wells. Figure E.14 shows the tracer breakthrough curves for Wells 3, 7, and 9. No data is presented for Well 1 because no tracer breakthrough curves were observed fig 40 at the well. At Well 3, the primary zone of tracer transport was near 60 m MSL. At Wells 7 and 9 tracer transport occurred primarily near 59 m MSL and near 55 m MSL. One should note that although both Wells 7 and 9 have

lenses of high conductivity located near the same elevations, there is an important difference between these lenses at the wells. At Well 7, the transport is fastest in the aquifer lense(s) near 55 m MSL, whereas at Well 13, the transport is fastest in the aquifer lense(s) near 59 m MSL. Table E.4 compares these values and the borehole flowmeter results. These comparisons vary from good (Well 3) to poor (Well 1).

## **E.5 RESULTS FOR TRACER TEST 5**

### **E.5.1 Data Presentation**

The major concern about the design of the large-scale tracer test was the potential for cross-contamination problems caused by the wells located between the injection and the withdrawal wells. One of the reasons that the cross-contamination problems was considered manageable is that the wells only intersect  $10^{-5}$  percent of the aquifer. Because cross-contamination would occur in only a relatively small volume, any cross-contamination between the aquifer layers would quickly dissipate with distance from the well and have a minor effect on the tracer profiles in downgradient wells. Because potential cross-contamination problems were a concern, groundwater samples were not taken from wells located in the immediate downgradient vicinity of a well. For this reason, all of the 27 interior wells were sampled except for Wells 14, 15, 19, 12, and 24.

**Table E.4 Comparison of hydraulic conductivity values from the borehole flowmeter and tracer test 4**

Withdrawal Well	ELEV (m)	R (m)	Time (min)	V (cm/min)	J	Tracer Test <sup>1</sup> K(cm/s)	Flowmeter <sup>2</sup>	
							Well W K(cm/s)	Well I K(cm/s)
9	59.3	8.87	1038	0.854	0.203	0.021	0.22	0.041
9	55.6	8.87	2178	0.407	0.203	0.010	0.30	0.011
7	59.3	7.28	1224	0.59	0.0846	0.035	0.11	0.091
7	54.3	7.28	444	1.64	0.0846	0.097	0.54	1.75
3	60.33	15.2	978	1.55	0.0249	0.311	0.71	0.125
1	-	15.8	>3,000	<8.8E-5	0.1605	<1.6E-4	.029 <sup>3</sup>	0.077 <sup>3</sup>

<sup>1</sup>From Equation 5

<sup>2</sup>Well W is withdrawal well, Well I is injection well, K is taken from Figures 30-32

<sup>3</sup>average values

Besides causing cross-contamination between aquifer layers, the vertical flows in the fully-screened wells were of concern. The mixing in a well could cause problems with interpreting the tracer profiles at that location. Because of this potential problem, the vertical flow profile in each well was logged during the tracer test. The flow profiles in the majority of the 27 interior wells had profiles similar to the examples shown in Figure E.15. In Figure E.15 the flow profiles have unidirectional flows that are less than .4 L/min. At every well, flow measurements were taken at 0.3-m increments. At selected wells, groundwater samples were taken at 0.6-m increments.

Although Figure E.15 cannot be used to determine the actual tracer concentrations in the aquifer at each elevation because the horizontal rate of groundwater flow through the



well is unknown, one can estimate from the data the elevation in the aquifer at which the tracer concentrations are highest and the time at which the peak concentration occurs in the well.

### **E.5.2 Water Table Elevations**

Table E.5 provides the temporal variations of the hydraulic gradients across the entire test area for the tracer test. The data indicates that the aquifer's hydraulic gradients were constant during the total tracer test. Figure 4.5 in the Chapter 4 shows the piezometric contours, which indicate that the aquifer material is considerably less resistant to groundwater flow toward Wells 3 and 7, than toward Wells 1 and 9.

### **E.5.3 Tracer Concentrations**

As the first half of the groundwater samples were being measured for chloride, problems occurred with adjusting and maintaining the calibration of the specific ion probes. The problems became more frequent and severe until the chloride probes were replaced midway through the chloride measurements. Because the accuracy of this portion of the chloride data was questionable, the electrical conductivity measurements were used to define the shape of the tracer breakthrough curve. All of the designated monitoring wells were sampled periodically throughout the duration of the test except for Wells 32 and 7. Unfortunately, the wells were sampled on a regular schedule only until 60 hours into the tracer test. After 60 hours, tracer breakthrough had not begun at Well 32 nor 7. Before the test ended, tracer breakthroughs were observed at all other wells except for Wells 1, 9, 8,



15	0.19	0.19	0.19	0.18	0.18	0.19	0.19	0.19
16	0.49	0.48	0.48	0.48	0.48	0.48	0.48	0.48
17	0.19	0.19	0.19	0.19	0.19	0.19	0.19	0.19
18	0.16	0.16	0.16	0.16	0.16	0.16	0.16	0.16
19	0.32	0.32	0.32	0.31	0.31	0.31	0.31	0.32
20	0.28	0.28	0.27	0.31	0.27	0.30	0.27	0.27
21	0.16	0.16	0.16	0.16	0.16	0.16	0.16	0.16
22	0.05	0.05	0.05	0.05	0.05	0.05	0.05	0.05
23	NM	NM	NM	NM	0.06	0.06	0.06	0.06
24	0.16	0.16	0.15	0.15	0.15	0.15	0.16	0.15
25	0.22	0.22	0.22	0.22	0.22	0.22	0.22	0.22
26	0.15	0.15	0.15	0.14	0.14	0.15	0.14	0.15
27	NM	NM	NM	NM	0.06	0.06	0.06	0.06
28	NM	NM	NM	NM	0.06	0.06	0.06	0.06
29	NM	NM	NM	NM	NM	0.05	0.05	0.05
30	NM	0.15	0.15	0.15	0.15	0.15	0.15	0.15
31	0.12	0.12	0.12	0.12	NM	0.12	0.12	0.12
32	0.10	0.10	0.10	0.10	0.10	0.11	0.11	0.10
33	NM	0.99	NM	NM	0.04	0.04	0.04	0.04
34	NM	0.99	NM	NM	0.04	0.04	0.04	0.04
35	NM	0.99	NM	NM	NM	0.04	0.04	0.04
36	NM	0.98	NM	NM	NM	0.04	0.04	0.04
37	NM	1.39	NM	NM	0.06	0.06	0.06	0.0

---

NM - No Measurement

HYDRAULIC CONDUCTIVITY REGIONS  
 $K_1 < K_2$

■ -  $K_1$     ▨ -  $K_2$

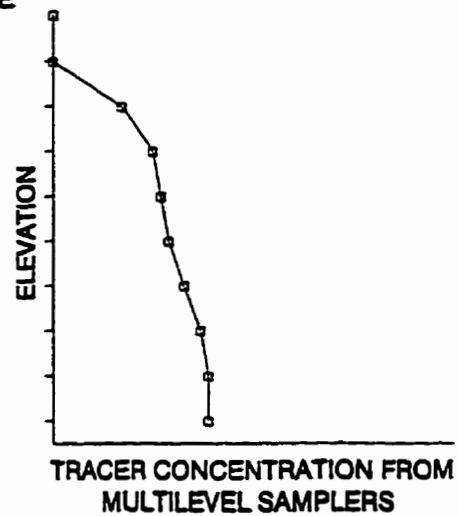
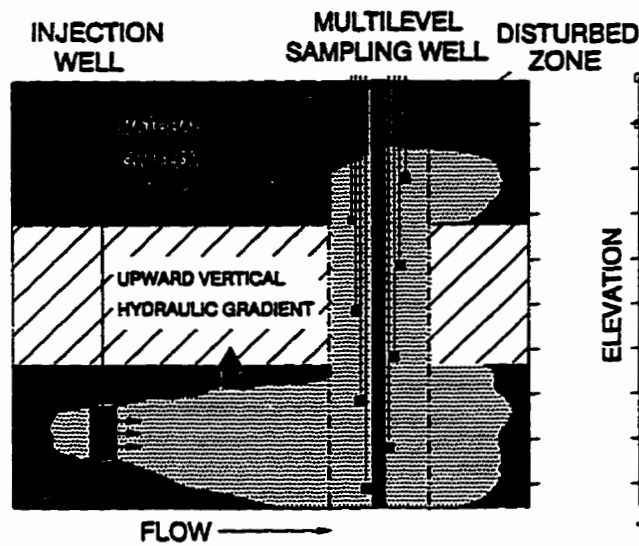
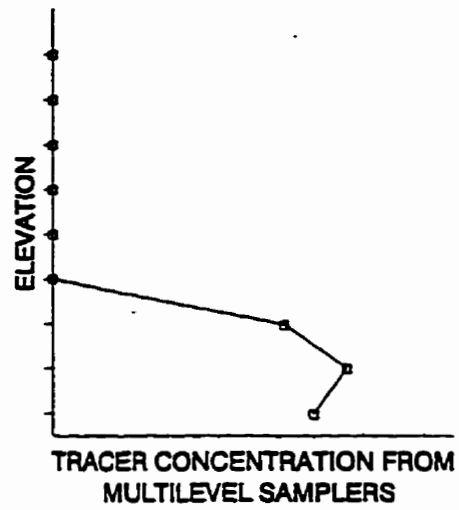
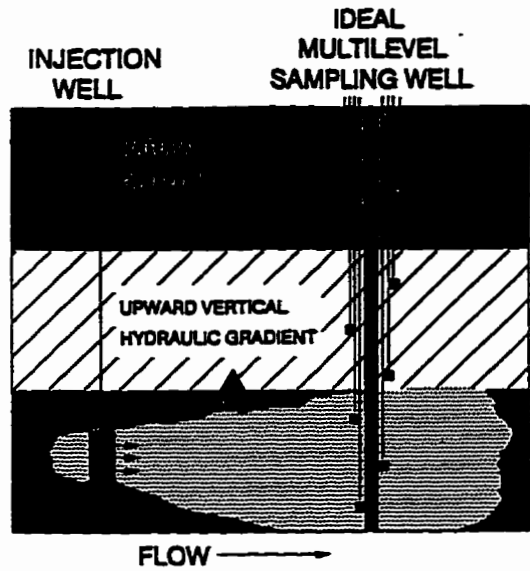


Figure E.1 Potential for mixing of concentration fronts in the annulus of multilevel samplers.

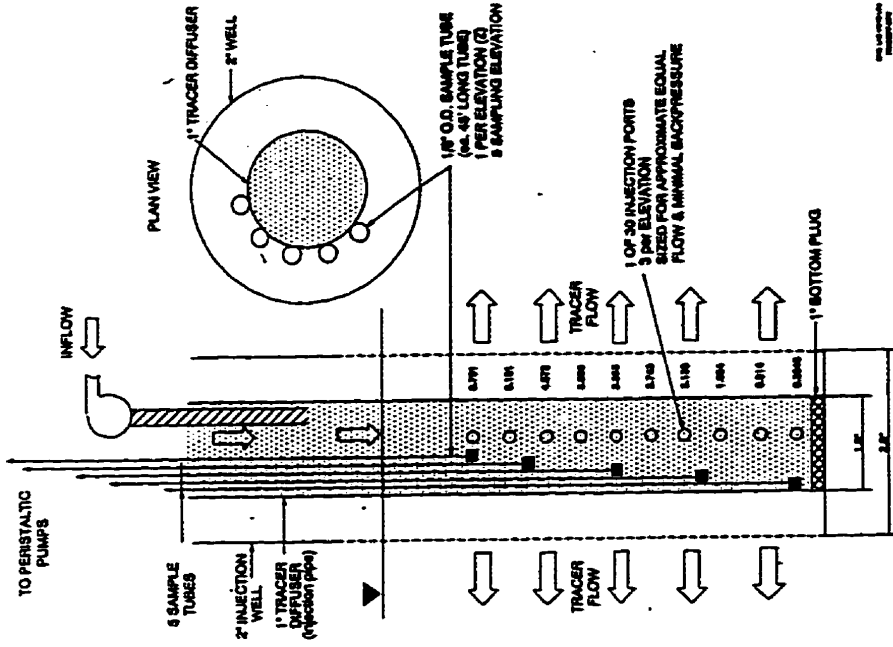
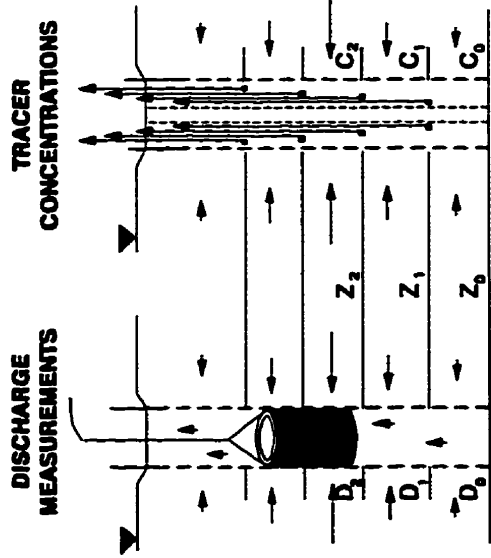


Figure E.3 Multilevel sampler for collecting groundwater samples from inside the injection wells.



LEGEND:  
 $Z_1$  - LOCATION OF LAYER I  
 $D_1$  - DISCHARGE FROM LAYER I  
 $C_1$  - AVERAGE TRACER CONCENTRATION IN LAYER I

EXAMPLE CALCULATION OF MASS FLUX

INTERNAL	VERTICAL DISCHARGE	TRACER CONCENTRATION	CUMULATIVE MASS FLUX OF TRACER	INCREMENTAL MASS FLUX OF TRACER
$Z_0$	$D_0$	$C_0$	$D_0 \cdot C_0$	$D_0 \cdot C_0$
$Z_1$	$D_1$	$C_1$	$D_1 \cdot C_1$	$D_1 \cdot C_1 - (D_0 \cdot C_0)$
$Z_2$	$D_2$	$C_2$	$D_2 \cdot C_2$	$D_2 \cdot C_2 - (D_1 \cdot C_1)$
$Z_1$	$D_1$	$C_1$	$D_1 \cdot C_1$	$D_1 \cdot C_1 - (D_2 \cdot C_2)$

Figure E.2 Borehole flowmeter and tracer concentration measurements at the injection and withdrawal wells.

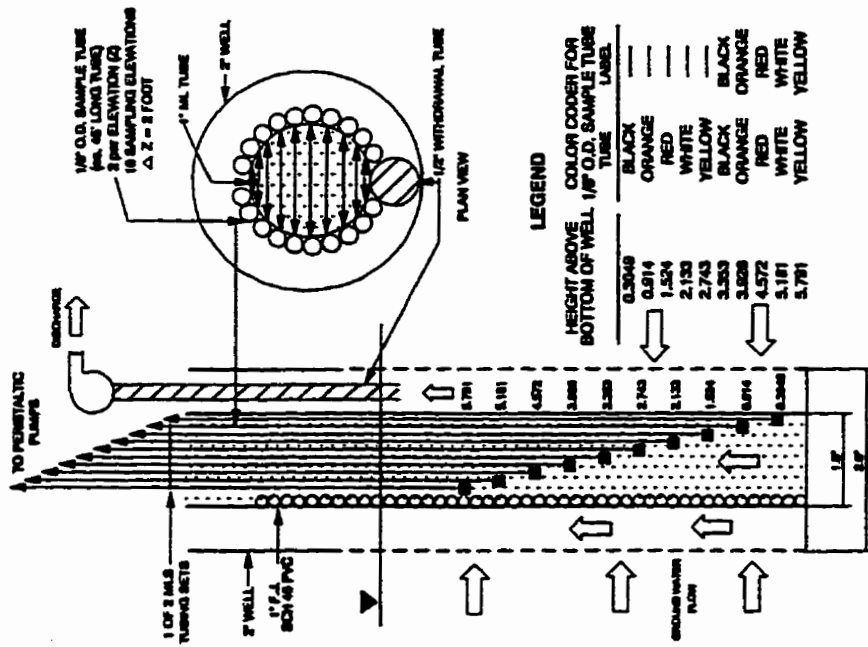


Figure E.4 Multilevel sampler for collecting groundwater samples from inside the withdrawal wells.

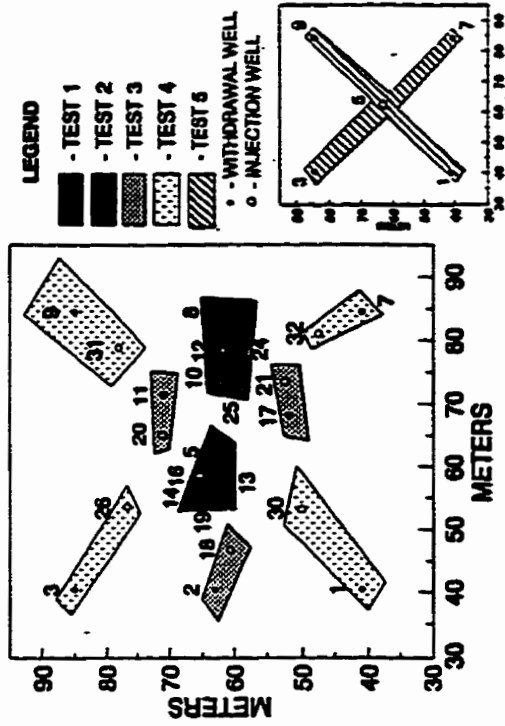
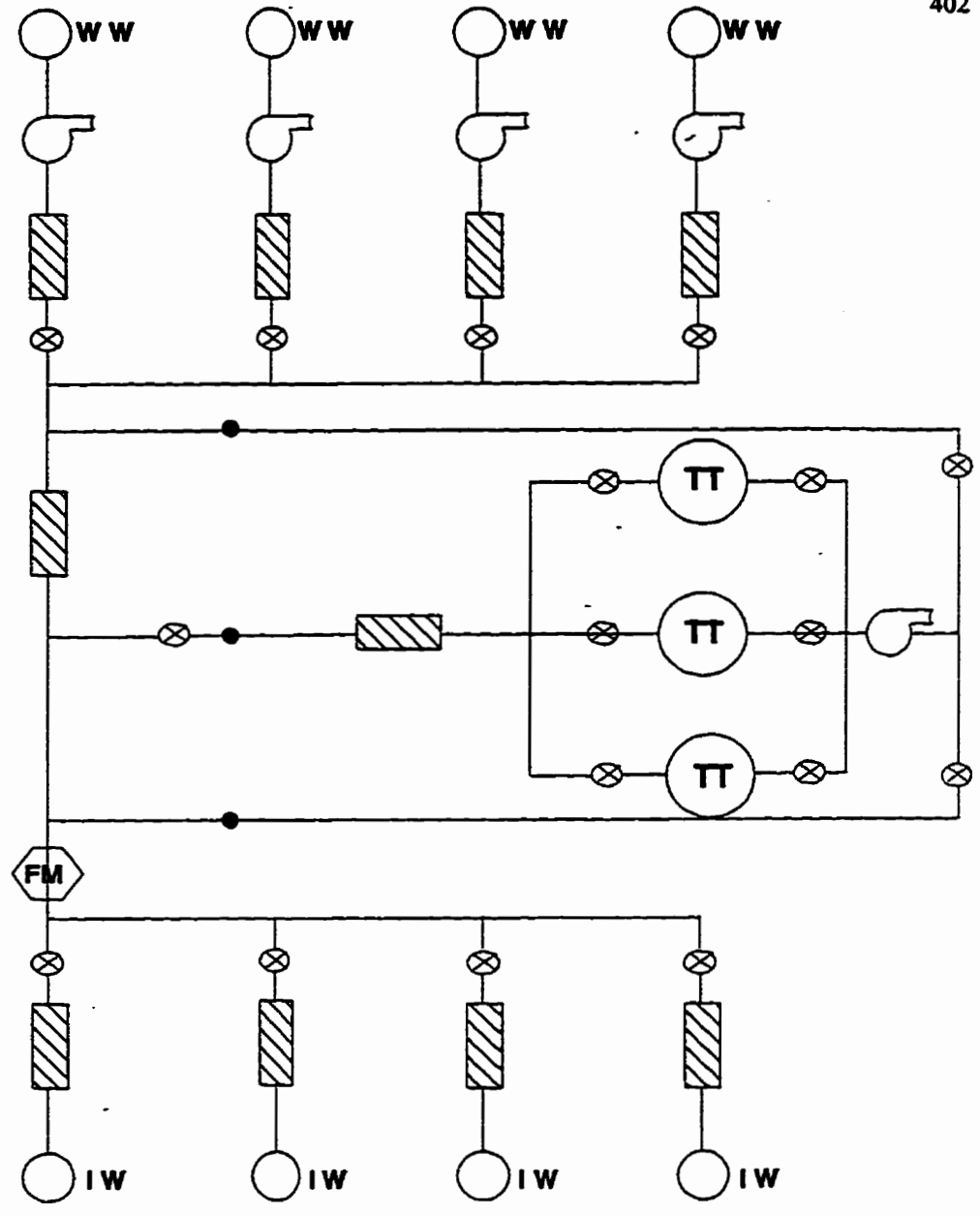







Figure E.5 Location of the small-scale recirculating tracer tests at the 1-Ha test site.



LEGEND

-  POSITIVE DISPLACEMENT PUMP
-  ROTAMETER (VISUAL INSPECTIONAL FLOWRATE)
-  FLOW RATE VALUE
-  TOTALIZING FLOW METER
-  LOCATION FOR IN-LINE SAMPLING
- TT : TRACER TANK
- WW : WITHDRAW WELL
- IW : INJECTION WELL

PHIL LEE AND LEO TRACERLAB

Figure E.6 Setup for the tracer injection and recirculation of groundwater from the withdrawal well(s) to the injection well(s).

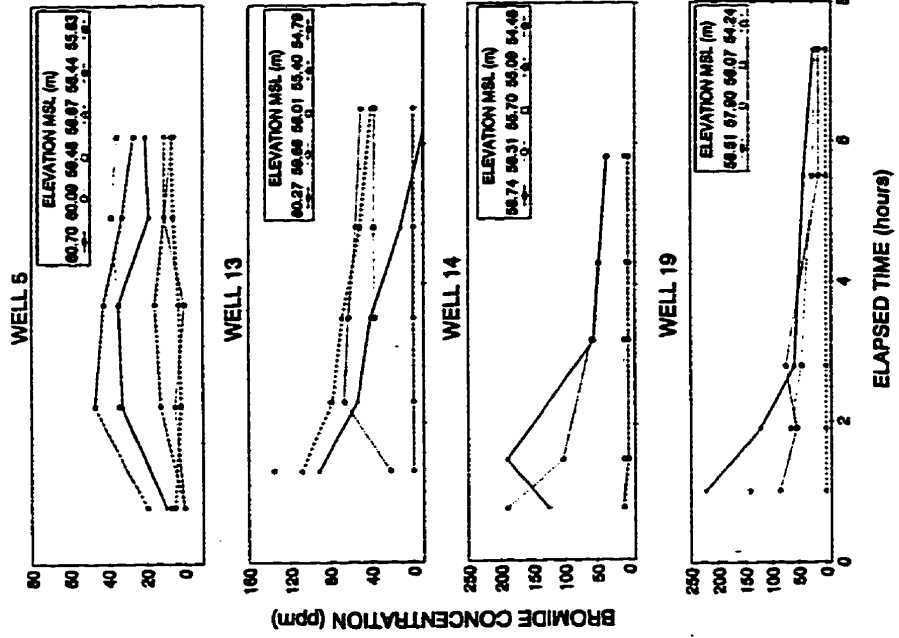


Figure E.8 Tracer concentration patterns at Wells 13, 14, 19, and Well 5 during Tracer Test 1.

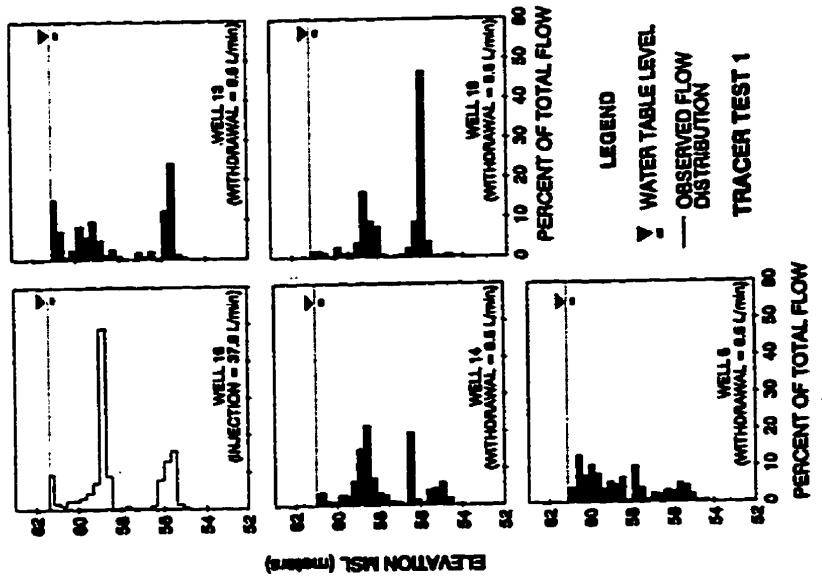


Figure E.7 Groundwater flow patterns at Wells 16, 13, 14, 19, and Well 5 during tracer Test 1.



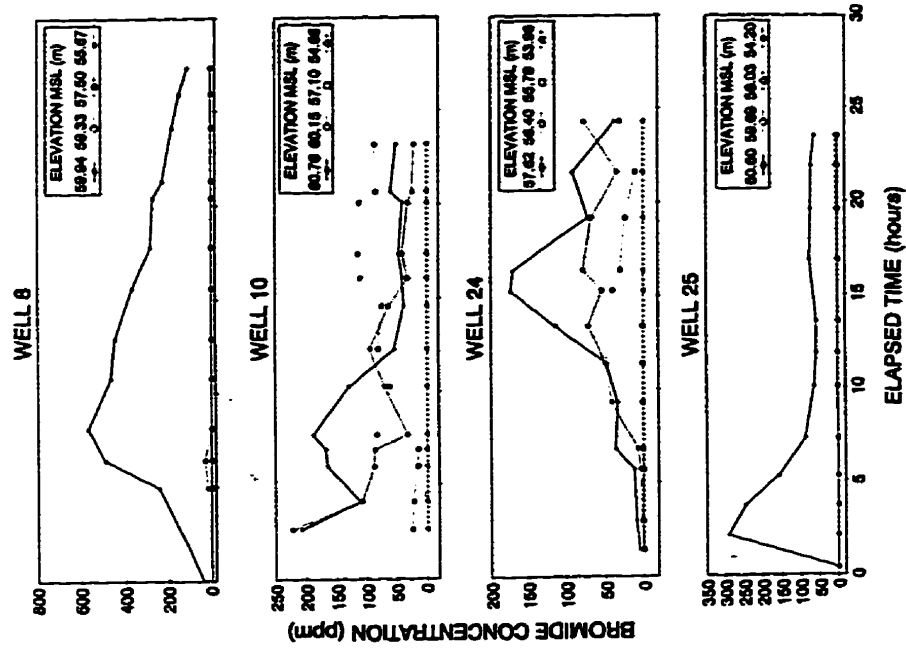


Figure E.10 Tracer concentration patterns at Wells 8, 10, 24, and 25 during Tracer Test 2.

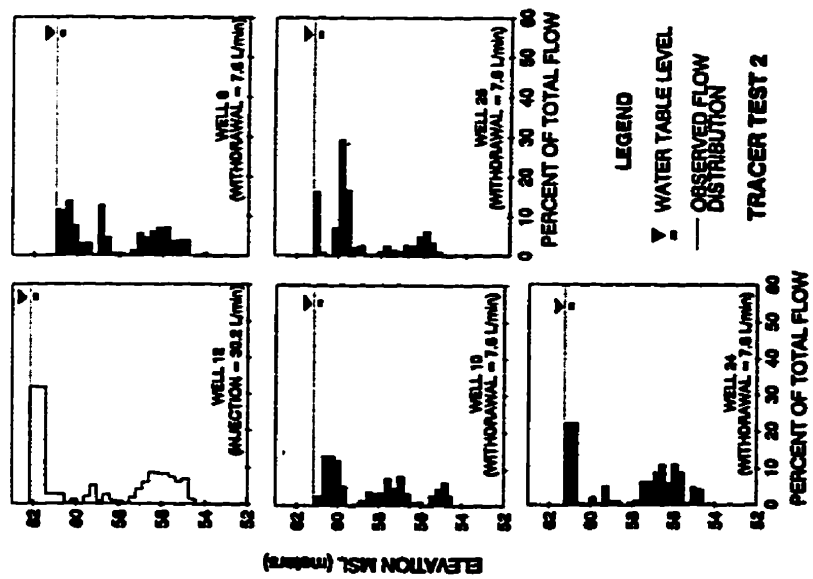


Figure E.9 Groundwater flow patterns at Wells 8, 10, 12, 24, and 25 during Tracer Test 2.

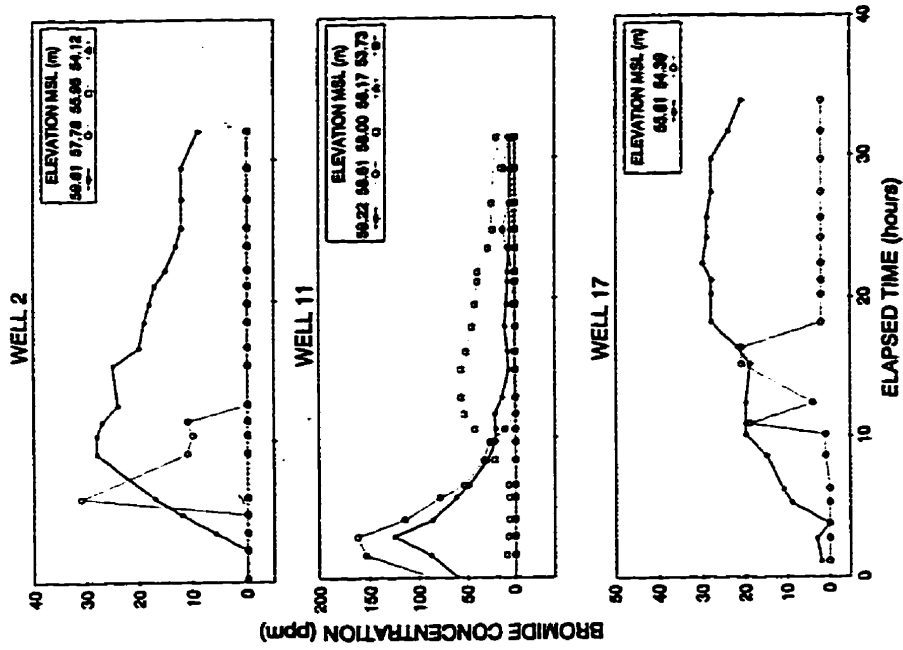


Figure E.11 Groundwater flow patterns at Wells 2, 11, 17, 18, 20, and 21 during Tracer Test 3.

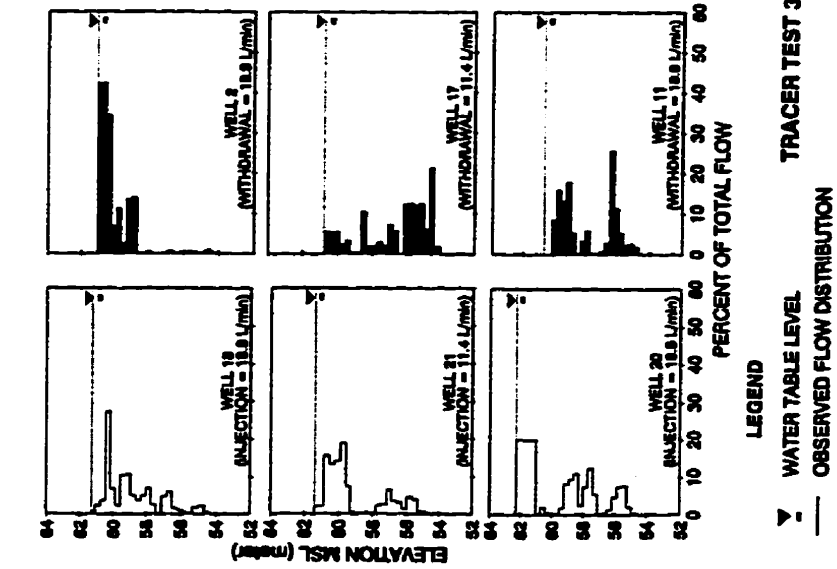


Figure E.12 Tracer concentration patterns at Wells 2, 11, and 17 during Tracer Test 3.

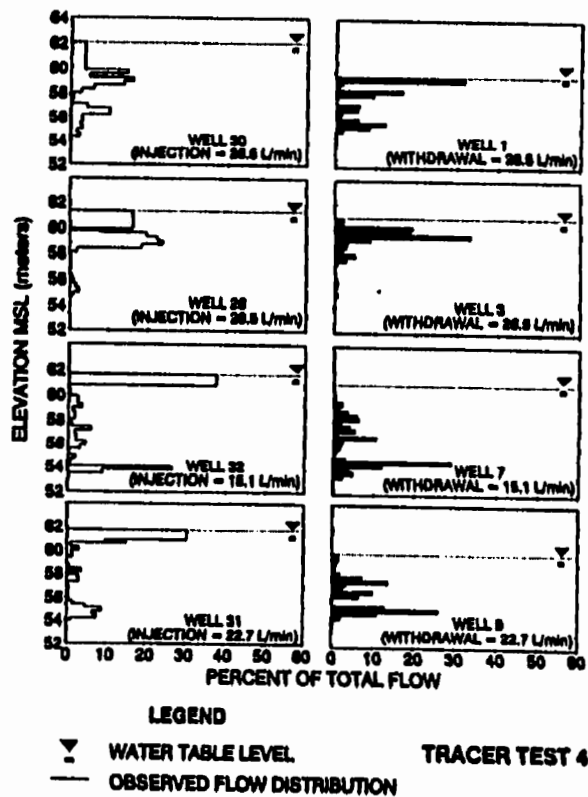


Figure E.13 Groundwater flow patterns at Wells 1, 3, 7, 9, 26, and 30, 31, and 32 during Tracer test 4.

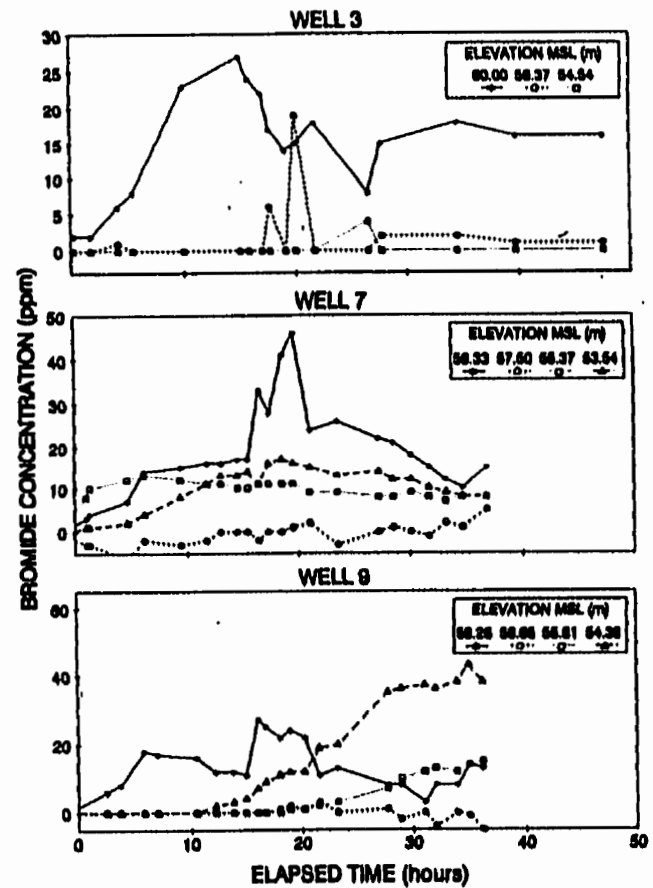


Figure E.14 Tracer concentration patterns at Wells 3, 7, and 9 during Tracer Test 4.

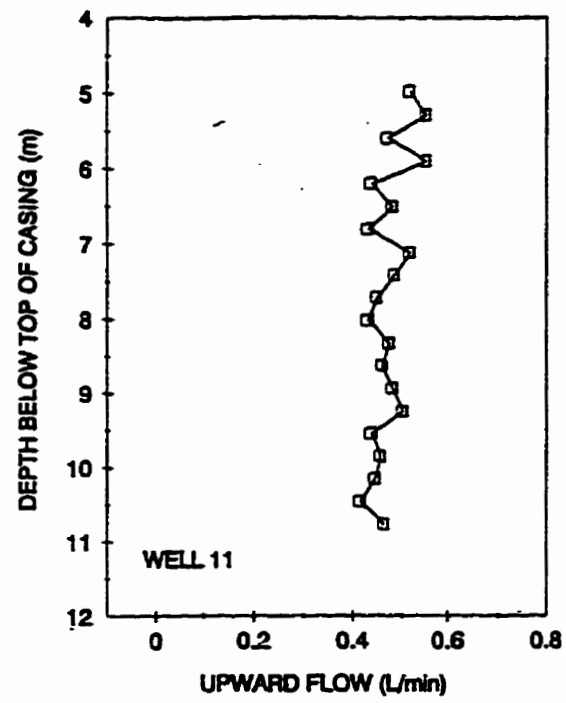


Figure E.15 Examples of vertical groundwater flow in wells during Tracer Test 5.